THE OHIO STATE UNIVERSITY

18th Annual Meeting
October 13-15, 1994

Conference Proceedings

AMERICAN SOCIETY OF BIOMECHANICS

edited by

Robert J. Gregor, Ph.D., The Georgia Institute of Technology
Alan S. Litsky, M.D., Sc.D., The Ohio State University

AMERICAN SOCIETY OF BIOMECHANICS

PROCEEDINGS
FOR THE
18TH ANNUAL MEETING

The Ohio State University
Columbus, Ohio

October 13-15, 1994

SPONSORS

The Ohio State University
Biomedical Engineering Center
College of Medicine
Division of Orthopaedic Surgery

The Cleveland Clinic Foundation
Department of Biomedical Engineering

The Whitaker Foundation

Edison BioTechnology Center

AMERICAN SOCIETY OF BIOMECHANICS

SUSTAINING MEMBERS OF THE AMERICAN SOCIETY OF BIOMECHANICS

The Society would like to thank the following organizations for their support as Sustaining Members:

Aircast, Inc.

DePuy, Inc.

Howmedica, Inc.

Kistler Instrument Corporation

Motion Analysis Corporation

MTS Systems Corporation

Noraxon U.S.A.

Peak Performance Technologies, Inc.

Orthofix, S.R.L.

Orthomet, Inc.

Zimmer, Inc.

AMERICAN SOCIETY OF BIOMECHANICS

The American Society of Biomechanics was formed in 1977 to foster among individuals in various disciplines in biomechanics research, such as anthropology, biology, engineering, ergonomics, exercise and sport science, orthopaedics, physiology, rehabilitation, speech and hearing, sports medicine, and zoology. In brief, Society members are persons applying principles of mechanics to the study of biological systems. The Annual Meeting provides an opportunity to exchange information and to broaden the perspectives on biomechanics in both formal and informal settings.

The Executive Board that had governed the Society during the past year is represented by the following individuals:

President:
Thomas D. Brown
University of Iowa

Past President:
Ronald F. Zernicke
University of Calgary

President-elect:
Philip E. Martin
Arizona State University

Secretary-Treasurer:
Mark D. Grabiner
The Cleveland Clinic Foundation

Meeting Chairperson:
Alan S. Litsky
The Ohio State University

Program Chairperson:
Robert J. Gregor
The Georgia Institute of Technology

Program Chairperson-elect:
Keith Williams
University of California, Davis

Membership Committee Chairperson:
M. Melissa Gross
University of Michigan

Education Committe Chairperson:
Jill McNitt-Gray
University of Southern California

PROGRAM COMMITTEE

Robert J. Gregor, Ph.D. *(Program Chair)*
Georgia Institute of Technology
Keith Williams, Ph.D. *(Program Chair-elect)*
University of California, Davis
Thomas Andriacchi, Ph.D.
Rush-Pres.-St. Luke's Medical Center
Donald Chaffin, Ph.D.
University of Michigan
Barbara Loitz, P.T., Ph.D.
Univeristy of Wisconsin
Jill McNitt-Gray, Ph.D.
University of Southern California
R. Natarajan, Ph.D.
Rush-Pres.-St. Luke's Medical Center
Clint Rubin, Ph.D.
SUNY, Stonybrook
William Whiting, Ph.D.
UCLA

EXHIBITORS

Human Kinetics
J.B. Lippincott Co.
Northern Digital Inc.
Human Kinetics
Kistler Instrument Corp.
Ariel Dynamics, Inc.
Bertec Corporation
Interlaken Technology
Innovision Systems, Inc.
Peak Performance Technologies, Inc.
MTS Systems Corporation
Noraxon, USA
B & B Microscopes, Ltd.
Novel Electronics, Inc.
Endura-Tec Systems
Motion Analysis Corporation

SESSION CHAIRS

1. **Mark Grabiner**, Ph.D.
   Department of Biomedical Engineering/Wb3
   The Cleveland Clinic Foundation
   One Clinic Center
   9500 Euclid Avenue
   Cleveland, OH 44195-5254

2. **Roger Enoka**, Ph.D.
   Department of Biomedical Engineering/Wb3
   The Cleveland Clinic Foundation
   One Clinic Center
   9500 Euclid Avenue
   Cleveland, OH 44195-5254

3. **Doris I. Miller**, Ph.D.
   University of Western Ontario
   Faculty of Kinesiology
   Thames Hall, 22
   London, Ontario
   CANADA N6A 3K7

4. **Christopher L. (Kit) Vaughn**, Ph.D.
   University of Virginia
   Health Sciences Center
   Children's Medical Center
   Kluge Children's Rehabilitation Center &
   Research Institute
   227 Ivy Road
   Charlottesville, VA 22901

5. **Melissa Gross**, Ph.D.
   University of Michigan
   Department of Movement Science
   401 Washtenaw Avenue
   Ann Arbor, MI 48109-2214

6. **Mary M. Rogers**, P.T., Ph.D.
   Wright State University
   School of Medicine
   Institute for Rehabilitation Research
   & Medicine
   3171 Research Boulevard
   Dayton, OH 45420

7. **Clint Rubin**, Ph.D
   State University of New York
   Musculo-Skeletal Research Laboratory
   Department of Orthopaedics
   Health Sciences Center T18-030
   Stonybrook, New York 11794-8181

8. **Louis F. Draganich**, Ph.D
   The University of Chicago
   Director of Orthopaedic Biomechanics
   Section Orthopaedic Surgery
   & Rehabilitation Medicine
   Department of Surgery
   5841 South Maryland Avenue, MC 3079
   Chicago, IL 60637-1470

9. **Irene S. McClay**, P.T., Ph.D.
   University of Delaware
   Physical Therapy Program
   School of Life & Health Sciences
   054 McKinly Laboratory
   Newark, DE 19716

10. **Ronald F. Zernicke**, Ph.D
    McCaig Centre for Joint Injury
    & Arthritis Research
    Department of Surgery
    3330 Hospital Drive NW
    Calgary, Alberta
    CANADA T2N 4N1

11. **Jill McNitt-Gray**, Ph.D.
    University of Southern California
    Department of Exercise Science
    Physical Education Building
    P.E.D. 107
    Los Angeles, CA 90089-0652

12. **Robert Shapiro**, Ph.D.
    Associate Dean, College of Education
    166 Taylor Education Building
    University of Kentucky
    Lexington, KY 40506-0001

AWARD WINNERS

Borelli Award:

Dr. Peter R. Cavanaugh
Distinguished Professor
Pennsylvania State University
"Rings in the Well: Adventures in the Study of Human Locomotion (xxiii)

Clinical Biomechanics Award:

Mr. Rodney Bristol
"Non-Uniformity of Contact Stress in Total Knee Arthroplasty" (xxiv)

Post-Doctoral Young Scientists Award:

Dr. J.J. Collins
"Developing and Implementing Techniques and Concepts from Nonlinear Dynamics and Statistical Mechanics to Study the Biomechanics and Neural Control of Posture and Locomotion" (171)

Pre-Doctoral Young Scientist Award:

Jeffrey A. Duncan
"Stair Climbing Gait to Evaluate Anterior Cruciate Ligament Reconstruction" (157)

POSTER SESSION I

SESSION 5: MUSCULOSKELETAL BIOMECHANICS
CHAIR: *Melissa Gross, Ph.D.*

SESSION 6: GAIT/POSTURE
CHAIR: *Mary Rogers, PT, Ph.D.*

SESSION 7: TISSUE MECHANICS
CHAIR: *Clint Rubin, Ph.D.*

SESSION 8: JOINTS
CHAIR: *Louis Draganich, Ph.D.*

SESSION 10: BONE
CHAIR: *Ronald F. Zernicke, Ph.D.*

SESSION 11: MOTOR CONTROL
CHAIR: *Jill McNitt-Gray, Ph.D.*

POSTER SESSION II

The 1994 Borelli Lecture

Rings in the Well: Adventures in the Study of Human Locomotion

Peter R. Cavanagh, Ph.D.
Center for Locomotion Studies
Penn State University, University Park, PA 16802

"These [ideas] dropped into my childish mind as if you should accidentally drop a ring into a deep well. I did not think of them much at the time, but there came a day in my life when the ring was fished up out of the well, good as new." Harriet Beecher Stowe, 1869.

Studies of human locomotion have, historically, played a pivotal role in the development of musculoskeletal biomechanics. The progression inherent in the activity under study can be considered a metaphor for the advancement that results from each experiment. New methods, results and ideas do not always find immediate application but, like rings in the well, they lie in wait for future rediscovery.

In an attempt to demonstrate the way in which previous experiments influence and contribute to new directions, this presentation will describe some of the studies conducted over the last 20 years by the author and his colleagues. Among the topics to be discussed are walking, running, and cycling mechanics; athletic and therapeutic footwear; and mechanical factors that affect the foot in diabetes.

Clinical Biomechanics Award Paper

Non-Uniformity of Contact Stress in Total Knee Arthroplasty

R.E. Bristol, MS, D.C. Fitzpatrick, MS, T.D. Brown, and J.J. Callaghan, MD

Depts. of Mechanical Engineering, Biomedical Engineering and Orthopaedic Surgery
University of Iowa
Iowa City, Iowa

SUMMARY

This study examined 15 commercially available TKR designs using PresSensor pressure sensitive film. There was found to be no consistent, statistically significant positive correlation between minimization of spatial mean contact stress and minimization of the amount of overloaded (>10 MPa) UHMWPe contact area. Furthermore, it was seen that machining cutter preparation of the UHMWPe insert not only left grossly visible A/P grooves on the articulating surface, but that substantial pressure non-uniformities corresponding to these grooves also appeared on the PresSensor contact stress recordings.

RELEVANCE

Because of the lack of statistically significant correlation between spatial mean contact stress and highly loaded UHMWPe area, we question the utility of spatial mean contact stress as a parameter for predicting the relative wear propensity of contemporary total knee designs.

Keynote #2

BIOMECHANICS OF SKELETAL MUSCLE INJURY

Richard L. Lieber, Ph.D.
Departments of Orthopaedics and Bioengineering
University of California, San Diego, La Jolla, California 92093-9151

Skeletal muscle injury was studied in rabbits and humans to understand the injury mechanism and to investigate methods for preventing injury. A human model of eccentric contraction was first created in the quadriceps femoris muscles which demonstrated that significant structural abnormalities are associated with eccentric contractions. In all cases, the earliest structural signs of injury were disruptions of the myofibrillar lattice at the level of the Z-disk.

A rabbit model was then developed to understand the fiber type-specific effects of injury and the injury mechanism. It was found that injury is most pronounced in the large, fast fibers with low oxidative capacity, i.e., the fast glycolytic or type 2B fibers. The mechanical basis for this injury was investigated by imposing a series of different stresses and strains on activated muscles. Using a multiple regression mode, we demonstrated that muscle fiber strain not stress was the mechanical factor most responsible for injury.

A noninvasive rabbit model was then developed to study the time-course of injury and recovery as well as muscle-specific damage after exercise. We found that injury was most pronounced in the extensor digitorum longus (EDL) muscle compared to the TA. Again, this was due to the high fiber strains achieved in the EDL during exercise. We also demonstrated significant disruption of the TA and EDL protein desmin suggesting cytoskeletal injury. In fact, such disruption was observed within minutes, indicating that these cellular changes were not controlled via gene regulation. Muscle fiber regeneration after injury was pronounced based on the expression of embryonic myosin during recovery.

Finally, the use of the nonsteroidal anthiinflammatory drug (NSAID), flurbiprofen, was administered to animals for three days following exercise-induced injury. We found that the NSAID exerted a potent short-term protective effect but resulted in a significant depression of muscle contractile properties in the long-term. These studies provide the basis for an improved understanding of muscle injury as well as data which may provide a rationale basis for treatment of muscle injury.

REFERENCES:

1. Friden, J., M. Sjostrom and B. Ekblom, Myofibrillar damage following intense eccentric exercise in man. Int. J. Sports Med. 4:170-176, 1983.

2. Lieber, R.L. and J. Friden. Selective damage of fast glycolytic muscle fibers with eccentric contraction of the rabbit tibialis anterior. Acta Physiol. Scand. 133:587-588, 1988.

3. Lieber, R.L. and J. Friden. Muscle damage is not a function of muscle force but active muscle strain. J. Appl. Physiol. 74:520-526, 1993.

4. Lieber, R.L. McKee-Woodburn and J. Friden. Muscle damage induced by eccentric contractions of 25% strain. J. Appl. Physiol. 70:2498-2507, 1991.

Keynote #3

Controlling Chaos

Alan Garfinkel, Ph.D.
Departments of Physiological Science and Medicine
University of California, Los Angeles

Simple deterministic systems can sometimes display erratic and irregular behavior. This behavior, called "chaos", represents a new way of looking at disordered phenomena. It has been successfully applied to fluid turbulence, to mechanical vibrations, and to cardiac arrhythmias, among other subjects.

By understanding the nature of the underlying process, we can sometimes eliminate undesirable chaos. But that requires, in addition to a model of the system, the ability to alter the key "chaotogenic" parameters. Recently another approach to chaos has been developed, called "controlling chaos", in which one does not attempt to take the system out of chaos, but rather, uses the chaos to facilitate control of the system. This method has been used by our group to successfully control a drug-induced arrhythmia in rabbit heart tissue *in vitro*.

Chaos and chaos control may also play a role in neural control systems. In particular, the control of neuromuscular systems and of locomotion may involve chaotic processes as pathological states. But the uses of chaos in the nervous system suggest, in addition, that chaos and chaos control may also be used in functional ways by the nervous system.

POSTER SESSION

I

COLLISION PHASE OF SOCCER KICKING

Nikitas Tsaousidis and Vladimir M. Zatsiorsky

Biomechanics Lab, Department of Exercise and Sport Science,
The Pennsylvania State University, University Park, PA 16802

The classical impact theory has been used in the literature to study ball-foot interaction during a collision phase of kicking (Wahrenberg et al., 1978; Huang et al. 1982; Lindbeck, 1983). It means that the duration of the collision has been assumed to be negligibly small. Engin and Tümer (1993) modelled the response of the lower leg to impact loading. They calculated the mechanical load experienced by the various knee joint structures when an impact load of rectangular shape was applied to the lower leg. The authors found that the classical impact theory cannot forecast mechanical effects of the impact when the collision time exceeds 15 msec. They did not study however the ball-foot interaction experimentally.

METHODS

Two experienced amateur soccer players were videotaped at a frame rate of 4,000 frames per second (Kodak SP2000). Each subject performed 10 consecutive kicks. The subjects were instructed to perform each kick with maximal effort with the tip of the foot. A FIFA approved soccer ball inflated at the regulation pressure was used in the tests. During filming, the distance from the camera to the ball was about 1.5 meters. Several points on the ball surface (up to 11) were digitized with Peak 3D from Peak Performance and analyzed on a PC in order to determine the ball deformation and the ball displacement. Since none of the individual points represents the ball's center of mass location, the point at the bottom of the ball was used to calculate the ball displacement and velocity. Two landmarks on the foot and two landmarks of the shank were digitized to obtain the kinematics of the lower leg. To estimate the depth of the foot penetration into the deformed ball, a simple geometrical model was constructed. The coordinates of the tip of the foot, invisible from the camera during the impact, were then reconstructed and used to determine the ball compression. The ball displacement data were filtered at a cutoff frequency of 200 Hz, and the ball compression data at a frequency of 400 Hz using a second order Butterworh filter. The period of 'near-maximal' ball compression was defined as a period during which the area enclosed by the 'ball deformation-time' curve and an imaginary horizontal line intercepting this curve does not exceed 5% of the total area under the curve. A special program was written to define the instant of the beginning and the end of the 'near-maximum' compression.

RESULTS

The following sub phases of collision are discerned:
1. Initial compression. This is the time from the instant of the initial contact of the foot with the ball to the beginning of the ball displacement. During this sub phase:
- the ball is being compressed (the compression begins practically immediately at the instant of initial contact) but does not move as a whole;
- the foot velocity decreases sharply.
2. Ball compression during the movement. The ball compression increases while the ball is beginning to move. This sub phase begins when the ball is losing its contact with the ground and it ends at the instant of the peak ball compression. During this sub phase:
- the ball velocity increases sharply;
- the foot continues decelerating.
3. Ball decompression during the movement. This sub phase begins at the instant of the peak ball compression. Exactly at this time the foot velocity is becoming equal to the ball velocity (in other words, the relative velocity of the ball with respect to the foot is equal to zero). During this sub phase:
- the ball is decompressing; its absolute and relative velocity increases;
- the foot velocity is almost constant.

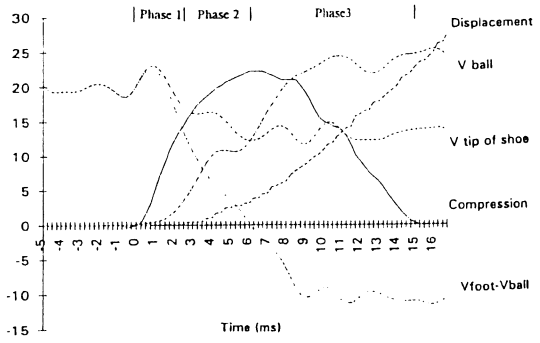

Figure: Data from a representative trial

In addition, the period of 'near-maximal' compression was determined. The main results for the ten trials of one subject are presented in the following Table (the results for the second subject were similar).

	Time, ms	Path, cm	End speed, m/s
Sub phase 1	2.95±0.9	N/A	N/A
Sub phase 2	3.28±1.3	2.72±0.7	13.6±2.4
Sub phase 3	10.2±1.3	23.3±2.2	25.2±1.5
Total	16.4±1.1	26±2.3	25.2±1.5
'Near-maximal' compression	4.3±1.7	5.99±2.5	19.4±3.7

It has been found that during and immediately after the collision the ball vibrates with a frequency which is in a sound emission range. Based on indirect evidence (the change of the shape of the curve after various smoothing procedures), the frequency of vibration was estimated between 400 and 800 Hz. A sound emission was registered directly.

DISCUSSION

Can colliding with a ball be considered a (classical) impact? In mechanics, colliding two bodies is considered an impact if the time of collision is *very short*. The definition of the *very short* interval of time depends upon a time scale of events. In case of collision of two stars, it may be millions of years; colliding nuclear particles takes nanoseconds. The most important presupposition which is made when interaction of the bodies is analyzed as a (classical) impact is the assumption about the conservation of momentum during the collision. In the case of human striking movements, the question arises: can we consider the time of collision *very* short and as a result neglect changes in the magnitude of the momentum of the 'human body-ball' system as well as in its mechanical energy? Also, can we neglect displacement of the system during the collision? If the displacement is large and the force is applied, the mechanical work done on the ball can be substantial. Note that during the collision phase the muscles are active and, if the displacement is visible, produce mechanical work.

Our data support the point of view, that the collision phase in kicking can barely be analyzed as a (classical) impact during which the total momentum of the system is conserved. There are at least three evidences in favor of the idea that the energy which is supplied by the muscles during the collision cannot be disregarded. First, during the period of contact the ball-foot displacement, compared with the range of human motion, is substantial (26±2.3 cm). Second, at the instant of maximal compression the ball possesses considerable velocity of 13.6 ±2.38 m/s, which is more than 50% of the velocity at loss of contact, 25.17±1.54 m/s. Thus, more than 50% of the ball's final velocity and at least 30% of its kinetic energy is imparted to the ball without any contribution of the potential energy of the ball deformation. Third, during the ball recoil (sub phase 3), the foot does not decelerate in spite of the force which is acting on it from the ball. This is possible only due to a counteracting muscle force. Since the muscles are shortening during this time and also generate force, they produce mechanical work which is supplied to the system. To visualize the described phenomena, let us consider two examples of a car crash. The car is colliding with an obstacle. In the first case, the engine is off. In the second, the engine is working. The first situation can be analyzed with classical equations of mechanical impact. The second, especially if the obstacle is deformable and the time of collision is not *very* short, cannot. Kicking resembles the second situation.

Hence, the classic impact theory is not applicable for modelling kicking because of not negilibly small duration of collision. As a result, (a) additional mechanical energy is supplied to the system due to the muscle work (this study), and (b) the classical impact theory cannot forecast the mechanical effect of the collision (Engin and Tümer, 1993).

Sound emission. The ball vibration during a collision is not a new discovery. Everybody knows a typical 'clapping' sound heard during any ball game. It has not been realized however that this sound can be used to collect information about the balls and striking instruments. In particular, registering sound emission is the simplest and less expensive way to determine frequency response of colliding bodies. This potential use of sound emission will be the focus of future investigation.

REFERENCES

Engin, A.E. and Tümer, S.T. (1993) ASME J. Biomech. Engng., **115**: 137-143.

Huang, T.C., Roberts, E.M. and Youm, Y. (1982) Human Body Dynamics: Impact, Occupational, and Athletic Aspects. Ghista, D.N. (Ed.) Oxford Medical Engineering Series, 409-443.

Lindbeck, L. (1983) ASME J. Biomech. Engng., **105**: 108-111.

Wahrenberg, H., Lindbeck, L. and Ekholm, J. (1978) Scandinavian J. of Rehab. Medicine, **10**: 93-98.

ACKNOWLEDGMENTS

The authors wish to thank Chris Spec for his assistance in data processing.

KINEMATIC AND EMG CHANGES DURING ASYMMETRIC AND SYMMETRIC LIFTING USING TWO TYPES OF WEIGHT BELTS

D. B. Aurslanian and R.E. Bahamonde

Biomechanics Laboratory, Ball State University, Muncie, IN. 47306

INTRODUCTION

EMG data of the erector spinae muscles synchronized with three-dimensional (3D) video techniques were used to determine the body's responses to asymmetric and symmetric lifting using two types of weight belts. Ten subjects performed static maximum voluntary exertions (SMVE) and dynamic lifts from 0^o and 45^o from the midline of the body. Three conditions were evaluated: WB1, an elastic belt with Velcro straps; WB2, a firm weight lifting belt; and WBO, a no belt condition. WB2 reduced the IEMG, peak voltage, and maximum frequency of the muscle recordings regardless of the type of lifting. No significant difference was found in the amount of time required to do the lifts, but significant differences were found in the maximum vertical velocity of the c.m. and the amount of trunk flexion. In the symmetric lifts the subjects flexed the trunk less but had a greater maximum linear vertical velocity of the c.m.

REVIEW AND THEORY

NIOSH (1981) reported that 68% of the overexertion injuries in the workplace involved lifting. Although symmetric lifting is recommended, asymmetric lifting is predominant in the workplace (Nussbaum, 1992; Plamondon et al., 1992). Disc compressive forces during lifting have been attributed to tension in the erector spinae muscles. Harman et al. (1989) and Lander et al. (1990) showed that the use of a weight belt increases the intrabdominal pressure (IAP) which theoretically reduces the spinal compressive forces by means of a decrease in the tension produced by the erector spinae muscles. To reduce the incidence of low back injuries in the workplace, many companies require the use of a weight belt. Most of the studies using weight belts have been limited to symmetric lifting and to a single type of weight belt (rigid leather). It was the purpose of this study to examine the muscle activity of the erector spinae muscles during symmetric and asymmetric lifts using two types of weight belts, a rigid weight belt and an elastic weight belt recommended by a physical therapist.

PROCEDURES

Ten male volunteers were asked to perform two trials of SMVE, symmetric lifts and asymmetric lifts. The SMVE was used to compare the EMG values during the dynamics lifts. Video analysis was used to record the 3D motion and surface bipolar electrodes (SensorMedics Corp. silver-silver chloride) were placed between the L3-L5 level of erector spinae muscle to record the EMG activity. The EMG signals were sample at 1000 Hz and processed using a high and low pass filter. Superscope II (G.W. Instruments) data acquisition program was used to collect, rectify, and integrate the EMG signals. A system of trigger mats was used to synchronize the lift. The subjects were instructed to lift a wooden box filled with sand (244.64 N maximum weight recommended by International Labor Office, 1988). For the symmetric lifts, the subjects lifted the box from a mat which triggered a light on. The subjects were instructed to lift the box about waist level and to lower the box down onto the mat which triggered the light off. The voltage passing through the light circuit was monitored and used to determine the lift period. In the asymmetric lifts, the subjects were asked to lift the box from a position of 45^0 to the right of the body to a position of 45^0 to the left of the body (without pivoting), lifting the box to about waist level. In both conditions, the box was placed at 0.3 m in front or to the side of the body. A factorial ANOVA with repeated measures was used to determine significant differences between the belts, lifts, sides, and trials.

RESULTS

Means and standard deviations for the EMG and kinematic variables are presented in Tables 1-5. WB2 (rigid weight belt) showed significant differences ($p < .05$) between the other two conditions in the burst area, peak voltage, and frequency (see Table 1-3).

Table 1. Means and standard deviations of the IEMG.

	WB1		WB2		WOB	
	RS	LS	RS	LS	RS	LS
Asy	.3398 ±.02	.2742 ±.02	.3279 ±.02	.2552 ±.02	.3685 ±.02	.3052 ±.02
Sym	.3587 ±.02	.2887 ±.02	.3402 ±.02	.2697 ±.02	.3575 ±.02	.2862 ±.02

Table 2. Means and standard deviations for the peak voltage.

	WB1		WB2		WOB	
	RS	LS	RS	LS	RS	LS
Asy	.6583 ±.07	.6420 ±.07	.6359 ±.07	.5675 ±.07	.7244 ±.07	.6632 ±.07
Sym	.7207 ±.07	.6746 ±.07	.6020 ±.07	.5754 ±.07	.7803 ±.07	.6848 ±.07

Table 3. Means and standard deviations for the maximum frequency (Hz).

	WB1		WB2		WOB	
	RS	LS	RS	LS	RS	LS
Asy	57 ±5	52 ±5	36 ±5	45 ±5	46 ±5	52 ±5
Sym	52 ±5	55 ±5	46 ±5	50 ±5	49 ±5	49 ±5

Table 4. Means and standard deviations for trunk flexion ROM (deg) (90° is the normal standing position).

LIFT	WB1	WB2	WOB
Asy	49 (± 2)	52 (± 2)	50 (± 2)
Sym	36 (± 2)	33 (± 2)	36 (± 2)

Table 5. Means and standard deviations for the maximum linear vertical velocity of the c.m. (m/s).

LIFT	WB1	WB2	WOB
Asy	.72 (±.04)	.71 (±.04)	.77 (±.04)
Sym	.83 (±.04)	.82 (±.04)	.81 (±.04)

Significant differences were also shown between the sides. The right side showed longer burst areas than the left side. No differences were found in the percent of SMVE (not shown) or between the two types of lifts. The kinematic variables showed a significant difference in the ROM during trunk flexion, with the asymmetric lifts producing a greater trunk flexion than the symmetric. The maximum linear velocity of the c.m. was greater in the symmetric lifts than in the asymmetric lifts. Elbow ROM was larger in the asymmetric lifts than in the symmetric lifts (not shown).

DISCUSSION

Harman et al. (1989) and Lander et al. (1990) have shown that wearing a rigid weight belt increases the IAP during lifting. An increase in IAP may produce a decrease in the tension of the erector spinae muscle which may be indicative of lesser spinal compression (Mcgill and Norman, 1989). The result of our study suggest that the type of weight belt may influence the changes in muscle activity produced during lifting. The rigid weight belt (WB2) decreased the electrical activity of the erector spinae muscles regardless of the type of lift performed. The WB2 belt was stiffer and could be tightened more; the subjects also reported that this type of belt prevented them from assuming an incorrect posture by cutting into the abdomen. In constrast, the elastic weight belt (WB1), recommended by a physical therapist did not produce any changes in the EMG activity. Although this belt is more comfortable to wear, it may not produce the benefits associated with wearing a weight belt during lifting.

REFERENCES

Harman, E. et al. Med. Sci. Spor. Exer., 21(2),186-190,1989.

Int. Labor. Office., Occupational Safety and Health Series, 1988.

Lander, J. et al. Med. Sci. Spor. Exer., 22(1), 117-126, 1990.

NIOSH Technical Report No. 81-122, 1981.

Nussbaum, M. NACOB II Proceedings, 525-526, 1992.

Plamondon, A. NACOB II Proceedings, 535-536, 1992.

ACKNOWLEDGMENTS

The authors appreciated the technical assistance of Doug Johnson, Tim Demchak, and Gary Lee.

KINEMATICS OF THE THROWING ARM SEGMENTS DURING A PENALTY THROW IN WATER POLO

Michael E. Feltner

Department of Sports Medicine, Pepperdine University, Malibu, CA 90263.

INTRODUCTION

The speed of the ball at release is an important variable affecting performance in throwing activities. As such, it is important to understand the motions of the body segments and their contributions to the speed of the ball at release. This paper reports the results of such an analysis conducted for the segments of the throwing arm during a penalty throw in water polo.

REVIEW AND THEORY

Previous studies on the mechanics of the throwing arm in water polo have been limited. Elliott et al. (1988) reported the flexion/extension angular displacement and velocity at the elbow and wrist, and the linear velocities of the segment endpoints, during a penalty throw. Davis et al. (1977) reported flexion/extension angular displacement data for the elbow and wrist, but only at the instant of release. Whiting et al. (1985) and Rollins et al. (1985) also have reported elbow flexion/extension angular displacement and velocity values. Nelson et al. (1993) reported pilot data that described the 3D angular displacements of the arm segments during a penalty throw. Thus previous studies have provided limited information about the motions of the arm segments during a penalty throw and no study has examined the role of the arm motions in producing the speed of the ball at release.

METHODS

Thirteen intercollegiate right-handed water polo players were videotaped (60 Hz) using the DLT method. To quantify the motions of the forearm and hand, a wooden stick (20 cm, 12 g) was affixed to the dorsal aspect of the distal forearm and a "T"-shaped wooden cross (22 g) was attached to the dorsal surface of the hand before the athletes entered the pool (Sakurai, 1993). Three-dimensional coordinate data of the relevant body landmarks and ball were obtained for two trials per subject using standard video analysis procedures and were smoothed via quintic spline functions. The linear velocity of the landmarks and ball was computed as the first derivative of the quintic spline functions.

Vector algebra techniques were used to calculate the abduction/adduction, horizontal abduction/adduction and internal/external rotation angles at the shoulder, the flexion/extension and pronation/supination angles at the elbow and the flexion/extension and radial/ulnar deviation angles at the wrist (Feltner et al., 1986; Sakurai et al., 1993) and the rotation of the trunk about its longitudinal axis (Feltner, 1987). The angular velocity along the longitudinal axes of the upper arm and forearm were computed using the procedure presented by Feltner et al. (1986). The methods presented by Sprigings et al. (1994) then were used to calculate the absolute and anatomical angular velocities of the arm segments. The contributions of the segment rotations to the speed of the right knuckle (the distal landmark on the throwing arm) during the throw were computed using the algorithm developed by Sprigings et al. (1994). This algorithm assumed that the valgus/varus anatomical rotation of the forearm and the anatomical rotation of the hand about its longitudinal axis were zero. Mean (standard deviation) values are reported for select kinematic data.

RESULTS AND DISCUSSION

The mean angular displacement data for the upper arm and forearm are presented in Figures 1 and 2. Although the data presented in Figures 1 and 2 are plots of mean (s.d) values for all subjects at each instant, the shape of each curve is representative of the shape of the respective plots for all subjects. Mean ball speed at release (REL) was 17.7 m/s (±1.8: range 14.4 - 21.3).

At an instant 300 msec before REL, the upper arm was in a position of external rotation, abduction and horizontal abduction, and the trunk was oriented so that a line connecting the shoulders was perpendicular to the plane of the goal. From this position the trunk began to rotate forward and the upper arm was simultaneously horizontally abducted, abducted and externally rotated. These actions continued until the upper arm reached its position of maximum horizontal abduction (30° ± 12° at t=9.81 ± 0.04s). The upper arm then was horizontally adducted and continued to abduct and externally rotate until it reached its positions of maximum abduction (22° ± 8° at t=9.91 ± 0.11s) and external rotation (-64° ± 12° at t=9.91 ± 0.03s). Between the instants of maximum external rotation (MER) and REL, the trunk continued its forward rotation and the arm was adducted, horizontally adducted and internally rotated.

The elbow was slowly flexed early in the penalty throw and reached its position of maximum flexion (105° ± 10°) near the instant of MER (t=9.90 ± 0.04s). The elbow then began to extend and was rapidly extended in the 50 msec prior to REL. All subjects reached their maximum elbow extension angular velocity (767°/s ± 153°/s) within ±20 msec of REL. The forearm was in a pronated position during the early portions of the throw, was supinated near MER and then rapidly pronated through REL.

The flexion/extension and radial/ulnar deviation motions of the hand were highly variable and are not presented. However, the wrist was flexed in the 20 msec period before REL in most subjects.

Figures 3 and 4 indicate that the segment rotations made small contributions to the linear velocity of the right knuckle (v_{RK}) prior to MER. Near MER, the linear velocity of the right shoulder (v_{SH}), associated with the forward trunk rotation, was primarily responsible for producing the v_{RK}. Between MER and REL, the linear velocity of the shoulder (v_{SH}), the horizontal adduction and internal rotation motions of the upper arm (ω_{HA} and ω_{IR}, respectively), and the extension of the elbow (ω_{EX}) were the main contributors to the rapidly increasing value of v_{RK}. However, the percent contributions of v_{SH}, ω_{HA}, ω_{IR} and ω_{EX} to v_{RK} at REL varied as the subjects used two different techniques to produce v_{RK} and ultimately the speed of the ball at REL (Table 1).

Table 1. Percent contributions [mean (s.d.)] to v_{RK} at REL, and v_{RK} and v_{BALL} at REL, during a penalty throw in water polo.

Source	Int. Rot. Technique		Hor. Add. Technique
v_{SH} (%)	11.3 (3.8)		11.8 (3.0)
ω_{HA} (%)	38.0 (5.8)	*	53.8 (8.1)
ω_{IR} (%)	24.5 (7.8)	*	3.5 (3.7)
ω_{EX} (%)	21.1 (7.4)		26.4 (7.9)
v_{RK} (m/s)	13.4 (1.5)	*	11.8 (0.6)
v_{BALL} (m/s)	18.0 (2.2)		17.3 (0.9)

* $p < 0.005$ (Student's t test) [Experiment wide error rate $p < 0.05$]

Eight of the subjects [Fig. 3; Int. Rot. Technique (IRT) in Table 1] used the internal rotation motion of the upper arm to make a significant contribution to v_{RK} at REL. The remaining five subjects [Fig. 4; Hor. Add. Technique (HAT) in Table 1] did not use an internal rotation motion and used a horizontal adduction motion of the upper arm to produce over 50% of v_{RK} at REL.

The IRT subjects had significantly greater internal rotation angular velocity and were in position of less external rotation at REL (Table 2). The IRT subjects also were in a position of increased elbow flexion at REL compared to the HAT subjects. Surprisingly, the IRT subjects had a significantly faster value for v_{RK} at REL, but the velocity of the ball at REL was not significantly different between the two groups (Table 1).

Table 2. Select angular kinematic variables [mean (s.d.)] at the instant of REL during a penalty throw in water polo.

	Int. Rot. Technique		Hor. Add. Technique
Ext. Rot Angle (°)	-25 (11)	*	-46 (7)
Elbow Ext. Angle (°)	137 (6)	*	148 (4)
Int. Rot. Ang. Vel. (°/s)	968 (364)	*	346 (288)

* $p < 0.005$ (Student's t test) [Experiment wide error rate $p < 0.05$]

The findings suggest that two techniques exist to produce the speed of the ball at release during a penalty throw in water polo. Further investigation is required to determine if one of the techniques is advantageous with regard to muscular activity and/or decreased risk of injury.

REFERENCES

Davis, T. et al. J. Sports Med. Phy. Fitness, 17, 5-16, 1977.
Elliott, B. et al. J. Sports Sci., 6, 103-114, 1988.
Feltner, M. E. Doctoral dissertation, Indiana Univ., 1987.
Feltner, M. Int. J. Sport Biomechanics, 5, 420-450, 1989.
Feltner, M. et al. Int. J. Sport Biomechanics, 2, 235-259, 1986.
Nelson, S. et al. Med. Sci. Sports Exerc., 25(5), S196, 1993.
Rollins, J. et al. In B. Zarins et al. (Eds.), Injuries to the Throwing Arm (pp. 311-317), W.B. Saunders, 1985.
Sakurai, S. et al. J. Applied Biomechanics, 9, 47-65, 1993.
Sprigings, R. et al. J. Biomechanics, 27(3), 245-254, 1994.
Whiting, W. C. et al. Am. J. Sports Med., 13(2), 95-98, 1985.

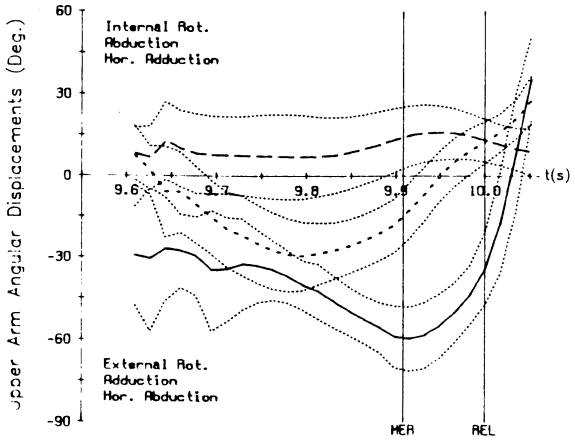

Figure 1. Mean upper arm angular displacement: int/external rotation (solid curve); abd/adduction (large dashed curve); horizontal abd/adduction (small dashed curve). The dotted curves indicate ± 1 standard deviation. The vertical lines represent the instants of maximum external rotation (MER) and ball release (REL), respectively.

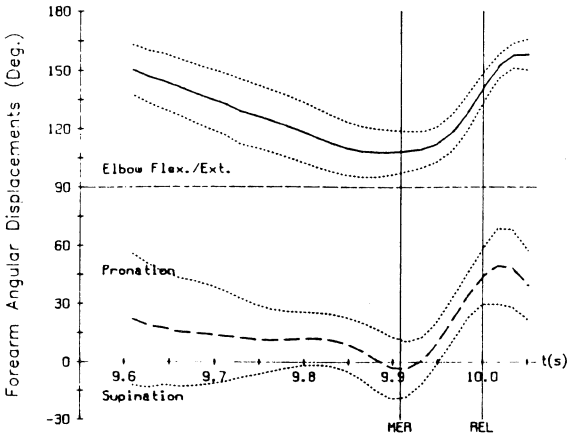

Figure 2. Mean forearm angular displacement: flexion/extension (solid curve); pronation/supination (dashed curve).

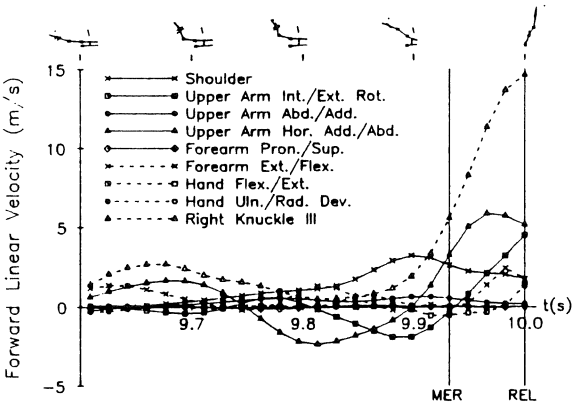

Figure 3. Contributions to v_{RK} during a penalty throw in water polo for a representative subject (v_{BALL} at REL = 20.6 m/s) who used the internal rotation technique. The stick figures represent the positions of the subject and markers applied to the forearm and hand. The crosses indicate joints on the right side of the body.

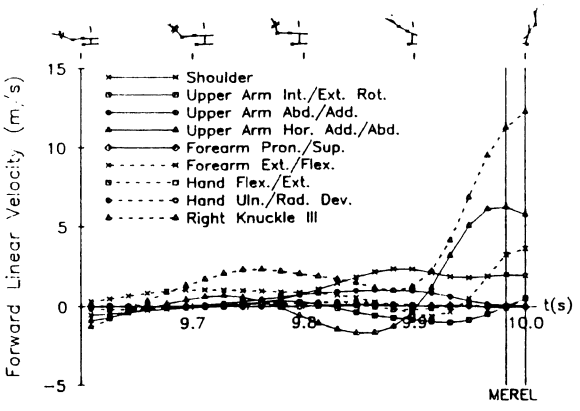

Figure 4. Contributions to v_{RK} during a penalty throw in water polo for a representative subject (v_{BALL} at REL = 18.4 m/s) who used the horizontal adduction technique.

THREE-DIMENSIONAL VIDEOGRAPHY OF SWIMMING WITH PANNING PERISCOPES

Toshimasa Yanai, James G. Hay, and John T. Gerot
Department of Exercise Science, The University of Iowa, Iowa City, IA. 52242

INTRODUCTION

A three-dimensional (3D) videography method with two stationary periscope systems was previously introduced for recording swimming techniques above and below the water surface (Yanai and Hay, 1993). This method had some methodological problems: (a) the projected size of the control object was relatively small, causing a large calibration error, (b) deformation was present in an under-water mirror, and (c) the lower body motion of the swimmer was obscured in front view by the upper body motion. The purpose of this paper is to describe a 3D videography method with panning periscope systems to overcome these problems.

SWIMMING ANALYSIS SYSTEM

One complete stroke cycle of a swimming motion generally (a) takes place in two media; (b) occupies a large 3D space; and (c) involves 3D, multi-joint motions. The first of these three conditions necessitates the use of two independent calibration fields to record the motions above and below the water surface. This need for two fields arises because a light ray refracts when it moves from one medium to another medium of different density, and this causes the recorded size of an object at a given distance to appear larger in an under-water field than in an above-water field (McIntyre and Hay, 1975).

The Direct Linear Transformation (DLT) method (Abdel-Aziz and Karara, 1971) can be used for 3D multi-joint motion analysis. An advantage of using the method in swimming analysis is that it requires no on-site measurement for the calibration, which may be physically difficult for below-water calibration. The second condition often presents a major disadvantage. In many cases, a competitive swimmer is displaced more than 2m in one complete stroke cycle. Since the displacement takes place in a horizontal direction, with the swimmer in a horizontal (or near-horizontal) position, each field of the camera must cover a length equal to the displacement plus the height and the arm length of the swimmer. The total length must be at least 5m for a stroke cycle. This generally makes the projected image size of the swimmer relatively small, causing large digitizing errors.

To solve this problem, the method described by Yu et al (1993) was adapted for the present study. In this method, each camera is allowed one degree of freedom of motion (rotation about a single fixed axis), and the DLT camera parameters are expressed as functions of the quantity which represents this angular motion (the panning orientation).

Two portable periscope systems were designed, constructed, and tested in our laboratory (Figure 1). Each system consisted of four parts; (a) a metal box with plexiglass bottom, (b) a metal table which supported a camcorder, (c) a pair of mirrors to reflect the above-water view to the camcorder, and another pair to reflect the below-water view, and (d) a metal frame which could be fixed to the pool deck, and which supported the metal box through two bearings. These bearings enabled the metal box to be rotated about a single fixed axis, holding a camcorder and four mirrors in the same relative locations. With this arrangement, the panning views of the above- and below-water motions could be recorded by a single camcorder.

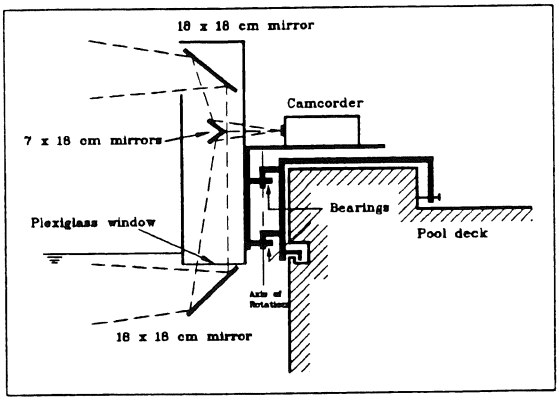

Figure 1: Side View of Panning Periscope System

PROCEDURES

The method was tested in the University of Iowa swimming pool. Two panning periscope systems were fixed on the side of the pool at a distance of 18.3m from each other, and so that oblique front and back views of the swimmer could be recorded. The calibration space was (1.5 x 9.4 x 2.0)m^3 in volume, and located in the middle of the farthest lane from the pool deck where the periscope systems were fixed. The angle between the optical axes of the two cameras ranged from 51 to 57°. Thirteen wooden blocks, on each of which a white circle of 30mm diameter was painted on a black background, were placed at 1.2m intervals on the pool deck adjacent to the object space. These wooden blocks served as reference markers to define a global reference system, and to define the panning orientation at a given instant.

A control object with 72 points (1.2 x 1.0 x 2.0m) was used for the calibration. The upper half and the lower half of the control object were used for the above-water and below-water calibration, respectively. A plumbline with two table-tennis balls was attached to the control object, and used to define the vertical axis in the global reference system. The control object was placed in seven consecutive locations along the calibration space. In each of these seven locations, the

position of the control object was recorded using Panasonic AG450-SVHS camcorders while panning the periscope systems. The two-dimensional (2D) coordinates of the points on the control object were digitized for eight fields recorded during the panning motion of each periscope system. The panning orientation of each camera at each instant was determined with the aid of the 13 black wooden blocks placed on the pool deck. The DLT camera parameters for these eight digitized fields were determined, and then each parameter was expressed as a function of the panning orientation by using a least-squares, second-order, polynomial regression equation.

Three steps were taken to determine the 3D coordinates of the points of interest: (a) these points and the reference markers were digitized in each field from each camera; (b) the DLT camera parameters of each camera were obtained, based on the determined panning orientation; and (c) the desired 3D coordinates for a given instant were determined from the digitized 2D coordinates and the two sets of DLT camera parameters.

VALIDITY TESTING

The validity of the method was tested by using a 2.5m scale rod with black and white stripes of 0.5m lengths. The scale rod was pulled through the calibration space, keeping half of the rod above the water surface and half below. Four intersections of the stripes (two above and two below the water surface) were digitized for each camera, and 3D coordinates of these intersections were obtained. The lengths of the stripes were computed from these coordinates of the intersections. The differences between the computed lengths of the stripes and their known lengths were then determined.

RESULTS AND DISCUSSION

Calibration error was estimated by the mean of the deviations between the known coordinates of points on the control object and the computed coordinates of the same points. The mean deviation (Mean) and the standard deviation (SD) in each single control object location are listed in Table 1. The result of the validation are presented in Table 2.

The calibration error tended to be larger in the below-water calibration than in the above-water, for each control object location. This could be attributed to two factors; (a) the under-water control object was much less well-lighted than the above-water, and (b) there were small but observable "pincushion" type distortions toward the lower edges of the below-water field. The illumination problem was due in part to the use of a single camcorder simultaneously recording the above- and below-water fields. This problem can only be solved completely by creating conditions in which the under-water lighting is equivalent to the above-water lighting.

The distortion problem was not caused by deformation of the under-water mirror, but instead, by the structure of the lens of the camcorder and the refraction at the interface of water and air. An independent laboratory test revealed that visually-observable "pincushion" distortion existed near the four edges of the frame when the camcorder was removed from the periscope and a target was placed over 10 m in front of it. In the present study, the distortion was perceivable only in the below-water field. This suggested that the distortion due to the camcorder was enlarged by the refraction at the interface of the two media to the degree that it could be recognized by observers. However, the accuracy of the 3D reconstruction of the scale used for the validation rod did not seem affected by the distortion. The scale rod was recorded in the middle of the frame, and it did not appear to be distorted in the field. In fact, the errors in computing dimensions of the scale rod were smaller than the mean calibration errors (see Table 2). This result was interpreted to mean that the non-linear component of the coordinate transformation, caused by the "pincushion" distortion, was not as serious as to invalidate the linear assumption in the DLT method.

The method described here solved all the problems identified in the previously-introduced method with stationary periscope systems. The method enabled the calibration of a large space and reconstruction of 3D motions above and below the water surface, and permitted a large image size to be obtained.

Table 1: Estimated Calibration Errors [mm]

	Control Object Locations						
	1	2	3	4	5	6	7
Above							
Mean	11.98	12.07	10.35	15.72	17.65	9.53	8.73
SD	6.08	5.14	6.62	6.51	7.75	5.21	5.77
Below							
Mean	14.00	15.80	12.35	18.23	17.64	10.32	10.69
SD	7.78	7.20	7.06	8.37	8.11	5.30	5.82

Table 2: Average Differences between Computed and Known Dimensions [mm]

Above water	Interface	Below water	Top to bottom
5.83	3.32	5.12	9.97
(1.16)	(0.66)	(1.02)	(0.67)

* percent in parenthesis

REFERENCES

Abdel-Aziz, Y. I., & Karara, H. M. ASP Symposium on Close-Range Photogrammetry, American Society of Photogrammetry, Falls Church, VA. 1971.

McIntyre, D. R. & Hay, J. G. Swimming II, pp 51-57, University Park Press, Baltimore, 1975.

Yanai, T., & Hay, J. G. ASB 17th Annual Meeting, American Society of Biomechanics, Iowa City, IA. 1993.

Yu, B., Koh, T. J., & Hay, J. G. Journal of Biomechanics, 26, pp 741-751, 1993.

THE EFFECT OF LIFTING BELTS ON TRUNK MOTIONS

SA Lavender, JS Thomas, O Chang, GBJ Anderson
Rush-Presbyterian-St. Luke's Medical Center
Department of Orthopaedic Surgery, Chicago, IL 60612

INTRODUCTION: Presently there is conflicting information in the literature regarding the effectiveness of lifting belts in controlling low back disorders in the workplace. The mechanism by which these belts reduce the mechanical loading on the spine is not clear. It has been hypothesized that a potential benefit of lifting belts may be their ability to reduce motions within the lumbar spine. Seguin and McGill (1992) showed that lifting belts did increase the passive stiffness of the torso. However, it remains to be seen if this affects the torso kinematics during lifting activities. The objective of the current investigation was to test the following hypotheses: 1) Lifting belts decrease the motion of the torso during asymmetric lifting, and 2) Foot motion during asymmetric lifting removes any potential benefit of the lifting belt.

MATERIALS AND METHODS: This study used a sample of 8 male and 8 female nursing personnel who routinely perform lifting tasks as part of their job demands. The independent variables were: 1)the use of the lifting belt, 2)the degree of asymmetry in the load placement following the lift (0, 45, and 90 degrees), and 3)whether subjects were permitted to move their feet (pivot) during the lift. Each subject attended three sessions scheduled approximately a week apart. Session 1 was an orientation session which included a test for maximum isometric strength. The lifting task performed in sessions 2 and 3 used a box weighing 20 percent of the peak force obtained during the strength test. Lifting belts were given to subjects either at the completion of session 1 or the completion of session 2. At this time the subject watched a short video describing how the belt was to be worn. The subject was then asked to wear the belt during the next week's work activities. The sequence of belt and no belt conditions was counterbalanced across subjects. The lifting task required subjects to lift a box from one of three positions with respect to a self. The box was lifted from 29 cm to a shelf at elbow height. In all 42 lifts were performed: 3 orientations, 2 foot movement conditions, and 7 replications. The lifts were temporally spaced at 2 per minute. The dependent measures were the motion variables obtained from the Lumbar Motion Monitor (LMM). This device provides torso kinematic data in the sagittal, frontal, and transverse planes. Statistical analyses were used evaluate the effectiveness of lifting belts for controlling coupled motions as a function of task asymmetry and foot movement.

RESULTS AND DISCUSSION: The lateral bending and twisting postural data were sensitive to the interaction between the belt, asymmetry, and foot movement conditions ($p<.005$). The effect of the belt on the amount of twisting was most apparent with 45 degrees of asymmetry. Here the belt reduced the twisting regardless of the foot motion. At 90 degrees of asymmetry in the load placement the twisting was minimized through the combination of the belt and foot motion (figure 1).

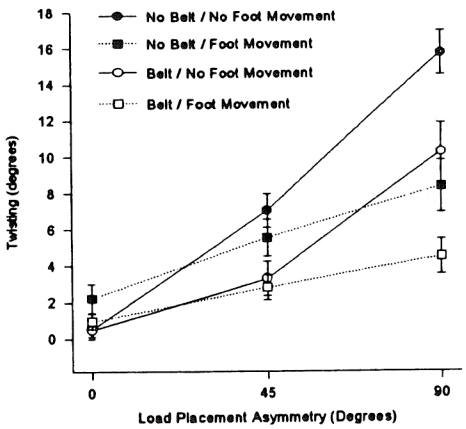

Figure 1. The average twist to the right across subjects as a function of the asymmetry, the lifting belt, and foot movement.

The belt's effect on lateral bending was essentially eliminated if foot motion occurred with 90 degrees of asymmetry in the load placement (figure 2). Foot movement with 90 degrees of load placement asymmetry reduced the lateral bending velocity and acceleration by 37 and 29 percent, respectively. Likewise, the twisting velocity was reduced by 34 percent, and the twisting acceleration was reduced by

30 percent under the same asymmetry conditions with foot movement. There were no significant changes in the sagittal plane motions due to the lifting belt, the foot motion, the asymmetry, or the combination of these factors.

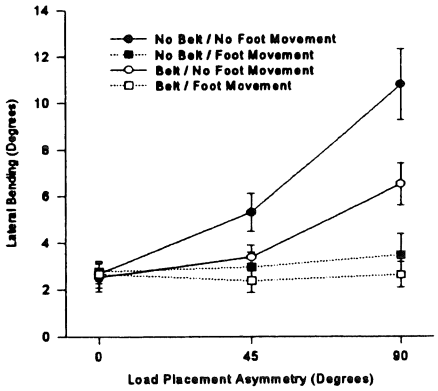

Figure 2. The average lateral bend to the right across subjects as a function of the asymmetry, the lifting belt, and foot movement.

CONCLUSIONS: 1) The belts do reduce the twisting and lateral bending particularly where there is extreme task asymmetry. 2) Foot motion by itself also works to reduce the lateral bending and to a lesser degree the twisting motions in the spine. Workers should be encouraged to step or pivot their lower bodies rather than relying on spine motion. 3) The net effect of the belts on the internal loadings placed on the spine is still not known, thereby, making any recommendations based only on this study premature.

Seguin, J. and McGill, S., Human Factors Association of Canada 25th Annual Conference, (pp67-72), 1992

Reaction Forces and Impulses Experienced During the Take-off and Landing of Tumbling Skills

Barry A. Munkasy, Jill L. McNitt-Gray, and Michelle Welch
USC Biomechanics Research Laboratory, Department of Exercise Sciences
University of Southern California, Los Angeles, CA 90089-0652

To produce the linear and angular momentum needed to successfully complete and land a tumbling skill, progressively more difficult gymnastics tumbling skills require larger impulses during the take-off phase (Bruggemann, 1987; Hwang et al., 1990). Generation of larger momenta also tends to produce larger impact peak forces and impulses during the landing (Panzer, 1987). Although Bruggemann (1987) has provided kinetic data pertaining to gymnastics tumbling take-offs and Panzer (1987) for landings neither study was conducted on competition springfloor surfaces. Therefore, the purpose of this study was to determine the load experienced on a tumbling springfloor during the take-off and landing phases of tumbling skills performed immediately following a run-hurdle-round-off-backhandspring series. Progressively more difficult tumbling skills (tuck single back salto (TSB), layout single back salto (LSB), and tuck double back salto (TDB) were hypothesized to produce different loading conditions during the take-off and landing phases. Of particular interest were the force-time characteristics of the vertical and anterior-posterior reaction forces.

METHODS

Eleven healthy male gymnasts, members of the Men's Junior National Team, consented to serve as subjects while attending a training camp at the U.S. Olympic Training Center. During data collection, gymnasts performed take-offs and landings of a series of progressively more difficult backward tumbling skills on a springfloor tumbling strip. Trials were blocked by skill and progressively increased in difficulty. Take-offs or landings were performed on an isolated portion of the springfloor, that was fully supported by a force plate (Kistler; 0.9 m by 0.6 m). The reaction forces at the floor-plate interface were quantified for both feet using a Kistler force plate (800 Hz).

RESULTS

Take-off Phase: Reaction force-time characteristics, quantified at the springfloor-force plate interface, were not significantly different between tumbling skills (Figures 1-3). However, as skill difficulty increased (TSB-LSB-TDB), the range of vertical reaction force impulses (Figure 2) and landing phase durations decreased (TSB: 0.039 - 0.061 s; LSB: 0.054 - 0.060 s; TDB: 0.041-0.058 s). The range and magnitude of peak vertical forces observed during the take-off phase also decreased with increases in skill difficulty (Figure 3).

Immediately after contact, a posteriorly directed (+) horizontal reaction force relatively was applied for a short time. The horizontal impulses (+) applied during this interval were relatively small and ranged from 0 - 0.2 BWs. Peak positive horizontal reaction forces ranged from 0.1 to 1.4 BW. Much larger anteriorly directed (-) horizontal impulses and reaction forces were observed during the remainder of the take-off phase (Figures 2 & 3).

Landing Phase: Reaction force-time characteristics, quantified at the springfloor-force plate interface, were not significantly different between tumbling skills (Figures 1-3). However, as skill difficulty increased (TSB-LSB-TDB), the range of vertical reaction force impulses decreased (Figure 2). The range and magnitude of peak vertical forces observed during the landing phase also decreased with increases in skill difficulty (Figure 3).

Immediately after contact, a posteriorly directed (+) horizontal reaction force was applied. The horizontal impulses (+) applied during this interval were relatively small and ranged from 0 - 0.7 BWs. Peak positive horizontal reaction forces ranged from 0.1 to 1.4 BW. Much larger anteriorly directed (-) horizontal impulses and reaction forces were observed during the remainder of the landing phase (Figures 2 & 3).

DISCUSSION

The force-time characteristics observed during TSB, LSB, and TDB take-off and landing phases are similar to forces and impulses observed by Bruggemann, 1987 (take-off) and Panzer, 1987

(landing). The hypothesis that progressively more difficult tumbling skills would produce different loading conditions during the take-off and landing phases was not supported. However, it was noted that as skill difficulty increased the range of peak reaction forces and impulses observed decreased. Although the impulse during the take-off was similar between skills, the initial conditions present at contact for the take-off phase may have been different. Finally, although high forces and impulses in gymnastic tumbling landings are well respected the results from this study indicate that equally high forces and impulses are experienced during the take-off phase.

References

Bruggemann, G.P. Med. Sport Sci., 25, 142-176, 1987.
Hwang et al. IJSB, 6, 177-186, 1990
Panzer, V. unpublished doctoral dissertation, U of Oregon, 1987.

Acknowledgements - This project was funded by the United States Olympic Committee. The authors would like to thank Sarah Smith, Ph.D. and the staff of the Division of Athletic Performance at the U.S. Olympic Training Center in Colorado Springs, CO, Larry Fie and American Athletic, Inc., Coach Mizoguchi and the Men's Junior National Team, Coach Brandt and the resident gymnastics athletes at the USOTC, and undergraduate research assistants in the USC Biomechanics Laboratory.

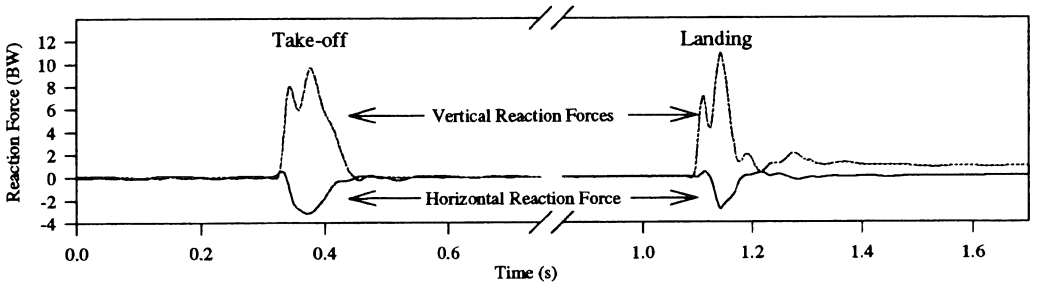

Figure 1 - Typical Reaction Forces Present During a Layout Single Back Salto Performed on a Springfloor

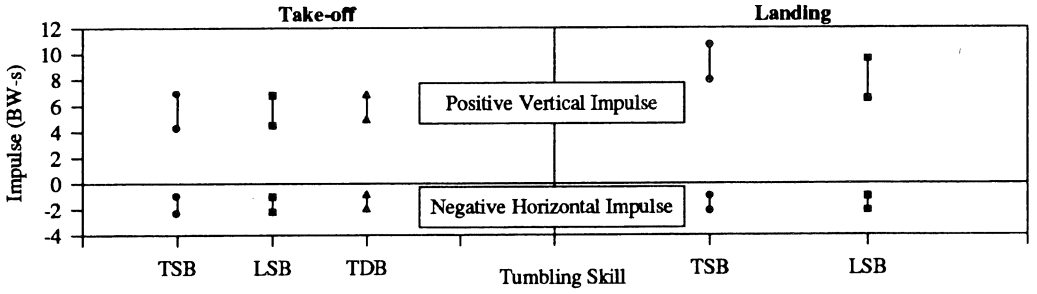

Figure 2 - Range of Reaction Force Impulses Experienced During the Take-off and Landing Phases of Tumbling Skills

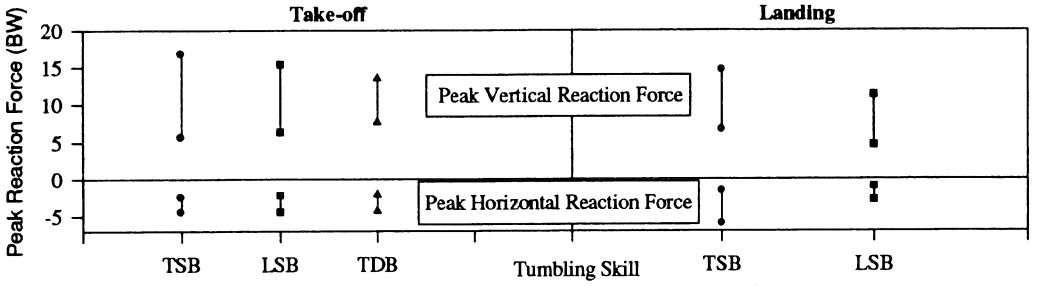

Figure 3 - Range of Peak Reaction Forces Experienced During the Take-off and Landing Phases of Tumbling Skills

ANGULAR MOMENTUM STRATEGIES IN AXEL JUMPING

D.I. Miller and W.J. Albert
Faculty of Kinesiology, University of Western Ontario
London, Ontario, CANADA N6A 3K7

INTRODUCTION

The axel (named the Axel-Paulsen after its originator) has been described as 'the king among jumps' by the International Skating Union. It is considered a 'break' jump by figure skaters and coaches as its physical, technique and psychological demands effectively separate competitors into novice (single), national (double) and international (triple) levels. A single axel theoretically consists of 1.5, a double 2.5 and a triple 3.5 rotations in the air with the skater taking off from the forward outside edge of one foot and landing on the back outside edge of the opposite foot. The number of revolutions actually completed may be significantly reduced by overrotation at the end of the takeoff and underrotation at the landing.

From a theoretical standpoint, the number of rotations achieved in a jump depends upon: 1) time in the air resulting from the vertical velocity of the center of gravity (CG) immediately before the flight; 2) angular momentum at the beginning of the flight; and 3) changes in the moment of inertia about the twisting axis during the flight.

The purpose of the current project was to investigate the angular momentum strategies employed by figure skaters to increase the number of rotations in the axel jump from a single to a double.

METHODOLOGY

Four VHS camcorders, positioned in the spectator area adjacent to the blue lines, videotaped skaters performing single and double axels at center ice. A 24-point control frame provided calibration data for determining DLT parameters (Marzan & Karara, 1975). Body segment endpoints were digitized using a Peak2D system. The sampling rate was 60 Hz and approximately 100 frames were included in the analysis of each jump. The data of one single and one double axel from 5 female and 6 male skaters were processed with custom software. The skater's body was modelled as 12 axis-symmetric rigid links with the feet and skates being considered together. Angular momentum of the system included remote contributions of all the segments with reference to the CG and their local contributions with respect to their transverse axes. The local angular momentum of the trunk relative to its longitudinal axis was also computed (Dapena, 1978).

RESULTS AND DISCUSSION

The analysis indicated that none of the skaters had a shorter flight time for the double than the single axel (Table 1). A similar trend was found by Aleshinsky (1987) who reported averages of 0.54 and 0.56 s for single and double axels of American Junior Elite female skaters and 0.57 and 0.59 s for their male counterparts. Absolute flight times for skaters in the current study were somewhat shorter than those reported by Aleshinsky suggesting that their skill level was not as high.

All else being equal, one would expect a skater to achieve greater height in a single axel. However, because singles can be performed with submaximal levels of effort, it is not surprising that there may be an increase in vertical velocity at the end of the takeoff for a double thereby increasing jump height and extending flight time.

During the takeoff, the largest angular momentum with respect to a vertical axis through the skater's CG was generated by the free leg. Its maximum value was followed by a significant decrease immediately prior to the initiation of the flight (Fig. 1). As the skater left the ice, the arms and free leg dominated the total angular momentum with respect to the vertical axis through the CG.

Somewhat surprisingly, there was no consistent increase in the magnitude

of the total angular momentum from single to double axels. Almost half the skaters had a smaller total body moment of inertia with respect to the vertical axis at the beginning of flight for their double than their single axel. These skaters appeared to be anticipating the need to lessen their resistance to rotation. All skaters significantly decreased their moments of inertia during flight (Fig. 2). The average moment of inertia for the double was 45-80% of its magnitude in the single axel. This was the dominant strategy employed by all skaters for increasing the number of revolutions in the jump. Previous research (Aleshinsky, 1986, 1987; King et al., 1994) has also stressed the importance of this general strategy. During the flight of the double, reductions in the angular momentum contributions of the upper and lower extremities resulted in corresponding increases in the angular momentum of the trunk. By contrast, in the single axel, the angular momentum of the extremities frequently overshadowed that of the trunk.

Data from the current study suggested that the role of the free leg during the takeoff may hold the key to understanding skill differences in axel performance.

REFERENCES

Aleshinsky, S.Y. **Prof. Skater** 18, (Jan/Feb) 24-28, 1987.
Aleshinsky, S.Y. **Skating** 63, (Dec.) 11-15, 1986.
Dapena, J. **J. Biomech.** 11, 251-256, 1978.
King, D.L. *et al.*, **J. Appl. Biomech.** 10, 51-60, 1994.
Marzan, G.T. & Karara, H.M. **Symposium Close-Range Photogrammetry**, Univ. Illinois, 420-476, 1975.

ACKNOWLEDGMENTS

Supported by Sport Canada.

Table 1: Descriptive statistics

Variable		Men (6)	Women (5)
Weight (N)		660 ± 154	524 ± 43
Height (m)		1.75 ± .08	1.56 ± .12
Age (yrs)		21 ± 4	17 ± 2
Flight (s)	S	0.52 ± .04	0.46 ± .05
	D	0.55 ± .03	0.50 ± .04

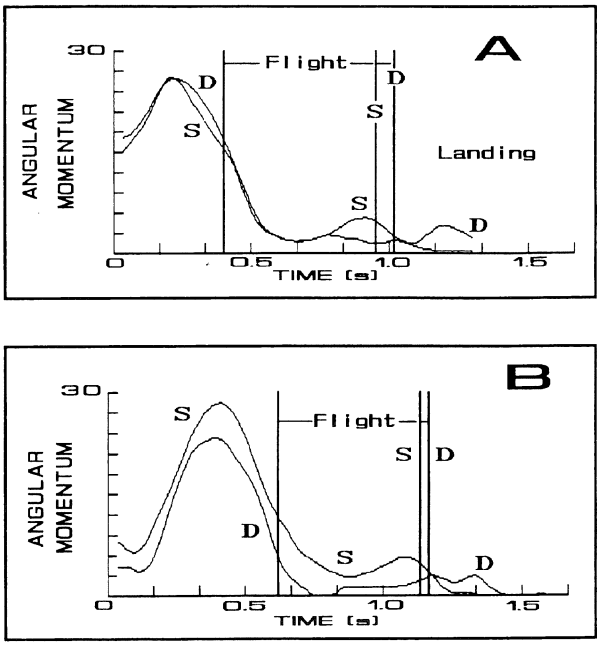

Fig. 1: Angular momentum (kg-m²/s) of the free leg with respect to a vertical axis through the CG for single (S) and double (D) axels of two male skaters. Skater A was the more highly skilled.

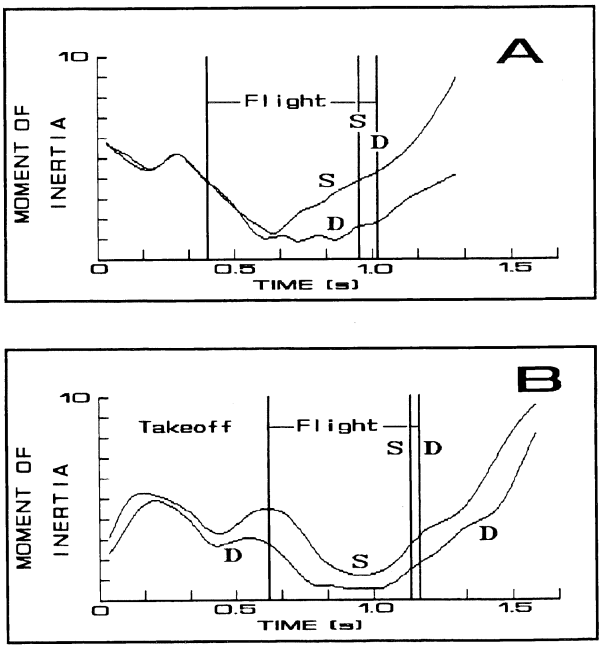

Fig. 2: Total body moment of inertia (kg-m²) with respect to a vertical axis through the CG for the same two skaters.

A COMPARISON OF SARGENT JUMP HEIGHT AND ACTUAL FLIGHT HEIGHT IN VERTICAL JUMPING

R.N. Hinrichs and P.F. Vint
Exercise and Sport Research Institute, Arizona State University, Tempe, AZ 85287-0404

INTRODUCTION

Sixteen male collegiate volleyball players were videotaped while performing two-footed vertical jumps with countermovement. The videotapes were digitized to track the whole body center of mass (CM) throughout the takeoff and flight. The purpose was to compare the "true" flight height of the body center of mass (CM) to that height obtained by conventional means using the Sargent vertical jump test protocol (Safrit, 1990). The results showed the Sargent jump height overestimated flight height by 36%. This discrepancy was reduced to 11% after making two modifications to the protocol. One modification involved taking the baseline reach measure from the tip-toes rather than standing flat-foot. The second modification involved using a reaction board to measure and correct for the shift in the CM location within the body between takeoff and peak.

REVIEW AND THEORY

For years the Sargent vertical jump test has been a standard technique for measuring raw vertical jumping ability. While the original Sargent test (Sargent, 1921) subtracted one's stature from the maximum height one could reach with the top of one's head in a jump, the modern day version of this test (still referred to as the Sargent vertical jump test; Safrit, 1990) uses the fingertips rather than the top of the head and allows a preparatory arm swing and countermovement prior to takeoff. The relative height (H_S) measured by this test is shown in Figure 1. When a certain athlete is reported to have a "40 inch vertical jump", for example, one is most likely referring to this height H_S.

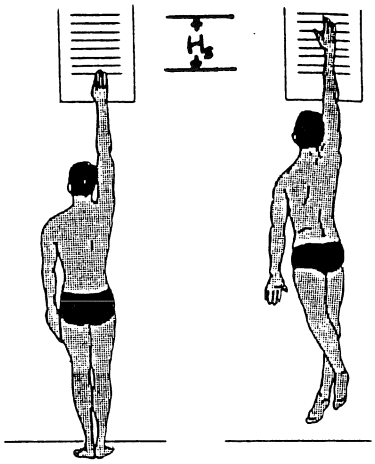

Figure 1. The (modern day) Sargent vertical jump test (adapted from Safrit, 1990).

How does H_S compare with the height that the body CM is elevated during the jump, a height which we believe more closely represents the "true" measure of raw vertical jumping ability? Using the simple deterministic model shown in Figure 2, the total height above the ground which an individual can jump and reach with the fingertips can be described by the sum of four lesser heights: takeoff height (H_1), flight height (H_2), reach height (H_3), and loss height (H_4, a negative number). Takeoff height is the height of the body CM at the instant of takeoff. Flight height is defined as the maximum height which the CM is elevated above its position at takeoff. Reach height refers to the height that one reaches with the fingertips above one's CM at the instant the maximum jump and reach height is evaluated. Loss height is the difference between the peak height of the CM and the height of the CM at the instant the maximum jump and reach height is evaluated.

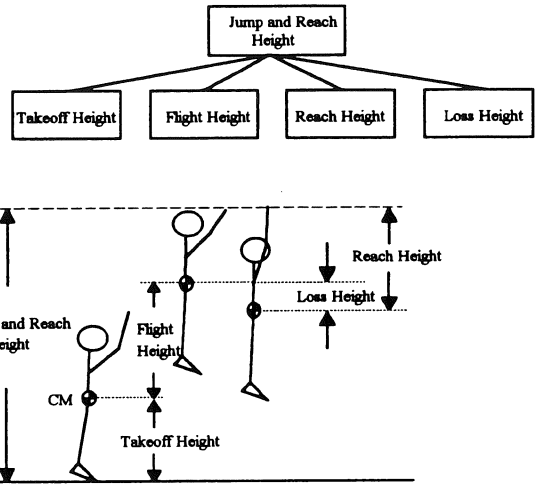

Figure 2. Deterministic model of vertical jump (following guidelines of Hay and Reid, 1988)

We believe the intent of both the original and modern day Sargent tests is to measure how high people can elevate themselves in the air independent of standing height or arm length. However, the point that best represents the body as a whole is the CM. In theory, the fingertips are elevated from takeoff to peak the same amount that the CM is elevated *only if* the body position at the peak of the jump is the same as at takeoff. In normal vertical jumping this is not the case. The takeoff usually occurs from the tip-toes with both arms overhead, but at the peak, the subject can reach higher if one arm is dropped to the side and the shoulders are tilted (e.g., see Hay, 1993, p. 133). In this case, the fingertips would be elevated more than the CM by two distances: [a] the distance which the CM moves within the body from lowering one arm to the side, and [b] the added reach that the shoulder tilt provides. The distance [a] can be measured easily with a reaction board (Hay, 1993). The distance [b] can be accounted for by insisting that all subjects use just as much shoulder tilt in the baseline standing reach as they do at the peak of their jumps. (Note that this does not appear to be the case in Figure 1.) In addition, since the subjects take off from their tip-toes, the baseline standing reach height should be measured on the tip-toes, not flat-footed.

The purpose of this study was to see how closely the height measured by the (modern day) Sargent jump test compares with the actual flight height in vertical jumping and make an attempt to correct for the discrepancies between the two.

PROCEDURES

Sixteen male collegiate volleyball players (mean age 20.9 years, height 186.9 cm, and mass 82.7 kg, both with shoes on) served as subjects. They each performed three standing two footed vertical jumps (with arm swing and countermovement) while being videotaped from the side at 60 Hz. The camera was placed approximately 30 m away to reduce perspective error. Heights reached by the fingertips while standing flatfoot, while standing on tiptoes, and when jumping for maximum height were measured with a Vertec vertical jump height measuring device which also served as a linear scale for the video analysis. The trial with the greatest jump and reach height for each subject was selected for analysis. Selected jumps were digitized with the Peak Performance video digitizing system. Twenty-one points on the body were digitized to define a 14 segment model and smoothed using a Butterworth digital filter. Segmental masses and centers of mass were obtained from the mean data of Clauser et al. (1969) as adjusted by Hinrichs (1990). Takeoff height, flight height, reach height, and loss height were calculated using the vertical location of the total body CM at the appropriate events.

A reaction board (Hay, 1993) was used to measure the CM distances from the bottom of the feet (with shoes on) for four supine body positions; both arms at the side, one arm up (i.e., shoulder of the reaching arm flexed 180°), one arm up with shoulder tilt, and two arms up. The distance [**a**] was computed to be the difference in CM location between the "two arms up" condition (the presumed body position at takeoff) and the "one arm up with shoulder tilt" condition (the presumed body position at the peak of the jump). Two adjustments were made to the measured Sargent jump height. First the measured jump and reach height was expressed relative to the tip-toe reach height to give an adjusted value H_S'. Second, the distance [**a**] was subtracted to correct for the CM shift within the body from dropping one arm and tilting the shoulders [$H_S'' = H_S' - a$]. These adjusted heights were then compared with the flight height (H_2) derived from video.

RESULTS

The takeoff, flight, and reach heights were found to be approximately 42%, 17%, and 41% of the total jump and reach height, respectively (see Table 1). Loss height was found to be sufficiently small as to be neglected, indicating that these subjects carefully timed their reaches to correspond closely with their peak CM height. The reaction board results revealed that the CM was lowered within the body by 3.4 cm on the average from lowering one arm alone without shoulder tilt (see Table 2). Tilting the shoulders lowered the CM an additional 0.4 cm. It appears that shoulder tilt increases both the distance [**a**] and the distance [**b**] thus providing a double benefit to the jumper. The Sargent jump results showed that H_S overestimated the actual flight height by more than 19 cm or 36% (see Table 3). Expressing height relative to tip-toe reach, however, reduced this difference to 10 cm or 19% (H_S'). Adjusting further for the CM shift [**a**] reduced the discrepancy to less than 7 cm or 11% (H_S'').

DISCUSSION

The (modern day) Sargent vertical jump test has become a standard tool for assessing vertical jumping ability. We believe that a truer measure of raw jumping ability, however, is flight height. Performing a segmental analysis from video or film is not practical in a school setting nor can it be used to provide immediate feedback. Reaction boards, on the other hand, are easily built and could be used to measure CM shift in a school setting without difficulty. The results of this study show that the Sargent jump height overestimates flight height by a large margin (more than 36%). If people interpret the Sargent jump height to be representative of flight height, then they are being misled into believing that they can raise their bodies into the air higher than they actually can. If the two modifications we suggest are incorporated into the test, it more closely approximates true flight height (within 11%).

It was hoped that these two adjustments would completely explain the difference between Sargent jump height and flight height. However, additional factors may still be present. Even though every effort was made to get these subjects to reach as high as they could in the baseline standing height measurements, it is likely that they could not duplicate in a static reach the same degree of plantar flexion and shoulder tilt that they achieved in their actual jumps (nor would they want to if they were interested in maximizing their scores!). Because of this, true flight height may always be overestimated in these vertical jump tests, regardless of the protocol used.

Table 1. Mean values (± STD) for sub-heights measured from video. Heights are also expressed as a % of total jump and reach height.

Variable	Height (cm)
Takeoff height	131.7 ± 5.9 (42.3%)
Flight height	51.8 ± 5.6 (16.6%)
Reach height	127.7 ± 4.8 (41.0%)
Loss height	–0.5 ± 0.8 (–0.2%)
Total jump and reach height	311.8 ± 9.9 (100%)

Table 2. Mean values (± STD) for reaction board CM measurements (distances from bottom of feet).

Body position	Distance (cm)
Two arms up	111.8 ± 3.8
One arm up, one down, no shoulder tilt	108.4 ± 3.8
One arm up, one down, *with* shoulder tilt	108.0 ± 3.9
Arms at sides	104.8 ± 3.7

Table 3. Comparison between mean values (± STD) for Sargent jump height (H_S), adjusted Sargent jump heights (H_S' and H_S''), and flight height (H_2). Heights are also expressed as a % of flight height.

Measure of jump height	Height (cm)
H_S (relative to flat foot reach)	70.7 ± 7.0 (136%)
H_S' (relative to tip-toe reach)	61.6 ± 6.2 (119%)
H_S'' (adjust for CM shift [**a**])	57.7 ± 6.5 (111%)
H_2 (Flight height from Table 1)	51.8 ± 5.6 (100%)

REFERENCES

Clauser, C.E. et al. (1969). AMTR Technical Report #69-70, Wright-Patterson AFB, Ohio. (AD-710-622)

Hay, J.G. (1993). *The Biomechanics of Sports Techniques*, Prentice Hall.

Hay, J.G. and Reid, J.G. (1988). *Anatomy, Mechanics, and Human Motion*, Prentice Hall.

Hinrichs, R.N. (1990). *J. Biomechanics*, **23**, 949-951.

Safrit, M.J. (1990). *Introduction to Measurement in Physical Education and Exercise Science*, Times Mirror/Mosby.

Sargent, D.A. (1921). *American Physical Education Review*, **26**(4), 188-194.

FORCES CREATED DURING GIANT SWINGS

R.J. Neal, V. Kippers, D. Plooy, and M. Forwood

Department of Human Movement Studies, The University of Queensland
Department of Anatomical Sciences, The University of Queensland
Brisbane, AUSTRALIA
Department of Anatomy, University of Indiana, USA

INTRODUCTION

A review of gymnastic literature has revealed an accumulating body of evidence suggesting that overuse injuries to the upper limbs of gymnasts have a greater incidence than previously thought, and overuse injuries involving the wrist have been identified as a specific problem (Carek & Fumich, 1992; Plooy & Forwood, 1990; Read, 1981; Roy *et al.*, 1985; Yong-Hing *et al.*, 1988). Traditionally the well known problem of wrist soreness in gymnastics has been associated with compressive and rotational forces at the wrist. Pommel horse is believed to be consistently responsible for wrist pain among males but Yong-Hing *et al* (1988) reported a case of chronic injury to the distal radial growth plates in an adolescent gymnast. The injury appeared to have an etiology due to excessive tensile loading of the joint. The authors hypothesised that the dowel hand guards reduced the amount of forearm muscle contraction that was necessary for the execution of giant swings

Epiphysial plate problems may be related to excessive loading which may also be the cause of stress fractures. In fact, Carek and Fumich (1992) reported a case of a 14 year old female non-elite gymnast with stress fractures of the distal radius. Although a number of authors suggest that stress injuries to the distal radius and ulna, and early closure of growth plates in gymnasts, are rare (Roy *et al.*, 1985), the increase of overuse injuries in children and the neglect of injuries incurred in supervised sport may not only lead to a decreased performance and participation, but may also lead to permanent injury to the young athletes body.

The use of dowel hand guards and the changes this guard may make to the biomechanics of the hand has not been well reported. The purpose of this study was to investigate the influence of gymnastic hand guards on bar forces and forearm muscle activity during backward giant swings on the high bar.

METHOD

Subjects

Ten experienced male gymnasts were chosen from a group of volunteers. They had all competed at State championships and were at least Level 6 in the General Stream of Gymnastics. Three of the subjects had international gymnastic experience and all subjects could perform at least five backward giant swings with bare hands.

Data collection and procedures

Areas of skin overlying the major flexor and extensor muscle groups of the left and right forearms were prepared by rubbing lightly with emery paper and then with cotton wool soaked in ethanol. Double-sided adhesive pads were attached to preamplified electrodes and gel was inserted into the wells overlying the two active and one reference electrode. Each electrode assembly was connected to a Bio-Sentry FM transmitter which sent signals to a receiver located approximately 5 m from the high bar.

The high bar was instrumented with train gauges in such a way that horizontal and vertical shear forces and torsion around the bar could be estimated. Excitation to and output from the bridges were provided by purpose built amplifiers. The input voltage was set at 10 V and the bridges were balanced with no load on the bar (other than its self-weight). The output voltage of the amplifiers was scaled so that peak forces on the bar did not produce voltages exceeding ± 10 V.

The fourteen channels of force data were sampled at 200 Hz using a PC based Burr-Brown data acquisition system and customised software for a total of 5.5 s. Triggering for the system was carried out using a photoelectric beam attached to the vertical support poles of the high bar. When the light beam was broken as the gymnast swung through, a 5V signal was sent to the data acquisition system and sampling commenced immediately. This signal was also used to simultaneously trigger the WASP system that was collecting the EMG signals.

The raw force data were stored on disk and used in the model described above to determine the loads applied to the bar by each of the gymnast's hands. These were then plotted as a function of time and the maximum forces for each revolution of the gymnast were determined.

Statistical analysis

Peak forces on each hand were submitted to a two-way ANOVA (condition of performance - dowel grips, loops & bare hands X hand - right & left). A one-way ANOVA was conducted on cycle time (i.e., the time taken for each revolution of the gymnast). Where necessary post hoc analysis using Scheffe or Neuman-Keuls methods were used to locate the source of significant differences.

RESULTS

The results of the statistical tests are summarised in Table 1 where the mean values of the dependent measures are presented.

A significant difference was found for swing time [$F(3,27)=25.6, p<.001$] and post hoc analysis indicated that the wind-up was different to all other conditions and that the bare hands condition was significantly different to both the webbing loops and dowel grips conditions. When peak force was analysed, there was no difference between the forces experienced by the left and right hands [$F(1,13)=3.3, p>.05$]. There was, however, a significant difference among conditions $F(3,39)=7.8, p<.001$] and post hoc tests indicated that the bare hands condition was different to all others. Perusal of the data in Table 1 indicates that the forces experienced by the gymnasts when they swung without anything on their hands were lower than all other conditions.

Normalised IEMG results form the forearm muscles were obtained from the period equivalent to 4% of the cycle time on either side of bottom dead centre. During the giant swing, activation of the flexor muscles was generally greater during the period around bottom dead centre (112% of reference signal) than during a maximum static hand grip measurement. The extensors were considerably less

active (25% ref) and the difference between flexor and extensor activity was highly significant [$F(3,27)=28.1, p<.001$]. The ANOVA of EMG results indicated a significant effect of condition on muscle activity [$F(3,27)=4.2, p<.05$]. Post hoc analysis revealed that higher activation occurred with bare hands than with webbing loops or dowel hand guards. There were no differences amongst any of the aided conditions of performance. With the hand guards, flexor activity decreased by between 3% and 28% whereas extensor activity decreased by between 14% and 60%.

DISCUSSION

It has been previously reported (Dainis, 1975) that the period of a well executed giant swing was 1870 ms, which compares favourably to the mean of 1846 ms observed in the present study. During the swings, the forces on the bar were of the order of 4 to 4.5 times body weight (BW) which is just below t he previously calculated forces of about 5 BW on the high bar (Cureton, 1939) and the higher of the asymmetric bars (Smith, 1981). However, the measured forces of the current study were higher than those reported by Hay *et al.*, (1981) and Kopp and Reid (1980).

As would be expected, the results showed a trend that force increased as swing time decreased. All gymnasts were requested to swing at the same angular velocity in all conditions except for the wind-up trials, but it would appear that they found it easier to swing faster with the hand guards. Not only do the hand guards help the gymnast swing with greater velocity, especially with the dowels inserted, but they do allow a greater number of repetitions to be performed during a training session. The EMG data indicated that the forearm muscles were generally less active when the hand grip was aided by either the dowel hand guards or the webbing loops. This event occurred even though the forces applied to the bar were greater and indicates that wrist stabilisation by the tendons crossing the joint is reduced when the hand grip is aided by the guards.

Differences between the finger/wrist flexor and extensor muscles indicate that a different type of hand grip is used to maintain contact with the bar, than is used for a maximum power grip. It is highly likely that the gymnast uses a hook grip on the bar. In this type of hand grip, the fingers would be curled around the bar and the thumb would not be used to the same degree as in the power grip. Also, the wrist would not be extended, which would provide another explanation for the low relative levels of extensor activity. The results indicate clearly that while the bar forces increased during giant swings with webbing loops and dowel hand guards, the EMG signals decreased significantly. This finding would indicate that passive structures such as the ligaments of the hand and wrist would have to contribute a greater proportion of the total force required to prevent wrist separation. In fact, they would be carrying an increased percentage of increased loads that cross the wrist joint. While some strain relief may be provided by the leather strap of the hand guard, its point of attachment at the wrist, distal to the epiphysial plate of young gymnasts, still means that the increased forces found during the swing may compromise the integrity of the epiphysial plate.

REFERENCES

Carek, PJ & Fumich, RM 1992 Stress fracture of the distal radius. Phys Sports Med 20:115-118.

Cureton, FK 1939 Elementary principles and techniques of cinematographic analysis. Res Quart 10:15-17.

Dainis, A 1974 Analysis and synthesis of body movements utilizing the simple n-link system. Biomechanics IV pp. 513-519.

Kopp PM & Reid, JG 1980 A force and torque analysis of giant swings on the horizontal bar. Can J Appl Spt Sci 5:98-102.

Plooy, D & Forwood, M 1990 Injuries to the distal radial epiphysis in women's gymnastics Sport Health 8(2):13-14.

Read MT 1981 Stress fractures of the distal radius in adolescent gymnasts. Br J Sports Med 15:272-276.

Roy *et al.*, 1985. Stress changes of the distal radial epiphysis in young gymnasts: a report of twenty-one cases and a review of the literature. Am J Sports Med 13:301-308.

Yong_Hing *et al.*, 1988 Chronic injury of the distal ulnar and radial growth plates in an adolescent gymnast: a case report. J Bone Joint Surg (AM) 70:1087-1089.

ACKNOWLEDGMENTS

The authors would like to acknowledge the contributions of the Australian Sports Commission for major funding and Queensland University of Technology for additional funds.

Table 1. Mean values (±SE) for the force and timing data.

Condition	Swing time (ms)	Peak force - L (N)	Peak force - R (N)
Dowel grips	1908 (41)	1316 (36)	1261 (35)
Loops	1863 (38)	1290 (33)	1249 (37)
Bare hands	2052 (65)	1185 (48)	1192 (32)
Wind-up	1560 (24)	1379 (33)	1350 (41)

Table 2. Mean values (±SE) for the EMG data collected in the study.

Condition	R Flex % ref	R. Exten %ref	L. Flex % ref	L. Exten %ref
Dowel grips	112 (32)	19 (8)	102 (49)	29 (22)
Webbing loops	117 (99)	16 (10)	105 (43)	21 (14)
Bare hands	121 (57)	35 (32)	142 (57)	36 (21)
Wind-up	95 (24)	14 (8)	102 (49)	29 (22)

MECHANICAL TESTING OF MATERIALS USED IN THE CONSTRUCTION OF PLAYING CASTS

R.E. Bahamonde & K. Malone

Biomechanics Laboratory, Ball State University, Muncie, IN. 47306
Methodist Sport Medicine Center, Indianapolis, IN. 46202

INTRODUCTION

Playing casts allow athletes with severe hands sprains, strains, or simple fractures to continue their participation without the risk of getting injured again. For many years a variety of materials have been used to prepare the casts without any scientific data to determine which material or combination of materials provide the rigidity and the force absorption needed in playing casts. The purpose of this study was to test the mechanical properties of the most common playing cast materials. These included the ability of the material to absorb an impact and its stiffness. A Shore A2 durometer was used to test the hardness of the materials. Force absorption properties were measured using a drop test, and the rigidity (stiffness) was measured using modulus of elasticity procedures. A performance coefficient was developed to take into account the force absorption properties of the material, the thickness of the cast, and the impact area.

REVIEW AND THEORY

A variety of materials are currently used in the construction of playing casts (polyurethane, fiberglass tape, silicone etc..) without any standard of construction. In some instances, a physician prescribes a cast and because of the type of material or its construction, the cast is declared illegal to use. The decision of whether a cast is legal or illegal is left to the game official, and this decision is often made based on subjective evaluation of the playing cast. Bahamonde et al. (1994) stated that a playing cast should provide sufficient internal rigidity to ensure immobilization of the injured part and provide the force absorption needed to cushion impacts during a game situation. Few studies have looked at the mechanical properties of the materials. Bergfeld et al. (1982) tested the hardness of a silicone material (RTV700) using durometer measurements. DeCarlo et al. (1994) used durometer and drop test measurements to evaluate a variety of materials and protective devices but did not test the rigidity of the materials. Therefore, it was the purpose of this study to evaluate the four most common materials used in the construction of playing casts in terms of their hardness, rigidity, and shock absorbing qualities, and to determine which of the materials provide the best protection to the injured part.

PROCEDURES

Four materials were tested: RTV11, a silicone rubber material (G.E. Corp.); Delta-Lite® (Johnson & Johnson Inc.) and ScotchCast™ (3M Corp.), are fiberglass tapes which undergo a chemical reaction to provide stiffness; and QuickCast™ (LANDEC Corp.), a fiberglass and rubber knitted sleeve impregnated with a polymer. When heat from a hair dryer is applied to the QuickCast™, the polymer softens, allowing the fabric to relax and conform to the anatomical part. After cooling, the material regains its stiffness and is ready to used in competition. A Shore A2 durometer was used to test the hardness of the materials. A drop test, consisting of dropping a known mass (m= .866 kg) from three predetermined heights (30, 50, and 75 cm) onto the surface of a Kistler 9281B force platform was used to measure the force absorbed by the materials. Modulus of elasticity procedures were applied to samples of the materials using a Universal Testing Machine (United Calibration Corp.) Impact velocity, impact area, and percentage of the force absorbed were computed. A performance coefficient, (P_c) was computed to account for the differences in impact area, thickness (typical thickness of playing cast made of such material), absorptive capacity of the materials.

$$P_c = \left[1.0 \div \left(F \times T \times A\right)\right] \times 100.0$$

F, was the vertical force produced by the impact, T, was the thickness of the cast, and A, was the impact area. One-way analysis of variance for independent means was performed on the

durometer readings. Descriptive statistics were used to present the other mechanical parameters.

RESULTS

Figures 1-5 show the results obtained in this study.

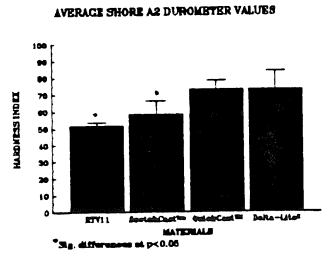

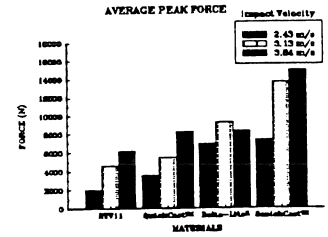

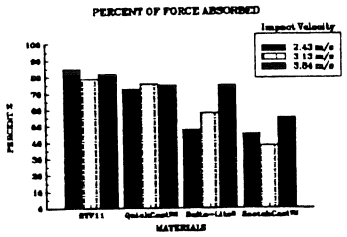

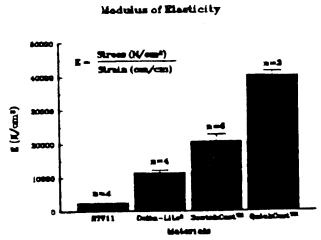

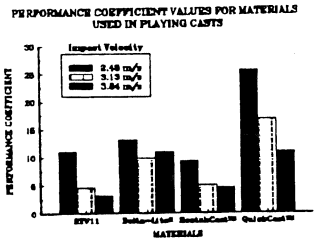

RTV11 and ScotchCast™ were the softer materials and showed significant differences in hardness from the other two materials. It was expected that the softer materials would be able to absorb a greater amount of the impact force. This assumption held true for RTV11 and ScotchCast™ but not for QuickCast™ or Delta-Lite®. The QuickCast™ material had a high durometer reading but was able to absorb a great deal of the impact force. The opposite trend occurred with ScotchCast™ which had a low durometer reading but produced high impact forces. The results of the modulus of elasticity (E) showed that although the RTV11 absorbed the largest percentage of the force, it had a low E value (very deformable). In contrast, QuickCast™ had the highest E value but was able to absorb a high percentage of the impact force. The P_c values were presented in Table 5. For all the impact velocities QuickCast™ had the largest P_c values, indicative of its ability to absorb a large percentage of the impact force over a small area and thickness.

DISCUSSION

Of the materials tested in this study RTV11 had the best shock absorbing properties, followed by QuickCast™. Although RTV11 is very deformable, it lacks rigidity. To obtain the necessary rigidity in a RTV11 cast more material is used to increase the thickness, which increases the weight and the bulkiness of the cast. In contrast, QuickCast™ showed force absorption properties comparable to RTV11, had less bulk, and was more rigid. This information could be valuable to trainers, physical therapists and sport medicine professionals in the determination of the type of materials used in the construction of playing casts. This information will also help in the development of standards to determine what type of protective equipment may be used in contact sports.

REFERENCES

Bahamonde, R. et al. JOSPT (in review).
Bergfeld, J.A. et al. Am. J. Sp. Med., 10, 293-296,1982.
DeCarlo, M. et al. JNATA, Spring 29(1), 1994.

ACKNOWLEDGMENTS

This study was supported by the LANDEC Corp.

CHANGES IN MUSCLE ACTIVATION PATTERNS DURING STATIC TASKS: A COMPARISON OF ISOMETRIC VERSUS ISOINERTIAL LOADING

Thomas S. Buchanan and David G. Lloyd

Departments of Rehabilitation Medicine and Biomedical Engineering, Northwestern University, and
Sensory Motor Performance Program, Rehabilitation Institute of Chicago,
345 East Superior Street, Chicago, IL 60611

INTRODUCTION

In this study we examined muscle activation levels during static joint moments. It was observed that for a specified posture and for specified load conditions, EMG activity varied depending on whether the limb was loaded isometrically or isoinertially (i.e., whether position was fixed and subjects were required to match a force or whether the load was fixed and subjects were required to match joint angles). We hypothesize that the differences may be due to the stiffness of the environment and the perceived need to stabilize the joint.

REVIEW AND THEORY

For a given person, muscle coactivation patterns during isometric contractions have been demonstrated to be rather consistent. That is, subjects tend to use their muscles in the same way for specified load conditions. Hence, synergic relations of muscle coactivation show consistent patterns which are functions of joint load state (Buchanan et al., 1989) and joint angles (Buchanan & Lloyd, 1994). However, muscle activation patterns measured from different investigators have been reported to show considerable differences despite that fact that the experimental conditions required the subjects to produce similar static joint moments (cf. Flanders & Soechting, 1990, and Buchanan et al., 1989).

In order to investigate this apparent inconsistency, we examined whether the way in which the static loads were applied was an important factor in determining muscle activation patterns. Whereas Buchanan et al. used an isometric protocol, Flanders & Soechting used an isoinertial protocol. The main differences between these protocols lies in whether the subjects were required to match a load while held at a fixed position or *visa versa* (i.e., required to match a position while under a fixed load).

De Serres and Milner (1991) examined the effects of isometric, stable and unstable loads on wrist muscle activation patterns. They observed increases in cocontraction of agonist and antagonist muscles as the enviornment became unstable.

PROCEDURES

Subjects were required to produce static elbow moments while sitting in a chair with the elbow at 90° flexion, neutral supination, and the shoulder at 0° extension and 90° abduction. EMGs were recorded from the biceps (BIC), brachialis (BRD), brachioradialis (BRD) and triceps (TRI). The BIC, BRD, and TRI were recorded with surface electrodes and the BRA was recorded using intramuscular fine wire electrodes. These were used for the BRA because it lies deeper in the arm and we wanted to minimize signal contamination from the biceps. For each subject a 5 cm wide cast was placed at the distal forearm just proximal to the wrist. Subjects were required to produce static forces either isometrically or isoinertially via loads attached at the wrist. In the isometric case, the cast was bolted to a six degree of freedom load cell and the subject was given visual feedback of the load produced on a computer screen. Subjects were required to produce the equivalent of 5, 10 or 15 lbs of flexion force at the load cell while keeping rotational (pronation/supination) and vertical (varus/valgus) forces at zero. This resulted in elbow torques of roughly 20-25, 45-50, 65-70 Nm, depending on the length of the subject's forearm. In the isoinertial case, a wire was attached to the cast which passed through a pulley from which weights were suspended. The subject was required to hold the arm in the same position as when the arm was in the load cell device. Once this was established, 1000 ms of data (from the EMGs and the load cell, if applicable) were collected on a Macintosh Quadra 950 at 1000 Hz. EMGs were preamplified at 60 db and bandpass filtered with a second order filter at 30–10,000 Hz. All signals were then amplified, lowpass filtered at 300 Hz with an 8th order Butterworth filter, and then sent to the computer for digitization.

In both cases, the joint angles as well as the loads at the cast, and, hence, at the elbow, were identical. In addition to the isometric and isoinertial tests described, a third case was examined. This was a modification of the isoinertial test with one addition. In this study, extra loads were placed on the cast via the wire and pulley systems to produce an extra 5 lbs of force in the flexion direction (20-25 Nm at the elbow) and the same amount was simultaneously applied in the extension direction. The net result was zero extra torque at the elbow joint but a considerable increase in forearm inertia. The extra 5, 10, and 15 lbs were then added via the same wire and pulley system and the tests were performed as described above for the isoinertial case.

RESULTS

The relationship between muscle activation (as measured by EMG) and joint torque was found to undergo considerable

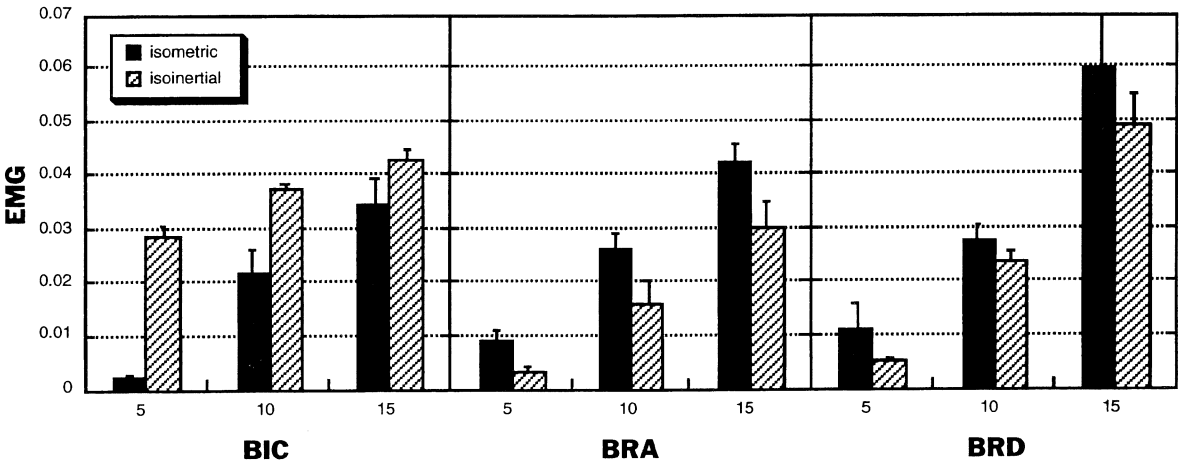

Figure 1. Changes in rectified, averaged EMG for three muscles during two different types of tasks which all required the same amount of elbow flexion torque. The subject was required to produce 5, 10, or 15 lbs of force at the wrist, which resulted in elbow torques of 23, 46, 69 Nm. The loads were either applied isometrically (i.e., with the limb fixed in a device with a load cell) or isoinertially (i.e., with weights suspended via a pulley system). In all cases, the elbow was at 90° flexion and the shoulder was at 90° abduction and 0° extension. The error bars indicate the standard deviations of five trials. Note that the EMGs vary considerably with the load paradigms.

change with the different protocols. Data for a typical subject (figure 1) show a greatly reduced BIC activation level for the isometric case compared to the isoinertial case. The opposite was observed for the BRA. In this subject, the BRD showed a similar pattern of activation to that of the BRA, that is, higher activation during isometric loads compared to isoinertial loads.

Muscle activation in the third protocol (where an increased inertial load was placed on the forearm prior to the isoinertial protocol) was not as revealing. The EMGs for this case were generally not statistically different from those of the isoinertial case. For all cases there was relatively little activation of extensor muscles during the flexion task, indicating that co-contraction was not used as a strategy. Thus, if, for a subject, one flexor muscle increased in activation with the isoinertial task (as the BIC did in figure 1), a corresponding decrease was observed in another flexor muscle (as in the BRA and BRD in figure 1). In this way an equal amount of elbow flexion torque was always maintained.

DISCUSSION

These data imply that muscle coactivation patterns (i.e., muscle synergies) may vary with the way joints are loaded. Even though the same amount of torque was required in all cases of this study and no movement was allowed, it was observed that significant differences could be observed for these static tests of muscle activation. The differences in these tasks can be characterized by a difference in the stiffness of the external environment. In the isometric case, the *world* is perfectly rigid (infinitely stiff). In the isoinertial case, the limb is free to move and the external environment is very compliant (near zero stiffness). It is our hypothesis that stiffness of the environment may play a role in determining muscle activation patterns. That may be because in the isometric case, joint stability is maintained by the environment whereas in the isoinertial case, the CNS may be using a strategy to stabilize the joint.

There is currently a debate among physical therapists as to whether closed kinetic chain (isometric) or open kinetic chain (isoinertial) treatment is better (see Palmitier et al., 1991). The data from this study indicate that different muscles may be emphasized in treatment depending on the type of protocol used.

REFERENCES

Buchanan T.S., Rovai G.P., and Rymer W.Z. *J. Neurophysiol.*, 62: 1201-1212, 1989.

Buchanan T.S. and Lloyd D.G. *Proc Second World Congress of Biomech*, 1994.

De Serres S.J. and Milner T.E. *Experimental Brain Research.* 86: 451-458, 1991.

Flanders M. and Soechting J.F. *J. Neurophysiol.*, 64: 1818-1837, 1990.

Palmitier R.A, An K.N, Scott S.G. and Chao, E.Y. *Sports Medicine* 11: 402-413, 1991.

ACKNOWLEDGMENTS

This work supported, in part, by NIH R29-AR40408 and NIDRR H133P20016.

DETERMINING SELECTED MUSCULOSKELETAL PARAMETERS OF THE QUADRICEPS MUSCLES USING MAGNETIC RESONANCE IMAGING AND RADIOGRAPHY

John W. Chow[1], James C. Ehrhardt[2], and Warren G. Darling[3]

[1]Department of Kinesiology, The University of Illinois at Urbana/Champaign, Urbana, IL 61801
Departments of [2]Radiology and [3]Exercise Science, The University of Iowa, Iowa City, IA 52242

INTRODUCTION

The purpose of this study was to develop a technique for the determination of selected musculoskeletal parameters of the quadriceps muscles *in vivo* using magnetic resonance imaging (MRI) and radiography. Two magnetic resonance (MR) scans were performed and axial images were obtained for the left thigh of a female subject at the anatomical position (AP). Muscle volume (V), coordinates of the origin and insertion, and muscle belly length at AP (L_a^b) of each quadriceps muscle were determined from MRI data. Six knee radiographs were used to determine the effective moment arm of the quadriceps force about the transverse axis through the knee joint (d_e) at different knee flexion angles ($\emptyset_K$s), defined as the angle between the distal extension of the thigh segment and the shank segment. Two hip radiographs were used to determine the amount of pelvis rotation from supine to sitting position. A combination of MRI and radiography data was used to compute the muscle lengths (Ls) at different $\emptyset_K$s.

REVIEW AND THEORY

Previous studies involving musculoskeletal modeling used musculoskeletal parameters measured from cadavers, dry-bone samples, and illustrations in anatomy literature (Yamaguchi et al., 1990). The extent of the errors caused by using these parameters in musculoskeletal modeling has not been examined. Despite the growing popularity of MRI and its advantages over computer tomography, few efforts have been made to use MRI to estimate musculoskeletal parameters. The purpose of this study was to develop a technique for the determination of selected musculoskeletal parameters of the quadriceps muscles *in vivo* using MRI and radiography.

PROCEDURES

A GE MRI scanner operating at 1.5 T was used to obtain axial images at 4 mm intervals for the left thigh of a female subject (24 yrs, 1.6 m, 574 N) at AP. There were a total of 114 MR images available and these images started at approximately 12 mm superior to the top of the femoral head (image #0) and ended at approximately 28 mm inferior to the distal articular surfaces of the femur (image #113). During the radiography session, six radiographs of the subject's left knee at different $\emptyset_K$s (25° to 100° at intervals of 15°) and two radiographs of the hip (supine and sitting positions) were obtained.

Femoral Reference Frame. The parameters determined in this study were referred to a femoral reference frame (O: x-y-z). The origin of the system was located at the knee joint center O, which was defined to be at the midpoint between the medial and lateral femoral condyles. The z-axis was defined as the line joining O with the center of the femoral head. The x-axis was directed anteriorly and perpendicular to a plane containing the z-axis and the medial and lateral femoral condyles. Finally, the y-axis was defined by the cross product of the x- and z-axes.

Effective Moment Arm. For each radiographic image, a tracing was made and the image of the metal ruler was the spatial reference for quantitative analysis (Figure 1). Lines IJ and FG were the lines of action (LOAs) of the quadriceps tendon and patellar ligament, repectively. Points B and L were the centers of contact area between adjacent bones. Using the coordinate data extracted from ecah tracing, d_e was determined by computing the shortest distances between point B and line FC (d_p), point L and line FG (d_1), and point L and line IJ (d_2) [Grood et al., 1984]:

$$d_e = (d_p d_2) / d_1 \qquad [1]$$

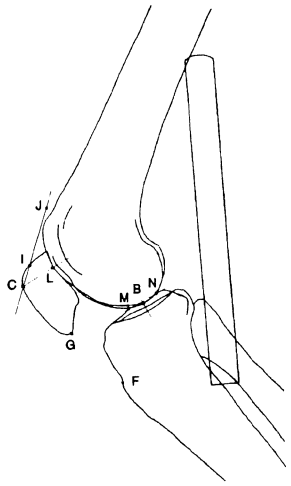

Figure 1. Tracing of a knee radiograph.

Patella Locations. Data for the patella locations relative to the femur at various $\emptyset_K$s were needed for the computation of muscle lengths. By superimposing the contour of the femur in each radiographic tracing, an additional tracing was made showing the patella locations at different $\emptyset_K$s (Figure 2). Coordinates of 10 points -- six locations of the bases of patella and four points along the curve UV -- were obtained for the computation of muscle length.

Muscle Volume. The MR image analysis was performed using the program SGITRACE (Image Analysis Facility, University of Iowa). To trace the contour of a muscle displayed on a monitor, a series of points was placed along the contour of the muscle and the software would connect consecutive points with straight line. Based on the inter-image space and the contours traced on the images, the software computed the volume of each quadriceps muscle.

Muscle Length. The SGITRACE program also allowed the user to digitize points on an image. In other words, there was a built-in reference frame attached to the MR images (MR reference frame, O′: x′-y′-z′) [Figure 3]. The z′-coordinate of a point was obtained as the product of the image # and inter-image space.

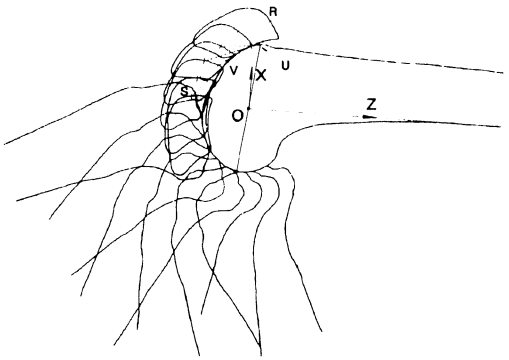

Figure 2. Patella Location at Different Knee Flexion Angles.

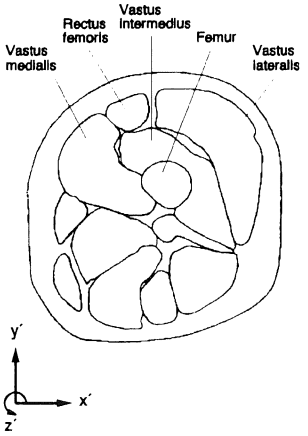

Figure 3. Tracing of a MR image.

The centroid of the attachment area was considered as the point representation of the muscle origin/insertion. Observations from MR images and illustrations in anatomy books were used to determine the locations of the origins of the rectus femoris (RF), vastus intermedius (VI), vastus lateralis (VL), and vastus medialis (VM). In addition, the coordinates of (1) the center of the femoral head, (2) the base of the patella (BP) at AP, and (3) the lateral and medial femoral condyles, were also determined. Transformation of coordinates from MR reference frame to femoral reference frame was completed in two steps. Linear transformation was first performed so that the two reference frames had a common origin. Rotational transformation was then executed using a direction cosine matrix.

The length of a quadriceps muscle was defined as the shortest distance between the origin and BP. The y-coordinate of BP was considered constant at different $\emptyset_K$s. The x- and z-coordinates of BP at different $\emptyset_K$s were obtained from Figure 2. In addition to the coordinates of the origin of RF (O_{RF}) at AP, coordinates of O_{RF} in the sitting position were obtained by rotating the coordinates of O_{RF} at AP about a transverse axis located at the center of the femoral head through an angle (pelvis rotation) measured from hip radiographs. When the quadriceps tendon wrapped around the femoral groove (i.e., $\emptyset_K \geq 55°$), the femoral groove was modeled as a pulley with the quadriceps tendon wrapping around it. The muscle length was still the shortest distance between the origin and BP given that the path of the muscle was altered by a pulley.

For the purpose of this study, LOA of the quadriceps force was a line passing through BP (or point U in Figure 2 for KFA $\geq$ 55°) and parallel to the z-axis. The angle between LOA of an individual muscle force and LOA of the quadriceps force for each quadriceps muscle was obtained using the dot product.

RESULTS AND DISCUSSION

Selected coordinate parameters determined in this study are presented in Table 1. For the purpose of comparison, coordinates of the origins of the vasti muscles given by Brand et al. (1982) are also included in the table. The comparison indicates a major discrepancy in the z-coordinate of VL. This is probably due to the difference in the location of the effective origin of VL chosen by Brand et al. (1982) and the authors of this study.

Table 1. Coordinates of Selected Anatomical Landmarks.

	Coordinate (mm)		
Anatomical Landmark	x	y	z
Muscle Origin (present study):			
Rectus femoris (supine)	30.3	4.0	385.3
Rectus femoris (sitting)	46.2	4.0	350.5
Vastus Intermedius	21.7	25.5	185.2
Vastus Lateralis	15.5	40.5	343.1
Vastus Medialis	20.2	-3.2	162.3
Base of patella	56.8	-1.8	24.2
Medial epicondyle	0.0	-42.6	-3.8
Lateral epicondyle	0.0	42.6	3.8
Center of femoral head	0.0	0.0	350.4
Muscle Origin (Brand et al., 1982):			
Average of 6 cadaver samples:			
Vastus Intermedius	23.2	17.6	206.7
Vastus Lateralis	1.0	36.5	212.7
Vastus Medialis	4.3	8.8	188.0
Scaled with anthropometric factors:			
Vastus Intermedius	24.6	11.1	184.1
Vastus Lateralis	1.3	21.4	188.9
Vastus Medialis	4.1	5.4	167.5

A survey by Yamaguchi et al. (1990) cited only one study (Friederich et al., 1990) that provided the volumetric data of the quadriceps muscles. The muscle volumes found in this study -- 226 (RF), 430 (VI), 655 (VL), and 420 (VM) mm^3 -- are much larger than the corresponding values Friederich et al. (1990) measured from a 63 yrs old female cadaver.

The shape of the d_e-$\emptyset_K$ relation found in this study is considered comparable to those reported in the literature, but the d_e values are relatively small. One possible explanation is that a female subject of average build was used in this study while male subjects or cadavers were used in most of the previous studies.

REFERENCES

Brand, R.A. et al. *J. Biom. Engr.*, 104, 304-310, 1982.
Friederich, J.A. et al. *J. Biom.*, 23, 91-95, 1990.
Grood, E.S. et al. *J. Bone Jt. Serg.*, 66A(5), 725-734, 1984.
Yamaguchi, G.T. et al. in Winters, J.M. et al. (Eds.) *Multiple Muscle Systems*, 717-749, 1990.

MAXIMUM MUSCLE STRESS OF THE QUADRICEPS MUSCLES

John W. Chow[1], James C. Ehrhardt[2], and Warren G. Darling[3]

[1]Department of Kinesiology, The University of Illinois at Urbana/Champaign, Urbana, IL 61801
Departments of [2]Radiology and [3]Exercise Science, The University of Iowa, Iowa City, IA 52242

INTRODUCTION

The purpose of this study was to determine the maximum muscle stress (σ), mathematically defined as the maximum isometric strength at optimum muscle length (F_o^{max}) divided by the physiological cross-sectional area (A), of the quadriceps muscles. One female subject performed maximum effort knee extension exercises on a LIDO dynamometer. The gravitational effect was taken into consideration when determining the isometric resultant knee torques (T_Ks) at different knee flexion angles ($\emptyset_K$s). The musculoskeletal parameters of the quadriceps muscles were obtained from radiography and magnetic resonance imaging (MRI). The σ value was computed using the measured T_Ks, musculoskeletal parameters data, and information reported in the literature. The σ values obtained from the data for nine different $\emptyset_K$s ranged from 18.9 to 27.3 N/cm^2. The average value of 22.8 N/cm^2 is notably smaller than the corresponding values reported in the literature.

REVIEW AND THEORY

The relation between the muscle size, specifically the cross-sectional area, and the maximum strength of the muscle has been a subject of interest for more than a century. A wide range of values for the so called "absolute muscle strength" of human muscles has been reported in the literature over the years. The large variation in strength values is probably due to the differences in the definition of cross-sectional area used by different investigators and the differences in muscle length at which the strength is measured.

The purpose of this study was to determine the maximum muscle stress of the quadriceps muscles. It is noteworthy that, because Hill's (1938) mechanical model is commonly used in musculoskeletal modeling, σ values are very useful because A and σ values can be used to predict F_o^{max}, which is a parameter in Hill's model.

PROCEDURES

A female (24 yrs, 1.6 m, 574 N) served as the subject. During the strength testing session, the subject performed maximum effort left knee extension exercises on a LIDO dynamometer in a sitting position. The session started with maximal isometric contractions at different attachment arm angles (isometric pre-tests). These were followed by 16 isokinetic and three isotonic trials. The session concluded with maximal isometric trials (isometric post-tests). Average values of the isometric pre-tests and post-tests were used for the determination of σ.

The resistance force acting on the shank-plus-foot (S+F) segment (F_R) was measured by a load cell located between the attachment arm of the dynamometer and the shank. The knee flexion angle ($\emptyset_K$), defined as the angle between the distal extension of the thigh segment and the shank segment, for each isometric trial was measured from sagittal view of the medial side of S+F segment recorded by a video camera. The T_K values were determined using the moment equation about the knee joint center:

$$T_K = F_R d_R + W_{SF} d_{SF} \quad [1]$$

where d_{SF} is moment arm of the weight of S+F segment (W_{SF}) [d_{SF}] and d_R is moment arm of F_R (d_R). The W_{SF}, d_R, and d_{SF} values were determined from video recordings and inertial parameters reported in the literature.

During the radiography session, six radiographs of the subject's left knee and two radiographs of the hip were obtained. During the MRI session, two scans were performed and axial images at 4 mm intervals were obtained for the left thigh. Based on the data reduced from radiography and MRI. The coordinates of the origins and insertions of the rectus femoris (RF), vastus intermedius (VI), vastus lateralis (VL), and vastus medialis (VM), and the effective moment arm of the quadriceps force about the transverse axis through the knee center (d_e) were determined (Chow et al, 1994). The muscle length was computed as the shortest distance between the origin and insertion of the muscle. In addition, muscle volume (V) and muscle belly length at the anatomical position (AP) [L_a^b] of each muscle were determined from MRI data.

In this study, A was defined as V divided by optimal muscle fiber length (L_o^f). For each muscle, L_o^f was obtained indirectly from L_a^b and sarcomere length (L^S) at AP (L_a^S) provided by Cutts (1988). The muscle fiber length at AP (L_a^f) was computed as the product of L_a^b and average L_a^f/L_a^b ratio reported by Friederich et al. (1990) and Wickiewicz et al. (1983). The number of sarcomeres per fiber was obtained by dividing L_a^f by L_a^S. The L_o^f was then computed as the product of the number of sarcomeres per fiber and optimum sarcomere length (L_o^S = 2.72 μm).

In addition to L_a^S data, Cutts (1988) also predicted L^Ss of the lower limb muscles at two different limb positions -- lying with $\emptyset_K$ = 115° (L-115) and sitting with $\emptyset_K$ = 13° (S-13). The L^Ss at sitting with $\emptyset_K$ = 115° (S-115) position were first estimated {S-115 = (L-115) - [(AP) - (S-13)]}. The Ls at S-13 and S-115 positions were than obtained using the L-$\emptyset_K$ relations obtained from radiography and MRI data. Assuming a linear relation between L and L^S, the L-L^S relation for each muscle was computed using the Ls and L^Ss at S-13 and S-115 positions (Figure 1). Using these relations, the optimal muscle length (L at which L^S = 2.72 μm, L_o) of each muscle was predicted (Table 1). Based on a normalized force-L^S ($\bar{F}$-L^S) relation of the human muscle reported by Walker et al. (1973) (Figure 2), $\bar{F}$s at Ls corresponding to S-13 and S-115, and at L_o were determined. For example, by applying the data points of VL in Figure 1 (3 triangles) to Figure 2, the $\bar{F}$s of VL at the above-mentioned three Ls were obtained as 76.5, 59, and 100 %, respectively. Becasue L_os of RF and VI fell outside of the working ranges of these two muscles in this study (i.e., 2 data points for each muscle), linear relations were applied to the $\bar{F}$-L data of these two muscles. The $\bar{F}$-L data of VL and VM (3 data points for each) were fitted with second-order polynomials because force-

length curves of isolated muscles are usually parabolic in shape (e.g., Woittiez et al., 1984).

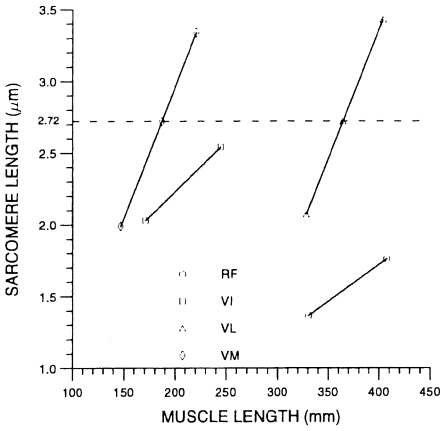

Figure 1. Relations Between Muscle Lengths of Individual Quadriceps Muscles and Sarcomere Length.

Table 1. Sarcomere and Muscle Lengths of the Quadriceps at Different Lower Limb Positions.

	Sarcomere Length (μm)				Muscle Length (mm)		
	L-115	AP	S-13	S-115	S-13	S-115	Optimal
RF	2.541	2.146	1.365	1.76	330.6	407.5	594.4
VI	2.482	1.97	2.03	2.542	170.9	244.7	513.8
VL	3.531	2.173	2.071	3.429	328.3	403.5	364.2
VM	3.401	2.048	1.988	3.341	146.8	220.6	186.8

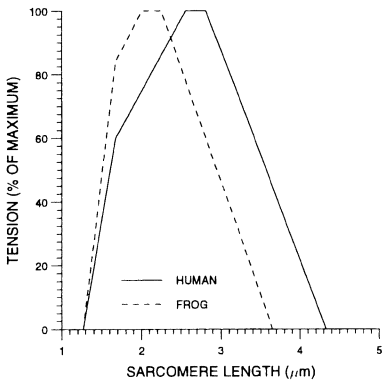

Figure 2. Relations Between Normalized Muscle Force and Sarcomere Length.

At a given L, the F^{max} of each muscle [$F^{max}(L) = \tilde{F}(L)\sigma A$, where (L) means a function of L] is related to T_K by

$$T_K = d_e \sum_{i=1}^{4} (\tilde{F}_i \sigma A \cos\theta_i) \qquad [2]$$

where θ is the angle between the lines of action of the quadriceps force and an individual muscle force, and i is the subscript for individual heads of the quadriceps muscle. Using the T_K-$\emptyset_K$, d_e-$\emptyset_K$, θ-$\emptyset_K$, $\tilde{F}$-L, and L-$\emptyset_K$ relations, T_K, d_e, θ_is, and $\tilde{F}_i$s at nine $\emptyset_K$s -- 25° to 105° at 10° intervals -- were computed. For each $\emptyset_K$, σ in Eq. [2] was solved using the *root* function in Mathcad (MathSoft, Inc.).

RESULTS AND DISCUSSION

The procedures used in determining the A in this study were similar to those used by Fukunaga et al. (1992). The only exception was that they used L_a^f in the computation of A. According to Cutts' (1988) data, L_a^Ss of the quadriceps muscles are shorter than L_o^S (Table 1). Therefore, A will be overestimated if L_a^f is used for any of the quadriceps muscles. For the given F^{max}, an overestimated A will cause an underestimated σ.

The σ and F^{max} values computed from the data for different $\emptyset_K$s are presented in Table 2. The relation between σ and $\emptyset_K$ is obvious -- σ increased with increasing $\emptyset_K$. This relation is probably due to ignoring pennation angle (α) in the computation of A. If α is considered, F_o^{max} ($= \sigma A$) can be expressed as

$$F_o^{max} = \sigma \left(\frac{V\cos\alpha}{L_o^f} \right) \qquad [3]$$

Considering the shape and the geometry of the muscle fibers of a unipennate muscle, α increases as the muscle gets shorter (i.e., $\emptyset_K \propto 1/\alpha$). For the given F_o^{max}, V, and L_o^f, σ becomes larger when α gets smaller (i.e., $\sigma \propto 1/\alpha$). The combination of these relations implies that σ increases with increasing $\emptyset_K$ if α is neglected or a constant α is assumed for different $\emptyset_K$s. Another possible reason for greater σ values at large $\emptyset_K$s is the introduction of passive force when a muscle is stretched beyond its resting length, which is the case for the quadriceps muscles at large $\emptyset_K$s.

Table 2. Maximum Isometric Strength and Muscle Stress.

	Maximum Isometric Strength (N)				
$\emptyset_K$ (°)	RF	VI	VL	VM	σ (N/cm^2)
105	423.3	1,369.8	1,854.9	1,051.5	27.3
95	353.7	1,196.9	1,854.7	1,034.5	24.3
85	319.9	1,133.4	1,937.6	1,067.9	23.4
75	295.8	1,101.8	2,034.5	1,109.8	23.1
65	271.8	1,073.6	2,112.5	1,140.9	23.0
55	242.6	1,031.9	2,138.9	1,143.1	22.5
45	206.5	968.9	2,087.0	1,102.9	21.7
35	164.3	886.0	1,940.0	1,012.4	20.4
25	118.6	790.2	1,689.4	868.9	18.9

The average σ value of 22.8 N/cm^2 is notably smaller than the σ values for human muscles reported in the literature, but is comparable to those found in animal muscles. To confirm the σ value found in this study, further studies using different human muscles are recommended.

REFERENCES

Chow, J.W. et al. *Proc. 18th ASB Annual Meeting*, 1994.
Cutts, A. *J. Anatomy*, 160, 79-88, 1988.
Friederich, J.A. et al. *J. Biom.*, 23, 91-95,1990.
Fukunaga, T. et al. *J. Ortho. Res.*, 10, 926-934, 1992.
Hill, A.V. *Proc. Royal Soc. B*, 126, 136-195, 1938.
Walker, S.M. et al. *Anatomical Record*, 178, 63-82, 1973.
Wickiewicz, T.L. et al. *Clin. Ortho. Rel. Res.*, 179, 275-283, 1983.
Woittiez, R.D. et al. *J. Morphology*, 182, 95-113, 1984.

BILATERAL DEFICIT IS DIFFERENTIALLY AFFECTED DURING CONCENTRIC AND ECCENTRIC CONTRACTIONS

M.D. Grabiner* and T.M. Owings**

Department of Biomedical Engineering*, The Cleveland Clinic Foundation, Cleveland, Ohio
Biomedical Engineering Center**, The Ohio State University, Columbus, Ohio

INTRODUCTION

The bilateral deficit is characterized by a reduction in muscular force generated by simultaneous maximum contraction of bilateral muscle groups, compared to the sum of the forces during individual maximum contractions. The exact mechanism responsible for this reduction in force has not been described, but has been broadly attributed to neurally mediated factors. It has been suggested that the deficit was due to an inhibition of small motor units (Secher et al, 1978) whereas others have reported that the deficit reflected large motor unit inhibition (Vandervoort et al, 1984; Koh et al, 1993). Although the bilateral deficit has been investigated for isometric and concentric isokinetic contractions there have been no investigations of this type of interlimb effect during eccentric contractions.

There is an increasingly convincing body of evidence that *the central nervous system specifically commands eccentric contractions*. This evidence cites decreased motor unit discharge frequencies during eccentric contractions, compared to concentric contractions; the inability to maximally activate the motor unit pool during eccentric contraction; and the possibility that large motor units may be selectively activated during eccentric contractions. The fundamental differences that may exist between motor unit activation during eccentric and concentric contraction give rise to the possibility that interlimb interactions may also differ. This study compared the activation and force characteristics of the bilateral deficit during concentric and eccentric isokinetic knee extensions. It was anticipated that (1) eccentric contractions would be found to demonstrate a bilateral deficit of smaller magnitude than concentric contractions and (2) that the bilateral deficit would be decreased during rapid and forceful contractions.

METHODS

Eight female and six male college students participated in this study. None of the subjects reported a history of knee injury. Two of the subjects reported previous experience with isokinetic testing. Bipolar electrodes were placed over the left and the right vastus lateralis and the left and right hamstrings of each of the subjects. A reference electrode was placed over the fibular head of the right leg. A Kin-Com isokinetic dynamometer was modified to allow measurement of both bilateral and unilateral isokinetic knee extension. The knee extension forces produced by the right and left limbs were measured independently using strain gauge load cells. The knee extension range of motion was from 90° of flexion to 20° of flexion. The isokinetic speeds that were tested were 30 and 150°/s.

Each subject performed a total of 18 trials, nine eccentric and nine concentric contractions. Each set of the nine contractions was comprised of three sequences of unilateral-right leg maximum voluntary effort (MVE), unilateral-left leg MVE, and bilateral MVE.

For each trial, the middle third of the knee extension range of motion was extracted for analysis. The variables extracted for analysis were the independently measured peak knee extension moment and peak rate of change of knee extension force (dF/dt), and the activation levels of the quadriceps femoris and hamstrings. The data for the subjects'

dominant leg were subjected to a 2 by 2 by 2 (contraction type by isokinetic speed by leg) repeated measures ANOVA.

RESULTS

The ANOVA revealed that the between-condition differences observed in the activation level of the hamstrings were not significant ($p>0.05$). Thus, changes in the knee extension variables were assumed to be independent of antagonist muscle activation.

A significant main effect of contraction type (concentric vs. eccentric) was revealed for the peak knee extension moment ($p<0.001$). The concentric bilateral deficit, pooled across leg and isokinetic speed condition,was -16.7 and -11.0 percent for the concentic and eccentric contractions, respectively.

The ANOVA revealed a significant speed by contraction type interaction ($p=0.001$) for dF/dt. For the 30 and 150 deg/s speeds, the concentric bilateral deficits for dF/dt were -31.6 and -15.4 percent, respectively. For the ecccentric contractions, the bilateral deficits for the 30 and 150 deg/s speeds were -7.8 and 1.4 percent, respectively, the latter value representing a *bilateral facilitation.*

The bilateral deficit data relative to the level of quadriceps femoris activation demonstrated a significant main effect of contraction type ($p<0.001$). The decreases observed during bilateral efforts for concentric and eccentric contractions were -8.6 and -6.6 percent, respectively.

The ANOVA revealed that the bilateral deficit demonstrated by the nondominant leg was not significantly different than that of the dominant leg. However, there were qualitative differences that intimated a tendency of the nondominant leg to be affected to a larger extent during bilateral contractions.

DISCUSSION

This study tested the hypothesis that maximum effort eccentric contractions would be affected to a lesser extent by the bilateral deficit than maximum effort concentric contractions. The data generally supported the first expected outcome which stated that eccentric contractions would be found to demonstrate a bilateral deficit of smaller magnitude than concentric contractions.

The second expected outcome stated that the bilateral deficit would be decreased during rapid and forceful contractions, that is during the 150 deg/s knee extensions. Although the data did not statistically support this expectation, there were qualitative trends in the data that suggest the bilateral deficit, for all variables, tended to be of smaller magnitude in the 150 vs. 30 deg/s conditions.

Within the limitations imposed by the underlying assumptions of the study, the results are in agreement with those of others (Vandervoort et al, 1984; Koh et al, 1993) and support the contention that the bilateral deficit is a manifestation of the influence of central nervous system restrictions on the ability to activate large motor units. The results also seem to be consistent with the contention that the central nervous system specifies different motor commands for eccentric contractions and that central and peripheral influences converge in such a way as to result in a different pattern of interlimb effects.

REFERENCES

Secher et al., *Acta Physiol Scand,* 103:456-462, 1978.

Vandervoort et al., *J Appl Physiol*, 56:46-51, 1984.

Koh et al., *J Appl Physiol*, 74:1200-1205,1993.

This work was supported by Chattecx, Corp.

DO RELATIVE CONTRIBUTIONS TO THE NET JOINT MOMENT CHANGE AFTER EXTENDED PRACTICE?

G.D. Heise and A. Cornwell
Department of Kinesiology, Louisiana State University, Baton Rouge, LA 70803.

INTRODUCTION

The components of the net joint moment at the elbow and shoulder and the relative contributions of those components were examined for subjects' nondominant arm during the practice of a maximal, planar, multijoint throwing motion. Subjects threw a 0.15 kg ball significantly farther after extended practice (200 trials) and analysis of segmental dynamics indicated that subjects increased generalized muscle moments as well as motion dependent moments at both joints. However, the ratios of moment components to the net joint moments at each joint did not change after extended practice. Restraining the throwing arm to a horizontal plane may partly explain why no changes were found in the contributions of joint moment components to the net joint moments. In addition, the throwing motion may be a skill pre-disposed to invariant dynamics due to limb structure.

REVIEW AND THEORY

Invariant kinematic and kinetic descriptors have been identified for the following whipping-type motions: throwing (Chapman & Sanderson, 1990; Jöris et al., 1985); kicking (Putnam, 1991); certain reaching motions (Hollerbach & Flash, 1982); and the motion of the leg during the swing phase of locomotion (Putnam, 1991). However, the response of these characteristics during skill acquisition has not been vigorously pursued. Schneider et al. (1989) examined the components of joint moments during practice of a maximal-speed vertical arm movement, of which only part of the movement can be considered a whipping-type motion. They found that as subjects performed faster movements, the interactive components and the generalized muscle moments (GMM) of all joints during all phases of movement increased. Their results were interpreted in light of Bernstein's hypothesis that individuals use reactive forces (represented by interactive or motion dependent moments) to complement active muscle forces (represented by GMM). Nevertheless, Schneider et al. (1989) did not comment on whether the movement strategy, as represented by the relative contribution of each component to the net moment, changed during practice. The purpose of the present investigation was to examine the relative contributions of the components of the net joint moment during the practice of a planar, multijoint throwing motion.

PROCEDURES

Seven healthy college-aged men volunteered as subjects for this study. Each subject performed 200 throwing trials equally distributed across 5 consecutive days. Subjects threw a 0.15 kg ball as far as possible with their non-dominant arm while the motion of their throwing arm was restrained to a horizontal plane. From video data, 2-D coordinates of joint centers defining a three segment model of the throwing arm were determined (Peak Performance Technologies, Inc. motion analysis) for two trials early in practice and two trials late in practice. Methods of Hatze (1979) were used to predict the inertial characteristics of each segment (i.e., upper arm, forearm, and hand). Joint moments were calculated at the shoulder, elbow and wrist. At each joint, the moment was partitioned into three components (Schneider et al., 1989): 1. interactive moments - motion dependent moments arising from the dynamic interactions between segments; 2. GMM - moment arising from muscle forces and other soft tissue forces crossing the joint; 3. net joint moment - sum of all positive and negative contributions from components 1 and 2. Gravity was not included in the kinetic analysis because the movement was restrained to a horizontal plane. Moment components were averaged, following the procedure of Putnam (1991), during the duration that the upper arm segment was accelerated in the direction of the throw. For each joint, average moment values of each component were calculated and ratios of GMM and interactive moments to the net moment also were calculated. The effect of practice on these variables was tested statistically with MANOVA procedures.

RESULTS AND DISCUSSION

Performance, as measured by the resultant distance of the throw, showed an expected, significant improvement over practice trials. The mean increase in distance, collapsed across subjects, was 1.8 m. The averaged net joint moments for the shoulder and elbow are presented in Table 1 along with the GMM and the two highest interactive moments for each joint. Moment components at the wrist were negligible. Ratios of moment components to the net joint moment are also presented in Table 1. Subjects showed expected significant increases in net moments and interactive moments (see average values in

Table 1). This is in agreement with the findings of Schneider et al. (1989) who also showed increased muscle moments with accompanying increases in interactive moments. However, in the present study, the relative contribution of muscle moments and interactive moments to the net moment did not change from early to late in practice (see ratios of Table 1). These ratio results are consistent with results of Hollerbach and Flash (1982) who found that subjects linearly scaled joint moments to produce faster movements in a horizontal plane, but are inconsistent with results of Zernicke and Schneider (1993) who showed different moment profiles during practice. The movement examined in the latter study and by Schneider et al. (1989) took place primarily in a vertical plane and gravity was a key moment component in earlier, slower trials. So, in the present investigation, restraining the throwing arm to a horizontal plane may partly explain why no changes were found in the ratio measures. The familiar nature of the throwing motion, even though it was performed by the nondominant limb in which the forearm remained pronated while against a horizontal surface, may also explain why the relative contribution of moment components did not change. The findings of the present study in combination with other experimental work on whipping-type motions (e.g., Hollerbach & Flash, 1982) and modeling studies (e.g., Chapman & Sanderson, 1990) may point to some dynamic-based theory describing multijoint throwing movements in which limb structure and segment dynamics dictate movement control rather than a memory-based representation of control (e.g., generalized motor program, Schmidt, 1975). In order to further address this speculation, it will be necessary to examine how the moment components change with practice when the throwing motion is not restrained to a horizontal plane.

Table 1: Average Moment Values and Ratios of Moment Components to the Net Joint Moment Early and Late in Practice. Positive moments represent horizontal shoulder abduction and elbow extension. Average moment values are in N m. Ratios are unitless. Numbers represent mean values across all subjects with standard deviations in parentheses. [1] Shoulder multivariate F ($p < 0.10$). [2] Elbow multivariate F ($p < 0.05$).
* Significant univariate F ($p < 0.05$), Late > Early.

	Early		Late	
	Average	Ratio	Average	Ratio
Components of Shoulder Joint Moment [1]				
Net Moment	2.99 (0.9)	——	4.83 (1.5) *	——
GMM	11.59 (3.7)	3.87 (0.5)	20.37 (5.6) *	4.26 (0.4)
UAA (upper arm angular acceleration)	- 5.97 (1.5)	- 2.02 (0.2)	- 10.29 (2.7) *	- 2.16 (0.2)
FAA (forearm angular acceleration)	- 3.65 (1.6)	- 1.21 (0.3)	- 5.86 (1.8) *	- 1.22 (0.2)
Components of Elbow Joint Moment [2]				
Net Moment	2.15 (0.7)	——	3.06 (0.9) *	——
GMM	3.92 (1.5)	1.82 (0.3)	6.45 (2.0) *	2.11 (0.1)
FAA (forearm angular acceleration)	- 1.67 (0.5)	- 0.80 (0.2)	- 2.43 (0.8) *	- 0.81 (0.1)
UAV (upper arm angular velocity)	- 0.35 (0.2)	- 0.16 (0.3)	- 0.89 (0.5) *	- 0.25 (0.1)

REFERENCES

Chapman, A.E. & Sanderson, D.J. in Multiple Muscle Systems, (Eds. Winters & Woo) Springer-Verlag, pp. 608-620, 1990.

Hatze, H. A model for the computational determination of parameter values of anthropomorphic segments. CSIR Tech. Report TWISK 79, Pretoria, South Africa, 1979.

Hollerbach, J.M. & Flash, T. (1982). Biol. Cybern., 44, 67-77, 1982.

Jöris, H.J.J. et al. J. Biomech., 18, 409-414, 1985.

Putnam, C.A. Med. Sci. Sport and Exer., 23, 130-144, 1991.

Schmidt, R.A. Psychol. Rev., 82, 225-260, 1975.

Schneider, K. et al. J. Biomech., 22, 805-817, 1989.

Zernicke, R.F. & Schneider, K. Child Dev., 64, 982-1004, 1993.

ACKNOWLEDGEMENTS

Faculty support was provided by the 1993 Summer Stipend Program from the Council on Research of Louisiana State University

A UNIQUE TREADMILL DEVICE FOR SYMMETRY ASSESSMENT AND REAL - TIME VISUAL FEEDBACK DURING GAIT

Jonathan B. Dingwell[1,2], Brian L. Davis[2], Dean M. Frazier[3], James H. Campbell[3]

[1]Department of Biomedical Engineering, The Ohio State University, Columbus, Ohio
[2]Department of Biomedical Engineering, The Cleveland Clinic Foundation, Cleveland, Ohio
[3]Department of Orthotics and Prosthetics, The Cleveland Clinic Foundation, Cleveland, Ohio

INTRODUCTION

Symmetry is an issue in the gait of amputees because of the unnatural asymmetry imposed on the patient by the amputation itself. This asymmetry, introduced to the mechanical system by the artificial limb, leads to a number of functional asymmetries which can be measured in the temporal, kinetic, and kinematic gait patterns of amputees. These asymmetries represent adaptations to the mechanical asymmetry imposed on the amputee by the prosthesis (Winter and Sienko, 1988). The most prominent asymmetries found in amputee gait have involved shortened stance times and decreased ground reaction forces for the prosthetic limb compared to the natural limb (Skinner and Effeney, 1985).

The purpose of the current study was to evaluate the effectiveness of a newly developed treadmill force plate device in making real-time gait symmetry evaluations. Asymmetries were assessed in the kinetic and temporal patterns of normal and Below-Knee (BK) amputee subjects. Three comparisons were made; asymmetries were compared between normal subjects and amputees, amputee subjects were compared before and after receiving real-time visual feedback, and were compared to quantify symmetry differences for two different heel bumper durometers available for the Otto Bock 1M1 multi-axis prosthetic foot. The 1M1 foot allows variable degrees of plantar- and dorsiflexion resistance by interchanging bumpers of varying durometers inserted behind the ankle joint.

METHODS

A treadmill device which has been developed at the Cleveland Clinic has two AMTI force plates mounted front to back underneath the treadmill belt. The treadmill and force plates have been mounted independently to the concrete foundation of the building to reduce any vibrational interference in the force plate signals from the treadmill. The advantages of this system are that it allows the collection and comparison of vertical loads under each limb during multiple, successive strides, at a constant, known speed, without forcing the subject to "target" their footsteps, and that data collection can be completed in a very short period of time (e.g. 10 to 15 complete strides can be collected in as little as 20 to 25 seconds).

Data was collected from the treadmill force plates using a Gateway 2000 486 computer, and Data Translations DT2812 A/D board. Software was developed in Borland Turbo Pascal v. 6.0 to continuously read and process data from the force plates, and display symmetry information to the subject in real time. Continuous collection, processing, saving, and displaying of data was possible at up to 100Hz. Three modes of visual feedback were developed, which graphically displayed Center Of Pressure (COP), Percent Stance Time (%ST), and relative Push Off Force (POF) information on a computer monitor. The setup for real-time feedback display is shown in Figure 1.

The study was conducted in three parts; (I) data was collected on six normal, right leg dominant subjects with no previous history of leg injury (mean age 42.7), (II) symmetries were evaluated for six unilateral BK amputees (three traumatic, two due to illness, one due to cancer; mean age 41.7) before and after receiving visual feedback, (III) symmetry was assessed for five unilateral BK amputees (all traumatic; mean age 42.8) using both durometer heel bumpers in the Otto Bock 1M1 foot. Two of the amputees participated in both parts of the study, at least two weeks apart. Amputee subjects had been wearing their prostheses an average of 9.4 years (range, 6mo. to 55yrs.), and were all judged to be good walkers. No specific attempt was made to match subjects by age.

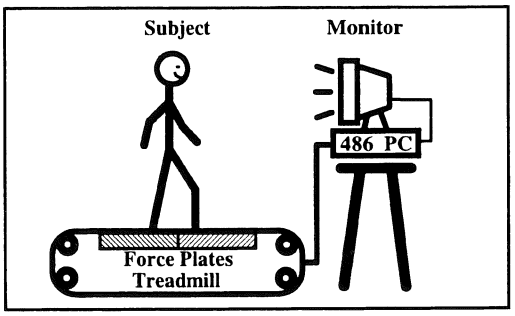

Figure 1. - Setup for Real-Time Gait Symmetry Feedback.

Normal subjects were given four minutes of walking time to acclimate to the treadmill, and data was collected at a walking pace of 2.5 km/hr. Amputee subjects for both Parts II and III were given four minutes to acclimate to the treadmill and asked to choose a comfortable walking speed. The same speed was used for all trials. Amputees walked at an average pace of 2.0 and 2.3 km/hr for Parts II and III, respectively. For Part II, initial data was collected without feedback. Subjects were then given four minutes of practice with each feedback routine, and data was collected. Subjects were instructed to adjust their gait patterns to achieve the most symmetrical gait possible for the particular feedback being displayed. The order of feedback given was randomized. For Part III, after initial treadmill acclimation, the subject's limb was fitted with the Otto Bock 1M1 foot with either the Hard or Soft durometer heel bumper. Subjects were given two minutes of practice walking on the treadmill with each heel bumper, and data was collected. The order of heel bumpers was randomized between subjects. Care was taken not to make any changes to the alignment of the prosthesis between trials. Subjects received no visual feedback, and no instruction was given other than to walk in a "normal and comfortable manner."

Twenty five seconds of data, representing 10 to 15 complete strides, was collected for all trials. Five variables were quantified for both left and right legs; foot position at heel strike (anterior-posterior center of pressure, COP), percent stance time (%ST),

maximum push off force (POF), and single and double support times (SST, and DST). All five variables were evaluated for normals and for amputees walking before feedback. For Part II, COP, %ST, and POF variables were evaluated after each feedback (COP, %ST, and POF, respectively) was given. Single and double support times were evaluated after all three feedback routines. For Part III, COP, %ST, and POF were evaluated for walking with both the Soft and Hard heel bumper conditions. Symmetry Indices (S.I.) were quantified for normals and amputees using the following equations, modified from Herzog, et. al., 1989:

$$S.I._{normal} = \frac{X_d - X_{nd}}{X_d + X_{nd}} \cdot 100\% \qquad S.I._{amputee} = \frac{X_n - X_p}{X_n + X_p} \cdot 100\%$$

where 'X' is the measured value, 'd' and 'nd' represent dominant and non-dominant limbs, and 'n' and 'p' represent the natural and prosthetic limbs, respectively. This equation represents an "asymmetry range" from -100% to +100%, with perfect symmetry being given by S.I. = 0.

RESULTS AND DISCUSSION

Ten to twelve full strides of data were obtained for each subject for each comparison. Two-way analyses of variance were performed to compare normals and amputees before feedback, amputees before and after real-time visual feedback, and amputees walking with the hard and Soft heel bumpers in the Otto Bock 1M1 prosthetic foot. ANOVA results are summarized in Tables 1 - 4.

Table 1. - Symmetry Indices for Normal and Amputee Subjects.
(n = 6 subjects * 10 strides = 60)

Variable	NORMALS	AMPUTEES	P
COP	-0.18%	-1.54%	**0.014**
%ST	+1.84%	+6.98%	**0.000**
POF	-1.36%	+2.56%	**0.000**
SST	+2.47%	+10.57%	**0.000**
DST	-10.50%	-11.78%	0.715

Table 2. - Symmetry Index Values Before And After Feedback.
(n = 6 subjects * 11 strides = 66)

Variable	BEFORE	AFTER	P
COP	-1.58%	-0.56%	**0.002**
%ST	+7.03%	+5.18%	**0.007**
POF	+2.47%	+1.38%	**0.033**

Table 3. - S.I.'s For Single And Double Support Times.
* - Significantly different to "Before Feedback" condition
(n = 6 subjects * 12 strides = 72)

Support Variable	Before Feedback	After COP	After %ST	After POF
SST	+10.54%	**+14.56%***	**+7.47%***	+8.43%
DST	-12.97%	-18.06%	-9.36%	**-5.31%***

Table 4. - Symmetry Index Values for Different Heel Bumpers.
(n = 5 subjects * 12 strides = 60)

Variable	HARD	SOFT	P
COP	-0.49%	-0.79%	**0.038**
%ST	+8.54%	+7.18%	**0.006**
POF	+2.32%	+2.88%	0.117

Data from normal subjects showed significant (non-zero, $p < 0.01$) asymmetries for all five variables quantified except foot position at heel strike ($S.I._{COP}$ = -0.18%; p = 0.336). Results of Table 1 verify that BK amputee subjects showed significantly greater asymmetries in their gate patterns than did normals. Significant decreases in the degree of asymmetry with real-time visual feedback were demonstrated in Table 2 for all three feedback variables (p = .002, .007, and .033, respectively).

Single and double support time symmetry data indicate that the amputees spent a greatly reduced time in single support on their prosthetic limbs. Changes in SST and DST values as a result of visual feedback shown in Table 3 suggest that decreases in asymmetry for those symmetry variables being displayed are not necessarily reflected in improved symmetry for other parameters of gait. Double support during gait is on the order of .1 to .2 sec., thus with a low (100Hz) sampling frequency, small errors (.01 sec.) may result in an error in calculating S.I. as great as +/- 10%. Values for DST symmetry data can therefore not be considered reliable. It is critical to achieving the most beneficial rehabilitation outcome to identify those variables for which achieving a more symmetrical gait are most important, and those which have the greatest consequence for long term benefit.

Results of Table 4 indicate that there were significant differences in the symmetry of gait patterns of BK amputees between using the Hard and Soft heel bumpers for both percent stance time (%ST) and foot placement (COP). Although push off force asymmetries were somewhat greater for the Soft heel bumper ($S.I._{Hard}$ = + 2.32%, and $S.I._{Soft}$ = +2.88%), this difference was not significant (p = .117). Changing the durometer of the heel bumper was primarily expected to effect plantar-flexion at heel strike, and so this result was not surprising.

CONCLUSIONS

Significant asymmetries in BK amputee gait patterns were found which were consistent with previous findings (Skinner and Effeney, 1985). Normal and amputee subjects both showed significant asymmetries in the gait parameters quantified, and amputee asymmetries were significantly greater than normals. Real - time visual feedback of gait symmetry information was shown to be effective in reducing the degree of asymmetry for the variable displayed. Changes in other gait symmetry variables did not necessarily follow those of the feedback variable displayed, indicating that amputees may alter their gait patterns to decrease one form of asymmetry by increasing other asymmetries. The significant differences between walking with two different durometers of heel bumper in the Otto Bock 1M1 multi-axis foot demonstrate that the CCF treadmill device is an effective tool for determining the effects on gait symmetry patterns of small changes in prosthetic componentry.

REFERENCES

Herzog, W. et. al., (1989), Medicine and Science in Sports and Exercise, **21** (1): 110 - 114.

Skinner, H.B., and Effeney, D.J., (1985), American Journal of Physical Medicine, **64** (2): 82 - 89.

Winter, D.A., and Sienko, S.E., (1988), Journal of Biomechanics, **21** (5): 361 - 367.

ACKNOWLEDGMENT

The authors would like to thank Otto Bock, Inc. for their cooperation in providing the components used in this study.

POST-ACTIVATION EFFECTS AND FACILITATION OF BALLISTIC MUSCLE ACTIONS

R.U. Newton[1], K. Colleran[2], and W.J. Kraemer[2]

[1]Center for Human Movement Science, Southern Cross University, Lismore, NSW 2480, Australia
[2]Center for Sports Medicine, The Pennsylvania State University, University Park, PA 16802, USA

INTRODUCTION

This study examined the post-activation effect of various modes of muscle action on subsequent performance in a ballistic upper body pushing movement. Such a study was designed to address the belief by many strength and conditioning specialists, that the post-activation effect can be used to enhance athletic training and performance. If a facilitation effect could be demonstrated for powerful, ballistic muscle action then this may have application in rehabilitation and training for athletic and work performance. However, no significant effect on any kinematic or kinetic variable of the powerful push movement using a 30% of maximum load was found . This may have been due to the observation by previous research, that the post-activation effect is greatest during high force rather than high power, high velocity muscle actions.

REVIEW AND THEORY

The post-activation effect was first detected by Hunt et al. (1951) in which they found that repetitive stimulation of the fusimotor supply of a muscle spindle is followed by a period during which the spindle's response to a subsequent single fusimotor transmission is enhanced. A brief stretch abolished this post-activation facilitation. Brown et al. (1969) found that responses of muscle spindles to stretch greatly increased if the stretch was preceded by a period of fusimotor stimulation. It was proposed that stable cross-bridges were formed between the actin and myosin filaments within sarcomeres of the intrafusal fibers. The hypothesis was that the intrafusal fibers became 'stuck' at the length at which stimulation had been applied (Brown et al., 1969). The after-effects of stretch and dynamic fusimotor stimulation appear to be due to the existence of stable cross-bridges (Morgan et al., 1984).

This alteration in the intrafusal fibers led Eldred et al., (1976) to suggest that the nuclear bag regions may not return to their initial set length due to the increase in tension. This property of plasticity of intrafusal muscle fibers causes the fibers to be more resistant to subsequent displacement (Brown et al., 1970; Hagbarth et al., 1985) and allows the transference of stretch to be more direct (Hutton, 1984). Therefore, post-activation stretch sensitivity is enhanced for most units (Brown et al., 1969; Durkovic, 1976; Suzuki et al., 1976).

Golgi tendon organs have also been linked to the mechanism of post-activation facilitation. Isometric contractions of greater than 25% maximum voluntary contraction (MVC) have been shown to cause a brief desensitization of the Golgi tendon organ receptors in response to tension (Hutton et al., 1986). This, when coupled to the autogenic inhibitory reflex role of the Golgi tendon organ (Granit et al.,1959) leads to disinhibition of the muscle. A conditioning contraction thereby allows for greater production of muscle force despite the facilitory adaptation being somewhat shorter (3 to 20 sec) for the Golgi tendon organ (Hutton et al., 1986).

Additional research has shown that the pre-contraction of antagonist muscle groups has a facilitatory effect on the subsequent contraction of the agonist group. It has been proposed that a tension-dependent, neural mechanism limits the excitation of agonist motorneurons during maximum voluntary contractions against high resistance (Perrine et al., 1978). The pre-contraction of the antagonists in some way counters the inhibitory influence and allows greater activation of the agonists in the subsequent contraction. Increases in low velocity isokinetic strength have been hypothesized to be the result of a neural adaptation that overcomes or modifies the inhibitory influence (Caiozzo et al., 1981).

The post-activation facilitation effect has yet to be examined in powerful ballistic movements. This is despite the fact that many practitioners in training and rehabilitation believe such an effect exists and is beneficial. If this facilitation effect can be demonstrated, improvements in the areas of muscular strength training, rehabilitation, and competitive performance should be forthcoming. This study is therefore designed to investigate the facilitory effects of intense eccentric, concentric, and isometric muscle actions, as well as the effects of pre-contraction of antagonists, on subsequent muscle action as measured by kinematic and kinetic variables during a powerful, ballistic upper body push movement.

PROCEDURES

Ten male subjects with at least 6 months bench press experience participated in the study. The mean (±SD) age, weight, and height of the subjects was 22 ± 2 yrs, 82 ± 10 kg, and 180 ± 94 cm respectively. All subjects read and signed an informed consent document prior to participation.

The test movement involved the performance of an upper body push using elbow extension and shoulder transverse flexion similar to that of the bench press movement, however, the mass was released from the hands (similar to a throw). A loaded barbell with a mass of 30% of the subjects one repetition maximum (1RM) bench press was used and the subject was instructed to project the bar vertically upwards for maximum height. Six trials were completed each involving a different conditioning muscle action. (1) Control (i.e.) no conditioning muscle action; (2) two repetitions at 90% of 1RM; (3) two repetitions at 70% of 1RM; (4) a 4 second maximal isometric contraction in the bench press position; (5) an eccentric action of lowering the bar to the chest with a load of 120% of 1RM; and (6) pulling the bar downwards against resistance (i.e. antagonist muscle activation).

All conditioning movements as well as the test movement were performed using an instrumented "Smith" machine linked to a computer (Wilson et al., 1993). The device measured bar displacement with time and the computer calculated velocity and acceleration through differentiation of the displacement-time data. Force-time data was also calculated based on acceleration data and the mass of the bar. The following

variables were then calculated to describe the kinematics and kinetics of the balllistic push movement: (1) time of the concentric muscle action; (2) total bar displacement; (3) peak velocity; (4) peak acceleration; (5) time to peak acceleration; (6) total work done; (7) average power output; (8) peak instantaneous power output; (9) average force output; (10) peak force output; (11) maximum rate of force development over 50 ms.

The results were examined statistically using analysis of variance with repeated measures followed up by Scheffe post hoc testing in the event of a significant interaction. An alpha level of 0.05 was the criterion for significance.

RESULTS

Analysis of variance revealed no interaction between type of conditioning muscle action and any of the measured variables. Subsequently the data was pooled and summary statistics are provided in the following table.

	Mean	S.D.
time for the concentric muscle action (s)	0.623	0.043
total bar displacement (m)	0.739	0.097
Peak bar velocity ($m.s^{-1}$)	1.519	0.152
Peak bar acceleration ($m.s^{-2}$)	4.715	0.715
Time to peak acceleration (s)	0.305	0.044
Total work done (N.m)	194.1	39.4
Average power (W)	315.5	80.1
Peak instantaneous power (W)	478.8	129.7
Average force (N)	329.5	63.3
Peak instantaneous force (N)	391.3	82.5
Maximum rate of force development over 50 ms ($N.s^{-1}$)	1482.9	456.1

DISCUSSION

The finding that there was no post-activation effect on powerful muscle action is surprising given the belief held by many practitioners in strength, conditioning and rehabilitation. However, if we are to examine the prior research and theoretical mechanisms proposed for the post-activation facilitation, the results may be more reconcilable.

The first mechanism, that of an increased stiffness of the intrafusal fibers (Brown et al., 1970) results in an increased post-activation stretch sensitivity. This study involved purely concentric muscle actions with relaxation of the agonists between the conditioning action and the test movement. Therefore, the contribution of enhanced stretch sensitivity may have been lost. Future research should address the effect of post-activation facilitation during stretch shortening cycle movement for which the contribution of the stretch reflex has already been well established. A further advantage to testing stretch shorten cycle movement is that it is much more common in human movement especially explosive muscular actions.

The second mechanism involved the Golgi tendon organ in which a disinhibition of the force limiting Golgi tendon organ reflex has been observed (Hutton et al. 1986) following agonist activation above 25% of maximum voluntary contraction. The Golgi tendon organ is also disinhibited by a prior activation of the antagonist muscles (Perrine et al., 1978). The activation of the agonists during the conditioning action was certainly of sufficient intensity to produce disinhibition (i.e. 70%, 90%, 120% of 1RM and maximum isometric). Similarly, the antagonist activation should have been effective. It is postulated that the lack of an experimental effect was due to the test mode used.

A load of 30% of 1RM was chosen for the testing protocol because this is the optimal load for the production of maximum mechanical power (Kaneko, et al., 1983), however, such a light load does not allow the muscle to produce very high forces. Thus, the disinhibition effect may not have had an influence because the force through the tendon was not high and so the Golgi tendon organ may not have inhibited the muscle activation even without a previous conditioning muscle action. Research by Perrine et al., (1978) supports this concept, finding that the effect of the disinhibition of the Golgi tendon organ reflex is substantial at slow movement velocities and high force but is not apparent during faster movements.

Based on the findings of this study it is concluded that post-activation facilitation is not effective for enhancing performance in ballistic muscle actions involving a load of 30% of 1RM.

Future research should address the effect that post-activation facilitation may have on other functional movements. In particular, the role of post-activation facilitation in high force, stretch shortening cycle movements such as those involved in resistance training and many manual work tasks needs to be investigated.

REFERENCES

Brown, M.C. et al. J. Physiol., 205, 677-694, 1969.
Caiozzo, V.J. et al. J. Appl. Physiol., 51(3), 750-754, 1981.
Durkovic, R.G. Exp. Neurology, 50, 99-112, 1976.
Eldred, E. et al. Progress in brain research, understanding the stretch reflex, Homma (Ed.), 1976.
Granit, R. et al. Acta Physiol. Scand., 46, 185-193, 1959.
Hagbarth, K.E. et al. J. Physiol., 368, 323-342, 1985.
Hunt, C.C. et al. J. Physiol., 113, 283-297, 1951.
Hutton, R.S. Neural and mechanical control of movement, Kumamoto (Ed.), 1984.
Hutton, R.S. Med. Sci. Sports Ex., 18, 69-74, 1986.
Kaneko, M. et al. Scand. J. Sports Sci., 5(2), 50-55, 1983.
Morgan, D.L. et al. J. Physiol., 356, 465-477, 1984.
Perrine, J.J. et al. Med. Sci. Sports Ex., 10(3), 159-166, 1978.
Suzuki, S. et al. Med. Sci. Sports Ex., 8, 258-264, 1976.
Wilson, G.J. et al. Med. Sci. Sports Ex., 25(11), 1279-1286, 1993.

ACKNOWLEDGMENTS

This study was supported in part by an Internal Research Grant from Southern Cross University, Lismore, Australia.

AN ITERATIVE SEGMENT LENGTH NORMALIZATION ROUTINE FOR USE WITH LINKED SEGMENT MODELS

G. A. Smith

Biomechanics Laboratory, Oregon State University, Corvallis, OR 97331

INTRODUCTION

Linked segment models assume that segment lengths are constant throughout movement. However, analysis methods involving digitizing of recorded images introduce error onto position-time data which results in varying segment length. An iterative segment length normalization routine was created which controls segment length along with smoothing of position data.

REVIEW AND THEORY

The collection of position-time data for linked segments by means of film or video recording and subsequent digitizing has been used for two and three dimensional analysis of a variety of human activities. This measurement process introduces some amount of random as well as systematic error into the positions determined for each end point of the segments being analyzed. Typically, the error introduced through the measurement process is dealt with through digital filtering algorithms which pass low frequency components of the signal while attenuating high frequency components containing most of the random measurement errors (Wood, 1982). Filtering algorithms based on spline functions, fourier analysis and the Butterworth filter have all been shown to be effective at removing much of the measurement error involved in digitizing film and video (Hatze, 1981; Wood, 1982). However, these algorithms deal only with the digitized positions as independent points without regard to the segments linking points in a model.

In an ideal linked segment model of a body, segments can be thought of as rigid bodies of fixed length connected to adjacent segments by simple hinge joints. Defining a model solely in terms of segment end point position-time data (as is conventionally done) ignores additional information associated with segment length. This additional information can be used in conjunction with filtering routines to smooth position data while constraining segment length to a nearly constant value (Ariel et al., 1993). The purpose of this study was to develop an algorithm to accomplish such segment length control in conjunction with a Butterworth filter for control of high frequency noise.

PROCEDURES

A three-segment compound pendulum was constructed for purposes of exploring segment length constraints on data smoothing. A planar swing pattern of the pendulum was recorded on video and subsequently digitized (128 frames at 60 Hz frame rate). The raw data segment lengths were found to vary by about 1 to 2% of the actual segment lengths. From a smoothed angle-time history of the pendulum, an ideal system position-time data set was created describing precisely the end points of each segment with constant segment lengths. This ideal data set was used as the reference motion for comparison of subsequent analysis methodologies. In simulation of the digitizing process, random noise was added to the ideal data set (with magnitude of approximately $\pm$ 1% of segment length). This noisy data set was subsequently smoothed and length normalized and compared to the ideal position-time data and segment lengths to assess effectiveness of the methodology.

Length normalization was accomplished through an iterative process which converged on a position-time solution for segment end points while controlling the segment's length. The normalization process involved initial determination of a mean length for each segment. Raw position data were smoothed with a Butterworth filter (6 Hz cutoff) and segment angle-time data were determined. Then, using each segment's angle, mean length and midpoint (from original position-time data), end point coordinates were determined. End points which were common between two segments had two coordinate predictions made; mean of the two predictions was used, thus slightly altering each segment's length. Succeeding iterations began with the previously calculated end points determining the segmental midpoints. From mean segment length and segment angle, new end points were redetermined. With each iteration, segment end points converged toward positions such that each segment's length was equal to the mean length determined from the original data set.

After each iteration, the RMS error of each point was determined (compared to the ideal data set positions) and the variability of each segment length was determined across the complete movement period.

RESULTS

The ideal data set used as the reference in this experiment had constant segment lengths across time. The noisy data set created from the ideal data had considerable variability of segment length: SD of approximately 1% of segment length. Simple digital filtering reduced this length variability to 0.2 to 0.3% of segment length. Further reduction of segment length variability was observed with each iteration of the normalization routine. After 10 iterations, the segment lengths had converged to nearly constant values equal to the mean segment length (SD of 0.004% of segment length). This convergence is illustrated in Figure 1.

Accuracy of the segment end point positions was also determined. The noisy data had positional errors of about 1% of segment length. Filtering reduced these positional errors to about 0.3 to 0.5% of segment length. The length normalization routine, while

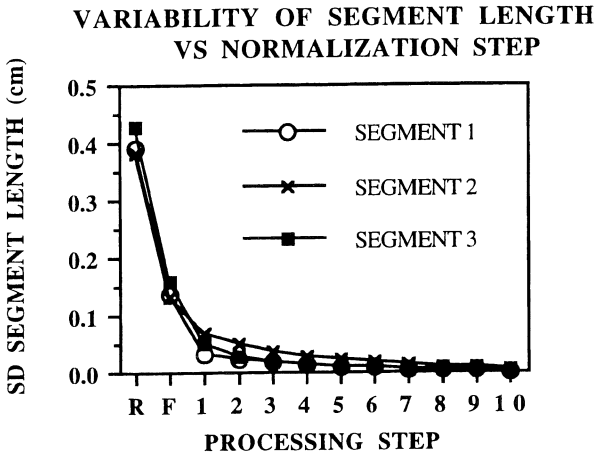

Figure 1. Standard Deviation of segment length for raw data (R), filtered data (F) and iterations 1 to 10.

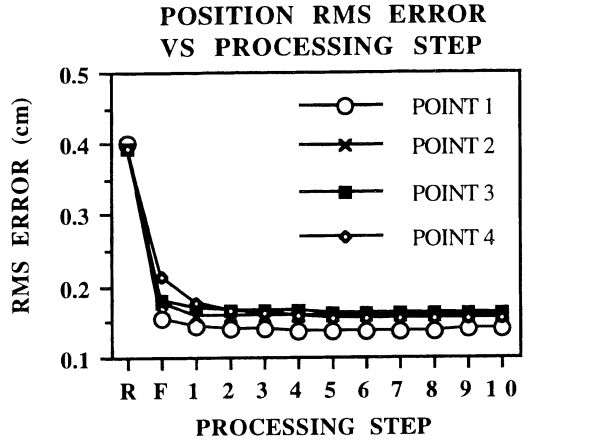

Figure 2. Root-mean-square error of point positions for raw data (R), filtered data (F) and interations 1 to 10.

slightly adjusting the end point positions to achieve nearly constant segment lengths, resulted in only marginal improvements in positional accuracy (Figure 2).

The normalization routine made small corrections in position from those determined by the Butterworth filter. As an initial assessment of the effect of these small positional changes on other kinematic variables, acceleration-time curves were generated for each point and direction for the ideal and the length normalized data. Only relatively small differences in accelerations were observed; a typical example is illustrated in Figure 3 for a single point.

DISCUSSION

Digitizing recorded motion introduces random error onto positional estimations. While filtering removes much

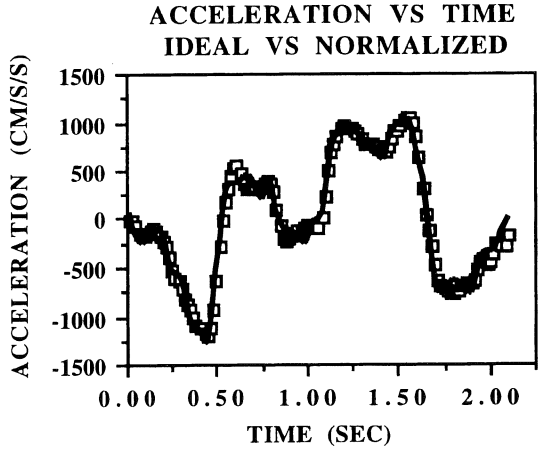

Figure 3. Horizonal acceleration of point 4 comparing the ideal acceleration (solid line) with the acceleration obtained from length normalized data (open squares).

of this error, segment lengths determined from position data are found to vary appreciably across movement time. Normalization of segment length uses additional information to "fine tune" position-time data from filtering to minimize segment length variation. Some previous normalization algorithms have been implemented using spline functions (Jennings & Wood, 1987) and weighted averages (Ariel et al.,1993). The approach suggested here is considerably simpler than the spline function normalization and offers better control of smoothing than the weighted average approach. In addition, the iterative technique allows the user to determine what is acceptable variability of segment length for a given situation.

The simulation used for this experiment was two-dimensional and involved perfectly constant segment lengths. In actual human motion, the situation is somewhat more complex. Segment lengths are known to be slightly variable, however the variability due to random and systematic errors in image digitizing are probably of considerably larger magnitude (and considerably larger than the noise introduced in this simulation as well). In addition, out-of-plane motion occurs which changes the projected lengths of segments in two-dimensional analyses. Further extensions of the segment length normalization routine developed here should be generalized to the three-dimensional situation and tested with kinematic data from human motion.

REFERENCES

Ariel, G. B. et al. *Proceedings of 14th Congress of the International Society of Biomechanics*, Paris, (pp. 112-113), 1993.

Hatze, H. *Journal of Biomechanics*, 14, 13-18, 1981.

Jennings, L. S. et al. *Proceedings of the 6th Meeting of the European Society of Biomechanics*, Bristol, 1987.

Wood, G. A. *Exercise and Sport Science Reviews*, (pp. 308-362), 1982.

THREE-DIMENSIONAL NORMATIVE DATABASES OF MUSCLE ORIGINS AND INSERTIONS FOR THE LOWER EXTREMITIES

T.M. Kepple, H. J. Sommer III*, K. Lohmann Siegel and S.J. Stanhope

Rehabilitation Medicine Department, Warren G. Magnuson Clinical Center,
Bldg. 10 Room 6S 235, National Institutes of Health, Bethesda, MD 20892
and
*Department of Mechanical Engineering,
336C Reber Bldg., The Pennsylvania State University, University Park, PA 16802

INTRODUCTION

In-vivo lines of action for individual muscles in the lower extremities, and concomitantly muscle lengths, velocities and moment arms, can be measured by filming the motion of external markers attached to palpable boney landmarks on subjects during locomotion. This requires a database of three-dimensional (3D) muscle origins and insertions relative to the palpable boney landmarks in order to extrapolate muscle motion. Unfortunately, the number of skeletal specimens used to accumulate existing databases of 3D origin and insertion locations for the lower extremities are relatively limited.

To this end, 3D locations of muscle attachments on the pelvis, femur, tibia/fibula, and foot were accurately digitized for 52 dried skeletal specimens from the Terry Collection of the National Museum of Natural History, Smithsonian Institution, Washington, DC. Thirteen specimens each were selected within four gender/race categories with representative stature. Normative 3D databases developed from these landmark data statistically extend currently available 3D databases by an order of magnitude, include expected gender/racial variation, and provide better effective lines-of-action for muscles which wrap over boney structures.

REVIEW

Knowledge of muscle kinematics such as lines-of-action, velocities and moment arms can be useful in both the clinical analysis of human motion and in computer aided assessment of surgical techniques (Delp, et.al. 1990). Although muscle kinematics can be extrapolated from surface landmark measurements using a database of muscle origins and insertions, existing 3D databases (White, et.al. 1989) have several limitations. First, the numbers of specimens used to create these databases were limited (pelvis N=9, femur N=9, tibia/fibula N=9, foot N=2). Secondly, the databases do not account for gender or racial variation in skeletal geometry. Lastly, previous databases do not completely represent muscle lines-of-action throughout a range of joint motion as muscles may wrap over boney structures rather than simply connect their origin directly to their insertion along a straight line (Kepple, et.al. 1994).

PROCEDURES

Three-dimensional muscle origin and insertion landmark locations as well as selected muscle connector landmarks were digitized from 52 dried skeletons in the Terry Collection of the National Museum of Natural History, Smithsonian Institution, Washington DC. Specimens were selected for equal representation within four gender/race categories (13 white males, 13 white females, 13 black males, and 13 black females) with stature spanning the 5th and 95th percentiles for each gender.

Data were collected on seven anatomical segments per skeleton (pelvis, two femurs, two tibias/fibulas, and two feet) with varying number of landmarks per segment as shown in Table 1. Distributed muscle origins and insertions were approximated by centroid locations. Three landmark locations that could be palpated externally on living subjects were also digitized for each segment.

Muscle lines-of-action connected origin and insertion centroid locations. When a single line-of-action was considered to be an insufficient representation because of widely distributed origins or insertions, the muscle was subdivided into two or more muscle units. When a line-of-action would be expected to wrap over a boney structure, connector points were selected as effective intermediate origins or insertions. A total of 43 lower extremity muscles and 60 muscle units per side were included in the database.

The locations of the muscle landmarks, the connector landmarks and the palpable landmarks were measured using a Bird three-dimensional electromagnetic digitizer (Ascension Technologies, Burlington, VT) with root-mean-square (RMS) calibration precision of approximately 2 mm. Affine scaling along three arbitrary axes (Sommer, et. at. 1982) was used to accumulate normative models and assess expected RMS landmark variation for each anatomical segment. Data from left and right segments were pooled. Procrustes multivariate statistical methods (Goodall, 1991) were then used to compare and statistically group the normative models.

As an additional test, the grouped normative models were regenerated excluding their second tallest and second shortest specimens. These independent specimens were then compared to the new modified models as an independent assessment of the models' predictive ability.

RESULTS

Procrustes comparisons were used to group the normative models nominally with 0.01 significance as shown in Table 1. The foot was characterized by clear differences between the black and white normative models but with insignificant gender variation. Expected RMS variation in foot landmarks is nominally 3.7 mm. Comparison of normative models for pelves indicated clear gender differences with additional variation between black and white female pelves. Racial differences in the female pelvis are corroborated by traditional anthropometry (Krogman and Iscan, 1986). Expected RMS variation in pelvis landmarks ranged from 6.1 to 7.8 mm. There was insufficient evidence to use more than one respective model for the tibia/fibula and femur segments. Expected RMS variation in tibia/fibula and femur landmarks was 5.8 mm and 6.6 mm respectively.

The overall RMS variation associated with each normative model resulted from comparing each individual landmark, on each individual specimen, to its homologue in the normative model. Additionally, individual variance-covariance matrices were accumulated for each landmark to assess directionality and relative variation between landmarks. The best results were obtained for the smallest segment (foot), with RMS variations tending to increase with segment size.

To test model performance, the second tallest and second shortest specimens were excluded from new modified normative models as independent specimens. Using both right and left segments for these independent specimens allowed 22 independent comparisons to respective normative models (4 for the white foot, 4 for the black foot, 4 for the tibia/fibula, 4 for the femur, 2 for the male pelvis, 2 for the white female pelvis, and 2 for the black female pelvis). Procrustes comparisons of these independent specimens to the modified models produced almost identical RMS variations as those obtained in generating the original normative models, with most comparisons differing by less than 1 mm from model RMS variations. These 22 comparisons indicate that independent specimens can be accurately mapped into the normative models with accuracy levels similar to that found in accumulating these databases.

DISCUSSION

With over 12,000 muscle origin and insertion locations digitized from 52 dried skeletons, the number of specimens used in this work represents an improvement over previous databases by an order of magnitude. These databases also account for gender and racial differences, and allow for more accurate representation of muscle lines-of-action by extensive use of connector points to account for muscle wrapping. These new normative databases should greatly enhance the ability to provide accurate estimates of muscle kinematics from surface landmark measurements.

ACKNOWLEDGMENT

The authors wish to thank Dr. David Hunt of the National Museum of Natural History, Smithsonian Institution, for his collaboration in this work.

REFERENCES

Delp, S., Loan, P., Hoy, M., Zajac, F., Topp, E., and Rosen, J. (1990) An Interactive Graphics-based Model of the Lower Extremity to Study Orthopedic Surgical Procedures. *IEEE Trans. Biomed. Engng 37*, 757-765.

Goodall, C. (1991) Procrustes Methods in the Statistical Analysis of Shape. *J. R. Statist. Soc. 53*, 285-339.

Kepple, T., Arnold, A., Stanhope, S., and Lohmann Siegel, K. (1994) Assessment of a Method to Estimate Muscle Attachments from Surface Landmarks: A 3D Computer Graphics Approach. *J. Biomechanics 27*, 365-371.

Krogman, W., and Iscan, M. (1986) *The Human Skeleton in Forensic Medicine*, C.C. Thomas, Springfield, IL.

Sommer, H., Miller, N., and Pijanowski, G. (1982) Three-dimensional Osteometric Scaling and Normative Modeling of Skeletal Segments. *J. Biomechanics 15*, 171-180.

White, S., Yack, J. and Winter, D. (1989). A Three-dimensional Musculoskeletal Model for Gait Analysis. Anatomical Variable Estimates. *J. Biomechanics 22*, 885-893.

SEGMENT	LANDMARKS	MODEL	SPECIMENS	BONES	RMS VARIATION (mm)
Foot	13	All Whites	26	52	3.6
Foot	13	All Blacks	26	52	3.7
Tibia/Fibula	38	All	52	104	5.8
Femur	41	All	52	104	6.6
Pelvis	54	All Males	25	25	7.8
Pelvis	54	White Females	13	13	6.7
Pelvis	54	Black Females	13	13	6.1

Table 1. Grouping of normative models based on Procrustes comparisons at 0.01 significance.

A HUMAN LOWER EXTREMITY MODEL FORMULATED USING KANE'S METHOD

R.D. Komistek [*], J.B. Stiehl [**], R.D. Paxson [*], R.W. Soutas-Little [***]

[*]Wright Medical Technology Inc., Applied Research Group, 5677 Airline Road, Arlington, TN 38002
[**]Columbia Hospital, 2015 East Newport Ave, Suite 703, Milwaukee, WI 53211
[***]Michigan State University, 4700 South Hagadorn, Suite 180, East Lansing, MI 48823

INTRODUCTION

A fully dynamic, three dimensional model of the lower extremity was derived using Kane's method of dynamics. The model includes 24 pertinent motions with respect to each leg and six pertinent motions at the pelvis and predicts hip, knee, and ankle joint interaction joint forces. These forces vary with respect to soft-tissue boundary conditions and motion speed. During gait, the interaction forces at the hip and knee joints were in the range of 1.9 to 2.6 and 1.7 to 2.3 times body weight, respectively. The value derived at the hip joint compared favorably with previously published telemetric studies. Interaction forces obtained from the model were varied under abnormal conditions, such as the removal of the cruciate ligaments. The implication is that normal joint kinematics need to be re-established after total joint replacement to optimize knee function. This model will allow for parametric studies using total knee implants to assess ultimate performance of a prosthetic system.

REVIEW AND THEORY

A mathematical model of the human lower extremity was derived using Kane's method [1] of formulating dynamical systems of equations. The author's proposed model is a fully dynamic, three dimensional representation containing 24 pertinent motions with respect to each leg and six pertinent motions at the pelvis. The objective of this work was to find accurate temporal interaction forcing functions across the hip, knee and ankle joints during various kinematic activities. Attempts have been made in the past to theoretically model the human lower limb [2,3,4], but they have unfortunately predicted values that are extremely high in comparison to experimental telemetric studies [5,6]. Davy, et. al. [5] writes, "Several investigators have approached the redundant force-distribution problem, using techniques that produce unique solutions by optimizing mathematically defined criteria for performance ... Hardt estimated peak contact forces of 5.7 times body weight for one subject. Recently, Rohrle, et. al. reported predicted peak forces of 4.1 to 6.9 times body weight ... Typically, the experimentally measured forces about the hip joint are lower than values that are predicted using analytical models.

The kinematics and the kinetics of the lower extremity were derived such that the pelvis initially coincided with the inertial reference frame. The pelvis, femur, tibia, patella and the foot were each modeled as rigid bodies with respect to the previously described reference frame in the sequence of rotations and then transformed to the inertial reference frame. Cadavers were used to identify muscle origin and insertion positions. Each muscle was then modeled as a distributive load at the rigid body attachment sites with respect to the corresponding interaction joint center. Muscle forces were then derived by decoupling the applied torques across the hip, knee and ankle joints.

The angular velocities, angular accelerations, velocities and accelerations were derived for each rigid body with respect to the inertial reference frame. Partial angular velocities and velocities of each respective body were derived for each generalized speed and dot multiplied with the active and inertial forces to obtain the equations of motion.

Twenty-four equations of motion were derived for each leg using Kane's equation,

$$F_r + F_r^* = 0, \quad r = 1, ..., n.$$

whereas F_r and F_r^* are the generalized active and generalized inertia forces, respectively. Equations for F_r and F_r^* are given by,

$$F_r^* = \sum_{u=1}^{N} \left[{}^A\underline{v}^S_{Ur} \cdot \underline{F}^{S*} + {}^A\underline{\omega}^S_{Ur} \cdot \underline{T}^{S*} \right],$$

$$F_r = \sum_{u=1}^{N} \left[{}^A\underline{v}^S_{Ur} \cdot \underline{F}^{S} + {}^A\underline{\omega}^S_{Ur} \cdot \underline{T}^{S} \right] [1].$$

EXPERIMENTAL METHODS

Seventy-five patients with Total Knee Arthroplasty and five people with normal knees were analyzed under kinematic conditions using fluoroscopy. A fluoroscopy video of each subject was filmed as they performed a prescribed kinematic activity to maximum flexion. The video was then analyzed using a still photograph from the video taken at 5 degree increments. Successive photographs were transposed in sequence as shown in Figure 1 to obtain femoral contact positions with respect to the tibia and patella contact position with respect to the femur patella relative to the tibia. The relative angle shown in Figure 1 ranges from 0 degrees to the maximum flexion, N degrees.

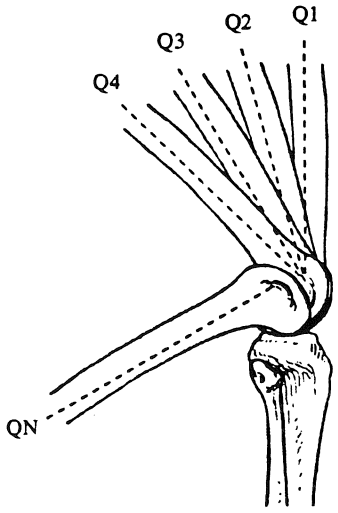

Figure 1. Flexion angle positions for analysis.

Two dimensional plots of these relative positions with respect to flexion angle were derived, as well as the patella and patella ligament relative rotations with respect to flexion angle.

Each two dimensional plot was then curve fitted to a $R^2 > 0.99$ so that an equation could be derived for each position and angle as a function of flexion angle. Each equation was then defined as a specified motion in the mathematical model that evaluates each respective relative motion with respect to flexion angle for the entire cycle. The obtained relative positions are used as boundary conditions at the knee for a mathematical model of the human lower extremity.

RESULTS AND DISCUSSION

Initial validation of the model was done under static and quasi-static conditions. Maximum hip joint interaction force during gait was compared to values obtained using telemetry. The telemetric studies [5,6] obtained maximum interaction force magnitudes for a total hip arthroplasty (THA) in the range of 2.0 - 3.0 x body weight (BW). The maximum resultant interaction force between the pelvis and the femur using the author's proposed model was in the range of 1.9 to 2.6 x BW for a normal hip and 1.7 to 2.3 x BW for a normal knee. A simulation was attempted with an implanted hip which predicted values slightly higher than those obtained for a normal hip. This simulation was derived by altering the femur/pelvis contact position and the gait data of the individual. Interaction forces at the hip, knee, patella and ankle for a slow gait cycle are shown in Figure 2. Figure 3. shows a caption of the computer program that is used to visually display the motion of the theoretical leg. A color bar displays lower extremity stress levels that change as the model replicates motion. As the leg moves, interaction forces are shown on the graph displayed on the lower portion of the screen. A bar sweeps through the graph depicting the same position the theoretical leg is at during the motion cycle. Other interaction and soft tissue forces have also been derived under varying conditions, but will not be published at this time. It is apparent that the interaction forces derived by the author's proposed model are less in magnitude than those previously reported. It is proposed by the authors that the use of optimization techniques may have contributed to the larger interaction force magnitudes in the hip that were previously reported in the range of 4.5 - 6.0 x BW during gait. The authors believe that the results derived using the proposed model are accurate and are partially attributed to the use of Kane's method of formulating dynamical systems of equations.

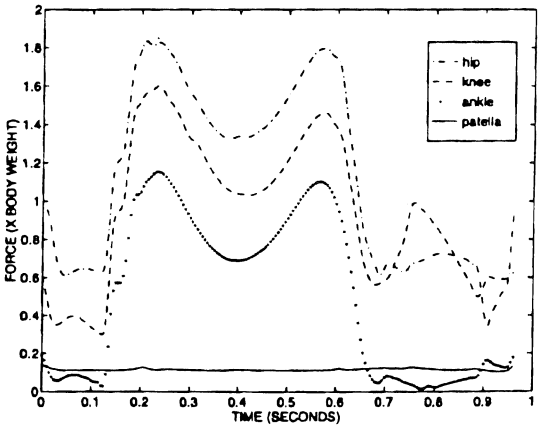

Figure 2. Interaction joint forces of the leg.

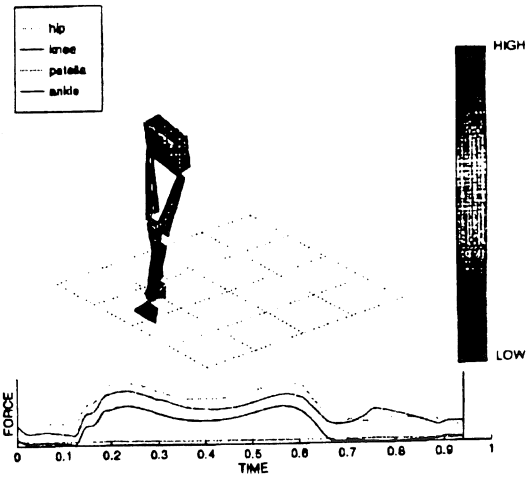

Figure 3. Visual display of the leg model.

The proposed model seems to accurately predict interaction forces in the normal human hip joint. This model should prove beneficial for determining normal loading forces in lower extremity joints and will be of great interest for investigating abnormal circumstances such as limb deformities and malalignment. The authors conclude that this model will be a valuable asset in understanding other interaction and soft-tissue forces in the lower extremity and will play a significant role in design evaluation of orthopaedic impants.

REFERENCES

[1] Kane, T.R. and D.A. Levinson. Dynamics: Theory and Applications. New York: McGraw-Hill Publishing Company. 1985.

[2] Seireg, A and R.J. Arvikar. The Prediction of Muscular Load Sharing and Joint Forces in the Lower Extremities During Walking. Journal of Biomechanics, 8:89-102. 1973.

[3] Paul, J.P. Approaches to Design: Force actions transmitted by joints in the human body. Proc. R. Soc., London, 192, 163-172. 1976.

[4] Hardt, D.E. Determining Muscle Forces in the Leg during Normal Human walking. Journal of Bio-mechanical Engineering, 100:72-78. 1978.

[5] Davy, D.T. et al. Telemetric Force Measurements across the Hip after Total Arthroplasty. Journal of Bone and Joint Surgery, Vol . 70-A. 1988.

[6] Rydell, N.M. Forces Acting on the Femoral Head-Prosthesis. Acta Orthop. Scandinavica, Supplementum 88. 1966.

ACKNOWLEDGEMENTS

The authors thank Dr. Thomas Kane for his consultation and to Columbia Hospital in Milwaukee Wisconsin for the use of experimental equipment.

THE EFFECT OF QUADRICEPS LOAD ON LIGAMENT LENGTHS IN THE KNEE

Yeou-Fang and Louis F. Draganich
Section of Orthopaedics And Rehabilitation Medicine
Department of Surgery
The University of Chicago
Chicago, Illinois

ABSTRACT
The relationship between quadriceps loading and length changes of the ligaments of the human knee has not been reported. The purpose of this cadaver study was to investigate that relationship for the anterior and posterior cruciate ligaments (ACL and PCL) and for the medial and lateral collateral ligaments (MCL and LCL) using a three-dimensional digitizer. For quadriceps forces ranging from low to physiological levels the relationship between ligament length and quadriceps force was found to be linear for nearly all of the superficial fiber bundles studied in these ligaments.

INTRODUCTION
Few studies have been performed to investigate the length changes of the major ligaments of the knee during extension by the quadriceps (1,2,3,4). In those studies, relatively low quadriceps forces were applied. Since no studies have been performed to investigate the effect of the magnitude of quadriceps load on the length changes of the ligaments, it is unknown whether the length changes generated with low quadriceps forces are representative of those occurring with physiological levels or whether the length changes can be extrapolated. Thus, the purpose of this study was to determine the relationship between the externally applied flexion moment in the knee equilibrated by the quadriceps and the lengths of the anterior and posterior cruciate ligaments and the medial and lateral collateral ligaments.

METHODS
Twelve cadaveric knees from twelve different donors with an average age of 47.6 years at the time of death were obtained fresh at autopsy and tested. The experiments consisted of applying four magnitudes of flexion moments, based on 1/12, 1/6, 1/4, and 1/3 of values reported in the literature for maximum isometric moments, equilibrating the knee with quadriceps forces at a particular flexion angle, and measuring the position of the knee using a three-dimensional digitizer. The loads were applied and measurements taken at 15^{o} increments from 0 to 120^{o} of knee flexion.
After the position data were collected the knee was dissected to remove all soft tissues except for the ACL, PCL, MCL, and LCL which were left intact. Selected superficial bundles of fibers were identified in the ACL, PCL, and MCL. The bundles were located according to the locations of their insertions into the tibia. Six bundles were identified for the ACL, six for the PCL, and three for the MCL. For the ACL and PCL these locations corresponded to the anterior (a), anteromedial (am), anterolateral (al), posterior (p), posteromedial (pm), and posterolateral (pl) aspects of the their attachments to the tibia. For the MCL these locations corresponded to the anterior, central (c), and posterior most aspects of the their attachments to the tibia. Tension was applied to each fiber bundle using forceps in order to identify the corresponding bundle's points of insertion into the tibia and femur for digitization. The centers of the LCL's insertions were also digitized. Thus, the LCL was represented by a single point-to-point attachment. In addition, anatomical reference points on the tibia and femur were identified and digitized in order to construct tibial and femoral coordinate systems. Ultimately, all digitized data were transformed to he femoral coordinate system for analysis.
The length of each bundle of fibers was

approximated as the straight line distance (using the Pythagorean theorem in three imensions) between the tibial and femoral points of insertion. The distance was modelled as a function of the applied external flexion moment using linear regression analysis. The method of least squares was used to determine *best fit*. The linear equation was derived and the correlation coefficient computed. Student's t statistic was used to test the significance, at the $p < 0.05$ level, of the differences of 1) the slope, m, and 2) the constant, b, from zero in the equation: distance = m(load) + b.

RESULTS

Quadriceps forces necessary for equilibrium of the knee ranged from approximately 100 N at full extension with the application of 1/12 of maximum isometric flexion moments reported in the literature to 1400 N at 90° of flexion for the application of 1/3 of maximum isometric flexion moments. Of the 144 equations developed to describe the relationship between distance and flexion moment for all of the fiber bundles studied, only twelve had slopes which were not significantly different from zero. For example, at 30° of flexion of the knee the slopes in the equations representing the distances for the anterior and central fibers of the MCL were not significantly different from zero, while the slopes in the equations used to model the rest of the distances were (Table 1).

DISCUSSION

The loads applied in this study ranged from very low levels to approximately 75% of those attained during stair climbing (5). Thus, for the knee loading paradigm and large range of quadriceps forces used in this study the results demonstrate that the relationship between ligament length and external flexion moment can be modelled with a linear equation for almost all of the fiber bundles studied between full extension and 120° of flexion.

Table 1. Linear regression analysis for 30° of knee flexion.*

Lig.	R^2	(b)**	p(m)***	b	m
MCL-a	0.800	< 0.001	0.106	8.055	0.048
MCL-c	0.800	< 0.001	0.106	8.090	0.090
MCL-p	0.966	< 0.001	0.017	7.940	0.156
LCL-c	0.982	< 0.001	0.009	5.230	-0.432
PCL-pl	0.997	< 0.001	0.002	3.055	-0.516
PCL-p	0.985	< 0.001	0.008	3.120	-0.384
PCL-pm	1.000	< 0.001	0.000	2.370	-0.120
PCL-am	0.997	< 0.001	0.002	2.605	-0.516
PCL-a	0.999	< 0.001	0.001	2.575	-0.672
PCL-al	0.999	< 0.001	0.001	2.565	-0.672
ACL-am	0.991	< 0.001	0.005	3.185	0.468
ACL-a	0.998	< 0.001	0.001	3.055	0.552
ACL-al	0.998	< 0.001	0.001	2.695	0.636
ACL-pl	0.997	< 0.001	0.002	2.175	0.516
ACL-p	0.997	< 0.001	0.002	2.425	0.408
ACL-pm	0.984	< 0.001	0.008	2.525	0.348

* ligament length = m(load) + b, where ligament length was measured in cm and load was a fraction of maximum isometric moments.

** p(b) is the p value for testing the significance of the difference of the constant, b, from zero.

*** p(m) is the p value for testing the significance of the difference of the slope, m, from zero.

REFERENCES

1. Arms SW et al: Am J Sports Med, 12:8-18, 1984
2. Draganich LF et al: J Ortho Res, 8:57-63, 1990
3. Renstrom P et al: Am J Sports Med, 14:83-87, 1986
4. White A et al: Acta Orthop Scan, 43:176-187, 1972
5. Andriacchi J Bone and Joint Surgery, 62A:749-757, 1980

ACKNOWLEDGEMENT

This work was supported by NIH grant AR40605.

COMPARISON OF MECHANICAL ENERGY EXPENDITURE OF DIFFERENT SOURCES OF MECHANICAL ENERGY DURING HUMAN LOCOMOTION: JOINT MOMENTS VS. MUSCLE FORCES

B. I. Prilutsky*, L. N. Petrova and L. M. Raitsin

Biomechanics Laboratory, Central Institute of Physical Culture, Moscow, Russia 105483.
*Current address: Human Performance Laboratory, Faculty of Physical Education, The University of Calgary, Alberta, Canada T2N1N4.

INTRODUCTION

Prilutsky et al. (1992a) and Prilutsky (1993a) showed using a theoretical analysis that two lower extremity models with different sources of mechanical energy - (1) muscles and (2) joint moments could have different mechanical energy expenditure (MEE) during the same movement. Model 1 with muscle sources could spend less mechanical energy than Model 2 with joint moment sources. This economy of MEE provided by two-joint muscles of Model 1 was possible if: (i) signs of the muscle powers produced by a two-joint muscle at both joints were opposite; (ii) antagonistic muscles were not active. In the present study, implementation of these two conditions during human locomotion was checked experimentally. Electrical activity of eight lower extremity muscles of ten subjects was measured during treadmill walking and running. Moments and powers at joints of the lower extremity of two subjects performing walking and running were calculated using kinematics and ground reaction force measurements, and an inverse dynamics approach. It was shown that MEE of models with different sources of mechanical energy appeared to be different during certain periods of the swing phase. However, the magnitude of this difference was probably relatively small.

REVIEW AND THEORY

Different approaches for estimating MEE of humans during movements give different results (Cavagna et al., 1965; Fenn, 1930; Pierrynowski et al., 1980; Prilutsky et al, 1992b; Williams et al., 1983; Winter, 1983; Zatsiorsky et al., 1982), depending on the assumptions about the sources of mechanical energy (term defined by Aleshinsky, 1986) which make movement possible. A detailed analysis of different approaches for determining MEE was made by Aleshinsky (1986). He showed, in particular, that if sources of mechanical energy producing human movement were assumed to be moments and forces at joints, the best estimate of MEE would be the summed mechanical work of net moments at joints. However, humans move because of forces created by muscles, some of which cross several joints. One can expect that mechanical work at a joint may not coincide with the summed mechanical work of muscles crossing this joint, even if antagonistic muscles around this joint are not active. For example, consider a movement during which only two muscle groups are active: the one-joint hip extensor muscles and the rectus femoris muscle. The hip joint is extended as a result of positive work done by the hip extensor muscles, and the two-joint rectus femoris muscle contracts isometrically, i.e., its length does not change. If there are no external constrictions, the knee joint will be extended because of the action of the rectus femoris and the one-joint hip extensor muscles. In this example, work done by the knee joint moment is positive (this work is equal to the product of the moment at the knee joint and the knee angular displacement). However, the work of muscles crossing the knee joint (defined as the product of force and change in the length of the muscles) is zero, because only the rectus femoris is active and the length of this muscle is constant.

To compare the mechanical energy expended by the models with different sources of mechanical energy during the same movement, the difference in MEE between these two models was estimated using theoretical analysis (Prilutsky et al., 1992a; Prilutsky, 1993a). The model of the lower extremity with muscle sources of mechanical energy (Model 1) consisted of 4 rigid segments (foot, shank, thigh, and pelvis) interconnected by frictionless joints, and eight muscles, three of which were two-joint muscles. It was assumed that sources of mechanical energy of this model, muscle forces, were not 'intercompensated' or 'recuperative' (Aleshinsky, 1986), that is, mechanical energy spent by a muscle cannot be reduced by simultaneous absorption of energy by another muscle at the same time, or by the same muscle during time. Model 2 had different sources of mechanical energy: moments at joints. It was assumed that these sources of mechanical energy were likewise not 'intercompensated' or 'recuperative' sources. For convenience of comparison of MEE between the models, Model 2, without muscles, was changed by 'identical transformations'; that is, the mechanical energy sources of Model 2 (joint moments) were substituted for muscle forces of Model 1 in such a way that the total MEE of the sources of Model 2 remained unchanged. Model 2 differed from Model 1 by the absence of two-joint muscles, which had been substituted by pairs of one-joint muscles having the same action at the corresponding joints. It can be shown that the above transformation ensures the same moments at the joints and their powers during the same movement of Models 1 and 2. On the other hand, it is easy to show that the conducted transformation of Model 2 does not change its MEE if antagonistic muscles are not active. The difference in MEE between Model 1 (W_1) and Model 2 (W_2) was estimated theoretically by Prilutsky et al. (1992a) and Prilutsky (1993a). It was shown that the difference in MEE between joint moments and muscles (W_2-W_1>0) was observed if signs of powers produced by a two-joint muscle at both joints were opposite and antagonistic muscles were not active.

The purpose of this experimental study was to check whether or not there are phases in human locomotion where powers at adjacent joints have opposite signs during which there is no activity of antagonistic muscles.

PROCEDURES

Recording and analysis of muscle electrical activity. Ten healthy males took part in the experiments. They walked and ran on a treadmill operated at a speed of 1.82 m/s (6.5 km/h). Electrical activity (EMG) of 8 muscles of the lower extremity (Fig. 1) was recorded using surface bipolar silver electrodes 8 mm in diameter. The recorded signals were amplified and fed into a computer at a sampling frequency of 2083 Hz for 2.8 s. The EMG was rectified and integrated every 40 ms. Discrete integrated EMG (IEMG) values were connected using an interpolation spline. IEMG values for each percent of a single locomotion cycle were calculated from the spline function. IEMG values of each muscle were normalized with respect to the peak IEMG value of the corresponding muscle in a given cycle of locomotion. For each percent of a cycle of locomotion, IEMGs of each muscle were averaged over all cycles and subjects available. A total of more than 20 cycles were

processed for both walking and running.

Registration of movement and inverse dynamics analysis. Two subjects participated in the second series of experiments. They walked and ran at constant speeds on a special wooden rostrum 40 m in length. In the middle of this rostrum, two force platforms were embedded. The force platforms were used for recording three components of the resultant vector of the ground reaction forces and coordinates of its point of application. A bilateral stereophotogrammetric filming was used for registration of kinematics (for details see Prilutsky et al., 1992b; Zatsiorsky et al., 1982). In all cases, reflective markers attached to the main joints of the subjects' body were flashed by stroboscopes operated at 100 Hz. Traces of the markers were exposed onto photoplates of four photogrammetric cameras (UMK-10, Carl Zeiss Jena, Germany). Coordinates of the body markers were digitized with a precision of 1 μm using a stereocomparator 'Stecometer' (Carl Zeiss Jena). Trials of walking and running at speeds of 1.82 m/s (6.5 km/h) and 1.57 m/s (5.6 km/h), respectively, were chosen for further analysis. A 16-link, 3D model of the human musculoskeletal system and the software HUMMOT (Prilutsky, 1993b) were used for computation of moments and powers at joints of the lower extremity in a sagittal plane. Input required for computing were the body marker coordinates, the force platform data, and the subjects' mass and inertia characteristics derived from the regression equations (Zatsiorsky et al., 1985).

RESULTS AND DISCUSSION

Fig. 1 show the mean and standard deviation of normalized IEMGs of lower extremity muscles during a running cycle. Fig. 2 shows the powers at joints of the lower extremity during a running cycle. The results of this study showed that during walking and running, two two-joint muscles -- the rectus femoris and the hamstrings -- appeared to be active without co-activation of antagonistic muscles during the swing phase (Fig. 1). Powers at the knee and hip showed that during the swing of the lower extremity there were phases where signs of these powers were opposite (Fig. 2). These results mean that these powers were produced by the rectus femoris and hamstrings without antagonistic activity. For example, during phase 3 in running, the rectus femoris muscle produced negative power at the knee and positive power at the hip. During phase 4, the hamstrings produced positive power at the hip and negative power at the knee (Fig. 1 and 2). Thus, it appears that during the swing phase in walking and running, MEE of Model 1 having muscle sources of mechanical energy may be less than that of Model 2 having joint moment sources of mechanical energy. The economy of MEE by two-joint muscles may be estimated using formula (5) from (Prilutsky et al., 1992a) and results from this study about activity of the muscles during walking and running. If one assumes that negative and positive powers at the knee and hip joints during the swing phase (see for example, phases 3 and 4 in running, Figs 1 and 2) are produced by the rectus femoris or hamstrings muscles exclusively, the economy of MEE that results from the action of these muscles will be 7.8 J and 12.7 J during walking and running, respectively. These values are less than 3% of MEE of the joint moments of the 16-link, 3D model of a human body estimated for the corresponding types of locomotion by Prilutsky et al. (1992b).

Thus, results of this study suggest that MEE of the models with different sources of mechanical energy, the joint moments and muscle forces, appears to be different during the swing phase of locomotion. However, this difference is probably relatively small.

REFERENCES

Aleshinsky, S.Yu. *J. Biomechanics*, 19, 287-315, 1986.

Cavagna, G.A. et al. *J. Appl. Physiol.*, 18, 1-9, 1965.

Fenn, W.O. Am. *J. Physiol.*, 92, 583-611, 1930.

Pierrynowski, M.R. et al. *Ergonomics*, 23, 147-156, 1980.

Prilutsky, B.I. *Proceedings of the 14th of I.S.B. Congress on Biomechanics*, pp. 1074-1075, Paris, France, 1993a.

Prilutsky, B.I. *Proceedings of the 14th of I.S.B. Congress on Biomechanics*, pp. 1076-1077, Paris, France, 1993b.

Prilutsky, B.I. et al. *Biophysics*, 37, 1101-1105, 1992a (in Russian).

Prilutsky, B.I. et al. *Human Physiology*, 18, 118-127, 1992b (in Russian).

Williams, K.R. et al. *J. Biomechanics*, 26, 115-128, 1983.

Winter, D.A. *J. Biomechanics*, 16, 91-97, 1983.

Zatsiorsky, V.M. et al. *Biomechanical Basis of Endurance*. FiS, Moscow, 1982 (in Russian).

Zatsiorsky et al. In *Biomechanics IX-B*, pp. 233-239, 1985.

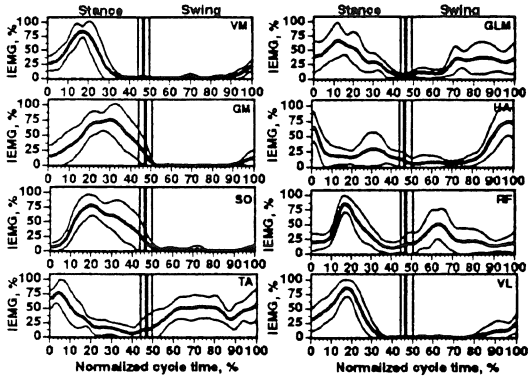

Fig. 1. Normalized IEMG of eight muscles as a function of normalized cycle time during running. Thick lines represent the average values of ten subjects; thin lines represent the standard deviation. The vertical lines separate the stance and swing phases. TA is tibialis anterior muscle; SO is soleus muscle; GM is gastrocnemius medialis muscle; VM and VL are vastus medialis and vastus lateralis muscles, respectively; RF is rectus femoris muscle; HA is hamstrings; GLM is gluteus maximus muscle. The nominal speed of running was 1.82 m/s (6.5 km/h).

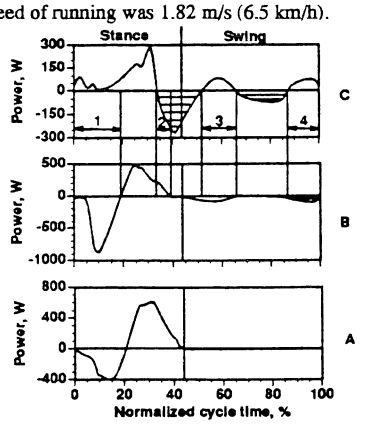

Fig. 2. Powers of net moments at the ankle (A), knee (B), and hip (C) joints in the sagittal plane as a function of normalized cycle time during running. Opened and closed areas represent powers produced by extensor and flexor muscles at the joints, respectively (the muscle groups producing the power were determined using the net moments at the joints). The arrows and numbers indicate phases where the powers at adjacent joints have the opposite signs. The speed of running was 1.57 m/s (5.6 km/h).

AN APPROACH FOR A DETAILED ANALYTICAL MODEL OF THE HUMAN LOWER EXTREMITY DURING A DROP LANDING

S. McGuan, L. Gutkowski and Q. Liu

Mechanical Dynamics, Inc., Ann Arbor MI 48105
NIKE Sport Research Laboratory, Beaverton, OR 97005

INTRODUCTION

A computer model of the human leg and foot was generated to explore the kinematic and kinetic properties of the human leg and foot during a drop landing. Experimental data from an actual drop landing was used to produce the model. A goal is to develop this modeling approach into a tool to investigate the effects of mechanical and geometric characteristics of sports shoes on acute injury such as an eversion-related injury to the lateral ligament complex.

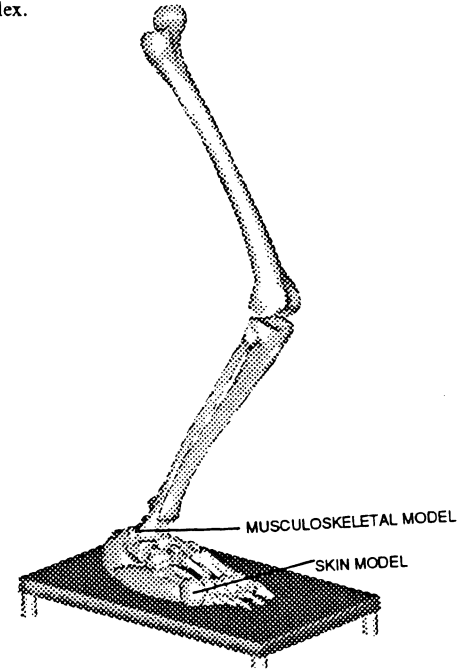

Figure 1. Musculoskeletal Model with Skin Model Overlay.

REVIEW AND THEORY

Rearfoot stability during running and general sports activities is related to foot anatomy and the kinematic changes that result from footwear, Nigg (1986). To study the effects of changes in footwear design variables, researchers have predominantly relied on laboratory analysis. Simple analytical models, Stacoff et al. (1988), Nigg (1986), Miller, et al. (1973), Jonsson (1987), have also been used, however, researchers continually stress the need to develop more detailed models to supplement and complement existing laboratory methods, Stacoff et al. (1988), Clark et al. (1984), Cavenaugh (1980), Cavenaugh (1990), Miller et al. (1973), Jonsson (1987).

As early as 1960, researchers have recognized that the human locomotor system can be characterized by a set of differential equations, Miller (1973). This characterization can be expanded to include a mechanical model of the shoe. Simple analytical models have been useful in obtaining relationships between rearfoot eversion and a changing moment arm due to varying midsole geometry and cushioning properties, Stacoff et al., (1988), Nigg (1986). Although a computer is used to find solutions to the set of differential equations characterizing the dynamics of these models, the set of equations themselves, were usually derived and assembled by hand, limiting the detail and complexity of the mechanical system described.

With the evolution of mechanical system simulation tools such as ADAMS™, it is now convenient to generate a system of non-linear (differential/algebraic) equations, representing a set of constrained six degree-of-freedom parts by working on a computer graphics analogy of the system. The system of equations are then assembled into matrix form and solved through time, Chase (1984). The simulation results are interrogated using computer animations and data graphs. This relatively new generation of software simulation tools removes the analyst from the complexity of the underlying mathematics allowing the focus to shift to model behavior and function.

Due to this increased convenience, the analytical models generated using mechanical simulation tools, will be of a higher order of sophistication and detail than of those used in the past for sport shoe evaluation, and will include many more interacting kinematic variables. For example, the model presented in this paper couples pronation/supination with full eversion/abduction/dorsiflexion, not just calcaneal eversion, to study the effects of pronation/supination on tibial rotation. In addition, the shoe model complete with flexure and cushioning properties, is capable of capturing the effects of a continuously varying moment arm during the jump landing. This cushioning surface can also be used to model the partial interaction between the shoe and obstacles, such as the landing on another player's foot. Through discretization, the foot and shoe model will better adapt to the ground surface, with or without obstacles, to provide increased kinematic accuracy of the entire human locomotor system.

PROCEDURES

Data Collection

A barefoot male subject dropped onto a Kistler™ force plate by releasing his grip from a "hang-bar." The drop height (distance from subject's toe to ground) was 14 cm. A Watsmart™ optoelectronic 3-D motion analysis system was used to collect the drop landing kinematic data for 2 seconds at 200 Hz. A

Watscope™ system was used simultaneously to collect force plate data at 600 Hz. Data collection was conducted on the subject's right lower extremity. Kinematic data were obtained using infrared markers at boney locations. A four-segment experimental model was assumed (Thigh, Shank, Rearfoot, and Forefoot) for data collection. Three-dimensional joint motions for the Hip, Knee, Ankle, and the "pseudo-joint" between Rearfoot and Forefoot were calculated using data analysis software provided with the Watsmart system. Data was collected for both a flat landing and a landing on a 3 cm obstacle under the 1st metatarsal head.

Computer Model

To simulate the lower extremity response to the drop landing, three types of computer models were constructed, a coarse model, a detailed model and a skin model (see figure 1). The coarse model was built with 4-parts to reflect the discretization employed during data collection. The degrees-of-freedom, DOFs, in this kinematic model would be driven with the experimental data produced by the Watsmart system. A detailed model of the complete musculoskeletal lower extremity was developed using 26 parts and a lumping scheme in the foot similar to Scott (1993). Mechanical joints were used to connect all parts in model except for the subtalar joint where a 3-D surface contact force was employed. A skin model was developed to provide a contact force between the musculoskeletal model and the environment (i.e., shoe, force plate, etc.)

Simulations

A model overlay technique was employed to drive the 26 parts of the detailed model with the 4 parts of the coarse model using the experimental displacement data. Spring-dampers elements were used to anchor the coarse model to the detailed model at the diode locations used in the experiment. The spring and damping rates of the connection elements were normalized to the specific accuracy of the diode, to allow for the more accurate diode locations to provide the dominant motion contributions. Viscous dampers were applied to the rest of the model to prevent any motion in the free DOFs during free-fall. The skin model was then overlayed over the detailed model to provide for foot to floor interaction. Dynamic simulations were performed with this overlay arrangement to record the relative rotational and translational displacements at the joint connections.

The coarse model was then stripped from the detailed model. Muscle-ligament forces acting at the joints were described using a controller element positioned at each DOF with the error function being based on the difference between the recorded instantaneous displacement from the previous simulation and the current simulation displacement. This controller would produce the internal muscular-ligament reactions necessary to guide the motion at each DOF in order for the segments of the model to match the segment motions in the experiment. Simulations were then performed with this dynamic model. The gains of the controller elements were iteratively adjusted using an optimization technique to match model results to experimental results (segment motion and external reaction forces).

RESULTS

Model verification was performed by comparing the ground reaction forces for model and experiment and the CP travel history. Figure 2 displays the vertical ground reaction force comparison between model and experiment. With the external reactions of the model correlating with the experiment in conjunction with a correlation of segment motion it is assumed that the internal reactions or muscle forces and ligament loadings of the model will also correlate to loads the experimental subject experienced.

DISCUSSION

Simulations using this method were performed for both flat landing and obstacle landing cases. With the model validated for both cases, the height of the obstacle is increased in the simulations to cause an ankle eversion in the model. Stresses on the spring elements representing the lateral ligament complex are monitored to gage injury and rupture. With this acute injury producing mechanism isolated, research is now focused on the development of a sports shoe model to overlay onto the detailed model to stabilize and reinforce the ankle.

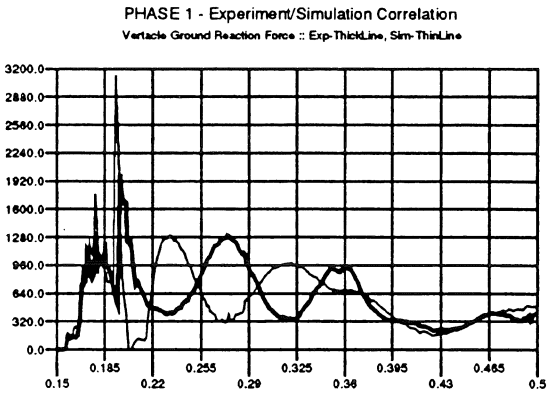

Figure 2. Experiment and Model Vertical Ground Reaction Force.

REFERENCES

Cavenaugh, P.R. (1980) The Running Shoe Book. Anderson World Inc. Mountain View, CA.

Cavenaugh, P.R. (ed.) (1990) Biomechanics of Distance Running. Human Kinetics, Champaign, Illinois.

Chase, M.A. (1984) "Methods and Experience in CAD of Large-Displacement Mechanical Systems." *Computer-Aided Analysis and Optimization of Mechanical Systems*, Springer-Verlag, Heidelberg.

Clark, T.E. et al (1984) Sport Shoes and Playing Surfaces. Human Kinetics, Champaign, Illinois.

Jonsson, B. (ed.) (1987) "Two Models Describing the Movement of the Foot During Impact- 2D v 3D Considerations." *Biomech. X.*

Miller, D.I. et al (1973) Biomechanics of Sport. Henry Kimpton Publishers, London.

Nigg, B.M. (ed.) (1986) Biomechanics of Running Shoes. Human Kinetics, Champaign, Illinois.

Scott, S. et al. (1993) "Biomec. Model of the Human Foot: Kinematics and Kinetics During the Stance Phase of Walking", *J.Biom.*

Segesser, B. (ed.) (1989) The Shoe in Sport. Year Book Medical Publishers, Inc. Chicago, Ill.

Stacoff, A., et al (1988) "Running Injuries and Shoe Construction: Some Possible Relationships." *Int. Journal of Sport Biomechanics.*

THE VOLUNTARY STRENGTH OF A HUMAN HAND MUSCLE CANNOT BE PREDICTED BY ITS SIZE

G. H. Yue, D. A. Keen, and R. M. Enoka

Department of Biomedical Engineering, The Cleveland Clinic Foundation, Cleveland, OH 44195-5254

INTRODUCTION

The capacity of skeletal muscle to exert force is determined by four factors: the level of activation (neural drive), the amount of agonist-antagonist coactivation, the cross-sectional area (CSA) of the muscle, and the specific tension (force generated per unit of CSA). If motivated humans are able to fully activate a muscle without coactivation during a maximal voluntary contraction (MVC), the MVC force should be directly related to its CSA, provided there is no change in specific tension. Furthermore, the increase in force due to strength training should be directly related to an enlargement in muscle size. To test these hypotheses, we examined the association between the abduction force exerted by the index finger during an MVC and the size (CSA and volume) of the first dorsal interosseus (FDI) muscle both before and after a strength training program. We found that the MVC force was poorly correlated with muscle size.

METHODS

Nineteen healthy subjects were assigned to an elderly group with an average age of 65 years or a young group with an average age of 23 years. All subjects were right-hand dominant and had no known neuromuscular disorders. Each subject participated in a 12-wk strength training program that involved a concentric-eccentric exercise by the FDI muscle of the left hand. The exercise was performed against a load that tended to adduct the index finger. The subjects performed 3 training sessions each week with each session comprising 6 sets of 10 repetitions of the exercise. The index finger was displaced through a 0.5-rad range of motion for each performance of the exercise. The training load was maintained at 80% of the maximum load that could be lifted. Subjects were instructed to increase the training load so that it remained difficult to complete all 10 repetitions in the final (6th) set.

Before and after the 12-wk training program, the index finger abduction MVC was measured during an isometric contraction. The MVC task consisted of a gradual 3-s increase to maximal effort with the MVC force maintained for 2-3 s before the subject relaxed. Each subject performed the MVC task 3-4 times with about a 60-s rest between trials.

The CSA and volume of the left-hand FDI before and after the 12-wk training program were measured with magnetic resonance imaging (MRI). The imaging protocol consisted of a volume gradient-echo pulse sequence (TR/TE = 50/7 ms; 60 degree flip angle; 256 x 192 acquisition matrix; and 10 cm field of view). Sixty cross-sectional slices (1.1 mm thick) were obtained in each MRI session. The boundary of the muscle in each slice was identified and the CSA of the muscle determined. The volume of FDI was calculated by summing the volume of each slice. Repeat measurements of the CSA and volume yielded a variability of less than 1%.

RESULTS

The correlations between the MVC force and the maximal CSA were $r^2 = 0.12$ (Fig 1A; before training) and $r^2 = 0.21$ (Fig. 2A; after training) while those between MVC force and volume were $r^2 = 0.18$ (Fig. 1B; before training) and $r^2 = 0.13$ (Fig. 2B; after training). The correlations between the training load and the CSA were $r^2 = 0.14$ (Fig. 1C; before training) and $r^2 = 0.12$ (Fig. 2C; after training) while those between traning load and volume were $r^2 = 0.16$ (Fig. 1D; before training) and $r^2 = 0.07$ (Fig. 2D; after training). Furthermore, after 12 wks training, the isometric MVC force increased 37% for the young subjects and 42% for the

elderly subjects, and the training load increased by 127% for the young and 148% for the elderly subjects. However, the increases in muscle CSA and volume were only 9.1 and 7.8% for the young subjects and 4.3 and 2.8% for the elderly subjects, respectively. The correlation between the increases in MVC force and muscle CSA was $r^2 = 0.08$ (Fig. 3A) and between MVC force and volume was $r^2 = 0.19$ (Fig. 3B). The correlation between the increases in training load and the CSA was $r^2 = 0.06$ (Fig. 3C) and for training load and the volume was $r^2 = 0.09$ (Fig. 3D).

DISCUSSION

These data suggest that the maximal voluntary strength of the FDI muscle does not depend exclusively on the size of the muscle, regardless of whether the task was novel (pre-training data) or learned (post-training data). The poor correlations were observed with both measures of size (CSA and volume) and force (MVC force and training load). The correlations obtained with the before-training data indicate differences between subjects in the extent of activation (less than maximal) and in the amount of coactivation. In addition, the after-training data could have been influenced by changes in specific tension. The similarity of the before- and after-training correlations is surprising because training is known to influence the neural drive to muscle (Yue & Cole, 1992), the amount of coactivation (Carolan & Cafarelli, 1992), and specific tension (Kandarian & Williams, 1993). We conclude that the maximal voluntary force of a hand muscle in healthy humans cannot be predicted reliably by the size of the muscle.

REFERENCES

Carolan, B. & Cafarelli, E. *J. Appl. Physiol.*, 73:911-917, 1992.

Kandarian, S.C. & Williams J.H. *Med. Sci. Sports Exerc.*, 25:999-1004, 1993.

Yue, G. & Cole, K.J. *J. Neurophysiol.*, 67:1114-1123, 1992.

Supported by NIH grant AG09000.

Figure 1 - Before Training

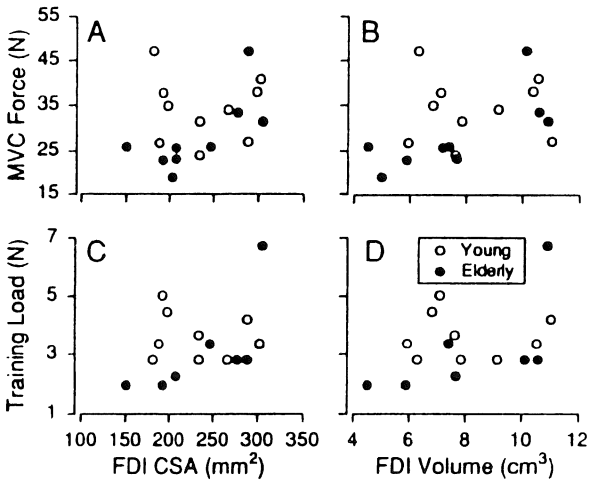

Figure 2 - After Training

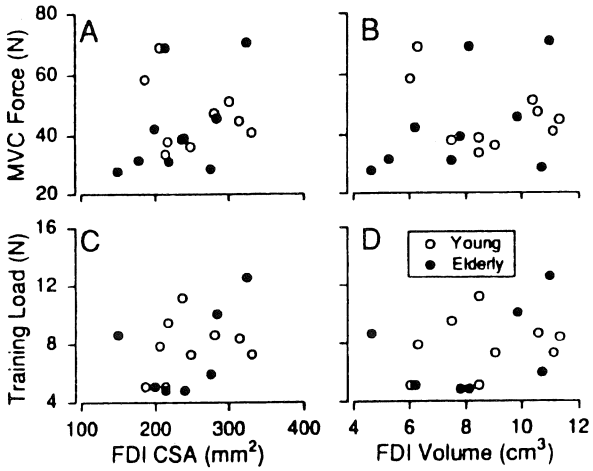

Figure 3

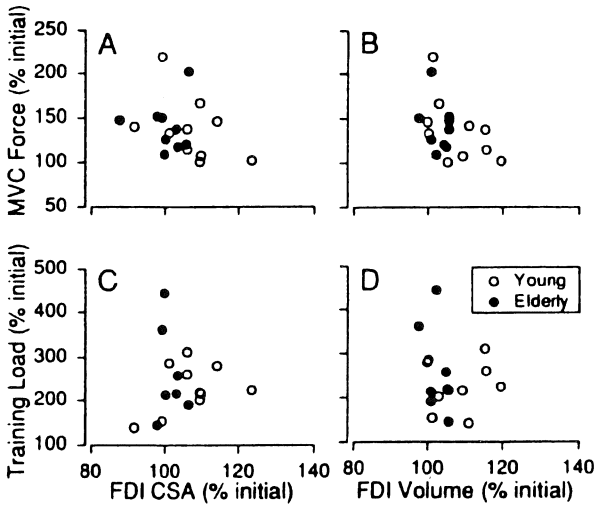

BIOMECHANICAL DETERMINANTS OF HUMAN WRIST JOINT STRENGTH

S.D. SHOEMAKER, T.J. BURKHOLDER, G.J. LOREN, M.D. JACOBSON AND R.L. LIEBER

Departments of Orthopaedics and AMES/Bioengineering
Biomedical Sciences Graduate Group
University of California and VA Medical Centers, San Diego, CA 92161 **USA**

INTRODUCTION

Strength is the most common clinical parameter used to assess neuromuscular function. It is therefore essential to understand the biomechanical determinants of strength to prescribe rational therapeutic methods for restoration of strength or function.

Maximal muscle force is determined primarily by muscle architecture (Gans, 1982) but is also influenced by sarcomere length (Gordon et al. 1966) and tendon compliance (Zajac, 1989). Moment arm can vary with joint angle (Brand, 1985) resulting in a system in which both muscle force and mechanical advantage are changing as a joint rotates. Since these components interact to produce the joint moment, it is of interest to determine their interrelationships. Thus, the purpose of this study was to measure muscle architecture, tendon compliance and moment arm of each of the five prime wrist torque generators (i.e., the muscle-tendon-unit acting across a moment arm) to model the human wrist torque-joint angle relationship.

METHODS

Maximum isometric tension of each wrist muscle-tendon unit (MTU) was predicted based on its physiological cross-sectional area. Architectural and tendon properties of the prime wrist MTU's (extensors carpi radialis brevis (ECRB) and longus (ECRL), extensor carpi ulnaris (ECU), flexor carpi radials (FCR), and flexor carpi ulnaris (FCU)) were determined as previously reported (Lieber et al. (1990). Maximum muscle tetanic tension (P_0) was calculated via multiplying PCSA on a specific tension of .25 MPa (Powell et al. 1974).

Tendon excursion was measured throughout FE and RUD in pronated, neutral and supinated forearm positions as described by An et al. (1983) and differentiated with respect to joint angle to obtain instantaneous moment arm. Moment arm data were fit using stepwise polynomial regression and averaged over the five different specimens.

A geometrical muscle force model was then developed after Zuurbier and Huijing (1990) which related sarcomere length to joint angle accounting for tendon elasticity. This scaled P_0 over FE and RUD. The resulting muscle force was multiplied by the corresponding moment arm to yield isometric joint torque throughout FE and RUD.

RESULTS

Moment arms magnitudes compared favorably to reported values (Brand, 1985; Horii et al. 1993). However, contrary to previous reports, moment arms varied substantially throughout the range of motion (Fig. 1). Extensor moment arms peaked in 10-30° of extension while flexor moment arms peaked at extreme flexion.

Maximum muscle force of the ECRB and ECRL coincided with their maximal moment arm in wrist extension (Fig. 1A), whereas maximum flexor muscle force (observed in extreme extension) did not coincide with flexor peak moment arm (observed in extreme flexion).

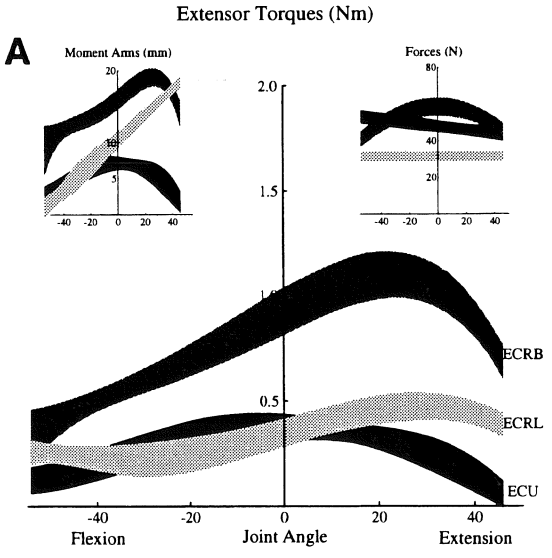

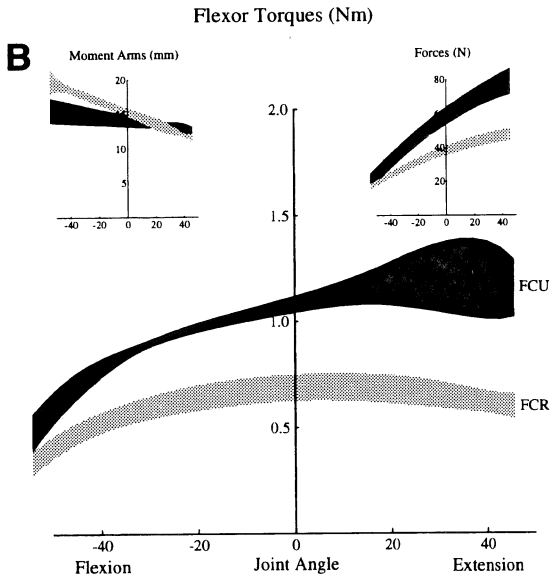

FIGURE 1: **(A)** Wrist extensor and **(B)** wrist flexors moment arm, muscle force and torque profiles. Mean ± SEM (n=5).

Sarcomeres within the extensors were predicted to operate almost exclusively at lengths corresponding to maximum tension (Fig. 2). Flexor sarcomeres had a greater range of sarcomere lengths during FE, shortening onto the steep ascending portion of the sarcomere length tension curve. This resulted in greater muscle force variation over FE for the flexors compared to the extensors (Figs. 1 and 2).

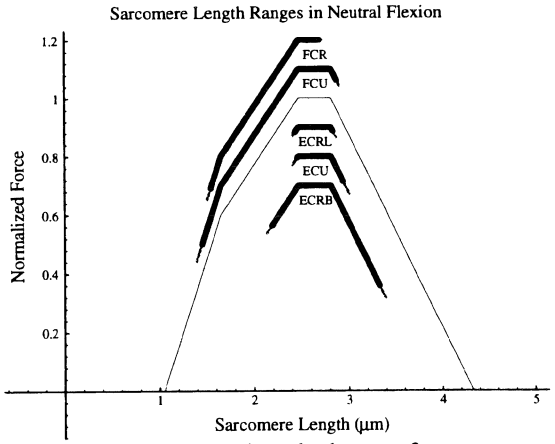

FIGURE 2: Sarcomere length changes for flexion/extension of the wrist flexors (above) and extensors (below) superimposed on the length-tension diagram.

Torque profiles varied markedly with joint angle. The shape of the extensor torque profiles were dominated by the moment arm and showed less dependence on muscle force. Tendon compliance had very little influence on the extensor torque profile.

Flexor torque profiles varied less from flexion to extension due to muscle force increases being attenuated by decreasing moment arm. As a result, neither muscle force nor moment arm dominated the flexor torque profiles. Tendon compliance had a much greater effect on the torque profiles of the flexors compared to the extensors.

DISCUSSION

These data illustrate that wrist strength results from interaction between muscle force, tendon compliance and moment arm and does not simply reflect either component alone. In addition, the relative influence of muscle, joint and tendon properties of wrist flexors and extensors differs considerably.

It may not be surprising that extensor muscle force and moment arms peaks in extension, since this is known to be the position of normal use. In contrast, the flexor system appears to be designed to generate a relatively high torque over a wide range of motion by means of an angular disparity between peak muscle force and moment arm.

These results have significant implications for surgical tendon transfers. For example, it would be nearly impossible to recreate a normal extension profile with either flexor muscle because the relationship between muscle and moment arm would be dramatically altered. In this case, however, the high force capacity of the FCU, more than twice that of the ECRB or ECRL may compensate for the lost elegance of design. A more thorough understanding of this design may enable improved decision regarding donor muscles and insertion positions of surgical tendon transfers.

REFERENCES

An *et al.* J. Biomech., 16:419-425, 1983.
Brand, Clinical Mechanics of the Hand Mosby, St. Louis, MO, 1985.
Gans, Ex. Sports Science Rev. 10:160-207, 1982.
Gordon *et al.* J. Physiol. 184:170-192, 1966.
Horii *et al.* J. Hand Surg., 18A:83-90, 1993.
Lieber. *et al.* J. Hand Surg. 15:244-250, 1990.
Lieber *et al.* Am J. Physiol. 261:C86-C92, 1991.
Powell *et al.* J. Appl. Physiol. 57:1715-1721, 1984.
Zajac, CRC Crit. Rev. in Biomed. Eng. 17:359-411, CRC Press, Inc., Boca, Raton, Fl., 1989.
Zuurbier and Hiujing J. Biomech. 25: 1017-1026, 1990.

ACKNOWLEDGMENTS

This work was supported by the Veterans Administration and NIH grant AR35192.

VALIDATION OF A FINITE ELEMENT MODEL OF THE FUNCTIONALLY LOADED ZYGOMATIC ARCH BY IN VIVO STRAIN GAGE DATA

E. C. Borrazzo†, W. L. Hylander‡ and C. T. Rubin†

†Musculo-Skeletal Research Laboratory, Department of Orthopaedics, State University of New York, Stony Brook, NY 11790

‡Department of Biological Anthropology and Anatomy, Duke University Medical Center, Durham, NC 27710

INTRODUCTION

Understanding the biomechanics of mastication may lead to design improvements of dental implants, retardation of alveolar bone loss, prevention of tooth loss, improved fracture healing of facial bones, and support for form/function assumptions in anthropologic and paleologic investigations.

In the study reported here, biomechanics of the zygomatic arch during mastication was investigated in an adult female macaque. Three 3-element rosette strain gages were applied to the lateral aspect of the zygomatic arch, and strain was recorded strain during functional activity (ie:chewing). A finite element analysis of the zygomatic arch was modeled and results of different boundary conditions compared to the surface strains measured *in vivo* . The approximate biomechanics of both the working-side and balancing-side zygomatic arches during mastication mimicked a moment applied anteriorly to a curved, built-in cantilever beam that caused the arch to bend superolaterally, a loading condition not anticipated based on results of previous *in vivo* experimental work.

REVIEW AND THEORY

Many analytic models have attempted to describe the strain distribution of the madible and zygomatic arch to improve our understanding of mastication. One of the most powerful experimental models has involved *in vivo* strain measurements made from various craniofacial bones of macaques during mastication (Hylander and Johnson, 1992). Although the bone strains can be measured, description of the resultant forces and moments are difficult due to the complexity of the loading and boundary conditions of muscles and food substance on the facial bones. Others have used finite element methods to study the mandible during mastication (Hart *et al.*, 1992; Korioth *et al.*, 1992). The results of these mathematical models, however, are vulnerable to speculation since loading and boundary conditions may produce erroneous results that cannot be compared to actual *in vivo* experimental measurements. Here, *in vivo* strain data are combined with a finite element model to more rigorously define the loading conditions of the zygomatic arch.

The strain analysis uses a technique derived from that described by Gross *et al.* (1992) to describe the biomechanics of the zygomatic arch of an adult female macaque during mastication. The accuracy of various *a priori* loading and boundary conditions will be checked by comparing the results obtained from the FEM with those obtained from the in vivo strain measurements, thus allowing approximation of the biomechanics of the zygomatic arch. This can serve as a first step in understanding the biomechanics of mastication in humans with possible future application of similar techniques to the mandible.

PROCEDURES

Under a general halothane anesthesia, three rosette strain gages were fixed to the lateral aspect of the right zygomatic arch of an adult female macaque (see figure 1). All experimental and surgical protocols were reviewed and approved by the Duke University Laboratory Animal Committee. One strain gage was located rostrally (or anteriorly), one was located caudally (or posteriorly), and the middle gage was located immediately rostral to the zygomatico-temporal suture. Details of the recording procedure are the same as described previously (Hylander et al., 1992). The strain data was recorded for two mastication series: chewing on the right side such that recorded strains represented working side strains, and chewing on the left side such that recorded strains represented balancing side strains. A sequence of 16 and 17 chewing cycles for analysis of working-side and balancing-side strains were averaged, respectively, to give representative peak principal strain values and the corresponding directions of those peak principal strains.

Fifty-three high-resolution CT scans of the animal's head were made at 1mm intervals to define the morphology and strain gage locations on the zygomatic arch. The finite-element model of the zygomatic arch was constructed from the CT images using a method similar to that described by Gross (1993). The model contained 4462 nodes with 2880 eight-node three-dimensional trilinear displacement bricks and 1440 six-node trilinear displacement triangular prisms. Because the CT scan showed mineralized tissue in the area of the zygomatico-temporal suture, the FEM model assumed this suture as fixed. The zygomatic arch was assumed to be a linearly elastic isotropic material with a Young's modulus of 100 MPa (for cancellous bone) and a Poisson's ratio of 0.32.

Over thirty different loading and boundary conditions were initially used in the FEM model. For example, loads were applied along axes representing pure axial compression and tension, pure bending, pure torsion, and three and four point bending as well as other simple loads. These loading conditions were then combined in ratios ranging from 0.1 to 1.0 of the load originally used for the single load cases, and FEM analysis was performed on these cases as well. The loading regimen also approximated an assumed action of the masseter muscle and temporalis fascia on the zygomatic arch.

Principal strains and directions were obtained for the three nodes corresponding to the approximate location of the three rosette strain gages. The results from the FEM for each loading condition and combination of loads were normalized to eliminate errors introduced by assumed load magnitudes and material properties. These values were compared to the *in vivo* results using functions that involved strain magnitudes and directions.

RESULTS

Using strain parameters at the point in the chew cycle where the peak principal tensile strain occurs on the working-side zygomatic arch, the results of FEM single load cases were compared with *in vivo* strain quantities using the scalar and angle comparison functions described above. When two loading conditions were combined in the FEM analysis in

varying proportions, 291 cases produced principal strain results that more closely approximate the *in vivo* scalar quantities than the best single load case. Values of the scalar comparison function ranged from 0.44 to 2950 with a value of 0 representing an exact comparison between *in vivo* and FEM results. Values of the angle comparison function ranged from 27 to 243, again with 0 representing and ideal case. The combined load case which best approximates the *in vivo* principal strain magnitudes and direction is a moment applied anteriorly acting superolaterally at the anterior zygomatic arch which is fixed posteriorly. Figure 2 shows the actual principal tensile and compressive strains for the *in vivo* experiment and the FEM model for this loading condition. This case has a scalar comparison function value of 0.59 and an angle comparison function value of 40. A moment applied in the opposite direction had a better scalar function value of 0.44, but the angle comparison function value was much worse at 214.

As on the working-side, the loading combination which best approximates the *in vivo* functional loading condition on the balancing-side is a moment applied anteriorly with the posterior end fixed that bends the arch superolaterally (slightly less laterally than superiorly, ratio of 0.8). The direction correlated well with an angle comparison function value of 24. This loading case, although it improved the correlation more than any simple loading case, had a scalar comparison function value of 0.99, reflecting the fact that many loading combinations that had good scalar function values with poor direction correlation.

The approximate biomechanics of both the working-side and balancing-side zygomatic arches during mastication mimicked a moment applied anteriorly to a curved, built-in cantilever beam that causes the arch to bend superolaterally (see figure). The finite element model was extremely sensitive to small changes in loading and boundary conditions.

DISCUSSION

By combining experimental and computational modeling, the biomechanics of the zygomatic arch of a macaque during mastication can be approximated. Knowing the principal strain magnitude and direction at three sites along the surface of the bone, the results calculated by the FEM were compared to the *in vivo* results, and the loading conditions of the FEM were systematically changed while the calculated principal strains approximated *in vivo* results.

As a first order approximation, this study shows that a bending moment applied anteriorly that deforms the zygomatic arch superiorly and laterally accurately describes the loading of the working-side and balancing-side zygomatic arches of an adult female macaque during mastication. This mimics a bending moment applied to the end of a curved, built-in cantilever beam. Importantly, other loading combinations also improved the correlations between mathematic and experimental results, but not as well as the bending moment case. Clearly, the actual biomechanics of the zygomatic arch may best reflected by a complex combination of bending, axial loading, and torsion.

The FEM is a useful tool in describing bone biomechanics, especially when we can validate the finite element model by comparing with *in vivo* strain data obtained during functional activity. Understanding the functional load environment of the zygomatic arch is a first step in describing the biomechanics of mastication. Such a complementary analytic/experimental methodology has great potential in describing the biomechanics of other bones during functional loading.

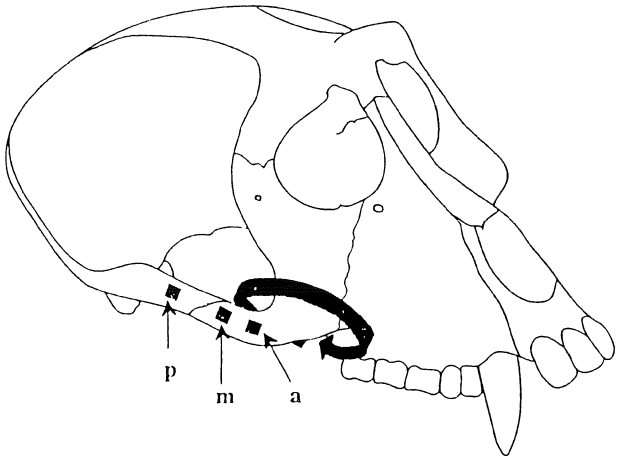

Figure 1: Placement of strain gages on lateral aspect of the zygomatic arch of the macaque: a, anterior rosette; m, middle rosette; p, posterior rosette. The large arrow shows the direction of the moment applied to the zygomatic arch in the FEM model which yields results that most closely resemble *in vivo* strain measurements.

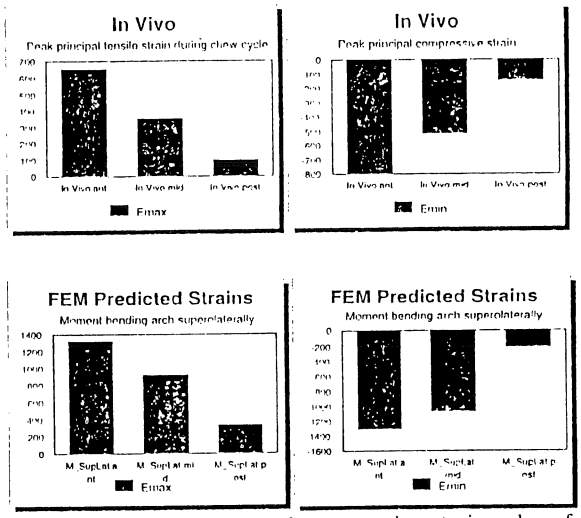

Figure 2: Principal tensile and compressive strain values for the *in vivo* experiment and the FEM predictions for the case of a moment applied anteriorly causing the arch to bend superolaterally. Values are in 10^{-6} strain. The strain gradients from anterior rosette (left) to posterior rosette (right) are remarkable similar.

REFERENCES

1. Gross, T. Isolating Strain Parameters Correlated to Skeletal Adaptation, Ph.D. thesis (SUNY-Stony Brook), 1993.
2. Gross, T. *et al.* J. Biomechanics, 25, 1081-1087, 1992.
3. Hart, R. *et al.* J. Biomechanics, 25, 261-286, 1992.
4. Hylander, W. and Johnson, K. Biological Mechanisms of Tooth Movement (ed. Davidovitch), 559-569, 1992.
5. Korioth, T. *et al.* Am. J. Phys. Anthrop., 88, 69-96, 1992.

AN EVALUATION OF THE BENDING AND TORSIONAL RIGIDITIES OF THE TIBIAE - INTRAMEDULLARY ROD CONSTRUCT IN COMMINUTED FRACTURES SUBJECTED TO PHYSIOLOGICAL LOADING:PRELIMINARY RESULTS

M. T. Archdeacon, A. E. Engin and R. F. Ostrum

Department of Biomedical Engineering, The Ohio State University, Columbus, Ohio 43210 U.S.A.

Department of Engineering Mechanics, The Ohio State University, Columbus, Ohio 43210 U.S.A.

Department of Orthopaedic Surgery, The Ohio State University, Columbus, Ohio 43210 U.S.A.

INTRODUCTION

In an attempt to evaluate the biomechanical properties of the tibia-rod composite in complex fractures of the tibia, a study of the biomechanical behaviors of intramedullary rods implanted in cadaveric tibias has been undertaken. The research consists of a series of biomechanical testing procedures applied to cadaver tibias artificially fractured to simulate comminuted long bone fractures, and implanted with 12mm open-section, slotted Biomet tibial intramedullary rods. The data obtained from the series of tests will be used toward the following objectives: 1) to develop methods for simulated physiological loading of a potted cadaver tibia, 2) to enhance the technique of measuring fracture fragment motion using specially designed displacement transducers, 3) to characterize the bending and torsional rigidities of the tibia-IM rod construct in comminuted fractures.

REVIEW AND THEORY

The intramedullary (IM) rod has proven to be a time-tested method of fracture fixation for midshaft diaphyseal fractures of the tibia, Weller et al. (1979); Hindley (1988); Gad et al. (1990); Court-Brown et al. (1991); Klemm and Borner (1986); Kessler et al. (1986); Whittle et al. (1992). Introduced in the 1940's by Kuntscher, the IM rod provides correct axial alignment in shaft fractures and good apposition of the fracture fragments, Lottes (1958). It provides semi-rigid fixation, and therefore minimal stress shielding, it absorbs rotational and bending stresses, thus allowing for early weight-bearing, and it has shown a reduced incidence of infection in closed tibial shaft fractures versus plating, Weller et al. (1979); Lotes (1958); Hindley (1988).

With the advent of the interlocking rod, the technique has been applied to more complex fractures of the tibia. The broader applications include fractures of the proximal and distal thirds of the tibia, fractures which have varying levels of comminution, and segmental fractures which are extremely unstable, Bone and Johnson (1986); Hindley (1988); Court-Brown et al. (1991); Klemm and Borner (1986); Kessler et al. (1986); Donald and Pope (1985); Whittle et al. (1992); Gleis et al. (1988). The loading which a fractured tibia fixed with an IM rod encounters during early weight-bearing (prior to bony union) is oftentimes sufficient to produce elastic and plastic deformation of the rod or transcortical screws, Martens et al. (1972). This distortion or failure of the IM rod may in fact be responsible for many post operative orthopaedic complications. Thus, the need for investigations which elucidate the behaviors of fractured tibias fixed with intramedullary rods is obvious.

Several studies have addressed the biomechanics of fracture fixation techniques for the tibia. In a study performed by Laurence et al. (1969), they simulated transverse midshaft fractures in the cadaver tibias and fixed the fractures with various fracture fixation plates or a Kuntshner IM rod. They then loaded the fixed tibias to determine the stiffness of the fixation device.

In a study by Minns et al. (1977), human cadaveric tibias were artificially fractured, fixed with various fracture fixation plates, loaded physiologically, and evaluated for regions of compressive and tensile stress. In order to test the fracture fixation plates in a realistic manner, the intersegmental forces and moments at the knee joint had to be applied to the tibias fixed with the fracture plates. The axial force and the cross-sectional resultant forces were applied to the cadaver tibias, and displacements were measured with dial gages in the plane of the applied loads.

In 1988 Gleis et al. (1988), attempted to measure the A-P displacement of distal fracture fragments fixed with G-K rods in cadaver femurs. They applied a known load to an exposed proximal end of a Gross-Kempf rod which was inserted distally in the cadaveric femur. Displacements of the proximal end were recorded and related to the number of distal screws and the percentage of proximal bony cortex which remained.

Henley et al. (1993), performed a series of biomechanical studies on cadaveric tibias to determine the effects of cortical contact in tibial fractures fixed with IM rods. His group artificially fractured the proximal tibia, rodded it with an AO intramedullary rod, and applied an axial load of body weight, and arbitrary torsional and varus/valgus bending moments using an MTS machine and a pneumatic actuator. They recorded fracture fragment deflections, and reported a significant increase in axial fragment displacement and varus/valgus translation with loss of cortical contact. However, they do not discuss the effects of variable amounts of cortical contact, and its relation to interfragmentary motion.

The orthopaedic literature is void of a thorough investigation of the biomechanical properties of comminuted tibial shaft fractures fixed with intramedullary rods. As an initial step in the investigation of tibial rods, we have attempted to characterize how the remaining cortex of a comminuted tibial shaft fracture fixed with an intramedullary rod contributes to the overall stability of the fracture-rod construct.

PROCEDURES

The experimental portion of this study involved six cadaveric tibias implanted with 12mm open-section, slotted Biomet tibial rods. The tibias were potted in dental plaster on their proximal and distal ends, then artificially fractured to simulate the Winquist (1984) comminuted fracture classification. Four tibias were then loaded experimentally with an appropriately applied single eccentric axial force to simulate two bending moments occurring at the 13th and 50th percentiles of the normal gait cycle. These positions were chosen because maximum forces or bending moments occur at these phases of the gait cycle, Bresler and Frankel (1950), Engin (1978). The remaining two tibias were loaded with a series of pure applied torques in the physiologic range. These loadings were performed on the intact tibias and after each fracture simulation.

Fracture fragment deflections were measured at the fracture site with specially designed displacement transducers for the tibia loaded with the axial force and corresponding bending moments. The applied axial load and the displacements of the proximal fracture fragment relative to the fixed distal fragment were recorded digitally with a data acquisition system.

A series of known torques was applied, and the relative rotation

of the proximal fracture fragment was recorded with small angle rotation transducers and digitized on the data acquisition system. The load versus displacement and torque versus angle of rotation diagrams were obtained. A representative "tibia-IM rod" bending rigidity and "tibia-IM rod" torsional rigidity was determined for each type of Winquist fracture pattern. Here, the term bending rigidity is used to indicate the ratio of eccentrically applied axial load to the relative proximal fragment displacement at the fracture site.

RESULTS AND DISCUSSION

Figures 1 and 2 demonstrate the relative bending rigidities in the A/P and M/L planes of the simulated comminuted fractures in a cadaveric tibia fixed with an IM rod. Figure 3 demonstrates the relative torsional rigidity of the various comminuted fracture patterns in a cadaveric tibia implanted with an IM rod. In the three figures, a filled square represents the intact tibia before fracture. The open diamond represents a type-I comminuted fracture in which less than 25% of the bony cortex has been removed. The open circle represents a type-II comminuted fracture. In this pattern, greater than 50% of the cortex remains intact. The type-III fracture, represented by the open square, is rotationally unstable with less than fifty percent of the bony cortex intact. In the type-IV comminuted fracture, no cortical stability exists. This fracture pattern is represented with the open triangle.

In Figures 1 and 2, the intact tibia load-deflection curve demonstrates bending deformation directly proportional to the applied load. In the type-I fractures, there is very little relative motion between the proximal and distal fragments; therefore, this construct appears very rigid. In the type-II and type-III fracture patterns, the data are much more difficult to interpret. For example, in Figure 1 the type-II fracture appears more stable than the type-III fracture. The relative bending rigidity in the A/P and M/L planes is probably dependent on not only cortical contact, but also on the loading configuration in each phase of the gait cycle. When the fractures are at the type-IV severity, the expected behavior of greater deflection with increasing load predominates. At this point, the cortex provides little if any stability.

The results of the purely applied physiologic torque in increasingly more unstable fracture patterns was more predictable. The intact, type-I, and type-II fracture patterns demonstrated similar behaviors in that the applied torque resulted in small angles of rotation. The type-III fracture resulted in a torsional rigidity that was about half that of the intact tibia, and the severe type-IV fracture resulted in a torsional rigidity that was almost one-tenth of the intact tibia value.

The results of this preliminary investigation are not sufficient to draw concrete conclusions. However, some general trends were observed. The goal of this research was to develop methods of physiologic loading that are reproducible, and to accurately measure the fracture fragment deflections and rotations. These goals have been accomplished. More data from additional test specimens are required in order to fully characterize the behaviors of the tibia-IM rod construct in comminuted fractures.

REFERENCES

Bone, L.B. et al. J. Bone Joint Surg, 68A, 877-887, 1986.
Bresler, C.H. et al. Trans Am Soc Mech Engrs, 72, 27, 1950.
Court-Brown, C.M. et al. J Bone Joint Surg, 73B, 959-964, 1991.
Donald, G.D. et al. Concepts in Intramedullary Nailing, Grune and Stratton, 1985.
Engin, A.E. Orthopaedic Mechanics: Procedures and Devices, Academic Press, 1978.
Gad, H.F. et al. Injury, 21, 217-219, 1990
Gleis, G.E. et al. Techniques Orthop, 3, 6-8, 1988.
Henley, M.B. et al. J. Orthop. Trauma, 7(4), 311-319, 1993.
Hindley, C.J. Injury, 19, 180-184, 1988.
Kessler, S.B. et al. Clin Orthop, 212, 18-25, 1986.
Klemm, K.W. et al. Clin Orthop, 212, 89-100, 1986.
Laurence, M. et al. J. Bone Joint Surg, 51B, 754- , 1969..
Lottes, J.O. Instructional Course Lectures, 65-77, 1958.
Martens, M. et al. Injury, 4, 18-24, 1972.
Minns, R.J. et al. J. Biomechanics, 10, 569-579, 1977.
Weller, S. et al. Clin Orthop, 138, 45-55, 1979.
Whittle, A.P. et al. J Bone Joint Surg, 74A, 1162-1171, 1992.
Winquist, R.A. et al. J. Bone Joint Surg, 66A, 529-539, 1984.

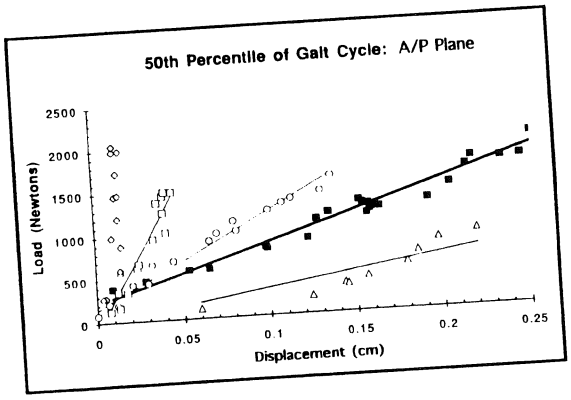

FIGURE 1. Eccentrically Applied Loads versus Relative Proximal Fragment Displacements in the Anterior / Posterior Plane.

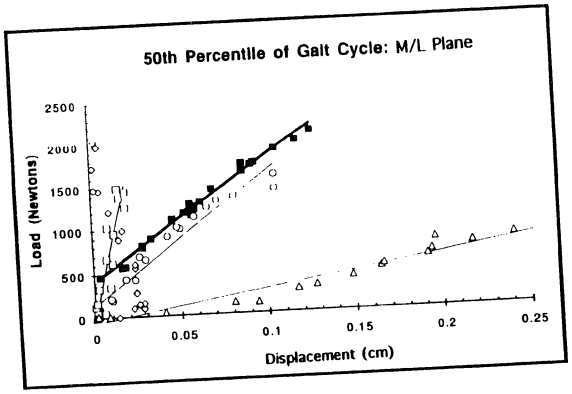

FIGURE 2. Eccentrically Applied Loads versus Relative Proximal Fragment Displacements in the Medial / Lateral Plane.

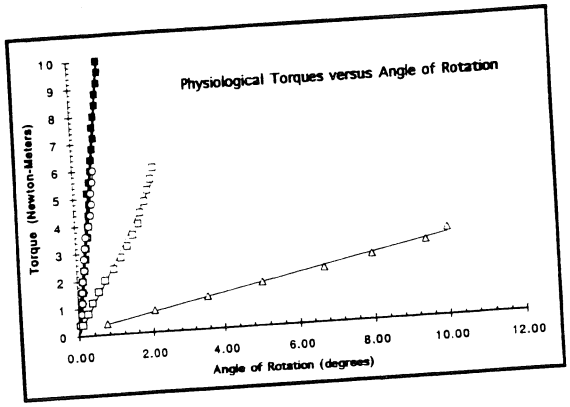

FIGURE 3. Applied Torques versus Relative Rotation of the Proximal Fragment .

ADVANTAGES OF DORSAL CORE SUTURE PLACEMENT TECHNIQUE IN FLEXOR TENDON REPAIR: A BIOMECHANICAL AND STRUCTURAL STUDY

O. Soejima, E. Diao, JC. Lotz* and JS. Hariharan

Hand and Microvascular Surgery Service, Department of Orthopaedic Surgery, University of California, San Francisco
San Francisco, CA 94143-0728

*Orthopaedic Bioengineering Laboratory, Department of Orthopaedic Surgery, University of California, San Francisco
San Francisco, CA 94143-0514

INTRODUCTION

We designed the present study to compare the strength of flexor tendon repair in the hand using dorsal side modified Kessler suture (dMKS) versus volar side modified Kessler suture (vMKS) using static loading. We also compared the relative strengths of dorsal portions (dFDP) and volar portions (vFDP) of flexor digitorum tendon to evaluate structural differences of these regions. The mean failure load of dMKS was 26.5% greater than that of vMKS, and the mean strength of dFDP was 58.3% greater than that of vFDP. We attribute the greater strength of dorsal core suture placement technique to the effect of suture placement on the tendon/suture construct.

REVIEW AND THEORY

Dorsally placed core sutures for flexor tendon repair have been previously discouraged due to concern about interfering with the vincular blood supply. However, as diffusion of synovial fluid has been shown to have a primary role in flexor tendon nutrition[1,2], these prohibitions may be unfounded. Dorsally placed core sutures have recently been described as a superior method of tendon repair compared to volarly placed core sutures in a dynamic-cadaveric model[3]. The authors attributed these results to decreased sheath friction and the biomechanics of the pulley system. However, this improved performance may also be due to suture placement and its effect on the strength of the tendon/suture construct.

The purpose of this study was to test our hypothesis that since the vincular vascular anatomy enters the tendon from the dorsal aspect of the tendon, the dorsal tendon should be stronger than the volar tendon; thus there would be biomechanical advantages to dorsal as opposed to volar placement of the core suture.

PROCEDURE

1) Measurement of breaking loads of dMKS and vMKS: Twenty FDP from fresh frozen cadaver hands were sutured with either of two suture patterns with 4-0 Dermalon (monofilament nylon) for the core suture and 6-0 Surgilene (monofilament polypropylene) for the running epitendinous suture. In one group (10 specimens), the core suture was placed in the dorsal portion of the tendon. In the other (10 specimens), this suture was placed in the volar portion of the tendon (Fig. 1). The specimens were mounted on a servohydraulic material testing machine (MMED, Materials Technology Corporation, La Canada, CA) with specially designed clamps. The distance between clamps was measured as the initial specimen length. The tendons were immersed in physiological saline at room temperature and distracted longitudinally at a rate of 2 cm/min to failure. Tendon load and grip travel were measured throughout the tests.

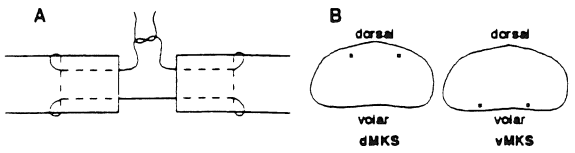

Fig. 1: A shematic diagram of a modified Kessler suture. The corner loops are retained. Only one strand of suture is used, with a single intratendinous knot (A). Cross section of the tendon ends. Core suture locate at dorsal side in dMKS and volar side in vMKS (B).

2) Measurement of the strength of dorsal and volar side FDP: Seven fresh frozen human cadaver FDP were removed from the hands and cut longitudinally with a razor. Tendons were loaded to failure as described above. After the testing, the volume of each specimen was determined gravimetrically. The average specimen cross-sectional area was determined by dividing the specimen volume by the specimen length[4]. The strengths (MPa) were calculated as the peak force divided by the tendon average cross-sectional area.

An analysis of histological differences between dorsal and volar side FDP was performed using an image analysis system (NIH image 1.54) on a personal computer.

RESULTS

1) Difference between dMKS and vMKS: The mean failure load of dMKS was 26.5% greater than that of vMKS (35.48±1.96 N and 28.04±1.89 N, respectively; $p<0.05$, Table 1). However, the stiffness of dMKS and vMKS were 8.02±1.00 and 7.19±0.83, respectively with no significant difference ($p=0.531$). During tensile testing, we observed that the running suture failed prior to the development of a small gap in the tendon repair.

2) Difference between dFDP and vFDP: The mean strength of dFDP was 58.3% greater than that of vFDP (18.33±2.75 MPa and 11.58±1.17 MPa, respectively, $p<0.05$, Table 1). In contrast, there was a tendency that the stiffness of dFDP was smaller than that of vFDP (17.52±2.36 N/mm and 18.10±2.19 N/mm, respectively), (Table 1, Fig. 2).

Table 1: The tensile properties (mean ± SEM) of all specimens

	(n)	Peak load (N)	Stiffness (N/mm)	Strength (MPa)
dMKS	10	35.48±1.96*	8.02±1.00	
vMKS	10	28.04±1.89	7.19±0.83	
dFDP	7	61.88±5.02	17.52±2.36	18.33±2.75+
vFDP	7	58.68±6.51	18.10±2.19	11.58±1.17

*Significantly different between dMKS and vMKS: $p<0.05$ (t-test)
+Significantly different between dFDP and vFDP: $p<0.05$ (t-test)

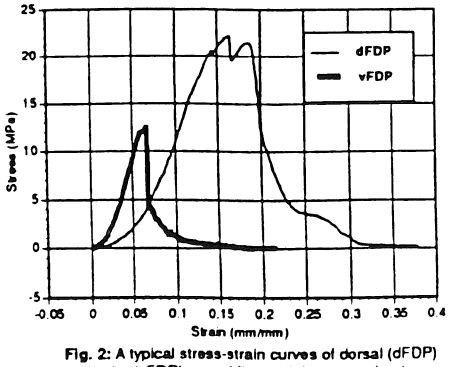

Fig. 2: A typical stress-strain curves of dorsal (dFDP) and volar (vFDP) part of flexor digitorum profundus tendon.

Histologic analysis revealed that the connective tissue elements of the vincular system were more prevalent in the dorsal side of flexor tendon.

DISCUSSION

Our results demonstrate that dorsal side modified Kessler suture sustained significantly higher load to failure than volar side modified Kessler suture. Moreover, dorsal portions of flexor digitorum profundus tendon had significantly greater strength than volar portions of flexor digitorum profundus tendon.

Komanduri et al.[3] were the first to state that a dorsally placed core suture is a superior method of tendon repair. The authors attributed the results of their dynamic-cadaveric model to sheath friction and the biomechanics of the tendon pulley system. They concluded that the dorsal suture placement prevented gapping as the tendon was deformed in a volar direction with digital flexion. However they did not analyze the relative strength of the tendon substance itself. Our data demonstrate that their results may well be explained by regional variation in tendon strength, and of the suture-tendon interface, between the dorsal tendon and the volar tendon. Similar results have been reported in the shoulder. Nakajima et al.[5] reported that the bursal-side of the supraspinatus tendon were different histologically and biomechanically from the joint-side. They suggested that biomechanical differences in the supraspinatus tendon were due to the differences of tendon fiber diameter and density.

Recent in vitro studies have shown that intermittently loaded connective tissue cells are sensitive to changes in cellular shape and hydrostatic pressures. Stretching and distortion of the cells enhances the production of fibrous matrix while hydrostatic pressure enhances the production of cartilaginous matrix[6,7]. Giori et al.[8] found that regions of cartilaginous matrix and fibrous matrix formation and turnover correlate well with the gradient of hydrostatic compressive stress and distortional strain when a tendon is pulled over a pulley. These results support the existence of tissue character differences between dorsal and volar side flexor tendon.

We anticipate that quantitative investigations of the tendon tissue with biochemical and histological analysis, e.g., collagen typing and counting, may help to further elucidate the structure of the FDP tendon in an effort to refine suture placement and repair techniques.

REFERENCES

1. Lundborg, G. et al. Scan. J. Plastic. Recon. Surg., 14, 99-107, 1980.
2. Manske, P.R., J. Hand Surg., 13B, 237-245, 1988.
3. Komanduri, M. et al. Proceedings of the 11th ASSH Residents and Fellows Conference, Kansas City, MO, (pp.28), 1993.
4. Matthews, L.S. et al. J. Biomechanics, 1, 65-71, 1968.
5. Nakajima, T. et al. Katakansetu, 16, 103-108, 1992 (in Japanese).
6. Harris, A.K. et al. Nature, 290, 249-251, 1981.
7. Nakatsuji, N. et al. Nature, 307, 453-455, 1984.
8. Giori, N.J. et al. J. Orthop. Res. 11, 581-591, 1993.

INITIAL STABILITY OF INTACT AND INSTRUMENTED CERVICAL SPINAL SEGMENTS AS DETERMINED BY FLEXIBILITY TESTING

A.G.U. Brantley*, T.R. Oxland+, J.B. Koeneman*
*Harrington Arthritis Research Center, Phoenix, AZ 85006
+SpineTech, Minneapolis, MN 55414

INTRODUCTION

Two common surgical techniques for stabilizing the lower cervical spine involve the insertion of intervertebral bone grafts and/or attachment of bone plates. A new method for stabilizing and promoting fusion of the cervical spine involves the insertion of one or two threaded, porous titanium cylinders [NEK interbody implants] in the disc space following discectomy. These hollow baskets are currently being used for lumbar spinal fusion as the BAK™ interbody fusion system[1]. The purpose of this study was to evaluate the initial stability of cervical spinal segments implanted with one or two NEK interbody implants, as compared to interbody bone grafts.

REVIEW AND THEORY

The complex neuromuscular control of the human spine cannot be attempted in vitro. However, several methods have been used to produce motion of spinal segments during in vitro tests, including the application of eccentric loads (which result in combined moments and loads, e.g., flexion *and* compression), or the application of "pure" bending moments. Three dimensional intervertebral displacements during the applied loads/moments have been measured using various stereophotogrammetric techniques[2,3], or with the use of extensometers or LVDTs. In this study we used a non-constraining flexibility mode of testing[4] while recording continuous intervertebral rotations using small electrolytic tilt sensors (during bending) and an image-analysis system (during axial rotation). Only main rotations were considered. Motion parameters such as the range of motion (ROM), neutral zone (NZ) and elastic zone (EZ) were determined from moment-angular displacement curves.

PROCEDURES

A total of five fresh frozen (-20^{o} C) human cadaveric spine segments (C3 to C7) were used (ages: 37 to 72). The specimens were cleaned of soft tissues, leaving the discs and ligaments intact, and mounted in fixture cups using a dental acrylic (PMMA). The specimens were allowed to thaw to room temperature before testing. Each construct was mounted in a servo-controlled hydraulic test machine (Shore Western Materials Testing System) in a test fixture which, through a set of cables and pulleys attached to the superior fixture cup, allows for the application of pure bending moments without constraining the motion of the spinal construct. Testing was performed in load control in increments of 0.5 Nm to a maximum of 1.5 Nm to simulate flexion, extension, lateral bending (right and left), or axial rotation (right and left). The spines were pre-conditioned at least three times before measurements were made. Each increment of 0.5 Nm was held constant for 45 seconds to allow for creep. Main motion (i.e., rotation) of three intervertebral bodies with respect to a global reference frame was recorded during the application of each moment. Rotations during flexion-extension and lateral bending tests were measured using small electrolytic tilt sensors (The Fredericks Company, Huntington Valley, PA) attached to the posterior processes of C4, C5 and C6. The output from the tilt sensors was recorded digitally, together with the applied load/bending moment, using a computer and LabTech Notebook™ software, and could be viewed continuously on the computer screen during testing. The angular positions of rigid posts extending from each of the three vertebral bodies during the axial torque tests were recorded and analyzed using Optimas™, an image analysis system. Each specimen was tested intact and again with the following instrumentations: one 10 mm NEK at C4-C5, an iliac crest bone graft at C5-C6 (using a modified Smith-Robinson technique), and two bilateral 6 mm NEKs at C6-C7. Contact radiographs were obtained before and after implantation. Intervertebral rotations were determined from the global rotations for each case by subtracting the adjacent inferior vertebral rotation. The ROM , NZ and EZ were determined for each case. Results were analyzed using a paired Student's t-test (two-tailed), with each spine as its own control.

RESULTS

The average ROMs for the intact spines are shown in Table 1. The average ROMs and NZs for the implanted constructs expressed as % of corresponding intact segments are shown in Table 2. There was a trend towards a decreased ROM at all the three instrumented levels during all three load configurations. However, the relative decrease in ROM became statistically significant only in the following cases: during flexion-extension with the 10 mm single NEK at C4-C5 ($P<0.01$), during lateral bending with the bilateral 6 mm NEKs at C6-C7 ($P<0.01$), and during lateral bending with the interbody bone graft at C5-C6 ($P<0.03$). The decrease in ROM (the sum of NZ and EZ) was due to a decrease in NZ to a greater extent than EZ. The relative decrease in NZ was significant ($P<0.02$) only in two cases: during flexion-extension with the single NEK and during lateral bending with the bilateral NEKs.

DISCUSSION

The average ROMs for the intact spines correlate well with what has been reported in the literature[5]. Some of the variability in the data could be correlated with implant and bone graft positioning, as seen from the contact radiographs, suggesting that the test method is capable of measuring differences in surgical placement. Although not statistically significant, there were trends towards decreased ROMs and NZs for both the NEK interbody implants (single 10 mm and bilateral 6 mm) and the interbody bone graft. A better control of implant/graft positioning would probably reduce the scatter and make the changes statistically significant.

In summary, the bilateral NEKs and interbody bone graft had a similar reducing effect on the ROM during lateral bending, while the single NEK did not seem to decrease the ROM as much. However, both NEK interbody implant configurations (single and bilateral) seemed to reduce the ROM more than the interbody bone graft during flexion-extension.

Table 1 Average ROM's for Intact Segments in Degrees (stdev)

Level	Axial	Flex-Ext	Lateral
C4-C5	12.2 (7.2)	16.8 (3.8)	14.6 (4.3)
C5-C6	8.6 (3.2)	12.7 (4.8)	7.2 (3.0)
C6-C7	9.0 (2.0)	12.2 (1.6)	9.6 (2.7)

Table 2 ROM (top) and NZ (bottom) as % of Intact (stdev)

ROM	Axial	Flex-Ext	Lateral
10 mm NEK	71.8 (35.7)	**58.5 (15.3)***	88.3 (52.6)
bone graft	91.2 (32.3)	78.5 (60.1)	**45.0 (34.5)*****
2x6mm NEK	64.2 (37.8)	64.0 (40.4)	**37.9 (21.6)***
NZ	**Axial**	**Flex-Ext**	**Lateral**
10 mm NEK	48.4 (31.9)	**57.2 (20.3)****	75.6 (54.5)
bone graft	67.3 (43.9)	74.8 (64.7)	42.2 (37.3)
2x6mm NEK	48.0 (63.2)	66.2 (66.0)	**26.8 (32.4)****

*P<0.01

**P<0.02

***P<0.03

REFERENCES

[1]Kuslich, S. et al. "The BAK Interbody Fusion System: Early Clinical Results of Treatment for Chronic Low Back Pain", Proceedings of the 8th Ann. Meeting of NASS, San Diego, CA (p.175), 1993.

[2]Sawa, A. et al. "Effects of Pedicle Screw Instrumentation and Disk Removal on 3-D Motion of Lumbar Spinal Columns Subjected to Various Loads", Proceedings of the 15th Ann. Meeting of the ASB, Tempe, AZ (pp.292-293), 1991.

[3]Oxland, T. et al. "Axes of Motion of Thoracolumbar Burst Fractures", J Spinal Disord, Vol. 7, No. 2, 1994.

[4]Crawford, N. et al. "An Apparatus for Applying Pure Unconstraining Moments to Spine Segments *In Vitro*", (Submitted to Spine, 1994).

[5]Panjabi, M. et al. "Basic Biomechanics of the Spine", Neurosurgery, Vol. 7, No.1, 1980.

ACKNOWLEDGEMENTS

This work was funded by SpineTech, MN. The authors wish to thank Dr. Thomas Fry for all the surgical procedures, and Thomas Hansen for assistance during testing.

DEVELOPMENT OF 3-D SURFACE RESPONSE OF TRUNK STRENGTH AS A FUNCTION OF TRUNK POSITION AND ANGULAR VELOCITY

K. A. Khalaf, M. Parnianpour, and P. J. Sparto

Biodynamics Laboratory, The Ohio State University, Department of Industrial and Systems Engineering, 1971 Neil Avenue, Columbus, OH 43210

INTRODUCTION

Occupationally related low back disorders continue to be a major concern in industrialized countries creating an increasing need for ergonomists and clinicians to develop effective means of quantifying trunk performance. Until recently, the majority of ergonomic assessment of trunk strength was static in nature. Marras et al. (1992) emphasized the significance of studying dynamic parameters such as trunk angular velocity and acceleration during trunk motion . The purpose of this study was to investigate the effect of trunk position angular velocity on trunk muscle strength during isometric, isokinetic, and isotonic exertions.

REVIEW AND THEORY

To determine the ability of any individual to complete a given lifting task, a series of models are being developed to quantify the required functional capacity of different joints during diverse lifting tasks. In addition, a data base of actual joint capabilities is being compiled for these joints (Khalaf et al., 1994). The question of how to best assess strength is still a topic of intense discussion. Khalaf et al. (1994) indicated that isometric and isokinetic modes of testing are more efficient methods of obtaining strength as a function of joint position and velocity as compared to the isotonic mode. In isotonic testing, it is difficult to obtain strength values for desired combinations of positions and angular velocities, since in this mode there is no prior knowledge what combination of joint position and velocity will be observed. This study attempts to expand the data base available for trunk performance by testing over a wide range of velocities.

PROCEDURES

Ten healthy male normal subjects participated in this study. The mean (s.d) age, mass, and stature of the subjects were 26..2 (3.8) years, 85.1 (14.0) kg, and 178.6 (10.7) cm, respectively. The strengths and speeds of the subjects were studied using the KIN-COM (Asymmetric Reference Frame) muscle testing and training system (Chattecx corp.) Three modes of testing were used: isometric, isokinetic and isotonic. In the isometric testing mode, the subjects were asked to flex and extend maximally at hold angles of 0, 10, 20, 30, and 40 degrees of trunk flexion. During the isokinetic mode, the subjects performed maximum exertions at velocities of 10, 20, 40, 60, 80, and 100 degrees/sec through a range of motion of 40 degrees. These values were selected based on values from literature as well as the results of the coordinated lifts performed in a previous study (Sparto et al., 1993). During isotonic tests, the velocities and torques were measured while the resistances were fixed. the resistances used were 50 , 100, 150, 200, and 250 Newtons in extension and 30, 60, 90, 120, and 150 Newtons in flexion.

RESULTS

The analysis of variance for the isometric and isokinetic tests are provided in tables 1 and 2. For the isometric exertions, a Tukey post-hoc test illustrated that the extension strength at higher angles (20, 30, and 40 deg) was significantly greater than that at lower angles (0 and 10 deg). For example, the extension strength at 40 deg was 26.4% higher than that at 0 degree. There was no difference between sagittal flexion and extension strength. There was also no interaction between the direction of exertion and posture. In the isokinetic mode, the MANOVA for the strength parameters was significant for the effect of velocity, as well as the effect of angular position. A test of pairwise comparisons showed that trunk extension strength was significantly lower at 10 degrees of trunk flexion than 20, 30, or 40 degrees. Conversely, for the effect of the velocity, the flexion torque was significantly greater at lower velocities. In addition, while there was no difference between sagittal flexion and extension, the interaction between the direction of exertion and posture was significant. The interaction between the direction of exertion and velocity was not significant. Figure 1 is a plot of the isometric extension torque as a function of the trunk position. Figures 2 and 3 are 3-D surface plots of torque as a function of position and angular velocity for trunk isokinetic extension and flexion respectively.

DISCUSSION

It can be seen from the tabular and graphical results that trunk strength is highly dependent on trunk position and angular velocity. This exemplifies that there is not one unique method to objectively quantify trunk performance. Since title I of the ADA went into effect, more than 17% of the 12,000 claims filed with the EEOC under the ADA have been related to back disorders. Therefore, quantification of trunk performance must take into consideration the demand of the job as well as the individual strength profile. This study will result in mathematical functions fitted to the generated surfaces and/or series of look-up tables that will aid in the determination of whether an individual can lift based on the demand profile established previously (Sparto et al., 1993). The results of the isotonic test were

inconclusive due to technical limitations of the dynamometer. The isotonic mode can best be called isoresistive: the dynamometer provides the resistance set by the experimenter. When the muscle torque exceeds the resistance, the initial isometric condition changes to isoresistive condition where the joint velocity is allowed to vary. Although the limit of 250 deg/sec was sufficient for the lower extremity testing, the device imposes a limit of 100 degrees/sec for back testing. This caused the subjects to switch to the isokinetic mode. Future studies should consider modifying the existing dynamometer in order to incorporate higher velocities.

ACKNOWLEDGMENTS

The authors acknowledge partial support from NIDRR, REC grant #H133E0009 and the Ohio Bureau of Worker's Compensation, Division of Safety and Hygiene. In addition, William Marras, Ph.D. is gratefully acknowledged for his invaluable assistance.

REFERENCES

1. Khalaf, K.A., Parnianpour, M., and Sparto, P.J, " The comparative evaluation of isotonic and isokinetic modes of testing with ergonomic and rehabilitation perspective," *RESNA*, Nashville, T.N., 1994, in press.
2. Marras, W.S., "Toward an understanding of dynamic variables in ergonomics," *Occupational Medicine*, Vol.7(4), 1992, pp. 655-677, 1993.
3. Sparto, P.J., Khalaf, K.A., and Parnianpour, M.," The effect of load, speed, and mode of lift on the joint energetics during unconstrained lifting and lowering activities," *ASME Advances in Bioengineering*, pp. 467-470, 1993.

Table 1. Results of MANOVA and ANOVA (p-values) on the effect of trunk position on isometric strength

	MANOVA	ANOVA
Sagittal Strength	.0001	
Extension Flexion		.0001 NS

Table2. Results of MANOVA and ANOVA (p-values) on the effect of trunk position and velocity on trunk strength

	MANOVA		ANOVA	
	ANG	VEL	ANG	VEL
Sagittal Strength	.053	.052		
Extension Flexion			.029 NS	NS .011

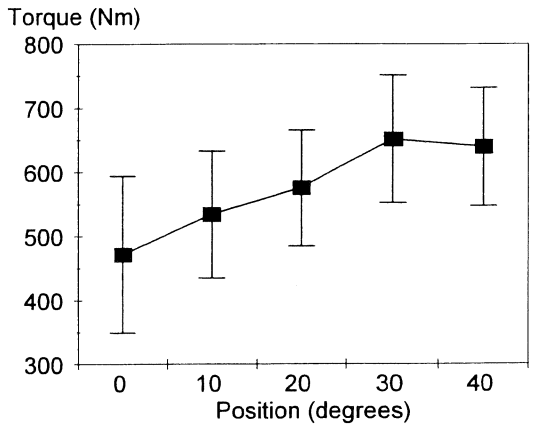

Figure 1. Isometric back extension strength as a function of trunk position

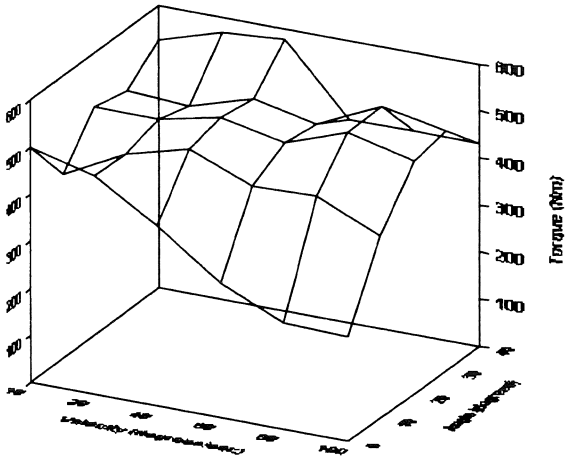

Figure 2. Trunk extension strength as a function of trunk position and angular velocity

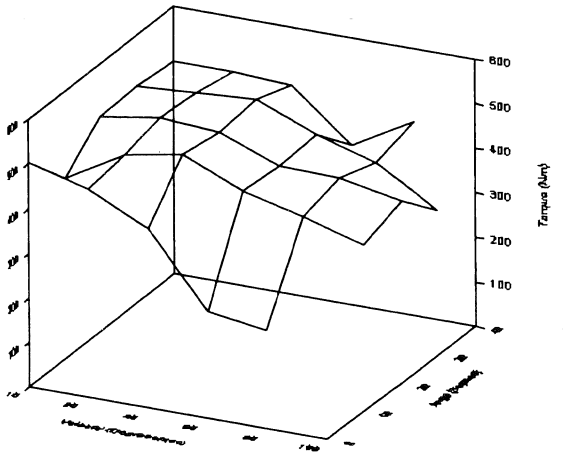

Figure 3. Trunk flexion strength as a function of trunk position and angular velocity

SESSION 1:
ORTHOPAEDICS

A BIOMECHANICAL ANALYSIS OF DEEP AND SUPERFICIAL EPITENDINOUS SUTURES

E. Diao, J.S. Hariharan, J.C. Lotz* and O. Soejima

Hand and Microvascular Surgery Services, Department of Orthopedic Surgery
University of California San Francisco, San Francisco, CA 94143-0728

Orthopedic Bioengineering Laboratory, Department of Orthopedic Surgery
University of California San Francisco, San Francisco, CA 94143-0514

INTRODUCTION

The aim of flexor tendon repair in the hand is to re-connect tendons that have been lacerated or ruptured and to restore maximal function. The particular anatomy of the flexor tendons, being within a sheath and pulley system, dictates that not only must tendons be repaired with sufficient congruity to allow healing, but the repair must be strong enough to allow some form of mobilization to reduce adhesion formation.

REVIEW AND THEORY

Recent studies [Gelberman et al. (1987); Seyfer et al. (1989)] have shown that early protected mobilization following primary tendon repair improves tendon gliding and function. However, currently popular repair techniques [Kessler (1987); Tsuge et al. (1977)] do not provide sufficient tensile strength to withstand the forces that would be associated with early active mobilization. Given the current knowledge about tendon healing, one can expect that an active motion mobilization program would offer substantial benefits.

While the running epitendinous suture was initially advocated as a cosmetic stitch to improve gliding, recent studies suggest that this peripheral suture can be an important structural component of the repair. However, no guidelines exist on epitendinous suture techniques. Moreover, the interaction between core and epitendinous suture in achieving repair strength has not been addressed. In order to determine whether the penetration depth of the epitendinous suture significantly affects the strength of the tendon repair, we performed tensile tests on two paired groups of repaired flexor digitorum superficialis (FDS) tendons: one group had superficial epitendinous suture (SES) placement, while the other group had deep epitendinous suture (DES) placement.

PROCEDURES

We isolated 12 FDS tendons from four fresh frozen human hands over a length of 12 cm. starting distally at the chiasm of Camper. We severed the distal section and repaired it using the SES technique. We severed the proximal section and repaired it by the DES technique.

- CORE: When performing all the tendon repairs, 4-0 Dermalon (monofilament nylon) was placed in the tendon using the modified Kessler (1987) grasping suture.
- SES: 6-0 Surgilene (monofilament polypropylene) was placed in a running fashion with needle passage through epitenon and only superficial tendon (Fig. 1A).
- DES: 6-0 Surgilene was then placed in a running fashion with needle passage through epitenon and tendon substance penetrating to half the distance to the center of the tendon (Fig. 1B).

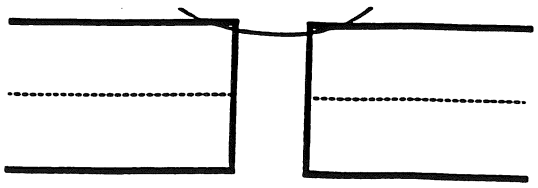

Fig 1A: SES repair

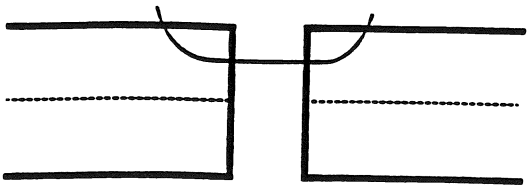

Fig. 1B: DES repair

The two repairs on each tendon were paired, and acted as an internal control. We then mounted them on a servo-hydraulic materials testing machine (MMED) and distracted them longitudinally at the rate of 2 cm/min. to failure. We recorded the tendon loads and grip displacements throughout the tests, with the tendons kept immersed in physiological saline at room temperature. We recorded each test on video (Kodak P6-120) to allow the analysis of the failure patterns of each repair. We tested differences between two means and between multiple means for statistical significance by Student's t test and by one way analysis of variance (ANOVA), respectively.

RESULTS

The breaking strength and the stiffness of the DES repair were observed to be 80 percent higher than those of the SES. The mean failure load of DES was 38.96 ± 13.88 N (SD), while that of SES was 21.68 ± 3.56 N (SD); P<0.005 (Fig. 2).

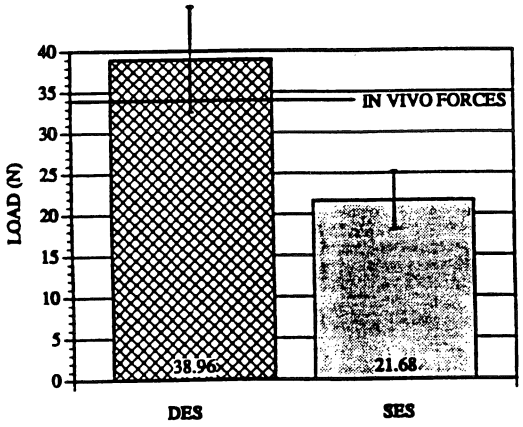

Fig. 2: Relative strength of DES and SES

DISCUSSION

We asked whether the depth of the epitendinous suture affects the strength of the tendon repair. Our data indicate that a deep penetration of the epitendinous suture can increase the strength of the repair by 80 percent over standard techniques. While the DES repair failed catastrophically with a rapid gap formation, the SES repair failed more gradually by a typical pattern of alternate breaking and unwinding of the peripheral sutures (Fig. 3). The core suture failed by pulling out of the substance of the tendon in each case and not by suture or knot failure. Failure of the core suture occurred after failure of the peripheral suture in both groups.

Our results show that the DES can tolerate loads up to 38.96 N before failure. Although ours is an in vitro study that does not look at tendon healing as a factor affecting the ultimate result, it gives us a scientific basis for evaluating the biomechanical properties of the peripheral epitendinous suture that was long thought to be merely a "cosmetic stitch". Our findings suggest that this peripheral suture can be an important structural component of the overall tendon repair and definitely imparts strength to the repair. Since digital flexor tendon forces up to 34.32 N (3.5 kgf) have been measured in vivo during active unrestricted finger motion [Schuind et al. (1992)]. DES theoretically allows for active unrestricted finger motion immediately after repair. Several techniques [Silfverskiold et al. (1993); Lee (1990); Pulvertaft (1965)] have been described recently, which are stronger than conventional methods. These methods have the disadvantage of being relatively complicated and time consuming in the hands of the average hand surgeon and have not enjoyed widespread use. Further, some of these techniques [Lee (1990); Pulvertaft (1965)] cause widening of the repair site, thereby, distorting the normal tendon anatomy.

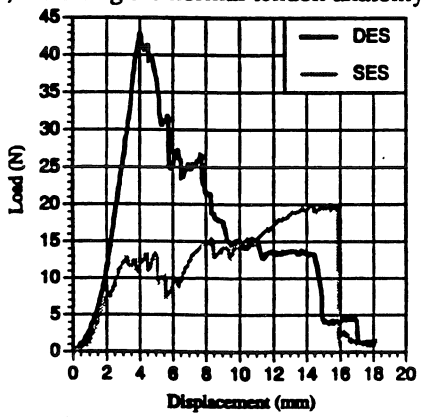

Fig. 3: Typical load-to-failure curves

CONCLUSION

Our results indicate that DES is a much simpler technique and yet offers the potential for early active mobilization.

REFERENCES

Gelberman, RH. et al. Tendon surgery in the hand, (pp. 170-177), St. Louis: The CV Mosby Company, 1987.

Seyfer, AE. et al. Plast. Reconstr. Surg., 83, 122-128, 1989.

Kessler I. Tendon surgery in the hand, (pp. 126-132), St. Louis: The CV Mosby Company, 1987.

Tsuge K. et al. J Hand Surg., 2, 436-440, 1977.

Silfverskiold KL. et al. J Hand Surg., 18A, 58-65, 1993.

Lee H. J Hand Surg., 15A, 953-958, 1990.

Pulvertaft RG. Am J Surg., 109, 346-352, 1965.

Schuind S. et al. J Hand Surg., 17A, 291-298, 1992.

RESTORATION OF LATERAL PINCH IN TETRAPLEGIA: A BIOMECHANICAL COMPARISON OF TWO SURGICAL METHODS

A. Matityahu *, A. Weiss **, B. Parks ***, and S. Siegler ***

* Hahnemann University, Philadelphia PA 19102
** Department of Orthopaedic Surgery and Rehabilitation, Hahnemann University, Philadelphia PA 19102
*** Drexel / Hahnemann Biomechanics Research Laboratory, Philadelphia PA 19102

INTRODUCTION

Patients who lose nerve function of the muscles in their arms and hands due to trauma of the spinal cord at level C5 - C6 lose hand function. Such people are, in many cases, quadriplegics who rely completely on others in their daily life. In order to help these people gain some autonomy, a surgical procedure was devised by E. Moberg (1975), which partially restores the use of the hand by re-establishing a key grip type of pinch. The flexor of the thumb is sutured to the radius. Therefore, when the wrist is extended, a passive flexion of the thumb occurs. This so-called "lateral pinch" allows patients to grasp small objects such as pens, keys, and screws between the thumb and the side of the index finger.

One problem with the surgical procedure above is that it is accompanied by an undesirable flexion of the interphalangeal (IP) joint of the thumb. To overcome this problem, Moberg suggested immobilization of the IP joint using a 2mm Kirshner (K) wire. The disadvantages of immobilizing the IP joint using this procedure include recurrent infections, and tenderness at the tip of the thumb, as well as lack of laxity during non-use. To solve the problems above, a modified Moberg procedure - the split FPL tendon transfer - was introduced by A. Weiss. In this procedure, stabilization of the IP joint during lateral pinch is achieved by transferring the radial half of the Flexor Pollicis Longus (FPL) tendon to the Extensor Pollicis Longus (EPL) tendon distal to the metacapophalangeal (MP) joint and proximal to the IP joint. The tendon transfer procedure provides an added extension moment about the IP joint which keeps it in a stable configuration during lateral pinch.

One concern of the modified Moberg procedure is that due to the tendon transfer, the efficiency of the lateral pinch is diminished. We therefore conducted a biomechanical study in which the efficiency (here defined as the ratio between the force applied to the flexor tendon and the pinch force - the smaller the ratio, the higher the efficiency) of the lateral grip of the modified Moberg procedure was compared with the original procedure in vitro.

REVIEW AND THEORY

The Moberg procedure is shown in Figure 1 and consists of two major steps. First, the attachment of the tendon of the FPL to the radius (tenodesis). Second, the stabilization of the IP joint of the thumb using a K wire.

To solve the clinical complications associated with the use of a K wire, the modified Moberg procedure was introduced by A. Weiss (Figure 2). As shown in this figure, the distal radial side of the FPL is cut and sutured to the EPL tendon distal to the MP joint and proximal to the IP joint. As can be further seen from this figure, when a force is generated in the FPL tendon (F_{FPL}), the radial half of the FPL creates an extension moment (F_{FPLe}) about the IP joint. This extension moment stabilizes the IP joint during thumb flexion.

This study was conducted to test, in vitro, the validity of the hypothesis that the modified Moberg procedure does not reduce the efficiency of lateral pinch.

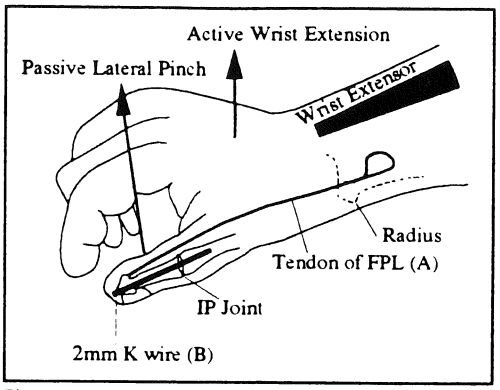

Figure 1 - The Moberg procedure. A) The tendon of the FPL is attached to the radius. B) A 2mm Kirshner (K) wire immobilizes the interphalangeal (IP) joint (Revised from Moberg, 1975).

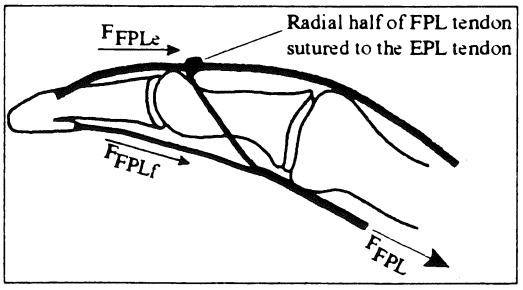

Figure 2 - The split FPL tendon transfer suggested by A. Weiss. F_{FPLe} is the extensor moment produced by the radial half of the FPL. F_{FPLf} is the flexor moment produced by the ulnar half of the FPL. F_{FPL} is the force applied by the FPL tendon.

PROCEDURES

The experiment was conducted on two fresh cadaver hands. The experimental setup is shown in Figure 3. The ulna and radius were immobilized with screws to the test board as shown in this figure. A metal plate was placed above the 3rd digit such that the thumb was positioned above it. Force transducer 1 was introduced between the plate and the tip of the thumb to measure the lateral pinch force. The FPL tendon was isolated and attached to a metal wire. The wire was placed over a pulley so that its direction approximated the line of action of the FPL tendon. This wire was then attached to force transducer 2, which monitored the force applied to the FPL tendon. The procedure consisted of applying forces to the FPL tendon and recording, on a computer, both the lateral

pinch force and the force applied to the FPL tendon. The experiment was conducted under five different conditions: 1) Intact thumb (Figure 4a). 2) IP joint mobilized with a K wire (Figure 4b). 3) With K wire in place and dissected A2 and oblique pulleys of the thumb (Figure 4c). 4) With K wire in place and the radial half of the FPL tendon cut at its most distal insertion (Figure 4d). 5) Suture of the radial half of the FPL to the EPL and removal of K wire (Figure 4e). Three repeated tests were conducted for each condition.

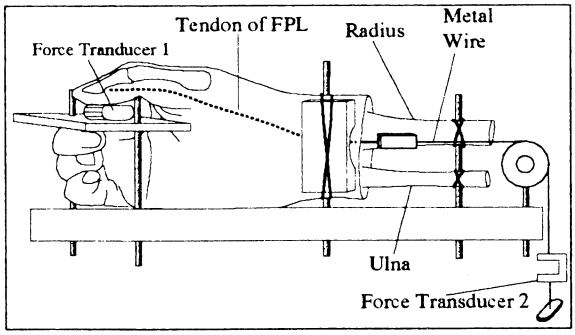

Figure 3 - Schematic diagram of the experimental setup using two force transducers and immobilizing the wrist, ulna, and radius. For illustration purposes, the second digit is not shown.

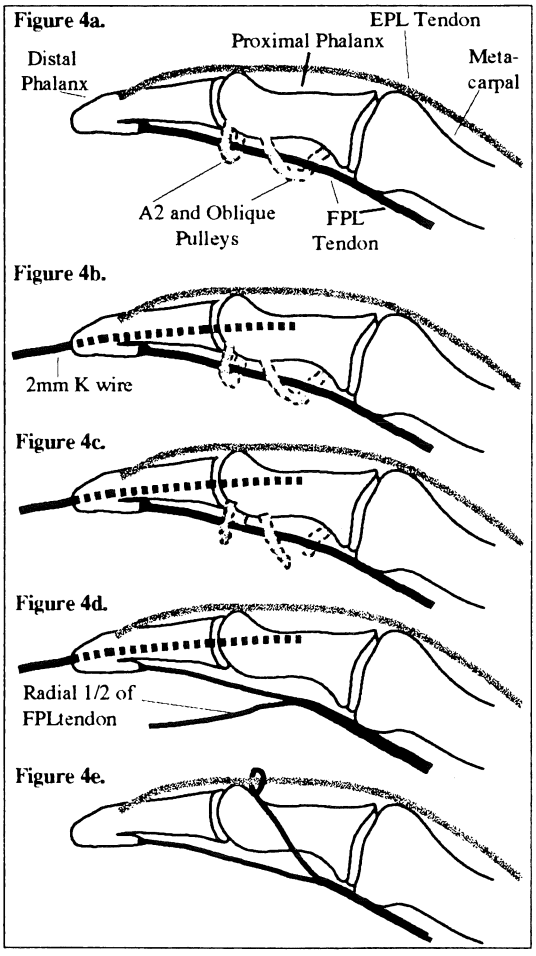

Figure 4 - a) In tact thumb. b) K wire immobilizing IP joint c) A2 and oblique pulleys cut. d) Radial half of FPL tendon cut. e) Radial half of FPL tendon sutured to EPL.

RESULTS

For each condition, the force applied to the FPL tendon was plotted as a function of the lateral pinch force. The results suggest that for the range of applied forces between 0 LB and 10 LB, the relation between the FPL force and lateral pinch force is linear. The least-square procedure was then used to find the best fit line for the applied FPL force versus the lateral pinch force. An example of this data, comparing the load transfer relationship with the IP joint stabilized using a K wire versus the IP joint immobilized through the use of the split FPL tendon transfer procedure, is shown in Figure 5. The slopes of all of the fitted lines for all the tested conditions were calculated. These are as follows: Condition 1 - 4.165, Condition 2 - 4.685, Condition 3 - 4.180, Condition 4 - 3.982, Condition 5 - 4.136. A multivariable Anova analysis of variance showed no significant differences (P>.05) in force transmission between any of the five conditions.

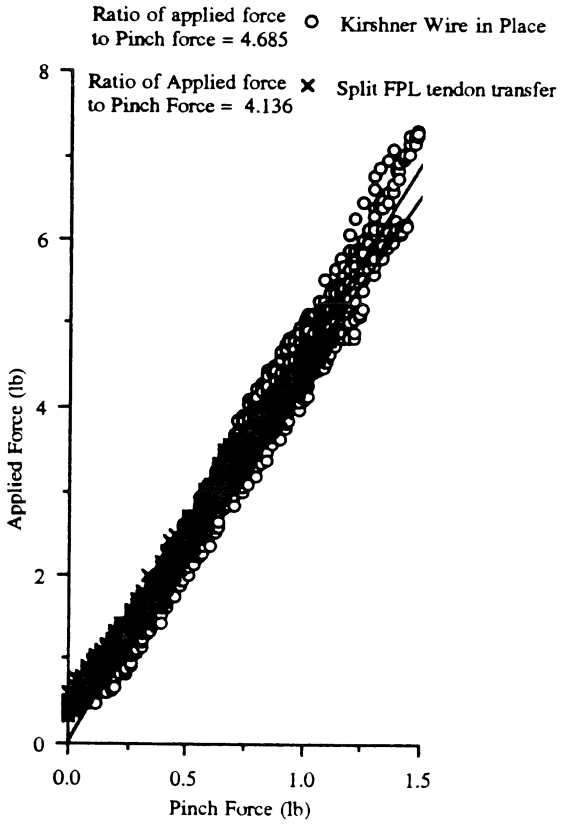

Figure 5 - Applied force to FPL tendon versus pinch force between thumb and index finger.

SUMMARY AND CONCLUSIONS

The preliminary results obtained in this study indicate that the modified Moberg procedure, which is based on the split FPL tendon transfer, does not decrease the efficiency of lateral pinch as compared to the original Moberg procedure. It therefore appears that this procedure is advantageous to the original Moberg procedure since it avoids the clinical complications associated with the use of a K wire.

REFERENCES

Moberg, E. Hand Surgery and the Development of Hand Prosthesis, Scandinavian Journal of Plastic & Reconstructive Surgery, 9(3), 227-30, 1975.

IN VITRO REPRODUCTION OF SPONTANEOUS HIP FRACTURE BY SIMULATED MUSCLE CONTRACTIONS

K. H. Yang, K. Shen, C. K. Demetropoulos, A. I. King
Bioengineering Center
P. Kolodziej, R. S. Levine, R. H. Fitzgerald, Jr.
Dept. of Orthopaedic Surgery

Wayne State University, Detroit, Michigan

ABSTRACT Two distinct loading conditions were developed to test proximal femurs *in vitro*. Cervical fracture was created when a femur was loaded along the line of the iliopsoas with an average fracture force of 3.4 kN. Trochanteric fracture was produced when a femur was loaded along the line of the gluteus medius with an average fracture force of 2.7 kN.

INTRODUCTION Hip fracture is most prevalent among the elderly who are prone to an exponential increase in the incidence with age [2]. Osteoporosis is commonly considered the leading cause of hip fracture. Additionally, a majority of investigators concurred that most hip fractures are the results of falls [6]. Hayes et al. [3] suggested that falls directly onto the hip in the elderly caused hip fracture.

Although previous studies have been able to consistently produce hip fractures employing several techniques, resultant fractures are not able to control the fracture site or pattern [4,9]. These discrepancies suggest the need for an alternative hypothesis. This study was designed to test the hypothesis of muscle induced spontaneous hip fracture. It was the goal of this study to establish two distinct loading conditions that can consistently produce clinical fracture patterns *in vitro* in the cervical and trochanteric regions of the femur.

MATERIALS AND METHODS Fourteen paired cadaveric femurs were harvested and stored at -20 C. All specimens were evaluated by X-ray before testing to assure that there were no defects. Before testing, each femur was thawed to room temperature. Soft tissues were removed and discarded. Testing was performed on an Instron testing machine (Canton, MA). Each femur was sectioned at midshaft and placed in a jig consisting of a collar mounted to a steel alignment shaft. The alignment shaft was composed of two segments joined at an angle of 135° so as to position the femur at 45° angle with respect to the Instron loading direction. The axis of the femoral neck was positioned perpendicular to direction of loading. The alignment shaft was inserted into a linear-bearing equipped holder to allow free linear displacement of femur in a direction orthogonal to the Instron table. The femoral head was placed in an acetabular cup fixture to permit free rotation of the head. The entire construct was fixed to the Instron table (see Figure 1). Force was applied to the femur, with a belt originating from either the greater or lesser trochanter and terminating at the Instron loading head, under displacement control at a rate of 50 mm/sec. All specimens were loaded to failure. Data were recorded using Tektronix TestLab (Beaverton, OR).

RESULTS All specimens loaded at the lesser trochanter, to simulate iliopsoas contraction, fractured at the femoral neck, while those loaded at the greater trochanter, to simulate gluteus medius contraction, fractured in the trochanteric region. Within each pair of specimens, force and energy at fracture were always greater when fracturing at the femoral neck. Statistical tests showed differences of force and energy to be significant ($p=0.00817$ and $p=0.00348$, respectively). The fracture force and energy at fracture are listed in Table 1. For all specimens, the average force at failure was 3040 ± 722 N, while average energy at failure was 57 ± 18 J.

DISCUSSION AND CONCLUSION Visual and X-ray inspection of tested specimens showed that fractures produced in this study resembled the patterns described in the AO manual. Unlike other studies [9], the testing procedure in this study did not cause any damage to the femoral head. The two loading conditions consistently produced exclusive fractures. Consequently, fracture type could be predicted from the loading site.

To date, the association between fall and hip fracture has been well documented. While the increased risk of fall among the elderly is thought to be responsible for the increased

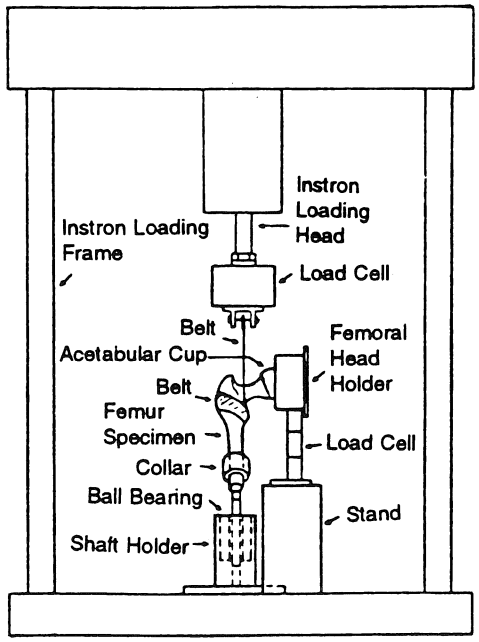

Figure 1: Testing Setup

TABLE 1. FRACTURE FORCE AND ENERGY

Cadaver No.	Loading At Greater Trochanter			Loading At Lesser Trochanter		
	Side	Fracture Force (N)	Work to Fracture (J)	Side	Fracture Force (N)	Work to Fracture (J)
187	L	2213	33.3	R	2778	44.6
588	R	2609	36.0	L	3924	57.5
607	L	2739	62.2	R	4077	82.1
768	R	2519	45.4	L	3244	79.7
900	L	3762	64.1	R	3820	81.1
894	R	3254	65.8	L	3486	67.1
886	L	1670	30.2	R	2471	48.7
Average	-	2680	48.1	-	3400	65.8
Std. Dev.	-	680	15.6	-	604	15.8

frequency of hip fracture in this population, the incidence of fall does not increase 30 fold as does the incidence of hip fracture between the ages of 50 to 80 [6]. Hayes et al. [3] reported that the energy required to fracture the femur *in vitro* was about 10% of the energy available in a typical fall. Yet, fewer than 2% of falls resulted in hip fractures. Additionally, should a person be moving forward, the resulting fall should be in the sagittal plane and not on the hip as hypothesized. Furthermore, a survey of side impact car accidents (National Accident Sampling System), a direct blow to the greater trochanter does not generally result in a femoral fracture, but rather a pelvic and an acetabular fracture. Therefore, although a well documented association between fall and hip fracture exists, a direct causal relation between the two has yet to be proven.

Periodically, literature in the field has cited reports of hip fracture without a history of violence. Kelly [5] reported that some patients receiving electro-convulsive therapy sustained fractures of the femoral neck due to sudden muscular contractions. Smith [8] reported two cases of hip fracture without a fall, in which the patients sustained femoral neck fracture due to sudden abnormal movements. It was the belief of Smith [8] that non-traumatic fracture was produced by the external rotators of the hip. Michele [7] proposed a mechanism for spontaneous fracture resulting from contraction of the iliopsoas muscle.

For spontaneous hip fractures, it has been hypothesized that because osteoporotic bone possesses a diminished capacity to repair microfractures, bone accumulates microscopic stress fractures with age that may diminish bone strength [2]. This study showed the average fracture force of all tested specimens to be approximately four times bodyweight (BW), given an average body weight of 778 N (175 lbs). It has been reported that during flexion of the extended hip, the peak force produced by the iliopsoas could be as high as 2.6 times BW, and during toe off, the peak force produced by the gluteus medius could be 1.2 times BW [1]. Thus, in an abnormal movement, it is reasonable to expect a muscle to generate a force equal to three or four times BW. Consequently, the misfiring of a muscle could produce forces capable of inducing fracture. Therefore, the combination of an osteoporotic bone and improper muscle contraction could cause an elderly individual to sustain a hip fracture prior to falling. Considering the chosen loading sites, a close parallel can be drawn between the force generated in testing and the force generated by a muscular contraction *in vivo*. Anatomical inspection shows greater trochanteric loading to simulate the force produced by the gluteus medius, while lesser trochanteric loading to simulate the force produced by the iliopsoas. Since these forces have produced fractures similar to those observed clinically, it seems possible that spontaneous fracture may offer a reasonable alternative to the theorized association between falls and hip fractures.

REFERENCES

1. Cheal, E.J., Spector, M., Hayes, W.C., 1992, "Role of Loads and Prosthesis Material Properties on the Mechanics of the Proximal Femur after Total Hip Arthroplasty", J. Orthop. Res., 10:405-422.
2. Cummings, S.R., Kelsey, J.L., Nevitt, M.C., O'Dowd, K.J., 1985, "Epidemiology of Osteoporosis and Osteoporotic Fractures", Epidem. Rev., 7:178-208.
3. Hayes, W.C., Myers, E.R., Morris, J.N., Gerhart, T.N., Yett, H.S., Lipsitz, L.A., 1993, "Impact Near the Hip Dominates Fracture Risk in Elderly Nursing Home Residents Who Fall", Calcif. Tissue Int., 52:192-198.
4. Hirsch, C., Frankel, V.H., 1960, "Analysis of Forces Producing Fractures of the Proximal End of the Femur", JBJS, 42B(3):633-640.
5. Kelly, J.P., 1954, "Fractures Complicating Electro-Convulsive Therapy and Chronic Epilepsy", JBJS, 36B(1):70-79.
6. Melton III, L.J., 1988, "Epidemiology of Fractures", *Osteoporosis: Etiology, Diagnosis, and Management*, Raven Press, New York, pp. 111-131.
7. Michele, A.A., 1962, *Iliopsoas*, Charles C. Thomas Publisher, Springfield, IL.
8. Smith, L.D., 1953, "Hip Fracture. The Role of Muscle Contraction or Intrinsic Forces in the Causation of Fractures of the Femoral Neck", JBJS, 35A(2):367-383.
9. Weber, T., Yang, K.H., Woo, R., Fitzgerald, R.H., 1992, "Proximal Femur Strength: Correlation of the Rate of Loading and Bone Mineral Density", ASME WAM, pp. 111-114.

A HYDROPHILIC SELF-ANCHORING COMPOSITE FOR ORTHOPEDIC DEVICES

A.N. Sharda, I.L. Kamel and R. Seliktar

Biomedical Engineering & Science Institute, Drexel University, Philadelphia, PA 19104
Department of Materials Engineering, Drexel University, Philadelphia, PA 19104
Department of Mechanical Engineering, Drexel University, Philadelphia, PA 19104

INTRODUCTION

A hydrophilic polymer matrix reinforced with a 3-D braided graphite structure is presented as a novel alternative to traditional metallic materials for orthopedic devices. This material has the mechanical properties of bone in the dry state. When fitted into a mold and immersed in an aqueous medium, its swelling tendency causes the application of a radial force on the mold, anchoring the material in place and enhancing bone deposition. A push-out test to determine the strength of the composite/mold interface yielded 8.3 MPa.; comparable to many porous-coated implants.

REVIEW AND THEORY

The adequate fixation of prosthetic components to bone represents the primary challenge of total joint replacements [Shirazi-Adl et al. (1993)]. There are two primary methods of fixing prostheses to bone; cementation and the use of a porous coating. The achievement of a permanent, stable joint remains elusive as loosening over the long-term remains the major complication [Shirazi-Adl et al. (1993); James et al. (1993); and Wang et al. (1993)]. In the case of cemented implants, many have suggested this is due to a poor cement-bone interface, while others maintain that the cement is too weak for use in these devices [James et al. (1993); and Nimb et al. (1993)]. To reduce the risk of loosening of cemented implants, efforts have been made to strengthen bone cement and reduce its crack propagation characteristics [Nimb et al. (1993)]. Suggestions to this effect have ranged from reinforcing the cement with fiber to using biodegradable cement that may allow bone ingrowth. More recent studies suggest that the cement/metal interface – not the cement/bone interface – is the weak link in these prostheses [James et al. (1993)].

Others have approached the bone-prosthesis interface by porous-coating the surface of prostheses to achieve fixation by bony ingrowth in the coating. Component stabilization by this method is achieved if the implant material is highly biocompatible and the coating has optimal pore size [Wang et al. (1993)]. Initial results of this fixation mechanism are encouraging, though with some limitations. For example, devices of this type need to be fully immobilized for days to weeks following surgery to allow bone to remodel in the pores [Shirazi-Adl et al. (1993); and Wang et al. (1993)]. The highest obtainable interfacial shear strength is approximately 35% of the shear strength of cortical bone [Wang et al. (1993)]. Also, the increase in metal ion release from these coated devices makes their long-term biocompatibility unclear [Wang et al. (1993)].

We propose a novel fiber-reinforced hydrophilic polymer material for the load-bearing portion of prostheses. When implanted in bone the swelling tendency of this material creates sufficient radial force to anchor the implant while stimulating bone deposition about the prosthesis. Indications from previous animal experimentation are that radiographic densification may be expected within 14-18 days post implantation. This accelerated healing if applied in a hip implant may be a distinct advantage to the patient; accelerating the schedule to use the prosthesis while eliminating the surgical cement problems altogether. In addition, the even force application by the implant should ensure a perfect fit and an even load distribution at the bone interface.

Preliminary work on a dynamic implant was carried out in our laboratory since the late 1970's [Greenberg, (1978); and Greenberg et al. (1978)]. In that research a crosslinked, hydrophilic polymer matrix was allowed to swell to a controllable level after implantation in a perfectly fitted location in bone. The tendency to swell permitted the implant to apply gradual pressure on the bone interface up to a maximum, predetermined level that can be tolerated without bone failure. This pressure induced the acceleration of the healing process at the implant site and resulted in increased bone mineralization at the implant interface [Greenberg et al. (1978)]. That material did not, however, possess the requisite mechanical properties for use in the weight-bearing component of an implant; maximum compressive yield stress and mean elastic modulus of the earlier material were 77.7 MPa and 4.4 GPa [El Basty et al. (1983)]. In the present investigation, composites with mechanical properties comparable to compact bone were produced. While details of the mechanical aspects of the composite cannot be discussed in the limited space available here, a summary of the mechanical properties, a push-out test, and a cytotoxicity test are presented.

PROCEDURES

Sample Preparation and Curing

Commercially available acrylic acid monomer inhibited with 200 ppm MEHQ, Allyl Methacrylate (AMA) monomer inhibited with 200 ppm HQ, and Azobisisobutyronitrile were used. All the ingredients were stored at room temperature and used as received except the AMA and Azobisisobutyronitrile, which were stored in a refrigerator (according to manufacturer directions) until used.

Polymer samples of 0.15–1.5M AMA in acrylic acid were produced by the free-radical method. A swelling study showed the optimum level of AMA as 0.37M. Similar solutions were combined with 3-D fiber structures to produce the composite samples. The fiber braids were

formed on a circular braiding machine with a 3 track by 28 column setup using 12K Celion® graphite fibers. The braids had outside and inside diameters approximately 13 mm. and 5 mm., resulting in fiber volume fraction approximately 0.25.

After polymerization the samples were incubated at 110°C for 1 hour to allow the consumption of unreacted species and to drive off free water. Then the temperature was raised to 150°C and held for 5 hours to allow the esterification reaction of the crosslinking agents with the unreacted carboxylic acid pendant groups of the poly(acrylic acid) chains.

Mechanical Testing of the Composite Samples

Compressive test

The composite samples were compression tested according to ASTM standard D-695-85 "Compressive Properties of Rigid Plastics." All tests were conducted without lubrication on an Instron Universal (model 1127) testing machine at a cross-head speed of 1 mm/min.

Tensile test

Samples approximately 11.2 cm. long were cut from the molds, representing a length to diameter ratio of approximately 8/1 and tested at crosshead speed of 1 mm-min. An extensometer with a 1 inch range was used in the tensile tests to accurately measure the change in length of the test section of the specimens.

Push-out Test

A composite specimen 25mm in length was placed in an aluminum mold approximately 7% oversized in diameter. The mold containing the specimen was immersed in Ringer's solution for 14 days. Afterward, the aluminum mold was mounted to allow clearance for sample extrusion on an Instron testing machine. An aluminum plunger was used to push the sample out of the mold at a crosshead speed of 5 mm/min.

Assessing the Cytotoxicity

A Direct Contact Test was conducted using rabbit corneal cells as described in the US Pharmacopoeia. This test is used to determine the cytotoxicity of various materials, and is related to the cells' suitability to be used in cell monolayer cultures due to their ability to attach to surfaces. The tests were conducted according to directions in 96-well plates where 3 wells contained the negative control, 3 the positive control, and 3 the test samples.

RESULTS AND DISCUSSION

Mechanical Properties

The compressive strength and modulus of the composite and, more importantly, the tensile modulus of the composite were all in the range of compact bone as shown in the table below:

Table 1 Mechanical properties of the composites.

	Comp. Str.	Comp. Mod.	Tens. Mod.
Compact Bone	180 MPa	18 GPa	18 GPa
Composite	280 MPa	20 GPa	25 GPa

The Push-out Test

The shear strength of the interface was calculated by dividing the maximum push-out force by the total mold area in contact with the specimen. This area is represented by the formula:

$$\text{Area} = \pi DH$$

where D is the diameter of the mold and H is the depth or thickness of its contact with the specimen. Using this method, the push-out strength of the composite was 8.3 MPa. This compares favorably with the 6-10 MPa values for Hydroxyapatite-coated specimens as described in literature [Cook et al. (1988); Dhert et al. (1991); and Soballe et al. (1990)].

The Cytotoxicity Test

The toxicity exhibited by the wells containing the test samples was near that of the negative control wells. Both the negative control and sample wells show a marked difference from the positive control wells, which contained a material designed to cause significant cell death. There were approximately 2.5× more cells in both the sample and negative control wells than in the positive control wells. In this protocol, then, the composite samples exhibited very slight toxicity. Using the grading method described in the US Pharmacopoeia, this material falls between grades 0 and 1, since less than 20% of the cells were "round, loosely attached, and without intracytoplasmic granules" but no "lysed cells" were present.

CONCLUSIONS

A few general conclusions can be derived from this work. These are:

- A material has been developed that in the dry state possesses the mechanical properties of bone.
- When immersed in an aqueous environment, it applies sufficient radial force to anchor itself in place. This force has been shown to enhance bone deposition about implants in previous animal experiments.
- The developed material exhibited little cytotoxicity in the Direct Contact Test protocol.

REFERENCES

Cook, S.D. et al. Clin. Orthop., 232, 225-243, 1988.

Dhert, W.J.A. et al. J. Biomed. Matr. Res., 25, 1183-1200, 1991.

El Basty, M.A. et al. J. Dent. Res., 62(6), 733-737, 1983.

Greenberg, A.R. Ph.D Dissertation, Biomed. Eng. Sci. Inst., Drexel University, 1978.

Greenberg, A.R. et al. J. Biomed. Matr. Res., 1978.

James, S.P. et al. J. Biomed. Matr. Res., 27, 71-78, 1993.

Nimb, L. et al. J. Biomed. Matr. Res., 27, 565-574, 1993.

Shirazi-Adl, A. et al. J. Biomed. Matr. Res., 27, 167-175, 1993.

Soballe, K. et al. Acta. Orthop. Scand., 61, 299-306, 1990.

Wang, B.C. et al. J. Biomed. Matr. Res., 27, 1315-1327, 1993.

BIOMECHANICAL INVESTIGATION OF BENDING RIGIDITY IN THE NORMAL HUMAN FEMUR AND ITS USE IN THE DESIGN OF A FEMORAL COMPONENT

Donald D. Anderson, Thomas A. Mutschler, and Scott A. Jones †

Biomechanics Research Laboratory, Allegheny-Singer Research Institute, Pittsburgh, PA 15212
† StelKast, Incorporated, Pittsburgh, PA 15212

INTRODUCTION

Investigators have established a high correlation between femoral implant bending rigidity and the presence of thigh pain following uncemented total hip replacement. Current femoral implants incorporate materials chosen to approximate the modulus of bone, novel distal stem geometries and the machining of slots in the distal stem, all features intended to decrease implant rigidity. While considerable effort has been expended in matching moduli and on distal stem geometry, little effort has been focused on the choice of a slot and its geometry. A general methodology was developed to consider the relationship between the details of a given implant and the bending rigidity of the bone/implant composite obtained with its use. The feasibility of a new slotted femoral implant design, with the orientation of the slot chosen so as to provide a bone/implant construct that more closely matches the bending properties of the intact femur, has been investigated.

REVIEW AND THEORY

Thigh pain following cementless total hip arthroplasty (THA) is common, occurring in 2-25% of patients in selected clinical series (Tronzo (1989)). Recent clinical study based on radiographic measures has linked the bending rigidity of an implant with the presence of thigh pain. Treating the femur as a hollow cylinder with a single characteristic bending rigidity and elastic modulus, Franks et al. (1992) established a high correlation between the ratio of bone to implant bending rigidity and the presence of post-operative thigh pain in a study group of 30 patients.

The manner in which a structure responds to bending moments is characterized by its bending rigidity, which is a product of its cross-sectional moment of inertia and its modulus of elasticity. As cross-sectional geometry of the femur varies along its length, its bending rigidity is also likely to vary. Since bone remodels to accommodate its mechanical environment, it seems reasonable to assume that the variation in bending rigidity along the femur is in some sense optimized to carry the moments to which it is subjected. Deviation from this characteristic bending rigidity owing to the implantation of a stiff femoral stem could directly explain the presence of thigh pain.

To date there have been few attempts at studying the relationship between bending rigidity in the intact femur and in the post-operative bone/implant composite. Based on simple design principles, Wright and Bartel (1988) presented a stem geometry chosen to minimize the decrease in bone tissue stress associated with implantation of a femoral component. Their analysis was based on assuming that endosteal and periosteal surfaces of the femur were, in cross section, concentric circles. Current implants feature materials chosen to approximate the modulus of bone, special stem geometries and the machining of slots in the distal stem of femoral implants, all intended to decrease implant rigidity. Of these approaches, the least effort has been focused on a choice of slot geometry.

The general methodology developed for the current investigation involves determining the bending properties of intact femurs *in situ*, characterizing the changes in bending properties associated with placing a given implant within those femurs, and finally modifying the implant design until some optimal bending properties are achieved in the final bone/implant construct. The specific objective was to assess the feasibility of an altered slot orientation, chosen to provide a bone/implant construct that more closely matches the bending properties of the intact femur.

PROCEDURES

Axial CT scans of the proximal femur were obtained from 8 subjects (3 female, 5 male) of mixed age. The scans were ported to a Sun workstation, running software capable of evaluating cross-sectional moments of inertia for bone CT sections (EXTRACT software - Bartel et al. (1988)). Briefly, the analysis involved slice-by-slice identification of the femur using interactively-guided boundary detection, the assignment of modulus values for each pixel within the femur based on CT #, and finally the computation of the modulus-weighted centroids and the modulus-weighted bending rigidity terms (EI_{XX}, EI_{YY}, EI_{XY}) for the femur at each cross-section.

Next, a computational means for evaluating the cross-sectional properties of the implant designs to be studied was developed. This process involved mathematically describing the implant, "assembling" the appropriately sized implant into each femur, describing the slot designs to be considered, and characterizing the bending properties of the oriented implant in anatomically-relevant planes. During formulation of the implant's bending properties, special emphasis was placed on treating the nature of the slot as a general variable for subsequent study.

Three specific implant designs were considered, all of which may be described as including a constant width slot whose angle ø with respect to the face of the implant may vary from a proximal start angle in a linear fashion along the length of the implant:

1) A current design, featuring a slot oriented to coincide with the plane containing the implant face;
2) A second design featuring a constant slot angle, with the angle to be chosen to minimize some critical mechanical parameters;
3) A third design involving a slot angle which varies linearly along the length of the implant containing a slot.

A FORTRAN program was written to numerically evaluate the inertial properties of the implant within the femurs. The cross-sectional moments of inertia for the bone/implant composite were expressed in terms of the geometry of the slot as it varies along the implant. Hence, the bending rigidity of the structure was expressed in terms of slot variables.

A least-square error approach to optimizing the variables of the slot orientation in the implant was adopted. For the purposes of the present investigation, the specific objective was to vary the slot orientation to retain as closely as possible the relationship between EI_{xx} and EI_{yy} present in the intact femur. While "minimizing the bending rigidity" of the bone/implant composite sounds like a good objective, in reality minimizing bending

rigidity about the x axis by changing slot orientation comes at the expense of increasing bending rigidity about the y axis, and vice versa. Assuming that in the intact femur there is a natural balance between these two properties, we have focused on maintaining that balance. The error term chosen represents a lumped error in the ratio of EI_{xx} to EI_{yy} across all CT slice levels over the region of the slot (we refer to this term as the lumped EI ratio error).

For the present implant design, this measure is the final result of the analysis. For design 2, the program must be run across a variety of slot angles, with a different lumped EI ratio error value being computed for each angle. Finally, in the case of design 3, the program must be run across a combination of the two design parameters (start_angle and angle_mult, a multiplier which determines how quickly the slot angle varies along the implant). This produces a contour of the error term plotted on an x-y mapping of the design parameters, from which a minimum of the error term may be identified.

RESULTS AND DISCUSSION

The lumped EI ratio error values obtained for the slot designs considered ranged from 0.408 to 1.135. Looking first at design 1 – the present design – a constant slot orientation of 0° generally decreases EI_{yy} at the expense of an increased EI_{xx} value (associated error value of 1.135). The variation in lumped EI ratio error for design 2 – with a constant slot orientation along its length – exhibited a peak near 0° with minima near ±60°. The lowest error value (0.411) was obtained at a slot orientation of -63°. The largest error value was that obtained with a slot orientation of 0°. Finally, the variation in lumped EI ratio error across the range of slot orientation parameters considered in design 3 is shown in contour form in Figure 1. A peak is noted in the vicinity of a constant slot orientation of 0° (i.e., angle_mult = 0., start_angle = 0.), while the minimum error value (0.408) is associated with a start_angle value of -70° and an angle_mult value of 13°. The effect of varying slot orientation along the implant had a minimal effect on the lumped EI ratio error value, when compared to the influence of the initial choice of slot orientation.

The aggregate result of the differing slot designs may be seen by considering the rigidity ratios obtained across all sixteen femurs (Figure 2). The position along the femur is normalized across the implant shaft, and the rigidity ratio has been normalized to the value for the intact femur. While it is clear that the new design produces ratios more closely in line with those in the intact femur across the 16 femurs considered, it is worth noting that there does

Figure 1. A contour of the variation in lumped EI ratio error term over a range of design variables across 16 femurs.

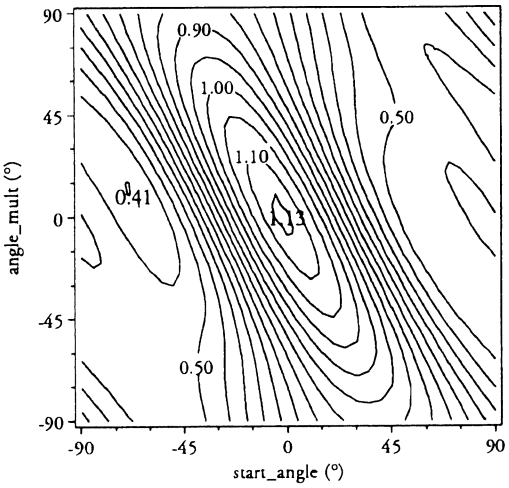

appear to be one pair of femurs whose properties differed from the rest.

The techniques used in the current analysis provided a powerful tool for considering the relationships between the details of a given implant design and the bending rigidity of the bone/implant composite obtained with its use. Given an objective of minimizing post-implantation bending rigidity by varying slot orientation in a femoral implant, it was found that linearly varying slot orientation along an implant can slightly improve bending rigidity properties.

REFERENCES

Tronzo, R. Orthopaedics, 12(9), 1161-1171, 1989.

Franks, E. et al. Trans. 38th ORS, Washington, (p. 296), 1992.

Wright, T. and Bartel, D. Encyclopedia of Medical Devices and Instrumentation, (pp. 2138-2141), John Wiley & Sons, Inc., 1988.

Bartel, D. et al. Computational Methods in Bioengineering, (pp. 199-210), ASME, 1988.

ACKNOWLEDGMENTS

This project was funded by a grant from StelKast, Incorporated.

Figure 2. Bending rigidity ratio for the femur/implant composite as it varies along the femur (16 femurs).

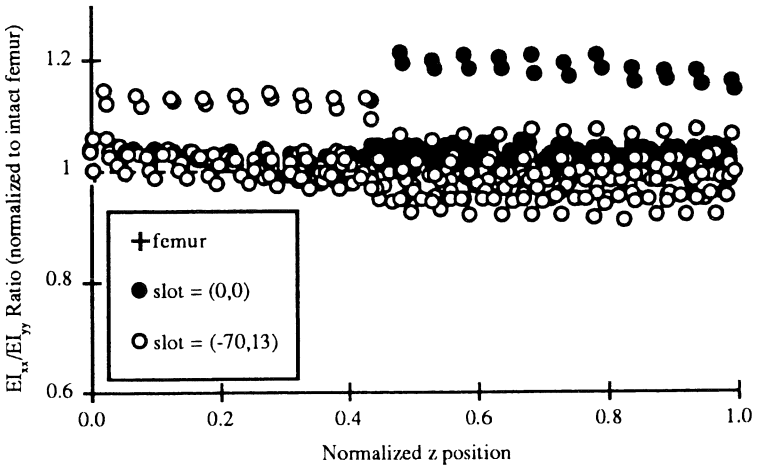

SESSION 2:

AGING

EFFECT OF AGE ON PERFORMANCE DURING A STRENGTH-TRAINING PROGRAM

J. Buck, M. Gross, and N. Alexander

Department of Movement Science and Department of Internal Medicine
The University of Michigan, Ann Arbor, MI 48109

INTRODUCTION

Muscle function is important for maintaining quality of life in the elderly. Adequate muscle strength may be important for improving functional ability or decreasing risk for falls in the elderly. Potentially, strength training programs can maintain or even increase muscle strength in the elderly. Design of effective strength-training programs depends on an understanding of muscle response under different loading regimes. The purpose of this study was to examine muscle performance in elderly subjects during a progressive resistance exercise program, and compare performance in young and elderly subjects in response to increasing resistive loads. Able and frail elderly subjects exercised three times per week for twelve weeks on a variety of lower extremity exercise tasks. Effort (product of repetitions and resistance level) during training was quantified for all sessions, and force and angular displacement data were recorded in other sessions. Results showed that both elderly and frail subjects improved their effort over the training program. Age-related differences in responses of young and elderly subjects to increased resistive loads were observed, however, and suggest that muscle power during exercise may be different in young and elderly subjects.

REVIEW AND THEORY

Muscle strength commonly decreases with advancing age (Schultz, 1992). Muscle power also decreases with age (Faulkner et al.,1990), even in athletic elderly individuals (More, 1975). Decrease in muscle strength has been associated with a decline in functional ability and an increase in risk for falling in the elderly (Tinetti et al., 1988). Investigators have shown that muscle strength can be increased, even in the very old (Fiatarone et al., 1990). More information is needed, however, regarding performance changes during a strength-training program in the elderly, especially frail elderly individuals, in order to better design strength training programs. The purpose of this study was to understand how performance changes during a training program using progressive resistive devices for able and frail elderly subjects.

PROCEDURES

Elderly subjects were residents of a local retirement center. Twenty-nine subjects ranging in age from 69 to 93 years (x=83.4 yrs) were tested. Subjects were excluded if acute disability existed. Elderly subjects were characterized as either able or frail based on use of assistive devices and other functional abilities. The mean age of young subjects was 21.7 years. Male and female subjects were included in both age groups.

Elderly subjects exercised three times per week for twelve weeks (36 sessions). Six different exercises were used: four hydraulic resistance machines (hip ab/adduction, knee extension/flexion, jump squat, and stair stepping), chair rise with weighted vest, and ankle plantar/dorsiflexion against resistance. Data are reported here only for the knee exercises. Subjects performed a series of repetitions at increasingly difficult resistance levels. Subjects were asked to work at maximum speed and range of motion while maintaining good form. Subjects' repetitions and resistance levels were recorded for each exercise session; "effort" was defined as the product of repetitions and level. In a separate session, young and elderly subjects performed the knee exercise at each resistance level. Force and angular displacement data were recorded. T tests were used to determine significant differences between groups.

RESULTS

Representative results for effort during the exercise program for able and frail elderly subjects are shown in Fig. 1. The effort exerted by able subjects increased over sessions of the training period. For the most able elderly, the effort profile was similar to the maximum profile allowed by the protocol. Frail subjects also worked at greater effort levels as training progressed, but the improvement was much less dramatic than in the able subjects.

Although effort profiles increased with training for most subjects, it was not known if subjects' ability to generate force increased with training. To better understand the relationship between effort profiles and limb function, maximum force and angular displacement were measured during the knee exercise

at each resistance level. Although knee range of motion was not different among subjects, duration of motion was greater in elderly than in young subjects ($p<0.05$), thus decreasing their average velocity (Fig. 2, top). Force was significantly greater for the young than for the elderly subjects at each resistance level ($p<0.05$) (Fig. 2, bottom). Force increased with resistance level for all subjects; force increased with resistance most for the young subjects, and least for the frail elderly subjects.

DISCUSSION

These data suggest an age difference in limb function while using resistive training devices. Elderly subjects accomodated increased resistive load by slowing their movements while only slightly increasing their force, thus decreasing their power. Young subjects, however, increased their force as resistive load increased, potentially maintaining or only slightly decreasing their power.

In this progressive resistive training program, elderly subjects increased their capacity to perform repetitions at increasingly difficult resistive loads. Ability to increase effort, however, may not parallel the subjects' ability to generate force or power at increasing resistive load levels. These data suggest that age-related differences exist in how young and old subjects perform while using progressive resistance devices, and that progressive resistance may not be an important feature of a strength-training program for frail elderly subjects.

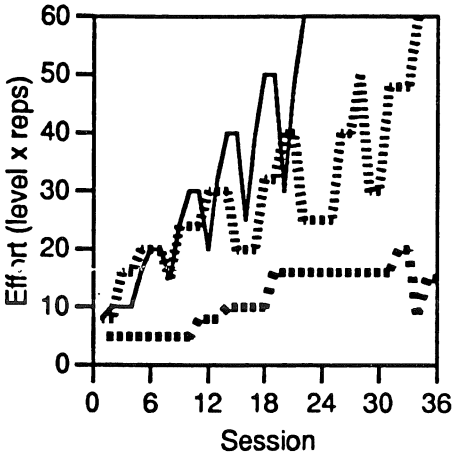

Figure 1. Effort profiles of representative able (dashed line) and frail (dotted line) elderly subjects during the training program. The solid line represents a maximum effort profile that would be performed by a young subject.

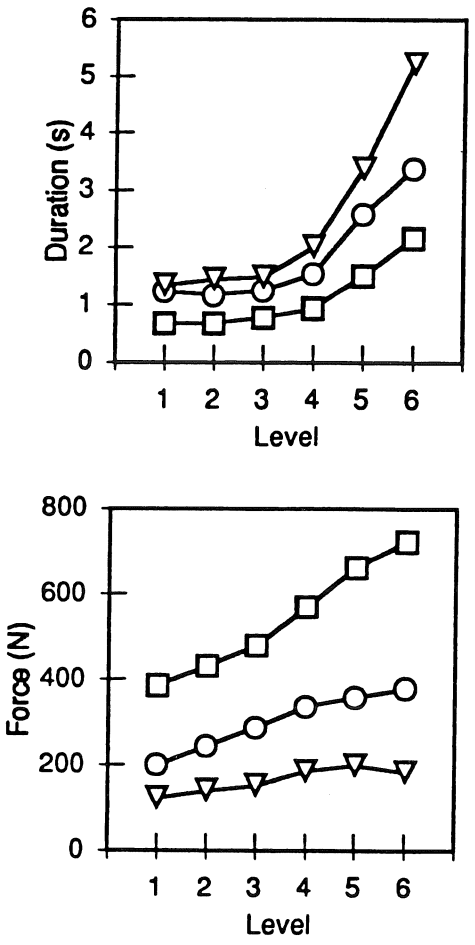

Figure 2. Duration and peak force of maximum knee extensions averaged for young (squares), able elderly (circle), and frail elderly (triangles) subjects.

REFERENCES

Faulkner, J.,et al., Ann. Rev. Gerontol. Geriatr., 10, 147-166, 1990.

Fiatarone, M. et al., JAMA, 263, 3029-3034, 1990.

Moore, D. H. , Nature, 253, 264-265, 1975.

Schultz, A. B. J. Biomechanics, 25, 519-528, 1992).

Tinetti, M.E. et al. N. Eng. J. Med., 319, 1701-1707, 1988.

ACKNOWLEDGEMENTS

The authors thank B. Luebke for her help in conducting the exercise training. This work was supported by a grant from the Department of Veterans Affairs.

TRAINING-RELATED CHANGES IN THE FORCE POWER SPECTRUM OF ELDERLY SUBJECTS

D. A. Keen, M. Bilodeau, G. H. Yue, and R. M. Enoka

Department of Biomedical Engineering
The Cleveland Clinic Foundation
Cleveland, OH, 44195.

INTRODUCTION

An increase in motor unit force that occurs with aging has been hypothesized to cause a detriment in the ability of elderly subjects to control force. This diminished ability has been previously associated with an increased amplitude of the prominent peak (3 - 12 Hz) in the force power spectrum (Galganski et al., 1993). To test the hypothesis that motor unit force is correlated with an individual's ability to control force, young and elderly subjects performed a 12-wk strength training program designed to increase motor unit force. The elderly subjects improved their ability to sustain constant forces at 2.5, 5, and 20% MVC force. This improvement, however, was unrelated to changes in the distribution of motor unit forces and to the energy in the power spectrum of the force record between the frequencies of 4 -12 Hz.

REVIEW AND THEORY

One consequence of aging is a decline in the number of motor units innervating a muscle and an increase in the average size of the surviving motor units (Brown et al., 1972; Campbell et al., 1973). Because this reorganization results in bigger motor units, it has been hypothesized to cause a decline in the ability of elderly subjects to maintain a constant submaximal force (Galganski et al., 1993). This impairment was evident as a larger amplitude for the prominent peak in the force power spectrum in the 6 - 8 Hz region for constant-force tasks. After 12-wks of strength training, we found that the ability of elderly subjects to sustain a submaximal effort at a constant force was improved significantly (Keen et al., in press). This adaptation, however, was unrelated to a change in motor unit force, as determined by spike-triggered averaging. The purpose of this study was to determine the association between the training-related decline in normalized force fluctuations (coefficient of variation) during a constant-force task and the energy in the power spectrum over the range of 4 - 12 Hz. This frequency range was chosen because it encompasses the range of physiological tremor.

PROCEDURES

Twenty-one healthy subjects were assigned to one of two age groups, an elderly group with an average age of 65 yrs (range = 59-74) and a young group with an average age of 23 yrs (range = 18-27). All subjects were right-hand dominant and had no known neuromuscular disorders.

Each subject participated in a 12 wk strength training program. The exercise involved concentric and eccentric contractions of the first dorsal interosseous (FDI) muscle of the left hand. The subjects performed 3 training sessions every week, each involving 6 sets of 10 repetitions of the exercise. The index finger was displaced through a 0.5-rad range of motion in the exercise. The training load was set and maintained at 80% of the maximum load that the index finger could lift.

Each subject participated in 4 experiments (0, 4, 8, and 12 wks). In these experiments, the subjects were required to perform an isometric MVC, a constant-force task, and a threshold task in which single motor units were recorded. For the constant-force task, a target force was displayed on the oscilloscope and the subject was encouraged to exert a steady abduction force with the index finger for 20 s to match the target force as closely as possible. Based on the MVC force of the subject for that session, target forces of 2.5%, 5%, 20% and 50% MVC force were calculated. The standard deviation (SD) and the coefficient of variation

(SD / mean x 100) of the force fluctuations about the target force were calculated. Power spectral analysis (1024 points multiplied by a raised cosine window, fast Fourier transform) of the force record was performed on successive windows across the whole trial for each sustained force level. A mean power spectrum was then obtained by averaging the results of all the single windows. The energy between 4 -12 Hz of this mean spectrum was obtained by integrating the power over this frequency band.

RESULTS

The training program caused a reduction in the coefficient of variation of the force fluctuations for the elderly subjects at the lower target forces of 2.5, 5, and 20% MVC force by -29.3, -20.5, and -11.6% respectively. The young subjects showed no significant changes with training. The majority of the improvement observed in the elderly subjects occurred in the first 4 wks of training. The improvement in the coefficient of variation was unrelated to changes in the distribution of motor unit forces or to the force power spectrum. In contrast, neither the absolute force fluctuations (SD) nor measures of the force power spectrum changed with training. Across all sessions (combining data for both age groups and for weeks 0, 4, 8, and 12), there was a high correlation (r^2 = 0.68) between the SD of the force fluctuations and the energy in the 4-12 Hz bandwidth of the power spectrum. This is apparent by the close association between the 2 variables across time (Figure 1).

DISCUSSION

The main finding of this training study was an improvement in the ability of the elderly subjects to maintain a constant submaximal force. This improvement occurred in the first 4 wks of training and was not associated with a consistent change in the energy in the force power spectrum between 4 - 12 Hz. The observation that strength training decreased the normalized force fluctuations appears to be a unique finding as there are several reports in the literature of conditions that enhance tremor amplitude (Furness et al., 1977; Young and Hagbarth, 1980) but there is little mention of a converse effect. The absolute (SD) force fluctuations, however, did not change with training and this was closely related with measures in the power spectrum.

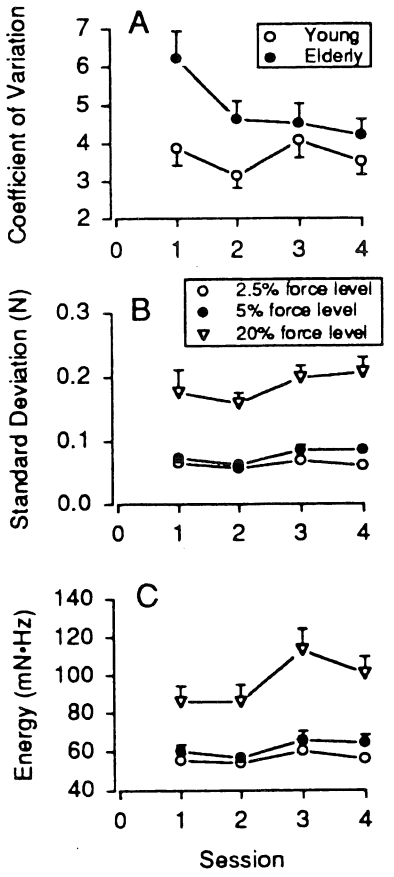

Figure 1. Changes in the normalized force fluctuations (A), the absolute force fluctuations (B), and the energy in the 4-12 Hz bandwidth of the power spectrum (C) over the 12-wk training program.

REFERENCES

Brown WJ: *J Neurol Neurosurg Psychiat.* 35: 845-852, 1972.

Campbell MJ et al: *J Neurol Neurosurg Psychiat* 36: 174-182, 1973.

Furness P et al: *J Physiol (Lond)* 265: 821-831, 1977.

Galganski M. et al: *J Neurophysiol* 69, 2108-2115: 1993.

Young R, Hagbath K: *J Neurol Neurosurg Psychiat* 43: 248-256, 1980.

Supported by NIH grant AG 09000 to RME.

Postural Control and Perceived Stability Limits in the Elderly

T. Lundin*, M. Grabiner* and M. Omlid**

* Department of Biomedical Engineering and ** Section of Geriatric Medicine
The Cleveland Clinic Foundation, Cleveland, OH 44195

INTRODUCTION

The aging process, in conjunction with some types of pathologies, contribute to the degeneration of postural control which, in turn, may lead to the high incidence of falls in the population over the age of 65. It is thus of significance to determine when the onset of disequilibrium takes place so that interventions can be made in an effort to reduce what could become irreversible degenerations of postural control.

Information regarding the maintenance of the center of pressure within the area of the base of support is derived from the somatosensory, the visual and the vestibular systems. These systems, under normal conditions, are at least partially redundant, thus making it difficult to evaluate the onset of disequilibrium through traditional measures of postural sway (Horak *et al.*, 1989).

The area of the base of support during upright stance can be defined by the limits of voluntary center of pressure excursion, or perceived stability limits (PSLs), in the anterio-posterior (AP) and medio-lateral (ML) directions. Examination of PSLs in the elderly may reveal important information regarding their postural control and may lead to a means by which instability can be diagnosed and intervened upon.

PROCEDURES

Thirty-five people volunteered to participate in this study and were divided into three age groups: mean(sd), GroupA, 25(2.3) years (n=11); GroupB, 71.2 (2.6) years (n=11) and GroupC, 78.3(2.2) years (n=13). PSLs were measured on an AMTI force plate statically and dynamically along with a twenty second neutral standing trial where the subjects were instructed to minimize sway.

Dynamic PSLs in the AP direction were defined as the minimum and maximum values of the center of pressure excursion over a twenty second trial. The subjects were instructed to oscillate to their limits of stability in the sagittal plane as rapidly as possible.

Static PSLs in the AP direction were found by averaging the center of pressure over a three second trial where the subjects were instructed to lean to their limit of stability and hold the position for three seconds. This was done in both the anterior and posterior directions.

Dynamic and static PSLs in the ML direction were calculated in a similar manner with motions occurring in the frontal plane. Postural sway amplitudes were defined as the standard deviations of the center of pressure excursions in the

AP and ML directions over the twenty second neutral standing trial.

The AP and ML variables were analyzed using a 2 by 3 (static/dynamic by age group) analysis of variance with repeated measures. A significance level of $p \leq 0.05$ was selected.

RESULTS

The values of postural sway amplitude were not significantly different between age groups in the AP or ML directions. Perceived stability limit results from this study are presented as the range (maximum-minimum) of the PSLs in the AP (Table 1) and ML (Table 2) directions.

Table 1
AP static and dynamic PSLs
mean(sd) cm

	AP static	AP dynamic
GroupA	13.1(1.7)[1,2]	17.0(2.1)[2]
GroupB	10.7(2.5)[2]	15.4(2.4)[2]
GroupC	8.4(1.5)	12.9(2.2)

1- significantly different from GroupB
2- significantly different from GroupC

Table 2
ML static and dynamic PSLs
mean(sd) cm

	ML static	ML dynamic
GroupA	10.0(1.9)[1,2]	14.8(2.0)[1,2]
GroupB	6.7(2.4)	13.4(1.5)[2]
GroupC	5.7(2.1)	11.4(2.3)

1- significantly different from GroupB
2- significantly different from GroupC

DISCUSSION

The results of this study show that as age increases the range of PSLs decreases. It is doubtful that the aging process alone contributed to these decreases. Although all patients were screened for neuromuscular impairment it is likely that the decreases in PSLs were due to some type of pathology (Gabell and Nayak, 1984).

The traditional postural sway amplitude values were not significantly different between age groups. However, significant differences in the PSLs were observed. Several factors which contribute to this may be muscular atrophy, decreased range of motion or loss of joint position sense at the ankle or even a fear of falling.

It follows that the postural sway, although not significantly different between age groups, made up a greater proportion of the available base of support in the eldest group compared to the younger groups. As this proportion grows larger the risk of a fall would also presumably increase.

The diagnosis and subsequent treatment of postural instability may be limited by general nonspecific tests of postural sway. By examining PSLs, greater information may be gained pertaining to postural control in the elderly.

REFERENCES

Gabell A and Nayak VSC (1984) *J. Gerontol.* **39**:662-666.
Horak FB et al. (1989) *Neurobiology of Aging.* **10**:727-738.

ACKNOWLEDGMENTS

This work was supported by the Aerex Corp.

THE USE OF STEPPING TO MAINTAIN UPRIGHT BALANCE: BIOMECHANICAL ANALYSES IN YOUNG AND OLD ADULTS

J.K. Sprague, J.A. Ashton-Miller, A.B. Schultz, N.B. Alexander

Department of Mechanical Engineering, University of Michigan, Ann Arbor, MI 48109

INTRODUCTION

Taking a step, or steps, is fundamental to locomotion. Toddlers through octogenarians also appreciate the importance of taking a step to avoid falling, which is known to become increasingly problematic with age (Tinetti 1988, 1989). Yet the factors leading to the decision to step in order to recover balance, rather than to rely on a sway response, remain poorly understood. What are the stimuli for a step, when should the step be initiated, in what direction and how long should a step be, and are multiple steps likely required? Are these decision processes affected by age? In what follows, we define balance for a given task as the act of manipulating the location, magnitude and direction of the support reaction vector in order to guide the whole body center of mass (CM) in a desired trajectory. The relative 3-D locations of the CM and the Center of Reaction (CR) determine the magnitude and direction of the gravitational moment accelerating the CM (Fig. 1).

Most research has either focused on standing balance (for example, Nashner 1971), the initiation of gait (Patla et al. 1993), locomotion (for example, Winter 1991), or on stepping responses to external perturbations (for example, Redfern, et al. 1993, Luchies, et al. 1994). McIlroy et al. (1993), studied "compensatory stepping" in response to external perturbations from a moveable platform, and found that subjects often initiated stepping well before limits of stability were reached. MacKinnon & Winter (1993) calculated and partitioned net joint moments in the frontal plane during gait. We are not aware of any studies that have addressed how stepped foot placement during gait relates to body angular tilt and velocity associated with the self-induced series of falls which constitute locomotion. In this experimental and theoretical study (see Sprague 1994 for more details) we tested the null hypothesis that age does not affect the ability to control upright balance through the use of stepping.

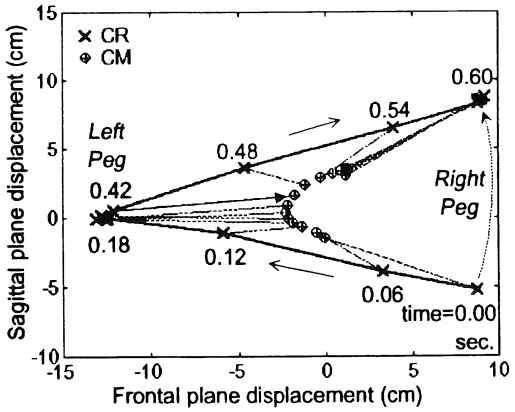

Figure 1. Sample detailed view of CM and CR motion over one cycle of stepping on pegs.

EXPERIMENTAL STUDY

Methods: In the experimental study, 24 young (YA:22.9 ±3.1 years) and 24 old (OA:73.2 ±5.4 years) subjects were asked to perform 11 trials of step-in-place tasks at a Steady Comfortable Rate (SCR) and using As Few steps As Possible (AFAP) while attempting to maintain their global position in the room as accurately as possible. Tasks were made increasingly challenging by systematically decreasing footprint area from full shoes, to half shoe, to a single 1 cm dia, 2 cm high, peg beneath each midfoot (Fig. 1) and occluding visual feedback. A safety harness and grab rails were used to prevent injury and subjects were allowed up to 30 seconds practice prior to each new task. Two sets of 6 infrared bilateral markers (Watsmart), a force plate for each foot and an anthropometric model were used to calculate the relative 3-D locations of the CR and CM over each of the 20 second trials.

Results: All subjects successfully completed all tests. No subjects could balance on the pegs for more than six seconds without taking a step. Step length (SL, defined as the perpendicular distance to the just loaded foot CR from the "stance line" joining the CR beneath each foot during midbipedal stance) and stepping rate were found to increase significantly ($p<0.05$) for all subjects as the tasks were made more difficult (Fig. 2). Multiple regression analysis indicated that the decision to step forward or backward relative to the stance line, and the magnitude of the SL itself, were highly correlated with linear combinations of the kinematic state vari-

ables: angular displacement (θ_{CM}) and velocity ($\dot{\theta}$) of the CM with respect to the CR, measured 200 ms prior to the step. For example, the combination of +0.4 deg (forward) θ_{CM} and +1.7 deg/sec $\dot{\theta}$ resulted in a 5.8 cm mean forward SL. The combination of -0.71 deg θ_{CM} and +1.7 deg/sec $\dot{\theta}$ resulted in a 0 cm mean SL, meaning no step was needed. The regression coefficients were not significantly altered by age. The resulting correlation coefficients ranged from 0.6 to 0.95 depending on task, subject group and time prior to stepping. In the peg AFAP task, YA were able to balance bipedally for significantly more time (p=0.018), they also took significantly smaller (p=0.036) and slower (p=0.014) steps. Similar results were found for the SCR task (p=0.005 and p=0.003, respectively). Analysis of over 4,000 steps showed both OA and YA used an average of two steps (ranging from 1 to 8), to arrest the momentum resulting from their self-induced forward falls.

THEORETICAL STUDY

Methods: A planar five degree of freedom, three rigid link, direct dynamic model was used to analyze the biomechanical factors that lead to the choice of step direction, when a step is initiated, and the direction and length of the new step needed to recover upright stance in a stepping-in-place task.

Results: The magnitude of whole body momentum arrested by a step was sensitive to both step length and timing (duration of unipedal stance and delay prior to stepping). Furthermore, the three link model predicted the experimentally-observed positive association between overstepping (the observed tendency to take a larger step than was needed to arrest momentum) and increased stepping frequency. The model results also predicted that SL will increase linearly with θ_{CM} and $\dot{\theta}$ evaluated 200 ms prior to the step.

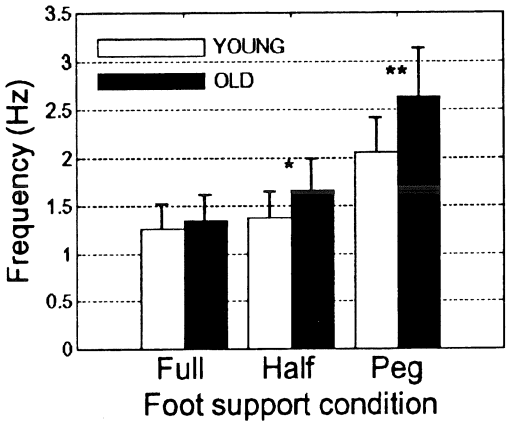

Figure 2. Mean (SD) subject stepping frequency for the first trials of SCR peg stepping tasks. *p=.002, ** p<.001

DISCUSSION

Balancing on two 1 cm diameter pegs in the AFAP task was challenging for both OA and YA. Despite this, no irrecoverable losses of balance occurred. The fact that less than 5% of steps taken were in an inappropriate direction indicates how reliable and accurate adult foot placement normally is. These healthy adults systematically used larger steps than were strictly necessary to arrest whole body linear momentum. In the AFAP task this may indicate conservatism and a desire to keep the CM "as still as possible" with as few steps as possible, in keeping with subject instructions. As the tasks were made more challenging, by removing visual feedback, both YA and OA increased the amount of overstep, again indicating conservatism. The model analyses suggested that the concomitant increase in step frequency is a corollary of this overstepping. We conclude that although the values of θ_{CM} and $\dot{\theta}$ that trigger a step do not alter with age, an age-related decrement in stepping balance was found. Healthy OA chose to lower the risk of losing dynamic stability by using a more energetic balance strategy involving the use of a larger SL and higher step frequency.

REFERENCES

MacKinnon CD & Winter DA (1993) *J. Biomech.* 6: 633-644.

Patla AE *et al.* (1993) *Clin. Biomech.* 8: 179-184.

Nashner LM (1971) *Acta Otolaryng* 72: 429-436.

Luchies CW *et al.* (1994) *J. Amer. Geriatr. Soc.* In press.

McIlroy WE & Maki BE (1993) *Brain Res.* 616: 30-38.

Redfern MS *et al.* (1993) *Amer. Soc. Biomech.* pp 59-60

Sprague JK. (1994) Ph.D. Thesis, University of Michigan.

Tinetti ME *et al.* (1988) *New Engl. J. Med.* 319: 1701-1707.

Tinetti ME & Speechley M (1989) *New Engl. J. Med.* 320: 1055-1059.

ACKNOWLEDGMENTS

We gratefully acknowledge the financial support of the Vennema Endowment, a Pre-Doctoral Fellowship from the Institute of Gerontology and the support of NIH grants AG 06621, AG 08808 and AG 10542.

TRANSMISSIBILITY OF GROUND VIBRATION TO THE AXIAL AND APPENDICULAR SKELETON: AN ALTERNATIVE STRATEGY FOR THE TREATMENT OF OSTEOPOROSIS

C. Rubin, K. McLeod, M. Pope*, M. Magnusson*, M. Rostedt*, C. Fritton, T. Hansson*
Musculo-Skeletal Research Laboratory, State University of New York at Stony Brook,
Institute for Orthopaedics, Sahlgrenska Hospital, Gottenberg, Sweden*

Introduction

Pain, loss of height, gross fracture and post-fracture complications of osteoporosis impair the quality of an individual's life, while treatment regimens impose a severe burden on our country's medical resources. Interestingly, the complications of osteoporosis occur predominantly at specific sites of the skeleton (e.g., femoral neck, lumbar spine), areas which are also associated with the greatest load bearing responsibility. Even though the disease is focal in nature, the most accepted treatment protocols are pharmacologically based and administered systemically (e.g., estrogens, bisphosphonates). As an alternative to a drug-based strategy, we believe that biophysical stimuli such as mechanical strain would facilitate a site-specific, endogenous regimen for the inhibition and/or reversal of osteoporosis.

Exercise, via the virtues of Wolff's Law, has been shown to inhibit bone loss in the elderly (Smith et. al., 1989). However, exercise as a generic treatment for the osteopenic patient must be prescribed with caution as it may produce the fracture it has been prescribed to prevent. As an alternative to a regimen of vigorous activity as a source of osteogenic stimuli, it has recently been demonstrated that bone tissue is highly sensitive to the frequency of the induced strain, so much so that strains below 500 microstrain ($\mu\varepsilon$) become osteogenic if induced between 15-40 Hz (Rubin et. al., 1990; McLeod & Rubin, 1994). Before such a mechanical prophylaxis can be safely prescribed for humans, it is necessary to devise a means whereby low magnitude, high frequency strains can be applied to those sites at greatest risk of symptomatic bone loss. Considering the relatively high (>10 Hz) frequencies of these strains, we believe they should be transmitted efficiently from the ground through the appendicular and axial skeleton to those regions at greatest risk of fracture.

Review and Theory

In the presence of 1 g-force of gravity, bones with weight supporting responsibility experience strains on the order of 1000$\mu\varepsilon$ (Rubin & Lanyon, 1984). This relationship between static strain and g-force suggests that 100-500 $\mu\varepsilon$ can be readily induced into the weight-bearing elements of the skeleton by perturbing the effective gravity by 0.1-0.5g.

The modulation of g-force can be accomplished by placing the standing human on a platform which is made to oscillate at a specific frequency and acceleration. However, little is known of transmissibility of ground based vibration at frequencies above 12 Hz (Griffin, 1990). Finally, an oscillating device capable of accelerating an 80kg subject to 0.4g at 30 Hz would require a mechanical actuator with an output rating of over 400N. An alternative to a "pure force" oscillating platform would be to design a resonant structure in which the human body becomes part of a spring-mass system. This abstract reports the first *in vivo* characterization of such a resonant system.

Methodology

Six human volunteers were used in this study (1 m, 5 f). In a surgical procedure approved by the Helsinki Accord for Human Experimentation, 2.3mm x 90mm trocar pointed Steinman pins were drilled into the spinous process of lumbar segment L4 and the greater trochanter of the right femur, just opposite the femoral head. This procedure was done under aseptic conditions and with the subject under a local anesthetic. Further, pin placement by the orthopaedic surgeon (TH) was validated by fluoroscopy. Immediately following surgery, accelerometers were fastened onto each of the two transcutaneous pins, and the subjects asked to stand on the portable vibration platform. The platform was driven by two solenoid actuators, each capable of delivering 9N of force when run at 1.7 amps. Data was collected as a function of both amplitude and frequency in the standing human. To determine damping as a function of posture, data was also collected from the subjects while standing with bent knees.

Acceleration data from the femur and spine was compared to that measured from the surface of the plate. Because the plate is based on a resonant design (supported by springs), it was important to demonstrate that the plate surface was translating vertically rather than rocking about the horizontal plane. Therefore, two accelerometers, one at the plate edge and one at the center, were used for this measurement. Subjects were positioned on the plate such that the plate accelerometers were in phase and of equal magnitude. Accelerometer data was conditioned through bridge amplifiers and digitized at 500 Hz. Data is reported as a function of frequency, with the transmissibility function reflecting the degree of energy lost from the ground to the femur and spine.

Results

For a constant force input (18 N), plate accelerations increased with frequency at both the femur and spinous process of L4. Peak accelerations measured at the plate surface and at the femur and spine show the phase shifts, increasing from 15 through 40 Hz, with the shift at 30 Hz to be 61 degrees in the hip and 81 degrees in the spine (Fig. 1). The transmissability of the ground acceleration to the femur and spine decreased as a function of frequency. There was negligible loss of acceleration in the lower frequency bands, transmissibility fell off by as much as 60% when the frequency approached 40 Hz (Fig. 2).

When the subject was asked to stand with bent knees, transmissibility fell to below 20% at the femur and spine when vibrated at 30 Hz. Presumably, this is due - at least in part - to the uncoupling of the body segments, and the segments no longer working efficiently as a fixed, stiff system.

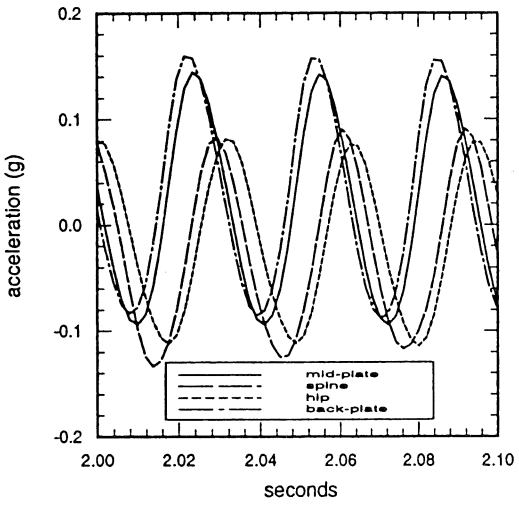

Fig. 1. Accelerometer reading from the center and back of the plate, as well as the vertical component of L4 and femur of a 52kg female oscillating at 29 Hz. While the amplitude of the plate and skeletal accelerations are similar, there is a distinct lag in the peaks.

Discussion

It has long been proposed that some corollary of Wolff's law would be an effective prophylaxis for osteoporosis. We have proposed that extremely low magnitude (< 500με), high frequency (15-40Hz) mechanical strains are extremely osteogenic, and could beneficially effect bone mass and morphology if some means of treating the vulnerable areas of the skeleton could be devised. By subtle variations in g-force, it is argued that proportional changes in strain could be induced in the bone tissue. Direct measurement of acceleration in the femur and spine of the standing human have shown the transmissibility of mechanical energy to remain above 50% for all frequencies up to 35 Hz. Using a resonant plate design with an ultimate force of 18N it was possible to accelerate 80kg humans by as much as 0.4g. While it will be necessary to incorporate this transmissibility and phase shift data into a model of the human body in order to determine actual induced strains in the axial and appendicular skeleton, we believe that accelerations of this magnitude will generate substantial dynamic changes in the baseline static strain caused by simple standing.

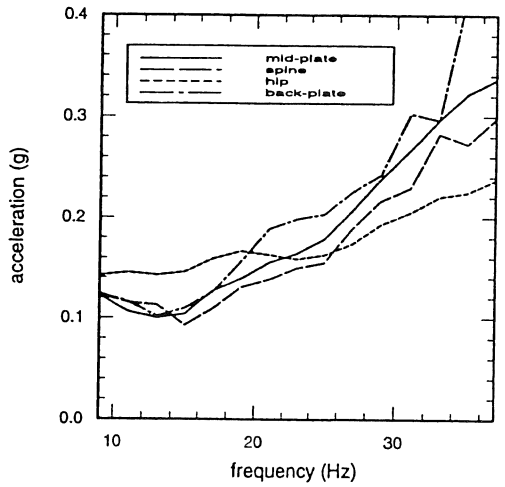

Fig. 2. Site specific accelerations as a function of frequency. As frequency increased, and therefore the effective g-force, the transmissibility of the ground reaction force fell in both the hip and spine.

A site which has adapted to induce 500 με while standing would increase to 700 με, while a site normally subject to 1500 με would increase to 2100 με. Net increases in strain of such small magnitude would not normally be considered osteogenic. That strains as low as 200 με become potently osteogenic when induced in the frequency band of 15-40 Hz potentiates their role as an effective, self-localizing therapy for osteoporosis. This abstract reports the first stage of characterizing the biomechanics of this novel treatment strategy.

Griffin (1990) Handbook of Human Vibration, Acd. Press, N.Y.

McLeod, K. & Rubin, C. (1994) Trans. 40th Orth. Res. Soc. 19:564

Rubin, C. & Lanyon, L. (1984) J. Bone Jt. Surg. 66A:397-402.

Rubin, C., McLeod, K & Bain, S. (1990) J.Biomech. 23s:43-54

Smith, E., Gilligan, C., McAdam, et. al. (1989) Cal. Tiss Int. 44:312-321

Work supported by NIH AR39278 and Exogen, Inc.

SESSION 3:

SPORT

THREE-DIMENSIONAL KINETICS OF THE SHOULDER, ELBOW AND WRIST DURING A PENALTY THROW IN WATER POLO

Michael E. Feltner & Grant Taylor

Department of Sports Medicine, Pepperdine University, Malibu, CA 90263.

INTRODUCTION

To understand the mechanics of any body motion, it is necessary to develop a model that links the kinematics of the motion with the kinetic parameters responsible for the production of the observed motion. The kinetic parameters include the net forces and torques (indicative of the net muscular activity) at the joints. This paper reports the results of such an analysis conducted for the segments of the throwing arm during a penalty throw in water polo.

REVIEW AND THEORY

Previous research by Feltner (submitted) demonstrated the use of two techniques to produce the speed of the right knuckle (the distal landmark of the throwing arm) at the instant of release (REL) in water polo. The linear velocity of the shoulder and the elbow extension angular velocity made approximately equal contributions (11% and 24%, respectively) to the speed of the knuckle at REL for both technique groups. However, the groups differed in the contributions from the horizontal adduction and internal rotation motions of the upper arm. The Horizontal Adduction Technique (HAT) subjects used the horizontal adduction angular velocity to produce 54% of the velocity of the knuckle at REL and the internal rotation angular velocity made a negligible contribution (4%) to the speed of the knuckle. The Internal Rotation Technique (IRT) subjects received a smaller contribution from the horizontal adduction angular velocity (38%), but an larger contribution from the internal rotation angular velocity (25%), to produce the speed of the knuckle at REL. The IRT subjects had a significantly greater internal rotation angular velocity at REL, and they were in positions of decreased external rotation and increased elbow flexion at REL compared to the subjects who used the HAT. It is unknown if the muscular activity required to produce the motions of the throwing arm segments differs between the two throwing techniques and no studies on the kinetic parameters at the joints of the throwing arm during a penalty throw have been conducted. The purpose of this study is to examine the roles of the kinetic parameters in the production of the motions of the throwing arm during a penalty throw in water polo.

METHODS

Thirteen intercollegiate right-handed water polo players were videotaped (60 Hz) using the DLT method. Three-dimensional coordinate data of the relevant body landmarks and ball were obtained for two trials of each subject using standard video analysis procedures and were smoothed via quintic spline functions. The inverse dynamics technique (Andrews, 1974, 1982) was used to compute the resultant joint force and torque (RJT) values at the shoulder, elbow and wrist of the throwing arm (Feltner et al, 1986). The computed RJT data were ultimately expressed in terms of anatomically relevant reference frames defined at the shoulder, elbow and wrist, respectively (Feltner et al., 1986). Subjects were divided into groups (IRT or HAT) based upon the findings presented by Feltner (submitted). Mean and standard deviation values were computed for select discrete RJT data. Group differences were determined using multiple t-tests and the experiment wide error rate was controlled at $p<0.05$ using a Bonferroni adjustment (Keppel, 1982).

RESULTS AND DISCUSSION

The mean RJT data at the shoulder, elbow and wrist during the penalty throw are presented in Figures 1-3, respectively. Although the data presented in Figures 1-3 are plots of mean values for all subjects at each instant, the shape of each curve is representative of the shape of the respective plots for all subjects in both the IRT and HAT groups. Discrete RJT values at the shoulder, elbow and wrist for the IRT and HAT groups are presented in Tables 1-3, respectively.

Table 1. RJT data [mean (s. d.)] at the shoulder for the subjects of the IRT (N=8) and HAT (N=5) groups during a penalty throw.

	Int. Rot. Technique		Hor. Add. Technique
Max. Int. Rot. RJT (Nm)	61 (17)	*	41 (6)
time Max. Int. Rot. RJT (s)	9.96 (0.01)		9.94 (0.02)
Max. Abd. RJT (Nm)	56 (21)		45 (10)
time Max. Abd. RJT (s)	9.93 (0.04)		9.93 (0.04)
Max. Hor. Add. RJT (Nm)	90 (25)	*	72 (8)
time Max. Hor. Add. RJT(s)	9.98 (0.01)		9.96 (0.02)
Int. Rot. RJT at REL (Nm)	8 (8)		9 (5)
Abd./Add. RJT at REL (Nm)	-5 (16)	*	22 (12)
Hor. Add. RJT at REL (Nm)	8 (26)		13 (13)

* Experiment- wide $p < 0.05$

Table 2. RJT data [mean (s. d.)] at the elbow for the subjects of the IRT (N=8) and HAT (N=5) groups during a penalty throw.

	Int. Rot. Technique		Hor. Add. Technique
Max. Varus RJT (Nm)	65 (17)	*	48 (5)
time Max. Varus (s)	9.97 (0.01)		9.95 (0.03)
Max. Ext. RJT (Nm)	11 (9)		9 (6)
time Max. Ext. RJT (s)	9.92 (0.04)		9.91 (0.06)
Max. Flexion RJT (Nm)	-22 (12)		-18 (5)
time Max. Flexion RJT (s)	10.00 (0.00)		10.00 (0.01)
Varus RJT at REL (Nm)	9 (11)		15 (8)
Flexion RJT at REL (Nm)	-22 (12)		-17 (5)

* Experiment- wide $p < 0.05$

Table 3. RJT data [mean (s. d.)] at the wrist for the subjects of the IRT (N=8) and HAT (N=5) groups during a penalty throw.

	Int. Rot. Technique	Hor. Add. Technique
Max. Flexion RJT (Nm)	14 (6)	10 (1)
time Max. Flexion RJT (s)	9.97 (0.01)	9.96 (0.02)
Flexion RJT at REL	1 (2)	1 (2)

At the shoulder, horizontal adduction, abduction and internal rotation torques were present throughout the throw. The

abduction and internal rotation torques reached their maximum values between the instants of maximum external rotation (MER) and REL, and then decreased through REL. The horizontal adduction torque reached its maximum value immediately before REL and then rapidly decreased. The absence of an external rotation RJT before the instant of MER indicates that the horizontal adduction and abduction RJTs at the shoulder are used to produce the external rotation of the upper arm through a mechanism similar to that reported by Feltner et al. (1986) and Feltner (1989). After the instant of MER, the horizontal adduction and internal rotation RJTs either maintain or produce their respective angular velocities of the upper arm. The subjects in the IRT group had significantly higher maximum values for the horizontal adduction and internal rotation RJTs during the throw.

The magnitude of the pronation/supination torque at the elbow was negligible throughout the penalty throw. As the upper arm was externally rotated, the varus torque at the elbow increased in magnitude and then rapidly decreased prior to REL. The presence of the varus torque at the elbow is due primarily to the internal rotation torque at the shoulder (Feltner et al., 1986). As expected, the subjects in the IRT group had a significantly higher peak varus torque due to their larger peak internal rotation torque.

The peak extension torque exerted at the elbow was quite small and suggests that the rapid elbow extension that occurred prior to REL was not due to the elbow extensor muscles, but to the joint force exerted by the upper arm on the forearm. This force would be associated with the centripetal acceleration of the upper arm as it rotated about the shoulder joint. Thus, the forward twisting rotation of the trunk and the horizontal adduction angular velocity of the upper arm that occurred during the throw would be responsible for producing an extension torque about the c.m. of the forearm (Feltner, 1989). Prior to REL, a flexion torque was present at the elbow to control the rate of elbow extension. The subjects in both the IRT and HAT groups exhibited similar flexion/extension RJT values at the elbow during the throw.

At the wrist, the RJTs in the pronation/supination direction (along the longitudinal axis of the hand) and the ulnar/radial deviation directions were small throughout the throw. Near the instant of MER, a flexion torque was present at the wrist to prevent an excessive extension motion of the hand. The flexion RJT reached its peak magnitude immediately prior to REL and then decreased through the remainder of the throw. The RJT values at the wrist were similar for the subjects in both the IRT and HAT groups.

The findings suggest that the athletes who use the internal rotation angular velocity of the upper arm to contribute to the speed of the ball at REL require greater muscular efforts from the horizontal adduction and internal rotation muscles. It is unknown if the IRT subjects had greater horizontal adduction and internal rotation muscular strength compared to the HAT subjects. The larger peak varus torque at the elbow for the subjects in the IRT group may indicate that they have an increased risk for elbow injury as the varus torque is produced primarily by tensile forces in the ligaments and articular capsule of the medial elbow and compressive forces on the bones of the lateral elbow joint (Feltner et al., 1986).

REFERENCES

Andrews, J.. Kinesiology 4, Wash., DC: AAHPERD, 1974.
Andrews, J. Med. Sci. Sports Exerc., 14(5), 361-367, 1982.
Feltner, M. Int. J. Sport Biomechanics, 5, 420-450, 1989.
Feltner, M. Proceedings of the 18th Meeting of the American Society of Biomechanics, Columbus, OH, submitted.
Feltner, M. et al. Int. J. Sport Biomechanics, 2, 235-259, 1986.
Keppel, G. Design and Analysis, Prentice-Hall, 1982.

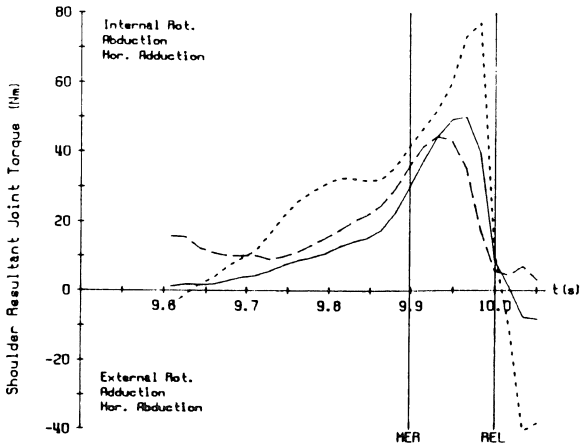

Figure 1. Mean RJTs at the shoulder: int/external rotation (solid curve); abd/adduction (large dashed curve) ; horizontal abd/ adduction (small dashed curve). The vertical lines represent the instants of maximum external rotation (MER) and ball release (REL), respectively.

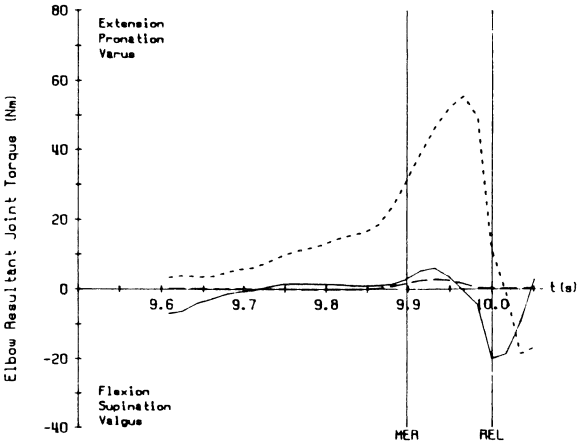

Figure 2. Mean RJTs at the elbow: flexion/extension (solid curve); pronation/supination (dashed curve); varus/valgus (small dashed curve).

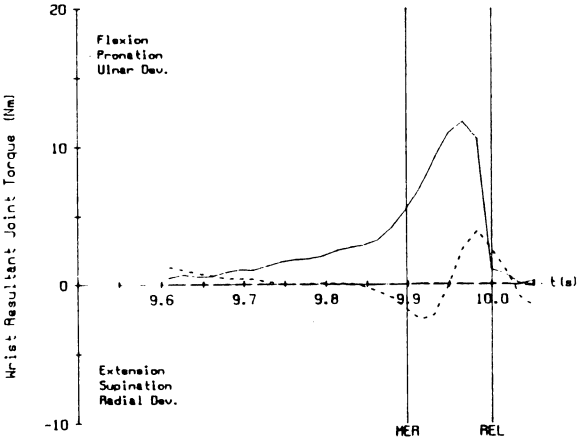

Figure 3. Mean RJTs at the wrist: flexion/extension (solid curve); pronation/supination (dashed curve); ulnar/radial deviation (small dashed curve).

STRATEGIES USED BY ELITE MALE GYMNASTS TO GENERATE HIGH FORWARD ANGULAR MOMENTUM DURING TAKEOFF IN VAULTING: A CLUSTER ANALYSIS

A. Hardyk, V. Fortney, V. Zatsiorsky

Biomechanics Lab, The Pennsylvania State University

Some stunts performed by elite gymnasts require the generation of high forward angular momentum (FAM). In particular, in horse vaulting, such extraordinary acts such as handspring with 2.5 forward somersaults (2.5 SS) and handspring with 1.5 forward somersaults and 1.5 twists (1.5 SS & 1.5 T) can be performed only if the gymnast can produce high rotation (Brüggemann, 1994). Only a few studies address FAM in handspring vaults. Brüggemann and Nissinen (1981) determined that the contact of the hands on the horse decreases FAM. Takei and Kim (1990) compared several groups of gymnasts at several competitions and found no significant differences between the FAM in the two groups in handspring vaults. There has been no attempt to determine the mechanism of the generation of the FAM at takeoff (as stated in a review of gymnastics biomechanics by Brüggemann).

The forward rotation produced in vaults must be generated by the ground reaction force (GRF) of the gymnast. To generate forward rotation, the line of action must pass behind the center of mass (CM). The GRF can be decomposed into its vertical and horizontal components. The horizontal component changes direction from negative (braking) to positive (accelerating) during the takeoff period. The vertical component of the GRF only passes behind the CM in the latter part of the takeoff when the CM is located anterior to the point of application. FAM is thus generated by two mechanisms: (a) during the first half of the support by the horizontal component of the GRF and (b) during the second half of the support by the vertical component of the GRF. From the considerations above, it follows that the horizontal component of the GRF plays an important roll in the generation of FAM.

The goal of this study was to examine the foot velocity landing patterns used by elite gymnasts in vaults requiring generation of high FAM. The issue of foot landing velocity (FLV) in vaulting has not been addressed in the sport biomechanics literature. In other activities such as walking, running, and triple jumping, the FLV with respect to the trunk is negative, especially in elite athletes.

PROCEDURES

Four 2.5 SS and three 1.5 SS & 1.5 T vaults were filmed at the 1992 Barcelona Olympic Games during various vault finals in competition. The films were digitized using Peak Performance Digitizing Software. Horizontal velocities of the CM both before and after the takeoff, the horizontal velocity of the CM of the right foot before takeoff, and FAM immediately after the takeoff were determined using the Kwon 3D Motion Analysis Package (1991). The data were smoothed with a second order Butterworth filter.

FAM was normalized by dividing the raw value by each competitor's mass and height squared. The relative horizontal FLV of the foot was computed by subtracting the horizontal velocity of the CM from the horizontal velocity of the foot.

Statistical methods were used with care due to the small number of subjects. The subjects are not randomly selected from a general population, rather they are the entire population of interest. The cluster analysis as it is presented in the S-Plus Statistical Package (1993) was used in the analysis.

RESULTS

The performance of the gymnasts showed similar trends in the following magnitudes:

- horizontal velocity of the CM before takeoff from springboard - 7.75 m/sec to 8.73 m/sec, 8.33 average.
- horizontal velocity of the CM after takeoff from the springboard - 3.62 m/sec to 6.21m/sec, 4.91 average.
- normalized angular momentum about the transverse axis - 0.472 sec^{-1} to 0.557 sec^{-1}, 0.449 sec^{-1}.

The performances differed, however, in the magnitude of FLV, both absolute and relative. Two distinct strategies for pre-landing were observed:

- highly positive values of the relative FLV, three gymnasts used this strategy, averaging 6.10 meters per second.
- relative FLV close to zero and negative (Figure 1).

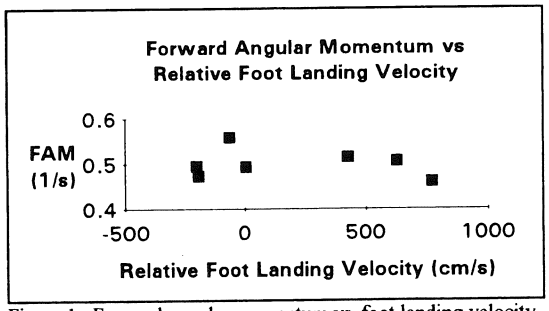

Figure 1. Forward angular momentum vs. foot landing velocity.

The first strategy is characterized by an active pre-landing where the foot landing velocity was positive and greater than four meters per second. The second strategy employed by the other gymnasts was a passive pre-landing where the relative foot velocity was close to zero or negative. A statistical cluster analysis showed that the two groups were distinct and separate.

Correlation of the angular momentum values with both absolute and relative FLV was low. This is expected since all of the gymnasts were elite athletes and performed the stunts successfully. Generation of maximum angular momentum is not the goal in gymnastics. The tasks during takeoff are to produce enough angular momentum to complete the stunt (all of the subjects were successful) and to maintain the highest possible velocity values. No strong correlations were found between FLV and other biomechanical variables.

Angular momentum was correlated with horizontal approach velocity at a level of r=0.6. A regression analysis was performed which resulted in a best fit line with the equation:

$$H_T = 0.00058 \cdot V + 0.017$$

where H_T = normalized angular momentum about the transverse axis in sec^{-1} and V = horizontal velocity in centimeters per second. Horizontal velocity of the center of mass decreased during the takeoff.

DISCUSSION

Based on the pattern of the FLV at takeoff, the athletes can be clustered into two groups as described above. The group employing the 'active' strategy of prelanding was characterized by the high positive values of the relative FLV. The athletes bring

their feet forward quickly into the springboard instead of pulling backwards. The gymnasts create a blocking action on the springboard with the forward velocity of the feet, producing rotation. The magnitude of this positive FLV was high: averaging 6.1 m/s with respect to the CM, and 14.32 m/s with respect to the ground.

In the second group, the relative FLV were close to zero or slightly negative. The feet are kept in the same position relative to the center of mass which tends to create a braking effect and generates desired angular rotation.

Neither of these strategies is used in running and jumping without somersaults. In running, forward angular momentum is not desired and the fact that the feet are moving in the opposite direction as the center of mass helps to accomplish this goal. The 'active' prelanding used by the gymnasts from the first group resembles the clawing action of the triple jump but in the opposite direction. Triple jumpers attempt to keep rotation to a minimum while still achieving the large forces necessary to jump in the horizontal direction.

The two strategies seem to be equally effective. As is shown in Figure 1, both positive and negative foot velocities with respect to the center of mass produce similar values of angular momentum. It should also be noted that both types of vaults had similar angular momentum requirements, and that both strategies were used to perform both vaults.

Although the differences in FLV strategies is interesting from an observational, or coaching, point of view, it is difficult to determine exactly what the two strategies accomplish in terms of angular momentum generation. Because there was no force data available, only assumptions as to what the forces might have been and how they might affect the generation of angular momentum can be made. The simple model presented in the introduction is evidently applicable in this case. Possible relative magnitudes of forces, their respective moment arms, and the resulting relative moments are presented in Table 1.

From this table, it can be seen that the horizontal GRF during the first half of the takeoff is one of the more important forces. What remains unclear is whether or not the two strategies of FLV do anything to increase the horizontal GRF and therefore generate more FAM.

Table 1
Relative forces, moment arms, and moments

	F_{horiz}	MA_{horiz}	F_{vert}	MA_{vert}	$M_{forward}$	$M_{backward}$
1st half of t/o	large	large	large	small	large	small
2nd half of t/o	small	large	large	small	small	small

A moderate positive correlation (r=0.6) was found between angular momentum and approach velocity and a low correlation was found between angular momentum and FLV. Higher horizontal velocity tended to produce higher angular momentum about the transverse axis independent of FLV. This may mean that the passive strategy is the only one necessary to produce the necessary FAM as long as a nominal velocity is achieved. The active strategy may only be necessary when the athlete cannot run fast enough. The data mildly supports this hypothesis. The slowest competitor was one of the athletes with an active strategy. However, one of the fastest gymnasts also utilized an active strategy and did not produce a FAM value which was predicted by the regression line. These conflicting results may indicate that there is a problem with the intrinsic assumptions in this study or that the active strategy does not really do what is postulated here. After all, the gymnast is not a rigid body and the increased FLV may not be transferred directly into FAM.

REFERENCES

Brüggemann, P., Biomechanics of gymnastic techniques: a review of recent research. To be published in Sport Science Review, 1994.

Brüggemann, P., Nissinen, M., Analyse kinematischer Merkmale des Handstützüberschlages beim Pferdsprung. *Leistungsport*, 11 Jhrg., Nr. 6, S. 537-547, 1981.

Statistical Sciences, Inc., *S-Plus for Windows User's Manual, Version 3.1*, Seattle: Statistical Sciences, Inc., 1993.

Takei, Y., and Kim, E.J., Techniques used in performing the handspring and salto forward tucked vault at the 1988 Olympic games. *International Journal of Sports Biomechanics*, Vol. 6, pp. 111-138, 1990.

ACKNOWLEDGMENTS

The authors would like to thank Liangchou Zou for digitizing the vaults used in this study, In-Sik Shin for videotaping, Yoshiaki Takei for filming the vaults at the 1992 Olympics, and Young Hoo Kwon for his technical assistance.

BODY ROLL AND BREATHING ACTION IN SKILLED AND UNSKILLED FRONT CRAWL SWIMMERS

B. Christina Kippenhan and James G. Hay

Department of Exercise Science, The University of Iowa, Iowa City, IA 52242

INTRODUCTION

Front crawl is considered to be the easiest of the four competitive strokes to learn and in many beginning swimming books it is the first stroke taught (American Red Cross, 1981; Thomas, 1989; Vickers & Vincent, 1989). Many beginning swimmers report problems in coordinating their breathing with the front crawl arm action. It was our opinion that many of these problems are caused by an inadequate body roll.

REVIEW

The inhalation phase of the breathing cycle is generally considered to take place at the end of the push phase and/or the beginning of the recovery phase of the arm on the breathing side (American Red Cross, 1981; Maglischo, 1982; Reischle, 1988; Vickers & Vincent, 1989; Wilke & Madsen 1988). Little attention has been paid to the body roll (clockwise and counterclockwise rotation of the transverse axis through the shoulders relative to the horizontal) in connection with the breathing action. Maglischo (1982) states that the turning of the head for breathing should be coordinated with the body roll and that a breath should be taken when the body is rolled maximally toward the breathing side. Others (Renner, et al., 1988; Vickers & Vincent 1989) have stated that the shoulders should be kept horizontal instead of rolling from side to side while breathing, to keep the body in good alignment. The purpose of this study was to evaluate the body roll during a breathing and non-breathing cycle of front crawl swimming for skilled and unskilled swimmers.

PROCEDURE

Fifteen students at the University of Iowa volunteered to take part in this study. Eight rated themselves beginning-to-intermediate swimmers with problems during breathing (unskilled) and seven as advanced swimmers with at least four years of competitive swimming experience and no such problems (skilled). Each subject swam six trials of 15m at their preferred speed (three trials holding the breath throughout and three trials breathing to the preferred side). All performances were videotaped from the front. A balsa fin was mounted on the subject's back to permit body roll angle vs. time data to be obtained (Beekman, 1988). The videotape was analyzed and the body roll vs. time data determined using the Peak 2D system. The obtained curves were analyzed qualitatively.

RESULTS AND DISCUSSION

Skilled Swimmers. The body-roll angle vs. time curves (hereafter referred to as the 'body roll curve') for the non-breathing condition had the same basic characteristics for all subjects (Fig.1, dashed line).

The mean value for the maximum body roll angle for the swimmers was 46° ($\pm$ 7°). The maximum body roll angle was obtained shortly after the hand of the arm on the breathing side exited the water. The body roll curve leveled off at about this point and assumed a plateau-like appearance. The swimmers held the maximum body roll angle for almost 20% of the stroke time.

The body roll curves for the breathing case (Fig.1, solid line) were generally similar to those for the non-breathing case. Some showed a small shift of the curve towards the breathing side (max. shift 8°) and/or a flatter plateau, but none changed their timing (the relative time between the entry and exit of the hands, and the coordination between the body roll and the push/pull or recovery phases of the arms). This indicates that the observed maximum body roll angle together with the observed plateau in the body roll curve (effectively a stop in body roll) allowed the subjects sufficient time to inhale conveniently.

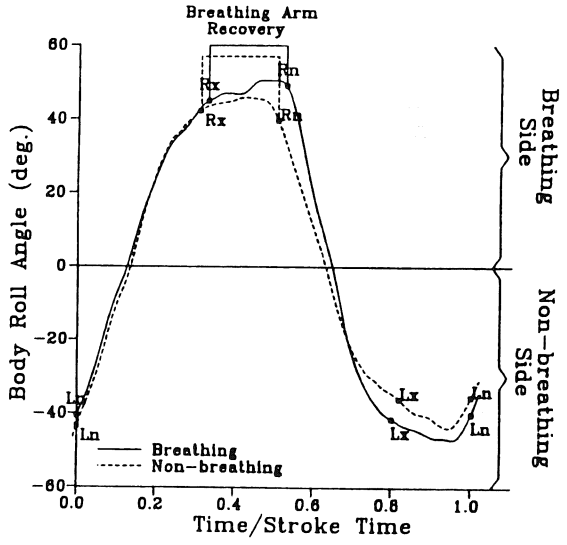

Fig.1: Body-roll vs. time curves for a typical skilled swimmer. Lx = exit of left hand, Ln = entry of left hand, Rx = exit of right hand, Rn = entry of right hand.

Unskilled Swimmers. The body roll curves for the unskilled swimmers revealed a lot of variability.

For the non-breathing case, some of these swimmers had very irregular curves and often small body roll angles (Fig.2). Others had regular curves with maximum angles reaching similar values to the skilled swimmers. Yet, even the most similar did not have a plateau as marked as the skilled swimmers (Fig.3). Often the subjects also showed a late hand exit (after the maximum body roll angle was obtained) and a late hand entry (body roll angle close to 0^{o}) compared to the skilled swimmers. In these cases, it would be reasonable to expect the swimmer to have some difficulty integrating the breathing and swimming actions because the body roll angle is too small to bring the mouth above the water, and/or because the maximum body roll angle is not held long enough to allow sufficient time to inhale conveniently unless changes are made in the body roll or in the timing.

For the breathing case, the unskilled swimmers exhibited a major increase in maximum body roll angle towards the breathing side of up to 40^{o}. The curves for all subjects included a plateau and this was generally near the exit of the hand on the breathing side (This is not the case for the subject in Fig.2). Most of the subjects still showed a late hand exit -- that is, an exit after the curve had already leveled off. It seems that with this timing, an extended period with the body at its maximum roll angle (as reflected by the plateau in the body roll curve) is not enough to allow the swimmer to inhale sufficient air and that a greater body roll is also needed.

In general, the hand on the breathing side entered the water later in the stroke cycle in the breathing case than in the non-breathing. Compared to the non-breathing case, more time (relative to the stroke time) was spent in the recovery (that is between exit and entry) of the hand on the breathing side in the breathing case.

All the mentioned changes elongate the part of the stroke cycle during which inhalation is possible, and therefore compensate for inadequacies evident in the non-breathing case. However, because all subjects altered their stroke rhythm and timing, the breathing can be said to have interfered with the stroke.

In comparison to skilled swimmers, unskilled swimmers demonstrate clear differences in body roll, manifested especially in differences in the amount of body roll, and in the timing for the non-breathing and breathing cases. Furthermore, while the body roll curves of the skilled swimmers are generally similar for both cases, the ones of the unskilled swimmers show clear differences between the two cases. The differences indicate that the breathing disrupts the stroke technique and they can thus be viewed as flaws in the swimming technique. A first step in eliminating the breathing problems would be to put an increased emphasis on achieving a consistently large body roll as shown by the skilled swimmers. If timing differences and breathing difficulties persist additional steps have to be taken.

REFERENCES

American National Red Cross. Swimming and Aquatics Safety,1981.

Beekman, K.M. et al. J. of Swim Res., 4(3), 11-14, 1988.

Maglischo, E.W. Swimming Faster, Mayfield Publ., 1982.

Reischle, K. Besser Schwimmen, sportinform, 1988.

Renner, W. et al. Schwimmen, Sportverlag, 1988.

Thomas, D.G. Advanced Swimming - Steps to Success, Leisure Press, 1990.

Vickers, B. et al. Swimming, Wm.C.Brown, 1989.

Wilke, K. et al. Das Training des jugendlichen Schwimmers, Karl Hofmann, 1988.

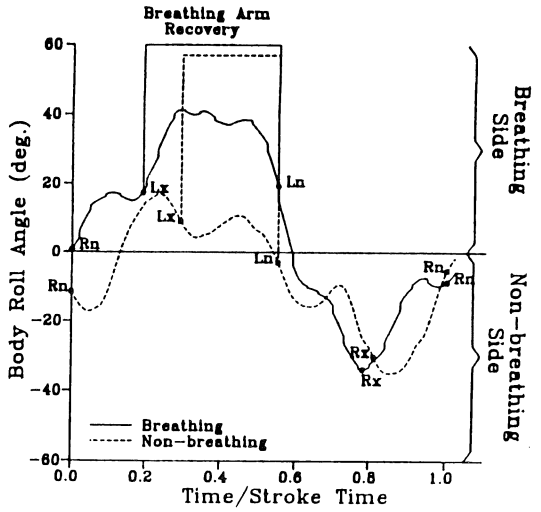

Fig.2: Body-roll vs. time curves for an unskilled swimmer. Lx = exit of left hand, Ln = entry of left hand, Rx = exit of right hand, Rn = entry of right hand.

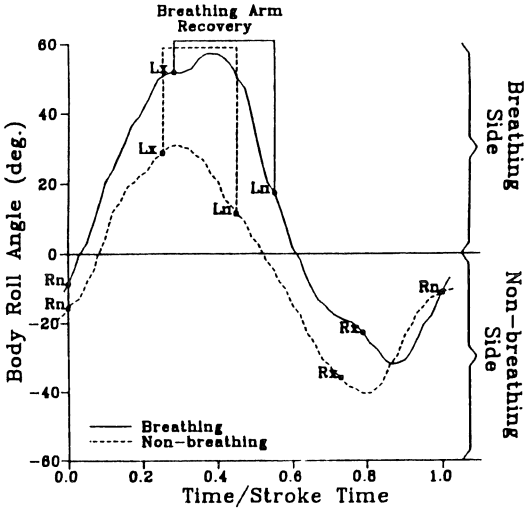

Fig.3: Body-roll vs. time curves for an unskilled swimmer. Lx = exit of left hand, Ln = entry of left hand, Rx = exit of right hand, Rn = entry of right hand.

Net Joint Moment Powers and Muscle Recruitment Patterns During Stop and Go Landing Movements

Jill L. McNitt-Gray, Barry A. Munkasy, Michelle Welch,
Jacklyn G. Heino, James P. Eagle, and Terry A. Smith

Biomechanics Research Laboratory
University of Southern California
Los Angeles, CA 90089-0652

INTRODUCTION

Injuries to the musculoskeletal system, close to the point of external force application (e.g. foot, shank, ankle, and knee; NCAA, 1987, 1990), account for the majority of injuries experienced by athletes involved in repetitive landing activities. Load experienced during contact may be dissipated by progressive attenuation of forces through the microstructures of bone or by lengthening of activated muscle (Radin & Paul, 1970). As an active muscle is lengthened, the muscle absorbs energy. This stored energy may then be dissipated within the musculoskeletal system, as in land and stop movements. Transfer of energy by biarticular muscle-tendon units from the distal to proximal joints may enable the proximal muscles to assist distal muscles dissipate the mechanical energy of the body during landing (Prilutsky & Zatsiorsky, 1994). Active lengthening of muscle, may also enhance the force production (Komi & Bosco, 1978), as in land and go movements.

In this study, the intended movement following landing (Stop vs. Go) was hypothesized to influence load dissipation within the lower extremity musculoskeletal system. This hypothesis was tested by comparing net joint force and moment powers and muscle recruitment patterns (EMG) between Stop and Go landings.

PROCEDURES

Collegiate female volleyball players at the University of Southern California (n=8) volunteered to serve as subjects. During data collection, a net and ball were suspended along side of the force plates so that the volleyball players could perform a realistic blocking movement without contacting the net. Stop landings were performed by moving laterally to the left using normal footwork, jumping from the floor, blocking a suspended ball with arms on each side of the ball, and landing. During Go landings, the subject landed and immediately moved laterally to the starting position. Trials were blocked within each experimental condition and randomized between subjects. Standardization of the ball height to stand and reach height of individual subjects was successful in minimizing differences in body center of mass (BCM) velocity at contact between trials and subjects. Reaction forces were sampled at 800 Hz. Saggital plane kinematics were recorded simultaneously using high speed video (200 fps; NAC Motion Analysis System). Activity of the soleus (SO), medial gastrocnemius (MG), vastus medialis (VM), vastus lateralis (VL), rectus femoris (RF), gluteus maximus (GM), and semitendonosis (ST) muscles prior to and during landing were monitored using surface electromyography (1800 Hz; Beckman Silver-Silver Chloride electrodes; Differential Amps, Data, Inc.). Each coordinate of the body landmarks (Zatsiorsky et al., 1987) were digitized (Peak Performance, Inc.) and filtered using a fourth order Butterworth Filter (Saito & Yokoi, 1982) with a cut-off frequency derived by the method of Jackson (1979). The EMG signals from each muscle were processed as specified by the International Society of Electrokinesiology (ISEK, 1985) using a high and low pass analog filters, rectified, and integrated during intervals prior to and during the landing. Synchronized kinematic and reaction force data were used to calculate the net joint forces, moments, and powers for the ankle, knee, and hip of the lead leg (left) using Newtonian mechanics. Significant differences in normalized kinematics, reaction forces, joint kinetics, and EMG patterns were compared between tasks using within subject analysis of variance ($p<.05$).

RESULTS AND DISCUSSION

The general shape of the vertical and horizontal reaction force-time curves observed during the landings of the Stop and the Go task were similar. However, greater asymmetry in reaction forces (RFs) between lead (left) and lag (right) legs were observed during Go, as compared to Stop landings. In some cases, lead leg peak vertical RFs during the Go task were 3.5 BW greater than those observed during the Stop task. Subjects demonstrating asymmetry in RFs between lead and lag legs have apparently modified their approach to the landing in preparation for the subsequent Go task.

Throughout the landing of both Stop and Go tasks, ankle, knee, and hip flexion velocities (-) and ankle extensor (+) moments were observed. In contrast, knee and hip netJMs tended to oscillate 180 degrees out of phase. During periods of knee flexor (-) and ankle extensor (+) netJMs, MG activity was observed. Biarticular muscle activity, observed in correspondence with ankle (-) and the knee (+) net JMPs, provides the potential for energy transfer by the biarticular MG muscle-tendon unit. During periods of hip extensor (+) and knee flexor (-) netJMs, ST EMG was observed. Biarticular muscle activity, observed in correspondence with ankle and hip (-) and the knee (+) net JMPs, provides the potential for energy transfer by the biarticular ST muscle-tendon unit. This correspondence between biarticular muscle activation and adjacent joint netJMPs provides experimental data in support of distal to proximal transfer of energy via biarticular muscles during mechanical energy dissipation, as proposed by Prilutsky and Zatsiorsky (1994). Mechanical energy dissipation by more proximal muscles may prove advantageous in reducing distal lower extremity injuries during landing.

REFERENCES

ISEK, Standards, 1985.

Jackson, K.M., IEEE Trans. Biomed. Eng., 26, 122-124, 1979.

Komi, P. & Bosco, C. Biomechanics VI-A, 79-85. University Park Press, Baltimore, MD, 1978.

NCAA Injury Surveillance System, 1986, 1990.

Prilutsky, B.I. & Zatsiorsky, V.M., J. Biomech. 27(1), 25-34, 1994.

Radin, E. L. & Paul, I. L., Arthritis & Rhuemat., 13, 139-144, 1970.

Saito, S., & Yokoi, T., Bull. of Hlth & Sports Sci., U of Tsukuba, 5, 201-206, 1982.

Zatsiorsky, V. , Seluyanov, V., & Chugunova, L.G. Contemporary problems of biomechanics, 272-289, 1988.

ACKNOWLEDGEMENTS

This project was funded in part by the NCAA. The authors would like to thank members of the USC Volleyball team and undergraduate research assistants in the USC Biomechanics Laboratory for their assistance with this project.

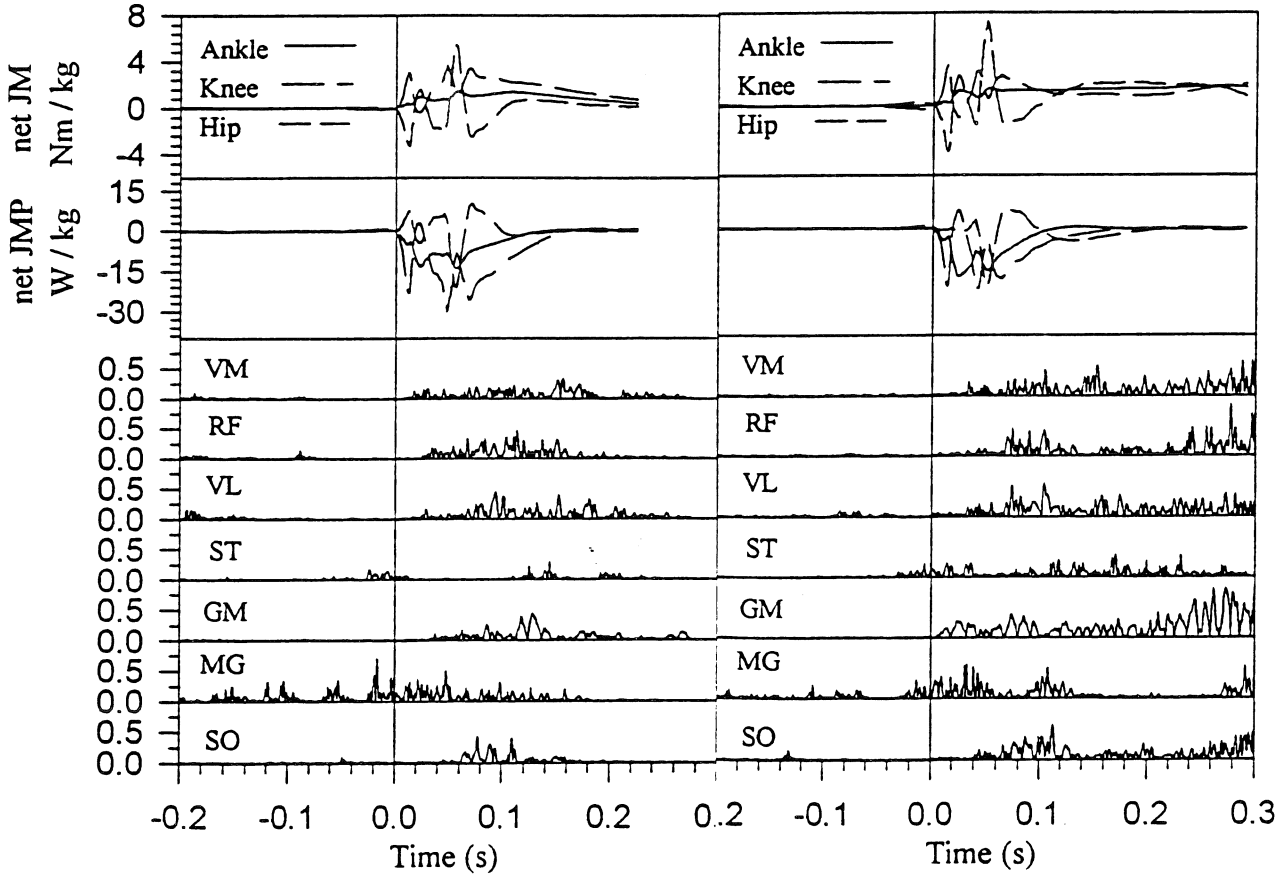

Figure 1. Representative ankle, knee, and hip net Joint Moments (netJM), net Joint Moment Powers (netJMP), and rectified EMG of lower extremity muscles during Stop and Go tasks. Note EMG is normalized to the peak amplitude observed for each muscle during all trials by one subject. The EMG is shifted to the right to account for a 50ms electromechanical delay.

DIFFERENCES BETWEEN ONE-FOOT AND TWO-FOOT VERTICAL JUMP PERFORMANCES

P.F. Vint, J.K. DeWitt, A.P. Marsh, S.P. McLean, R.D. Seidler, C.P. Sherwood, R.N. Hinrichs, and P.E. Martin

Exercise and Sport Research Institute, Arizona State University, Tempe, AZ 85287-0404

INTRODUCTION

The purpose of this investigation was to quantify kinematic differences between one- and two-foot vertical jumping performances for maximal height. Fifteen subjects performed both jump styles with a four step approach at a self-chosen distance. Although overall jump and reach heights were not different, one-foot jumps elicited significantly greater CM heights and horizontal CM velocities at takeoff, while two-foot jumps demonstrated greater flight heights. Horizontal approach velocities were not different between jump types, but two-foot jumps had significantly greater negative vertical CM velocities prior to takeoff. It was concluded that different strategies were utilized during the approach-takeoff transition to attain similar overall performance results during one- and two-foot jumping.

REVIEW AND THEORY

During the performance of a maximal effort vertical jump, the goal of the task is to jump and reach as high as possible. During the takeoff phase, both upward momentum and large ground reaction forces are induced in order to propel the center of mass (CM) in the vertical direction. Using the simple deterministic model shown in Figure 1, it can be shown that the maximum vertical height to which an individual can jump and reach may be described by the sum of four lesser heights: takeoff height, flight height, reach height, and loss height. The overall vertical height may be considered to be the absolute maximum height an individual can jump and reach. Takeoff height defines the height of the CM at the instant the individual leaves the ground. Flight height refers to the actual vertical height to which the CM was elevated during the in-flight phase of the jump. Reach height describes the vertical distance from the CM to the fingertips at the instant the maximum jump and reach height is evaluated. Loss height refers to the difference between the absolute peak height of the CM and the height of the CM at the instant the maximum jump and reach height is evaluated.

Based on anecdotal evidence, it appears that some performers seem to prefer one-foot takeoff jumps, while other athletes favor two-foot takeoffs. When attempting a two-foot jump, the performer has the advantage of utilizing force generated from two legs to impart propulsive forces upon the ground (Van Soest et al., 1985), while during the one-foot jump the performer may gain advantage from the elevated CM at takeoff which is attributable to the elevation of the non-support leg. However, the fundamental differences between one-foot and two-foot jumps from an approach run have not been quantified in the literature. The purpose of this investigation was to examine the kinematic differences between one- and two-foot vertical jumping performances for maximal height in the context of the deterministic model shown in Figure 1.

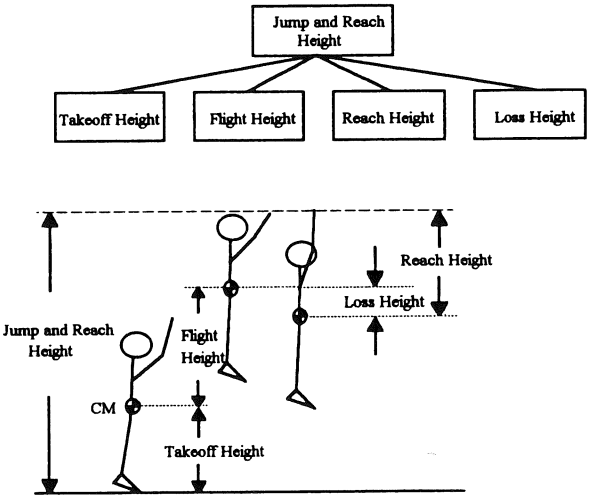

Figure 1. Factors determining vertical jump and reach height.

PROCEDURES

Fifteen male physical education students volunteered to participate in this study. After a brief warm up period, each subject performed a block of five one- foot jumps and five two-foot jumps while being videotaped at 60 Hz in the sagittal plane. Each style of jump was preceded by a four step run up at the performer's freely chosen velocity. Trial blocks were randomized across subjects. Jump and reach heights were measured for each trial using the Vertec vertical jump height measuring device. The highest jump and reach height for each style for each subject was considered for further analysis. Selected jumps were digitized with the Peak Performance Technologies Motion Measurement System. Twenty-one points were digitized to define a 14 segment model of the body. Segmental masses and center of mass locations were obtained from Clauser et al., (1969) as adjusted by Hinrichs (1990) and

were used to compute the whole body CM location during the entire trial. Prior to CM calculations, the 2-D coordinate data were rotated from the camera reference frame into a true vertical-horizontal lab reference frame. Horizontal and vertical coordinates of each point were smoothed with a fourth order, zero-lag, Butterworth digital filter using individually selected cutoff frequencies. Takeoff height, flight height, reach height and loss height were calculated using the vertical location of the CM at selected events. Whole body CM velocity was also computed throughout the entire trial. A matched-pairs MANOVA was utilized to examine differences between mean results over the set of dependent variables.

RESULTS

Table 1 summarizes the performance characteristics of one-foot and two-foot jumps. Takeoff height was significantly higher in one-foot jumps ($p < .001$) while flight height was significantly higher in two-foot jumps ($p < .001$). Overall jump and reach height, reach height, and loss height were not different between jumping styles. Upon finding differences in flight height, a post-hoc analysis of the velocity profiles was initiated to try to better understand the differences which were noted between one-foot and two-foot jumps (Table 2). From this follow up analysis, it was determined that the horizontal approach velocity was not different between one- and two-foot jumps. However, both the horizontal flight velocity and the minimum vertical velocity prior to takeoff were significantly different between jump styles ($p < .001$).

Table 1. Mean Values for Selected Performance Variables during One- and Two-Foot Jumps ± STD

	One-Foot (cm)	Two-Foot (cm)
Overall Height	304.7 ± 14.5	303.1 ± 11.2
Takeoff Height	133.6 ± 6.3*	125.5 ± 4.7
Flight Height	43.0 ± 6.8	50.4 ± 6.7†
Reach Height	128.1±7.2	127.2 ± 6.5
Loss Height	0.4 ± 0.3	0.5 ± 0.6

*1-foot significantly higher than 2-foot

†2-foot significantly higher than 1-foot

Table 2. Mean Values of Selected CM Velocity Parameters during One- and Two-Foot Jumps ± STD

	One-Foot (cm/sec)	Two-Foot (cm/sec)
Avg. Horizontal Approach Velocity	353.1± 51.4	326.3 ± 56.3
Avg. Horizontal Flight Velocity	183.8 ± 19.4*	111.4 ± 21.2
Min. Vertical Velocity Prior to Takeoff	-14.8 ± 18.4	-81.9 ± 23.7†

*1-foot significantly faster than 2-foot

†2-foot significantly faster negative velocity than 1-foot

DISCUSSION

Overall jump and reach height is dependent upon the height and the vertical velocity of the CM at takeoff, and the position and orientation of the body about the CM at the instant the maximum height is evaluated. The results of this study indicated that while overall jump and reach heights were similar between one-foot and two-foot jumps, the strategies employed to achieve these results were notably different. During one-foot jumps, subjects benefited from an increased takeoff height which was attributable to the elevation of the non-support leg. During two-foot jumps, subjects were able to achieve greater flight heights, perhaps because of the greater availability of musculature which could be used for the generation of vertical impulses against the ground.

It was interesting to note that while the difference between one-foot and two-foot flight height was statistically significant, the magnitude of this difference was only 7.4 cm. During two-foot jumps, a significantly higher negative vertical velocity prior to takeoff was observed. This finding could be an indication that the subjects were utilizing a more rapid vertical countermovement action during two-foot jumps than for one-foot jumps. One-foot jumps elicited a much lower negative vertical velocity prior to takeoff and demonstrated a less pronounced change in horizontal velocity during the approach-takeoff transition. From the analysis of the velocity profiles, it was apparent that the difference in flight height may be explained, at least in part, by a difference in the strategies which were adopted during the approach-takeoff transition. While the two-foot performances demonstrated vertical CM velocity profiles which were consistent with traditional countermovement actions, it was possible that one-foot jumps were able to derive a beneficial eccentric loading from the radial motion of the CM moving over the support leg which has been described by Dapena and Chung (1988) for high jumping. Briefly, during the approach-takeoff transition, the radial motions of the segmental and whole body centers of mass with respect to the support foot may have helped in the development of faster eccentric and slower concentric conditions of the takeoff leg musculature (Dapena & Chung, 1988).

Further research should be directed at identifying the mechanisms which would help explain the differences which were observed between one- and two-foot vertical jumping performances.

REFERENCES

Clauser, C.E., et al., (1969). AMRL 69-70, Wright-Patterson Air Force Base, Ohio, NTIS #AD-710-622.

Dapena, J., & Chung, C.S. (1988). *MSSE*, **20** (3), 290-302.

Hinrichs, R.N. (1991). *JOB*, **23**, 949-951.

Van Soest, A.J., et al. (1985). *MSSE*, **17** (6), 635-639.

A 3D COMPARISON OF GOLF SWING STYLES

R.J. Neal, A. Hanna and K. Meredith

Department of Human Movement Studies, The University of Queensland
Brisbane, AUSTRALIA

INTRODUCTION

Central to elite performance in golf is the execution of a powerful, controlled and consistent swing. Dependable replication of a swing pattern involves the precise, sequential coordination of various body parts. Accordingly there has been much conjecture surrounding the optimal kinematic and kinetic characteristics of the golf swing.

Numerous studies have used 2D and 3D cinematographical techniques to verify dynamic models (Budney & Bellow, 1982; Jorgensen, 1970), describe motion (Milburn, 1982; Neal & Wilson, 1985; Vaughan, 1981) and optimise swing kinematics and kinetics (Lampsa, 1975). These studies rarely extended to a comparison of different skill level golfers or to different swing styles of elite level players. Forceplates have been used to analyse the centre of pressure (CP) and ground reaction force (GRF) characteristics of a golf swing. Initial studies in this area provided "normative" or descriptive data pertaining to the kinetic characteristics of the golf swing (Cooper *et al* 1973), while later investigations used CP and GRF data in an attempt to discriminate between high and low handicap golfers (Richards *et al* 1985; Williams & Cavanagh, 1983).

Two styles of swinging are in currently vogue, namely the traditional left-to-right (LR) and the more modern rotational (LB) style. In the LR (e.g, Greg Norman) much of the player's movement is lateral as the hips move away from and then toward the target, with the leading arm held nearly straight during the back swing and downswing. The LB style, (e.g. Nick Faldo), is typified by a rotating action about the body's longitudinal axis. The shoulder is held tightly retracted throughout the movement with the leading elbow flexing slightly at the top of the swing.

No scientific studies have been found that have verified the qualitative differences noted above. The intention of this study was to identify mechanical differences between these two styles of swinging in golf and then to determine which of the two styles had the greatest consistency of execution.

METHOD

Subjects

Twenty low handicap or professional male golfers were subjects in this study. On the basis of their previous training experience and after examination by a professional golf coach, the subjects were categorised as either the LR or LB groups.

Data collection and procedures

After a warm-up period subjects were required to hit fifteen shots with their driver and seven (7I) iron. A trial consisted of the subject striking a golf ball from a customised driving range mat into a net placed approximately two metres away. During each trial time synchronous data were collected from a force platform and a high speed video (HSV) system (Motion Analysis Corp).

CP data were obtained through an AMTI (LG64-1) force plate while club, arm and shoulder motion were obtained using the HSV system. The period from the commencement of the backswing to the point of impact was determined through the use of a photocell and a microphone. When the clubhead broke the photocell beam at the start of the backswing, data acquisition commenced. The microphone picked up the sound of impact and a pulse was sent to the computer that collected the force data.

Customised software identified temporal information, CP movement and normalised the data to stance position on the plate and time. The maximum and minimum excursions in the AP and lateral directions were determined and an excursion score (EXC), the ratio of the lateral to the AP displacements was calculated for each trial. Total swing time (TT), the time between the start of the take away and impact was used to provide normalised values of the times to maximum and minimum displacements of the CP in the lateral and AP directions.

The Motion Analysis 3D tracker was used to generate 3D coordinates of the reflective markers. These data were then used to calculate the following variables which were hypothesised as measures that could be used to discriminate between the two swing styles: the maximum and minimum displacement of the clubhead and the times of these occurrences; the velocity and acceleration of the clubhead; the maximum and minimum elbow angles.

Statistical analysis

The dependent variables (e.g., EXC) were submitted to a two-way (style and club) repeated measures ANOVA. The source of significant differences ($\alpha = .05$) among club conditions was detected using Newman-Keuls post-hoc test. A coefficient of variation (after Winter, 1979) was used to measure the consistency of swing kinematics. This score was also submitted to a two way ANOVA. Discriminant analysis was used to ascertain which mechanical variables were able to distinguish between swing styles.

RESULTS

Qualitative examination of the CP traces indicated that the LR group produced a more elongated CP pattern than the LB group. This finding was supported by the EXC scores of the golfers where the LR group was significantly greater ($p < .05$) than the LB group.

The temporal data for the LR and LB groups displayed in Table 1 revealed some further differences between the groups. While both groups had extremely similar values for the normalised time taken to reach minimum excursion in the lateral direction (tY_{min}), the groups differed significantly in the time to reach maximum lateral excursion (tY_{max}) ($p < .05$). The LB group transferred their weight from back to front foot at a greater rate than that of the LR group.

When using the driver players produced a longer ($p < .05$) total excursion in the lateral direction than with the two irons. Furthermore there was an incremental increase in the in the maximum CP excursion in the AP direction as club length increased. This increase reflected the change in position of the centre of mass of the club (relative to the feet) as shaft length increased.

Under all club conditions the LB golfers displayed a positive velocity at impact in the AP direction while the LR golfers had small positive or negative velocities. This difference was statistically significant ($p < .05$) indicating that while the LB players consistently hit from inside the

line of the target, the LR group approached the ball from positions either marginally inside or outside the target line.

Although it was anticipated that the minimum elbow angle of the LB group would be smaller than that of the LR group a non-significant difference ($p > .05$) between them was found.

DISCUSSION

To date studies examining the golf swing have assumed that the swings of elite golfers conform to a standard swing and differences were attributed to individual idiosyncrasies. This study has shown that identifiable swing styles exist amongst low handicap golfers, dependent upon the coaching received by the player.

The intention of both swing styles is to produce a repeatable whole body movement that will result in a powerful but controlled striking action. The results of this study show that differences exist in the way in which they attempt to achieve this goal. Fundamentally the LB style involves rotation of the body around its longitudinal axis, the player winding up and then uncoiling, while the LR group derives power through the transfer of weight in an exaggerated back foot to front foot movement.

The differences in swing styles between the two groups were evident in both the CP and kinematic data. Not only were consistent patterns of weight transfer found (cf. Williams and Cavanagh, 1983) but distinguishable differences were found in the amount of AP and lateral movement of the CP for the two swing styles. The difference between the groups on the EXC score coupled with the large lateral displacement of the LR group illustrated the tendency for this group to transfer weight from back to front foot to a greater extent than the LB group.

Kinematic analysis revealed differences in the movement of the clubhead, with the LR group reaching minimum displacement in the AP direction earlier as well as displaying tendencies to displace the club further along the lateral direction than the LB group. This result may be understood in terms of a simplified model of the swing of both groups of golfers. After the initial cocking of the wrists the swing of the LB group loosely approximates the uni-planar models assumed by previous studies (Budney & Bellow 1982; Jorgensen, 1967; Lampsa, 1975). The LR swing can be thought of occurring in two planes, the first inclined more steeply than the second and used during the backswing, and the second, used on the downswing.

The clubhead velocity in the AP direction at impact showed that the LB group hit consistently from inside the target line while the LR group were more variable, approaching the ball from both inside and outside the target line. Further study examining the angle of the club face at impact and the flight of the ball would be needed to determine if this difference would influence ball projection characteristics and flight patterns.

The groups did not differ significantly on a number of important variables. Firstly, for both groups of golfers the minimum excursion of the CP along the AP direction occurred in the last 10% of the downswing. Thus, regardless of swing style, at impact the weight of the golfers was centred close to the heel of their front foot, indicative of the golfers' need for stability at impact.

Secondly, the velocities in the lateral direction at impact for both groups were not significantly different ($p > .05$). Thus, although the styles were distinguishable in terms of mechanical factors, the extremely important characteristic of clubhead speed was not different.

Golf coaches have qualitatively described differences between the two most common swing styles of modern golf but no scientific research has been conducted to quantitatively investigate these differences. CP motion as well as clubhead kinematics were investigated and differences in the mechanical factors of excursion ratio and clubhead velocity were found to differentiate the two styles.

REFERENCES

Budney, D & Bellow D 1982 On the swing mechanics of a matched set of golf clubs. R Quart Exer Sport 53:185-192.

Cooper, JR et al. 1973 Kinematic and kinetic analysis of the golf swing, Biomechanics IV pp. 298-305.

Jorgensen, T 1970 On the dynamics of the swing of a golf club. Am J Physics 38:644-651.

Lampsa, MA 1975 Maximising distance of the golf drive: an optimal control study. ASME 97 (Series G):362-367.

Milburn, PD 1982 Summation of segmental velocities in the golf swing. MSSE 14:60-64.

Neal, RJ & Wilson, BD 1985 3D Kinematics and kinetics of the golf swing. Int J Sport Biomech 1:221-232.

Richards, J et al 1985 Weight transfer patterns during the golf swing. R Quart Exer Sport 56:361-365.

Vaughan, CL 1981 A three dimensional analysis of the forces and torques applied by a golfer during the downswing, Biomechanics VII-B pp. 325-331.

Williams, KR & Cavanagh, PR 1983 The mechanics of foot action during the golf swing and implications for shoe design. MSSE 15:247-255.

Table 1: Temporal data (Mean (SD)) for the two groups.

	Group	
	LR	LB
TT(ms)	1120 (68)	925 (113)
tX_{max}*	58 (47)	21 (19)
tX_{min}*	92 (5)	92 (4)
tY_{max}*	99 (1)	87 (14)
tY_{min}*	54 (24)	56 (15)

*Values presented as a percentage of the total swing time.

SESSION 4:

PROSTHETICS/ORTHOTICS

MICROMOTION OF AN UNCEMENTED FEMORAL COMPONENT UNDER SIMULATED IN VIVO GAIT LOADS

F. C. Barich, T. D. Brown, J. J. Callaghan

Departments of Orthopaedic Surgery and Biomedical Engineering, University of Iowa, Iowa City, IA 52242.

INTRODUCTION

Micromotion is defined as small-scale recoverable interfacial displacement between bone and prosthesis. A study was undertaken to characterize the motion of a new uncemented total hip arthroplasty femoral component and to determine the effects of proximal and distal fit. To that end, a method was developed to apply three-dimensional quasi-physiologic loads to the head of the component and to quantify interfacial micromotion everywhere on the component surface. The simulated loading encompassed both level walking and stair climbing gait cycles. Displacement measurements were taken with triads of liquid-metal strain gages (LMSG) outrigger-mounted to the surface of the component. Rigid-body kinematics were used to estimate three-dimensional component motion. The result of each test procedure was a full temporal and spatial mapping of micromotion over the entire surface of a component. Preliminary results indicate that tight-proximal fit is critical to maintaining micromotion within acceptable levels for bone ingrowth.

REVIEW AND THEORY

Excessive micromotion tends to inhibit bone ingrowth into porous coatings on the surface of prostheses. The maximum amount of micromotion which allows ingrowth to occur is not precisely known, but an accepted upper limit is around 150μm [6]. For new component designs, an accurate prediction of motion is obviously desirable before clinical application. Two significant problems in determining micromotion in vitro are reproduction of the complex loading observed in vivo, and measurement of micromotion over the entire porous coated region. Previous studies simplified the loading by applying only axial or torsional loads separately. Some work has applied axial and torsional loads simultaneously, but only statically [2], and measurements of micromotion have generally involved only one or two sites on the prosthesis.

A clinical concern of uncemented hips is the persistence of thigh pain, particularly during stair climbing and rising from chairs, for up to two years in a relatively high percentage of patients [3]. Exact anatomical fit with uncemented hips is desirable, but difficult to achieve in practice. It is suspected that less than optimal fit may lead to greater magnitudes of micromotion and may be a factor in the occurrence of thigh pain.

A study was undertaken to characterize the micromotion of femoral components with less than ideal component fit in the medullary canal. Time-variant, three-dimensional, quasi-physiologic loads simulating level walking and stair climbing were applied to surgically implanted femoral components. Rigid-body motion kinematics were used to estimate micromotion and subsidence, defined as permanent displacement, over the entire surface of the component.

PROCEDURES

Noncemented femoral components (BIOMET Ranawat/Burstein Total Hip System) were implanted in eight fresh-frozen cadaver specimens by an experienced surgeon following standard operating procedures. Tightness of fit was determined based on radiographs and on the insertion process itself. Templates were used to determine optimal component size for tight fit, both proximally and distally. An undersized component was used to achieve loose-proximal fit. Distal fit was based on whether isthmus cortical reaming was performed prior to insertion. Classification of loose-distal fit was when little or no cortical reaming was performed. Both fit classifications were verified radiographically after implantation. Three categories of fit were used: tight proximal/tight distal (T/T); tight proximal/loose distal (T/L); loose-proximal/tight-distal (L/T).

A digitally controlled dual-actuator materials testing machine (MTS Bionix 858) was used in conjunction with a hemi-pelvis simulation fixture to apply three-dimensional cyclic loads to the head of the component. The load cycles consisted of a series of axial and torsional ramps designed to match the dynamic loading pattern observed in vivo for level walking (LW) and stair climbing (SC) gait cycles [1,4]. A complete test cycle for a specimen consisted of 1000 load cycles. Table 1 shows the pattern of loading.

Table 1. Femoral Component Load Regime

Cycle Number	Gait	Cycle Number	Gait
1-5	LW	105-110	SC
6-10	SC	111-155	LW
11-55	LW	156-255	LW
56-60	SC	256-260	SC
61-105	LW	261-1000	LW

Two orthogonal triads of LMSG's were used to measure three-dimensional displacement. One triad was positioned at the porous coated region and one near the distal tip of the component. A seventh gage was used to measure linear displacement at the third location. The displacements were used to compute three-dimensional

rigid-body kinematics of the femoral component [5]. LMSG output was recorded at a frequency of 100Hz for five consecutive load cycles. The five cycles recorded are the last five of each set listed in Table 1 except for the series from 261-1000. In this set data was recorded beginning with cycles 261, 501, and 1001. The reported micromotion was an average over the five cycles. Micromotion was calculated at over 100 locations on the component and supplied to a contouring routine to assemble continuous mappings.

RESULTS AND DISCUSSION

To our knowledge, this is among the first micromotion studies to use realistic load histories patterned after actual gait data. The maximum micromotion experienced at a significant number of locations on the component does not occur at the instant of maximum joint resultant, maximum axial, or maximum torsional loading. This was observed in all specimens at every stage of testing. Micromotion of seven of the eight specimens stabilized after 150 cycles. The eighth became stabilized after 200 cycles.

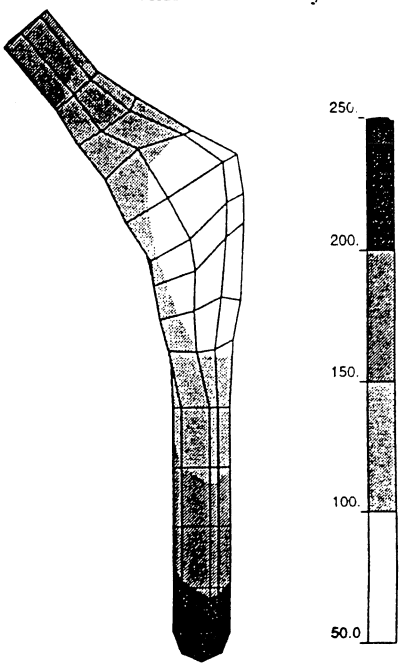

Figure 1. Micromotion (μm) After 1000 Cycles for a Typical T/T Fit Specimen

Figure 1 shows a typical distribution of micromotion over the component surface. As shown here the component experienced more motion at the distal tip than near the porous coated region. This trend held for both level walking and stair climbing and was consistent for all three fit categories. All but one component showed less micromotion on the lateral aspect than on the medial aspect. The trend for all specimens indicated that micromotion could be approximated by rotation about an axis through the proximal-lateral apex of the component and directed at approximately 45° downward in the coronal plane.

The micromotion mappings were used to determine the percentage of the porous coated region that underwent certain ranges of motion. Table 2 shows these percentages for the various fit categories and loading cycles. The percentage reported is the average of the components in the category. Three of the specimens failed due to trochanter breakage before completing the full 1,000 cycle regime (two specimen failed after 120 cycles and one after 350). The L/T components showed excessive micromotion. Only one of the four components in this category showed micromotion of less than 150μm at any portion of the coated region. Micromotion was less during stair climbing than during level walking. This was surprising considering the reports of thigh pain. However, micromotion was greater at the distal tip for stair climbing than for level walking. For all three categories the amount of motion at the distal tip was significant, averaging more 200μm.

Table 2. Percentage of Porous Coated Region Displaying Specific Range of Micromotion

Micromotion (μm)	Percentage of Porous Coated Region					
	T/T		T/L		L/T	
	LW	SC	LW	SC	LW	SC
50-100	40	75	55	80	0	10
100-150	10	25	40	20	20	15
150-250	50	0	5	0	40	35
>250	0	0	0	0	40	40

Due to the size of the required data files, subsidence was computed at two point, one on the porous coated region and at the distal tip. The results show that the T/T and T/L specimens underwent only one-half to one-third of the displacement magnitude of L/T specimens. The L/T specimens averaged 700μm at the porous coated location, with a maximum of 1200μm. The displacement was primarily in the S-I and M-L directions. Subsidence was greater, by 50-100μm, at the distal tip location.

It should be noted that the load cycles simulated normal gait. Clinically there will be some bone ingrowth before the prosthesis experiences this magnitude of loading. Coupled with the fact that many of the components were deliberately implanted in a less than optimal manner, the micromotion values reported here probably overestimates those in the clinical situation.

REFERENCES

1. Barich, F. *et al.*, Proc. 17th ASB, 85-86, 1993
2. Burke, D. *et al.*, JBJS, 73-B:33-37, 1991.
3. Callaghan, J. *et al.*, JBJS, 70-A:337:346, 1988.
4. Kotzar, G. *et al.*, J. Orth. Res., 9:621:633, 1991
5. Panjabi, J. *et al.*, J. Biomech., 25:329-340, 1981.
6. Pilliar, R. *et al.*, Clin. Orth., 208, 108-113, 1986.

ACKNOWLEDGMENTS

The authors wish to thank Zimmer for their financial support and BIOMET for supplying the prostheses.

THE EFFECT OF CEMENT MODULUS ON THE SHEAR PROPERTIES OF THE BONE-CEMENT INTERFACE

Michael J. Funk, MS and Alan S. Litsky, MD, ScD

Orthopaedic BioMaterials Laboratory
The Ohio State University, Columbus, Ohio

INTRODUCTION

Shear tests of the bone-cement interface were performed, "in vitro", using two types of bone cement, PMMA and PBMMA (a reduced-modulus cement, designed to decrease contact stresses at the bone-cement interface). Tests were also conducted on the cancellous bone and cements alone. Ultimate shear strengths and shear moduli were calculated. The tests were done with the Iosipescu shear test method. This method generates a pure shear force in a zero-moment section of the specimen. By doing so, shear properties can be determined at specified locations throughout the specimen. Tests were performed across the entire interface region.

REVIEW AND THEORY

Polymethylmethacrylate (PMMA) is a self-curing thermoplastic which has a glass-transition temperature of 114°C. When cold-cured, it is an amorphous polymer, and therefore, glassy below its glass-transition temperature. Thus, at body temperature (37°C), PMMA is glassy and fractures in a brittle manner.

Polybutylmethylmethacrylate (PBMMA) incorporates polybutylmethacrylate (PBMA) beads into a methyl methacrylate matrix. This cement is the same as PMMA in many aspects; the PBMA beads have no active part in the curing process (1). However, there are two important differences in the material properties of PBMMA and PMMA; the reduced elastic modulus and increased ductility of PBMMA. Because the glass-transition temperature of PBMA is 27°C (as opposed to 114°C for PMMA), the beads become rubbery at body temperature and allow the cement to take on the aforementioned properties. PBMMA has an elastic modulus of 0.27 GPa at 37°C, an ultimate tensile elongation of over 40%, and a much greater work to fracture than PMMA (1).

Contact stresses are a result of one body exerting pressure on another body over a small surface area. The solution of the idealized contact problem was first obtained by Hertz in 1881 (2). In solving for contact stresses, it is assumed that the two materials in contact are homogeneous, isotropic, and elastic. Locally, and for small deformations, this assumption holds relatively well (3). For a given load and geometry, and assuming that Poisson's ratios are approximately equal ($\nu_1 \approx \nu_2$), the solutions for the maximum principal and shearing stresses follow the proportionality

$$\sigma_{max},\ \tau_{max} \propto \sqrt{\frac{1}{E_1}+\frac{1}{E_2}}^{-\frac{2}{3}}. \qquad (1)$$

The peak stress in the bone will vary with the modulus of the cement. For a relatively soft cement,

$$Peak\ Stress \propto Const\ x\ \frac{\mu_{(cement)}}{\mu_{(bone)}} \qquad (2)$$

where $\mu_{(cement)}$ is the shear modulus of the cement, and $\mu_{(bone)}$ is the shear modulus of the bone (1). The contact stresses are thus diminished by reducing the shear modulus of the cement or by the presence of a membrane.

The development of a biological membrane to reduce local stresses to an acceptable level is the physiological response to excessive contact stresses. Local contact stresses are reduced and distributed with the interposition of a soft membrane, which acts as a 'shear spring' (4). The amount of local stress reduction is increased with increasing membrane thickness. However, the thickness of the membrane needs to be kept to a minimum to prevent the mechanical decoupling of the bone-cement bond. This necessitates an alternative method of reducing peak contact stresses, such as a reduced modulus cement.

PROCEDURES

The shear tests in our work were performed on cancellous bone and both PMMA and PBMMA cements, as well as interface specimens utilizing bovine cancellous bone and both types of cement. Iosipescu shear testing procedures were followed (5). An MTS Iosipescu Shear Test Fixture [MTS, Eden Prairie, MN] and strain gages designed for Iosipescu testing [type: N2A-00-C032A-500, Measurements Group, Inc., Raleigh, NC] were used. Cement penetration was held constant (6 mm) to remove any effect that depth of penetration may have on the strength and modulus results. PBMMA specimens were held at 37°C until testing; PMMA specimens were kept at 20°C to alleviate testing difficulties. (For PMMA strength and modulus, no significant difference was found between the 20° and 37° tests.) Force and strain gage data were collected using a loading rate of 2.5 mm/min.

RESULTS AND DISCUSSION

The shear test results are summarized in Table 1. PM1 refers to the bone-composite interface; PM2 refers to the composite; and PM3 refers to the cement-composite interface, using PMMA. PB1, PB2, and PB3 refer to the same type of specimens using PBMMA. Figures 1 and 2 display these results.

The PBMMA cement, because of its ductile nature, did not fail in the shear test. Although not quantified, the deformation was observed to contain an elastic component. Specimens kept at 37°C after testing began to return to their original shape, though not completely. However, this elastic component of PBMMA was slow in acting, and in the short-term case, the viscous characteristics seem to dominate the behavior of PBMMA.

The shear modulus of the PBMMA, found to be 41.50 ± 3.42 MPa, is considerably less than the determined shear modulus of the PMMA. This, coupled with PBMMA's greatly reduced elastic modulus, should alleviate much of the contact stress. Using values of 0.27 GPa, 2.12 GPa, and 0.93 GPa for elastic moduli of PBMMA, PMMA, and cancellous bone (ρ_{app} = 591 kg/m^3, the mean apparent density for all bone samples used here) (1,6), respectively, the compressive contact stresses in **Eq 1** are reduced by a factor of 2. Using the mean shear modulus values found here, namely 41.5 MPa, 1560 MPa, and

Table 1
Mean shear strengths, and shear moduli for PMMA, PBMMA, Cancellous bone and interface specimens

	τ_u (MPa)	G (MPa)	ρ_{app} (g/cm^3)
PMMA	21.78 ± 6.19	1560 ± 81.9	-
PBMA	*	41.50 ± 3.42	-
BONE	7.61 ± 2.94	513.0 ±131.0	.577 ± .121
PM1	7.17 ± 1.83	706.0 ± 149.5	.588 ± .086
PM2	9.04 ± 1.56	1119.2 ± 160.0	.605 ± .085
PM3	9.48 ± 3.05	1126.8 ± 350.7	.610 ± .112
PB1	5.46 ± 0.47	635.0 ± 286.0	.580 ± .063
PB2	5.52 ± 1.37	684.2 ± 133.9	.558 ± .083
PB3	*	234.0 ± 59.6	.620 ± .043

mean ± s.d.
* Strained beyond equip. limits w/o failure

Figure 1: Mean interface shear strengths (MPa) PMMA vs. PBMMA

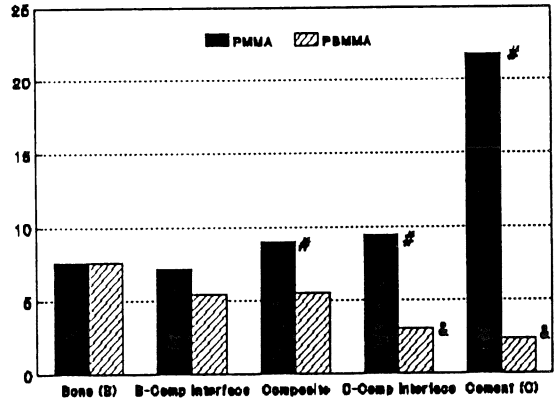

#: significant at $p < 0.01$
&: 0.2% offset yield stress for PBMMA

Figure 2: Mean interface shear moduli (MPa) PMMA vs. PBMMA

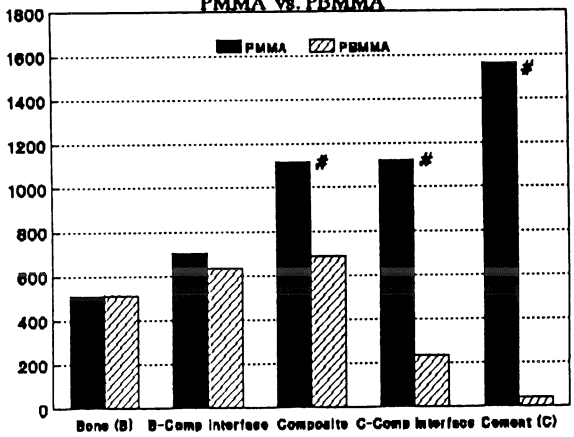

#: significant at $p < 0.007$

526.5 MPa for PBMMA, PMMA, and cancellous bone (normalized to ρ_{app} = 591 kg/m^3), respectively, the peak stresses at an interface under shear in Eq. 2 are reduced by a factor of 37.5. Although these are two idealized situations, it can be seen that PBMMA will reduce both compressive and shear contact stresses at the bone-cement interface.

Additionally, the experimental results point to the conclusion that, for either type of cement, the shear strength and shear modulus at the interfaces on either side of the composite region is controlled by the pure material. Thus, at the bone-composite interface, the shear properties are driven by cancellous bone regardless of the cement used. At the cement-composite interface, for both PMMA and PBMMA, the shear properties are cement driven. Through the composite region, it seems that the shear strength and shear modulus is driven by the stronger and stiffer material, which is PMMA for the bone-PMMA composite and cancellous bone for the bone-PBMMA composite.

The bone-cement interface shear strength is significantly less for PBMMA through the composite region in these experiments. The cancellous bone used here was completely dry, which reduces the strength of the bone (8). Cancellous bone which is kept wet will give a more accurate representation of the natural state.

The ductile nature of the PBMMA offers an additional advantage, beyond reducing contact stresses, at the bone-cement interface. This would be resistance to formation of debris at the interface. PMMA, being brittle, is subject to microfractures, which can deposit cement debris at the interface. This acrylic debris will elicit a foreign body reaction in the surrounding tissues (9). A small amount of debris can be successfully removed by the lymphatic system; larger amounts may cause an overload of the lymphatic system. The nearby tissues will then be affected resulting in bone necrosis and resorption, which is the first step in the loosening cascade (1). The ductility of PBMMA, displayed here, and its increased toughness compared to PMMA, will allow it to resist fracture and, therefore, the formation of acrylic debris at the interface, reducing the likelihood of a foreign body response.

The Iosipescu method, by focusing on the test plane, eliminates the bulk energy absorbing capacity of the cement. This artificially reduces the influence of the cement properties on the cement-composite interface. When forces are transmitted through the bulk of the cement mantle, as it is in total joint arthroplasties, the choice of cement has a profound effect on the mechanical environment of the bone and, thus, on bone resorption.

REFERENCES

1. Rose, R. M. and Litsky, A. S. "Biomechanical Considerations in the Loosening of Hip Replacement Prostheses" in Current Perspectives on Implantable Devices, Vol I, (pp. 1-45), D. F. Williams, JAI Press, 1989.
2. Boresi, A.P. and Sidebottom, O.M. Advanced Mechanics of Materials, 4th Ed., (pp. 599-642), John Wiley and Sons, 1985.
3. Clech, J.P., et al. J. Biomech. Eng. 107, 175-182, 1985.
4. Albrektsson, T. "Implant fixation by direct bone anchorage" in The Bone-Implant Interface, Workshop Report, (pp. 157-171), J.L. Lewis and J.O. Galante, 1985.
5. Adams, D.F. and Walrath, D.E. Exp. Mech. 27, 113-119, 1987.
6. Hodgskinson, R. and Currey, J.D. Proc. Instn. Mech. Engrs., Part H 204, 43-51, 1990.
7. Litsky, A.S., et al. J. Orthop. Res. 8, 623-626, 1990.
8. Black, J. Orthopaedic Biomaterials in Research and Practice, (p. 116), Churchill Livingston, 1988.
9. Mjöberg, B. Acta. Orthop. Scand. 62(5), 500-508, 1991.

THE RELATIONSHIP BETWEEN BONY INGROWTH AND THE MECHANICAL ENVIRONMENT AROUND A POROUS-COATED IMPLANT

Y. QIN, F. GUILAK, K.J. McLEOD, and C.T. RUBIN
Musculo-Skeletal Research Laboratory
State University of New York at Stony Brook, NY 11794-8181

Introduction

The use of porous-coated implants to facilitate biological fixation in total joint arthroplasty is an area of great interest in orthopaedic research. It is well accepted that early mobilization is essential for ensuring rapid bone ingrowth into cementless prostheses. Moreover, recent work showing the importance of a dynamic strain environment in the promotion of bony ingrowth suggests that mobilization may enhance ingrowth through the strain induced at the bone-implant interface[1]. The possibility that bony ingrowth could be enhanced, rather than deterred, by the mechanical milieu of the bone-implant interface may provide an excellent alternative to cemented fixation. Unfortunately, the osteogenic parameters of the mechanical environment have proven difficult to identify. Current research involves a variety of strain stimuli as the dominant influence of skeletal morphology and remodeling. The diverse nature of the loading environment makes it difficult to even define the biophysical milieu of the bone-implant interface, much less to determine the specific components of the regimen responsible for remodeling response. In an effort to address this issue, we have begun a characterization of the relationship between the stress-strain distribution around and the ingrowth into a simple, porous-coated cylindrical implant in an animal model in which the mechanical loading environment can be accurately controlled. In this paper, theoretical predictions based on a three-dimensional orthotropic finite element model (FEM) were validated using both strain gages and high resolution optical strain measurement techniques. The FEM calculations of the mechanical environment at the bone-implant interface were then correlated with the experimentally measured bony ingrowth around the bone-implant interface.

Methods

***In vivo* Animal Experiment:** Twelve, one-year-old, skeletally mature male turkeys were randomly subdivided into disuse and disuse plus loading groups[1]. A 4.1-mm diameter Ti-6A1-4V implant, surfaced with titanium beads, was press fit across the cortices of the ulna of the adult male turkey which had undergone isolation surgery[1]. The isolated ulna of each animal was loaded with a 20 Hz, 80 N load for 100 cycles per day for eight weeks. After sacrifice, the ulna was embedded in methacrylate and a modified surface grinder was used to cut five 150-μm sections transverse to the cylindrical implant in the dorsal cortex, starting from the periosteal surface. The bone-implant interface was then examined using backscatter electron imaging (AMRAY 1810D). The distribution of new bone was quantified as the fraction of radial ingrowth between the drilled bone surface and the implant core surface.

Finite Element Analysis: A 3-D elastic orthotropic finite element model of the ulna preparation was developed to evaluate the stress and strain distribution induced by the experimental loading regimen. The geometry of the model was determined from digital images of microradiographs made from a series of 1-mm sections of a zero-time control ulna. In the mid-diaphyseal region containing the implant, serial sections were taken every 500 μm. The mesh consisted of 4608 8-noded elements. Because the boundary conditions at the bone-implant interface were unknown, the stress-strain distribution was solved for conditions with rigid contact between the implant and bone, and no contact. Bone material properties were determined using ultrasound,[3] and the implant was assumed to be isotropic with a Young's modulus of 200 GPa. The loading conditions were applied by fixing the proximal end of the model and applying a load of 80 N distributed over the nodes of the distal end of the model. Twenty-six candidate mechanical parameters were calculated, including the six independent strain components, the six independent stress components, the three principal strains and the three principal stresses, strain energy density, dilitational stress and deviatoric stresses and strains. The global FEM stress and strain solutions at the bone-implant interface were transformed to a local polar coordinate system in order to correlate local mechanical parameters to the bony ingrowth from the animal experiment. The relationship between the mechanical environment at the bone-implant interface and the extent of osseointegration was examined using a linear correlation analysis.

Validation of FEM Solutions: Two techniques were used for validating the finite element model: strain gages and moire interferometry. The FEM-calculated strain environment was first validated using four triple rosette gages. Gages were mounted at the cranial, caudal, and ventral surfaces of the turkey ulna a distance of five times the implant radius away from the midshaft, and one gage was mounted distal to the implant on the cranial surface. Compression was applied in a trapezoidal ramp waveform using a pneumatic loading apparatus. The longitudinal normal strain measured by the three strain rosettes mounted in the same plane and their respective coordinate locations within the cross section were used to solve for the periosteal surface normal strain along the longitudinal direction.

The FEM-calculated strain environment immediately surrounding the bone-implant interface was validated using moire interferometry. This method provides significantly higher spatial resolution of surface strains than resistance strain gages. The specimen grating is made of epoxy with cross lines of 1200 line/mm. A layer of specimen grating approximately 0.3 mm thick was firmly attached to the bone-implant interface. A reference grating of the same pitch was superimposed on the specimen surface by applying a laser interferometry. The specimen was

loaded by a mechanical testing machine and the distribution of normal and shear surface strains were determined from the moire interference patterns using digital image processing methods.

Results and Discussion

Bone ingrowth into the cylindrical implants demonstrated a distinct spatial pattern around the implant (Fig.1). Both dorsal and ventral cortices showed bony ingrowth to be symmetric about a transversely bisected plane.

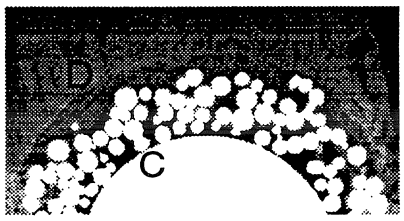

Fig. 1. Backscatter electron image of the bone-implant interface following eight weeks of loading. Visible is the region of the drill hole surface (D) and core surface (C).

Excellent agreement was observed between the FEM calculations and strain gage measurements of the longitudinal normal strain ε_{33} (R^2=0.98), indicating that the global FEM strain results were accurate.

Excellent agreement was also observed between the optically measured strain distribution around the implant and the FEM prediction of the strain environment assuming rigid contact between the bone and implant. (R^2=0.90, Figure 2). On the other hand, the FEM-predicted strain distribution matched poorly with the experimental results of the moire interferometry when no contact was assumed, supporting the assumption of rigid contact boundary conditions.

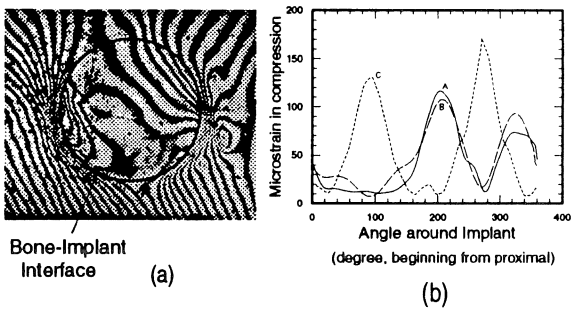

Fig. 2. (a) The longitudinal field moire interferometry pattern of the ventral surface of the ulna, showing the bone-implant interface while subjected to a longitudinal load. (b) The longitudinal normal strain distribution around the bone-implant interface. A--determined by moire interferometry, B--determined by FEM with rigid contact interface, C--determined by FEM with no contact boundary condition.

Axial loading of the ulna resulted in a highly non-uniform stress-strain distribution at the bone-implant interface. In the vicinity of the implant, FEM results showed that the stress and strain concentrations were symmetrical about a plane transverse to the bone mid-shaft through the center of the implant. The distribution of three mechanical parameters from the FEM results correlated to the site specificity of bony ingrowth is shown in Figure 3. Correlation of ingrowth to normal radial strain around the implant, σ_{rr}, was one of the poorest correlates (R=0.15), with strain energy density not much of an improvement (R=-0.25). The correlation of ingrowth improved with the normal radial strain gradient (R=0.4). The deviatoric stress component, S_{zz}, demonstrated a good correlation (R=0.68). Interestingly, the best predictor of bony ingrowth was demonstrated by an inverse relationship to the shear stress component, $\sigma_{r\theta}$ (R=-0.7).

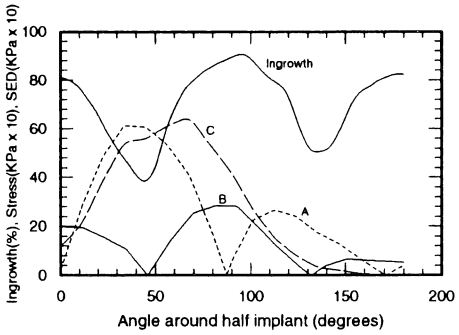

Fig. 3. Correlation between bone ingrowth around the implant (dark solid line) and shear stress $\sigma_{r\theta}$(A), deviatoric stress S_{zz}(B), and strain energy density (C).

This animal model, when combined with the finite element method and validated by strain gaging and by optical strain techniques, has provided a unique model for the direct, systematic comparison of ingrowth patterns with specific parameters of the mechanical milieu.

These preliminary results suggest that local deviatoric stress and shear stress[4] may play an important role in osseointegration. Further, to maximally stimulate bony ingrowth, it appears important to *minimize* any shear stress at the bone-implant interface. This is further evidence that micromotion is deleterious to the long term success of total joint procedures.

Further experimentation and analysis will be required to test this observation as well as to investigate the possible role of alternative stimulus parameters.

References

1. Rubin & McLeod (1994) Clin. Orth. 298:165-175.
2. Huiskes (1987) J. Biomech. 20:793-804.
3. Ashman et al. (1984) J. Biomech. 17:349-361.
4. Wong & Carter (1990) Bone 11:127-131.

Acknowledgements

Supported by NIH grant #AR-39278 and NSF-EET8658105.

TEST PROCEDURES FOR COMPARING CEMENTLESS ACETABULAR CUP FIXATION METHODS UNDER AXIAL AND ROTATIONAL LOADS

J.L. Pavlovic*, D.M. Zapzalka*, K. Terajima*†, J.E. Bechtold*, R.B. Gustilo*, R.F. Kyle*

*Orthopaedic Biomechanics Laboratory, Hennepin County Medical Center, 701 Park Ave. S., Minneapolis, MN, 55415

†Graduate School of Science and Technology, Niigata University, Japan

INTRODUCTION

A study was performed to develop test procedures for measuring the initial stability of uncemented acetabular cups under simulated physiologic loading in an in-vitro laboratory setting. The test procedures were designed to minimize differences due to surgical technique and specimen quality. Four different fixation methods, press-fit only, two screws, one screw and one peg, and two pegs, were tested in a study performed on fresh-frozen human cadaver hemi-pelves. Cup motion was measured relative to the bone under repeated non-destructive loading, with the cup either loaded axially and measured in three dimensions, or loaded and measured rotationally about an axis normal to the cup rim. Data analysis methods for comparing fixation methods were developed and are described.

REVIEW AND THEORY

Cementless fixation of acetabular components is used for younger patients and revision hip replacements. To achieve long-term biologic fixation, cementless components must be rigidly stabilized to prevent initial micromotion and subsidence which could interfere with bony ingrowth. Although many laboratory studies have been performed to evaluate initial fixation of cementless components (Dodge et al. (1991), Hollis et al. (1991), Perona et al. (1991), Stiehl et al. (1990), Takedani et al. (1991)), test methods and results have varied widely. Thus, no consensus has been reached regarding the best type of uncemented acetabular fixation. The test procedures described below were designed for comparative evaluation of cementless fixation methods.

PROCEDURES

Eight fresh frozen human cadaver hemi-pelves without evidence of musculoskeletal disease were tested. Four acetabula were under-reamed by 1mm (axial loading) and four acetabula were under-reamed by 2mm (rotational loading), maintaining subchondral bone. The difference in under-reaming was due to a change in surgical practice between the time the axial and rotational tests were performed. Since comparisons were not made across loading modes, this difference did not influence the results. The cups (Reflection Cup, Smith & Nephew Richards, Inc., Memphis, TN) were implanted as shown in Fig. 1. The pelves were dissected of soft tissue and potted in dental Die-Stone (Miles Inc., South Bend, IN).

To minimize variations due to anatomical differences and surgical technique, all four types of cementless fixation were tested on each hemi-pelvis in the following order: (1) press-fit, (2) two screws, (3) one screw and one peg, (4) two pegs. This test sequence was chosen to maximize purchase, using the smaller diameter cancellous screws before the larger diameter radial pegs. The same two cup holes, in the posterior superior quadrant (Fig. 1), were used for each type of screw and peg fixation. These hole locations were chosen based on surgical practice. Loads were applied by a servohydraulic materials testing machine. To keep test conditions consistent, the specimens remained mounted on the test machine while the screws and pegs were inserted and removed.

Axial Load: Four hemi-pelves were potted with the symphysis pubis and anterior superior iliac spine aligned in the frontal plane, represented by the anterior side of the potting box (Fig. 2). A femoral head driver mounted on the test machine applied axial loads to the polyethylene liner in the metal cup. Static and cyclic axial loads were applied to each hemi-pelvis at a 25 degree angle to simulate stance phase of walking. A 2,000 N static pre-load was applied to each specimen for 60 sec. to make sure the cup was well seated. Then a cyclic load between 25 N and 3,000 N, about 3.5 times body weight (Brand et al. (1980)) was applied for 30 cycles at 0.5 Hz as in a previous study (Takedani et al. (1991)). This sequence represented the loading and unloading occurring during movement. The cyclic load was followed by a 3,000 N static load for 46 sec., then a 25 N static load for 46 sec.

The orientation of the cup relative to the bone was measured in the coronal (y-z), transverse (x-y), and sagittal (x-z) planes with a six degree-of-freedom instrumented spatial linkage (ISL). For one-point sampling, ISL linear accuracy was ±50 microns and angular accuracy was ±0.5° (Terajima et al. (1991)). Relative motion between the cup and the bone was defined as the difference in cup orientation under the final 3,000 N and 25 N static loads.

Rotational Load: The remaining four hemi-pelves were potted as shown in Fig. 3. A loading fixture was made to fit into the splined rim of the metal cup, in place of the polyethylene liner. This fixture, mounted on the test machine, applied a torque to the cup about an axis perpendicular to the plane of the cup rim. The applied loads were representative of the *in vivo* range of loads transmitted from the polyethylene liner to the cup to the bone, with a range of 1.6 N-m to 3 N-m, and an average torque of 2.2 N-m (Davidson (1989), Schryver (1992)). Applying these known loads directly to the cup eliminated test variables (such as friction at the femoral head/poly liner interface) that would be present if the test load were applied by a femoral head through a poly liner. Ramp loading was used to simulate continuous human movement. The 1 N-m/sec. rate, representing loading from 0 to the average load in 2.2 sec., was used to avoid overshoots. This rate was half as fast as the typical rate of a person walking at one step per sec. The 15 sec. dwell periods were used to enable accurate measurements of multiple data points at the 1.6 N-m, 2.2 N-m, and 3 N-m loads. Cup rotation was measured by a rotational variable differential transformer (RVDT) mounted on the test frame, aligned with the loading axis. The RVDT needle, attached to a fixture mounted perpendicular to the cup rim, moved with the fixture as the cup rotated. RVDT resolution was ±0.03 degrees for each measurement.

RESULTS AND DISCUSSION

Axial Load: Translation vector magnitudes ranged from 0 mm to 3.14 mm, with individual x, y, and z translations ranging from -2.2 mm to 0.96 mm. Since ISL linear accuracy was ±50 microns for one-point sampling, measurement errors were negligible. Rotations about the x, y, and z axes ranged from -4.9 to 2.13 degrees. Since ISL angular accuracy was ±0.5°, rotational measurement errors could be relatively large, but were unlikely to mask trends. The data were normalized to the press-fit condition by dividing the translation for each fixation method by the translation for the press-fit condition for that hemi-pelvis (Fig. 4). A quotient of "100" indicates the fixation method was

equivalent to the press-fit method; a quotient greater than "100" indicates the method was less stable; and a quotient less than "100" indicates the method was more stable.

Rotational Load: The difference between the angular cup position at the initial 1.6 N-m dwell and the final 3 N-m dwell represents the net angular cup shift over two loading cycles. This was determined for each specimen by calculating the mean of thirty points at the initial 1.6 N-m dwell and at the final 3 N-m dwell, then subtracting the initial mean from the final mean. The net angular cup shift ranged from 0.01° to 0.42°, with most values between 0.1° and 0.2°. For this range, the RVDT errors are ±15-30%. Means for the four specimens are shown in Fig. 5. The total range of rotation was calculated as the difference between the maximum and minimum cup angles reached between the initial 1.6 N-m and final 3 N-m loads. This parameter ranged from 0.15° to 0.48°, with most values between 0.2° and 0.3°. For these values, RVDT errors are ±10-15%. Means for the four specimens are shown in Fig. 5.

The fixation methods were tested for initial stability under physiologic loading conditions. Although the cups were not moved when changing from screws to pegs, some loosening of the cups within the bone due to cyclic loading of each fixation method could be expected. Thus, the efficacy of the later fixation methods tested may have been affected by the earlier testing, in which case the later tests would consistently show more loosening. The test results indicated that no fixation method was predictably superior, suggesting that the test order did not significantly influence the data to favor one method. However, it is possible that no overall change would occur if the cup gradually loosened and the later fixation methods were superior. The effects of test order should be examined further when a larger study is performed. To determine whether significant loosening occurs, the press-fit condition can be tested at the beginning and end of the test sequence.

This study provided useful information for evaluating the test instruments and procedures. However, due to the lack of statistical significance of the small sample size, no conclusions were made regarding the relative efficacy of the fixation methods. With a larger sample size, the data could be statistically analyzed, leading to comparative conclusions.

A non-destructive test method for comparing acetabular cup fixation methods was developed, and a study was performed on eight fresh-frozen hemi-pelves. The test method was designed to minimize differences due to surgical technique and specimen quality. Since the ISL provided precise three-dimensional measurement of cup movement during axial testing, this method provided more information than previous studies measuring linear motion. Data analysis techniques, including normalization to the press-fit condition and calculation of net angular cup shift and total range of rotation, were described. The methods developed in this study are well-suited for a larger comparative study of fixation methods. Tests could be performed on synthetic bone substitute material to eliminate variations in bone quality (Litsky et al. (1994)), or on fresh-frozen cadaver specimens.

REFERENCES

Brand, R.A. et al. Clin. Orthop., 147, 181-184, 1980.
Davidson, J. Adv. Bioengr., BED-Vol. 15, (pp.83-84), 1989.
Dodge, B.M. et al. Clin. Orthop., 269, 16-24, 1991.
Hollis, J.M. et al. Trans. Comb. Meet. Orthop. Res. Soc. of USA, Japan, and Canada, Banff, Alberta, Canada, (p. 238) 1991.
Litsky, A.S. et al. Orthopedics, 17:1, 53-57, 1994.
Perona, P.G. et al. Trans. Comb. Meet. Orthop. Res. Soc. of USA, Japan, and Canada, Banff, Alberta, Canada, (p. 218) 1991.
Schryver, J. Ortho. Trauma Sem., Mpls., MN, Oct. 22-24, 1992.
Stiehl, J.B. et al. Proc. 14th Am. Soc. Biomech. Meeting, Miami, FL, (pp.45-46), 1990.
Takedani H. et al. Trans. A.A.O.S., Anaheim, CA, 1991.
Terajima K. et al. Trans. Comb. Meet. Orthop. Res. Soc. of USA, Japan, and Canada, Banff, Alberta, Canada, (p. 262) 1991.

ACKNOWLEDGEMENTS: Smith & Nephew Richards Inc.

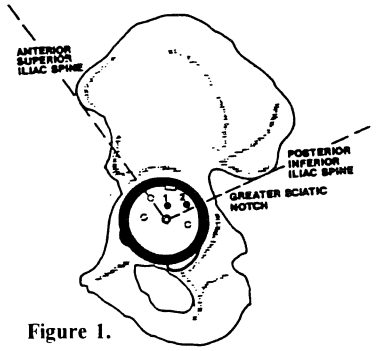

Figure 1.
Locations of Peg and Screw Holes

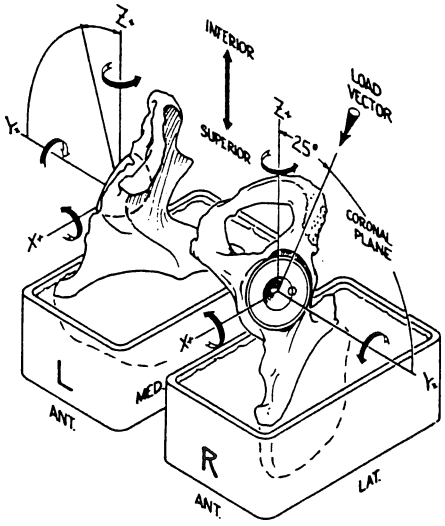

Figure 2. Axial Test Configuration

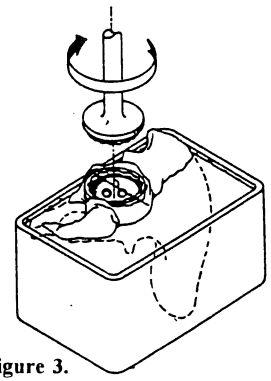

Figure 3.
Rotational Test Configuration

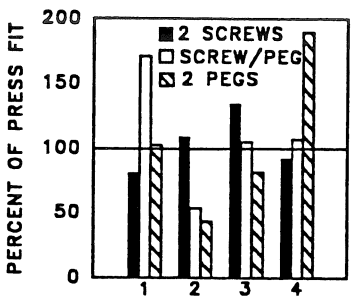

Figure 4.
Magnitude of Translation Vector, % of Press-Fit

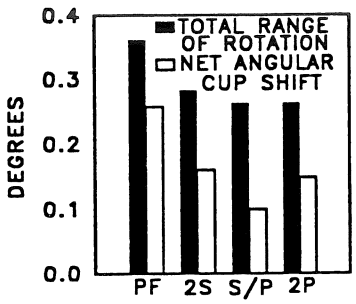

Figure 5.
Total Range of Rotation and Net Angular Cup Shift, Means for Four Specimens

THE ROLE OF MUSCLES IN GENERATING ROTATORY TORQUES ABOUT THE IMPLANT STEM AXIS

[1]D.E. Hurwitz, [1]T.P. Andriacchi, [2]S.L. Delp
[1]Rush-Presbyterian St. Luke's Medical Center, Department of Orthopedic Surgery Chicago, Illinois
[2]Departments of Biomedical Engineering and Physical Medicine and Rehabilitation, Northwestern University
Sensory Motor Performance Program, Rehabilitation Institute of Chicago, Chicago, Illinois

INTRODUCTION

Micromotion in total hip replacements (THRs) can prevent bony ingrowth from occurring in uncemented THRs or lead to destruction of the cement mantle in cemented ones. Micromotion often results from rotatory torques about the stem axis (1). In some instances rotatory torques measured during activities of daily living in subjects with instrumented THRs have approached those that caused micromotion in cadaveric experiments (2,3).

The rotatory torques about the stem axis during functional activities result from both the kinetics of the hip joint as well as the muscle forces. The objective of this study was to examine the role of muscles in generating rotatory torques about the stem axis during gait. Muscles capable of generating relatively high rotatory torques were first identified. The contribution to the rotatory torque from the muscles was compared to the contribution from the hip kinetics during gait in subjects with THRs.

METHODS

Loading at the hip joint during gait was examined using the hip kinematics and kinetics of 51 subjects with THRs. All subjects were at least one year postoperative (28$\pm$17 months) and had a good clinical result (Harris score, 97$\pm$3). The data were obtained with an optoelectronic system and a multicomponent force plate (4). The average walking speed analyzed was 1.1$\pm$0.1 m/sec.

A biomechanical model of the lower extremity was used to generate the isometric forces of the muscles crossing the hip joint (5). This model included a Hill type representation of the muscles. The rotatory torque generated by a muscle was calculated about the longitudinal axis of the implant stem. The maximum muscle rotatory torque was calculated using the maximum isometric muscle force at hip angles representative of the peak hip flexion and extension angles measured during gait. Rotatory torques that caused the femoral head to rotate anteriorly were referred to as anteversion torques (positive) while those that caused the head to rotate posteriorly were retroversion torques (negative).

Published electromyographic data were used to determine which muscles were active during gait (6). A parametric approach was then used to determine the range of agonist muscle force distributions needed to balance the external moments in the sagittal and frontal planes and the moment from a selected level of antagonistic muscle activity. The distributions of agonist muscle forces were evaluated at incremental levels of antagonistic muscle activity that ranged from 0%, indicating no antagonistic activity, to 100%, meaning the antagonistic muscle forces were at their maximum isometric forces.

The relative contribution of the muscles to the stem rotatory torque was compared to that resulting from the hip kinetics (sagittal and frontal plane moments and intersegmental force) at several instances during gait. The instances examined were the peak hip flexion moment (7 $\pm$ 6% stance), the initial peak hip adduction moment (30 $\pm$ 4% stance), the transition in the sagittal plane moment from flexion to extension (46 $\pm$ 12% stance), the second peak hip adduction moment (74 $\pm$ 4% stance) and the peak hip extension moment (83 $\pm$ 3% stance). In the first two cases the agonists were the abductors and extensors and in the last two cases the agonists were the abductors and flexors while the antagonists were the adductors. During the sagittal moment transition the agonists were the abductors, rectus femoris and tensor fasciae latae while the antagonists were the semitendinosus and semimembranosus.

RESULTS

Almost all muscles generated an anteversion muscle rotatory torque (Figure 1). Only the gluteus minimus and tensor fasciae latae generated

a retroversion muscle rotatory torque. The stem rotatory torque due to the muscle forces would therefore predominately be a retroversion moment.

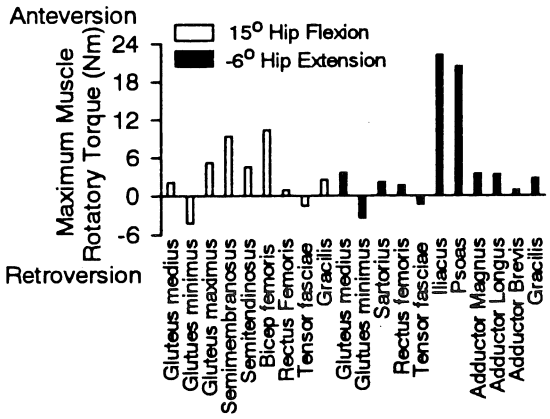

Figure 1. The maximum muscle rotatory torques for muscles active during the beginning and end of the stance phase of gait.

The magnitude of the maximum rotatory torque of most muscles was less than 5 Nm. However, the maximum rotatory torques of the iliacus and psoas were about two to three times greater than that of the other muscles. The maximum rotatory torques of these two muscles were approximately 20 Nm which resulted from their relatively large anterior force components. The semimembranosus and long head of the biceps femoris also had somewhat larger maximum rotatory torques (10Nm). This was due to their posterior attachment sites with respect to the implant reference system which resulted in relatively large moment arms for their medial-lateral force components.

During gait the average stem rotatory torques ranged from -16 Nm to -43 Nm when no antagonistic activity was present (Figure 2). With 40% antagonistic activity the average stem rotatory torque ranged from -22 Nm to -49 Nm. The external sagittal and frontal plane moments and the intersegmental hip force during gait contributed from -12 Nm to -19 Nm to the stem rotatory torque. The muscle forces were therefore responsible for 19 to 58% of the average stem rotatory torque when no antagonistic muscle activity was present and for 41 to 63% of the average stem rotatory torque when 40% antagonistic activity was present.

DISCUSSION

The greatest variation in the rotatory torques resulted from variations in the iliacus and psoas muscle forces. The stem rotatory torques during the peak hip extension moment varied by approximately two fold depending on the relative activation levels of these two muscles. Any gait adaptations that would decrease the iliacus and psoas muscle forces might increase stem stability by decreasing the overall rotatory torques. This could be achieved by either decreasing the overall demand on the hip flexors through a reduced hip extension moment or by increasing the relative contribution of the other hip flexors.

The gluteus minimus and tensor fasciae latae may also have a stabilizing effect on the implant stem as their rotatory torques were in the opposite direction of the other muscles.

The muscle forces were responsible for a substantial portion of the stem rotatory torque. It would be important, therefore, to consider the muscular contribution to the stem rotatory torques in addition to the contribution from the hip kinetics.

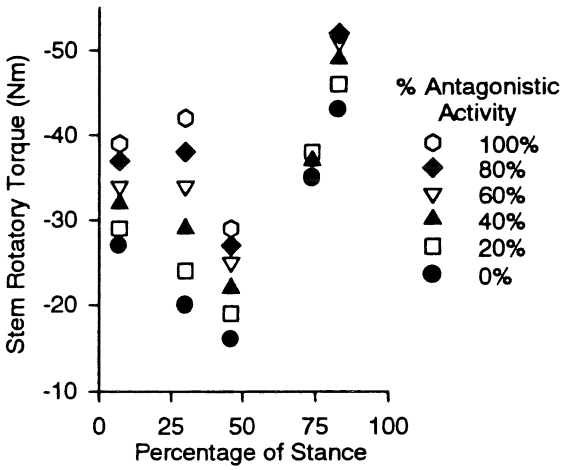

Figure 2. The average stem rotatory torque during stance at each level of antagonistic muscle activity.

REFERENCES

1)Berzins et al., JOR 11(5):758-69, 1993.
2)Bergmann et al., J. Biomechanics 969-990, 1993.
3)Phillips et al., J. Biomechanics 37-48, 1991.
4)Andriacchi et al., NATO ASI E:83-102, 1985.
5)Delp et al., IEEE Biomed. Eng. 757-67, 1990.
6)Univ. Calif. Prosth. Dev. Res. Rep. 2(25), 1953.

ACKNOWLEDGEMENT NIAMS #AR39239

BIOMECHANICAL ANALYSIS OF BONE MINERAL DENSITY, SCREW TORQUE AND HOLDING STRENGTH OF ANTERIOR CERVICAL PLATE SCREWS

J. Clausen, T. Ryken*, V. Goel, V. Traynelis*

Department of Biomedical Engineering, The University of Iowa, Iowa City, IA 52242
*Division of Neurosurgery, University of Iowa Hospitals and Clinics, Iowa City, IA 52242

INTRODUCTION

The bone mineral density of 99 cadaveric cervical vertebral bodies (C3-C7) was determined using dual x-ray absorptiometry. The vertebral bodies were randomly assigned to receive either a unicortical (n=51) or bicortical (n=48) Caspar cervical plating screw. The mean bone mineral density (BMD) for the total group (n=99) was 0.787 ± 0.154 g/cm^2, the mean insertion torque was 0.367 ± 0.243 Nm, and the mean pullout force was 210.4 ± 158.1 N. A significant correlation was noted between BMD and torque ($p<0.0001$, $r=0.42$), BMD and pullout force ($p<0.0001$, $r=0.54$), and torque versus pullout force ($p<0.0001$, $r=0.88$). The insertion torque and pullout force differed significantly ($p=0.02$ and $p=0.008$, respectively) for the unicortical and bicortical groups. The bone mineral density of the unicortical and bicortical groups did not vary significantly ($p=0.92$). A holding index for each screw and insertion technique was defined as the product of the bone mineral density and insertion torque which was found to be significantly correlated with pullout force for both techniques of screw insertion ($r=0.92$). A significant difference in holding index was observed with unicortical versus bicortical screw placement ($p=0.04$). The determination of bone mineral density and measurement of insertion torque to create a unique holding index provides an assessment of bone-screw interaction and holding strength of the screw, both of which impact on the resultant stability of the construct.

REVIEW AND THEORY

The anterior approach to the cervical spine has been successfully utilized to treat degenerative cervical spine disease, vertebral body fractures, tumors, and infection. In the presence of instability, anterior plates of various sizes and shapes have been used to secure the spine until fusion occurs. These plating systems may utilize either bicortical or unicortical screws. Anterior cervical plate stabilization is dependent upon the holding strength of the bone screws. Inadequate holding strength may result in failure of the stabilization procedure. A significant factor in the holding strength of this type of instrumentation is the quality of the vertebral bone, and a major contraindication for placement of plate and screw devices is the presence of osteoporosis (Tippets and Apfelbaum, 1988). A variety of techniques have been used to assess bone quality; however, recently dual x-ray absorptiometry (DXA) has been recognized as the modality of choice for determination of bone mineral density (BMD) in multi-center longitudinal studies of osteoporosis (Duboeuf, et al., 1992).

A previous study by Maiman et al. compared the pullout strength of Caspar screws placed unicortically and bicortically in cervical vertebral bodies. Twenty-one screws were placed in unicortical fashion and 22 were placed bicortically. Two screws were placed in each vertebral body and the required pullout force determined. The mean for the bicortical group was greater than the unicortical group, comparing 412 N with 371 N, although the difference was not statistically significant. This may be due in part to a small sample size, placement of two screws per vertebral body, and difficulties in achieving a pure axial pullout.

The goals of this experimental study were twofold: (1) to evaluate DXA as a means of obtaining a reproducible assessment of cervical vertebral bone quality and; (2) to examine the relationship of BMD to the peak insertion torque and holding strength of anterior unicortical and bicortical cervical plating screws in a reproducible biomechanical model. The BMD and insertion torque were used to define a mathematical holding index which can accurately predict the holding strength of these screws.

PROCEDURES

Thirty cervical spines were harvested from fixed cadavers obtained from the University of Iowa Department of Anatomy. The average age of the donors was 75.2 years (range 59 to 95 years). A total of 99 vertebral bodies ranging from C3 to C7 were obtained from the spines for this study. The male to female ratio was 5:4. The distribution by cervical level was as follows: C7 (n=22), C6 (n=23), C5 (n=22), C4 (n=19), and C3 (n=13). There were no significant differences between the unicortical (n=51) and bicortical (n=48) groups with respect to age, sex, or distribution of cervical level (unpaired two-tailed Student's t-test, $p>0.05$).

Prior to dissection, each spine was scanned in the lateral plane using a Hologic QDR-1000 Bone Densitometer (140/70 kVp, 2.0 mA average, 60 Hz) with a scan width of 8.0 cm, a scan length of 15.25 cm, line spacing of 0.1003 cm, and a point resolution of 0.0952 cm to determine the areal bone mineral density (Hologic Inc., Waltham, MA).

Following determination of the bone mineral density, each vertebral body was randomly assigned to receive a unicortical (n=51) or bicortical (n=48) Caspar cervical plating screw (donated by Aesculap, South San Francisco, CA). The screws were inserted using the instrumentation from the Caspar Trapezial Osteosynthetic anterior cervical plating system. The guide hole traversed the central region of the vertebral body and, for the bicortical screws, pierced both the anterior and posterior cortices. Each vertebral body received only one screw to avoid stress artifact from repeated testing. The anterior cortex was tapped, and each screw was inserted through a pullout cylinder (described below) into the vertebral body. Following insertion, the peak insertion torque (Nm) was determined by tightening the screw with a digital electronic torque wrench (Snap-On, Inc., Kenosha, WI).

A specially designed stainless steel holding frame was used to immobilize the vertebral body (Figure 1). A 4 mm titanium rod was placed through the transverse foramen or against the anterior tubercle on either side of the vertebral body and mounted in the holding frame. The level of the two rods could be varied to maintain perpendicular alignment of the screw despite minor anatomic irregularities between sides of an individual specimen. Motion in the rostral-caudal direction was minimized by tightening a screw clamp onto the spinous process of the body through the sides of the holding frame. The base of the frame contained a threaded recess to allow direct coupling to a hydraulically servo-controlled Materials Testing System device (MTS Systems Corp., Minneapolis, MN). A threaded stainless steel screw pullout cylinder was designed to allow perpendicular pullout of the screw and avoid coupling of motion with pullout (Figure 1). The inner and outer surfaces of the distal end of the cylinder were machined to the exact specifications of the Caspar anterior cervical plate to ensure accurate reproduction of the clinical placement of the screws. After the body was secured in the holding frame and the screw inserted through the pullout cylinder, the entire construct was mounted in the MTS machine. A distraction load was applied collinear to the screw axis with a displacement rate of 0.25 mm/s. The maximum force (N) achieved was plotted as a function of displacement (mm) with a standard chart recorder.

Comparisons between the unicortical and bicortical groups were made using standard two-tailed unpaired Student's t tests and a mixed-model analysis of variance (MANOVA). A multiple regression model and a MANOVA were performed in analyzing correlations between variables for each of the unicortical, bicortical, and total groups.

RESULTS

The average values for BMD, torque, and pullout force for the total group and after stratification into unicortical and bicortical groups are presented in Table 1. A typical pullout curve for a bicortical Caspar screw is shown in figure 2.

TABLE 1 Summary of BMD, torque, and pullout force. The mean and standard deviation values (in brackets) for the entire group and the unicortical and bicortical subgroups are listed.(p-values shown compare unicortical and bicortical groups [unpaired two-tailed Student's t-test])

	BMD (g/cm^2)	Torque (Nm)	Pullout (N)	Index (kg^2/sec^2)
All specimens (n=99)	0.787 (0.154)	0.367 (0.243)	210.4 (158.1)	0.304 (0.224)
Unicortical (n=51)	0.785 (0.152)	0.312 (0.230)	170.1 (152.6)	0.258 (0.211)
Bicortical (n=48)	0.788 (0.158)	0.426 (0.246)	253.3 (154.1)	0.354 (0.228)
p-value	0.92	0.02	0.01	0.04

Regression analysis of BMD with peak insertion torque yields a significant linear relationship ($p<0.0001$); however, the correlation coefficient is low ($r=0.42$). The linear regression analysis of BMD with pullout force for the group also yields a significant linear relationship ($p<0.001$), the correlation coefficient of which is 0.54. Regression analysis of peak insertion torque with pullout force results in a p-value of 0.0001 and a correlation coefficient of 0.88.

A multiple regression analysis was performed to evaluate the relative contribution of BMD and torque on the variability observed in pullout force. BMD accounted for 28.3%, and peak insertion torque accounted for 76.9% of the observed variability in pullout force. The relative differences in the effects of BMD and torque on pullout strength which were identified with multiple regression analysis are consistent with the correlation coefficients obtained using a simple linear regression models. Overall, these results indicate that although both BMD and insertion torque are statistically significant variables, torque has the greater influence.

BMD and torque were examined using a series of mathematical equations, including a weighted sum of BMD and torque, in an attempt to improve their predictive power of pullout strength. We found that the simple multiplicative index obtained as the product of BMD and torque yielded the best improvement in the correlation coefficient of the multiple regression model. We therefore defined a holding index as the product of the BMD and the peak screw insertion torque.

$$\text{Holding Index} = \text{BMD} \times \text{Torque}$$

This creates a torque value which is weighted by the BMD of the bone in which the screw is being inserted. The improvement in the correlation coefficient ($r=0.92$) reflects the reduction in scatter of the data around this linear plot.

Including this holding index in the multiple regression analysis improves the predictive power of the model, with holding index alone accounting for 84% of the variability observed in pullout force. The linear relationships obtained by separately plotting the unicortical and bicortical subgroups do not significantly alter the slope, intercepts, or correlation coefficients of the plots ($r=0.91$ and $r=0.93$, respectively); however, the mean holding index for the unicortical group and the bicortical do differ significantly, comparing 0.258 ± 0.211 for unicortical versus 0.354 ± 0.228 for bicortical placement. Thus, while the mean holding index for the two groups differs significantly, this does not impact on the basic relationship between BMD, torque, and pullout strength. For these groups, the comparison of holding index can be used to assess the ability of similar screws placed with different techniques to withstand pullout.

DISCUSSION

We have found the determination of cervical bone density using DXA to be a reliable indicator of bone quality in the cervical vertebral body. Both BMD and torque play a role in the holding strength of cervical vertebral body screws. In this study, bicortical placement improved the holding strength of anterior cervical plating screws. Although this study used fixed vertebral bodies it is expected that these findings will be supported by testing of unfixed vertebral bodies currently underway by the authors. Studies involving bone quality, torque, and screw holding strength begin to analyze the complex interaction at the bone screw interface. The extension of bone mineral density and holding index determination into clinical practice may result in guidelines for minimal acceptable values prior to consideration of anterior cervical plating constructs. Extensive variability in screw design exists between manufacturers, and these results cannot be extrapolated to other cervical screws without further testing.

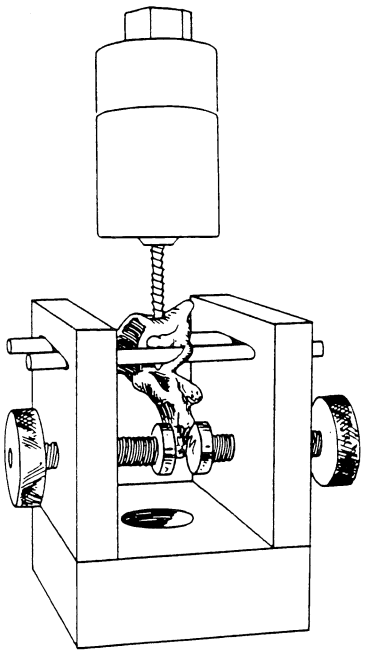

Figure 1 Schematic of the pullout cylinder (top) and the holding frame (bottom).

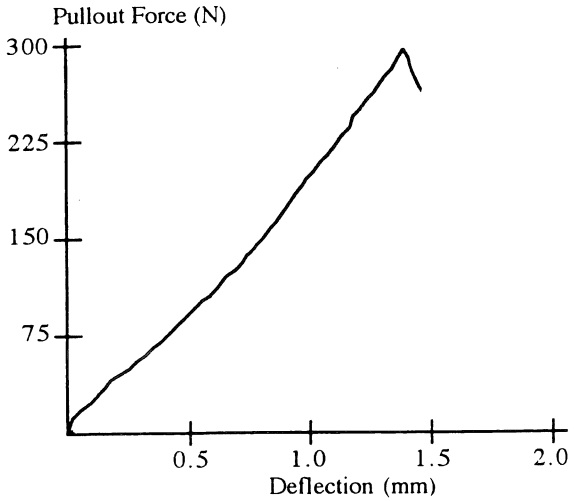

Figure 2 Typical pullout curve for a bicortical Caspar screw.

REFERENCES

Tippets RH. et al. Neurosurgery 22:1008-1013, 1988
Duboeuf F. et al. Bone Miner. 17:S1, 1992.
Faulkner KG. et al. Am. J. Roentgenol. 157:1229-1237, 1991.
Maiman DJ. et al. Neurosurgery 31:1097-1101, 1992.

SESSION 5:

MUSCULOSKELETAL BIOMECHANICS

IN VIVO MUSCLE FORCE AND MECHANICAL POWER OUTPUT OF MAJOR HINDLIMB EXTENSORS IN A CAT DURING VERTICAL JUMPING

T.A. Abelew and R.J. Gregor
Department of Health and Performance Sciences,
The Georgia Institute of Technology, Atlanta, GA 30332

INTRODUCTION

Muscle forces were directly measured using implanted transducers placed on the tendons of the medial and lateral gastrocnemius muscles of four cats. Net joint powers and individual muscle powers were calculated using smoothed coordinate data acquired from high speed film records. Results indicate that the medial and lateral gastrocnemius muscles generated different forces and powers during jumping to various heights and that an intermuscular difference in output remained. At lower heights power generated at the ankle joint was supplemented by power transported from the knee extensors through the active lateral and medial gastrocnemius muscles. At higher heights this phenomenon was absent and it is postulated that different neuromuscular strategies were used at different heights in response to physical demand and in light of physiological properties of the hindlimb extensors.

REVIEW AND THEORY

In vivo muscle-tendon forces of various hindlimb muscles have been reported in cats during overground walking (Fowler et al., 1993), treadmill locomotion (Herzog et al., 1992) and jumping (Tjoe et al., 1991) to quantify the contribution made during movement. While muscle force is a critical parameter in examining the resulting movement, quantifying the influence of muscle velocity is perhaps of equal importance. Calculations of mechanical power produced by muscle-tendon units have been made in an attempt to combine force and velocity parameters for the soleus and medial gastrocnemius muscles during treadmill locomotion (Gregor et al., 1988,Whiting et al., 1984) and for the medial and lateral gastrocnemius muscles during jumping (Abelew et al., 1993). Recent reports indicate that the lateral and medial gastrocnemius muscles play different roles in contributing to the load sharing at the ankle joint. Muscle moments during walking (Fowler et al., 1993) and muscle power during jumping (Abelew et al., 1993) have been shown to be different.

The significance of generation, absorption and transfer of mechanical power by individual muscles has been previously described (Ingen Schenau et al.,1990, Robertson and Winter, 1980). These investigations examined the changes in net joint and segmental power yet could not assess individual muscle force output. The relationship between joint and segmental power and the mechanical output of individual muscles, therefore, remains unclear.

The purpose of this investigation is to examine the differential mechanical output of the medial and lateral gastrocnemius muscles by quantifying the mechanical power produced by the individual extensor muscles of the hindlimb and directly comparing these values to the *in vivo* force output and to the net joint power at the ankle joint during jumping in cats.

PROCEDURES

Four adult female cats were trained to jump from specially designed force platforms concealed in the floor of a Plexiglas enclosed walkway to heights ranging from 0.31 to 0.67 meters. Tendon transducers were surgically placed, under sterile conditions, on the tendons of the individual medial and lateral gastrocnemius muscles in one hindlimb and on the plantaris and soleus tendons in the contralateral hindlimb. Displacement of segment endpoint markers were obtained for the hip, knee, ankle, metatarsophalangeal joints and toe using reflective markers and high speed film. Displacement data were hand digitized, smoothed and differentiated and, together with body segment parameters, used as input to Newtonian equations of motion for calculation of joint moments. Muscle-tendon unit velocities for all trials were calculated by differentiation of muscle lengths acquired using a trigonometric algorithm (Goslow et al., 1973). Joint powers were calculated as the product of joint moment and angular velocity and the muscle powers calculated as the product of muscle force and muscle-tendon unit velocity (Abelew et al., 1993).

RESULTS

Exemplar data for one cat are presented for jumps to 0.31 and 0.67 meters. Medial and lateral gastrocnemius muscle forces are presented in figures 1 and 2. Lateral gastrocnemius magnitude regularly exceeded that of the medial gastrocnemius at all jump heights and consistently exhibited a bi-modal shape at the low heights. At higher heights, force patterns in both muscles became more parabolic in shape though medial gastrocnemius continued to rise to its peak magnitude prior to the lateral gastrocnemius. Muscle powers are presented in figures 3 and 4 along with the net ankle joint powers. At 0.31 meters, summed extensor muscle powers reached approximately 40% (2.3W)of peak ankle joint power (5.7W) during propulsion. Summed muscle powers at 0.67 meters reached 33W which was 107% of peak ankle joint power (31W).

DISCUSSION

Results of this investigation indicate that large differences exist between calculated muscle and joint power at low jump heights. While errors due to sampling muscle forces from opposite limbs are included in these differences we feel that they do not account for all of the observed differences.

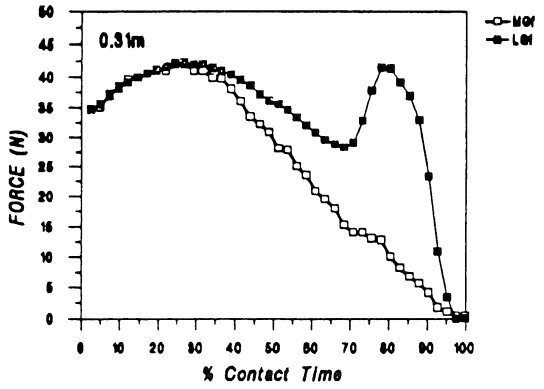

Figure # 1. Medial and lateral gastrocnemius forces

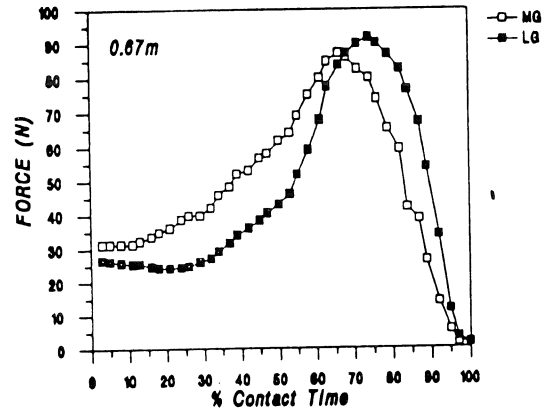

Figure # 2. Medial and lateral gastrocnemius forces

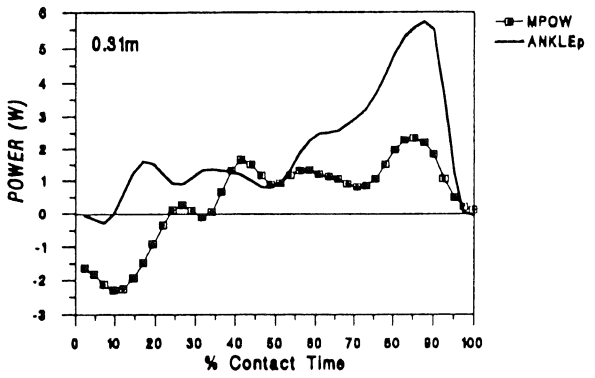

Figure # 3. Total muscle and ankle joint power

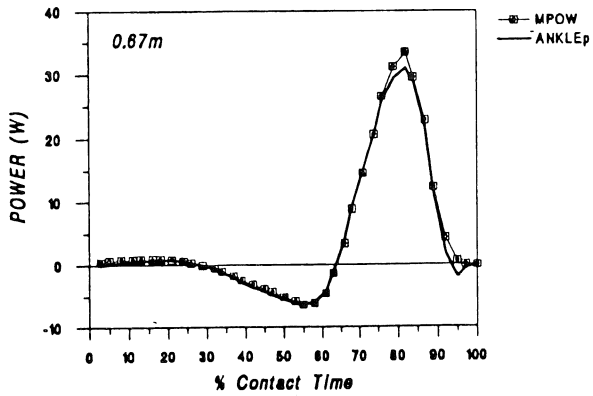

Figure # 4. Total muscle and ankle joint power

This suggests that power calculated at the ankle joint was derived from sources other than ankle musculature. It is further suggested that the additional power was transported from the knee joint through the active gastrocnemius and possibly plantaris muscles to the paw. A similar strategy has been previously suggested by Ingen Schenau et al.(1990) for jumping in humans. At the higher jump heights the transported power was apparently not required and was derived directly from the ankle extensors. It is suggested that these differences in the occurrence of transport are attributed to physiological differences between muscles and the reliance on what is ultimately most "efficient" for the nervous and muscular systems of the cat during a given activity.

Enhancement of the soleus force above the isometric tetanic tension (Po) measured *in situ* has been reported *in vivo* during treadmill locomotion (Gregor et al., 1988). Similar comparisons between *in situ* and *in vivo* force output of the medial gastrocnemius found no enhancement even during high jumps (Gregor et al., 1991). These differences in enhancement have been attributed to differences in physiological needs of the system implying that it may be more beneficial to enhance a muscle or transfer power from adjacent joints in one circumstance while relying on recruitment of additional muscles in another.

REFERENCES

Abelew, T.A. et al., Proceedings of the 14th Congress of the International Society of Biomechanics, Paris, France (pp67-68),1993

Fowler, E.F. et al., J. Biomech., 26,465-483, 1993.

Gregor, R.J. et al., J. Biomech., 21,721-732, 1988.

Gregor, R.J. et al., Proceedings of 14th annual meeting of the American Society of Biomechanics, Miami, (pp67-68), 1991

Goslow, G.E. et al., J. Morph. 141, 1-42, 1973

Herzog, W. et al., J. Biomech, 26, 945-953, 1993

Ingen Schenau, van G.J. et al., Multiple Muscle Systems, (pp639-652), Springer-Verlag, 1990

Robertson D.G.E. et al., J. Biomech., 13,845-854, 1980

Tjoe J.A. et al., J. Biomech.,24,267,1991

Whiting, W.C.et al., J. Biomech., 17,685-694, 1984

Acknowledgments

We would like to thank Dr. Roland Roy and Dr. John Hodgson for sharing their time and expertise during the calibration experiments and helping us develop our surgical techniques for implanting the tendon transducers. This study was supported by NSF grant # IBN-9311398

MECHANICAL POWER AND WORK OF CAT SOLEUS, GASTROCNEMIUS, AND PLANTARIS MUSCLES DURING LOCOMOTION: FUNCTIONAL SIGNIFICANCE OF MUSCLE DESIGN, FORCE- AND ACTIVITY-PATTERNS

B. I. Prilutsky*, W. Herzog and T. R. Leonard

Human Performance Laboratory, Faculty of Physical Education, The University of Calgary, Alberta, Canada T2N1N4.
*Permanent address: Biomechanics Laboratory, Central Institute of Physical Culture, Moscow, Russia 105483.

INTRODUCTION

In order to study the functional significance of the design features of the cat soleus (SO), gastrocnemius (GA), and plantaris (PL) muscles and their force- and integrated electromyogram (IEMG)-patterns during locomotion, mechanical power and the relative contribution of these three muscles in absorption and generation of mechanical energy during cat walking and trotting were estimated experimentally. Forces of SO, GA, and PL were measured using standard force transducers in three freely moving cats at walking and trotting on a motor-driven treadmill. Video records and a geometrical model of the cat hindlimb were used for calculating the rates of the length changes in SO, GA, and PL muscles. Mechanical power and work of SO, GA, and PL were calculated for 144 step cycles. The results of this study suggest that the design features of the ankle extensor muscles and the control of their activity are advantageous for the generation of mechanical energy for locomotion.

REVIEW AND THEORY

In order to understand the functional significance of the design of the musculoskeletal system and the organization of muscle activity during movements, it is useful to know the goal of the movements studied. In animal experiments, where submaximal activity is studied, muscle forces may be measured during normal movements (Herzog et al., 1993a,b; Hodgson, 1983; Walmsley et al., 1978). However, the goal of the movement may not be obvious, and the role of the muscles in achieving the goal of the movement cannot be interpreted easily. For example, if the main function of the ankle extensor muscles during cat locomotion is assumed to be the control of the direction of the ground reaction forces (Lawrence et al., 1993), interpretations of corresponding muscle force- and IEMG-time histories might be different compared to the case where the main function of the muscles is assumed to be the production of mechanical energy. In some cases, reasonable assumptions about the goal of an animal movement (e.g., hunting for food, or escaping from predators) may be made. Presuming that locomotion is performed in an 'efficient way', it may be assumed that the design of the ankle extensor muscles, SO, GA, and PL, and the control of these muscles during locomotion are advantageous for the production of mechanical energy.

The aims of this study were (1) to estimate mechanical power and work of the cat SO, GA, and PL during locomotion at different speeds, and (2) to explain force-, power-, and IEMG-patterns, the work done by these muscles, and the features of their design in terms of physiological and mechanical advantages which they might have in generating mechanical energy during locomotion.

PROCEDURES

Forces of SO, GA, and PL were measured using standard force transducers in three freely moving cats at walking and trotting speeds of 0.4, 0.8, 1.2, 1.5, and 1.8 m/s on a motor-driven treadmill. Video records (60 Hz) and a geometrical model of the cat hindlimb were used for calculating the rates of the length changes in SO, GA, and PL muscles. Power of the muscles was calculated as the scalar vector product of the muscle's force and the relative velocity of the attachment points. Muscle powers were obtained at each one percent of each step cycle using an interpolation cubic spline, and were then averaged over all step cycles available for a given animal and speed of locomotion. Negative and positive mechanical work done by a muscle for a given step cycle was calculated as the time integral of the negative and positive muscle power, respectively. The total mechanical power of SO, GA, and PL was equal to the algebraic sum of the powers of the individual muscles. The contributions of negative (-RC) and positive (+RC) work done by SO, GA, and PL to the total work of the three muscles were expressed as a percentage of the total negative and positive work done by the three muscles, respectively.

RESULTS AND DISCUSSION

Typical average power-time, force-time, and velocity-time histories of SO, GA, and PL obtained from one cat are shown in Fig. 1. The patterns and magnitudes of the velocity of SO, GA, and PL are similar to those reported by Gregor et al., 1988 and Goslow et al., 1973. Patterns and magnitudes of muscle forces recorded in this study are consistent with the results reported by Fowler et al., 1993; Gregor et al., 1988; Herzog et al., 1993a,b; Hodgson, 1983; Walmsley et al., 1978. Changes in power of SO and GA with increasing speeds of locomotion obtained in this study were similar to those reported by Whiting et al., 1984.

The positive mechanical work done by SO, GA, and PL during the step cycle increased with increasing speeds of locomotion from 0.4 m/s to 1.2 m/s. When speed increased from 1.2 to 1.8 m/s, the positive work of SO, GA, and PL did not change substantially. The positive work done by SO, GA, and PL per cycle of locomotion at the speeds of 0.4 - 0.8 m/s were -28±10 to 86±13 mJ, 20±8 to 111±29 mJ, and 28±9 to 99±17 mJ, respectively. The corresponding values of the positive work of the three muscles at speeds of 1.2 - 1.8 m/s were 36±6 to 100±3, 114±36 to 354, and 89±21 to 255±20, respectively. Relative contributions of SO, GA, and PL to the total negative and positive work are illustrated in Fig. 2. At slow speeds of locomotion, the slow, low threshold SO did approximately the same amount of positive work as the fast and strong GA and PL. The amount of work required to extend the ankle at slow speeds of locomotion could be done by GA and PL exclusively by recruiting additional motor units with a higher threshold (Walmsley et al., 1978). However, an increase in the percentage of fast motor units participating in the generation of mechanical energy might increase metabolic energy expenditure (Gibbs et al., 1972; Wendt et al., 1973). SO could produce more force and do more work at speeds of 1.2 - 1.8 m/s (Figs 1 and 2), because this muscle probably does not reach its maximum isometric force at these speeds (Herzog et al., 1992). However, the stiff muscle-tendon complex of SO (Prilutsky et al., 1994a) and its slow maximum velocity of shortening (Spector et al., 1980) compared to GA and PL causes a substantially faster decrease in the contractile abilities of this muscle in the late support period at fast compared to slow speeds of locomotion (Prilutsky et

al., in press, 1994; Prilutsky et al., 1994a). Therefore, the observed sharp decrease in muscle activity of SO in this period (Prilutsky et al., in press, 1994) may be considered useful. The decrease in the contractile abilities of SO during the late phase of support at fast speeds of locomotion seems to be compensated by an increase in activity (Prilutsky et al., in press, 1994), forces and powers (Figs 1 and 2) of GA and PL, and by a transfer of mechanical energy from the knee to the ankle through GA and PL (up to 67 mJ, Prilutsky et al., 1994b). The transfer of mechanical energy through two-joint muscles allows muscles located more proximally on the extremity to compensate for the deficiency in work production of muscles located more distally (Prilutsky et al., 1994c). Because of the design features of GA and PL (high intrinsic velocity of shortening and maximum isometric force [Herzog et al., 1992; Spector et al., 1980], multi-joint nature of these muscles, and about five times more compliant muscle-tendon complexes compared to SO [Prilutsky et al., 1994a]), these muscles are better suited to function at speeds of locomotion higher than 0.8 m/s. It seems that the central nervous system uses the features of GA and PL by activating them for a prolonged period of time during the late support phase (Prilutsky et al., in press, 1994; see also Fig. 1). The relatively larger increase in force and power of PL during the late phase of support compared to that of GA (Fig. 1) may be useful in flexion of the metatarsalphalangeal joints, because PL has two partial insertion sites, one on the calcaneus and another one on the tendon of the flexor digitorum brevis on the plantar surface of the foot (Abraham et al., 1985; Goslow et al., 1972). Also, PL has a larger moment arm about the knee than GA. This feature gives PL an advantage over GA in using energy generated by the knee extensor muscles to extend the ankle (Prilutsky et al., 1994b). During the early support phase, force and power produced by PL were low (Fig. 1) and the amount of negative work done by this muscles was usually less than 15% of the total negative work of the three muscles (Fig. 2). This behavior of PL in the early support phase might prevent a premature flexion of the metatarsalphalangeal joints. According to Goslow et al., 1972, initial contraction of PL causes immediate digit flexion, because forces from the plantaris are transmitted 'relatively undiffused' to the tendon of the flexor digitorum brevis to which the tendon of PL is partly attached.

In conclusion, the results of this study suggest that the design and control of the ankle extensor muscles are advantageous for the generation of mechanical energy for locomotion.

ACKNOWLEDGEMENTS

This study was supported by an operating grant of NSERC of Canada to W.H. and postdoctoral grants of the University of Calgary (1992-1993) and the Alberta Heritage Foundation for Medical Research (1993-1994) to B. I. P. We would like to acknowledge the technical expertise of T. L. Allinger and H. Nguyen in this study.

REFERENCES

Abraham et al. Exp. Brain Res., 58, 580-593, 1985.
Fowler, E.G. et al. J. Biomechanics, 26, 465-483, 1993.
Gibbs, C.L. et al. Am. J. Physiol., 223, 864-871, 1972.
Gregor, R.J. et al. J. Biomechanics, 21, 721-732, 1988.
Goslow, G.E. et al. J. Morphology, 137, 335-352, 1972.
Goslow, G.E. et al. J. Morphology, 141, 1-42, 1973.
Herzog, W. et al. J. Biomechanics, 25, 1329-1335, 1992.
Herzog, W. et al. J. Biomechanics, 26, 945-953, 1993a.
Herzog, W. et al. J. Biomechanics, 26, 1463-1471, 1993b.
Hodgson, J.A. J. Physiology (Lond.), 337, 553-562, 1983.
Lawrence, J.H. et al. J. Neurophysiology, 69, 282-285, 1993.
Prilutsky, B.I. et al. Proceedings of the 8th Biennial Conference of Canadian Society for Biomechanics, 1994a.
Prilutsky, B.I. et al. Proceedings of the 2nd World Congress of Biomechanics, Amsterdam, 1994b.
Prilutsky, B.I. et al. J. Biomechanics, 27, 25-34, 1994c.
Prilutsky, B.I. et al. J. Biomechanics, in press, 1994.
Spector, S.A. et al. J. Neurophysiology, 44, 951-960, 1980.
Walmsley, B. et al. J. Neurophysiology, 41, 1203-1216, 1978.
Wendt, I.R. et al. Am. J. Physiol., 224, 1081-1086, 1973.
Whiting, W.C. et al. J. Biomechanics, 17, 685-694, 1984.

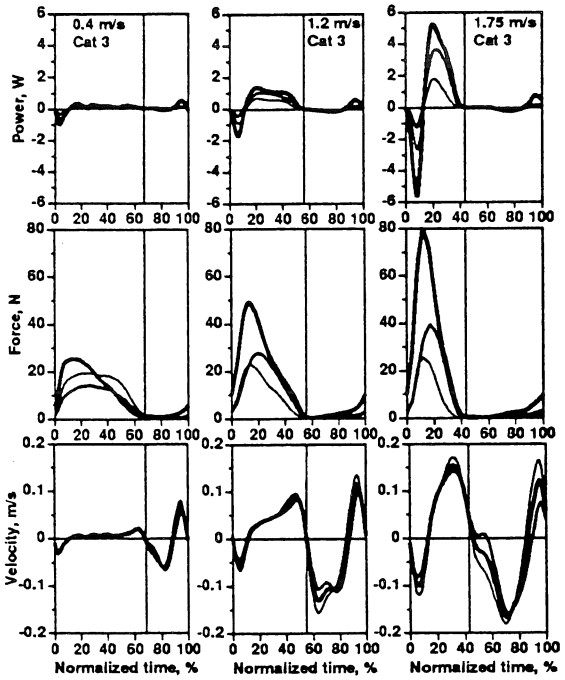

Fig. 1. Average velocities, forces, and powers of SO (thin lines), GA (thick lines), and PL (intermediate lines) as a function of normalized step cycle time for different speeds of locomotion. Touch down occurs at time 0%. Vertical lines separate the support and swing phases.

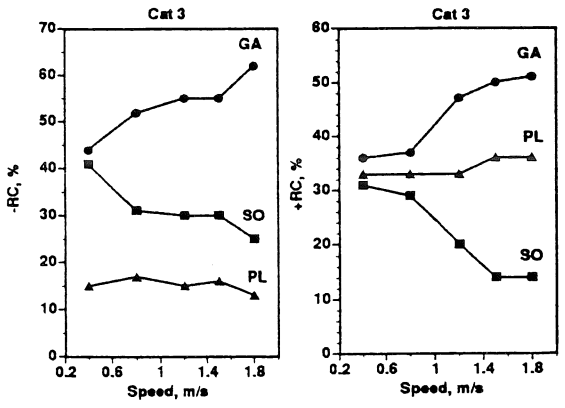

Fig. 2. Averaged relative contribution of the negative (A) and positive (B) mechanical work of SO, GA, and PL to the total negative and positive work of these muscles, respectively, as a function of speed of locomotion.

IN VIVO UTILIZATION OF THE "Z" TENDON TRANSDUCER

V. Venkateswaran, T. Basham and C.S. Enwemeka

Department of Physical Therapy Education
University of Kansas Medical Center, Kansas City, KS, 66160.

INTRODUCTION

A number of technical difficulties are encountered when tendon forces are monitored via a tendon force transducer. This report describes our experience in using a newly developed "Z" tendon transducer in the course of our experiments designed to determine the intensity of electrical stimulation required to impose safe therapeutic loads on repaired rabbit Achilles tendons. First, the repaired Achilles tendons were used to calibrate the tendon transducer. The "Z" transducer was hooked on the tendon and connected to a specially designed peak-hold meter. Via a wire sutured above the calcaneal attachment of the tendon, weights totaling up to 2.2 Kg were used to pull the tendon in 0.45 Kg increments. Following satisfactory calibration the maximum safe load transmitted by the repaired Achilles tendon of rabbits were determined on each of post-operative days 1, 3 and 5 as the triceps surae was electrically stimulated. A maximum of four bouts of stimulation was achieved before appreciable fatigue of the muscle became evident. Furthermore, 10 volts of electrical stimulation was the maximum safe load tolerated by the animals without rupture of the repaired tendons. The "Z" transducer was calibrated in Newtons/millivolts (N/mV), and hence the load transmitted through the tendon was derived by converting the amount of mV monitored on the peak-hold meter, to Newtons (N)

REVIEW AND THEORY

Several types of transducers are used to measure tendon and ligament forces (1-4). In 1990, An et al., described the "Z" tendon force transducer, which compensates for changes in temperature and allows measurement of tendon forces without slippage or assembly of parts (5). In this study, we present our findings in calibrating the "Z" tendon transducer, and the preliminary results of our study designed to determine the maximum safe load transmitted by surgically repaired rabbit Achilles tendons when the muscles are subjected to electrical stimulation.

PROCEDURE

I. Calibration of The "Z" Force Transducer: Eight 9 weeks old rabbits were weighed, anesthetized, and the fur overlying the right Achilles tendon shaved. A longitudinal incision was made, then after separating the tendon from its sheath, its diameter was measured. With the tendon intact, steel monofilament sutures were sutured to the tendon 8 mm above the calcaneal insertion. The suture wires were then looped and used to anchor the standard weights used for calibrating the transducer. With the "Z" tendon transducer appropriately attached midway between the calcaneal insertion and the musculotendinous junction of the tendon, and connected to a specially designed peak-hold meter (Rochester Electronics, Rochester, MN),.weights were added to the wire in 0.45 Kg increments up to a total weight of 2.2 Kg. The peak force transmitted through the tendon as weights were added, was read off the peak-hold meter and recorded.

II. The Peak Force Tolerated By The Tenotomized Achilles Tendon (Without Rupture) Upon Electrical Stimulation of The Triceps Surae: Eighteen rabbits, 9 weeks of age, were equally divided into three groups. Animals were weighed, anesthetized, and the right lower hind limb of each rabbit prepped. Under sterile conditions, the right Achilles tendon was severed sharply and transversely midway between its calcaneal attachment and musculotendinous junction. Subsequently, the severed ends of the tendon were approximated, sutured, and the limb immobilized in a rigid polycaprolactone cast. On each of post-operative days 1, 3 and 5, the skin sutures on six rabbits were removed, the tendon exposed, freed from the surrounding tissue, and the transducer implanted proximal to the site of tenotomy under anesthesia. With the transducer connected to the peak-hold meter, and the active and dispersive electrodes placed on the skin overlying the belly of the triceps surae and the lumbosacral areas respectively, a Mettler Electronics Sys. Stim 207 electrical stimulation unit (Mettler Electronics, Anaheim,, CA) was used to deliver pulsed DC current at an intensity of approximately 10 volts. Our preliminary study reveals that this was the maximum intensity tolerated by the animals. The current was surged to mimic a slow-twitch contraction. The maximum force transmitted by the tendon during each contraction, was read and recorded from the peak-hold meter.

RESULTS

Our calibration of the transducer revealed a linear relationship between the load imposed on the tendons and that obtained from the transducer (Fig 1). The weights applied to the tendon and the transducer output have been fitted on a line using linear regression (r=0.997). A maximum of four stimulations was achieved without appreciable fatigue of the muscle. Furthermore, 10 volts of electrical stimulation was the maximum safe dose tolerated by the animals without rupture of the tendons (Fig 2). In both of these experiments we encountered easy and simple installation of the transducer yet allowing its secure attachment to the tendon.

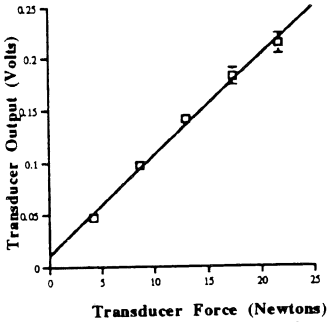

Fig. 1: Calibration of the "Z" tendon transducer

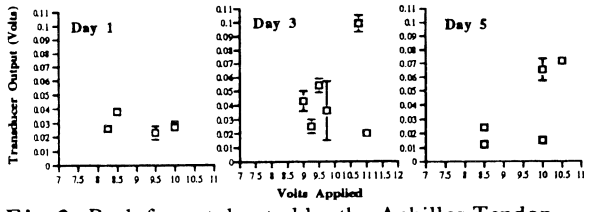

Fig.2: Peak force tolerated by the Achilles Tendon upon electrical stimulation of the triceps surae on day 1, 3 and 5 following tenotomy

DISCUSSION

This preliminary study reveals that: 1) tendon force can be accurately monitored using the "Z" force transducer. These results are highly reproducible with proportional linearity and without hysteresis. 2) Using our electrical stimulation parameters, a maximum of four stimulations can be achieved without appreciable fatigue of the triceps surae. 3) Higher than 10 volts of current intensity level was not tolerable to the animals and resulted in rupture of the repaired tendons. 4) The installation of the transducer on the tendon was easy and simple, allowing secure attachment to the tendon.

The "Z" tendon force transducer functions on a principle which involves converting longitudinal tension into transverse load that can then be measured. This concept has been used in the past for both tendons and ligaments (5). After four bouts of electrical stimulations, the force of muscle contraction wanes. This may be due to the onset of muscle fatigue. Data obtained from this study is currently being used in the biomechanical, ultrastructural, biochemical and molecular effects of a combination of functional loading, therapeutic ultrasound and laser photostimulation on the healing process of repaired tendons.

REFERENCES

1. Salmons, S. Biomed. Engng., 4,467-474, 1969.
2. Barnes, G.R.G and Pinder. D.N. J. Biomechanics., 7,35-42, 1974.
3. Lewis, J.L. et al. J Biomed Engng., 104,125-128, 1982.
4. Abraham, L.D and Loeb. G.E. Expt. Brain Res., 58,580-593, 1985.
5. An, K.N. et al. J. Biomechanics., 23(12),1269-1271, 1990.

ACKNOWLEDGMENT

This work was funded by the U.S. Department of Education-NIDRR.

AFFECTS OF ASSUMED GEOMETRY, FLEXIBILITY, AND INTRINSIC STRENGTH ON OPTIMIZATION-BASED FORCE PREDICTIONS

M.A. Nussbaum, D.B. Chaffin, and S.A. Lavender[+]
Center for Ergonomics, The University of Michigan, Ann Arbor, MI, 48109-2117
[+]Rush Presbyterian-St. Luke's Medical Center, Chicago, IL, 60612

INTRODUCTION

The present study considers the affects of assumed subject flexibility and intrinsic muscular strength on patterns of predicted muscle recruitment. A single type of exertion is evaluated, involving static loading of the torso in a laterally bent posture. The practical significance of these assumptions is evaluated by comparison of optimization-based force prediction with experimental data. Results showed that predictions are dependent on these assumptions. However, the interplay between accuracy in force prediction and geometry was not clear, indicating that recruitment strategies are altered with postural asymmetry. The use of a single optimization strategy for non-neutral postures is thus debatable and the dependency on geometrical and physiological assumptions is emphasized.

REVIEW AND THEORY

Muscle force predictions are commonly achieved using optimization-based methods as part of a biomechanical analysis. The predictive ability of these models, and their potential for simulating recruitment strategies, provides the motivation for the use of these types of methods. Existing reports have demonstrated that optimization model predictions are sensitive to assumptions regarding muscle moment arms and lines-of-action. The dependency on assumptions of subject flexibility and intrinsic strength is examined here. It is typically presumed that the accuracy of muscle force predictions will increase with increasing geometric realism. The implication is that force estimates should improve along with our ability to model the anatomical system. This was assessed for one optimization model by successive incorporation of geometric detail and comparison to experimental data. Thus, two hypotheses are examined: 1) Do optimization-based predictions depend on assumed flexibility and strength, and 2) does the veracity of force predictions increase with increasing geometric fidelity?

PROCEDURES

Lumbar muscle force levels were predicted using an optimization formulation (Crowninshield et al., 1981; Hughes, 1991), that minimized the sum of the cubed muscle intensities and maintained muscle forces within physiologic bounds. Variation in muscle strength was simulated by proportionally changing the cross-sectional areas (CSA) of all muscles in the model. For a given predicted force, an increase in CSA reduced the muscle intensity (and cubically decreased its contribution to the objective) and increased the muscle's maximal force (upper bound). It was assumed that differences in subject flexibility in lateral bending were largely due to passive forces generated by muscle stretching. Thus, variation in flexibility was simulated by shifting the passive component of the length-tension (L-T) relationship. Muscle resting length is nominally that in an upright posture, and a decrease in flexibility (or an increase in stiffness) was achieved by decreasing the resting length. In the work presented here, a 15% shift was employed. All simulations were performed assuming a 50th%-ile male, with a 40Nm moment load at L3/L4 and the thorax laterally bent 20^{o} to the right.

Geometric changes that are induced by postural asymmetry, including changes in muscle lines-of-action, muscle length-tension properties, and passive restorative moments, were incorporated in a step-wise fashion. Following each step, predicted forces were statistically compared to observed muscle activity. EMG data for these comparisons were obtained from a previous experiment by Lavender et al. (1993). In their study, 15 subjects resisted static lumbar moments of 20 and 40 Nm while the thorax was laterally bent 20^{o}. EMG records from the pairs of Erector Spinae (ES), Rectus Abdominus (RA), External Oblique (EO), and Latissimus Dorsi (LD) were normalized (NEMG) using maximal and resting values.

RESULTS

Altering muscular strength had a large influence on the magnitudes of predicted lumbar forces for a given moment load. The *patterns* of predicted muscle use, though, were essentially unchanged. An example is considered for the left EO (Figure 1). Compared to a normal subject, a subject with twice the lumbar muscle strength has predicted muscle activity at nearly half the level, and the opposite for a weaker subject with half the strength. Despite the non-linear penalty imposed by the objective function, muscle activities are apportioned consistently across a four-fold variation in assumed muscular strength.

Shifting the passive muscle L-T curve caused the contralateral muscles to have higher levels of passive forces. Since the net muscle forces on this side were predicted to remain relatively constant, the predicted active component was reduced. Changes in the patterns of predicted force were most dramatic on the ipsilateral side. The right EO is considered for a normal subject and one with increased stiffness (Figure 2). For a low load (20Nm), a stiff subject needed additional REO force for postural maintenance. For a higher load (40Nm), the stiffer subject

recruits the REO at larger magnitudes and over a larger range of load orientations.

Step-wise inclusion of increasing geometric detail had inconsistent effects on the correspondence between predicted forces and experimental NEMG (Figure 3). With only body weight (BW) accounted for, and excluding the LD, the average coefficient of determination was 0.72. After incorporating the active and passive effects resulting from the bent posture (Post.), the average rose slightly to 0.76. For individual muscle, however, improved correspondences were not always associated with more geometric information. Further, if all postural effects are ignored, and the posture is assumed to be upright, the average coefficient is 0.78!

DISCUSSION

Predicted forces using an optimization-based model were found to be moderately dependent on assumptions regarding subject strength and flexibility. The sensitivity to strength, which was simulated by varying muscle cross-sectional areas, was previously shown by Brand et al. (1986), and sensitivity to assumed muscle lines-of-action is evident in our ongoing work. Variations in strength appeared to cause proportional changes in predicted forces, whereas differences in flexibility, simulated by changing muscle stiffness, showed shifts in the *patterns* of predicted activity. Optimization-based methods have proven useful in characterizing the overall behavior of the lumbar musculature, but mainly in terms of subject averages. These techniques have generally been less robust when applied to individual subjects. Indeed, subjects exhibit large differences in observed muscle activity, even for simple static loads (Nussbaum et al., 1993). Given that optimization-based estimates are sensitive to almost all groups of assumptions upon which they are developed, their use in subject-specific modeling will be especially challenging. Present efforts are continuing to examine whether the recruitment patterns that result from simulation of strength and flexibility differences are supported by empirical measures of these qualities.

The inclusion of increasing geometric detail was somewhat equivocal in terms of increasing the veracity of muscle force predictions. While correlation of predicted forces with NEMG has been criticized as a validation technique, it nonetheless provides a reasonable indication of model performance. The results here do not clearly indicate that predicted forces became more realistic with better anatomic and physiologic approximations. The present optimization model has been relatively more successful in predicting behavior during static loading in upright postures. These results give evidence, then, that recruitment patterns and perhaps strategies are altered in asymmetric postures. Thus, the single strategy inherent in the model objective may not be applicable.

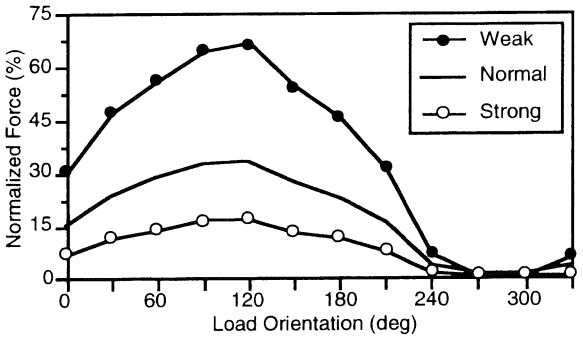

Figure 1. Predicted response of the left External Oblique with variable lumbar muscle strength.

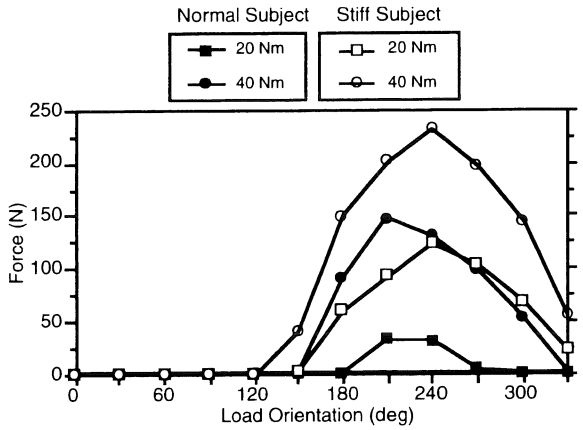

Figure 2. Predicted response of the right External Oblique with changes in assumed subject flexibility.

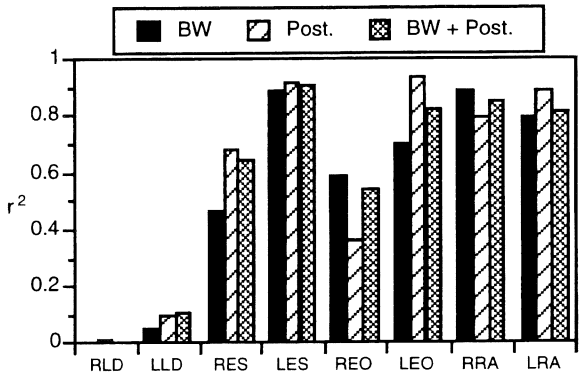

Figure 3. Correspondence between predicted forces and NEMG using three sets of input geometric information.

REFERENCES

Brand, R.A. et al. J. Biom., 21, 59-66, 1988.

Crowninshield, R.D. et al. J. Biom. 14, 793-901, 1981.

Hughes, R.E. PhD Thesis, Univ. of Michigan, 1991.

Lavender, S.A. et al Proc. of 37th HFES, Seattle, (688-692), 1993.

Nussbaum, M.A. Proc. of ASB, Iowa City, (xi-xii), 1993.

ACKNOWLEDGMENTS

This work was supported by NIH Grant 1R01-AR39599.

EXTENT OF MUSCLE ACTIVATION IN NON-IMMOBILIZED AND IMMOBILIZED HAND AND ELBOW JOINTS

M. Bilodeau, G. H. Yue and R. M. Enoka

Department of Biomedical Engineering
The Cleveland Clinic Foundation
Cleveland, OH 44195

INTRODUCTION

The aim of the study was to investigate the effect of immobilization on the level of activation of the first dorsal interosseus (FDI) and biceps brachii muscles. EMG signals were recorded for 24-hr periods prior to and during immobilization of the thumb and index finger and of the elbow joint. Immobilization produced a decrease in the activation level of both muscles, but the extent of the reduction was variable across subjects.

REVIEW AND THEORY

Immobilization has been shown to induce morphological and functional changes in skeletal muscles of animals (Robinson et al., 1991) and humans (Duchateau & Hainaut, 1987). These adaptations are thought to be due to the immobilization-induced decrease in muscle activity. However, Alford et al. (1987) observed that the level of muscle activity (24-hr EMG) in rat hindlimb muscles during hindlimb suspension returned to control values by the 7th day of suspension. Consequently, they concluded that muscle activity per se does not play a major role in maintaining muscle properties in the rat hindlimb suspension model.

It is not known, however, how much muscle activity occurs during immobilization in humans, although there is evidence that muscle is not completely silenced by immobilization in animal models (Mayer et al., 1981). The purpose of this study was to quantify the level of muscle activity in the FDI and biceps brachii muscles of normal human subjects in non-immobilized and immobilized conditions. This should explain some of the variability observed in the responses of different subjects to immobilization and allow investigators to determine the role of activity in the determination of various physiological parameters.

PROCEDURES

Three normal subjects volunteered for experiments on the FDI and two for experiments on biceps brachii. Each subject was tested for 24-hrs once before immobilization (non-immobilized control session) and then for 1-28 days of immobilization. For the FDI, two subjects had their thumb and index finger immobilized in a splint for a period of 24-hrs and one subject for 4 consecutive days during which EMG signals were monitored continuously. For the biceps brachii, one subject wore a cast and another a sling that immobilized the elbow joint at a 1.57 rad (90^{O}) angle for a period of 4 weeks. For these two subjects, EMG signals were monitored for 24-hr periods on several scattered days throughout the 4 weeks of immobilization. EMG signals were detected with surface electrodes and could be recorded continuously for 24-hr periods with a unit that was fitted inside a hiney pack tied at the waist of the subject.

The chronic EMG unit consisted of a differential input amplifier that provided common mode rejection and switchable gain of 100 and 1000. The output of the amplifier was then fed through an integrator unit where the signal was rectified and filtered with a time constant of 0.05 seconds. The rectified and filtered signal was recorded on a Sony HR-10 Model J Cassette data recorder at a tape speed of 0.15 cm/s, which yields a frequency range between DC

and 39 Hz. The data were then played back at a speed of 4.8 cm/s and digitized at a frequency of 500 Hz for further analysis on a PC.

The EMG was quantified in terms of bursts of the rectified and integrated activity. EMG bursts were determined by an automatic process that identified an increase in the signal above a chosen threshold level. The threshold was determined as 3 to 5 standard deviations above the mean signal amplitude derived from a 1 min silent period, when the subject was resting. Muscle activity was quantified with the following parameters: number of bursts per time period, burst rate, average burst amplitude, average burst duration, average burst area and relative duty cycle ("on" time/total time).

RESULTS AND DISCUSSION

Preliminary analysis of the data shows that there was a decrease in the level of activity during immobilization for all subjects. Figure 1 shows 24-hr recordings for both the non-immobilized (A) and the immobilized (B) conditions for the FDI muscle of one subject. The extent of the decrease in muscle activity, however, was variable across subjects, muscles (FDI vs. biceps brachii), and time. The activity in the biceps brachii muscle of both subjects was depressed to a much greater extent than FDI during immobilization.

Because of this variability in the extent to which muscle activity is reduced, it is critical that the amount of activity in several subjects be determined for each immobilization protocol.

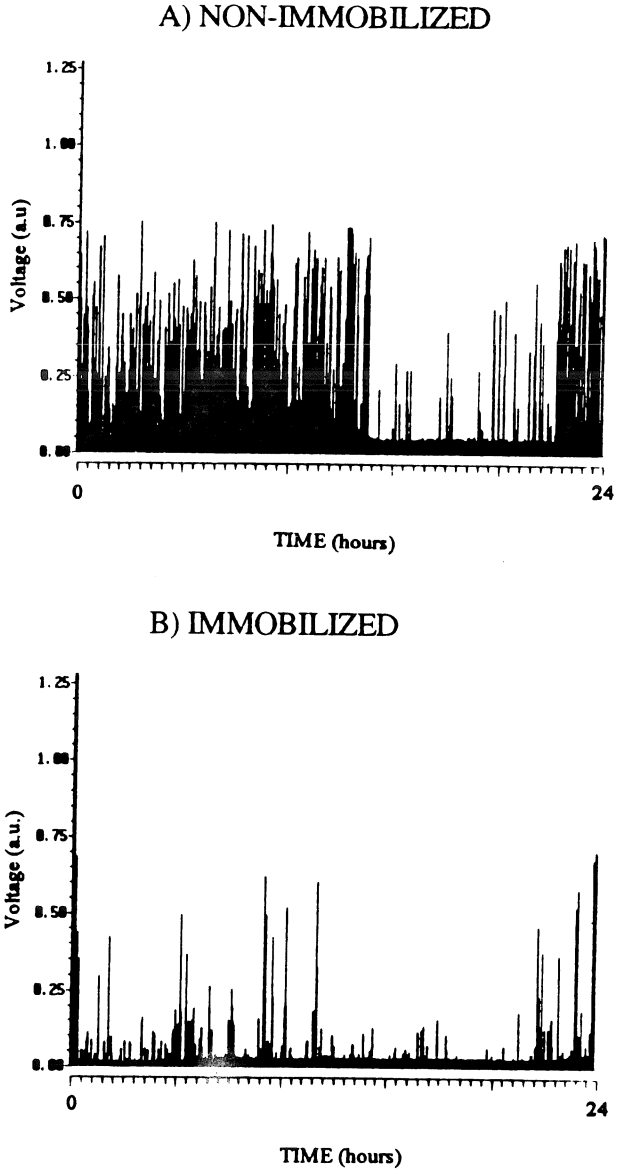

Figure 1. *24-hr records of EMG activity in the FDI muscle of one subject for the non-immobilized (A) and the immobilized (B) conditions.* Voltage is in arbitrary units.

REFERENCES

Alford EK et al: *Exp Neurol* 96: 635-649, 1987.

Duchateau J, Hainaut K: *J Appl Physiol* 62: 2168-2173, 1987.

Mayer RF et al: *Neuroscience* 6: 725-739, 1981.

Robinson GA et al: *Muscle & Nerve* 14: 563-573, 1991.

ACKNOWLEDGMENTS

The authors acknowledge the technical assistance of D. Keen in the data collection. Supported by NIH grant NS20544.

A METHOD FOR THE DETERMINATION OF THE FORCE-LENGTH-VELOCITY RELATION OF HUMAN SKELETAL MUSCLES

John W. Chow[1], Warren G. Darling[2], James G. Hay[2], and James G. Andrews[2]

[1]Department of Kinesiology, The University of Illinois at Urbana/Champaign, Urbana, IL 61801
[2]Department of Exercise Science, The University of Iowa, Iowa City, IA 52242-1111

INTRODUCTION

The purpose of this study was to propose and evaluate a method for the *in vivo* determination of the force-length-velocity (FLV) relations of individual quadriceps muscles. One female subject performed maximum effort knee extension exercises on a LIDO dynamometer. The gravitational and inertial effects were taken into consideration when determining the resultant knee torque (T_K). The musculoskeletal parameters of the quadriceps muscles were obtained from radiography and magnetic resonance imaging (MRI). Hill's (1938) mechanical model was used to represent the force-velocity (FV) relation of a muscle and the constants in Hill's model were assumed to vary with muscle length (L). Experimentally determined T_K and muscle shortening velocity ($\dot{L}$) data were used to determine the unknown parameters in the muscle model. The predicted T_Ks using the muscle model were consistently greater than the measured T_Ks. The overestimations resulted from the lack of low T_K-high $\dot{L}$ data for the determination of muscle model parameters.

REVIEW AND THEORY

Over the last three decades, musculoskeletal models have been used by biomechanists in various tasks. One major criticism of musculoskeletal modeling is the inclusion of many assumptions involved in the modeling process. For example, Hill's (1938) mechanical model -- $F = (F^{max}b - a\dot{L})/(\dot{L} + b)$, where F is muscle force, a and b are Hill constants -- is commonly used to represent the FV characteristic of muscle contraction. Because of the difficulties in determining individual muscle forces *in vivo*, muscle model parameters (e.g., a and b) used in musculoskeletal modeling are typically taken from experiments performed on animal muscles under *in vitro* conditions.

The purpose of this study was to propose and evaluate a general method to determine the FLV relations of individual human skeletal muscles *in vivo*. Specifically, it was the intent of this study to derive muscle model parameters for individual knee extensors. To make the musculoskeletal modeling more manageable, the muscle tissue and the related tendons for each muscle were treated as a single functional unit. If the mechanical characteristics of individual muscles can be estimated *in vivo*, use of generic FLV and stress-strain relations can be avoided. Consequently, fewer assumptions are required in the modeling process.

PROCEDURES

Strength Data. During the strength testing session, a female subject (24 yrs, 1.6 m, 574 N) performed maximum effort left knee extension exercises on a LIDO dynamometer in a sitting position. The session started with maximal isometric contractions at different attachment arm angles (isometric pre-tests). These were followed by 16 maximal isokinetic trials (25 to 400 °/s at intervals of 25 °/s) at different preset angular velocities (PAVs) and three maximal isotonic trials at different preset resistance torques (two repetitions per trial) . The session concluded with maximal isometric trials (isometric post-tests).

The resistance force acting on the shank-plus-foot (S+F) segment (F_R) was measured by a load cell located between the attachment arm of the dynamometer and the shank. The knee flexion angle ($\varnothing_K$), defined as the angle between the distal extension of the thigh segment and the shank segment, was measured by an electrogoniometer attached to the lateral side of the left leg. Sagittal views of the medial side of the S+F segment during the trials were videotaped.

Musculoskeletal Parameters. During the radiography session, six radiographs of the subject's left knee and two radiographs of the left hip were obtained. During the MRI session, two scans were performed and axial images at 4 mm intervals were obtained for the left thigh. Based on the data reduced from radiographic and magnetic resonance images, the coordinate data of the origins and insertions of the quadriceps muscles and the effective moment arm of the quadriceps force about a transverse axis through the knee center (d_e) were determined. The muscle length was computed as the shortest distance between the origin and insertion of the muscle (Chow et al., 1994a).

Resultant Knee Torque. Video pictures of four isokinetic repetitions -- 25, 150, 275, and 400 °/s -- were analyzed and three relations were established: (1) shank angle ($\varnothing_S$) vs. $\varnothing_K$, (2) moment arm (d_{SF}) of the weight of S+F segment (W_{SF}) vs. $\varnothing_S$, and (3) moment arm (d_R) of F_R vs. $\varnothing_S$. The T_K values were determined using the moment equation about the knee joint center:

$$T_K = F_R d_R + W_{SF} d_{SF} + I_{SF}\ddot{\varnothing}_S \qquad [1]$$

where I_{SF} is the moment of inertia of the S+F segment about a transverse axis through the fixed knee joint center and $\ddot{\varnothing}_S$ is the angular acceleration of the shank segment. Using the relations established from data of selected isokinetic repetitions, d_R and d_{SF} were determined indirectly from the $\varnothing_K$ data obtained from the goniometer. Inertial parameters reported in the literature were used to obtain W_{SF} and I_{SF}. The $\ddot{\varnothing}_S$ values were determined by differentiating $\varnothing_K$ twice with respect to time.

Muscle Model. Application of Hill's characteristic equation to individual quadriceps muscles yields

$$T_K = d_e \sum_{i=1}^{4} \left(\frac{F_i^{max} b_i - a_i \dot{L}_i}{\dot{L}_i + b_i} \cos\theta_i \right) \qquad [2]$$

where θ is the angle between the lines of action of the quadriceps force and an individual muscle force, and i is the subscript for individual heads of the quadriceps muscle. The number of unknowns in the above equation is 12 (4 F_i^{max}s + 4 a_is + 4 b_is). At the completion of data collection, one repetition was selected from each isokinetic trial and there were 17 sets of T_K-$\dot{L}$ data (16 from isokinetic and 1 from isometric trials) for a

given $\emptyset_K$. Each set of T_K-$\dot{L}$ data provided T_K and $\dot{L}$ values for one independent equation.

Determination of Muscle Parameters. To find the unknown parameters at different Ls, T_K-$\dot{L}$ data, d_e, and θ_is at nine $\emptyset_K$s -- 25° to 105° at 10° intervals -- were extracted from the data files or computed. For each $\emptyset_K$, the over-determined system of equations could only be solved using an optimization approach.

The optimization program used required the user to supply a guess value for each variable to be determined. The F^{max} values determined from the data reduced from isometric trials (Chow et al., 1994b) were used as guess values for F_i^{max}s. Because a is usually expressed as a fraction of F^{max}, four different a/F^{max} ($= b/V^{max}$) values -- 0.2 to 0.8 in steps of 0.2 -- were used as guess values for each muscle. Therefore, 256 combinations [4 (a/F^{max} values) to the power 4 (muscles)] were supplied as guess values. Using the maximum shortening velocity (V^{max}) values reported in the literature, a V^{max} value of four optimum fiber lengths per second (L_o^f/s) was assumed in determining the guess value of b [i.e., $b = 4\ L_o^f$ x (b/V^{max})]. For each muscle parameter of each muscle, the parameter values from selected converged combinations were plotted against L and a polynomial was fitted to the data using regression analysis.

Model Evaluation. To evaluate the effectiveness of the present muscle model, T_Ks predicted by the muscle model (T_K^Ps) were compared to the measured torques (T_K^Ms) in eight isokinetic and six isotonic repetitions. To evaluate the sensitivity of each parameter, T_K^P resulting from a 10% increase in either F^{max} ($T_K^{P(+F)}$), a ($T_K^{P(+a)}$), b ($T_K^{P(+b)}$), L ($T_K^{P(+L)}$), or $\dot{L}$ ($T_K^{P(+V)}$) was computed. In addition, the T_K^P when fixed Hill constants ($a/F^{max} = 0.275$, $b = 4\ L_o^f$/s) were used for all Ls and muscles ($T_K^{P(FC)}$) was also computed.

RESULTS AND DISCUSSION

For those repetitions of PAV > 300 °/s, the T_Ks recorded at the instants of peak angular velocity ($\dot{\emptyset}_S^{pk}$) ranged from 56.6 to 67.9 Nm. Because $\ddot{\emptyset}_S$ at the instant of $\dot{\emptyset}_S^{pk}$ was zero and the knee torque due to W_{SF} was small, the T_Ks recorded at these instants were largely due to F_R.

Two quantities are used to compare the torque-time curves obtained in each repetition (Figure 1). The average absolute error (AAE), defined as the average vertical distance between the two curves, is used to compare the T_K^P curves with the T_K^M curve. The average vertical location (AVL), defined as the average vertical location of one curve relative to another, is used for the sensitivity analyses. A negative AVL indicates that a curve is located below the T_K^P curve.

On average, the developed muscle model overestimated T_K by 13.3 Nm in the selected isokinetic repetitions, and by 25.4 Nm in the isotonic repetitions. When the AAE is expressed as a percentage of the average T_K^M of the repetition (AAE_R), the average AAE_R of the T_K^P curves is 15.5±5.1% for the isokinetic repetitions, and 25.4±7.6% for the isotonic repetitions. Results of detailed analysis suggest that the overestimated T_K^Ps are due to a combination of underestimated a values and overestimated b values, which in turn resulted from a lack of low T_K-high $\dot{L}$ data for the solving of muscle model parameters. The AVLs of $T_K^{P(FC)}$ indicate that the $T_K^{P(FC)}$ curve is located at a relatively constant distance below the T_K^P curve, irrespective of the PAV.

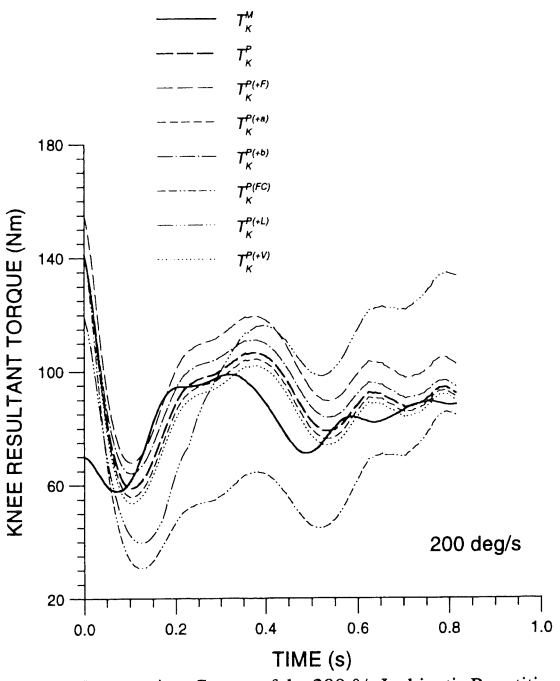

Figure 1. Torque-time Curves of the 200 °/s Isokinetic Repetition.

This suggests that using constant values of a and b has little effect on the shape of the predicted torque-time curve. However, the large AAEs of $T_K^{P(FC)}$ demonstrate that the predicted torques can be very remote from the measured torques if inappropriate constant values are used.

The results of the sensitivity analyses are presented in Table 1. The AVL values clearly demonstrate the prominent influence of F^{max} on predicted torque values.

Table 1. Results of the Sensitivity Analyses.

	Average AVL (Nm)				
	$T_K^{P(+F)}$	$T_K^{P(+a)}$	$T_K^{P(+b)}$	$T_K^{P(+L)}$	$T_K^{P(+V)}$
Isokinetic Trials (N = 8)	11.7 ±1.3	-2.0 ±0.5	3.8 ±0.7	7.1 ±1.9	-3.9 ±0.7
Isotonic Trials (N = 6)	13.3 ±0.5	-1.5 ±0.2	3.1 ±0.3	6.7 ±1.3	-3.3 ±0.3

Given the fact that high $\dot{L}$-low T_K data were not available for determining the muscle model parameters, the average AAE_R in T_K^P of 15.5% found in selected isokinetic repetitions is considered satisfactory and implies the practical feasibility of the method proposed in this study. Further study is recommended to examine the extent to which the AAE_R is reduced if a full range of T_K-$\dot{L}$ data are available for determining the model parameters.

REFERENCES

Chow, J.W. et al. *Proc. 18th ASB Annual Meeting*, 1994a.
Chow, J.W. et al. *Proc. 18th ASB Annual Meeting*, 1994b.
Hill, A.V. *Proc. Royal Soc. B*, 126, 136-195, 1938.

Acknowledgement. This study was supported in part by a grant from the University of Iowa Student Association.

SESSION 6:

GAIT/POSTURE

STRIDE FREQUENCY AND MUSCULOSKELETAL STIFFNESS

Claire T. Farley and Octavio Gonzalez
Department of Human Biodynamics,
University of California, Berkeley, CA. 94720. USA.

INTRODUCTION

When humans and other mammals use running gaits, the body's complex system of muscle, tendon and ligament springs behaves like a single linear spring ("leg spring"). In all of the running, trotting and hopping mammals studied to date, the stiffness of the leg spring remains nearly the same at all speeds. The spring system is adjusted to bounce off the ground in less time at higher speeds by increasing the angle swept by the leg spring during the ground contact phase rather than by increasing the stiffness of the leg spring. The goal of this study was to determine how the musculoskeletal spring system is adjusted to accommodate different stride frequencies at a given running speed. Our findings show that the body's spring system is adjusted to operate at different stride frequencies by changing the stiffness of the leg spring. This finding has implications for understanding how the musculoskeletal system is adjusted for running on a variety of terrain and for designing spring-based prostheses for running.

REVIEW AND THEORY

When animals run, they bounce along the ground using muscles, tendons and ligaments as springs that store and return elastic energy. This observation has led to the development of a simple model for running gaits. This model consists of a single linear "leg spring" and a mass equivalent to the animal's mass (Fig. 1; Blickhan, 1989; McMahon & Cheng, 1990). This model has been shown to describe and predict the mechanics of running gaits remarkably well (Blickhan & Full, 1993; Farley et al., 1991, 1993; He et al., 1990).

Biomechanical studies of running, trotting and hopping mammals have revealed the general principle that the stiffness of the leg spring remains nearly the same at all forward speeds (Farley et al., 1993; He et al., 1990). In all of the mammals studied to date, including humans, the spring system is adjusted to bounce off the ground in less time at higher speeds by increasing the angle swept by the leg spring during the ground contact phase rather than by increasing the stiffness of the leg spring.

The goal of the current study is to examine how the spring system is adjusted when humans alter their stride frequency at a given running speed. We examine the relative importance of changes to the stiffness of the leg spring and changes to the angle swept by the leg spring during the ground contact phase. This study will reveal new insight into whether it is possible to change the stiffness of the leg spring during forward running.

PROCEDURES

Four male subjects ran at 2.5 $m \cdot s^{-1}$ while using a range of stride frequencies: their preferred stride frequency, four below their preferred (-5%, -11%, -18%, -26%) and four above their preferred (+17%, +25%, +30%, +36%). The subjects ran on a treadmill-mounted force platform that was used to measure the vertical ground reaction force (Kram & Powell, 1989). The vertical force was integrated twice to obtain the vertical displacement of the center of mass (Blickhan & Full, 1993).

The spring-mass model consisted of a mass and a single "leg spring" that connects the foot and the center of mass of the runner (Fig. 1). Figure 1 depicts the model at the beginning (left-most position), middle (middle position) and end of the ground contact phase (right-most position). The leg spring has an initial length, L_0, at the beginning of the ground contact phase, and its maximal compression is represented by ΔL. In Figure 1, the dashed spring-mass model represents the length of the uncompressed leg spring, Δy represents the vertical displacement of the center of mass, and θ represents half of the angle swept by the leg spring during the ground contact phase.

The stiffness of the leg spring (k_{leg}) was defined as the ratio of the force in the spring (F) to the displacement of the spring (ΔL) at the instant that the spring was maximally compressed. The peak displacement of the leg spring (ΔL) was calculated from the following relationship:

$$\Delta L = \Delta y + L_0 \cdot (1 - \cos \theta). \quad (1)$$

The vertical motions of the system during the ground contact phase were described in terms of a "vertical stiffness" (k_{vert}). The vertical stiffness does not correspond to any physical spring in the model. Rather, k_{vert} describes the vertical motions of the mass during the ground contact phase and is important in determining how long the spring-mass system remains in contact with the ground. Because it is probable that the time available for the spring-mass system to bounce off the ground changes with stride frequency, it is likely that there will be changes in k_{vert} to accommodate different stride frequencies. The vertical stiffness (k_{vert}) was calculated from the ratio of the peak force (F) to the peak vertical displacement (Δy) of the center of mass.

The vertical stiffness depends on a combination of several characteristics of the spring-mass system:

$$k_{vert} = F / [(F / k_{leg}) - L_0 \cdot (1 - \cos \theta)]. \quad (2)$$

Equation 2 shows that k_{vert} increases if k_{leg} increases. In addition, it shows that when the angle swept by the leg spring (θ) increases, k_{vert} increases relative to k_{leg}.

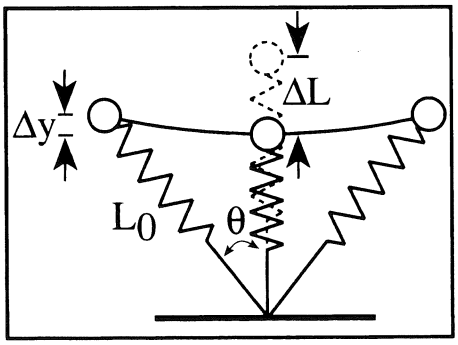

Figure 1: The spring-mass model. See "procedures" section for explanation.

RESULTS

As stride frequency was increased, the general pattern of vertical ground reaction force and displacement of the center of mass remained the same (Fig. 2). At all frequencies, the force reached its maximum at the same time as the vertical displacement reached its minimum. However, several observations show that there were adjustments to the mechanical properties of the musculoskeletal spring system as frequency was changed. First, the time of foot-ground contact decreased by 32% between the lowest and highest stride frequencies (Fig. 2; 0.365 ± 0.009 s to 0.248 ± 0.008 s, SE). Second, over the same range of frequencies, the vertical displacement of the center of mass decreased by 76% (0.107 ± 0.011 m to 0.025 ± 0.001 m).

As stride frequency was increased from the lowest to the highest stride frequency, the vertical stiffness (k_{vert}) increased by 3.5-fold (15.1 ± 0.713 $kN \cdot m^{-1}$ to 52.4 ± 2.34 $kN \cdot m^{-1}$) (Fig. 3). This increase in k_{vert} was the result of a stiffer leg spring at higher stride frequencies (Fig. 3). Between the

lowest and highest stride frequencies, k_{leg} more than doubled (7.03 ± 0.21 kN • m^{-1} to 16.3 ± 0.42 kN • m^{-1}).

The angle swept by the leg spring (θ) decreased at higher stride frequencies, partially offsetting the effect of the higher leg spring stiffness (Fig. 4). Equation 2 shows that when θ decreases, k_{vert} decreases relative to k_{leg}. The angle swept by the leg spring decreased from 28.2° (± 0.4°) to 18.7°(±0.3°) between the lowest and the highest stride frequency.

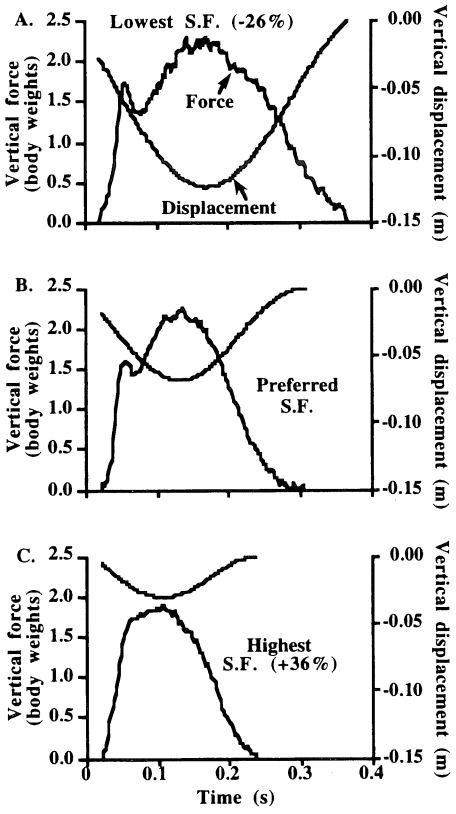

Figure 2: Vertical ground reaction force and vertical displacement of the center of mass for one ground contact phase. (A) Lowest stride frequency, (B) the preferred stride frequency, and (C) the highest stride frequency. Note the decrease in the ground contact time and the vertical displacement of the center of mass at higher frequencies.

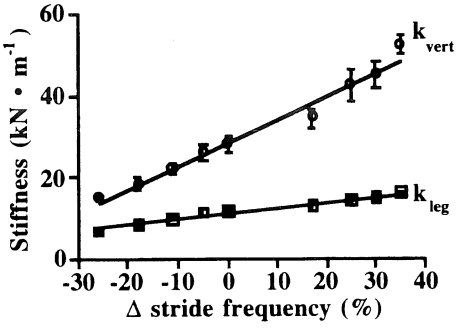

Figure 3: Vertical stiffness and leg stiffness increased at higher stride frequencies. "Δ stride frequency" refers to the % difference from the preferred stride frequency.

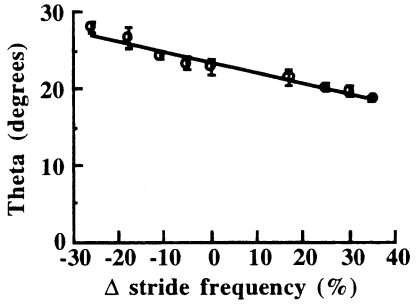

Figure 4: Theta decreased at higher stride frequencies.

DISCUSSION

We conclude that the primary adjustment to the spring system for different stride frequencies is that the stiffness of the leg spring is altered. Thus, the mechanism for adjusting the spring system for different stride frequencies is not the same as the mechanism for adjusting the spring system for different forward speeds. Earlier studies have shown that when forward speed is increased in running humans as well as other mammals that trot and hop, the time available to bounce off the ground decreases. This change is accommodated by increasing the vertical stiffness of the spring system. The higher vertical stiffness is achieved by increasing the angle swept by the leg spring rather than by increasing the stiffness of the leg spring (Farley et al., 1993; He et al., 1991). In the present study, we find that when stride frequency is increased at a given speed, the shorter time available to bounce off the ground at higher stride frequencies is accommodated by increasing the vertical stiffness. In this case, the mechanism for increasing the vertical stiffness is increasing the stiffness of the leg spring.

These findings about the capacity for adjustment of the stiffness of the leg spring during forward running parallel those of an earlier study showing that the stiffness of the leg spring is altered substantially when humans hop in place at different frequencies (Farley et al., 1991). When humans hop in place, the stiffness of the leg spring increases by about two-fold when they increase their hopping frequency by 65%. Similarly, when humans run at a given forward speed, the stiffness of the leg spring increases by about two-fold when they increase their stride frequency by 65%. Thus, the relationship between leg stiffness and stride frequency is the same for hopping in place and for forward running. Although our study did not address the issue of the mechanism of stiffness adjustment, earlier studies (Greene & McMahon, 1979; McMahon et al., 1987) suggest that alterations in limb posture may lead to changes in leg stiffness.

Our observation that it is possible to vary leg spring stiffness during forward running has implications for understanding how the musculoskeletal system is adjusted for running over variable terrain, for the design of spring-based prostheses for running, and for the design of legged robots.

REFERENCES

Blickhan, R. J. Biomechanics 22, 1217-1227, 1989.

Blickhan, R. & Full, R. J. J. Comp. Physiol. A 173, 509-517, 1993.

Blickhan, R. & Full, R. J. Biomechanics: structures and systems, (pp. 75-96), Oxford University Press, 1993.

Farley, C. T. et al. J. Appl. Physiol. 716, 2127-2132, 1991.

Farley, C. T. et al. J. exp. Biol. 185, 71-86, 1993.

Greene, P. R. & McMahon, T. A. J. Biomechanics 12, 881-891, 1979.

He, J. et al. J. Appl. Physiol. 71, 863-870, 1991.

McMahon, T. A. et al. J. Appl. Physiol. 62, 2326-2337, 1987.

McMahon, T. A. & Cheng, G. C. J. Biomechanics 23 (suppl.. 1), 65-78, 1990.

MUSCLE AND LIGAMENT CONTRIBUTIONS TO THE SUPPORT OF VARUS-VALGUS KNEE MOMENTS DETERMINED BY BIOMECHANICAL MODELING AND EXPERIMENTAL DATA

David G. Lloyd and Thomas S. Buchanan

Departments of Rehabilitation Medicine and Biomedical Engineering, Northwestern University, and Sensory Motor Performance Program, Rehabilitation Institute of Chicago, 345 East Superior Street, Chicago, IL, USA, 60611

INTRODUCTION

Although both ligaments and muscles can contribute to stabilizing the knee joint against varus and valgus loads, their respective roles have yet to be determined. To this end, experiments were conducted where subjects actively performed tasks that applied various combinations of flexion-extension (FE) and varus-valgus (VV) moments to the knee. During the experiments EMGs and external knee moments were measured. These measures were then used as inputs to a biomechanical model that estimated the contributions of each muscle to the external moment. The required ligament forces to balance the VV moments could then be predicted. It was found for the tasks performed that muscles were not principally activated to stabilize the knee during VV loads. Hence the neuromuscular control system relies upon the tension to be developed in ligaments.

REVIEW AND THEORY

Poor knee joint stability during varus-valgus loading has been implicated as a possible reason for development of osteoarthritis of the knee (Noyes et al. 1992, Schipplein et al. 1991). It also known that most muscles that cross the knee have moment arms that allow them to produce varus or valgus moments. Such muscles could therefore actively contribute to stabilizing the knee during VV tasks relieving ligaments from some of this role.

Previously, biomechanical models of the knee have been used to estimate the muscle and ligament moments contribution to total knee moments. These models, however, have used lumped equivalent muscle methods to overcome the model's indeterminacy (Noyes et al. 1992, Schipplein et al. 1991, Morrison 1968). Subsequently, these models could not account for the possibility of muscles being specifically activated to stabilize the knee.

The purpose of this work is to see if the neuromuscular control system actively controls knee joint stability. To this end, the specific aim of this work was to determine the individual contributions of each muscle to the total knee joint load and joint stability. Subsequently, contributions to knee stability from ligaments and other soft tissues could be estimated.

PROCEDURES

A biomechanical model of the knee was developed which allowed muscle and ligament loads about the knee to be estimated using experimentally obtained data. The EMGs from 10 muscles and all components of the external knee joint loads were measured during a series of experiments. In these experiments each of the 8 seated subjects, with their ankles cast in a fixed cuff, were required to produce various combinations of VV and FE isometric forces, with no internal-external rotation moment by the hip and no load directed along the long axis of the leg. Visual feedback of all these 4 force types was given to the subject and the data was only recorded when the subject matched the required forces for a period of 1 second. Each subject's hip flexion angle was kept constant at 85° and their knee flexion angles varied from 40° to 90° in 10° increments.

Biomechanical Model

The biomechanical model was based on SIMM (Delp *et al.*, 1990), with added VV displacements. The varus rotations were centered beneath the medial femoral condyle, 25 mm from the center of the tibial plateau. The center of the valgus rotations were similarly located 25 mm from lateral from the center of the tibial plateau. The model provided the muscle moments arms and musculo-tendon lengths for the muscles around the knee joint.

The muscles were modeled as musculo-tendon units with a Hill based muscle model and a non-linear tendon function (Zajac, 1989). The forces generated by musculo-tendon units were determined using, EMGs and musculo-tendon lengths as inputs. The musculo-tendon model parameters which also determined the force output were; optimal fiber length (OFL), maximum isometric force (MIF), pennation angle (PA) and tendon rest length (TRL). The musculo-tendon moments were determined by the multiplying the individual muscle forces with their moment arms.

The externally measured moments must be equal to the sum of the internally generated moments, which is the sum of the musculo-tendon, ligament and joint contact moments, i.e.,

$$M^{external} = M^{musc} + M^{joint}_{contact} + M^{lig}$$

In the FE plane it was assumed that the ligaments had a negligible contribution to the total FE moments. In addition, the joint contact moments were assumed to be zero since the joint contact points in the FE plane are the instantaneous centers of rotation. Therefore, the model's estimated net musculo-tendon FE moments should have been equal to the active external FE moments generated by each subject during the experiments. The model's estimated passive (zero activation) musculo-tendon moments were also required to match the values for passive knee moments found in literature. Therefore, for both the active and passive FE cases the following equation must have held

$$M^{external} = M^{musc}$$

Using the initial musculo-tendon parameters, however, the model's prediction of the active FE external and the FE passive knee moments was poor. It was therefore necessary to adjust the model. A possible source of variation between the model's estimated moments and the actual moments was in the selection of the various musculo-tendon model parameters. There is a large variation in OFLs reported in literature, and very few reports of values for the TRLs. Variation of the pennation angle has only a small affect on the force output from the muscle model (Zajac 1989). It was therefore decided to vary each muscle's OFL and TRL within 2 standard deviations of reported values. Two global

gain factors were also used, one for the flexor muscles and one for the extensors, to account for the different strength capabilities of these muscle groups across people. The total moments produced by the muscles was therefore given by

$$M_{musc} = \left[G^{flx} \cdot \sum_{\text{Flexors}} r_i^{musc} \times F_i^{musc}\left(EMG, l^{mt}; l_0^m, l_0^t\right) \right] + \left[G^{ext} \cdot \sum_{\text{Extensors}} r_j^{musc} \times F_j^{musc}\left(EMG, l^{mt}; l_0^m, l_0^t\right) \right]$$

The adjustment of the muscle parameters was performed using a non-linear least-squares conjugate Newton method. The function minimized (see following equation) was the squared difference between the model's FE musculo-tendon moments and the a) active external FE experimental moments, and b) passive knee moments. The parameter starting values were based on those found in literature.

$$U = \sum_{\substack{\text{Joint} \\ \text{angle}}} \sum_{\substack{\text{Force} \\ \text{Dir.}}} \left[M_{ext}^{FE} - M_{musc.}^{FE} \right]^2_{\text{active}} + \sum_{\substack{\text{Joint} \\ \text{angle}}} \left[M_{ext}^{FE} - M_{musc.}^{FE} \right]^2_{\text{passive}}$$

Using the estimated muscle forces from the adjusted model, the contributions from the muscles and ligaments to the total joint load was obtained. Ligament contributions were assumed to be the residual between the externally applied VV loads and the VV load contributions by the muscles. When the residual was negative it was assumed that there was compression under both condyles and no ligament forces, i.e., for external VV moments:

for $M^{musc} > M^{external}$

$$M_{contact}^{joint} = M^{musc} - M^{external}$$

$$M^{lig} = 0$$

and for $M^{musc} < M^{external}$

$$M_{contact}^{joint} \approx 0$$

$$M^{lig} = M^{musc} - M^{external}$$

RESULTS

Results from the model indicate that FE load generated by the muscles matched the externally measured FE load very well for all joint angles (figure 1A). However, in varus-valgus directions, the muscle contributions were insufficient to counter the external loads and, hence, ligament forces were required (figure 1B).

As shown in figure 2 the need for ligament forces increased as the external force direction moved further away from

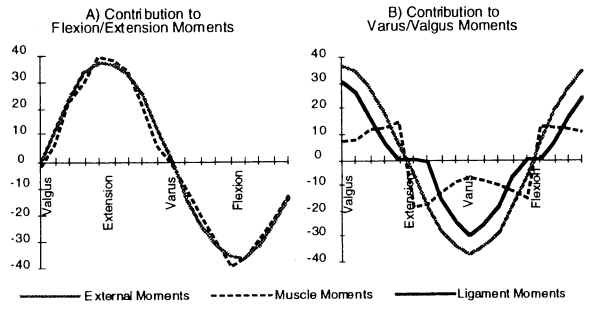

Figure 1. Contribution of muscles and ligaments to the sup port of the external loads at a knee flexion angle of 80°.

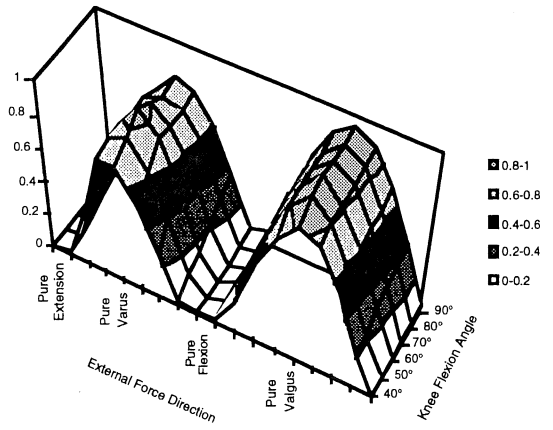

Figure 2. The ratio of ligament loads to total knee load for the different external load directions and the knee joint angles. This data is the average from 5 subjects.

pure flexion or pure extension and peaked at pure varus or pure valgus. Generally the ligament loading also decreased as knee flexion angle decreased. This was due to the increase in the passive muscle forces as the knee went closer to full extension. All these subjects used minimal amounts of muscle co-contraction for these tasks, although there was a little VV directionality with the muscle activations. One subject however exhibited greater levels of muscle co-contraction with which the model predicted lower required ligament forces.

DISCUSSION

For the isometric tasks performed the subjects' muscle activation patterns and subsequent muscle forces could not support the external VV knee moments. This indicates that ligaments forces would have been required to help support VV moments. These results show that, at least during the tasks described, the muscles are not to any great extent activated to stabilize the knee during VV loads. Hence the neuromuscular control system relies upon the tension to be developed in ligaments.

There was a general decrease in the required ligament forces as the knee was closer to full extension which corresponded with increasing passive forces in the hamstring muscles. This suggests that the hamstrings passive forces could be important for knee stability during gait when the knee is close to full extension during the stance phase.

REFERENCES

Delp, et al. *IEEE Trans. Biomed. Eng.*, 37, 757-767, 1990.

Morrison, J.B. *J. Biomech.*, 3, 51-61, 1970.

Noyes, F.R. et al. *Amer. J. Sports Med.*, 20:707-716, 1992.

Schipplein, O.D. et al. *J. Orth. Res.*, 9:113-119, 1991.

Zajac, F.E. *Critical Reviews in Biomedical Engineering*, CRC press, 17, 359-411, 1989.

ACKNOLEDGEMENTS

This work is supported, in part, by NIDRR Training Grant H133P20016 and the Dr. Ralph C. and Marion Falk Medical Research Trust.

COMPARISON OF TWO- AND THREE-DIMENSIONAL MODELS USED TO CALCULATE FOOT SEGMENTAL POWER AND ENERGY DURING THE STANCE PHASE OF GAIT

K. Lohmann Siegel †, T. Kepple†, and G. Caldwell‡

†National Institutes of Health, Warren G. Magnuson Clinical Center, Rehabilitation Medicine Department, Biomechanics Laboratory, Bethesda, MD, 20892.
‡University of Massachusetts, Department of Exercise Science, Amherst, MA, 01003.

INTRODUCTION

Segmental power (P) and energy (E) reflect the role of the musculature in producing and controlling limb movement during locomotion. The purpose of the present study was to evaluate the effect of calculating foot segmental power and energy in only the sagittal plane (2D) and in three dimensions (3D) on the agreement of foot segmental power and rate of change of foot segmental energy (dE/dt). Foot function of fifteen adult subjects was evaluated during the stance phase of gait. Results revealed excellent agreement between P and dE/dt for the 3D model, but poor to excellent agreement for the 2D model. The level of agreement for the 2D model decreased with increasing toe-out angle and foot inversion/eversion excursion during gait. This was because out-of-plane power terms were larger than out-of-plane energy terms. When compared to 3D results, 2D estimates of foot segmental energy are relatively insensitive to non-planar foot movements during gait, but 2D foot segmental power estimates are affected by foot toe-out angle and foot inversion/ eversion excursion.

REVIEW AND THEORY

Mathematically, it can be shown that segmental power equals the rate of change of segmental energy (Aleshinsky, 1986). Traditional sagittal plane analyses of segmental power have found low pearson correlations (rp) between P and dE/dt only at the foot during the stance phase of gait (Robertson et al., 1980, rp=-0.163; Smith, 1991, rp=0.085). Although usually assumed to equal zero, distal foot segmental powers can be significant in stance phase, and this power may provide a way to quantify energy absorbed by the soft tissues of the foot. Including distal terms in the calculation of total foot power dramatically reduces the discrepancy between P and dE/dt (Siegel, 1993, rp=0.693). Sagittal plane analyses of power and energy during gait include an assumption that components acting in other planes and about other axes are small. Certainly when lower extremity joint flexion/extension axes are perpendicular to the sagittal plane, the component terms of power and energy in the sagittal plane account for most of their totals in three dimensions. However, even in normal gait, foot angle to the line of progression can range from 10 deg of toe-in to 25 deg of toe-out (Inman et al, 1981) resulting in lower extremity joint axes of movement that are not perpendicular to the sagittal plane. As lower extremity movements become less planar, total segmental power and energy can be expected to differ for the 2D as compared to the 3D case. This may affect the agreement of P and dE/dt, although no reports of these model comparisons have been found in the literature. The purpose of the present study was to calculate foot segmental power and energy in the sagittal plane (2D) and in 3D and to evaluate the effect on the agreement of P and dE/dt.

PROCEDURES

The subject sample included 8 men and 7 women. On average, the subjects were 36±11 years old, 1.71±0.08 m tall, and 75.3 ±14.4 kg in mass. Data collection procedures and equipment have been described previously (Siegel et al., 1993). Non-colinear, reflective, spherical targets were affixed securely to the dorsum of the right foot (3 targets) and lateral aspect of the right shank (4 targets). 3D kinematic gait data were sampled at 50 Hz simultaneously from 4 video cameras with infrared strobes. Synchronized ground reaction forces were sampled at 200 Hz. Subjects ambulated at a freely selected velocity with a mean cadence of 115 steps/min and a velocity of 1.27 m/s or 0.74 statures/s. Data were smoothed using a second-order dual pass Butterworth filter cutting off at 6 Hz for target data and 25 Hz for force data. Data analysis was performed during the stance phase of gait on three repeated trials per subject.

Foot segmental power was calculated from proximal and distal joint force powers and muscle moment powers. Foot segmental power and segmental energy terms were computed in two forms, from only the 2D sagittal plane components, and from 3D components. The agreement of P and dE/dt was evaluated with a concordance correlation coefficient (rc) (Lin, 1989). Rc values for the 2D and 3D models were compared using a t-test for correlated means. Additional output data thought to reflect non-sagittal plane behavior of the foot during gait included toe-out angle and foot inversion/eversion excursion. Toe-out angle was defined as the average angle during stance phase between the longitudinal axis of the foot and the laboratory axis parallel to the walkway direction. Foot inversion/eversion was defined as the angle between the foot and shank in the frontal plane of the shank. The excursion was defined as the difference between peak inversion angle and peak eversion angle during gait.

RESULTS

The t-test revealed that the agreement of P and dE/dt was significantly less ($t=4.99$, $p<0.0005$) for the 2D as compared to the 3D model (Table 1). For the 3D model, rc values reflected excellent agreement of P and dE/dt with low variability across subjects. For the 2D model, mean rc values were lower than for the 3D model, and ranged from very low to very high values. The standard deviation in rc values across subjects was nearly ten times greater for the 2D model as compared to the 3D model.

Table 1 Agreement of Foot Power and Rate of Energy Change

	P vs. dE/dt AGREEMENT (rc values)			
MODEL	MEAN	STD DEV	MIN	MAX
2D	0.648	0.253	0.025	0.911
3D	0.956	0.031	0.862	0.987

Differences in foot function during gait were noted between the subjects with the best and worst agreement of P and dE/dt for the 2D model. Subject 13 displayed the lowest agreement of 2D P and dE/dt, rc=0.025 (Figure 1), the second highest toe-out angle of 11 deg, and the largest inversion/eversion excursion of 20 deg. Subject 5 demonstrated the highest agreement of rc=0.911 (Figure 1), the second lowest toe-out angle of 1 deg, and the second lowest inversion/eversion excursion of 12 deg.

Although average toe-out angle during stance phase was poorly correlated with total inversion/eversion excursion (rp=0.13, p=0.64), both parameters were significantly and negatively correlated with the 2D model agreement of P and dE/dt. The

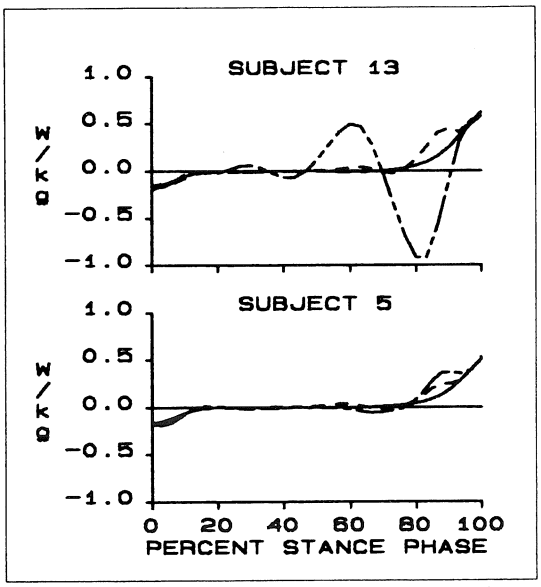

Figure 1. Two-dimensional rate of energy change (solid line), two-dimensional power (long and short dashed line), and three-dimensional power (short dashed line) for Subject 13 (top) and Subject 5 (bottom).

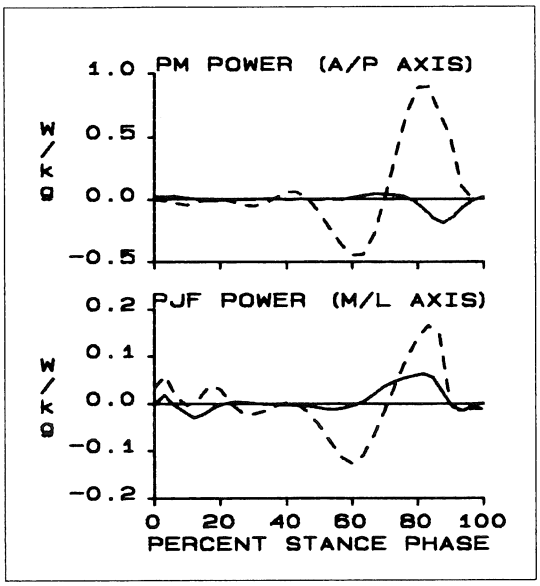

Figure 2. Foot proximal muscle moment power about an anterior/posterior axis (top) and proximal joint force power along a medial/lateral axis (bottom) for Subject 13 (dashed line) and Subject 5 (solid line).

pearson correlation (rp) of 2D model agreement of P and dE/dt with toe-out angle was -0.69 (p=0.005) and the correlation with inversion/eversion excursion was -0.68 (p=0.005). A multiple regression analysis was performed to determine how well the combination of toe-out angle and inversion/eversion excursion could predict agreement of P and dE/dt for the 2D model. The multiple R was 0.91 ($p<0.00005$) yielding an R^2 value of 0.83. This suggests that the combination of toe-out angle and inversion/eversion excursion could predict 83% of the variability in the agreement of P and dE/dt for the 2D model.

The rate of change of foot segmental energy was nearly identical for the 2D and 3D models. Differences in agreement of P and dE/dt between the 2D and 3D models were due to changes in total foot power for the two models. As toe-out angle or inversion/eversion range increased, proximal muscle power terms about the anterior/posterior (A/P) axis and proximal joint force powers along the medial/lateral (M/L) axis increased in magnitude. Corresponding increases in rotational kinetic energy about the A/P axis and translational kinetic energy along the M/L axis also were noted. However, the non-sagittal plane power terms composed 15% of the total 3D foot power, while the non-sagittal plane energy terms made up less than 0.5% of total foot energy. As a result, total foot powers were more sensitive to model condition than total foot energy as toe-out angle and inversion/eversion excursion increased.

DISCUSSION

Energy flows in and out of the foot during gait may be studied with either kinematic (dE/dt) or kinetic methods (P) (Aleshinsky, 1986; Robertson et al., 1980; Smith, 1991). However, the discrepancy between P and dE/dt at the foot has limited segmental power studies to swing phase (Caldwell et al., 1992). In the present study, both the 2D and 3D models of foot segmental power included distal segmental power terms unlike previous studies of foot segmental power. As a result, both the 2D and 3D foot power estimates showed better agreement with the corresponding 2D or 3D rate of energy change than previous studies in the literature (Robertson et al., 1980; Smith, 1991). However, the 3D model produced high agreement of P and dE/dt more consistently than the 2D model. Discrepancies between 2D P and dE/dt increased with increasing toe-out angle and foot inversion/eversion excursion during gait. As toe-out angle increased, the ankle dorsi/plantar flexion axis was no longer perpendicular to the sagittal plane. Some of the dorsi/plantar flexion was measured as proximal muscle moment power about an A/P axis and proximal joint force power along a M/L axis. As foot inversion/eversion excursion increased, proximal muscle moment power about an A/P axis and proximal joint force power along a M/L axis also increased. Because the out-of-plane power terms reflected these non-planar foot movements more dramatically than the out-of-plane energy terms, agreement of P and dE/dt was better for the 3D model than the 2D model.

These results suggest that sagittal plane studies of foot energy changes during the stance phase of gait are adequate when using kinematic methods (rate of energy change), but have potential errors when using kinetic methods (power), especially as subject toe-out angle and inversion/eversion excursion increase. If a 3D analysis of gait is performed, 3D estimates of foot segmental power appear accurate. This is an advantage over current techniques described in the literature because of the documented advantage of power techniques over energy techniques to document energy flow in and out of segments (Caldwell et al., 1992).

REFERENCES

Aleshinsky, S. J Biomech., 19, 287-293, 1986.
Caldwell, G. et al. Med Sci Sport Ex 24,1396-1412, 1992.
Inman V. et al. Human Walking, (p. 57), Williams & Wilkins, 1981.
Lin, L. Biometrics, 45, 255-268, 1989.
Robertson, D. et al. J Biomech. 13, 845-854, 1980.
Siegel, K. Segmental Power and Energy Calculations at the Foot During Gait, Masters Thesis, Univ of MD, College Park, 1993.
Siegel, K. et al. Clin Biomech, 8, 147-155, 1993.
Smith, A. Proc. of the 15th Annual Meeting of ASB, Tempe, (pp. 38-39), 1991.

A COMPARISON OF KNEE KINETICS FROM SURFACE-MOUNTED AND BONE-MOUNTED TARGETS DURING GAIT

S. J. Stanhope[1] and J. P. Holden[2]

[1]Rehabilitation Medicine Department, Warren G. Magnuson Clinical Center
[2]National Institute of Arthritis and Musculoskeletal and Skin Diseases
Biomechanics Laboratory, National Institutes of Health, Bethesda, MD 20892.

INTRODUCTION

The purpose of this study was to examine the differences during gait between proximal shank kinetic estimates derived from surface mounted targets (SMT) and from targets fixed to the bone. A percutaneous skeletal tracker (PST) was attached to the distal right shank of three healthy male subjects. In addition, plastic shells holding clusters of reflective targets were attached to the dorsum of the foot and the mid-shank. Independent rigid-body inverse dynamics analyses were performed utilizing the PST and SMT techniques to obtain proximal shank forces and moments. Ensemble averages and estimates of variability were generated for intra-subject and normalized inter-subject data. Differences between SMT and PST techniques were most prominent during stance. While intra-subject variability was low, the magnitude and timing of kinetic differences were subject dependent. The transformation of SMT data to the PST-based shank coordinate system virtually eliminated differences in forces but not in moments. The results show that the differences found in kinetic estimates due to target attachment technique would likely not affect clinical interpretations.

REVIEW AND THEORY

The fundamental measurements in gait analysis consist of joint motion and net joint kinetic estimates. The fact that such measurements are referenced to joints implies the knowledge of motion of the skeleton. Gait analysis kinematic data, however, are routinely obtained using individual or clustered optical targets attached to the surface of segments. Stanhope et al. (1994) and Holden et al. (1994) have reported kinematic inaccuracies approaching 8 degrees in shank skeletal orientation estimates and 9 mm in position estimates due to surface target mounting techniques and soft tissue movement relative to bone. While the magnitude of these relative displacements may have little effect on the clinical interpretation of kinematic test results, their effect on subsequent kinetic data has not been reported.

The three-dimensional (3-D) equations of motion include several terms which are derived from segment kinematics. In general, these terms can be thought of as related to segment movement (derivative terms) and/or segment position and orientation (pose). For example, a_{cg} in equation 1 is the translational acceleration of a segment's center of gravity and is a derivative dependent variable. The expression of a_{cg} and g, the acceleration due to gravity, within a segment coordinate system depends on the segment orientation.

$$F_p = m a_{cg} - F_d - mg \qquad (1)$$

The rotational equation of motion (equation 2) contains similar derivative terms, such as the segment angular velocity ω and angular acceleration α. However, the magnitude and expression of the moments created by applied forces is largely dependent on the segment pose.

$$M_p = -M_d - R_p \times F_p - R_d \times F_d + I_{cg}\alpha + \omega \times (I_{cg}\omega) \qquad (2)$$

Hence, the purpose of this study was to compare proximal shank (knee) kinetics derived using surface and bone mounted targets during gait.

PROCEDURES

Three male subjects of varying body types (height: 1.83, 1.93, & 1.78 m; weight: 961, 903, & 667 N) participated in this study after providing their informed written consent. A percutaneous skeletal tracker (PST) device, supporting four passive spherical targets, was attached to the bone of each subject's right distal shank using a total of four modified halo pins that were inserted into the periosteum of the medial and lateral malleoli. In addition, four surface-mounted targets (SMT) were attached to the mid-shank using a neoprene wrap and Velcro-backed polyform shell, and three targets were attached to a polyform shell that was held on the dorsum of the foot with adhesive wrap.

Subjects were allowed ample time to accommodate to walking with the PST in place. A six-camera, 50 Hz video-based (Vicon, Oxford Metrics, Botley, Oxford, England) target tracking system and two force plates (AMTI, Newton, MA, USA) sampled at 200 Hz were used to measure target locations and ground reaction forces during six free-speed barefoot walking trials by each subject. The data collection volume, which surrounded both force plates, extended 1.78 m in the direction of progression and was .99 m high and .61 m wide. AMASS software (Adtech, Adelphi, MD, USA) was used for system calibration and 3-D target reconstructions. Low-pass digital filtering was applied to target trajectories at 6 Hz and force plate data at 15 Hz.

A static subject calibration trial employing landmark targets was used to create anatomically-based, orthogonal coordinate systems for the foot and shank (SCS). The SCS longitudinal (Z) axis projected superiorly, passing through mid-condylar and mid-malleolar points. The shank X axis projected laterally in the plane created by the Z axis and the bi-malleolar axis. The foot and shank segments were modeled as frusta of right cones, and segment masses were determined using modified Dempster equations (Winter, 1990). The six degree-of-freedom motions of the foot, SMT-based shank, and PST-based shank were estimated using a least-squares technique.

Inverse dynamics analysis was performed using Move3D software (NIH, Bethesda, MD, USA) for one complete right stride per trial during the interval defined by 20 N of vertical loading on the two force plates. The 3-D rigid body equations of motion were solved to produce two sets of estimates of proximal shank kinetics using the SMT and PST targets. For inter-subject comparisons, forces were normalized by body weight and moments were normalized by the product of body weight and height. Intra- and inter-subject ensemble averages and coefficients of variability (CVR) (mean standard deviation/signal range) were generated for the kinetic data from the SMT and PST analyses, and for SMT kinetic data transformed into the PST-based shank coordinate system.

RESULTS

The three subjects reported little difficulty in walking with the PST attached. Stride lengths ranged from 1.2-1.4 m, and avg. walking speed (stride length/stride time) was 1.1-1.3 m/s.

The intra-subject PST data produced CVRs that averaged 3.5% for force parameters and 4.7% for moments. The normalized inter-subject data produced mean CVR values of 6.6% for forces and 8.2% for moments. Ensemble averages (n=6 trials) of force data using the SMT and PST are depicted for one representative subject in Figure 1. Differences due to the two target attachment techniques were primarily confined to the stance phase of the gait cycle (0-60%). The largest average difference for any subject was 39, 16, and 9 N for the X, Y, and Z force components. The X force component contained the greatest relative differences. All force differences were virtually eliminated when the SMT force data were transformed into the PST-based shank coordinate system. As with the force data, differences between proximal shank moments were greatest during stance phase (Figure 2). The maximum mean difference in the moment data X, Y, and Z components for one subject were 9, 9, and 2 Nm, respectively. Transforming the SMT data into the PST-based shank coordinate system was not as effective at reducing differences in moment data as in force data.

DISCUSSION

This study is the first of its kind to compare joint kinetics derived from surface mounted targets to those derived from in-vivo bone mounted targets. The fact that each subject tolerated the PST procedure well, returning to work immediately after the procedure and reporting no adverse effects on follow-up, is an indication of the PST's utility for making these comparisons. The general shapes of the kinetic time histories are similar to those reported by Winter (1987); more direct comparisons are unwarranted because the data are reported in the shank coordinate system, which was externally rotated with respect to a laboratory sagittal plane or the femoral coordinate system. The differences found in shank kinetic estimates due to soft tissue motion would likely not affect the clinical interpretation of results, but may be important for other applications. The primary cause of discrepancies between surface and bone mounted target attachment techniques relates to the effect of segment pose on the expression of forces and on the magnitude and expression of moments. The finding that derivative term contributions to kinetic differences is small is consistent with the reports of the relative contribution of inertial terms to the calculation of knee joint kinetics (Wells, 1981).

REFERENCES

Stanhope S.J. et al. Gait and Posture 2(1), 58, 1994.

Holden J.P. et al. Proc. 13th Southern Biomed. Engr. Conf., Washington, DC, (pp. 1035-1038), 1994.

Wells R.P. Bull. Prosthet. Res. 18, 15-19, 1981.

Winter D. Biomechanics and motor control of human movement (pp. 56-57), John Wiley & Sons, 1990.

Winter D. The biomechanics and motor control of human gait (p. 34), Univ. of Waterloo Press, 1987.

ACKNOWLEDGEMENTS

The authors wish to acknowledge the assistance of John Orsini, Karen L. Siegel, and Tom Kepple with this project.

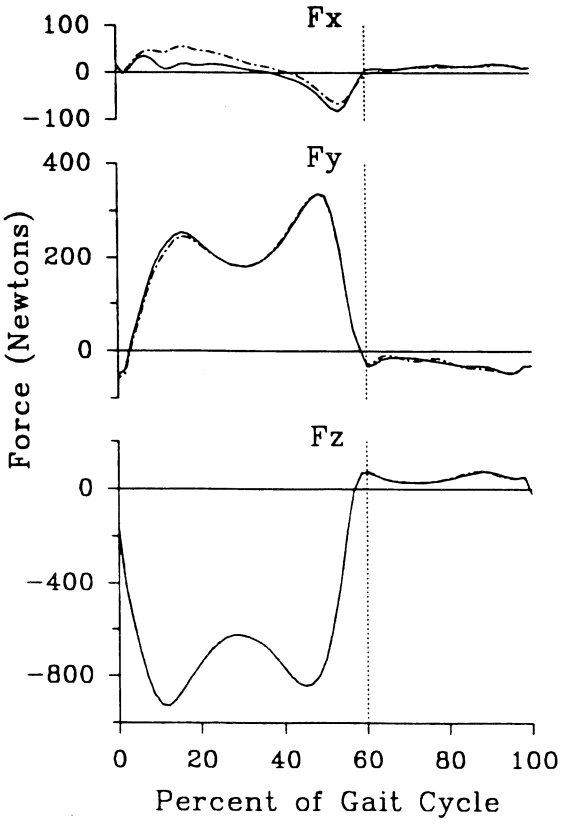

Figure 1. Ensemble averages (n=6) of shank X, Y, and Z forces for one subject. Solid lines are from bone (PST) based and dashed from surface (SMT) methods. Stance is 0-60%.

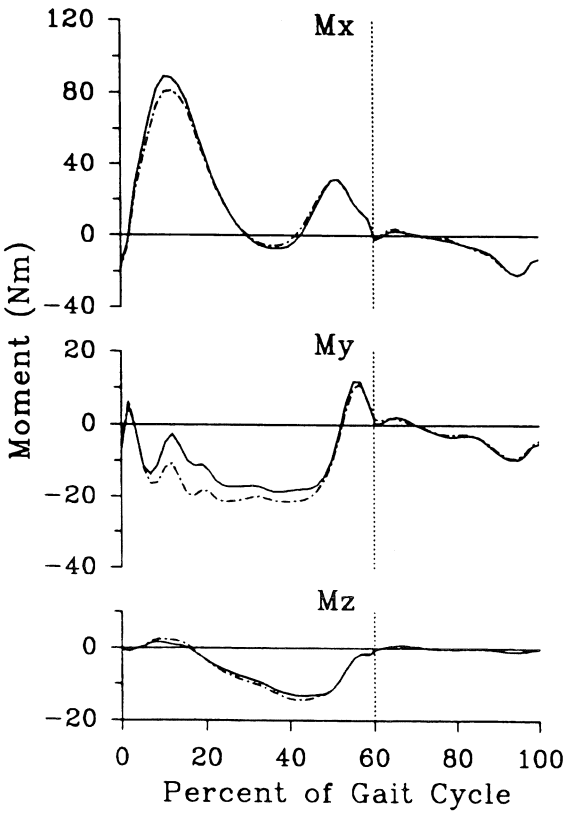

Figure 2. Ensemble averages (n=6) of shank X, Y, and Z moments for one subject. Solid lines are from bone (PST) based and dashed from surface (SMT) methods. Stance is 0-60%.

PREDICTING FUNCTION FROM STRUCTURE: THE RELATIONSHIP BETWEEN PLANTAR PRESSURE AND RADIOGRAPHIC MEASURES OF THE FOOT

E Morag, AJM Boulton+, MJ Young+, KT Galvin, SE Pammer and PR Cavanagh

Center for Locomotion Studies, The Pennsylvania State University, University Park, PA 16802,
+University Department of Medicine, Manchester Royal Infirmary, Manchester, UK

INTRODUCTION

This study explored the relationship between structural factors measured from standardized radiographs and plantar pressure during barefoot walking. In diabetic patients with a history of ulceration, almost 60% of the variance in plantar pressure under the first metatarsal head could be explained using only three predictor variables. This suggests that the future addition of dynamic biomechanical variables may result in a fairly complete model to predict plantar pressure.

REVIEW AND THEORY

While elevated plantar pressure has been implicated in ulceration of the insensitive foot (Boulton et al. 1983), the precise reasons for elevated plantar pressure are still a matter of speculation. It has been suggested that structural factors such as a cavus foot type, clawing of the toes, loss of the plantar fat pad can lead to increased pressure. It is also likely that dynamic factors such as limb kinematics and walking speed play a major role. Many of the structural factors can be quantified by measurement from plane radiographs (Renton et al. 1982) and this study was designed to examine the relationship between such static measurements of foot structure and dynamic barefoot plantar pressure during walking.

PROCEDURES

Standardized lateral and dorsi-plantar weight bearing plain radiographs of the right foot and ankle of 155 subjects were taken by a single radiographer. The subjects (mean age 54.0 yrs., 44 females) were divided into four groups: diabetic patients with no history of ulceration or neuropathy (NNP, n=32), those with a history of neuropathy but not of ulceration (N, n=39) and those neuropathic diabetic patients with a history of plantar ulcer (U, n=34). A group of age matched control subjects without diabetes (C, n=50) was also included.

The films were scanned with a high resolution video camera and captured with a frame grabber card and *Color Snap* onto a Macintosh Quadra 950. A number of angular and linear measurements were then made using the NIH *Image* program. Plantar pressure distributions were collected using an optical pedobarograph, and subsequent manual analysis allowed the mean pressure from three walking trials at discrete sites, such as the first metatarsal head (MTH1), to be determined. The resulting peak plantar pressure values were log transformed to stabilize the error variance. Eight measurements from the dorsi-plantar film and twelve from the lateral film were chosen as potential predictors of MTH1 pressure which had anatomical relevance. A stepwise regression model of the form:

$$y = \beta_0 + \beta_1 \bullet x_1 + \beta_2 \bullet x_1^2 + \ldots \beta_{2n-1} \bullet x_n + \beta_{2n} \bullet x_n^2$$

was applied to predict the $\log_e$(pressure) under the first metatarsal head using the SAS procedure "PROC REG". The criterion for entry and exit of the regressors to and from the model was set at 0.05. The analysis was performed on the entire group of subjects and on each of the four groups separately.

RESULTS

In each of the five models $\log_e$(pressure) under the first metatarsal head was predicted by only three or four structural variables, but the actual variables selected were found to be group dependent. Some factors, such as sesamoid height and Morton's index, appeared in more than one model. For the entire group of 155 subjects, the predictors of MTH1 plantar pressure are summarized in Table 1. The multiple correlation coefficient was 0.59 and the coefficient of determination (r^2) was 0.35.

The corresponding regression model is:

$$\log_e(pressure) = 6.409 - 0.062(mort) - 0.059(sesht) - 0.029(p1) + 0.007(lsx)^2$$

The equation for the U group was:

$$\log_e(pressure) = 4.033 + 0.214(lsx) + 0.00047(navicht)^2 - 0.004(calcht)^2$$

This model had a multiple correlation coefficient of 0.77 and an r^2 of 0.59

DISCUSSION

The interpretation of the equation for the entire group is that a low Morton's index (head of MTH2 less distal to head MTH1), a lower sesamoid height (less plantar soft tissue), a small inclination of the first

phalanx, and a large deviation of the fibular sesamoid from the midline, are features which tend to be associated with higher MTH1 plantar pressures.

In the group of diabetic patients with ulcers, lateral deviation of the fibular sesamoid was again selected as a predictor of high pressure, together with a large navicular height, and a small sub-calcaneal soft tissue thickness.

While the contribution of structural factors to the variance in plantar pressure in all subjects taken together was only modest (35%), it is rather remarkable that almost 60% of the variance in dynamic plantar pressure could be predicted in the ulcer group from structural variables measured under static conditions. Since factors such as walking speed and individual kinematics of gait were not measured in the present study, it is likely that the addition of these and other dynamic variables would result in more comprehensive models to predict plantar pressure. This approach also appears promising as a quantitative screening tool to identify individuals at risk for ulceration in the setting of diabetic neuropathy.

REFERENCES

Boulton, AJM. et al. Diabetes Care, 6, 26-33, 1983.

Renton, P. et al. The Foot and its Disorders, (pp. 305-377), Blackwell Scientific, 1982.

ACKNOWLEDGMENTS

The radiographic expertise of Ms. Karen Vickers is gratefully acknowledged.

Table 1

Contribution of the various predictors to plantar pressure under the first metatarsal head in the entire group of subjects

Variable	Description	Effect	Mean	sd	r	r^2	β_i	ΔP per unit (kPa)	ΔP per sd (kPa)
$(lsx)^2$	Fibular sesamoid x coordinate	+	75.2	42.2	0.39	0.15	0.007	25.3#	164.2
mort	Morton's index	-	1.3	3.3	0.29	0.09	-0.062	26.7#	89.1
p1	Proximal first phalanx inclination	-	6.9	7.5	0.28	0.08	-0.029	12.5+	93.8
sesht	Sesamoid height	-	8.2	2.7	0.20	0.04	-0.059	26.1#	71.6

(Mean MTH1 pressure in all subjects = 470.1 kPa)

model r = 0.59; model r^2 = 0.35

$kPa*mm^{-1}$ + $kPa*deg^{-1}$

A Comparison of Three-Dimensional Lower Extremity Kinematics during Running between Pronators and Normals

I McClay and K Manal

Motion Analysis Laboratory, University of Delaware, Newark, DE 19716

INTRODUCTION

Excessive rearfoot pronation is often linked with overuse injuries of the lower extremity. The purpose of this research was to compare the 3D lower extremity kinematics of runners who pronate to those with normal rearfoot mechanics. Eighteen subjects (9 Pronators-PR, 9 Normals-NL) were studied during treadmill running at 3.35 m/s. The mean eversion for the NL was 11.1 degrees vs. 21.2 degrees for the PR. Despite this significant difference in rearfoot mechanics, peak 3D values were similar across the two groups with only a few exceptions. Time to peak eversion was sooner in the PR group. A trend towards increased dorsiflexion was also seen in this group, but not significant. Only 10 subjects' knee data were available for analysis. At the knee, the PR group demonstrated significantly less abduction and significantly greater flexion than the NL. No difference was found between the 2D and 3D peak eversion angle across all subjects, however, a significant relationship was found between the difference between these 2 angles for each subject and the amount of foot abduction they exhibited in a global reference frame.

REVIEW AND THEORY

Until recently, the focus of lower extremity kinematics during running has been limited to sagittal plane motion of the knee and ankle and frontal plane motion of the rearfoot. This frontal plane motion between the tibia and calcaneus is often referred to as pronation. However, pronation is actually a three-dimensional movement involving components of motion in all three cardinal planes of the body occurring between the talus and calcaneus. However, difficulty in measuring talar movements with external markers has led researchers to using the tibia as a reference for the movement.

Although the largest component of knee motion is in the sagittal plane, this information has lent relatively little insight into etiology of running-related injuries. Recent attention has been focused on the transverse plane motion of the tibia, with suggestions that increased pronation will result in greater internal rotation, however, this has never been objectively tested. There is a dearth of 3D data on the foot and knee during running. The papers that are available (Soutas-Little et al., 1986, Areblad et al., 1990) focus on methodology using 1-2 subjects. Along with presenting a method for calculating 3D foot angles, Soutas-Little et al. demonstrate mathematically how orientation of the foot to the cameras will effect calculation of the 2D rearfoot angle. Areblad et al. experimentally examined this by altering placement of the cameras. There have been no studies, to date, which have studied the 3D kinematics of the knee and foot in normal runners and those who excessively pronate or assessed the influence of foot abduction on the 2D eversion angle.

Therefore, the purpose of this research is to begin to examine the 3D patterns of motion at the foot and knee during running and to explore whether differences in these patterns exist between runners with normal rearfoot motion and those who pronate. In addition, the effect of foot abduction (toe-out) on the 2D eversion angle is also assessed.

PROCEDURES

Eighteen recreational runners, previously screened for rearfoot mechanics were used in this study. Nine subjects each were assigned to the Pronator (PR) or the Normal (NL) group based upon their peak 2D eversion values measured during running. Values between 8-15 degrees placed one in the NL group while values greater than 18 degrees placed on in the PR group. The right foot was used in all cases, except when the left foot demonstrated the greater amount of eversion.

Three markers were placed on the femur, lower tibia and rearfoot segments (figure 1) in a manner similar to that described by Soutas-Little et al (1986). This particular orientation enabled the markers to define the anatomical coordinate system and to track the motion of the segments.

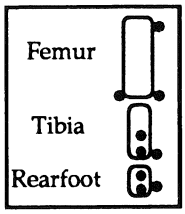

Figure 1. Lower Extremity Marker Placement (rearview of right lower extremity)

Following a standing calibration trial, subjects ran on a treadmill operating at 3.35 m/s. Data were collected with a 4 camera (200 Hz) Motion Analysis System (Motion Analysis Corp., Santa Rosa, CA). Five footstrikes were collected from each subject. The contact phase of three of these trials was used for analysis. Custom software was developed in order to calculate 3-D joint coordinate system angles (Grood and Suntay, 1983). All angles were referenced to standing with the exception of inversion/eversion of the foot. The 3D foot eversion angles were compared to the 2D rearfoot angles calculated from the markers on the longitudinal axes of the tibia and rearfoot.

Analysis of variance techniques were utilized to compare peak angular data and excursions for both the rearfoot and the knee. A regression analysis was used to assess the effect of foot abduction on 2D and 3D eversion angles. As the difference between these measures is often attributed to out of plane movement, the 3D-2D difference was also correlated to foot abduction (in a lab reference frame) across all subjects.

RESULTS and DISCUSSION

The following represents the mean data for three footstrikes from each of the 18 subjects. Due to problems encountered during data reduction, knee data were available for only 10 subjects (5 PR and 5 NL).

3D rearfoot and knee data from a typical normal subject are presented in figures 2 and 3. In general, it can be seen that following footstrike, the foot dorsiflexes, everts and abducts, then reversing its trend until toe-off. The knee

exhibits flexion, adduction and external rotation with the reverse motions occurring in the last half of stance.

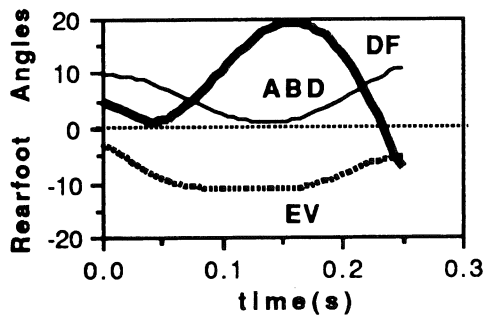

Figure 2. Typical Normal 3D Rearfoot patterns

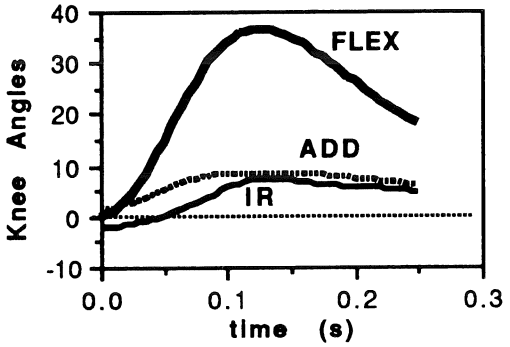

Figure 3 Typical Normal 3D Knee Joint patterns

Figure 4 demonstrates the eversion patterns of a typical PR and NL subject. Note the differences both in the magnitude and time to peak eversion between the two subjects.

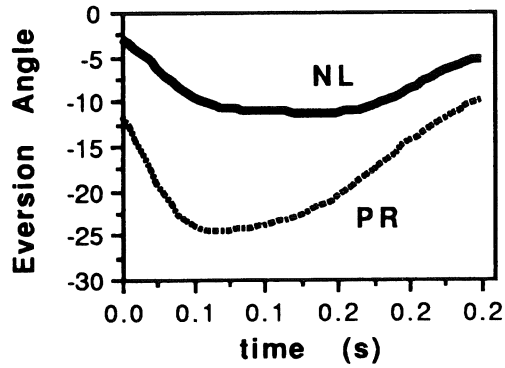

Figure 4. Comparison of a typical eversion curve for a PR and a NL subject.

It is surprising to see the remarkable similarity between peak values and times to peaks between the two groups (Table 1) in light of the twofold increase in eversion seen in the PR group. The lack of more significant findings is due, in part, to the relatively large intersubject variability present. The only significant differences found were in rearfoot eversion (which the subjects were screened upon), time to eversion and knee flexion and adduction. A trend of greater dorsiflexion in the PR group was seen, but not significant. Knee flexion and dorsiflexion are associated with pronation and are thought to be part of the cushioning mechanism. Genu valgum is often associated with a pronated foot posture and may be related to the lower knee adduction seen in the PR group. Internal rotation was not found to be greater in the PR group as is often suggested.

Variable	PR (sd)	NL (sd)
Foot df	19.8 (4.4)	17.7 (4.5)
time to df	0.14 (0.02)	0.15 (0.02)
Foot ev	-21.7 (4.9) *	-11.1 (2.7)
time to ev	0.08 (0.03) *	0.10 (0.02)
Foot abd	-5.7 (10.5)	-3.1 (9.4)
time to abd	0.10 (0.04)	0.10 (0.01)
Knee flex	43.3 (3.8) *	36.5 (7.7)
time to flex	0.11 (0.02)	0.15 (0.02)
Knee add	2.6 (3.5) *	9.6 (5.5)
time to add	0.09 (0.07)	0.12 (0.07)
Knee IR	8.3 (4.8)	7.1 (4.0)
time to IR	0.13 (0.04)	0.14 (0.09)

Table 1. Comparison of mean peak and time to peak for the 3D parameters of the foot and the knee across the NL and PR. Significant differences are marked by * ($p<.002$)

It was interesting to note that there was no difference in the mean peak 2D vs. 3D eversion angle when comparing across all subjects. Values of -11.1 and -11.5 deg. were noted for the NL group (2D and 3D respectively). The PR group exhibited -21.2 vs -21.1 deg. However, a significant relationship was found between the 3D-2D difference for each subject and their amount of foot abduction in a lab coordinate system (Figure 5). A second order polynomial equation produced the best fit of the data with 63% of the variance being explained by this model. This supports the suggestions of Soutas-Little et al. (1986) and provides further experimental evidence that as the frontal plane of the foot moves out of the frontal plane of the lab in either direction (abduction/adduction), the 2D eversion angle under-estimates the true 3D eversion angle.

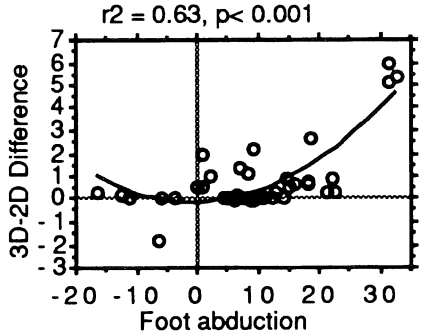

Figure 5. Relationship between foot position and 2D vs 3D eversion angle

The findings of this study suggest fairly similar mean peak foot and knee kinematics in runners who pronate versus those with normal rearfoot mechanics. Some trends were apparent, however, the small subject number and large variability may have contributed to the non-significance. A significant influence of foot abduction on the calculation of the 2D eversion angle was found suggesting caution when interpreting these angles, especially when increased foot abduction is present. More work is needed to establish normative 3D kinematics of the foot and knee during running and to examine these kinematics in identified clinical populations in order to further understand the etiology of running-related injuries.

REFERENCES

Areblad, M et al. J. Biom.. 23(9)933-940, 1990
Grood,ES &Suntay, W. J. Biom. Eng. 105,136-144. 1983
Soutas-Little et al. MSSE 19(3):285-293, 1983

SESSION 7:

TISSUE MECHANICS

THE OBSERVATION OF TISSUE LOAD, DEFORMATION AND STRAIN IN AND AROUND THE LUMBAR FACET JOINT

Q.H. Li, J.M. Cavanaugh, A.C. Ozaktay, K.H. Yang and A.I. King

Bioengineering Center, Wayne State University, Detroit, MI 48202, U.S.A.

INTRODUCTION

The etiology of low back pain is complex. Mechanical loading of the spine, especially the facet joint has been hypothesized as a possible source for this common ailments. A number of investigators have found that the capsule of facet joint is well innervated by the nerve fibers belonging to groups III and IV, as well as free nerve endings. Yang and King (1984), and El-Bohy et al. (1989) found that the facet joint is a load-bearing structure and its capsule can undergo extensive stretching under physiological loading. Cavanaugh et al. (1989) and Yamashita et al. (1990) have found that the high threshold slowly conducting units serve a nociceptive function, while the low threshold afferent units serve a proprioceptive function.

The purpose of the current study was to investigate the relationship between loading of the facet joint and surrounding soft tissue and facet capsule deformation and nerve discharge. The deformation of the capsule of facet joint and soft tissue were recorded by two video cameras. The displacements and strains of the facet joint capsule and surrounding soft tissue were calculated using finite element methods.

METHODS

Rabbits (3-4 kg, male) were anesthetized with ketamine, xylazine and butorphanol, i.m. A left L6 ventral ramus rhizotomy and L5-L6 laminectomy were performed. The left L6 dorsal rootlets were cut at their proximal ends, split and draped over a dual bipolar platinum recording electrodes. Latency between the electrodes was used to determine conduction velocity (CV). If the dorsal rootlets were not long enough, a bipolar electrodes and a stimulator were used to determine the CV. In this case, distance between receptive field and the electrodes was measured. The left L6-L7 facet joint and adjacent tissue were exposed and searched with 1-2 mm diameter glass probes for the receptive field of the mechanosensitive unit. The dorsal roots and receptive field were covered with warm (36.5°C) mineral oil. The left L6 inferior articular process was freed and fixed with silk suture connected to a load cell (Entran Ultra-Miniature Load Cell, ELF-TC500-100). After the receptive field of an afferent neuron was identified, it was markered with 4x4 grid-like array of square black markers which diameter was approximately 0.5 mm. The nerve discharge rate and load cell output were sequentially recorded on an analog tape recorder for later digitized computer analysis (EGAA, R.C. Electronics, INC.) Two video cameras with an 18-108 mm macro-zoom lens, an image splitter and a super-VHS monitor were used to collect the data of marker position during the test. The split image from the two video cameras was captured on super-VHS tape and played back as digitized still frame images through a video-audio mixer. Each marker in the digitized image was tracked with a mouse and the coordinates stored on a frame-grabber. The 3D coordinates of the grid array were obtain using an in-house 3D reconstruction software (JSW3D). The volume reference scale in the 3D system was a metal calibration frames with 15 known coordinates. The calibrated volume was 30x40x40 mm. The digitized data from nerve discharge rate and load cell output were synchronized with digitized image data. A Fortran computer program was developed to interpolate the grid to 144 elements. The measurements of nodal displacements were used to compute the components of the Lagrangian finite strain tensor for the element. A finite strain tensor is used because in most soft tissue problems, the strains are not small. Two methods were used to express the displacements and strain in the grid area. Firstly, the position of each node after the stretch in different directions was superimposed to the original position of each node to compare the displacements of the grid area. Secondly, the strain in each element was expressed at different grey levels to demonstrate the high strain fields

in the grid area.

RESULTS

Validation of the calibration field showed that the mean error rate for 1-5 mm distance was 5%. The error rate tended to increase as distance between markers decreased. In initial studies, 10 trials of stretch loading were applied to the facet joint in each of several directions. In the caudal-to-rostral direction, the peak loads reached 6.29 N, the biggest displacement between two markers reached 34% and related peak multi-unit neural discharge rate increased from 112 to 156/sec (39.3%). In the lateral-to-medial direction, peak values were 5.24 N, 53% and from 186 to 250/sec (34.4%) respectively. In the medial-to-lateral direction, peak values were 5.6 N, 40% and from 120 to 208/sec (73.3%) (Figure 1 and 2). In the rostral to caudal direction, peak values were 4.8 N, 20% and from 120 to 156/sec (30%).

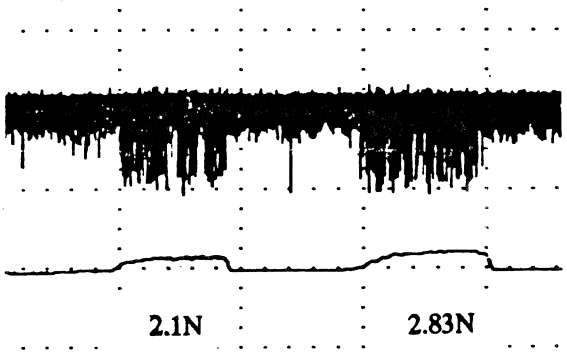

Figure 1. Loading of the facet joint and correlated nerve discharge rate during stretch in the medial-to-lateral direction.

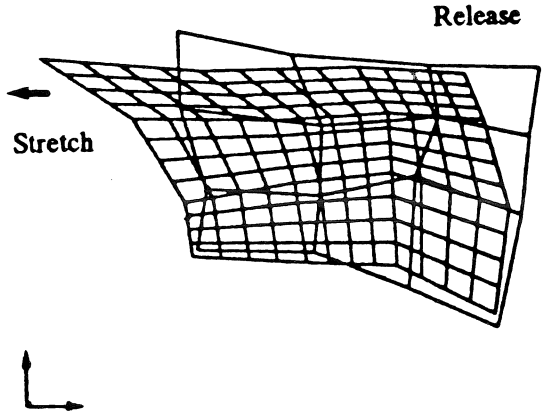

Figure 2. The deformation of grid area during stretch in the caudal-rostral direction.

CONCLUSIONS

The relationship between facet joint deformation, loading, strain and neural response were obtained for different loading directions. Stretch of the facet joint with peak loads of 4.8-6.3 N, caused nerve discharge to increase 30 to 73% over baseline rates. These data suggest that movement of the lumbar facet joint can cause large strains and greatly increased neural discharge. This suggests that excessive soft tissue strain at this joint may cause low back pain.

REFERENCES

Cavanaugh, J.M., El-Bohy, A., Hardy, W.N., Getchell, T.V., Getchell, M.L. and King, A.I. Sensory Innervation of Soft Tissues of the Lumbar Spine in the Rat. J. Orthop. Res. 7, 378-388, 1989.

El-Bohy, A., Yang, K.H. and King, A.I. Experimental Verification of Facet Load Transmission by Direct Measurement of Facet Lamina Contact Pressure. J. Biomechanics 22, 931-941, 1989.

Yamashita, T., Cavanaugh, J.M., El-Bohy, A., Getchell, T.V. and King, A.I. Mechanosensitive Afferent Units in the Lumbar Facet Joint. J. Bone and Joint Surgery 72-A, 865-870, 1990.

Yang, K.H. and King, A.I. Mechanism of Facet Load Transmission as a Hypothesis for Low Back Pain. Spine 9, 557-565, 1984.

ACKNOWLEDGEMENTS

This research was supported by NIH Grant No. NS-28994 and the WSU Office of Research and Sponsored Programs.

Radial Tensile Properties of the Lumbar Annulus Fibrosus

J. C. Lotz, Y. Fujita, and O. Soejima
Orthopaedic Bioengineering Laboratory, Department of Orthopaedic Surgery,
University of California, San Francisco, CA 94143-0514

INTRODUCTION

Though our understanding of degenerative disc disease is only half a century old, low back pain is the most prevalent and costly illness in today's society, affecting up to 70% of people at one time in their lives (Biering-Sorensen, 1982). To supplement existing data on the material properties of the annulus fibrosus that can be used to clarify the process of degenerative disc disease, we measured the tensile properties of radially oriented annular specimens. Further, we asked whether these properties vary between the anterior and postero-lateral regions. Our results suggest that the interlaminar matrix of the anterior annulus is both stiffer and stronger than that of the postero-lateral annulus.

REVIEW AND THEORY

Disc disruption has historically been attributed to acute traumatic loads of a magnitude sufficient to produce sudden tensile failure of the collagen fibers of the annulus (Adams and Hutton, 1982). Yet, observations that the disrupted annulus often displays circumferential clefts suggests that disruption of the annulus may be the result of failure of the matrix ***between*** lamina rather than the collagen fibers of the lamina (Friberg and Hirsch, 1949; Harris and Macnab, 1954; Lipson, 1988; Saunders and Inman, 1940; Yasuma et al., 1986). In support of this, significant radial stresses have been predicted within the annulus during flexion and subsequent to a reduction of nuclear pressure (Shirazi-Adl et al., 1986). However, rigorous testing of this hypothesis requires data on the interlaminar stiffness and strength, such that appropriate failure criteria can be developed. The objectives of this study were to determine the stiffness, ultimate strain and ultimate strength of radially oriented annular specimens. Further, since most clinically observed annular disruptions occur in the postero-lateral annulus, we also asked if significant differences exist for these properties measured for specimens harvested from the anterior versus the postero-lateral annulus.

PROCEDURES

We prepared 57 rectangular specimens from the anterior (28) and postero-lateral (29) quadrants of six intervertebral discs harvested from fresh-frozen human lumbar spines. The quadrants of tissue were cut parallel to the anatomic horizontal plane into 1 mm thick specimens using a vibratome (Micro-Cut, H1200). During vibratome cutting, the tissue was chilled in physiologic saline at 0°C. Subsequently, the specimens were cut to a width of 3.2 mm using a precision dye. The long dimension of the rectangular specimens ranged from 3.0 mm to 7.6 mm and was oriented in the anatomic radial direction, perpendicular to the annular lamina. The ends of each rectangular specimen were attached to a sandpaper frame using cyanoacrylate adhesive (Permabond 101) to facilitate easy transfer and attachment to the materials testing machine grips (MTS Model 858.2 Bionix). The testing protocol consisted of submersion in 0.15M NaCl at room temperature, preconditioning with five cycles at 0.4 Hz of tension to 0.5 N, and distraction to failure at a rate of 1.2 mm/min (0.4% strain/sec). The applied load was measured using a precision force transducer (Sensotec, Model 31), and the specimen deformation was measured as the grip travel using the testing system LVDT. Stress and strain were calculated based on the initial undeformed dimensions. The elastic modulus was calculated from the linear region of the stress versus strain curve. The ultimate strain was calculated as the strain occurring at the ultimate stress. These tensile properties for the anterior and postero-lateral regions were compared using a two-tailed t-test (Systat, Version 5.2). The strength data for those specimens which failed at the grips were excluded from the analyses.

RESULTS

There was significant difference in the mean failure load, ultimate stress and elastic modulus for the two groups of specimens. The mean failure load for the anterior specimens was 25% greater than that for the postero-lateral

specimens (Table). The mean ultimate stress of the anterior specimens was 23% greater than for the postero-lateral specimens. The mean elastic modulus for the anterior specimens was 41% greater than that for the postero-lateral specimens. However, the mean ultimate strain was not statistically different between groups.

	Harvest Location	
	Anterior	Postero-lateral
Ultimate Load (N)	1.22 (0.39)	0.98 (0.29)*
Elastic Modulus (MPa)	0.62 (0.30)	0.44 (0.22)†
Ultimate Stress (MPa)	0.38 (0.12)	0.31 (0.09)*
Ultimate Strain (%)	98.9 (39.9)	105.9 (33.3)‡

*P=0.01 †P=0.02 ‡P=0.5

DISCUSSION

Our objective was to characterize the radial, tensile properties of the human annulus fibrosus. Further, we asked whether these tensile properties differed for the anterior versus the postero-lateral annulus. Our results indicate that there is a significant difference in the ultimate load, ultimate stress and elastic modulus between the two groups, with the anterior specimens being stronger and stiffer. However, there was no significant difference in the ultimate strain.

Marchand and Ahmed (1989) were the first to measure tensile properties of radially oriented annular specimens. Their mean failure stress (0.187 MPa), mean elastic modulus (0.160 MPa), and mean failure strain (161%) are different from those we report here. These disparities may be due to both differences in the biochemical content of the host tissues and differing techniques used to maintain tissue hydration during testing.

Best et al.(1994) reported the radial compressive stiffness of the annulus derived using confined compression testing and biphasic theory. Their data indicate an average compressive stiffness of 0.38 ± 0.16 MPa. In contrast to our findings, they report that the compressive modulus does not vary between the anterior and postero-lateral regions. Importantly, they also demonstrate a significant trend of compressive modulus versus tissue water content and sulfated glycosaminoglycan content.

Shirazi-Adl and coworkers's (1986) predicted the radial strains developed in the human annulus during flexion and extension with a moment of 60 N-m. Their data show a peak radial strain of 35% in the anterior annulus during flexion and 19% in the posterior annulus during extension. With a loss of nuclear pressure, the anterior radial strain increase to near 50% in flexion, while the posterior radial strain remain near 20%. Their results plus our data suggest that critical radial strains are not achieved during hyperflexion and hyperextension. However, their applied loading did not include axial compression in combination with the bending moments, and hence their data may be underestimates of *in vivo* annular stains.

The results of our study suggest that there are significant differences in the tensile, intralaminar properties between the anterior and postero-lateral annulus, with the anterior annulus being stronger and stiffer. These results may be significant for the development of analytical models used to clarify the pathomechanics of disc disruption and degenerative disc disease.

REFERENCES

1. Adams, M.A. *et al.* The mechanics of prolapsed intervertebral disc. International Orthopaedics, 6, 249-253, 1982.
2. Best, B.A. *et al.* Compressive mechanical properties of the human annulus fibrosus and their relationship to biochemical composition. Spine, 19, 212-221, 1994.
3. Biering-Sorensen, F. Low back trouble in a general population of 30-,40-,50-, and 60-year-old men and women: Study design, representativeness and basic results. Dan Med Bull, 29, 289-299, 1982.
4. Friberg, S. *et al.* Anatomical and clinical studies on lumbar disc degeneration. Acta Orthop Scand, 19, 222-242, 1949.
5. Harris, R.I. *et al.* Structural changes in the lumbar intervertebral discs. J Bone Joint Surg, 36B, 304-322, 1954.
6. Lipson, S.J. Metaplastic proliferative fibrocartilage as an alternative concept to herniated intervertebral disc. Spine, 13, 1055-1060, 1988.
7. Marchand, F. *et al.* Mechanical properties and failure mechanisms of the lumbar disc annulus. 35th Annual Meeting, Orthopaedic Research Society. Las Vegas, Nevada, 1989.
8. Saunders, J.B. *et al.* Pathology of the intervertebral disk. Arch Surg, 40, 389-416, 1940.
9. Shirazi-Adl, A. *et al.* A finite element study of a lumbar motion segment subjected to pure sagittal plane moments. J Biomechanics, 19, 331-350, 1986.
10. Yasuma, T. *et al.* Histological development of intervertebral disc herniation. J Bone Joint Surg, 68A, 1066-1072, 1986.

STRUCTURAL STIFFNESS OF THE TRIANGULAR FIBROCARTILAGE COMPLEX

B.D. Adams, R.L. Aper, and K.A. Holley*

The University of Iowa Orthopaedic Biomechanics Laboratory, Iowa City, IA 52242.
* The University of Vermont, Burlington, VT 05405.

INTRODUCTION

Triangular fibrocartilage complex (TFCC) tears are among the leading causes of wrist pain. Current injury theory implicates excessive compressive loading across the ulnocarpal joint (ulnar impaction syndrome). The purpose of this study was to 1) evaluate TFCC structural stiffness across and within regions of the disk at different positions of forearm rotation, and 2) evaluate the biomechanical validity of two common surgical alternatives: the shaft osteotomy and partial head resection. Indentation testing (with a 1 mm metallic porous cylindrical head) was performed at seven sites across the intact TFCC disk. Stiffness in the central regions decreased with both pronation and supination. The volar regions became more compliant with pronation while the dorsal regions became more compliant with supination. Both ulnar shortening procedures produced increased compliance over most of the disk.

REVIEW AND THEORY

The TFCC is a fibrocartilaginous and ligamentous structure interposed between the ulnar head and the ulnar carpus at the wrist, arising from the radius and inserting into the distal ulna and ulnar carpus. The TFCC has been shown to have three major biomechanical functions: 1) it functions as a cushion for the ulnar carpus, carrying approximately 20% of the axial load across the wrist; 2) it is the major stabilizer of the distal radioulnar joint; and 3) it is a stabilizer of the ulnar carpus [4]. Variable loads are borne on the ulnar aspect of the wrist by the TFCC as the forearm moves through pronation and supination [3]. Forearm rotation causes changes in the relative lengths of the ulna and the radius (ulnar variance), resulting in relatively small but potentially significant changes in total load borne by the TFCC. In addition, support for the TFCC changes during forearm rotation as the ulnar head moves dorsally under the TFCC in full pronation and palmarly in full supination. This results in changes in load distribution across the TFCC [2].

Current injury theory implicates excessive compressive loading across the ulnocarpal joint as the cause of tears in the TFCC. Based on the concept of "unloading" the ulnocarpal joint, ulnar shortening procedures (shaft osteotomy and partial head resection) are common surgical alternatives.

Purpose. The purpose of this study was to 1) evaluate TFCC structural stiffness across and within regions of the disk at different positions of forearm rotation, and 2) evaluate the biomechanical validity of the shaft osteotomy and partial head resection procedures.

PROCEDURES

Indentation testing was performed at seven predefined sites (Fig. 1) across the distal articular surface of the TFCC in nine fresh-frozen upper extremity specimens disarticulated

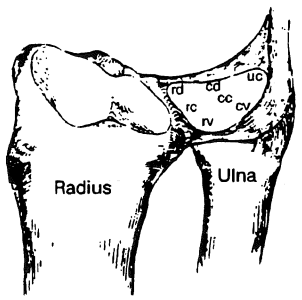

Figure 1. Indentation testing was performed at seven regions defined as: radial-central (rc), central-central (cc), ulnar-central (uc), radial-dorsal (rd), central-dorsal (cd), radial-volar (rv), and central-volar (cv).

through the wrist joint (TFCC intact and neutral ulnar variance in all specimens). A loading apparatus was designed to perform indentations with a 1 mm metallic porous cylindrical head. The apparatus was interfaced to a microcomputer to provide indentor positioning, load-feedback control, and to acquire load-deformation data. Data were acquired at 0.015 N intervals from a preload of 0.01 N

to a maximum of 0.75 N (a maximal 1 MPa nominal stress). Distraction of the distal radioulnar joint (DRUJ) was applied (0.63 lb or 5 lb) during testing to create the transverse TFCC tension that is naturally present during wrist axial loading. A series of conditions were tested: 1) forearm positioned in neutral, pronation, and supination with a 0.63 lb DRUJ distraction load; 2) 5 lb DRUJ distraction load with forearm in neutral; 3) ulnar shaft osteotomy (4 mm segment removed), forearm in neutral, 0.63 lb DRUJ distraction load; 4) partial head resection (distal 4 mm of the ulnar head removed, leaving TFCC attachment sites intact), forearm in neutral, 0.63 lb DRUJ distraction load.

RESULTS

In neutral forearm rotation, the central-central (cc) and ulnar-central (uc) regions were stiffer than the remaining regions of the disk. Increased DRUJ distraction load (0.63 lb to 5 lb) produced increased stiffness over the entire disk, with the greatest increases occurring ulnar and central. Stiffness in the central regions (rc, cc, uc) decreased with both pronation and supination (Fig. 2). The volar regions (rv, cv) became more compliant with pronation while the dorsal regions (rd, cd) became more compliant with supination. Both ulnar shortening procedures produced increased compliance over most of the disk (Fig. 3). However, despite a decrease in structural stiffness, the general shape of the load-deformation curve remained similar to the unoperated joint.

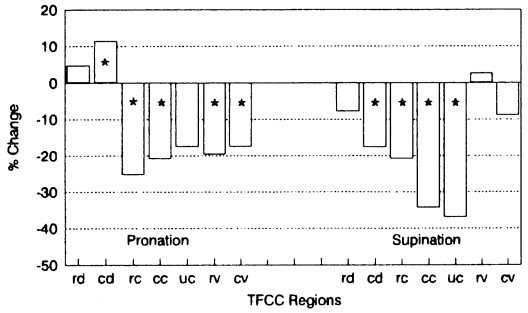

Figure 2. Change in TFCC disk stiffness due to forearm rotation. Percents indicate changes from the neutral position.

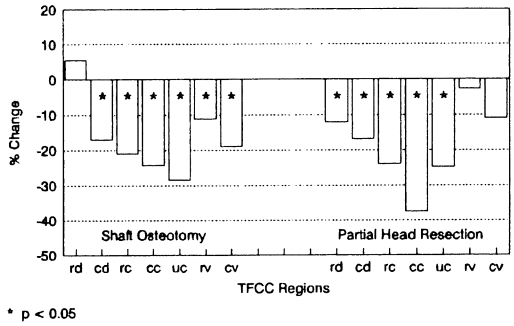

Figure 3. Change in TFCC disk stiffness following operative procedures. Percents indicate changes from the unoperated joint.

DISCUSSION

The results support the concepts that structural compliance varies across regions of the disk and is dependent upon the position of forearm rotation. Variations are most likely due to changes in support by the ulnar head. However, contrary to theory regarding the ulnar impaction syndrome, the central disk regions become more compliant rather than stiffer in pronation. Thus, the radiographic finding of increased positive ulnar variance with pronation may not have the significant clinical implications previously reported [1]. Shaft osteotomy and partial head resection produced similar increases in compliance. However, as the maximal indentation loads were reached, stiffness still increased. Thus, although ulnar shortening procedures reduce load transmission to the ulna, they may not sufficiently reduce the stresses that cause injury to the intact disk.

REFERENCES

[1] Chun, S. and Palmer, A.K. J Hand Surg, 18A:46-53, 1993.
[2] af Ekenstam, F. Clin Orthop, 275:14-18, 1992.
[3] Kauer, J.M.G. Acta Anat, 93:590-605, 1975.
[4] Palmer, A.K., J Hand Surg, 14A:594-606, 1989.

ACKNOWLEDGEMENTS

This work was supported by a research grant from the Orthopaedic Research and Education Foundation (#91-001).

INFLUENCE OF SITE, EXERCISE AND SYNOVITIS ON INTRINSIC MATERIAL PROPERTIES OF EQUINE THIRD CARPAL ARTICULAR CARTILAGE

A.L. Bertone+, J.L. Palmer+, and J. Mansour*

+Department of Veterinary Clinical Sciences,
The Ohio State University,
601 Vernon L Tharp,
Columbus, OH 43210

INTRODUCTION

Aggregate modulus, Poisson's ratio and permeability constant were determined in 12 sites of the articular cartilage of the equine third carpal bone of exercised horses and nonexercised horses; and in exercised horses with and without synovitis. Sites anterior on the bone had decreased aggregate modulus; exercise increased Poisson's ratio and increased permeability constant, particularly in the posterior joint subjected to constant low loading. Synovitis induced a decrease in Poisson's ratio. These changes reflect alterations in cartilage matrix that would be expected for the loading characteristics of the bone/joint. Indentation testing is able to detect subtle changes in matrix composition or organization.

REVIEW AND THEORY

Intrinsic material properties of articular cartilage, as measured by indentation and KLM model analysis, have been shown to correlate with the biomechanical characteristics, and biochemical content of the cartilage. [Mow et al. (1989), Athanasiou et al. (1991), Palmer et al, (1994)] Specifically, aggregate modulus, and Poisson's ratio are reduced in areas of lower-weight bearing (patellar groove) as compared to areas of high-weightbearing (femoral condyles) and aggregate modulus is inversely correlated with articular cartilage water content and directly correlated with proteoglycan content. We have previously reported the loading characteristics of the equine third carpal bone and documented sites of low-load constant weightbearing and high-load intermittent weightbearing. [Palmer et al. (1994)] Subsequently, we have performed a series of experiments on equine third carpal articular cartilage to investigate several factors that may influence these properties; including location on the cartilage surface (site), joint loading (exercise) and exposure to synovitis. The purpose of this report is to summarize these results and report the alterations in aggregate modulus (H_A), Poisson's ratio (υ_s) and permeability constant (k) at 12 sites in exercised and unexercised horses, and in exercised horses with carpal joints exposed to synovitis or no synovitis for 1 or 5 weeks.

PROCEDURES

Six horses were exercised on a Swedish Sato high-speed treadmill for 30 minutes three times per week at 2m/sec (weeks 1 and 2), 4m/sec (weeks 3 and 4), and 6m/sec (weeks 5 and 6) [exercised group]; and 6 horses were confined to a boxstall for 6 weeks [nonexercised group]. Ten additional horses were exercised for 30 minutes at 4m/sec three times weekly for ten weeks. One carpus from each horse had synovitis induced with four intra-articular injections of 0.125ng of purified lipopolysaccharide at week 5 or 9 of the 10 week study. At the end of these studies, horses were euthanized and the third carpal bone isolated, grossly evaluated for defects, sectioned sagittally in the medio-lateral plane and frozen at -80° C. Bones were thawed and maintained in saline solution and enzyme inhibitors and indentation tests performed using a plane ended circular porous microindentator (1.5mm). At each site, equilibrium was reached after applying an initial tare load of 2g. An instantaneous 20 g load was then applied and cartilage displacement recorded until equilibrium. The biphasic material properties of the cartilage were determined in a PC adapted version of the mathematical model of cartilage developed by Mow, and included fluid and solid phases. Differences in material properties were determined by repeated measures mixed ANOVA for site and exercise, or site and synovitis with significance set a $p < 0.05$. Post-hoc contrasts were evaluated after Bonforoni correction.

RESULTS

Aggregate modulus was significantly lower for the nests of sites located on the anterior/anteriomedial aspect of the radial facet and on the intermediate facet as compared to nests of sites on the posterior aspect of the radial facet. (Fig 1) Exercise significantly increased the permeability constant irrespective of site as compared to nonexercise. (Fig 2) Exercise resulted in a significant increase in Poisson's ratio on the nest of sites on the posterior aspect of the radial facet. (Fig 3) Poisson's ratio was significantly decreased in articular cartilage exposed to synovitis for 1 and 5 weeks as compared to limbs with arthrocentesis only and no synovitis.

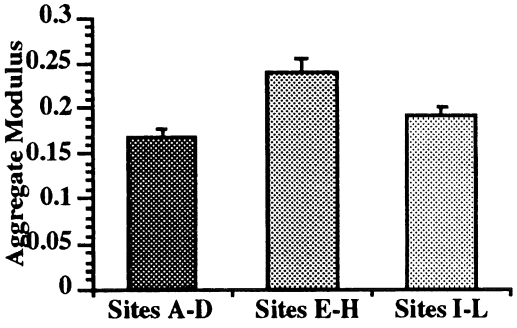

Figure 1. Sites A-D (anterior) < sites E-L(posterior)

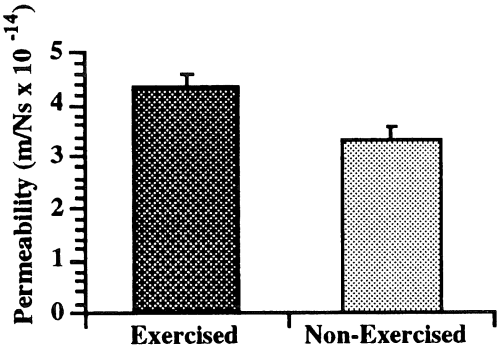

Figure 2. Exercised > nonexercised (p<0.05)

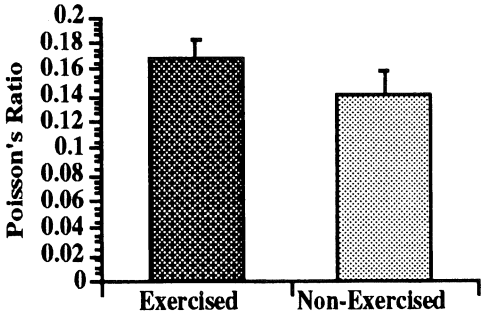

Figure 3. Exercised > nonexercised (p<0.05)

DISCUSSION

These results imply that 1) articular cartilage has less proteoglycan and more water content in the intermittent high loading sites (anterior), that 2) exercise induces an increased capability of fluid movement (k) and that 3) exercise induces a decreased cartilage compressibility (υ_s), particularly in the posterior aspect of the joint. Articular cartilage also has increased compressibility in the anterior and posterior aspect of the joint after exposure to moderate synovitis for as long as 5 weeks earlier. A high permeability constant and a lower Poisson's ratio

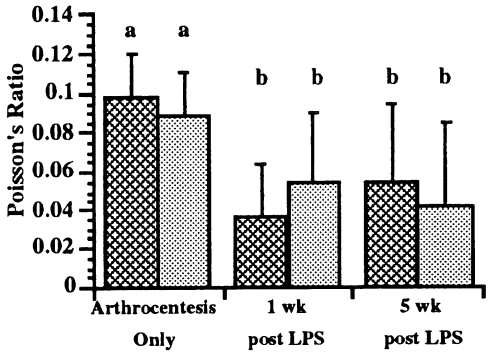

Figure 4. Different letters are different (P<0.05) Dots posterior, cross-hatch anterior.

(anterior aspect) seen with exercise would enable the cartilage to rapidly deform to an applied load. This might be most necessary in the anterior intermittently high-loading areas of the third carpal bone.Adaptation of this cartilage may be an adjustment to stress, as this is the site of traumatic cartilage injury in racehorses. The lower Poisson's ratio (greater compressibility) in cartilage exposed to synovitis suggests a change in matrix organization secondary to inflammation that results in more deformable cartilage. This cartilage may be prone to mechanical injury under normal loading. Indentation testing appears to be a sensitive assessment of differences in articular cartilage matrix composition or organization.

REFERENCES

Mow V.C., et al. Biphasic indentation of articular cartilage-II. J Biomech 22,853-861,1989.

Athanasiou K.A., et al.Interspecies comparisons of in-situ intrinsic mechanical properties of distal femoral cartilage. J Orthop Res 9,330-340, 1991.

Palmer J.L., et al. Site specific biochemical characteristics of third carpal articular cartilage in exercised versus non-ercercised horses: Comparison with indentation properties. Transactions of the 40th Annual Meeting of the Orthopedic Research Society, New Orleans,(p147), 1994.

Palmer J.L., et al. Contact area and pressure distribution changes of the equine third carpal bone during loading. In Press Equine Vet. J., 1994.

ACKNOWLEDGEMENTS

This work was supported by a grant from NIAMS, NRSA fellowship, Veterinary Orthopedic Society, and by Equine Research Funds, The Ohio State University.

*Dept of Mechanical and Aerospace Engineering, Case Western Reserve University, Cleveland, Ohio 44106.

EVALUATION OF A CLASS OF HYPERELASTIC CONSTITUTIVE MODELS FOR FINITE ELEMENT ANALYSIS OF EXPERIMENTALLY INDUCED DEFECTS IN THE GOAT PATELLAR TENDON

Balakrishna Haridas, David L. Butler
Noyes-Giannestras Biomechanics Laboratories
Department of Aerospace Engineering & Engineering Mechanics
University of Cincinnati, Cincinnati, Ohio.

INTRODUCTION

We present a nonlinear hyperelastic finite element model for simulation of in vivo stress distributions within and around an experimentally induced injury in the goat patellar tendon. This is part of a larger study, the goal of which is to establish a mathematical basis for Wolff's law for soft tissue healing. This law, originally proposed for bone [4], states that *a tissue's structure is regulated in part by its in vivo loading regime.* Our immediate goal was to evaluate strain energy functions for modeling the response of the tendon just after creation of a square window defect. We used the ABAQUS finite element code [6] to model material nonlinearities using two strain energy functions; **a)** the Mooney-Rivlin function [9] and **b)** a five term function. The Mooney-Rivlin function was found to be unsuitable for modeling the tendon's nonlinear response. However, we were able to model this behavior successfully using the five term function. Our results show that though the model predicts strains at in vitro load levels fairly accurately, its efficacy under varied in vivo loading and deformation modes is still under evaluation. We conclude that this approach is a better alternative compared to those used to date in our laboratory. Further investigation into strain energy functions for representing the anisotropy of the patellar tendon is warranted.

REVIEW AND THEORY

The finite element method (FEM) has become a method of choice in modeling soft tissue mechanics [1,3]. Models have evolved from being linear, small strain, elastic to the present ones which can account for many inelastic phenomena. FEMs have been applied to tissues like lung parenchyma and cardiac muscle [1], articular cartilage [7], intervertebral disks, and tendons [2,3]. We have also recently used poroelastic FEM in ABAQUS [6] to model the interaction of the goat patellar tendon with a transducer [2]. This was a 2D finite element model using poroelastic continuum elements reinforced with nonlinear springs. These spring elements were used to model the typical nonlinear toe region of the σ-ε relationship (Fig 1). In this work, we investigated a hyperelastic material model as an alternative for modeling this nonlinearity. All the modeling has been performed using the IDEAS [5] and ABAQUS [6] commercial finite element codes.

Hyperelasticity: Hyperelastic material models describe materials which exhibit nonlinear elastic response up to finite strains. Stresses in such materials can be derived from a *strain energy function, U* [8] as,

$$S_{ij} = \frac{\partial U}{\partial E_{ij}} \qquad (1)$$

where S_{ij} is the 2nd Piola-Kirchoff stress tensor, and E_{ij} is the Green-Lagrange strain tensor. For incompressible materials, U is a function of the invariants of the deviatoric part of E_{ij}.

ABAQUS uses a strain energy function of the following general form for isotropic materials,

$$U = \sum_{i+j=1}^{N} C_{ij}(I_1-3)^i(I_2-3)^j + \sum_{i=1}^{N} \frac{1}{D_i}(J-1-R)^{2i} \qquad (2)$$

where, C_{ij} and D_i are contants to be determined by fitting the above expression to experimental Lagrangian stress-strain data. If the material is almost incompressible (a good assumption for soft tissue), then all the D_i are zero. I_1 and I_2 are the first and second deviatoric strain invariants and J is the determinant of the material deformation gradient F, where

$$F_{ij} = \frac{\partial x_i}{\partial X_j} \qquad (3)$$

x is the current position of a material point and X is its reference position. When $N = 1$ and the material is incompressible, the equation for U corresponds to the Mooney-Rivlin function [9].

$$U = C_{10}(I_1-3) + C_{01}(I_2-3) \qquad (4)$$

The two constants C_{01} and C_{10} need to be determined from uniaxial tension, biaxial tension, and pure shear tests. Theoretically, while just one of these experiments is sufficient to compute these constants, it is advisable to obtain data from as many deformation modes as possible. When $N = 2$, we obtain the five term function,

$$U = C_{10}(I_1-3) + C_{01}(I_2-3) + C_{20}(I_1-3)^2 + C_{11}(I_1-3)(I_2-3) + C_{02}(I_2-3)^2 \qquad (5)$$

PROCEDURES

Modeling: We modeled the goat patellar tendon as an elliptical cylinder (Fig. 2) 55mm in length. The elliptical cross section had a minor axis of 3mm and major axis of 12mm. Quadratic brick elements (C3D20H) and triangular prisms (C3D15H). were used for discretization. The defect region (5×5×3mm) was not meshed corresponding to no material in the injury at time zero. Both the classes of 3D elements used were of the "mixed-hybrid" type with quadratic displacement and linear pressure interpolation.

Boundary conditions (B.C's): Displacement B.C's were applied to both ends of the tendon (Fig 2). Nodes on one end were completely restrained while the nodes on the other end was restrained in the y and z directions and allowed to move freely in the x-direction (Fig 2). These B.C's were applied to simulate the insertion sites. A uniformly distributed stress of 36.0 MPa was

applied in the x-direction (Fig 2). This simulated an in vivo tensile force of 1200N typically experienced during trotting [10]. Material models: The finite element models were run using the two proposed strain energy functions. The nominal stress-strain data used to derive the model coefficients C_{ij} is shown in Fig 1.

RESULTS AND DISCUSSION

The analyses performed represent the response of the tendon just after creation of the defect. The Mooney-Rivlin formulation, performed poorly and the system matrix was non-positive definite and highly unstable resulting in unconverged solutions. The analysis which was run using the five term function converged at all the load steps. The computed C_{ij} for this function are shown in Table 1. Peak stresses and strains observed in this model were 120.0 MPa and 17.8% respectively (Figs 3 and 4). They appear to be fairly accurate when compared with our experimental data on in vitro failure tests on normal tendon. These predictions are under physiological load levels at which we would expect strains of this magnitude to occur. Load levels at higher strains could not be investigated because the model was assessed by ABAQUS using the Drucker's Stability criterion [11] to be stable only up to 39% tensile strain. Moreover, since uniaxial stress-strain data was the only information used to compute the C_{ij}, the material stability limits on strain level for the other possible deformation modes were much lower. Additional tests are required to accurately compute the C_{ij} for a more stable material model.

Limitations to this study include the fact that the tendon was assumed to be isotropic while in reality it is transverse isotropic. An appropriate strain energy function needs to be developed to represent such a material. The hyperelastic material model also neglects time dependent response. This drawback can be circumvented by using a poro-hyperelastic model with the material being modelled as biphasic (solid/fluid). In conclusion, hyperelastic constitutive models offer us an alternate route to model soft tissues. Our future studies will address these issues and we will try to overcome some of the limitations of the current approach. A continuum FEM model has been developed, however, which can simulate the nonlinear stress-strain response of the tendon without having to use nonlinear springs which render model development cumbersome. This model will ultimately be used to study the evolving stress distribution within and around the healing tissue over time.

ACKNOWLEDGEMENTS

This study was supported by Grants AR38719 from the NIH and PES498 from the Ohio Supercomputer Center to the Noyes-Giannestras Biomechanics Laboratories, University of Cincinnati.

REFERENCES

1. Gallagher RH, et al. (eds): *Finite Elements in Biomechanics.*, John Wiley & Sons Ltd. 1982.
2. Herrin DW, et al: *ASME, Summer Bioeng Conference*, 1993.
3. Spilker RL, Simon BR (eds.): *Computational Methods in Bioengineering*, ASME, New York, 1988.
4. Wolff J: *The Law of Bone Remodelling*, Springer-Verlag, 1986.
5. IDEAS, *SDRC, Cincinnati, OH*
6. ABAQUS v5.2, *HKS Inc.* Providence, RI.
7. Mow VC, et al. (eds): *Biomechanics of Diarthrodial Joints*, Springer-Verlag, 1990.
8. Fung YC: *Biomechanics, Mechanical Properties of Living Tissues*. Springer-Verlag, 1993.
9. Mooney M: *J. Appl. Phy.*, **11**, 582-592, 1940.
10. Korvick DL, et al: *Advances in Bioengineering*, 99-101, 1992
11. Chen WF, Mizuno E: *Nonlinear Analysis in Soil Mechanics, Theory & Implementation*, Elsevier Science Publishers, 1990.

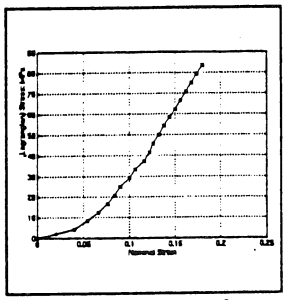

Fig 1. Subfailure σ-ε response of normal goat patellar tendon

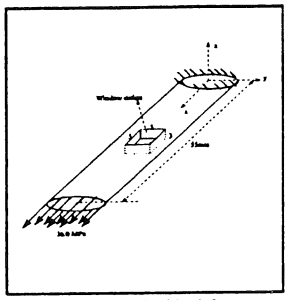

Fig 2. Tendon model with defect: Boundary conditions

Coefficient	Fitted value (MPa)
C_{10}	-743.1
C_{01}	767.1
C_{20}	0.6114E+05
C_{11}	-0.1462E+06
C_{02}	0.8868E+5

Table 1. Material coefficients computed using nonlinear least squares curve fitting

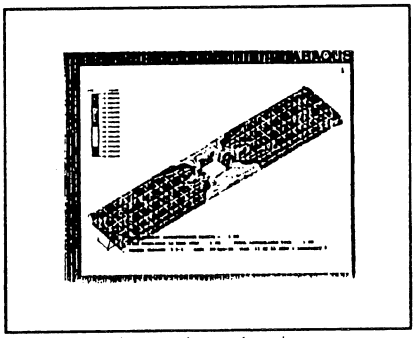

Fig 3. Contours of stresses along tendon axis

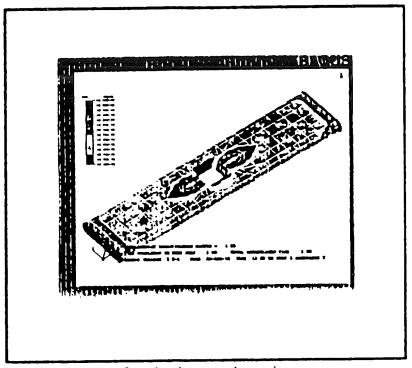

Fig 4. Contours of strain along tendon axis

SESSION 8:

JOINTS

MEASUREMENT OF TIBIOFEMORAL CONTACT FORCE FOLLOWING TOTAL KNEE ARTHROPLASTY USING A SIX-DEGREE-OF-FREEDOM TRANSDUCER

R. Singerman*, H. Pagan§, J. Berilla§, D. Davy*

Dept. of Mechanical & Aerospace Engineering* and Orthopaedics§
Case Western Reserve University, Cleveland, Ohio 44106

INTRODUCTION

Both the magnitude and location of the tibiofemoral contact force following total knee arthroplasty (TKA) may be related to successful outcome. This force may influence component wear, loosening of cemented tibial components, and stability of tibial implants fixed by means of bone ingrowth. In particular, the three orthogonal components of the resultant contact force are needed to define completely the applied load to the tibial component. We have developed a six-degree-of-freedom transducer designed to measure the tibiofemoral contact force following TKA. A typical application is presented comparing the contact forces following TKA with Insall/Burstein™ total condylar and posterior stabilized knee components (Zimmer, Inc). The contact forces were similar for both component designs at low flexion angles but differed slightly at high flexion angles.

REVIEW AND THEORY

Perry *et al.* (1975) used a single-degree-of-freedom transducer to measure the component of the tibiofemoral contact force aligned with the tibial axis. They reported contact forces determined for the normal articular surface with the collateral and curciate ligaments intact. Engin and Weis (1977) reported that the axial force component decreased with increasing flexion angle from 20° to 100°. Carmines and MacMahon (1991) reported the use of a force-plate type transducer used to determine the normal component of the contact force and the center of pressure. Our purpose was to develop a force transducer capable of simultaneous determination of (i) three orthogonal components of the tibiofemoral contact force and, (ii) the location of the center-of-pressure on the tibia.

PROCEDURES

We modified a previously reported six-degree-of-freedom transducer for use in the tibiofemoral joint (Singerman *et al.* (1994)). The transducer consists of two concentric cylinders with flanges at one end (Fig. 1). Twenty-four metal-foil strain gages arraigned in

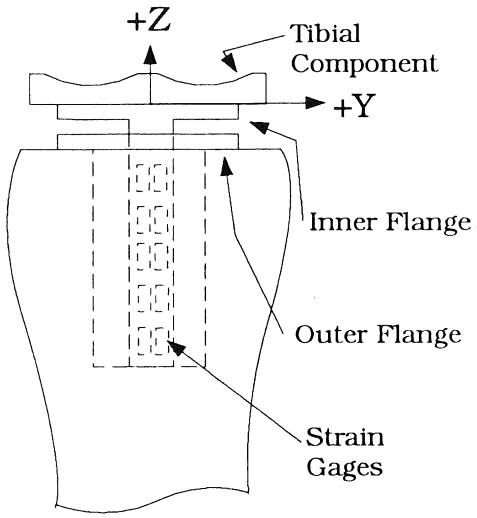

Fig. 1. Schematic of tibiofemoral transducer. Although not shown, the collateral ligaments, posterior joint capsule, and patellar ligament are left intact. (Positive-x normal to paper.)

six circuits are bonded to the inner piece. Calibration loads estimated to be similar in magnitude and direction to those expected to occur experimentally in the tibiofemoral joint were applied. The design loads are 450 N in the z-direction (F_z) and 100 N in the x- and y-directions (F_x and F_y). The accuracy of the transducer is estimated to be 2% of full-scale for F_x and F_y and 6% of full-scale for F_z. Standard total knee arthroplasty was performed. The tibial resection was inferior to the standard location. The tibial transducer was inserted into a hole drilled normal to the tibial resection. The plastic tibial components (Insall/Burstein™ posterior stabilized and total condylar) were machined to approximately 0.25cm thick at their thinnest part and securely attached to the inner flange. Shims inserted between the transducer and the tibial components were used to control joint laxity and

tibiofemoral joint-line location. Forces were recorded during continuous flexion-extension cycling. The quadriceps extensor force was directed along the anatomical axis of the femur and the hip and ankle joints were modeled as spherical joints.

RESULTS

The anterior-posterior component was posteriorly directed on the femur at low flexion angles and anteriorly directed at higher flexion angles (Fig. 2). This corresponds to the anterior component of the patellar ligament force at low flexion angles and the posterior component of this force at high flexion angles.

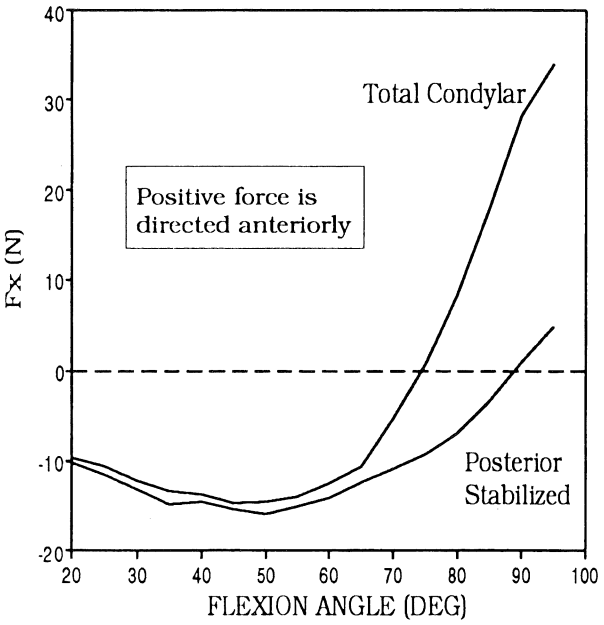

Fig. 2. The anterior-posterior component of the contact force on the tibia for two component designs.

The force measured for the total condylar component was higher than for the posterior stabilized at flexion angles above 70°. The medial-lateral component was directed laterally for all flexion angles studied, increased approximately linearly with increasing flexion angle, and was higher for the posterior stabilized component than for the total condylar. The inferior-superior component of the contact force was similar for both components (Fig. 3). At flexion angles above 85°, this force component decreased for the posterior stabilized design.

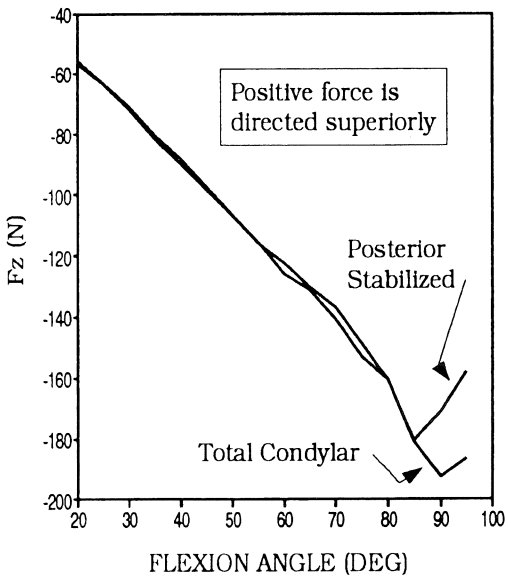

Fig. 3. The inferior-superior component of the contact force on the tibia for two component designs.

DISCUSSION

We have demonstrated the use of a six-degree-of-freedom transducer capable of measuring simultaneously the magnitude and direction of the tibiofemoral contact force. This force can be determined while the knee is loaded in continuous flexion-extension cycling. The transducer can be used with a variety of component designs, including posterior cruciate sacrificing and retaining components. The transducer also allows for evaluation of important geometric characteristics of knee arthroplasty such as joint-line location and component orientation.

REFERENCES

Carmines, MacMahon, Ortho. Res. Soc., 16, 578, 1991.

Engin & Weis, Biomech. Symp., Applied Mech. Div., 23, 207, 1977.

Perry *et al.* J. Bone Jt. Surgery, 57-A, 961-967, 1975.

Singerman *et al.*, J. Biomechanics, 27, 233-237, 1994.

ACKNOWLEDGEMENTS

This study was supported in part by National Institutes of Health Grant No. AR40004 and Zimmer, Inc.,

One-Stage Versus Two-Stage Bilateral Knee Arthroplasty: A Biomechanical Assessment

JE Perry, BL Davis, LS Borden* and TM Owings

Departments of Biomedical Engineering and *Orthopaedic Surgery
The Cleveland Clinic Foundation, Cleveland, OH 44195

INTRODUCTION

With recent advances in orthopaedic surgery, bilateral total knee replacements can be performed as a one-stage procedure. While these patients appear to do as well as those having their knees replaced at separate times, no comparative studies have quantified this from a functional point of view. This study undertook such a comparison by evaluating indices of right/left leg symmetry between one-stage and two-stage bilateral knee arthroplasty patients. For all variables studied there were no significant differences between the two groups.

REVIEW AND THEORY

It is becoming increasingly important to provide cost-effective health care. In the case of arthritic patients who require bilateral knee replacement, a one-stage procedure seems to be a viable option considering that it is significantly less costly. However, it remains to be seen how these patients' functional capabilities compare to those of patients who have had their knees replaced at separate times.

Although a number of biomechanical studies have quantified the efficacy of total knee replacement (TKR) with regard to unilateral and two-stage bilateral arthroplasty (Berman et al. 1987, Chao et al. 1980, Murray et al. 1983) there are no reports comparing one-stage versus two-stage bilateral knee replacements.

The purpose of this study was to make such a comparison by evaluating the symmetry between right and left sides for one-stage and two-stage bilateral TKR patients. It was hypothesized that for each variable studied the two groups would be indistinguishable.

PROCEDURES

To date, data has been collected and analyzed on 8 subjects (4 one-stage and 4 two-stage). All subjects were at least 2 years post-operative to insure complete rehabilitation (Chao et al. 1980).

Three-dimensional gait characteristics were collected using a six-camera Motion Analysis system and two AMTI forceplates. The subjects performed five walks at a speed of 1.2 m/s. Knee flexor and extensor strength was assessed with a Kin-Com dynamometer during three 1 second trials of maximum isometric contraction. The subjects were seated with the knees in 45° of flexion.

Analysis consisted of determining a symmetry index for each variable of interest (Table 1) for each subject. The

index compares right and left sides to give an indication of functional performance.

RESULTS

Table 1 summarizes the results for each of the two subject groups. There were no significant differences between the groups with regard to symmetry indices.

Table 1. Comparison of one-stage vs two-stage bilateral knee arthroplasty patients.

Variable	One-Stage mean ± SD	Two-Stage mean ± SD
Age (yrs)	72 ± 7	66 ± 5
Height (m)	1.61 ± .07	1.62 ± .05
Weight (N)*	789.9 ± 36.6	991.3 ± 117.8
knee flexor strength (% wt. x ht.)	2.1 ± 0.9 **.75 ± .21**	1.8 ± 1.0 **.67 ± .15**
knee extensor strength (% wt. x ht.)	4.5 ± 0.9 **.92 ± .08**	4.2 ± 1.0 **.91 ± .07**
peak ground reaction force (% wt.)	104.0 ± 1.2 **.99 ± .01**	99.3 ± 4.8 **.97 ± .03**
knee range of motion (degrees)	50.4 ± 3.7 **.91 ± .04**	47.2 ± 5.2 **.86 ± .11**
step length (cm)	58.3 ± 4.5 **.93 ± .04**	57.6 ± 3.1 **.95 ± .05**
stance time (% gait cycle)	61.5 ± 1.0 **.99 ± .01**	63.4 ± 1.2 **.97 ± .01**
swing time (% gait cycle)	38.5 ± 1.0 **.98 ± .02**	36.6 ± 1.2 **.95 ± .02**

Note: number in regular typeface is the average raw value for right and left sides combined, boldface number is the symmetry index (leg with smaller value/leg with larger value), 1 = perfect symmetry

* significant difference ($p \leq 0.05$)

DISCUSSION

For both groups the time spent in stance and swing was very near the normal ratio of 60/40 (Vaughan et al. 1992). Stance and swing times, range of motion during gait, and ground reaction force values were similar to those found in unilateral or two-stage knee arthroplasty patients one year post-op (62%, 38%, 53° and 100% body weight, respectively, Chao et al. 1980).

Although the differences between groups were not significant it is interesting to note that except for step length, the one-stage patients had higher symmetry indices and, with the exception of knee flexor strength, the symmetry indices were very high (a value of 1.0 represents perfect symmetry). These preliminary results indicate that individuals with one-stage operations have functional capabilities at least equal to the more traditional two-stage knee replacement patients. This suggests that one-stage operations are a viable alternative for individuals facing bilateral knee arthroplasty.

REFERENCES

Berman, A. et al. J. Bone Joint Surg., 69A, 1340-1345, 1987.

Chao, E. et al. Arch. Orthop. Traumat. Surg., 97, 309-317, 1980.

Murray, M. et al. Clin. Orthop., 173, 191-199, 1983.

Vaughan, C. et al. Dynamics of Human Gait, (p. 11), Human Kinetics Publishers, 1992.

Effects of Patellar Thickness on the A-P Drawer of Tibia after Total Knee Arthroplasty

Anna X. Zhang, Mark C. Miller, Richard A. Berger, Yesh A. Navalgund, Harry E. Rubash, Savio L-Y. Woo

MSRC, Department of Orthopaedic Surgery, University of Pittsburgh, Pittsburgh, PA 15213

Introduction:

Total knee arthroplsty (TKA) has become the standard treatment for a variety of knee disorders and has proven long-term success. While many surgeons agree that restoration of the tibiofemoral joint line is crucial, there is debate concerning restoration of patella thickness. Yoshii, et al[4] suggested that restoring normal patellar thickness promotes the return of kinematic function better than does making the patella either thicker or thinner. Reuben, et al.[3] suggested that the bony patellar strain increases with thickness of the overall patellar arthroplasty and that the overall thickness of the patellar arthroplasty should be maintained or restored while maintaining a bony patella thickness of at least 15 mm. The aim of current study was to add to the research effort by comparing the tibial A-P drawer for different patellar thickness after total knee arthroplasty.

Materials and Methods:

In three whole knee specimens, the native patella thickness was measured. The patella was transected in the coronal plane and instrumented with a multiaxial force plate between the base and the articular surface of the patella. One threaded intracortical pin (with five reflective markers on it) was inserted into patella, femur, and tibia respectively. The knee was then placed into the Oxford rig knee simulator and flexed and extended from 0-90° by applying force on the quadriceps tendon. A data acquisition system continuously recorded the magnitudes of the patellofemoral forces and moments. Motions of reflective markers on femur, tibia, and patella were recorded at 60 Hz with a video-based MotionAnalysis™ system. They were tracked to obtain the positions of reflective markers, which were then transformed into simple geometric descriptions of the patellofemoral and tibiofemoral joints through the use of joint coordinate system.

After testing the native knee, a standard PCL retaining TKA was performed. Three patella thicknesses were tested for each knee: +5, +0, and -5 mm relative to the native patellar thickness. The patella thickness was altered by loosening the rod collars on the force transducer, allowing the rods to slide freely in the patellar-thickness direction, and extending the force plate attachment rods.

Results:

Tibial A-P drawer versus knee flexion angle for one knee flexion cycle with 44.5 Newtons simulating the half-body weight in the Oxford-rig are shown in Figures 1-3 for three specimens. All three graphs show only small differences between arthroplastic cases with different patellar thicknesses.

All three specimens show similar anterior tibial motion after arthroplasty, but one specimen shows a different tibial movement in the native case. For specimens 2 and 3, the tibias moved anteriorly about 20 mm as the knee flexed from 0° to about 90°. This is comparable to the in vivo result from Lafortune et al.[1], in which tibia moved anteriorly 15 mm during 60° knee flexion.

In specimens 2 and 3, the joint arthroplasty repositioned the tibias anteriorly about 10 mm. The differences in A-P drawer between arthroplastic and native cases are larger than differences after arthroplasty caused by variations in patellar thickness (Figures 2 and 3). These differences were larger at the beginning of the knee flexion, as shown in Figure 4.

Discussion:

Results indicate that changes in patellar thickness have negligible effect on the tibial A-P drawer. While a thicker patella provides a larger moment arm for the quadriceps and a larger factor of safety against patellar fracture, it also increases the normal patellofemoral force during the first 30° of knee flexion[2]. Complications associated with this potential difficulty must also be considered. The use of 44.5 Newtons as a half-body weight may have

some effect[5] and more specimens should be tested before a final conclusion concerning patellar thickness is drawn.

Acknowledgment:

This project was supported by University Orthopaedics Inc. and Zimmer Inc.

References:

1) Lafortune M, Cavanagh P, Sommer H and Kalenak A: Three-dimensional Kinematics of the Human Knee During Walking. *Journal of biomechanics*, 25(4):347-357, 1992.

2) Miller M, Zhang X, Berger R, Crossett L, Navalgund Y and Rubash H. Patella tracking before and after TKA. in *40th annual meeting, ORS*. 1994. New Orleans, LA.

3) Reuben J, McDonald C, Woodard P and Hennington L: Effect of patella thickness on patella strain following total knee arthroplasty. *Journal of Arthroplasty*, **6**:251, 1991.

4) Yoshii I, Anouchi YS and Whiteside LA. The Effect of Placement of the Patellar Button and Design of Femoral Component on Patellar Tracking. in *36th Annual Meeting, ORS*. 1990. New Orleans, LA.

5) Zhang X, Miller M, Berger R, Rubash H and Woo SL-Y. Effects of Scaled body-Weight on the Patellofemoral Forces and Patellar Tracking. in *13th Southern Biomedical Engineering Conference*. 1994. Washington DC.

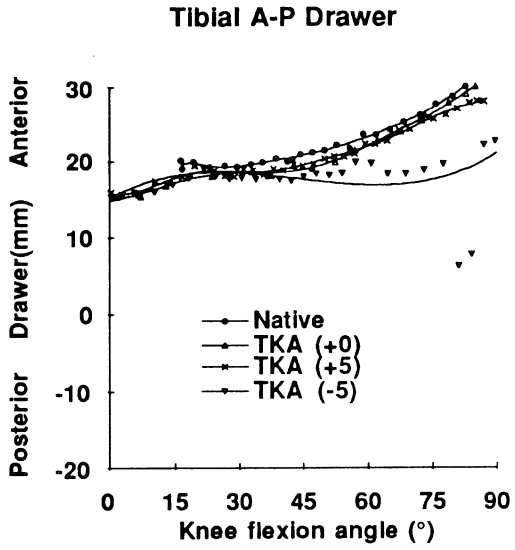

Figure 1 Tibial A-P Drawer (Specimen 1)

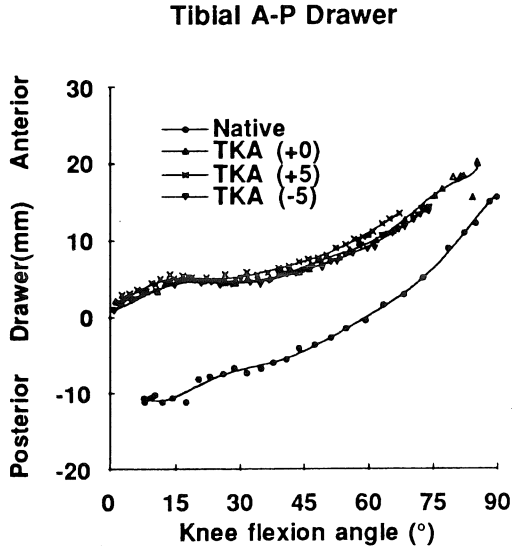

Figure 2 Tibial A-P Drawer (Specimen 2)

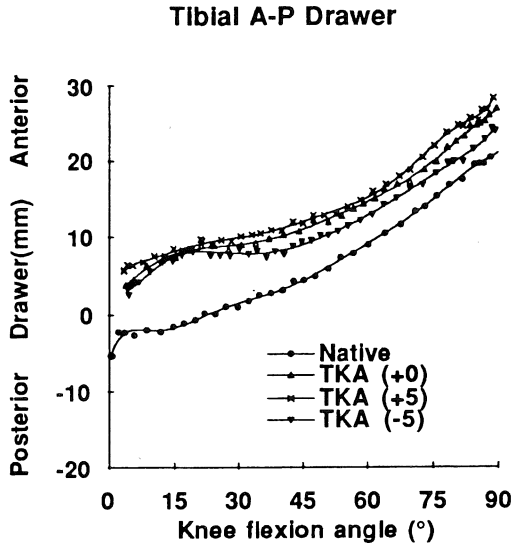

Figure 3 Tibial A-P Drawer (Specimen 3)

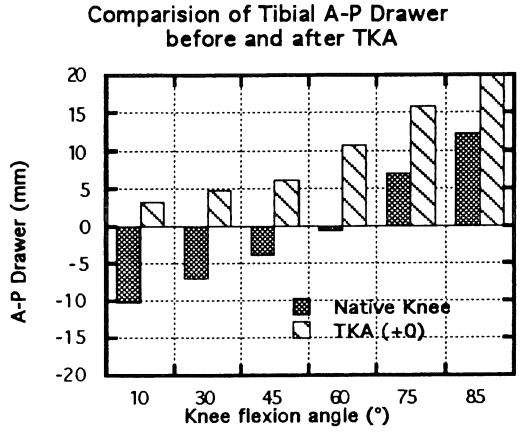

Figure 4 A-P Drawer before and after TKA (Specimen 2)

OFFSET HINGES IN THE WRIST JOINT: MODEL PREDICTIONS AND VERIFICATION

K. Hollerbach[1,3], A. Hollister[2], C. Chen[3], S.Burastero[3], M.Shih[3]
[1]Institute for Scientific Computing Research, LLNL, Livermore, CA
[2]Adult Brain Injury Services, Rancho Los Amigos Medical Center, Downey, CA
[3]Ergonomics Laboratory, Department of Health Services, LLNL, Livermore, CA

INTRODUCTION

The objective of the present study is to demonstrate the use of a 2D offset hinge model to describe wrist motion by (1) comparing trajectories predicted by the offset hinge model with those predicted by a 3D Euler angle model, (2) introducing a motion analysis system that incorporates an offset hinge model and can be used conveniently in quantitative ergonomic analyses of work tasks and tools involving use of the hand, and (3) experimentally verifying the accuracy of the offset hinge model in predicting movement of the wrist in 3D space. In this study, data from a mechanical wrist and an actual human wrist are presented.

REVIEW AND THEORY

Human joint kinematics are frequently described in terms of Euler angles and other models [1,2,3,4,5], and are only rarely described using offset hinges that more accurately represent the physical joint axes. The joint discussed here is the human wrist joint. To initiate this discussion, a brief definition of the significant terms and concepts used in this abstract are presented.

The most general kinematic relationships of two bodies (e.g. hand and forearm) in 3D space have six degrees of freedom. Any particular joint, however, may have significantly fewer actual degrees of freedom: the human wrist joint has two. This fact does not contradict the observation that the wrist joint can produce motion throughout 3D space. The number of degrees of freedom of a set of two bodies is the minimum number of parameters needed to describe the bodies' relative positions in space. Parameters such as X, Y, Z, and orientational angles (such as Euler angles) should not be confused with degrees of freedom. It is possible for a one degree of freedom mechanism to effect changes in any or all of the six parameters used to describe the body's position and orientation in 3D space. Prudent choice of coordinate systems and definition of joint axes may, however, lead to a significant reduction in the number of dimensions needed to accurately model the actual joint motion. Furthermore, such a choice may lead to a greater intuitive understanding of the joint motion when the model's axes are aligned with the true joint axes, resulting in a physical interpretation for each joint angle that is meaningful in the context of the real system.

An offset (arbitrary) axis of rotation (or hinge) is defined as any axis of rotation that is not coincident with one of the reference frame coordinate axes. In nature, the offset hinge is much more common than the reference coordinate axes; there are an infinite number of possible offset hinges for each arbitrarily chosen reference frame. Moore et al. [4] have postulated that the healthy, intact human wrist can be described by a 2D offset hinge model. A mechanical device, the axis finder, was used to locate the axes of rotation of the wrist. There are two offset hinges of rotation. The flexion-extension (FE) axis makes an angle of about 15 degrees with the longitudinal axis of the forearm in the coronal plane and lies in the coronal plane. The radio-ulnar (RU) axis is just distal to the FE axis; the offset of the RU axis from the sagittal and transverse planes varies from about 10 to 15 degrees.

The primary objective of the present study is to demonstrate the use of a 2D offset hinge model to accurately describe 2D wrist motion in 3D space. Data from a mechanical and a human wrist joint are presented, together with an analysis of these data with an Euler angle model. The second objective is to introduce a new tool (DataGlove) to analyze in vivo wrist motion. The DataGlove incorporates an offset hinge model, in which each joint axis corresponds to a physical joint axis, and can be used conveniently in quantitative ergonomic analyses of work tasks and tools involving use of the hand.

PROCEDURES

The mechanical wrist is a 2 degree of freedom mechanism with two non-orthogonal, non-intersecting axes. The proximal axis models the FE axis of the human wrist, while the distal axis models the RU axis of the human wrist. If the long axis of the forearm is chosen as one of the reference coordinate frame axes, and the other two axes of that coordinate frame are chosen orthogonal to it, the FE axis is offset from the reference frame by a single rotation of 15 degrees. Similarly, the RU axis of the mechanical wrist is offset from the reference frame by two rotations of 15 degrees each and is, in addition, translated distally, in such a way that it does not intersect with the F/E axis.

The MacReflex Motion Analysis System (QualiSys, Inc.) used is a two camera system. XYZ coordinates for each of six infrared markers are measured at 50 Hz and are converted into three Euler angles describing the relative orientation (FE, RU, and rotation) of the hand and forearm. The MacReflex system is used both in the mechanical wrist experiments and in the human wrist experiments.

The DataGlove (Greenleaf Medical Systems) is a thin, strain gauge instrumented lycra glove. Two strain gauge sensors are affixed to the glove on the forearm and hand, one measuring FE, the other measuring RU. Sensor position and calibration are fitted to each subject's hand and forearm,. Recorded data angles (50 Hz) represent the

offset hinge joint angles directly. The DataGlove system is used in the human wrist experiments only.

The offset hinge angles are converted into a set of XYZ coordinates of the hand markers relative to the forearm reference frame. The XYZ coordinates are converted into predicted Euler angles, using the model that was used to calculate experimental Euler angles from the MacReflex data. Finally, a direct comparison is made between the predicted and the measured values of the Euler angles.

RESULTS AND DISCUSSION

The mechanical wrist was used to produce 1D and 2D movement in 3D space. This movement can be described by a 3D Euler angle model. However, only a 2D model is required to completely describe the entire motion of the mechanical wrist, because the device itself has only 2 degrees of freedom (or even 1, when one axis is fixed). The offset hinge model predictions of the Euler angles confirms this assertion: The correlation coefficients relating the Euler angles predicted by the offset hinge model and the experimental Euler angles (Column 2 in Table 1) demonstrate that no information is lost in describing the RU deviation movement of the mechanical wrist in 3D space. Figure 1 demonstrates graphically the effect of axis offsets on the results (c.f. also Col. 3 in Table 1): When using offset hinges to predict motion, accurate measurement of the axis orientation is critical in establishing the validity of the angle predictions. Even a small (< 5 deg) error in the orientation causes a decrease in the correlation coefficient (to as low as 0.760).

	Human RU	Mech. RU	Mech. FE
FE angle	0.978	0.999	0.994
RU angle	0.976	1.000	0.760
ROT angle	0.958	0.998	0.993

Table 1: Correlation coefficients relating the predicted and measured Euler angles of the human and mechanical wrists.

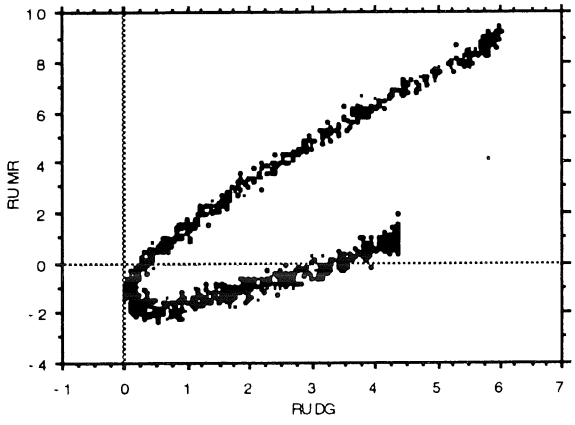

Figure 1: Correlation between the RU Euler angles predicted by the offset hinge angles of the mechanical wrist and by the data measured by MacReflex; the primary movement was FE (corr. coeff. 0.760).

Following the mechanical wrist measurements, we confirmed that the human wrist behaves like the 2D mechanical wrist (Col. 1 in Table 1 and Figure 2). A strong correlation is observed between the Euler angles predicted by the 2D measuring device (DataGlove) and the Euler angles calculated from the 3D MacReflex data.

As a 2D mechanism, the wrist can be characterized by a minimum of 2 variables, when properly parameterized. Higher dimensional models (such as Euler angle models), though at times more conveniently based on arbitrarily placed reference frames, merely confuse the description of the movement, because they provide redundant information, where all model parameters are completely determined whenever any two independent parameters are specified. The DataGlove, with its 2D data acquisition system, provides a convenient research and ergonomic analysis tool that adequately describes wrist joint motion in 3D space.

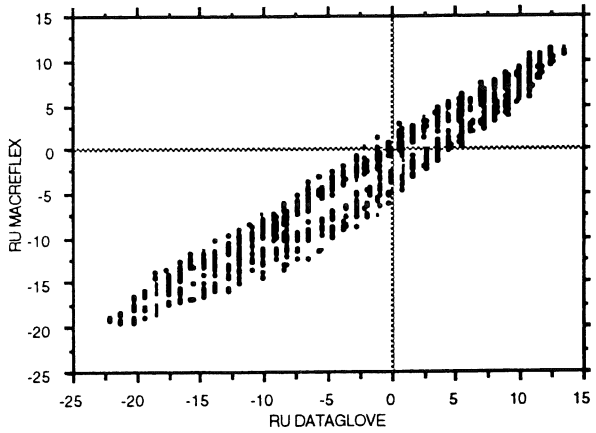

Figure 2: Correlation between the RU Euler angles predicted by the DataGlove and the data measured by MacReflex; the primary movement was RU deviation of the human wrist (corr. coeff. 0.976).

REFERENCES

[1] Andrews, J. G. et al. (1979) A biomechanical investigation of wrist kinematics. J. Biomech, **12**:83-93.

[2] Brumbaugh, R. B. et al. (1982) An in vivo study of normal wrist kinematics. J. Biomech. Engr., **104**:176-181.

[3] de Lange, A. et al. (1985) Kinematic behavior of the human wrist joint: a Roentgen-stereo-photogrammetric analysis. J. Orthop. Res., 3:56-64.

[4] Moore, J. A. et al. (1994) A kinematic technique for describing wrist joint motion: analysis of configuration space plots, J. Eng. Med (in press).

[5] Youm, Y. et al. (1979) Analytical development in investigation of wrist kinematics. J. Biomech., **12**:613-621.

CHANGES IN CARPAL KINEMATICS WITH DISPLACED INTRA-ARTICULAR FRACTURES OF THE DISTAL RADIUS

John D. Des Jardins, Thomas E. Daniel, Mark E. Baratz†
Donald D. Anderson, and Joseph E. Imbriglia†

Biomechanics Research Laboratory, Allegheny-Singer Research Institute, Pittsburgh, PA, 15212
†Department of Orthopaedic Surgery, Allegheny General Hospital, Pittsburgh, PA, 15212

INTRODUCTION

Displaced fractures of the distal radius have been shown to significantly alter the contact stress distribution across the joint. It is hypothesized that these aberrant stresses in the presence of displaced fractures may alter the kinematics of the joint as well. This study utilized the Polhemus 3Space electromagnetic tracking device to record the kinematics of the scaphoid and lunate in four unembalmed cadaver specimens. Results of this study show significant changes in carpal motion with increasing fracture displacement and confirm clinical observations of joint instability following these fractures.

THEORY AND REVIEW

Clinical study has shown that intra-articular fractures of the distal radius that heal with residual incongruity often develop post-traumatic osteoarthritis (OA)(Knirk et al., 1986). In an attempt to explain this phenomena, Baratz et al. (1993) reported significant increases (roughly 1.5-fold) in mean contact stresses after creating a lunate "die-punch" fracture with increasing displacements of up to 3 mm. A study by Hadley et al. (1989) however has suggested that articular cartilage can over time tolerate up to a two-fold increase in local pressure before the onset of OA. It remains necessary to further characterize fracture dependent changes in wrist mechanics in an attempt to explain these degenerative changes.

In addition to variations in contact stress magnitude, Baratz et al. (1993) noticed a spatial migration in the focus of maximum contact stress toward the fracture, suggesting altered carpal kinematics. There was also a dramatic increase in "over-loaded" areas in the vicinity of the fracture, defined as areas on the articular surface that experienced approximately twice the average stress measured across intact specimens. It is our hypothesis that a change in carpal kinematics associated with displaced fractures may act in conjunction with elevated contact stresses to accelerate wear of the articular surface. The present study was intended to examine, in-vitro, the effects of fracture malreduction on the kinematics of the proximal carpal bones. The carpal motion of human cadaveric specimens was measured with the 3Space electromagnetic tracking device.

PROCEDURES

Four cadaver arms were transected at the midhumeral level and were dissected preserving the elbow capsule, interosseous membrane, wrist flexor and extensor tendons and the wrist capsule. An electromagnetic source was secured to the dorsal aspect of the radius, and three sensors were mounted on the hand and wrist. Two sensors were secured to K-wires that had been inserted into the dorsal aspect of the scaphoid and lunate. A third sensor, measuring overall wrist motion, was attached to the third metacarpal. Specimens were mounted in a plexiglass jig with the elbow at 90° flexion. A load of 100N was applied across the wrist joint through the wrist flexor and extensor tendons. Starting from neutral position, the hand was taken through a full range of two separate motions: flexion/extension and radial/ulnar deviation. After testing the intact specimen, a precise osteotomy was performed to simulate a fracture of the lunate fossa (Baratz et al., 1993). Each specimen was re-tested with 0, 1, 2, and 3 mm displacements of the fracture fragment. Sensor measurements were reduced to describe the motion of the scaphoid and lunate (relative to the radius) as three successive Euler rotations about the three clinically familiar axes: flexion-extension, radial-ulnar, and pronation-supination.

RESULTS

The maximum ranges of wrist motion for this study were determined to be from 30° of extension to 45° of flexion, and from 15° of radial deviation to 20° of ulnar deviation. Table 1

presents the average changes in scaphoid and lunate flexion at two of these wrist angles with respect to the fully-reduced configuration.

Table 1 Decrease in flexion angle of scaphoid(s) and lunate(l).

Wrist Position	Fracture Step-off 1 mm	2 mm	3 mm
Fully Flexed	4.3°(s) *4.8°(l)	7.1°(s) 6.9°(l)	7.8°(s) 8.3°(l)
Radially Deviated	4.1°(s) 4.2°(l)	6.0°(s) 6.4°(l)	5.7°(s) 6.0°(l)

• all values statistically significant ($p<.05$), except *($p=.07$)

The data show a significant decrease in carpal bone flexion with increasing fracture displacement. Figure 1 illustrates this change for the measure of lunate flexion as as the wrist is flexed to its maximum position. During wrist flexion, no significant differences in radial/ulnar deviation or axial rotation of the carpals was measured with increasing step-off.

DISCUSSION

The factors involved in the development of post-traumatic arthritis are thought to include the initial injury to cartilage, intra-articular incongruity and associated joint instability. In this model we have attempted to isolate the mechanical effects of the most commonly involved fracture pattern in displaced intra-articular fractures of the distal radius. Previous studies examining contact stresses following displaced intra-articular fractures have reported only modest increases in mean and maximum local contact stresses. However the stresses measured appeared to concentrate along the edge of the experimentally created fracture.

Using the 3Space electromagnetic tracking device we have observed a change in carpal motion with fracture displacements as small as 1 mm, changes which increased with increasing fracture displacement. The most obvious changes were a loss of scaphoid and lunate flexion with wrist flexion or radial deviation. The loss of carpal motion observed in this experiment may, in vivo, lead to restricted wrist motion while creating abnormal wear patterns on the articular surface. These findings taken together with the previously observed changes in contact stresses may begin to explain the mechanical factors contributing to the onset of post-traumatic arthritis in displaced intra-articular fractures of the distal radius.

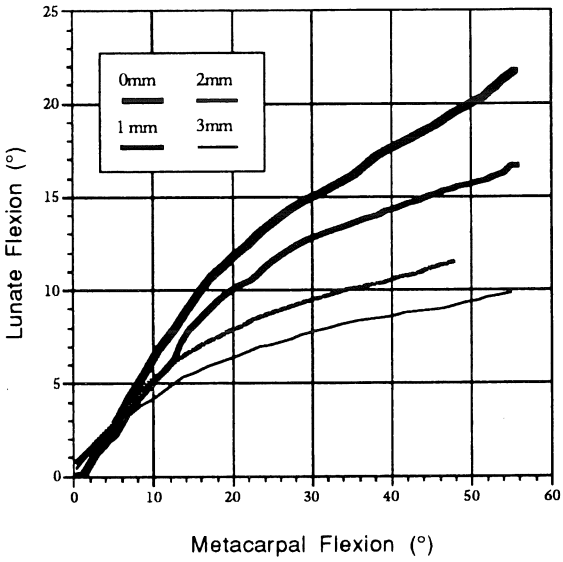

Figure 1 Lunate flexion vs. metacarpal flexion with increasing step-off

REFERENCES

Knirk, J.L., Jupiter, J.B., Journal of Bone Joint and Surgery, Vol 68A, pp. 647, 1986.
Baratz, M.E., et al., Proceedings of the 39th Annual Meeting of the Orthopaedic Research Society, pp. 106, 1993.
Hadley, N.A., et al., Proceedingsof the 35th Annual Meeting of the Orthopaedic Research Society, pp. 54, 1989

ACKNOWLEDGMENT

Supported by a grant from the Albert B. Ferguson, Jr., M.D. Orthopaedic Foundation.

SESSION 9:

REHABILITATION

POST-ROTATIONPLASTY, ANKLE JOINT MOTION ANALYSIS - EFFECTIVE AXIS CHANGES UNDER LOAD SIMULATING NORMAL GAIT

Melissa C. Carson*†, Stephen Naumann*‡ and William Cleghorn†
*Institute of Biomedical Engineering, University of Toronto
†Department of Mechanical Engineering, University of Toronto and
‡Rehabilitation Engineering Department, The Hugh MacMillan Rehabilitation Centre

INTRODUCTION

Previous studies of people who have undergone Van Nes rotationplasty have shown varying degrees of achievable gait efficiency, functional characteristics, and range of joint motion with a Van Nes prosthesis. The present goal is to examine affected ankle joint motion post-surgery, for management of proximal femoral focal deficiency (PFFD), in order to determine device independent joint characteristics for motion both unloaded and loaded.

The pilot study results presented show significant differences in affected ankle joint motion path and curvature in the sagittal plane. The effective centre of rotation moves within a range of 2.0 to 10.0 cm, or an average of 0.3 cm/cm foot length. This was found through the full range of ankle motion under applied moments simulating average loads about the knee joint in normal walking.

Study of individual patterns of ankle motion could later form the basis for Van Nes prosthesis knee joint modification. Currently a single hinge joint is used. The aim is to harness range of affected ankle motion in order to maximize range of motion of the prosthetic knee and to enhance clinical quality and standards of fit, thus improving functional results.

REVIEW & THEORY

Affected ankle joint motion post-rotationplasty has not been studied resulting in prosthesis knee joint designs lacking function-specific guidelines. As well, prosthesis fit depends on clinical experience of the prosthetist. The goal of this research is to evaluate and modify prosthetic knee joint design and fit to improve overall functional success when combined with prosthetic alignment guidelines (Hall et al., 1969), and surgical prerequisites (Friscia et al. 1989; among others).

Prosthesis knee joint designs have not generally harnessed affected ankle joint range of motion, which in many studies has not even been measured independent of the prosthesis. Comparing results of those who did measure range of motion of the affected ankle and that of the prosthetic knee, Murray et al.(1985) reported a loss of 45° and 34° in two cases. Knahr et al. (1987) also reported a loss of 9° of motion on average in 12 cases, however, Friscia et al. (1989) showed no difference on average in 11 subjects. Friscia et al. (1989) also reported on one subject who achieved 70° with the prosthesis knee joint and had only 30° of affected ankle joint motion. Another subject achieved only 90°, and had 105° natural joint motion. No basis for prosthesis design or fit was presented. This research aims to harness affected ankle joint motion in a modified prosthesis design through its measurement independent of the prosthesis.

Ankle joint motion measurement techniques have included roentgen stereophotogrammetry (accurate but invasive) (Lundberg et al., 1989), goniometry (less accurate and requires tester-defined joint axis) (Elveru et al.,1988; Hardy et al., 1987), motion analysis systems (quite accurate) (Allinger et al. 1993), and cadaver bone study (*in vitro)* (Inman et at., 1976). Errors in *in vivo* studies include subjective definition of ankle joint neutral position, nonsystematic variation of ankle joint complex loads and orientations, goniometer accuracy of only ±5° and unreliable inter-tester results (Elveru et al., 1988). This research aims to minimize these errors through use of a motion analysis system (accuracy of ± 2°), repeatable loading methods and a tester independent procedure.

The main considerations in simulating normal gait during data collection are hip joint angles which vary from -10° to 30° of flexion (Apkarian et al., 1987), and knee joint moments in flexion-extension, which can range from -0.7 to 0.5 Nm/kg of body weight (Winter et al., 1987). Power generated and absorbed at the knee joint is large at weight acceptance and push-off (Winter et al., 1982), and is primarily negative indicating eccentric work about the knee joint. The present joint motion measurement aims to simulate gait through application of loads building upto those experienced in normal gait while hip angle is maintained in the normal range.

PROCEDURES

The data collection entails measuring flexion-extension motion of the affected foot and ankle joint in 3D, first unloaded and subsequently under low applied moments. Positive and negative moments are applied, inducing eccentric and concentric muscle work. Hip angles are maintained at 0° which falls in the normal range, primarily because the PFFD study group tend to push the hip into extension during stance (Sheil, et al. 1994).

The VICON motion analysis system, described by Apkarian et al. (1989), consists of four cameras sensitive to infrared light, which reflects off markers adhered to anatomical landmarks on the subject's affected limb (*figure.1*). The moment is applied using a simple rotating bar and weights, and requires that the approximate joint axis around the malleoli be lined up with the centre of rotation of the bar (*figure.2*).

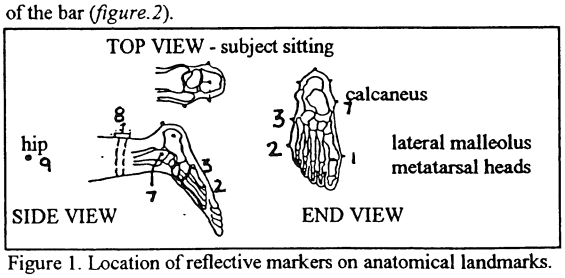

Figure 1. Location of reflective markers on anatomical landmarks.

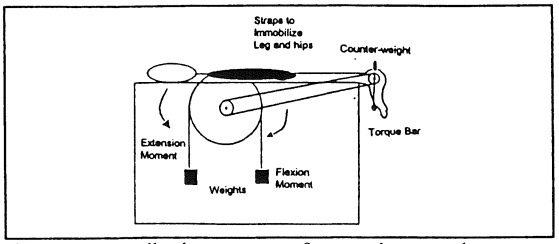

Figure 2. Data collection apparatus, frame and moment bar.

Data manipulation involves first transforming the laboratory global reference frame to a body fixed frame (fixed to the upper shank). The 3D data is projected onto the sagittal plane since this is the plane in which the prosthesis moves. This 2D data curve is then divided into portions for which each tangent and its perpendicular are calculated, giving the path of the instantaneous centre of rotation and characteristics of the ankle foot motion through flexion and extension motion. These paths are compared for the no-load case, positive applied moment and negative applied moment cases.

RESULTS

Results from a pilot study on a normal subject, indicate changes in the ankle motion under different applied loads. *Figure 3* shows the physical representation of foot position in the sagittal plane corresponding to the subsequent graphical data. Results, shown in *figure 4*, are of forefoot motion, markers #1, #2 and #3, with an applied load of -1.78 Nm, (-0.034 Nm/kg of body weight). The relative locations of the marker paths in the sagittal plane indicate a twisting motion of the foot. The contact point between the foot and socket would be that furthest forward in the trial, and could also be substantiated by noting calloused areas on the foot. In this case marker #2 on the medial metatarsal head would represents this contact.

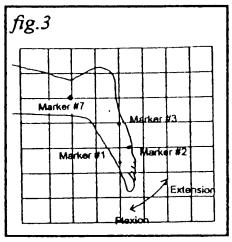

Figure 3. Foot position corresponding to graphical output.

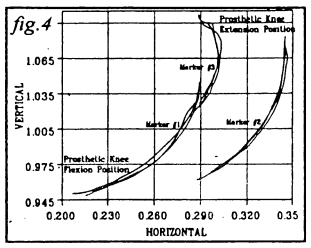

Figure 4. Foot motion under applied flexion moment.

The paths of marker #2 for two opposing loads (±0.034 Nm/kg of body weight) are shown in *figure 5* (positive moment in counter clockwise direction - i.e. extension) & *figure 6* (negative moment in clockwise direction - i.e. flexion). The lines extending from the curve are perpendicular to the instantaneous tangents to the curve for 8 divisions. The axis of the shank is determined by the position of markers #7, #8 and #9, and marker #7 is on the malleolus.

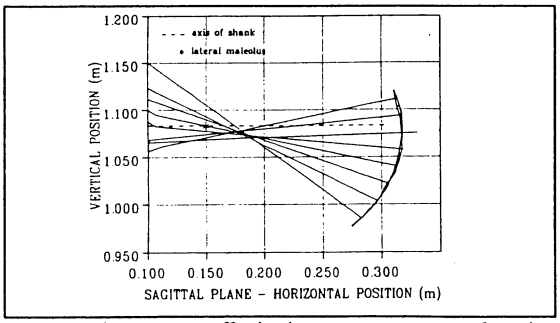

Fig.5.Extension moment, effective instantaneous centres of rotation.

The perpendicular rays, in figures 5 & 6, coincide within an area of about 4 cm by 3 cm in both cases. However, they intercept with the axis of the shank in different patterns. Under the extension moment, they run close to the malleolus and close to the axis of the shank. Under the flexion moment they cross the axis of the shank distal to the malleolus. The envelope of ray coincidence is also much closer to the maleolus, about 3 cm distal, in the first case and occurs distal, about 9 cm, and slightly anterior to the maleolus in the second case.

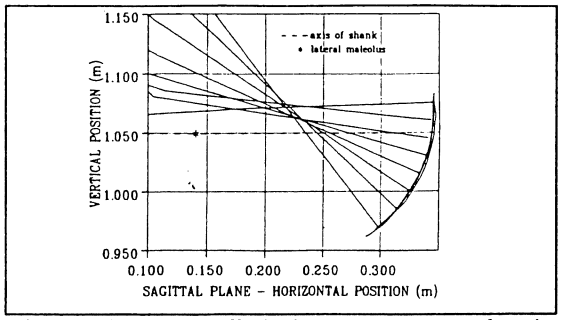

Fig. 6. Flexion moment, effective instantaneous centres of rotation.

Since the moment direction is not isolated from the direction of motion, both eccentric and concentric muscle work is done about the affected ankle joint in one trial. No significant difference in the pattern of motion is found between these two types of muscle work.

DISCUSSION

Significant differences are evident between the ankle joint characteristics under applied flexion moments and extension moments. Different patterns of motion exist and there is an average difference of approximately 6 cm between the areas of coincident perpendicular rays to the curve, suggesting that consequential variance in joint motion could also exist in other subjects.

The differences between the curves also indicates the challenges of fitting a hinge joint, as currently used, to the client in a clinical setting and harnessing the maximum range of motion of the natural joint. In both cases presented here, for instance, the more distal a hinge joint is located, the greater the range of motion. However, more cases need to be examined.

In the next step, three case studies will be carried out in the same manner, to examine individual patterns. A computer model will combine the empirical results with the prosthesis knee joint mechanical design, to evaluate range of motion and positioning for each unique case. Parameters for scaling and positioning the design to an individual will be developed. This parametric model will be verified through evaluation of other subjects. Ultimately, a more clinically practical measuring tool will be developed to apply the parametric design in the clinical setting.

The potential for this research is to both improve the function of people with a Van Nes prosthesis and to broaden the scope of people who might otherwise not be suitable for a rotationplasty due to a low level of ankle joint motion.

REFERENCES

Apkarian, J, et al. J Biomechanics, 22, 143-155, 1989.
Allinger, T.L. et al. J Biomechanics, 26, 1, 69-76, 1993.
Elveru, R.A. et al. Phys. Therapy, 68, 5, 672-677, 1988.
Elveru, R.A. et al. Phys. Therapy, 68, 5, 678-682, 1988.
Friscia, D.A. et al. J Bone & Joint Surg.,71-A, 9,1386-1392, 1989.
Hall, J.E. et al. Proximal Femoral Focal Deficiency: A Congenital Anomaly, (pp. 77-99), Nat. Acad. of Sciences, 1969.
Hardy, A.E. et al. J Bone & Joint Surg., 838-830, 1987.
Knahr, K. et al., Orthop., 10, 1241- 1248, 1987.
Lundberg, A, et al. J Bone & Joint Surg., 71-B, 94-99, 1989.
Murray, M.P. et at. J Bone & Joint Surg., 67-A, 392- 399, 1985.
Sheil, E., et al. Second World Congress of Biomechanics, accepted, 1994.
Winter, D.A. The Biomechanics & Motor Control of Human Gait: Normal, Elderly and Pathological. (pp.31,102-103), 1982
Winter, D.A. The Biomech. & Motor Cont. of Human Gait. (pp.33-35), 1987.

ACKNOWLEDGMENTS

This work is supported by the Natural Sciences and Engineering Research Council, Canada, and The Easter Seals Research Institute, Canada.

KINETIC ANALYSIS OF PREFERRED AND FAST CADENCES IN SUBJECTS WITH PROXIMAL FEMORAL FOCAL DEFICIENCY

D. IRVINE[1], E. FOWLER[1], R. ZERNICKE[2], Y. SETOGUCHI[3] AND W. OPPENHEIM[4]

Functional Assessment Laboratory[1], Department of Orthopaedics[4], UCLA, Los Angeles, CA
Department of Surgery, University of Calgary, Calgary, Alberta, Canada[2]
and
Child Amputee Prosthetics Project, Shriners Hospital, Los Angeles, CA[3]

INTRODUCTION

Proximal femoral focal deficiency (PFFD) is a congenital deformity of the proximal femur associated with varying degrees of hip instability, malrotation, insufficient proximal musculature, and leg length discrepancy. In severe cases, treatment options have included primary prosthetic fitting or secondary prosthetic fitting following Syme amputation with knee fusion. An alternative procedure, initially described by van Nes, involves rotating the tibia 180 degrees allowing the ankle to serve as a surrogate knee joint. Theoretically, this allows the patient to ambulate as a below knee amputee. However, questions have arisen as to whether the latter procedure offers a true biomechanical advantage over the more conventional Syme procedure. In particular, the van Nes rotational osteotomy is controversial in terms of cosmetic appearance and the tendency to derotate requiring additional surgical procedures. It is unknown which of these two procedures produces better results.

Preliminary kinematic, kinetic and energy expenditure results during natural cadence have been reported for these two groups (Fowler et al., 1993). The data showed evidence of ankle muscular control of the prosthetic knee joint by van Nes subjects. This was observed by: 1) appearance of a loading response (knee flexion during weight acceptance) in some subjects, 2) production of knee extensor moments during single limb support, and 3) production of small knee flexor/extensor moments during swing. Syme subjects had a higher incidence of natural limb compensatory mechanisms. This was evident from 1) excessive hip extensor and knee flexor moments and power generation following initial contact due to diminished propulsive forces on the prosthetic side and 2) stance phase vaulting (plantarflexion) to clear the prosthetic limb during swing resulting in excessive ankle extensor moments and power generation. Mean O_2 cost was also greater for the Syme group. An issue of concern is to see if functional gains are maintained through faster cadences. Therefore, the purpose of this study was to examine the gait mechanics during preferred and fast cadences for PFFD patients who have received the Syme amputation versus those who have received the van Nes rotationplasty.

METHODS

Subjects were recruited from Shriners Hospital, Los Angeles or the Child Amputee Prosthetics Project at the UCLA Institute for Rehabilitation and Chronic Disease and studies were performed at least five years after their surgical procedures. Fourteen subjects have been studied to date, seven with Syme amputation and seven with a van Nes procedure.

Movement was recorded unilaterally by two video cameras at 60 Hz while the subject walked along a walkway. Force plate information, synchronized to the video, was simultaneously acquired from a force plate concealed in the walkway. Ground reaction forces were sampled at 1000Hz (Kistler 40x60 cm force platform). The force data was normalized to body weight. Trials were accepted only if the limb being filmed hit the force plate in isolation. A total of five trials from each condition were collected. Three characteristic features were selected from the vertical force for analysis: first maximum following foot contact, minimum amplitude during stance, and second maximum amplitude prior to toe off. Two characteristics were selected from the horizontal force: maximum breaking force in the aft direction during the initial part of stance and maximum propelling force in the fore direction during the later phase of stance.

RESULTS

Characteristic maxima and minima of the vertical and horizontal components of force are reported in Table 1.

In general, vertical force maxima, and maximum braking and propelling forces were reduced on the prosthetic side compared to the natural side for both van Nes and Syme subjects. This was observed at both preferred and fast cadences. Stance time was also prolonged on the natural side in all subjects and all speeds. Two of the Syme subjects had a unimodal shaped curve on the prosthetic side where all van Nes subjects had bimodal shaped curves. Within subject consistencies were high; however, differences in curve shapes were observed between subjects and between groups.

Natural limb vertical forces had inconsistent shapes within each group (Syme and van Nes). While all subjects had a bimodal vertical curve on the natural side, some curves displayed multiple oscillations during initial stance. This observation was more frequent in several Syme subjects.

Preferred Cadence

On the prosthetic side, both braking and propelling horizontal forces were observed for all van Nes subjects; however, propelling components were absent in four out of seven Syme subjects.

On the natural side, the horizontal component of force appeared normal in shape in the van Nes subjects and most of the Syme subjects. Three out of seven Syme subjects had horizontal propelling forces.

Fast Cadence

Comparing the fast to preferred cadence, horizontal forces increased in the van Nes subjects. The horizontal propelling force observed in three Syme subjects slightly increased with the faster walking trials.

During fast walking trials, all subjects displayed a reduced vertical minima (unweighting) during mid stance. On the prosthetic side, van Nes subjects exhibited greater unweighting from preferred to fast trials which was within normal limits; however, no change was observed for Syme subjects. On the natural side, the observed unweighting was within normal limits for van Nes subjects. Syme subjects also had greater unweighting on the natural side; however it was excessive. This corresponded with excessive plantarflexion during midstance (vaulting) to assure prosthetic limb clearance.

Syme subjects exhibited greater asymmetry between the natural and prosthetic side during preferred cadence trials and this was more pronounced during fast cadence trials.

TABLE 1. Ground Reaction Force Data Normalized to Body Weight

		PREFERRED CADENCE				FAST CADENCE			
		Prosthetic		Natural		Prosthetic		Natural	
		Avg	*Stdev*	Avg	*Stdev*	Avg	*Stdev*	Avg	*Stdev*
Syme	Horiz -	-0.13	*0.05*	-0.20	*0.11*	-0.14	*0.05*	-0.24	*0.27*
	Horiz +	0.08	*0.08*	0.22	*0.09*	0.12	*0.09*	0.36	*0.10*
	V-max 1	1.09	*0.09*	1.28	*0.14*	1.18	*0.15*	1.46	*0.37*
	V-min	0.80	*0.07*	0.67	*0.09*	0.73	*0.11*	0.41	*0.18*
	V-max 2	0.98	*0.06*	1.15	*0.09*	1.00	*0.13*	1.33	*0.27*
van Nes	Horiz -	-0.16	*0.03*	-0.23	*0.08*	-0.21	*0.03*	-0.31	*0.11*
	Horiz +	0.16	*0.05*	0.26	*0.05*	0.19	*0.04*	0.34	*0.05*
	V-max 1	1.11	*0.13*	1.21	*0.15*	1.20	*0.10*	1.43	*0.10*
	V-min	0.79	*0.08*	0.75	*0.07*	0.68	*0.12*	0.57	*0.10*
	V-max 2	1.02	*0.09*	1.10	*0.11*	1.09	*0.11*	1.29	*0.18*

(Horiz -) represents braking forces
(Horiz +) represents propelling forces

DISCUSSION

Few studies have quantified patterns of ground reaction forces in the child amputee during gait (Hoy et al., 1982; Zernicke et al., 1985; Engsberg et al., 1991, 1993); however, no studies have included comparisons of below-knee and above-knee amputations. Adult studies on gait mechanics have demonstrated that above knee amputees have diminished stability as compared to below knee amputees who have preserved knee function (Susuki, 1972).

Susuki, 1972 compared patterns of ground reaction forces during gait in adult above- and below-knee amputees. Similar trends in vertical and horizontal maxima and minima were observed in the current study.

The results of this study show that the observed knee function in these van Nes subjects was maintained through faster walking cadences. In the Syme subjects, the compensatory measures, such as greater unweighting of the natural limb during mid stance and greater asymmetry in horizontal and vertical forces between the prosthetic and natural side, were amplified in the faster walking trials. Further kinetic and kinematic analysis of the fast walking trials is needed to confirm the inferred compensatory mechanisms involved with this patient population.

REFERENCES

Engsberg JR; Lee AG; Tedford KG; Hardner JA. *J Ped Orthop* 13: 169-173, 1993.

Engsberg, JR, Lee AG, Patterson JL, Harder JA. *Arch Phys Med Rehabil* 72 (8):657-661, 1991.

Fowler E, Irvine D, Zernicke R, Setoguchi Y, Oppenhiem W. *Proceedings for 17th Annual American Society of Biomechanics*, 167-168, 1993.

Suzuki K. *J Jap Orthop Assoc* 46: 503-516, 1972.

Zernicke RF; Hoy MG; Whiting WC. *Arch Phys Med Rehabil* 66: 736-741, 1985.

ACKNOWLEDGMENTS

Supported by Shriners Hospital Grant #15956.

EFFECTS OF GROWTH ON GAIT CHARACTERISTICS OF BELOW-KNEE-AMPUTEE AND ABLE-BODIED CHILDREN

J.R. Engsberg, K.G. Tedford*, and J.A. Harder*

Motion Analysis Laboratory, St. Louis Children's Hospital, St. Louis, MO, U.S.A.
*Alberta Children's Hospital, Calgary, Alberta, CANADA

INTRODUCTION

This study described ground reaction forces during gait of below-knee-amputee (BKA) and able-bodied (AB) children over a five year period. No investigations have been published describing changes in gait characteristics of BKA and AB children over an extended period of time. The nonprosthetic leg had consistently greater external loading than the other two leg types. The prosthetic leg was approximately the same as the legs of the AB children or slightly lower. The force variables indicated a steady decline in magnitude as the study progressed and was probably due to the fixed walking speed used throughout the investigation. Results indicated gait patterns of BKA children do not substantially change over time.

REVEIW AND THEORY

Investigations describing characteristics related to the gait of BKA and AB children have been cross-sectional in nature (e.g., Engsberg et al., 1993). No investigations have been published describing changes in gait characteristics of BKA children over an extended period of time. The purpose of this investigation was to describe ground reaction force characteristics during gait of BKA and AB children over a five year period.

METHODS

Ten AB (mean age, 8.2 years at onset of investigation, range 7-9 years, 5 males) and three BKA (mean age, 7.0 years, range 6-8 years, 2 males) children volunteered for this investigation. The children visited the Human Performance Laboratory approximately every six months over a five year period. Height and mass of each subject were recorded at each session.

The details of the data collection have been described elsewhere (Engsberg et al., 1993). Briefly, two force platforms were used to collect ground reaction forces (1000 Hz) for two consecutive steps of each child. A fixed speed of 1.2m/s $\pm$ 10% was used and at least three trials of data were collected for each subject on each occasion. Ground reaction forces were normalized by dividing by subject weight and total time spent on both plates was normalized to a value of 1 (i.e., time 0 was touchdown of the first foot and time 1 was takeoff of the second foot). Average force-time curves were determined for the right and left legs of the AB children, and for the prosthetic and nonprosthetic legs of the BKA children. Discrete variables analyzed were the ratio of support time for each foot (ToTime), two local maxima from the vertical force-time trace (ZMax1, ZMax2), and peak anterior and peak posterior forces from the anterior-posterior force-time trace (RMax, PMax). Means and standard deviations were determined for each subject for each session and leg type (i.e., AB, nonprosthetic and prosthetic) and were then averaged within groups, for each session.

RESULTS

As expected the height and mass of the children steadily increased during the five year period (Figures 1 and 2). While the AB children were both taller and heavier than the BKA children through the initial stages of the study both groups were about the same size at the end of the study. The apparent rapid change in size of the BKA group from 36 to 42 months was not a physiological phenomenon but was due to the withdrawal of the female child from the study.

The support time ratio (ToTime) for the AB children ranged from 0.548 to 0.564 (Figure 3). The support time for the nonprosthetic leg of the BKA children ranged from 0.555 to 0.574 and for the prosthetic leg from 0.528 to 0.553. The trend throughout the investigation was that the nonprosthetic leg was in support longer than both the prosthetic leg and the legs of the AB children.

The force variables (i.e.,ZMax1, RMax, PMax) indicated a steady decline over time (Figures 4,5,6). However the relationship between the leg types remained relatively the same. The nonprosthetic leg had consistently greater external loading than the other two legs. The prosthetic leg had approximately the same or slightly lower loading than the legs of the AB children.

DISCUSSION

The results of the present investigation offer information relevant in at least two areas. The first is that the results fall within the values reported for cross-sectional studies of similar groups of children (Engsberg et al., 1993). In the cross-sectional investigation ToTimes for AB children were reported to be 0.55 with a standard deviation of 0.04. Means and standard deviations for the nonprosthetic and prosthetic legs were 0.58 (0.09) and 0.55 (0.06), respectively. Further, the ground reaction force patterns were also consistent with the cross-sectional data. Similar to the cross-sectional investigation the nonprosthetic leg consistently indicated forces of greater magnitude than the results for the other leg types while the prosthetic leg was the same or less than the results for the legs of the AB children. It has been reported that a mature gait of AB children is established by 3 years of age (Sutherland et al., 1980). While the cohort of BKA subjects for this investigation was small, results appear to indicate that like AB children a gait pattern for BKA children is established and does not vary substantially over time.

The second area focuses on the result of decreasing force magnitudes as the study progressed. We believe this result was due to the imposed walking speed of 1.2 m/s throughout the investigation. Several methods exist for determining speeds of subjects (e.g., fixed speed, fixed cadence, freely chosen speed); each method has its own attributes and limitations. Since it has been shown that rate of walking can influence the magnitude of force variables for children with above-knee amputations (Zernicke et al., 1985) and to better control this influencing factor, we decided to use the same walking speed throughout the investigation. However, fixing the speed may have had the same effect as having children in a cross-sectional study gradually reduce their walking speed. This is due to growth and the concomitant reduction in stride length and stride frequency over the duration of the investigation.

REFERENCE

Engsberg, et al. J Pediatr Orthop. 13(2), 169-173, 1993
Sutherland, et al. J Bone Joint Surg, 62A(#), 336-353, 1980.
Zernicke, et al. Arch Phys Med Rehabil. 66, 736-741, 1985.

ACKNOWLEDGMENT

Funding provided by the George Reed Foundation for the Handicapped, Variety Club of Southern Alberta - Tent 61, and the Human Performance Laboratory, University of Calgary.

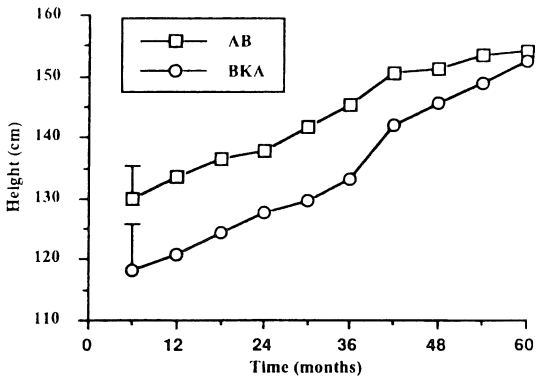

Figure 1. Means and representative SD for height for BKA and AB children over a 5 year period.

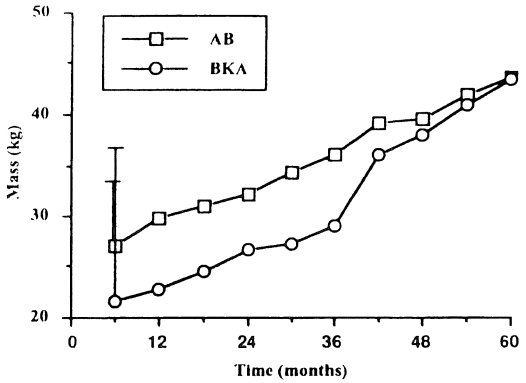

Figure 2. Means and representative SD for mass for BKA and AB children over a 5 year period.

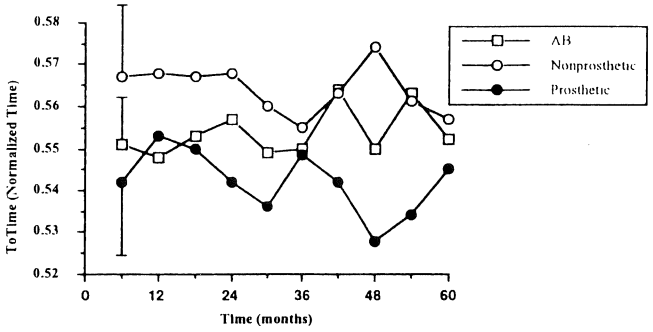

Figure 3. Means and representative SD for ratio of support time for BKA and AB children.

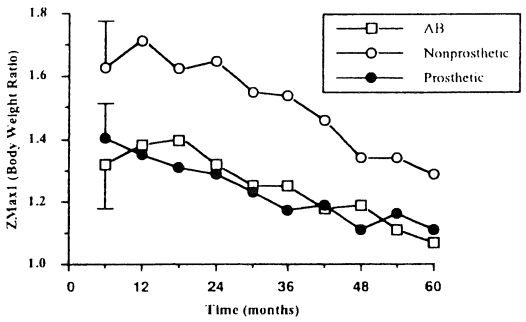

Figure 4. Means and representative SD for first local maximum of vertical force-time trace for BKA and AB children.

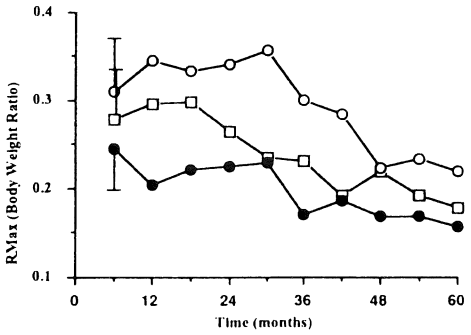

Figure 5. Means and SD for maximum retarding force from the anterior-posterior force-time trace for BKA and AB children.

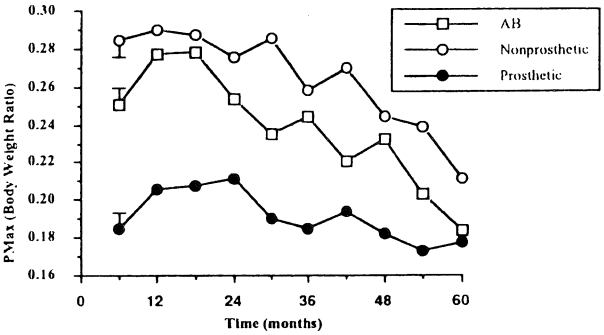

Figure 6. Means and SD for maximum propulsive force from the anterior-posterior force-time trace for BKA and AB children.

GAIT CHARACTERISTICS OF MULTIPLE SCLEROSIS PATIENTS PRE AND POST AN EXERCISE TRAINING PROGRAM

Mary M Rodgers, PhD, Janet A Ponichtera-Mulcare, PhD, and Deborah L King, MS

Department of Veterans Affairs Medical Center, Dayton, OH 45428
Institute for Rehabilitation Research and Medicine, Wright State University School of Medicine, Dayton, OH 45420

INTRODUCTION

Multiple sclerosis is a progressively debilitating disease whose symptoms often include reduced muscular strength, spasticity and gait ataxia. Thirty MS patients were recruited to participate in an exercise program to determine if they would exhibit similar benefits of exercise as do normal healthy adults. Particular areas of interest were the patients' gait characteristics and walking capabilities. Gait analyses have thus far been conducted on 6 patients pre, during, and post a 6 month exercise program involving cycle ergometry. No significant changes were observed in walking velocities, ground reaction force (GRF) patterns, or electromyography (EMG) of selected muscles. However, significant differences were noted in passive hip range of motions from pre to post exercise, as were changes in ankle and knee kinematics.

REVIEW AND THEORY

One of the most common affects of multiple sclerosis is a decline in physical activity, particularly in a person's walking capabilities. This decline in physical activity is probably due to the reduced muscular strength and endurance and the gait ataxia observed in MS patients. Little research has been done to determine if MS patients respond positively to exercise - demonstrating improvements in strength and endurance and ultimately daily activity capabilities. Gehlsen et al. (1986) studied the gait characteristic of 9 MS patients pre and post an aquatics exercise program. No significant changes in the subjects' gait were found following the exercise program. However, the exercise program in this study was not well defined varying from subject to subject, and the subjects involved were all of relatively low disability. Thus, the purpose of this study was to examine the gait characteristics of a wide range of MS patients pre and post a standardized exercise program.

PROCEDURES

Six adult MS patients (5 females and 1 male) of differing disability participated in this study. The Kurtzke Expanded Disability Status Scale (EDSS) was used to quantify the severity of the disease for each subject. EDSS scores are determined through a neurological exam, with scores ranging from 0 (normal neurological exam) to 10 (death from MS). Scores greater than 7 indicate restriction to a wheelchair. The range of scores for the 6 subjects was 1 to 6.5 with a mean of 2.75. The subject with a score of 6.5 utilized a cane while walking.

The subjects were instructed to walk at their normal walking velocities on a 6.5 m walkway while 3D kinematic, ground reaction forces, and EMG data were collected. Retro-reflective markers were placed on 5 sagittal landmarks and surface electrodes were attached to monitor the gluteus maximus, biceps femoris, lateral gastrocnemius, anterior tibialis, vastus lateralis, and rectus femoris muscles. The EMG and GRF data were obtained with a Noraxon telemetered EMG unit (Noraxon USA, Inc, Scotsdale, AZ) and Kistler force plate (Kistler Instrument Corp, Amherst, NY), respectively, and were sampled at 1000 Hz.. Kinematic data were collected with three 60 Hz. video cameras positioned to attain left and right side data separately. A PEAK5 Motion Measurement System (Peak Performance Technologies, Inc., Englewood, CO) was used to analyze the kinematic and kinetic data. EMG data were normalized to percent average contact and percent stride. Passive range of motion measurements, using hand goniometers, were taken prior to the gait analysis.

Analyses were conducted prior to (pre), 3 months into (3 mo), and following (post) a 6 month exercise program. The exercise program consisted of a cycle ergometry protocol in which the subjects exercised three times a week for 30 minutes while maintaining a heart rate of 55 to 65 % of their maximal heart rate. The subjects utilized either an upright or recumbent ergometer depending on their ability level. Statistical analysis consisted of analysis of variance between the three conditions (pre, 3mo, and post) at a .05 level of significance. Tukey's post hoc test was used to test for differences between means of variables with p values less than .05.

RESULTS AND DISCUSSION

Passive range of motion measurement indicated several trends at the hip joint. Hip external rotation significantly increased pre to post exercise going from 32 $\pm$ 6.5 degrees pre exercise to 42 $\pm$ 9.0 degrees post exercise. Hip adduction also increased from 29 $\pm$ 12 degrees to 44 $\pm$ 16 degrees, though the increase was not significant. Hip flexion demonstrated a non significant decrease of 5 degrees - probably due to the great demand that cycling places on the hip flexors coupled with the lack of a stretching protocol in the exercise program.

Mean temporal results included: velocity, .86 $\pm$ .35 m/s, percent stance, 64$\pm$ 3.6 %, stride length 1.04 $\pm$ .3 m, and cadence .81 $\pm$ .1 strides/s. There were no significant changes in velocity, stride length, cadence, or percent stance from pre to post exercise.

Two kinematic parameters did show significant changes pre to post exercsie. Ankle angle at contact was greater during the post condition, as shown in Figure 1, indicating that the subjects contacted the ground with less dorsiflexion. This change, however, was not reflected in the vertical or anterior/ posterior GRF impact peaks or in the anterior tibialis EMG activity as might be expected.

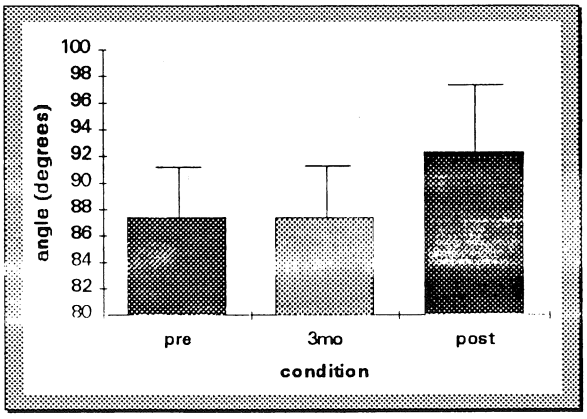

Figure 1. Ankle angles at contact pre, 3 months, and post exercise.

Knee angle at toe off, shown in Figure 2, increased from pre to post exercise such that the subjects had a more extended knee at toe off following the exercise program. While having greater extension of

the knee at toe-off theoretically allows for a more effective push-off, the GRF results did not indicate greater vertical or anterior/posterior thrust peaks during toe off.

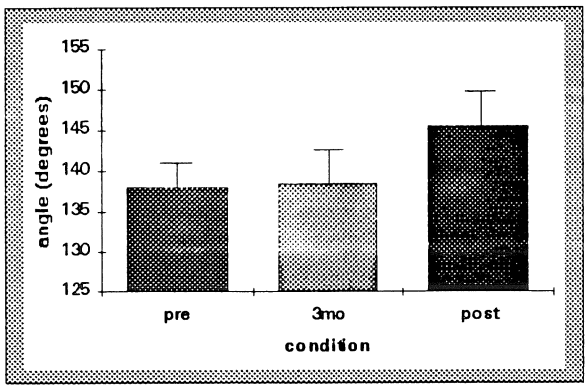

Figure 2. Knee angle at contact pre, 3 months, and post exercise.

EMG patterns showed no consistent changes pre to post. Four of the 6 subjects demonstrated inappropriate biceps femoris activity during late stance during the pre condition, with 2 of these 4 demonstrating more normal patterns during the post exercise condition. The decrease in biceps femoris activity during late stance in these two subjects may have allowed them to attain the greater knee extension which was observed at toe off.

Despite the limited number of subjects who have thus far completed the exercise program, several conclusions appear to be warranted. No significant changes were observed at the 3 month interval, though significant differences in gait characteristics were observed after 6 months of cycling. Most promisingly, knee extension was increased at toe off, possibly allowing for a more effective propulsive phase of the gait cycle. This increase in knee extension at toe off may have been caused by a decrease in inappropriate biceps femoris activity during late swing (observed in two subjects). However, no increase in stride length, velocity or GRF thrust peaks accompanied the increased knee extension at toe off. Thus, though the study is still ongoing, it tentatively appears that in contrast to the aquatics exercise program of Gehlsen et al. (1986), a long term cycling program may be beneficial to MS patients.

REFERENCES

Gehlsen G. et al. Arch. Phy. Med. Rehabil., 67, 536-539, 1986.

ACKNOWLEDGMENTS

This work was supported by the Rehabilitation Research and Development Service of the U.S. Department of Veterans Affairs. (grant #92-421A).

SIX DEGREE OF FREEDOM JOINT POWER TO EVALUATE ANTERIOR CRUCIATE LIGAMENT DEFICIENCY IN STAIR CLIMBING

J. Duncan[§], D. Kowalk[†], C Vaughan[§†]

§ Department of Biomedical Engineering, University of Virginia, Charlottesville, VA 22903.
† Department of Orthopaedics, University of Virginia, Charlottesville, VA 22903.

INTRODUCTION

Anterior cruciate ligament (ACL) injuries are the most common ligament injuries of the knee (Johnson, 1983). The ACL provides support to the knee, preventing anterior displacement of the tibia on the femur and hyperextension of the knee joint (Moore, 1992). While previous studies have shown a tendency for patients with ACL deficiency to avoid a knee extension moment in level walking, this tendency has not been shown in stair activities (Berchuck et al., 1990). It has been shown that the knee extension moment in stair activities exceeds that of level walking even in the ACL deficient knee but the mechanism for handling this moment has not been addressed thus far. In this study we investigated these mechanisms to further our understanding of the biomechanical changes in the ACL deficient knee, its reconstruction, and to introduce a six degree of freedom (DOF) model for calculating joint power.

REVIEW AND THEORY

Joint power has been calculated several different ways to date. Most of the published data on joint power consists of a one DOF model: the product of the sagittal plane moment and angular velocity terms.

$$\text{Joint Power} = \mathbf{M} \bullet \omega$$

Buczek and his colleagues (1992) presented a six DOF power model including both rotational and translational terms. However, they neglected to present a true six DOF power curve for the joint as a whole but instead presented three planar graphs. By dividing the power into three graphs instead of presenting one value for power, the importance of the additional degrees of freedom can not be understood. Buczek et al. (1992) presented the equation:

$$\text{Joint Power} = \mathbf{M} \bullet \omega_j + \mathbf{F} \bullet \Delta v$$

This equation was used in the current study by calculating two joint velocity terms and employing two equations for each joint based on the location of passive markers placed according to the Helen Hayes Hospital marker set (Kadaba et al., 1990).

PROCEDURES

Gait analysis was conducted on ten normal subjects (6 male, 4 female, ages 22-40, mass 65.8±11.9 kg) and eight ACL deficient patients: pre-operatively an average of 6.8 months (±6.0) after injury (6 male, 2 female, ages 18-38, mass 90.4±15.8 kg), and post-operatively an average of 6.7 months (±2.2) after their reconstruction (ages 18-39, mass 93.3±13.9 kg). A patellar tendon graft reconstruction was performed on each of the ten patients by the same surgeon. Figure 1 shows the procedure graphically. In this procedure the central third of the patellar tendon is removed with bone wedges on both ends. The tibia and femur are drilled in the original location of the ACL. The graft is passed distal to proximal endoscopically through the holes and held in place using an interference screw at both the proximal and distal ends.

Each subject ascended and descended a staircase which consisted of three steps (22 cm rise, 25 cm run) six times: three trials beginning with the right leg and three with the left. Kinematic and force plate data were collected and analyzed to calculate joint

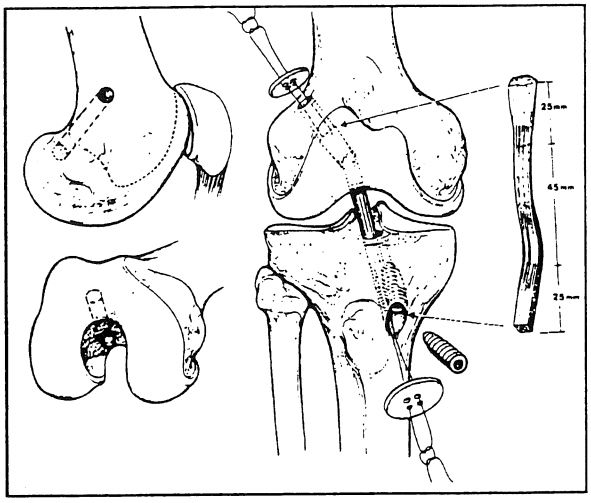

Figure 1 Patellar tendon graft reconstruction.
(Used with permission, O'Brien et al., 1991)

angles, moments, and powers. The data were pooled and statistical analysis of the data using repeated measures MANOVA ($p<0.05$) was performed to identify any adaptations used by the patients to accommodate for the ligamentous deficiency. Repeatability of the six DOF joint power approach was tested using a variance ratio (VR) (Hershler and Milner, 1978).

RESULTS AND DISCUSSION

It was established that six degree of freedom power was significantly different from one degree of freedom power ($p=0.013$ ascending, $p=0.001$ descending) and that the six degree of freedom model presented for calculating joint power had an important contribution to the understanding of trends observed. Figure 2 shows the hip joint power for both one and six DOF models descending stairs for the normal subject population.

It was further established that the six DOF joint power was repeatable both within and between subjects with the inter-subject

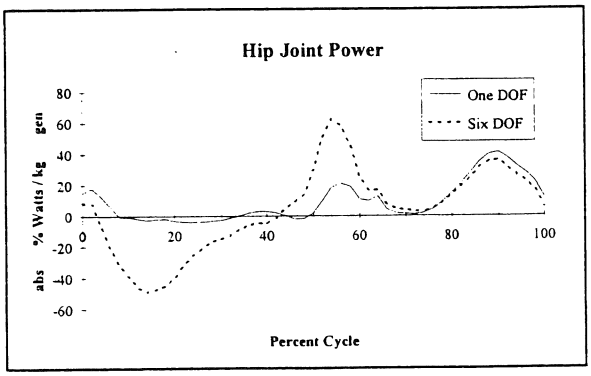

Figure 2 Hip joint power descending stairs

VR's for the hip = 0.17, knee = 0.13, and ankle = 0.20. These compare with the inter-subject VR's of the flexion extension moments of the hip = 0.09, knee = 0.14, and ankle = 0.10.

To understand why patients tend to have more difficulty during level walking than stair ascent, even though the maximum extension moment during stair ascent is larger, the joint forces and moments for a normal knee were observed. It was found that the anterior posterior joint force at the knee does not load the ACL during stair ascent while it does load the ACL during level walking. The decrease in the loading was caused by a decreased step length and tibial orientation during stair ascent. Figure 3 illustrates normal stair ascent. Note first that the step length can be altered even while maintaining the stride length by varying the depth of foot placement on the step as can be seen in the varying placement in the figure. Also note that the proximal end of the tibia never becomes posterior to the distal end throughout the gait cycle. This is the primary difference in stair ascent which allows a more stable gait for ACL deficient patients than level walking.

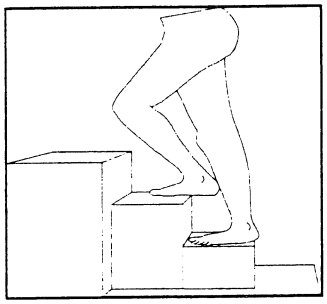

Figure 3 Stair ascent

Post-operatively the patients made one other significant adaptation. They significantly reduced the amount of work done at the affected knee (p=0.001). This was accomplished by altering the step length, as previously discussed, and transferring work away from the injured knee. They transferred the work by reducing the amount of work performed at the knee and increasing the amount of work performed across the hip and ankle, both ipsilaterally and contralaterally. This maintained a constant amount of total work performed. Table 1 shows the net work performed across each joint and the net totals for normal and post-operative subjects. Figure 4 illustrates the power curves for the hip, knee and ankle for normal, injured and uninjured knees post-operatively. Note the decrease in knee power during mid-stance and the increase in power at the ankle just prior to toe-off. In stair ascent, the primary means of elevating the body from one step to the next is the simultaneous extension of the ipsilateral hip and knee with the plantarflexion of the contralateral ankle. This can be seen in Figure 3 where the upper leg has the hip and knee both flexed and the ankle dorsiflexed just prior to lifting the body while the lower leg has the hip and knee fully extended and the ankle in a slightly dorsiflexed position after being raised to the next step. By increasing the work performed at the ipsilateral hip and contralateral ankle, the work performed at the reconstructed knee was decreased. Similar work transfer trends were also observed descending stairs. This trend was not observed pre-operatively. The decrease in post-operative work performed at the injured knee suggest that harvesting of the graft from the ipsilateral patellar tendon decreases the ability for the knee to generate work and may have long term adverse effects.

(J/kg)	Normal		Post-Operative	
	Right	Left	Injured	Un-Injured
Hip	0.59	0.48	0.68	0.72
Knee	0.18	0.35	-0.03	0.27
Ankle	0.47	0.40	0.47	0.50
Total	2.47		2.61	

Table 1 Joint work ascending stairs

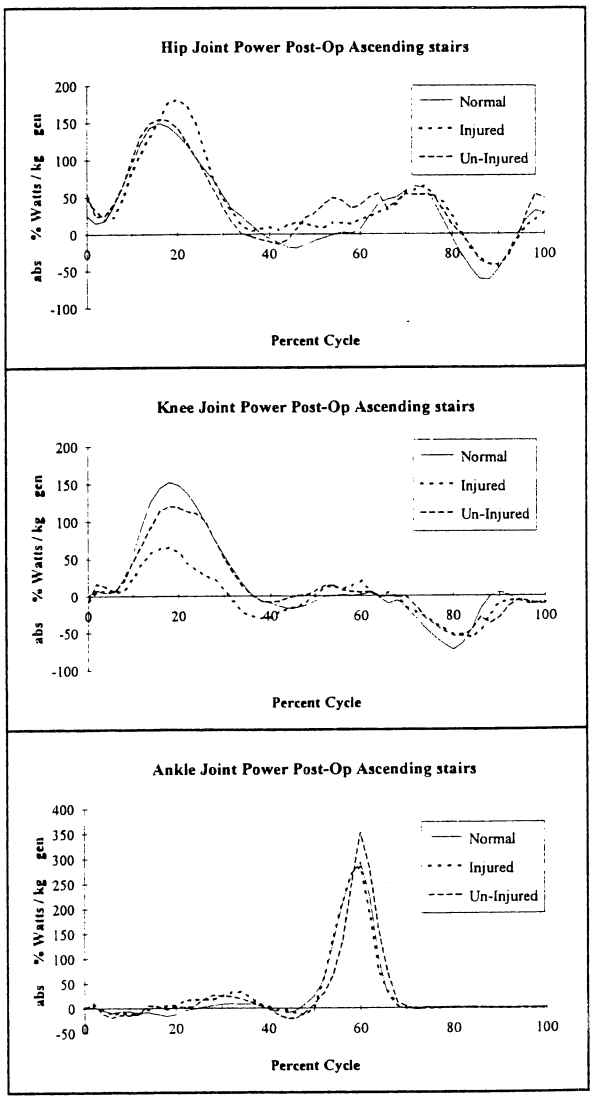

Figure 4 Joint power, post-operative, ascending stairs

REFERENCES

Berchuck, M et al. JBJS, 72-A(6), 871-877, 1990.
Buczek, F et al. NACOB II, Chicago, IL, 503-504, 1992.
Hershler, C, Milner, M IEEE Trans. BME, 25, 413-420, 1978.
Johnson, RJ Clin. Orthop., 172, 14-18, 1983.
Kadaba, M et al. J Orthop. Res., 7, 849-860, 1990.
Moore, K Clinically Oriented Anatomy, Will. & Wilkins, 1992.
O'Brien S et al. JBJS, 73-A(2), 278-286, 1991.

ACKNOWLEDGMENTS

This work was supported in part by grants from the US Department of Education under a Rehabilitation Engineering Training Grant H133P10006-92, and the National Institutes of Health 1 R01 HD30134-01, 5 T32 AR07482.

SESSION 10:

BONE

CHARACTERIZING THE HOMEOSTATIC REMODELING STIMULUS WITHIN THE TURKEY ULNA

D.J. Adams, A.A. Spirt, R.A. Brand, C.T. Rubin*, and T.D. Brown

Departments of Orthopaedic Surgery and Biomedical Engineering, The University of Iowa, Iowa City, IA 52242
*Department of Orthopedics, State University of New York at Stony Brook, Stony Brook, NY 11794

INTRODUCTION

This study reports an account of animal activities and their resultant cortical bone surface strains over a 24 hour period. Quantification of these activities and strain characteristics provides a basis for further testing of bone remodeling rules which examine departures from homeostasis. *In vivo* measurement of longitudinal mid-diaphysis surface strains revealed magnitudes ranging from 30 to 700 με for four wing activity patterns. Observation of a population of male turkeys within their normal commercial environment over 24 hours quantified the number of daily occurrences of each activity pattern. This study demonstrates that higher strain activity patterns occurr less frequently than lower strain activity patterns in the turkey ulna.

REVIEW AND THEORY

Several theoretical bone remodeling rules have recently considered departures from normal daily occurrences of stress/strain stimuli within a bone (Beaupre et al., 1990, Huiskes et al., 1987, Whalen et al., 1988). To implement these theoretical concepts, a complete appraisal of an animal's daily activities and resulting stress/strain histories is essential. As a practical matter, however, very little is known of habitual natural activity patterns and the resulting homeostatic stimuli passed to individual bones.

The isolated avian (turkey) ulna has been the subject of numerous studies of cortical bone adaptation, including direct comparison between experimental surface adaptation and the artificially engendered stress/strain milieu (Brown et al., 1990). Given that normal activities maintain bone mass in homeostatic equilibrium, that functional isolation causes bone resorption, and some regimens cause new bone formation (Rubin and Lanyon, 1984), we assume normal activities provide a background "homeostatic remodeling stimulus." To further investigate the departure of a regimented experimental remodeling stimulus from the background homeostatic remodeling stimuli within the turkey ulna, a survey of ordinary wing activities and resulting stress/strain distributions within the ulna is necessary. The purpose of this study was to document the strains occurring within the turkey ulna for activities observed within a population of commercially-raised turkeys over a complete 24 hour cycle.

PROCEDURES

The study had two parts. First, surface strains on the ulna of one male adult turkey were recorded for various wing activities. Following administration of anesthesia and aseptic exposure of the left ulna, three stacked rosette strain gages (FLA-2-11, Tokyo Sokki Kenkyujo, Inc.) were bonded to the periosteal surface at mid-diaphysis using established *in vivo* techniques (Lanyon, 1975). All wires extended through a small incision in the skin to a connector box clipped to the bird's back, from which a single cable extended via an overhead boom to data acquisition equipment. Following recovery from anesthesia, the bird was returned to the animal facility containing 12 other male turkeys. All 9 channels from three rosettes were recorded in FM analog format on magnetic tape (SE7000, EMI Technology, Inc.). Gage voltages were recorded intermittently over a 24 hour period, providing 6 full hours of strain recordings. Simultaneous video recordings provided a visual record of all activities. Individual activities producing ulnar strains were sampled digitally at 200 Hz, converted to units of microstrain, and resolved into anatomical components.

The second part of the study involved diurnal observation of turkeys within their "normal" commercial habitat. A sub-group of 27 turkeys was followed within a population of approximately 5,000 commercially raised, 19 week old Nicholas turkeys (99% male, average weight 15 kg). A circular pen (11' diameter, 3' high) constructed of welded-wire fence was placed within the confines of a commercial habitat (17,500 square feet single-room building), to provide an area suitable for observation. The pen provided 3.5 square feet per bird, identical to that of the entire habitat. All birds within the observation pen were allowed normal access (ad libidum) to water and feed, as well as routine interactions with other birds and humans.

A VHS format video camera was mounted above the pen, such that the observation group was within the field of view. The video recorder and a monitor were placed in an adjoining room to prevent atypical interaction with the birds. Video recording began at 7 AM, and continued for 24 hours. Dim lights allowed continuous recording through the night. These video recordings subsequently yielded a catalog of wing activities which were categorized and counted. Then, based on *in vivo* strain signals from the first part of the study, representative strain signals from each category were analyzed, to elucidate background remodeling stimuli.

RESULTS

The entire population of 5,000 turkeys remained quiescent for extended periods during night hours, while the highest level of activity occurred at sunrise. Activities which produced ulna strains were grouped into four categories: (1) moderate wingflap, (2) small wingflap, (3) wing extension, and (4) wing adduction. Strain signals corresponding to these four wing activities demonstrate great variability in strain magnitude (Figure 1). Peak *in vivo* (mid-diaphysis) ulna strains ranged from approximately 30 microstrain (με) for wing adduction to as high as 700 με for moderate wingflap (Table 1). Direct observation of turkeys over 24 hours revealed substantially fewer high strain magnitude events than low strain magnitude events (Table 2).

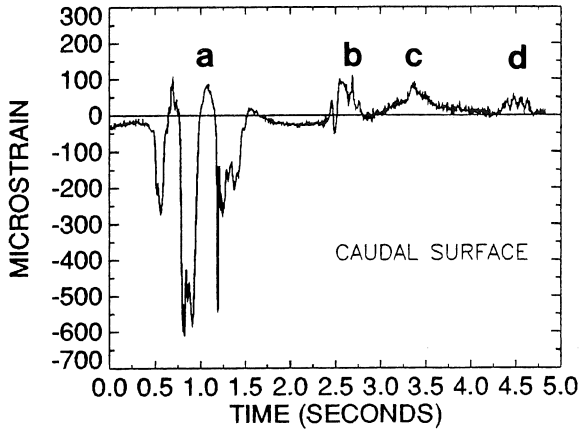

Figure 1: *In vivo* mid-diaphysis longitudinal strain recordings for four types of observed wing activity: (a) moderate wingflap, (b) small wingflap, (c) wing extension, (d) wing adduction.

Wing Activity	Peak Long. Strain (με)
Moderate wingflap	600-700
Small wingflap	150-300
Wing extension	80-120
Wing adduction	20-30

Table 1: Approximate range of peak *in vivo* mid-diaphysis longitudinal strain on the caudal surface of the turkey ulna for normal wing activities.

Wing Activity	Average Daily Number
Moderate wingflap	1.3*
Small wingflap	6.2 **
Wing extension	17.6
Wing adduction	34.7

* episode of 1-2 beats ** episode of 2-3 beats

Table 2: Average daily wing activities of male turkeys in their normal environment (#/bird/24 hrs).

DISCUSSION

An important observation of our study is that higher strain activities occur less commonly than lower strain activities. Rubin and Lanyon (1984) demonstrated that as few as four loading cycles at peak physiological magnitude (wingflap) maintained cortical integrity of the isolated turkey ulna. Given that only 2-3 cycles of moderate wingflap were observed over a 24 hour period in this study, experimental stimuli consisting of a small number of high magnitude strain cycles do not necessary reflect a "small" homeostatic stimulus.

Recent experimental data (McLeod and Rubin, 1994) suggest that strain magnitude interacts with cycle frequency and daily number of cycles in a dose-response fashion to maintain bone mass. This suggests that the relative contribution of each wing activity to homeostasis is a function of magnitude, frequency (and/or strain rate), and number of daily occurrences. Further elucidation of this relationship will provide a basis upon which the effects of departures from homeostasis can be determined.

REFERENCES

Beaupre et al., *J Orthop Res* 8(5):651-661, 1990.
Brown et al., *J Biomech* 23:893-905, 1990.
Huiskes et al., *J Biomech* 20:1135-1150, 1987.
Lanyon et al., *Acta Orthop* 46:256-268, 1975.
McLeod & Rubin, *40th Trans ORS*, 19:564, 1994.
Rubin and Lanyon, *JBJS* 66A:397-402, 1984.
Whalen et al., *J Biomech* 21:825-837, 1988.

ACKNOWLEDGEMENTS

Financial assistance provided by NIH AR-40411. The authors appreciate the technical assistance of Xi-Yia Qin and Ted Gross, and the cooperation of Gene Troyer, Mike Knerr and Louis Rich, Inc.

CONTRIBUTION OF BONE'S CONSTITUENTS TO THE ANISOTROPIC PROPERTIES OF OSTEONAL BONE

A. Chandran*, R. M. V. Pidaparti*, and C. H. Turner**

*Department of Mechanical Engineering, **Department of Orthopaedic Surgery
Biomechanics and Biomaterials Research Center
Indiana University and Purdue University at Indianapolis, IN 46202

INTRODUCTION

The anisotropic elasticity of whole bone and its constituent materials (collagen and mineral) were obtained experimentally. Rule of mixture theory was applied to predict the stiffness of whole bone in the off-axis directions (longitudinal - radial plane) as a function of its constituent materials.

Ten specimens with different angular orientations from 0 (longitudinal) - 90 (transverse) at 10 degree increments, were collected from each of 24 canine femora. Whole bone stiffness for all orientations was obtained using 50 MHz (high frequency) pulse-echo ultrasonic techniques. Of these 24 femora 11 were demineralized in 10% EDTA solution, and 13 were decollagenized in 7% hypochlorite solution. The anisotropic elasticity of the individual constituents was measured using the 50 MHz (high frequency) pulse-echo ultrasonic techniques.

The mineral phase exhibited a large anisotropy ratio (C_L/C_T) of 1.4, close to the anisotropic ratio of 1.5 measured for whole bone. The anisotropy ratio for collagen was found to be 1.1. A modified rule of mixture theory was used to fit the experimental data. The empirical relation developed was found to closely match the experimental data obtained.

REVIEW AND THEORY

Bone is a complex composite material. Many theories have been proposed to describe its microstructure, and anisotropic elasticity. This study presents the most complete data available on cortical bone's anisotropic elasticity and the anisotropic elasticity of its major constituents collagen and mineral. An empirical model including microstructural components is presented to better understand bone's macroscopic behavior.

Traditionally bone is thought to be composed of 60% mineral, 25% collagen, and 15% water. There has been much debate as to the actual microstructural arrangement of mineral and collagen in bone. Weiner and Traub (1992) proposed that the basic building blocks of bone are the small plate shaped crystals of carbonate apatite (several hundred angstroms long and wide and 20 - 30 angstroms thick). These crystals are arranged in parallel arrays inside the collagenous framework. The mineral filled collagen fibers are then organized into arrays. Weiner and Traub (1992) further speculated that bone material is arranged in a rotated plywood configuration.

There have been many other theories on collagen orientation. Gebhardt(1906), Von Ebner (1874), and Weldenresch (1923) proposed that fiber orientation is abruptly changed from longitudinal to transverse orientation from lamellae to lamellae. Ranvier (1875) and Zeigler (1908) proposed that the appearance of lamellae was caused by alternating differences in collagen - mineral ratio, and not orientation. Ruth (1947) and Roullier (1956) concluded that the differences in appearance from lamellae to lamellae were partly due to collagen orientation. They proposed that the differences in appearance were due to alternating "compact lamellae" (transverse structure proposed by Ruth, and vertical structure proposed by Roullier), and "diffuse cementing lamellae".

Marotti and Muglia [1988], based on studies of a cross- and longitudinally-sectioned single lamellae, proposed that there is no difference in orientation of collagen fiber bundles from lamellae to lamellae. They postulate that the difference in appearance of alternating lamellae is caused due to differences in collagen packing density. These SEM findings do not illustrate any clear orientation for the collagen fiber labyrinth.

As indicated earlier and emphasized by the preceding discussion there are many confounding theories on collagen fiber orientation. One of the objectives of this study is to provide evidence of any orientation of collagen fiber or apatite crystals by studying their anisotropic elasticity.

PROCEDURES

Twelve pair of canine femurs were obtained from skeletally mature mongrel dogs. Ten sections with different angular orientations 0 (longitudinal) - 90 (transverse) at 10 degree increments, were collected from each of 24 canine femora. Bone tissue elasticity for all orientations was obtained using a UH3 acoustic microscope (Olympus) with a 50 MHz lens (V-390, Panametrics, Waltham, MA). Specimen preparation, and measurements required to calculate stiffness are described in the next section.

High Frequency Techniques::

Specimen Preparation:
The proximal 5 cm of the mid-diaphysis of each femur was used in the high frequency (50 MHz) tests. First, the proximal 5 cm is mounted onto specimen holder, with mid-diaphysis exposed. Specimen holder is then attached to the appropriate interface (0 - 90 degrees) using a metal leaf. The assembly is then mounted on the wire saw. A 500 μm thick specimen is obtained and removed of marrow. The thickness was measured using a Mitutoyo micrometer (resolution of 1 μm). The specimen was placed in a biopsy cassette in a physiological saline solution. These steps are repeated to obtain 10 specimens at 10 degree increments from the longitudinal - radial direction.

Density measurements
Specimens were trimmed leaving only the anterior portion of the cross-section. Wet weights and submerged weights were made using a Mettler AJ100 balance (Mettler Instruments Corp., Highstown, NJ). The submerged weight was measured by immersing wet bone in 70% EtOH solution. Wet density of the specimen was calculated using Archimedes' principle .

Acoustic Velocity Measurements
The high frequency measurements were made using the Olympus UH3 Scanning Acoustic Microscope. Specimens were mounted to the bottom of a chamber in the UH3 SAM. The chamber was then filled with distilled water and brought to a temperature of 24 °C. A 50 MHz lens (V-390, Panametrics, Waltham, MA) was used to transmit, and receive acoustic waves in pulse-echo mode. Delay time between acoustic waves reflected at the top of the specimen and those reflected from the bottom of the specimen was measured using a digital oscilloscope (TDS 620, Tektronix Inc., Beaverton, OR). Acoustic velocity for the pulse echo technique described above is calculated as twice the specimen thickness divided by the delay time. The elastic stiffness coefficient at each angular orientation was obtained as the product of density and velocity squared for each specimen.

Demineralization:

The right femur of sets 1 - 11 were subsequently placed in 10% Ethylenediaminetetraacetic acid (EDTA) solution, for demineralization. The specimen contained in Biopsy cassettes were left in solution (refrigerated) for a period of 72 hours. This procedure dissolves and removes hydroxyapatite crystals leaving behind the organic framework. After demineralization, the specimens were rinsed in distilled water. Wet weight

measurements were taken to determine the mass of collagen in specimen. Using the same volume calculated for the whole bone specimens, density was calculated for the demineralized specimens. Methods used for the acoustic velocity measurements for collagen were the same as those employed for bone tissue.

Decollagenization:

The left femora of sets 1 - 11, and both femora of set 12, were placed in 7% hypochlorite solution for decollagenization. The specimen to be decollagenized contained in biopsy cassettes were left in 7% hypochlorite solution (refrigerated) for a period of 120 hours. This procedure dissolves and removes collagen fibrils (and other organic constituents) leaving behind the mineral platelets. Density and velocity measurements were obtained using the same procedure as for collagen.

Composite Model:

A composite model was developed based on the modified rule of mixture theory, and component data. Bone tissue data, and collagen data obtained from this study were used in the model.

A third degree polynomial of the form,

$$\text{Stiffness}(\theta)=6.6e\text{-}06(\theta)^3-0.001(\theta)^2+0.03(\theta)+3.48$$

was used to fit the collagen data, and predict the off-axis stiffness of collagen. Results indicate a collagen orientation of 30 degrees from the long bone axis.

Literature based values were used in an orthotropic model for the mineral phase. Values for the orthotropic stiffness constants as reported by Katz and Ukraincik (1971) were used. The constants C11, C22, C12, and C66, were respectively 172 GPa, 137 GPa, 54.9 GPa, and 39.6 GPa. Volume fractions of 60% mineral (25% inside collagen, 75% outside collagen), and 25% collagen were assumed in this study. Collagen and the mineral component inside the collagen were taken to be oriented at 30 degrees. The orientation of mineral outside collagen fibrils was varied to fit the experimental data for whole bone. Correction factors dB and AR were applied to mineral properties to account for imperfect bonding between collagen and mineral, material flaws and geometric effects.

RESULTS

The mean longitudinal and transverse elastic coefficients for bone tissue were calculated to be 34.46 and 22.9 GPa, respectively. The anisotropic ratio (ratio of longitudinal to transverse elastic coefficients) for bone was calculated to be 1.5. The mean longitudinal and transverse elastic coefficients for mineral were found to be 22.44 and 16.22 GPa, respectively. The anisotropic ratio calculated for mineral was found to be 1.4. The mean longitudinal and transverse elastic coefficients for collagen were calculated to be 4.09 and 3.57 GPa, respectively. The anisotropic ratio for collagen was found to be 1.1. There was a local maxima in collagen elasticity found at 30 degrees. These results are shown in Figure 1.

The composite model developed best fit whole bone data when dB was assumed to be 0.285, and AR was assumed to be 1.15. These results are shown in Figure 2.

DISCUSSION

The mineral data obtained has a large standard deviation, and are non-uniform. The data shows a great deal of scatter. Scatter in the data might be due to variability of the effect of sodium hypochlorite on bone specimens. They may also be due to inhomogeneous microstructure. It is known that hydroxyapatite crystals themselves have a high modulus when compared with bone modulus. A higher local concentration of mineral at the location of measurements might cause large deviations.

The composite model closely fits the experimental data for whole bone. However, the physical meaning of the values used for constants dB and AR in the model is not known. Further study into the nature of the bonding between organic and inorganic constituents of bone is warranted.

ACKNOWLEDGMENT

The authors thank the Whitaker Foundation for their support..

REFERENCES

Weiner and Traub, The FASEB Journal, Vol. 6, pp 879 - 885, 1992..

Gebhardt W., Arch. Entw Mech. Org.,Vol. 20, pp. 187 - 322, 1906.

Von Ebner V., Arch Mikrosk Anat., Vol. 29, pp. 213 - 236, 1887.

Weldenresch F., Zeitschrift fur. Anat. und Entwick., Vol. 69, pp. 382 - 466, 1923.

Ranvier J., Traite technique d'histologie, 2nd ed., Savy, Paris., 1889.

Zeigler O., Dtsch. Z. Chir., Vol. 85, pp. 248 - 262, 1906.

Ruth E. B., Am. J. Anat., Vol. 80, pp. 35 - 47, 1947.

Rouiller C., The Biochemistry and Physiology of Bone, Academic Press NY, pp. 104 - 147, 1956.

Marotti and Muglia, Arch. Ital. Anat. Embriol., Vol. 93, pp. 163 - 175, 1988.

Katz J. L. and Ukraincik K., J. Biomechanics, Vol. 4 pp. 221 - 227, 1971.

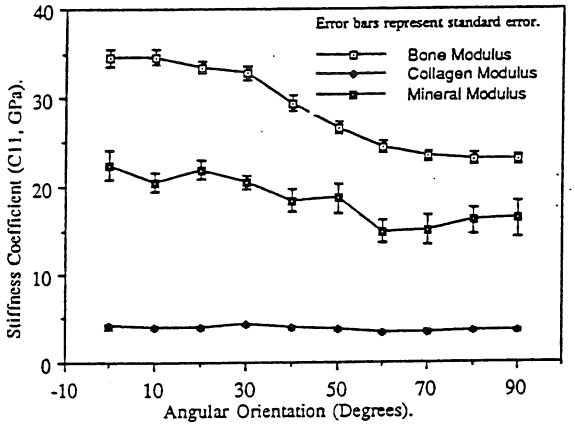

Fig 1: Experimentally obtained anisotropic elasticity of bone and its constituent materials.

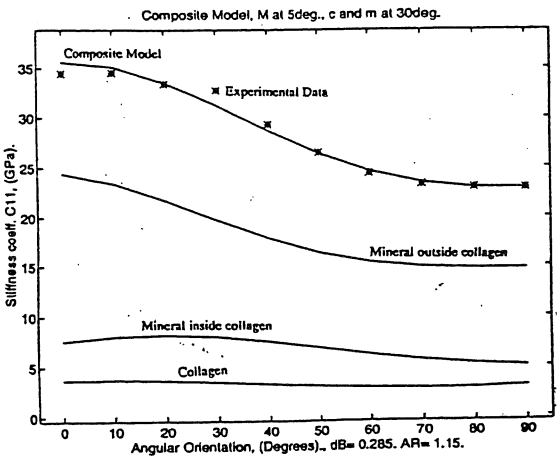

Fig 2: Composite model compared with experimental data.

DETERMINANTS OF LONG BONE STRUCTURAL PROPERTIES

T.M. Cleek, B. Katz and R.T.Whalen

Life Science Division, NASA/Ames Research Center, Moffett Field, CA. 94035

INTRODUCTION

The objective of our research is to determine whether a non-invasive determination of long bone cross-sectional areal properties using only the mineral component of bone accurately predicts the true structural properties. In this study section properties of a whole long bone were compared using two methods: (1) special analysis of bone densitometry data (Martin & Burr, 1984, Cleek & Whalen, 1993), and (2) experimental determination of flexural rigidities from bone surface strain measurements during controlled loading (Gies & Carter, 1982).

REVIEW AND THEORY

Cross-sectional area, centroid, and the second moment of area of the mineralized tissue in the plane of the x-ray beam can be computed by integrating pixel bone mineral content or aluminum thickness across the scan width as proposed by Martin and Burr (1984). The discretized equations are

Cross-sectional area, A_t: $A_t = \Sigma\, t_i\, \Delta x$

Centroid, x^*: $x^* = (1/A_t)\, \Sigma\, x_i\, t_i\, \Delta x$

Second moment of area, I_y: $I_y = \Sigma\, (x_i^2 - x_i\, x^*)\, t_i\, \Delta x$.

The summation is across the phantom or bone width, t_i is the phantom or bone mineral thickness at the ith pixel obtained from raw attenuation data, and Δx is the pixel width (see fig. 1).

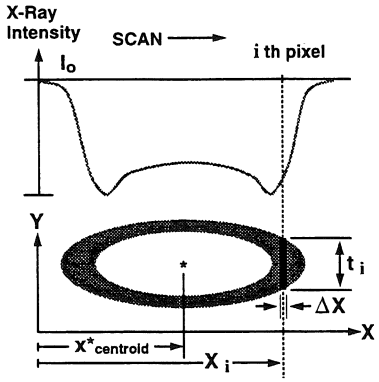

Figure 1: Cross-sectional area, centroid, and moments of inertia are computed by integrating pixel bone mineral content (BMC) across the scan width.

Independent analyses of 3 non-coplanar scans are used to obtain principal moments and orientations at each cross-section. Maximum and minimum second moments of area are calculated by the diagonalization of the moment matrix. Components of the transformation matrix are direction cosines of the principal axes which are orthogonal to each other (see figure 2). Section properties from cross-sections along the length of the bone are then combined.

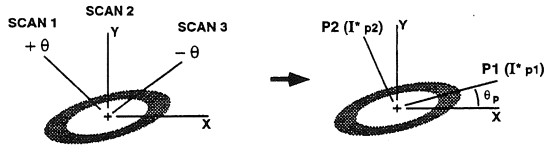

Figure 2: Principal moments of inertia (Imin, Imax) and orientations of principal axes (θp, θp + 90°) are determined from independent analyses of 3 scans.

PROCEDURES

Section principal area moments of inertia and major axis orientation from bone densitometry: The proximal end of an embalmed human female right tibia was potted with bone cement and inserted into a precision indexer. Using a precision (±0.1°) inclinometer, the tibia was oriented with the medial-lateral plane normal to gravity, which was chosen as the reference orientation for the experiment. Three scans were taken of the entire tibia with an Hologic QDR-1000/W densitometer at rotations of 0°, 45°, and 90° about the tibia long axis. The tibia long axis was perpendicular to the scan plane and all scans started at the same point. Pixel attenuation data from the high energy beam were first converted to equivalent aluminum thicknesses using an aluminum calibration wedge, and then used to compute area moments (zeroeth, first, and second) line by line for each of the scans (Martin & Burr, 1984). The principal area moments of inertia and orientation of the principal major axis at each line, i.e., bone cross-section, were determined by combining the areal properties obtained from independent analyses of the three scans (Cleek & Whalen, 1993).

Section principal flexural rigidities and major axis orientation from surface strain measurements: After scanning, four single element strain gages, aligned along the long axis of the tibia were bonded uniformly around the circumference at each of four cross-sections (0.35, 0.49, 0.63, and 0.77 l_0 measured from the proximal end, sections 1-4 respectively). Beginning with the medial-lateral plane in the reference orientation, a known load producing a known bending moment at each cross-section was hung vertically from the distal end of the tibia. Strain data were recorded from all strain gages as the indexer was rotated through 360° in 45° degree increments. To compute flexural rigidities (defined as $I^*_x = \int E(x,y) y^2 dA$, $I^*_y = \int E(x,y) x^2 dA$) from strain gage data, curvatures were computed from strain data; the section centroid was then calculated from curvatures and strains; and finally, section flexural rigidities about the centroid were derived from simultaneous solution of equations using the known curvatures and known bending moments (Gies & Carter, 1982).

	Principal Angle (deg)		Isotropy Index		Effective E (GPa)	
Section	Strain measurement	Densitometry	I*min/I*max (strain)	Imin/Imax (densitometry)	I*max/I_1	I*min/I_2
1	-57.4	-53.7	.47	.48	29.94	29.11
2	-53.7	-55.2	.56	.58	33.46	32.18
3	-40.8	-43.4	.63	.59	33.26	35.52
4	-17.0	-25.3	.88	.84	30.06	31.32

Table 1. Summary of bone section data

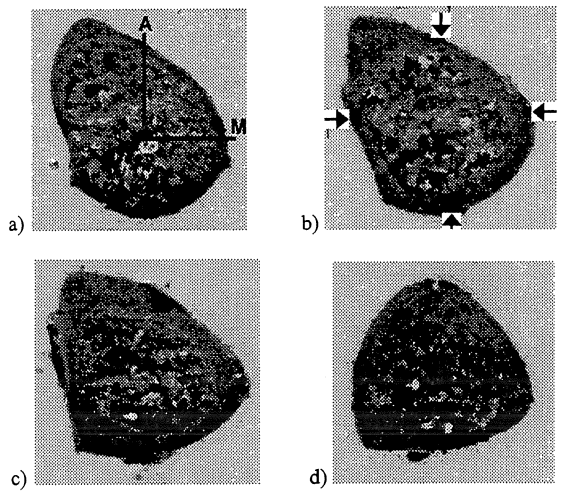

Figure 1 a-d. The tibia was sectioned following completion of testing. Sections 1-4 from a to d Section 1: Anterior and medial directions are identified as "A" and "M". Section 2: arrows indicate gage locations. Coordinates of gages with respect to the reference plane and coordinate system were obtained using an x-y table.

RESULTS

The principal major axes of the bone mineral computed non-invasively by densitometry compared well with those for flexural rigidities computed from surface strain measurements (Table 1 and Figure 2). The mean difference in the angle was 2.2 ± 4.9°. The principal area moments of inertia of bone mineral were linearly related (r=0.99) to the principal flexural rigidities (Figure 3). The isotropy indices (I*min/I*max derived from strain measurements and Imin/Imax from densitometry) were also very similar at each of the four bone sections.

About each principal flexural plane, we computed an "effective" elastic (flexural) modulus, $E_{effective}$, as the experimental flexural rigidity (I*max or I*min) normalized by the area moment of inertia (I_1 or I_2) of the bone mineral transformed to the principal flexural coordinate system. These values for $E_{effective}$ differed by only -0.33 to 0.39% from calculations using Imin and Imax since the principal angles from the two methods were closely aligned. From Table 1, effective moduli are somewhat higher in the mid-section, and are not consistent with respect to the major and minor flexural plane. The average value of $E_{effective}$ from Table 1 is 31.8 ± 2.2 GPa, while the value from pooled data is 29.7 GPa (see Figure 3).

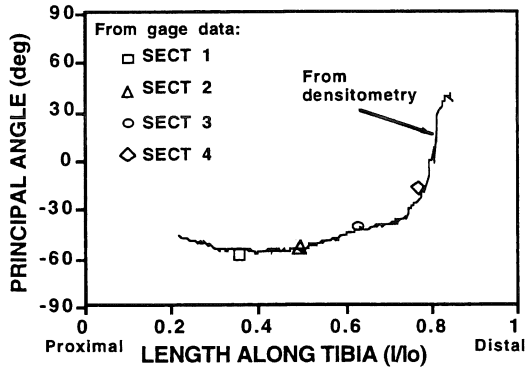

Figure 2. Principal angle of the major axis. Coordinate frame (viewed from distal end): 0°-medial; 90°-anterior; -90°- posterior.

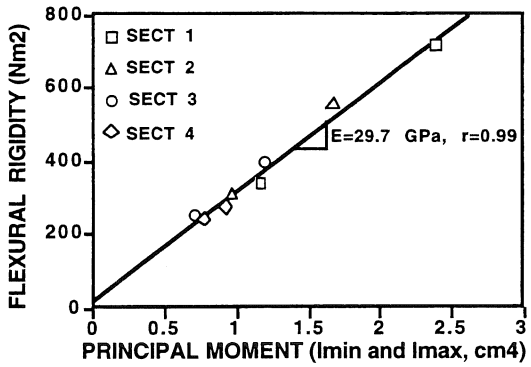

Figure 3. Principal flexural rigidities from strain vs. Imin and Imax from densitometry. Slope E (effective elastic modulus) is calibrated to aluminum. Preliminary calibration to bone tissue using Hologic software yielded an effective elastic modulus of bone of 27.3 GPa. This compares well to measures of E = 26.9 GPa for fresh (bovine) bone with ~3% porosity (Schaffler & Burr, 1988).

DISCUSSION

The results and correlations from this tibia are striking. We have recently done the contralateral tibia and found very similar results. The mean difference in principal angle for four sections on the left tibia were 0.16 ± 1.52° and the value of $E_{effective}$ from the pooled data was 26.56 GPa (r=0.96). The agreement we found using two different methods was excellent and may improve as we continue to refine our experimental technique. Independent of bending orientation or measurement site, the variation in the effective elastic (flexural) modulus is significantly less than the range of values reported in the literature for compact bone (Schaffler & Burr, 1988, Mammone & Hudson, 1993). The value we obtained from our preliminary calibration to bone tissue is close to the value reported for compact bone of low porosity indicating that non-linear factors associated with porosity and microstructure, measured from excised machined specimens (Schaffler & Burr, 1988), may be modulated in whole bone.

Our measurements of elastic modulus may not be surprising for predominantly dense cortical bone regions (sections 2 and 3), which are expected to be more uniform. Remarkably, section 4 with a higher concentration of cancellous bone, with a tissue modulus reported to be considerably below cortical bone (Ryan & Williams, 1989), also yielded a high $E_{effective}$ (see Figure 1d). It appears that the amount and distribution of bone mineral are the predominant contributors to whole bone mechanical properties. We would expect these relationships to change, or change the $E_{effective}$, in young or diseased bone.

REFERENCES

Martin , B. & Burr, D. J. Biomech., 17, 195-205, 1984.
Cleek, T.M. & Whalen, R.T. Conf. Proc. of American Society of Biomechanics, (p. 125), 1993.
Gies, A.A. & Carter, D.R. J. Biomech., 15, 297-303, 1982.
Schaffler, M.B. & Burr, D.B. J. Biomech., 21, 13-16, 1988.
Mammone, J.F. & Hudson, S.M. J. Biomech., 26, 439-446, 1993.
Ryan, D.R. & Williams, J.L. J. Biomech., 22, 351-355, 1989.

ACKNOWLEDGEMENTS

Thanks to B. Jenny Kiratli, Ph.D. for her assistance.

INCREASED BONE BLOOD FLOW PRECEDES DISUSE INDUCED BONE LOSS

Ted S. Gross, Michael R. Doschak, Robert C. Bray, and Ronald F. Zernicke

McCaig Centre for Joint Injury and Arthritis, Department of Surgery
University of Calgary, Calgary, Alberta, Canada T4N 2N1

INTRODUCTION

Bone is able to rapidly alter its mass and morphology in response to mechanical stimuli. Although the process by which bone's resident cells perceive and respond to these stimuli is complex and poorly understood, recent research suggests that the vascular supply of the tissue may actively mediate bone adaptation. By examining blood flow alterations in a model of disuse osteopenia, this study begins to assess whether the induced vascular adaptations precede, occur concurrently with, or follow the cellular and tissue adaptations precipitated by disuse. After four weeks of disuse, resorptive activity was evidenced by heightened intracortical porosity and scalloped endosteal borders, but cross-sectional areal properties had not yet been significantly altered. Blood flow within the bones deprived of mechanical stimuli was, however, significantly increased compared to intact contralateral controls.

REVIEW AND THEORY

Description of bone's vascular supply as an active mediator of tissue adaptation (as opposed to an entirely passive mechanism of cellular and nutrient transport) was reported in the early 1800's (1). These initial observations have been recently complemented by data at the cellular and molecular levels indicating that endothelial cells express peptides that directly act upon bone cell populations (2), and that these factors may act as paracrine regulators of bone cell activity (3). In a preliminary study, we assessed subchondral bone degradation and bone blood flow alterations induced by joint laxity and found that *increased* subchondral bone blood flow was associated with *enhanced* bone tissue degradation (4). In order to further pursue the general hypothesis that vascular adaptation mediates skeletal adaptation, we have developed the ability to assess bone blood flow in a model of disuse osteopenia. As the time course of osteoclastic recruitment and subsequent bone resorption concomitant with disuse is well established in this model (5), this study begins to identify the temporal relationship between blood flow alterations and the cellular and tissue adaptation precipitated by the loss of function.

PROCEDURES

The left ulna of three adult leghorn roosters (1 yr) were isolated from mechanical stimuli via parallel metaphyseal osteotomies (6). Small (2 mm thick) wafers of bone were removed at either metaphysis, and the exposed diaphyseal bone ends were covered with methacrylate filled delrin caps. The right ulna served as an intact, contralateral control. After 4 wk in which the animals freely ambulated (but the left ulnae remained unloaded due to the osteotomies), the animals were again anesthetized, and the left ventricle cannulated retrograde from the right carotid artery. Placement was confirmed by a pressure transducer in line with the cannula. Colored microspheres in mixed suspension with saline (4 million, 15.5 μm dia.) were sonicated, vortexed for 5 min, and then injected into the left ventricle over a 30 s period. Starting 10 s prior to the injection, a reference blood sample was drawn for 1 minute at 3 ml/min from a second catheter placed in the anterior tibial artery. After sacrifice, kidney, lung, and reference blood samples were removed and digested in 7 ml of 4M KOH. Using a diamond wafer saw, 200 μm cross-sections were extracted from the mid-diaphysis of the experimental and control ulnae. An 8 mm long section extending distally from the mid-diaphysis was then removed from each bone. The 200 μm sections were ground to 125 μm, photographed, enlarged and digitized to determine areal properties (total area, periosteal envelope, endosteal envelope, and intracortical porosities). The thick sections were cleansed of marrow, decalcified for 3 days in 10% HNO_3, and then digested in 4M KOH. The microspheres within these samples were isolated by filtering the digested tissues through a 7 μm polyester filter, and then directly counted with an epi-fluorescent microscope. Spheres within the reference blood sample, kidney, and lungs were assessed by eluting the dye from the trapped spheres with DMF and applying spectrophotometer readings to manufacturer calibration curves. Standardized blood flow within a sample (ml/min/100g) was determined by relating the sphere count to that determined for the reference blood sample and normalizing to the mass of the sample. Differences between the experimental and control ulnae were assessed using paired t-tests ($p=0.05$).

RESULTS

Mean standardized blood flow values (± S.D.) for the left (406 ± 208) and right (448 ± 313) kidneys were statistically equivalent. Lung blood flow was also symmetric between the left (95 ± 49) and right (90 ± 44) organs. Mean standardized blood flow in the experimental ulnae (18.1 ± 6.7) exceeded that of the control ulnae (14.6 ± 5.8) by 24.0% (Fig 1). Within animals, increased flow to the experimental bones ranged from 21.9% to 29.6%. However, four weeks of disuse was not sufficient to alter the areal properties of the experimental ulnae as compared to their intact, contralateral controls (Fig 2). Cross-sectional area was nearly identical for the control (12.5 ± 1.3 mm^2) and experimental (12.6 ± 1.4 mm^2) ulnae. The periosteal (2.7%) and endosteal envelopes (4.8%) were both slightly elevated in the experimental sections. The total area incorporated by intracortical porosities was small, but elevated two-fold in the experimental sections (0.4 ± 0.3 vs 0.2 ± 0.2 mm^2).

DISCUSSION

The left/right symmetry of standardized blood flows measured in the kidneys and lungs indicates adequate mixing and distribution of the injected microspheres. Standardized blood flow determined for the control ulnae was greater than that previously reported for canine cortical bone (8 ml/min/100g; (7)), but this difference may be due to elevated avian blood pressure and/or unique microcirculation patterns as compared to mammals. The 4 wk of disuse was sufficient for the recruitment of pre-osteoclasts and the onset of resorption (evidenced by heightened intracortical porosity, and the presence of scalloped endosteal borders), but insufficient for the demonstration of significant tissue level bone loss. Each of the three animals, however, demonstrated similarly elevated blood flow in the bone deprived of mechanical stimuli. We conclude, therefore, that vascular adaptations are initiated by disuse, are evident at the onset of resorptive activity, and precede tissue bone loss. Future studies will assess whether these blood flow changes precede the onset of resorptive activity.

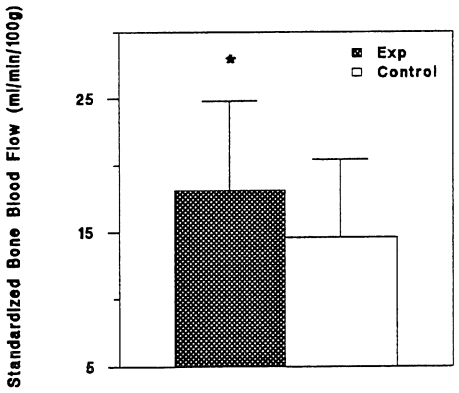

Figure 1. *Mean (± S.D.) standardized cortical bone blood flow in the experimental and intact, contralateral control ulnae. Blood flow in the experimental bones was significantly increased by 4 wk of disuse (p=0.05).*

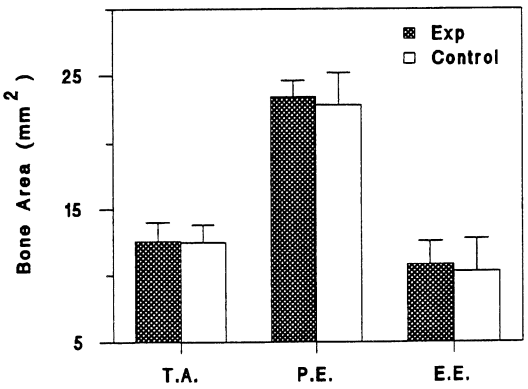

Figure 2. *Mean (± S.D.) mid-diaphysis cross-sectional areal parameters for the experimental and control ulnae. No statistical differences were noted in total area (TA), periosteal envelope (PE), endosteal envelope (EE), or intracortical porosities (not shown).*

REFERENCES

1. Jaffe, *Arch Surg,*20(3): 355-385, 1930.
2. Alam, et al., *Endocrinology,* 130:3617-3624, 1992.
3. Fiorelli, et al., *J Bone Miner Res,* 9(3): 329-337, 1994.
4. Gross, et al., *2nd World Congress*, in press.
5. Bain, et al., *J Bone Miner Res,* 5(S2):S217, 1990.
6. Rubin, et al., *J.B.J.S.*, 66A: 397-402, 1984.
7. Li, et al., *J Orthop Res*, 7:61-67, 1989.

ACKNOWLEDGEMENTS

This work was supported by The Arthritis Society, Medical Research Council, and the Alberta Heritage Foundation for Medical Research.

An Analysis of Strains Surrounding Lacunae and Canaliculi

BA Riemer and SJ Hollister
Orthopaedic Research Laboratories
University of Michigan
Rm. G-0161 400 N. Ingalls, Ann Arbor, MI 48109-0486

INTRODUCTION

It is generally believed that bone adapts to its mechanical environment. How bone cells sense the need to adapt has not been determined. Strain levels at the whole-bone level have been determined, and cell stretching experiments have been used to determine the response of cells to various strain environments. The relationship between the whole-bone strains and those seen by the cells, however, has not been sufficiently described. Since it is impossible to directly measure cellular level strains within the bone, analytical methods must be used to estimate these strains. This paper describes a method to estimate, using homogenization theory, the strains surrounding a representative lacuna and canalicula within a portion of trabecular bone previously analyzed by Hollister and co-workers (Hollister and Kikuchi, 1994; Hollister and Goldstein, submitted). The results show that the peak strain levels in the matrix surrounding both the lacuna and canaliculi are similar, approximately two times those determined for the trabecular level, and three to four times those at the whole-bone level. This suggests that the cell stretching experiments in general investigate strains which are of the same order as or greater than those seen in a physiologic in vivo state.

REVIEW AND THEORY

Many investigators have shown that the bone cells respond to various levels of strain. For example, increases in prostaglandin (PGE2) production have been induced by strains of 10,000 με (Harell et al) and between 50,000 and 100,000 με (Yeh and Rodan). Most cell-stretching experiments, including these, have been carried out at strain levels which are much higher than those measured at the whole-bone level, and therefore appear to be difficult to extrapolate to the physiologic *in vivo* case. However, it has been shown (Hollister and Kikuchi, 1994) that there is an amplification of strain as one looks at more microscopic levels of structure. In order to compare strain levels in the bone matrix surrounding cells and the strain applied to cells in the *in vitro* cell-stretching experiments, it is important to determine the mechanical environment in the bone tissue at the level of lacunae and canaliculi.

Modeling the mechanical environment of an individual cell using a whole-bone model is impossible even with today's computing technology. Homogenization theory is a technique which has been used to analyze the mechanical behavior of composites, including bone, at different microstructural levels. The details of homogenization theory as applied to bone have been discussed elsewhere (Hollister et al., 1994; Hollister and Kikuchi, 1994). The basic assumptions of the method are the following: the total displacement may be written as an asymptotic expansion of displacements at each level of microstructure; the coordinates at one level are related to the next microscopic level by

$$x_{i+1}=x_i/\eta$$

where x_{i+1} is the more microscopic level and η is the characteristic size of the microstructure; and displacements at the representative volume element boundaries are periodic. Using the equilibrium equation on the more microscopic level, the local structure matrix may be determined. The effective stiffness may then be calculated as:

$$[C_{i-1}]=\{\int_{RVE}[C_i][M_i]dV_{RVE}\}/V_{RVE}$$

where $[C_{i-1}]$ is the stiffness of the i-1 (more global) level, $[C_i]$ is the stiffness of the i^{th} structural level, V_{RVE} the representative volume element volume, and $[M_i]$ is the i^{th} level local structure matrix. The global level strain is found from the equilibrium equation under applied boundary conditions. The strains at any given level may then be obtained from the strains at the next more microscopic level with the equation:

$$\{\varepsilon_i\}=[M_i]\{\varepsilon_{i-1}\}$$

where $\{\varepsilon_i\}$ is the strain at the more microscopic level, $\{\varepsilon_{i-1}\}$ is the strain at the more macroscopic level, and $[M_i]$ is the local structure matrix for the i^{th} level.

Hollister and Kikuchi (1994) have shown that a whole-bone strain of 495 με result in strain levels of -1000 to 7000 με in the trabecular bone tissue. They found strains of 782 to 2530 με around the lacuna, when the applied strain was the vector {1325, 287, 80} με. Their study, however, did not investigate the strains surrounding the canaliculi or the effects of varying lamellar properties. This study, then, will utilize the strain level at the trabecular level found by Hollister and Kikuchi, but determine the state of strain around a lacuna and canaliculi, and the effects of varying lamellar properties.

PROCEDURES

Model of Lacuna -- The lacunar level model consisted of a block with an ellipsoidal void cut from the center. The block was 50 microns in each direction. The ellipsoidal diameters were 23, 15, and 6 microns (see fig. 1 or 2), taken from experimentally determined values (Sissons and O'Conner, 1977). The model geometry was created using SDRC's I-DEAS, then transferred to PATRAN to create the mesh. The model contained 1920 three-dimensional solid elements. The lacunar model was verified by applying a uniaxial strain to the model, and comparing the resulting strain distribution to that of an analytical analysis of voids in homogeneous media (Tandon and Weng, 1986), which showed very good correlation.

Model of Lamellae -- The model used to investigate the effect of variations in lamellar properties was created using two layers of material, each 3 microns thick, with different Young's moduli. The overall dimensions of the model were 6 microns on each side. Lamellae moduli were set to 3.9 GPa for both lamellae, 3.8 and 4.0 GPa, and 2.9 and 4.9 GPa respectively for three analyses. This model was created and meshed in PATRAN, and contained 256 solid three-dimensional elements. Maximum principal strains from the lacunar model were used as macroscopic strains in these analyses.

Model of Canaliculi -- The models representing bone with canaliculi were created with from two layers of material, with a 0.2 micron cylindrical void perpendicular to the plane of the lamellae, and running the entire thickness of the model (see fig. 3). This model was used to determine how strains in areas of low strain in the lacunar model would be amplified by the canalicular shape. Therefore, strains from the ellipsoidal face perpendicular to the z-axis (see fig. 1 or 2) were used as the macroscopic strains in this model.

RESULTS

The principal strains at each level are shown in fig. 4. The results suggest that the strain level surrounding the lacunae and canaliculi are approximately two times the strain at the trabecular level, while varying the lamellar properties does not appear to affect the strain levels.

Lacunar Model -- The maximum principal strain, approximately twice that found at the trabecular level, was found at the ends of the ellipsoid which had greatest curvature (see fig 1). However, the greatest strain energy density was found in a different region (see fig 2).

Lamellar Model -- The lamellar model suggests that the strain in both materials is approximately the same. The stresses, however, vary because of the difference between the Young's modulus of the different materials. Since the principal strains were oriented

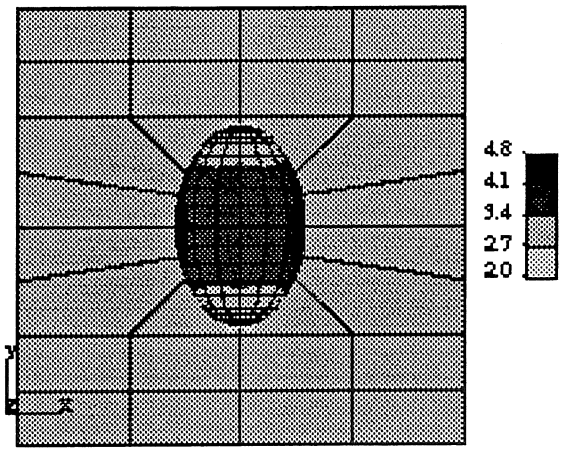

Fig. 1: Relative strain energy density.

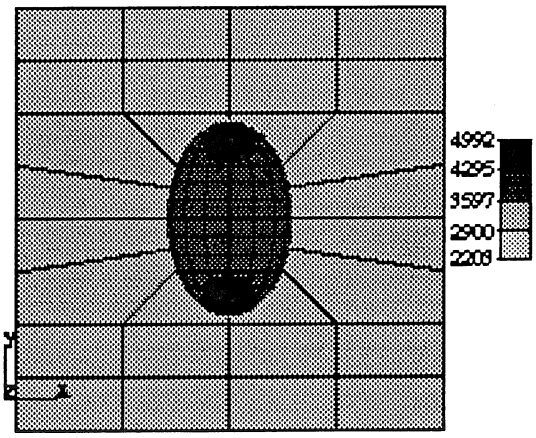

Fig. 2: Maximum principle strain (με).

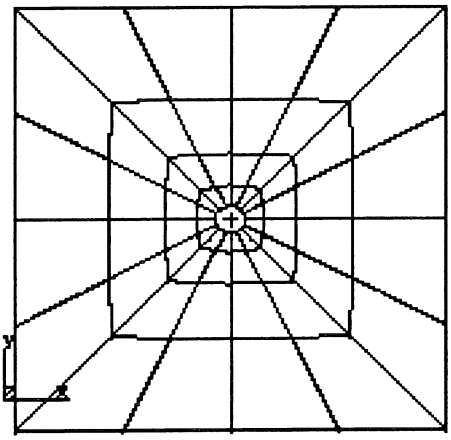

Fig. 3: Model of canaliculi.

fig. 4: Principal strains at various levels and regions for two sets of lamellar properties.

	Young's modulus of lamellae 3.9, 3.9 GPa	2.9, 4.9 GPa
trabecular level	{1325,287,80}	{1325,287,80}
lacunar level maximum principal strain	{2255,575,-1174}	{2278,576,-1202}
lacunar level strain in canalicular region	{1163,649,-896}	{1665,647,-894}
canalicular level maximum principal strain	{2660,-256,-896}	{2666,-263,-866}

with respect to the lamellae, there were no shear component to the principal strains. If the lamellae were not oriented along the directions of principal strain, however, one would expect a shear component.

Canalicular Model -- The maximum principal strain seen around the canaliculi was approximately two times the strain at the trabecular level, and 1.6 times the strain in the corresponding region of the lacunar model. Thus, the strain level around the canaliculi and at the region of maximum strain around the lacunae are approximately the same. This block was found to have nearly the same elasticity matrix as that of the solid block, although the strain distribution differed as a result of the void.

DISCUSSION

This study confirms that there is indeed a strain magnification phenomenon creating higher strain around the osteocyte than is seen at the whole-bone or even trabecular level. Strain levels of up to two times that of the trabeculae were found around the lacunae. The canaliculi were also shown to have strains of up to two times that of the trabeculae. Thus, strains of up to three or four times that of the whole bone may be common-place around the osteocytes within trabecular bone.

The strains found in this specific region of the trabecular bone do not appear large enough to elicit a response to strain as seen in the cell-stretching experiments. If the strain surrounding the lacunae and canaliculi are everywhere approximately twice that at the trabecular level, then the greatest strain found in the model by Hollister and Kikuchi (1994) may result in strains surrounding the osteocyte which are on the order of those used in some cell-stretching experiments.

In the future, it will be possible to expand this model to include an "osteocyte" with "integrin" connections to the matrix, and a "cytoskeleton" structure to transfer loads within the cell. This should allow a better representation of the strains seen by the cell as opposed to the strains of the matrix. In conclusion, this model is a feasible method to investigate the strain level and distribution of strains surrounding the osteocytes and osteocytic processes within bone.

REFERENCES

Hollister et al., Journal of Biomechanics, vol. 27, p. 433-444, 1994
Hollister and Kikuchi, Biotechnology and Bioengineering, vol.43, p 586-596, 1994
Sissons and O'Conner, Calcif Tissue Res (1977 May) 22 Suppl:530-3.
Tandon and Weng, Journal of Applied Mechanics, vol. 53, p 511-518, Sept. 1986.

ACKNOWLEDGMENTS

This study was funded by the Whitaker Foundation and the National Science Foundation.

SESSION 11:

MOTOR CONTROL

DIRECTIONAL SPECIFICITY OF POSTURAL MUSCLES DURING FAST ARM MOVEMENTS

A.S. Aruin, M.B. Shapiro, M.L. Latash

Department of Physical Medicine and Rehabilitation
Department of Molecular Biophysics and Physiology
Rush University, Chicago, IL 60612

INTRODUCTION

Human subjects stood on a biomechanical platform and performed fast bilateral, symmetrical shoulder movements in different directions. Mechanical variables and EMGs of leg and trunk muscles were recorded. Anticipatory changes in the activity of the postural muscles demonstrated a clear dependence on direction of the arm movement. Commonly, postural muscles were activated prior to the movement in a certain range of movement directions. Their activity was unchanged or suppressed during movements in other directions. Each muscle demonstrated a specific "preference" towards a certain range of movement directions. These findings suggest that postural muscles can gradually modify anticipatory changes in their activity depending on the direction of planned voluntary movement..

THEORY AND REVIEW

Voluntary movements are frequently performed in conditions that require maintenance of a certain posture in a joint, or of a limb, or of the whole body. Movements, particularly fast ones, may be considered postural perturbations (Bernstein, 1967). In particular, when a standing person performs fast voluntary arm movements, the postural equilibrium becomes endangered because of two reasons. One reason is related to the involved changes in the limb and body geometry leading to a change in the projection of the center of gravity. The other reason is related to the dynamics of the arm voluntary movement which induces dynamic forces at other joints of the body. One may say that the transmission of forces and torques from the moving limb through the body's linked segments is the primary reason for postural perturbations.

Two components of postural control are commonly invoked with respect to the changes in the levels of activation in postural muscles observed during fast voluntary movements (see review in Masion, 1992). The first component is addressed as anticipatory postural adjustment and involves changes in the levels of activation of postural muscles prior to the voluntary movement . This mechanism is supposed to estimate possible balance perturbations and induce changes in the activity of postural muscles that would oppose the expected postural disturbances. The efficacy of this mechanism is, however, commonly suboptimal, so that a postural perturbation occurs. Then, signals from the peripheral receptors are used as triggers to launch the second, corrective component which comes at a relatively short latency (about 70 ms) and deals with the actual postural perturbation.

A series of studies by Buchanan et al. (1989) have demonstrated, in isometric experiments, that human arm muscles may be involved into force increase in a rather wide range of direction. These studies have suggested that a commonly used classification of muscles into flexors-extensors or abductors-adductors may be too crude to account for the complexity of the muscle function during actual motor tasks. Postural muscles are also frequently classified into flexors-extensors or abductors-adductors. However, they frequently need to counteract perturbations in directions that do not coincide with the preferred direction of action of either of the muscles. Clearly, postural muscles are able to do so. The purpose of this work has been to study the directional specificity of postural muscles when they participate in corrections of the vertical posture in anticipation of a perturbation induced by arm movements in different directions.

PROCEDURES

Five healthy adult males participated in the study after giving an informed consent. The subjects stood barefoot on a biomechanical platform (AMTI OR-6). The signals from the platform were amplified and used to measure reaction forces in three orthogonal directions and moments of forces in two directions (in the saggital, My, and in the frontal, Mx, planes). Four two-axis goniometers (Penny & Giles) were taped on corresponding segments and measured angles in the ankle joint (saggital plane), knee joint, hip joint (saggital plane), and shoulder joint (saggital and frontal planes). Velocity was derived from the angle signals by differentiation after filtering at 100 Hz. Acceleration was measured by miniature unidirectional accelerometers (Sensotec) that were taped to the subject's right wrist and oriented so that their axes of maximal sensitivity were parallel to the sagittal or to the frontal plane. Disposable pediatric electrocardiographic electrodes were used to record the surface EMG activity of the following muscles: anterior deltoid, posterior deltoids, rectus abdominus, erector spinae, rectus femoris, biceps femoris, medial gastrocnemius, soleus, and tibialis anterior. A Mac-IIci computer was used to control the experiment, collect the data, and perform most of the analyses.

The experimental procedure involved 7 series of movements. Each series involved 10 bilateral shoulder movements in different directions, starting from forward (+90°, according to our convention) and ending by backwards (-90°) with increments of 30° were required. Prior to each series, the subjects were given 3 to 5 practice trials. The nominal amplitude of the shoulder movements was about 25°. Accuracy requirements were not stressed, and the subjects were

free to choose their preferred movement amplitude under the instruction to be fast and consistent. Movement direction was shown to the subject by a pole that was placed at a point on a circle just outside the subjec'ts reach. Three out of 5 subjects took part in experiments with additional loads (0.45 and 2.2 kg each) attached to the wrists bilaterally.

The trials were viewed off-line on a monitor screen and aligned according to the first visible change in the deltoid EMG signal. This time was used as "time zero" (t_0) for all the later data processing. Anticipatory changes in the EMG activity were assessed by integration of the rectified EMGs from -100 ms to +50 ms with respect t_0. These values were corrected for the background activity and normalized. Horizontal displacements of the center of pressure and center of gravity in the anterio-posterior and in the lateral directions were calculated.

RESULTS AND DISCUSSION

Typically, EMG patterns of the agonist-antagonist pair controlling the primary shoulder movement demonstrated the commonly observed tri-phasic pattern. Depending on the direction of the movement, the role of the agonist was played either by the anterior deltoid muscle (movement directions of 90°, 60°, 30°, and 0°) or by the posterior deltoid (movement direction of -30°, -60°, and -90°). Similar, tri-phasic patterns of muscle activity were commonly seen in the leg and trunk postural muscles. Postural muscles demonstrated a pronounced preference to be activated during movements in certain directions. This dependence for an "agonist-antagonist" pair of postural muscles could demonstrate a virtually non-overlapping, reciprocal pattern typical for the erector spinae-rectus abdominus pair. On the other hand, the background activity of soleus demonstrated an anticipatory decrease during movements in the opposite directions (90° and -90°) when tibialis anterior demonstrated an increase in its background activity. Fig. 1 summarizes these findings in polar diagrams. Movements against higher inertial loads attached to the wrists bilaterally demonstrated qualitatively similar patterns of the anticipatory changes in the background activity of the postural muscles although depth of the EMG modulation was higher. Anticipatory changes in the activity of postural muscles were accompanied by corresponding mechanical events including changes in ankle, knee, and hip joints, as well as shift of the center of pressure and center of gravity. Fig. 2 illustrates an example of the shifts in the center of pressure for one of the subjects who was moving with additional 2.2 kg loads attached to the wrists.

Our observations show that postural muscles can gradually modify anticipatory changes in their activity depending on the direction of planned voluntary movement. The patterns of the directional dependence of these changes are rather similar to the patterns reported by Buchanan et al. (1989) for arm muscles during isometric contractions.

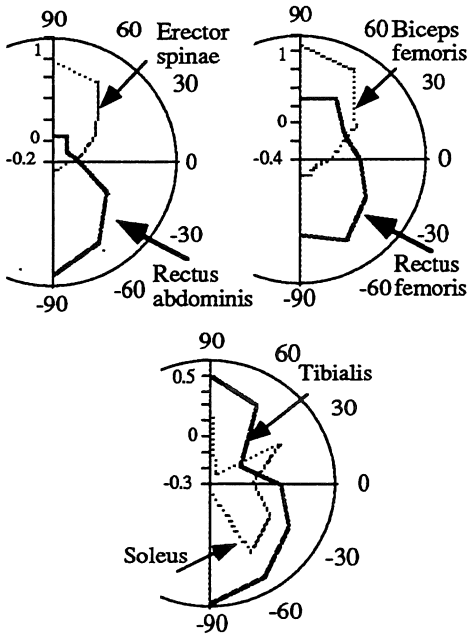

Figure 1
Averaged across subjects distributions of integrated anticipatory activity of postural muscles during fast shoulder movements in different directions.

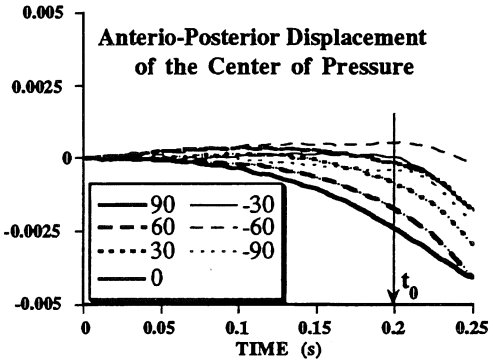

Figure 2
Examples of the anterior-posterior displacements (in m) of the center of pressure in a subject who performed shoulder movements from 90° to -90° with additional 2.2 kg loads attached to the wrists.

REFERENCES

Bernstein, N.A. The co-ordination and regulation of movements. Pergamon Press, 1967.
Buchanan, T.S. et al. J Neurophys39: 925-935, 1989
Massion, J. Prog Neurobiol 38: 35-56, 1992.

ACKNOWLEDGMENTS

The study was in part supported by an NIH grant HD30128 and a grant from the Rush University Research Fund.

IS POSTURAL SWAY STOCHASTIC OR CHAOTIC?

J.J. Collins and C.J. De Luca

NeuroMuscular Research Center and Dept. of Biomedical Engineering, Boston University, 44 Cummington St., Boston, MA 02215.

INTRODUCTION

During quiet standing, the human body continually moves about in an erratic, and possibly chaotic, fashion. Here surrogate data techniques and algorithms from dynamical systems theory were used to show that postural sway is indistinguishable from correlated noise. These analyses indicated that balance regulation is better represented as a stochastic process, as opposed to a chaotic one.

REVIEW AND THEORY

Noise-like fluctuations abound in physiological systems and processes. It has been suggested that the complex, unpredictable behavior exhibited by the mammalian nervous and muscular systems may be instances of deterministic chaos. A likely candidate for physiological chaos is the human postural control system, the output of which is highly irregular (Collins and De Luca, 1993). The identification of postural sway as an instance of chaos would suggest that there is a simple, dynamical mechanism at work in balance regulation and may make possible new therapeutic and preventive strategies for postural instability.

Chaotic systems are typically characterized by the existence of an attractor that has a fractal structure and a sensitive dependence upon initial conditions. Numerical algorithms which quantify either of these properties have been developed to detect the presence of deterministic chaos in experimental time series. (In the case of scalar time series, such algorithms usually require one to reconstruct firstly the system's attractor by embedding the time series in m-dimensional phase space.)

The most common way to approximate the fractal structure of a system's attractor is to calculate the correlation dimension, D_2 (Grassberger and Procaccia, 1983). Chaotic systems are generally characterized by finite, non-integer, i.e., fractal, values for D_2. To compute D_2, one firstly calculates the correlation sum, $C(\varepsilon)$, which is the fraction of pairs of points (on the reconstructed attractor) that are separated by a distance less than ε, for various values of ε. The correlation dimension can then be determined from the slope of a suitable, linear scaling region in the plot of $\ln C(\varepsilon)$ versus $\ln \varepsilon$.

A system's sensitivity to initial conditions can be quantified by computing its Lyapunov characteristic exponents. Lyapunov exponents provide a measure of the rate at which initially nearby trajectories on an attractor diverge or converge as time progresses. The presence of a positive Lyapunov exponent is sufficient for diagnosing chaos and reflects the fact that nearby trajectories diverge at an exponential rate. For experimental time series, the largest Lyapunov exponent, λ_1, can be determined from the slope of a suitable, linear scaling region in the plot of $\langle \ln d_j(i) \rangle$ versus $i\,\Delta t$, where $d_j(i)$ is the distance between the jth pair of nearest neighbors (on the reconstructed attractor) after i discrete-time steps, the symbol $\langle\cdot\rangle$ denotes an average over all values of j, and Δt is the sampling period of the time series (Rosenstein et al., 1993).

With short, noisy time series, the aforementioned algorithms can give spurious results, i.e., they can indicate the presence of chaos in systems that are not chaotic. Recently, surrogate data techniques have been developed to detect such 'false chaos positives' (e.g., Theiler et al., 1992). Surrogate data sets are created by randomizing some property of the original time series. (For example, a surrogate data set can be formed by taking the Fourier transform of a time series, randomizing the phase information, and then taking the inverse Fourier transform; this procedure yields a data set of correlated noise with amplitude spectral characteristics identical to that of the original time series.) The surrogate sets are then processed according to the identical algorithms that are applied to the original time series, and the results are analyzed to test the null hypothesis that the properties of the surrogate data sets are sufficient to account for the results obtained from the original time series. (The null hypothesis tested with phase-randomized surrogates is that the original time series is correlated noise.) If the results from the surrogates and the original time series are not significantly different, then the null hypothesis cannot be rejected.

In the present study, we tested the null hypothesis that postural sway can be modelled as a correlated noise process.

PROCEDURES

Ten healthy subjects—five males and five females—of similar age (19–24 yr, mean: 22 ± 2 yr), height (1.60–1.80 m, mean: 1.69 ± 0.08 m), and body weight (54.4–77.1 kg, mean: 64.3 ± 8.4 kg) were included in the study. Postural sway was quantified by using a Kistler force platform to measure the time-varying displacements of the center of pressure (COP) under each subject's feet. Each subject stood barefoot in an upright posture in a standardized stance on the platform for a series of five 90-s trials. All subjects were tested under eyes-open conditions. The COP trajectories were processed according to the aforementioned dynamical systems algorithms. In particular, for each COP time series, the Grassberger-Procaccia algorithm (1983) was used to compute $C(\varepsilon)$ for embedding dimensions 2–20, in increments of 2. Likewise, the algorithm of Rosenstein et

al. (1993) was used to compute the average separation of nearest neighbors on the reconstructed attractor and to estimate the largest Lyapunov exponent (λ_1). In addition, an ensemble of 10 different phase-randomized surrogate data sets were generated from each original COP time series (Theiler et al., 1992) and subsequently analyzed using the above techniques. The significance of the differences between the computed λ_1 values for the original COP time series and the surrogates was calculated according to the method described by Theiler et al. (1992). (We also used techniques described therein to estimate error bars on the significance.) With this approach, the significance is defined by the difference ($\Delta\lambda_1$) between the value of λ_1 for the original COP time series and the mean value of λ_1 for the surrogates, divided by the standard deviation (σ_s) of the λ_1 values for the surrogates.

RESULTS

The plots of ln $C(\varepsilon)$ versus ln ε for the original COP data (Fig. 1a) and the phase-randomized surrogates (Fig. 1b) were virtually indistinguishable. In each case, there was no clear linear scaling region of significant length and the slopes of the plots failed to converge with increasing embedding dimension, m. (Thus, it was not practical to extract values for D_2.) These qualitative results are those expected for a stochastic system. The Lyapunov exponent results were similar — the plots of $\langle \ln d_j(i) \rangle$ versus $i\,\Delta t$ for the original posture data (Fig. 1c) and the phase-randomized surrogates (Fig. 1d) were essentially identical. Although there was no clear linear scaling region in the respective plots, the region between 0.5 and 1.5 s (in particular, for $m < 14$) could be mistaken as appropriate for extracting a positive Lyapunov exponent. We therefore estimated λ_1 over this region for the original COP data and found that the computed values (Δ) appeared to converge for embedding dimensions of 6, 8 and 10 (Fig. 1e). However, a similar convergence was found in the results (+) for the ensemble of surrogate data sets (Fig. 1e). In addition, this anomalous scaling region, in the original and surrogate data sets, flattened out with increasing embedding dimension (Fig. 1e), as would be expected for a stochastic system. For $m > 4$, there were no statistically significant differences between the computed values of λ_1 for the original posture data and the phase-randomized surrogates (Fig. 1f). (A dashed line is plotted in Fig. 1f at the significance level which corresponds to a p-value of 0.05. The significant differences found for $m \leq 4$ can be attributed in part to the ill-defined nature of the scaling region for these small values of m (Figs. 1c,d).) Similar findings were obtained for all 10 subjects — shown in Figs. 1g,h, for example, are the computed λ_1 results for $m = 12$.

DISCUSSION

Given these findings, we were unable to reject the null hypothesis that postural sway is correlated noise. We therefore concluded that the postural control system should not be modelled as a chaotic process and that it is better represented as a stochastic one. These general results are consistent with those obtained from surrogate analyses of other physiological time series, such as electrocardiograms, electroencephalograms, and H-reflexes. Although deterministic chaos has been observed in perturbed biological preparations, e.g., periodically stimulated chick heart cells and squid axons, we are not aware of any documented cases wherein the 'steady-state' behavior of a physiological system has been definitively identified (using surrogate data techniques) as an instance of chaos.

REFERENCES

Collins, J.J., De Luca C.J., Exp. Brain Res. 95, 308-318, 1993.

Grassberger, P., Procaccia, I., Phys. Rev. Lett. 50, 346-349, 1983.

Rosenstein, M.T., Collins, J.J., De Luca, C.J., Physica D 65, 117 - 134, 1993.

Theiler, J. et al., Physica D 58, 77-94, 1992.

ACKNOWLEDGEMENTS

This work was supported by the National Science Foundation and the Rehab R&D Service of the Department of Veterans Affairs.

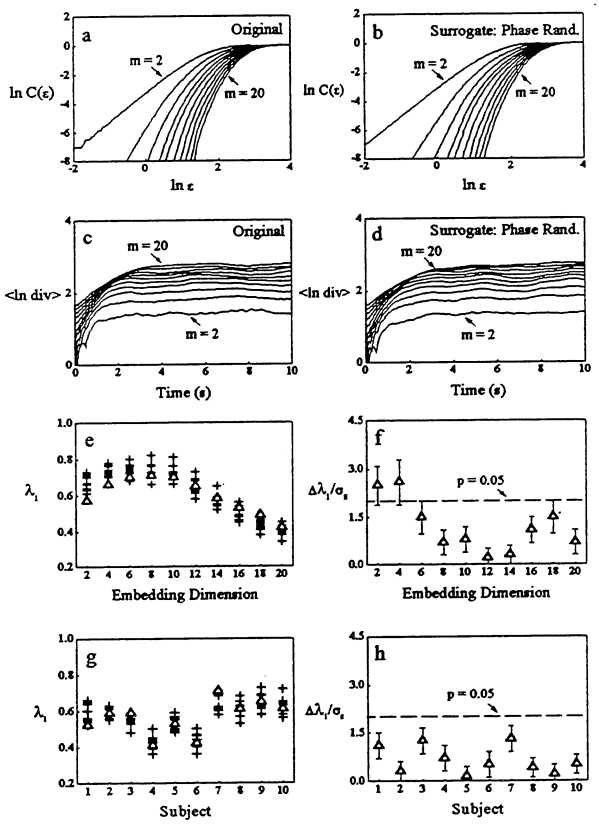

Fig. 1

DEVELOPMENT OF NEW EXPERIMENTAL PROTOCOL TO QUANTITATIVELY ASSESS THE NEUROMUSCULAR CONTROL CAPABILITY OF THE TRUNK MUSCLES

J. Y. Kim, M. Parnianpour, and W. S. Marras

Biodynamics Laboratory, The Ohio State University, Department of Industrial and Systems Engineering,
1971 Neil Avenue, Columbus, OH 43210

INTRODUCTION

Controlling range of motion and target tolerance has been proven to minimize the variability of dynamic motion parameters such as angular velocity and acceleration during repetitive trunk movement based on Fitts' law paradigm (Fitts, 1954; Kim et al., 1993). Based on that, new experimental protocol was developed to quantify the neuromuscular control capability of the trunk muscles during dynamic oscillatory movement. Twenty healthy male subjects participated in the study and each subject performed 23 oscillatory sagittal trunk bendings at self-selected maximal level of effort. The time series of ROM data were collected by Lumbar Motion Monitor (LMM). Peak angular velocity, peak angular acceleration, and movement time were computed and used as dependent variables. Individual dynamic motion parameters such as velocity and acceleration were rank-ordered and compared across different indices of difficulty (ID) conditions . Spearman Correlation Analysis was used to see the relationship between the dynamic parameters with and without ID conditions as well as amongst ID conditions. Wilcoxon Signed Ranks test was used to see the significance of difference in individual rankings among ID conditions. New experimental protocols were suggested based on the results and the use of information processing capacity was also discussed.

REVIEW AND THEORY

Range of motion and strength test have been used to quantify the function of the trunk muscles (Keeley et al., 1986; Triano & Schultz, 1987; Beimborn and Morrissey, 1981) for low-back patients. McIntyre et al (1991) measured preferred motion characteristics between normal and low-back patients, and found a significant difference between those two groups. Recently, Marras et al. (1993) examined the functional differences of normal and injured populations in terms of ROM, velocity and acceleration during dynamic oscillatory bending motion, and successfully classified them into normal and injured group. Furthermore, this motion measurement has an advantage over strength measurement because patients do not need to expose their injured body part to excessive loading. Therefore, having an accurate and easy-to-use method of measuring the dynamic trunk motion can greatly assist clinicians or ergonomists to quantitatively evaluate the functional capacity of the trunk muscle especially for low-back pain patients. Fitts' law describes the speed-accuracy trade off in reciprocal movements (MT=a+b*ID; ID= $\log_2(2A/W)$, A=range of motion, W=target tolerance, MT= movement time, a=intercept, b=slope). Kim et al. (1993) used this paradigm to investigate the dynamic neuromuscular control capability of the trunk. They found a great reduction in within group variability of performance parameters such as angular velocity during dynamic trunk movement. The purpose of this study was to determine the generalizability of functional assessment and the consistency of parameter during dynamic trunk movement at different ID.

PROCEDURES

Twenty healthy male subjects whose ages ranged from 20 to 47 (mean=30, s.d.=8.0) were used. Their mean height was 177.3 cm (s.d.=6.4) and mean weight was 80.5 kg (s.d.=12.0). First part of the experiment was to measure the dynamic performance of the trunk during ballistic movement at the subject's preferred range of motion without specification of any target tolerance. This method of trunk assessment is currently utilized with various technologies. For the second part of the experiment, different amplitudes of movement and target tolerance were used to create 11 IDs during oscillatory bending movement. The order of 22 trials (two trials for each ID condition) were randomly selected for each subject to minimize possible learning or fatiguing effect. The subject was told to flex and extend as fast as he can during 10 seconds period for the first part of experiment. In the second part, the subject was instructed to continue oscillatory bending movement as accurately and fast as possible while he was monitoring the real time feedback of his motion trajectory on the screen. If the subject missed the target more than twice, they were asked to try it again. The subject were verbally encouraged to perform at their best level during the trials. The triaxial trunk motion was collected by LMM at 60 Hz via portable data acquisition system. This experimental set up is shown in figure 1.

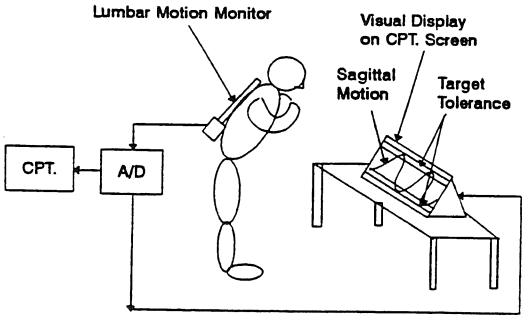

Figure 1.
Data acquisition system

RESULTS

The dynamic motion parameters such as velocity and acceleration in different IDs were used to see the consistency of dynamic trunk performance. First, since velocity and acceleration covaried with ROM (γ=.89 with flexion vel, γ=.93 with ext. vel., γ=.55 with flex. acc., and γ=.69 with ext. acc.), the adjusted means of velocity and acceleration were computed through analysis of covariance. Second, the adjusted means were normalized based on the maximum value to obtain non-dimensional adjusted composite scale for consistency of dynamic performance parameters. The consistency scale was computed as a square root value of difference between the dynamic parameters as follows:

$$((flex.vel.-ext.vel)^2+(flex.vel.-flex.acc)^2+(flex.vel-ext.acc.)^2+(ext.vel.-flex.acc.)^2+(ext.vel.-ext.acc.)^2+(flex.acc.-ext.acc.)^2)^{\frac{1}{2}}$$

The smaller value in this scale indicates a more consistent performance across the dynamic parameters. That is, the value of zero indicates complete agreement on the relative performance across the dynamic parameters. As a result, trial 3,5,6,8,9,10 showed relatively small numbers in this scale. This result is displayed in table 1. Furthermore, this adjusted means of dynamic performance parameters were rank-ordered and Spearman correlation coefficients were computed by SAS. The spearman correlation coefficients between trial 1 and other trials showed relatively low correlation coefficients ($-1.0 < \gamma < .57$). On the other hand, ID 1.32, 1.59, 2.00, 2.33, and 2.59 are highly correlated amongst each other ($.68 < \gamma < .90$); ID 2.74 and 3.00 are highly correlated ($\gamma=.76$); and ID 3.73, 3.91, and 4.32 ($.70 < \gamma < .81$) are highly correlated too. These results are summarized in table 2. ID conditions highly correlated amongst each other were grouped and numbered together in table 1. In addition to that, arbitrarily selected trial 5,8,10 from each group and information processing capacity were tested by Wilcoxon Signed Rank test. The result indicated those conditions are not significantly different each other even at $\alpha = 0.1$ level. Besides, information processing capacity of the subjects was computed as 4.23 bits ± 1.43 bits/second.

Table 1
Summary of consistency scale and ID grouping based on Spearman correlation coefficients

	trial	ID	scale	ROM (deg.)	target (deg.)
Part I	1	n/a	.68	self-selected	none
Part II	2	1.32[1]	.42	10&15	8&12
	3	1.59[1]	.32	10&15	6&9
	4	2.00[1]	.44	15&20	7.5&10
	5	2.33[1]	.31	10&20	4&8
	6	2.59[1]	.29	15&30	5&10
	7	2.74[2]	.35	20&30	6&9
	8	3.00[2]	.31	30&40	7.5&10
	9	3.33	.27	20&40	4&8
	10	3.73[3]	.33	30&40	4.5&6
	11	3.91[3]	.40	30&40	4&5.3
	12	4.32[3]	.44	30&40	3&4

1,2,3: groups highly correlated each other

DISCUSSION

Low correlation coefficients between the trial 1 and other ID conditions suggest that the highly ranked subjects during maximal performance may not score high during the trials with index of difficulty (ID). That is, the trunk control capability measured in this study can show an unique trunk motion characteristics which cannot be measured from the traditional maximal performance test. Moreover, the smaller consistency scale during ID conditions proved that this experimental protocol with ID measures the dynamic parameters more consistently than the maximal trunk performance test. Furthermore, some ID conditions showed high correlation coefficients and no significant difference in Wilcoxon Signed Rank test amongst them. Thus, the number of ID conditions can be reduced without losing ordinal information of the trunk control capability. Hence, only several ID conditions can measure the dynamic trunk performance over a full range of motion. Therefore, the best strategy to develop new experimental protocol could be to select several ID conditions which have low consistency scales as well as cover a full range of the trunk motion. For example, trial 5, 8, and 10 can be a set of trials which not only shows relatively consistent information in terms of scale but also shows the control capability over the full ROM from 10 to 40 degrees. Likewise, these or possibly other combination of three experimental conditions can be used as a new experimental protocol. Moreover, ranking of information processing capacity of subjects was not significantly different from the rankings of dynamic parameters such as velocity and acceleration. Therefore, individual's control capability of the trunk can also be described in terms of information processing capacity (bit/second). This is in contrast to our previous observation that information processing capacity has low correlation with the maximum dynamic performance parameters based on trial 1 (Kim et al., 1993).

The importance of coordination of trunk muscle during sport and work related activities has been recognized, but this paradigm provides a quantitative method for its assessment for the first time at the best of authors' knowledge. Future studies should include patient groups, and the hypothesis that this method increases the separability of patients and normals should be investigated.

Table 2
Spearman correlation coefficients of rankings of dynamic parameters among indices of difficulty

ID	1.32	1.59	2.00	2.33	2.59	2.74	3.00	3.33	3.73	3.91	4.32	trial 1
1.32	1.00	.78	.84	.82	.68	.53	.11	.03	-.09	.04	.01	.57
1.59	-	1.00	.80	.89	.78	.66	.30	.36	.16	.29	.14	.29
2.00	-	-	1.00	.90	.79	.78	.37	.30	-.02	.15	.03	.47
2.33	-	-	-	1.00	.80	.75	.44	.33	.14	.27	.15	.39
2.59	-	-	-	-	1.00	.75	.54	.40	.17	.34	.16	.61
2.74	-	-	-	-	-	1.00	.76	.46	.40	.44	.41	.45
3.00	-	-	-	-	-	-	1.00	.55	.54	.55	.49	.33
3.33	-	-	-	-	-	-	-	1.00	.54	.42	.30	-.10
3.73	-	-	-	-	-	-	-	-	1.00	.70	.81	.06
3.91	-	-	-	-	-	-	-	-	-	1.00	.73	.15
4.32	-	-	-	-	-	-	-	-	-	-	1.00	.15

$p<.001$ if $\gamma>.74$, $p<.01$ if $\gamma>.55$

ACKNOWLEDGEMENT

Ohio Bureau of Worker's Compensation

REFERENCES

Beimborn, D. S. and Morrissey, M. C. (1981). *Spine*, 13(6), 655-660.

Fitts,P.M. (1954). *J of Exp Psych*, 47(6), 381-391.

Keeley et al.(1986). *Spine*, 11(1), 31-35.

Kim et al. (1993). *ASME Winter Annual Meeting*, 471-474.

Marras et al. (1993). *Eur J of Physi Med*, 3(6), 218-235.

McIntyre et al. (1991). *J of Spinal Disorders*, 4 (1), 90-95.

Triano, J.J., and Schultz, A.B. (1987). *Spine*, 12(6), 561-565.

EFFECTS OF MANIPULATING HEAD ORIENTATION ON SENSORIMOTOR TRANSFORMATIONS

W.G. Darling, A.J. Butler, A. Eversmeryer and G. Entsminger

Department of Exercise Science, The University of Iowa, Iowa City, IA 52242

INTRODUCTION

The purpose of this experiment was to evaluate the effects of manipulating head orientation on the performance of sensorimotor transformations for reaching movements. We examined the effects of experimenter manipulation of head position after presentation of a target but prior to initiation of the reach to the remembered target location. Such manipulations of head orientation produced small increases in directional and distance errors. This suggests that moving the head has little influence on the performance of sensorimotor transformations.

REVIEW AND THEORY

Transformations of information between the visual and kinesthetic coordinate systems are necessary for controlling upper limb movements to external targets (Flanders et al. 1992). Recently, experiments in this laboratory have shown that the axes of these two coordinate systems at the perceptual level are defined by a trunk-fixed anterior/posterior (a/p) axis and the gravitational axis (Darling 1993, Darling et al., in preparation). Because the coordinate systems are fixed in the trunk and earth, it might be expected that manipulating head orientation would have little influence on performance of sensorimotor transformations for reaching. However, because the eyes are located in the head, varying head orientation might influence such transformations because the visual information must initially be specified in retinotopic and head-fixed coordinate systems. Previous research showed that extreme rotations of the head significantly influenced direction errors but not distance errors (Smetanin et al. 1993).

PROCEDURES

Six college-aged undergraduate students with no history of neuromuscular disease participated in these experiments. Subjects made pointing movements to remembered targets presented either visually or kinesthetically (the subject's fingertip was moved to the target and returned to the start position). An experimenter then moved the subject's head by rotation and/or flexion/extension (i.e., to vary orientations of the head longitudinal and a/p axes) to a new position in some conditions. The alterations in head position were wide ranging but the limit of the range of motion was not reached. After the change in head position the subject reached with their hand to place their fingertip in the remembered target location under visual or kinesthetic guidance. Six different experimental conditions were studied: (1) VTHMVR - visual target, head orientation manipulation, reach with vision, (2) VTHMBR - same as 1 except reach blind, (3)KTHMBR - same as 2 except the target was presented kinesthetically (4) KTHMVR - same as 3 except the reach was visually guided, (5) VTBR - same as 2 except there was no manipulation of head orientation, (6) KTVR - same as 4 except there was no manipulation of head orientation. In conditions 2 and 5 a transformation of visual information on target location into a kinesthetic representation of upper limb orientation was required since subjects could not see their hand during the reach. In conditions 4 and 6 subjects may use a transformation of kinesthetic information on target location into a visual representation because they can see their hand throughout the reach (Darling and Miller 1993). The order of experimental conditions was varied for the different subjects. One hundred trials were performed for each of conditions 1 - 4, fifty trials for each of conditions 5 and 6.

Positions of the target, the head and of the upper limb were recorded optoelectronically using the WATSMART system (Northern Digital, Waterloo, Canada). Infrared emitting diodes were attached to an aluminum cross-bar device fixed to goggles to define head orientation. The longitudinal axis of the humerus was defined by two IREDs. Three IREDs were placed on the hand (two defining its long axis and one on the index fingertip).

Target and fingertip locations were measured in a shoulder-fixed spherical coordinate system (i.e., position defined by distance and azimuth and elevation of the target or fingertip relative to the shoulder). Variable errors were used as a measure of random error and rms errors as a measure of overall error. In addition, the dependence of the errors on changes in head position were evaluated using regression techniques.

RESULTS AND DISCUSSION

Manipulating head orientation generally produced decreased accuracy for reaching to remembered visual targets (Fig. 1). Overall directional errors (mean of azimuth and elevation rms errors) were significantly larger when head orientation was manipulated ($p < 0.04$, compare VTHMBR to VTBR in Fig. 1. Because reaches to visual targets were

kinesthetically guided in these two conditions, this result shows that varying head orientation produces errors in transformation of visual information into the kinesthetic coordinate system. However, the increases in the errors were remarkably small, showing that changing position of the head has little influence on programming of reaching movements. Furthermore, use of vision to guide reaches to remembered visual targets after head orientation manipulation resulted in much smaller reach errors that were significantly lower ($p < 0.05$) than for kinesthetically guided reaches (compare VTHMBR to VTHMVR in Fig. 1).

Reach distance errors in the visual presentation conditions were similar to those described previously and were not significantly affected by manipulation of head orientation. Subjects overshot targets close to the shoulder and undershot targets far from the shoulder as shown previously (Darling and Miller 1993, Soechting and Flanders 1989). Thus, varying head orientation between target presentation and reaching has little influence on transforming visual information on target location into an upper limb configuration for reaching.

When the target was presented kinesthetically, there were no significant changes in directional or distance errors due to head orientation manipulation (compare KTHMVR to KTVR in Fig. 1). This suggests that manipulating head orientation does not influence visual guidance of reaching to a kinesthetically remembered target. It is likely that the subjects ignored visual information in this condition and simply guided their hand kinesthetically to the remembered target location. Indeed, this appeared to be the case even in the KTVR task in which there was no manipulation of head orientation. The pattern of reach distance errors was approximately random, in contrast to the findings of a previous study in which such errors were similar to those for reaches to remembered visual targets (Darling and Miller 1993).

Regression analysis showed that the directional errors depended partially on the changes in head longitudinal axis and a/p axis orientations between target presentation and reach initiation. Coefficients of determination were largest for prediction of azimuth errors in the VTHMBR (mean $R^2 = 0.31$, range = 0.1 - 0.55). Prediction of directional errors was generally poor for the conditions in which the target presentation was presented kinesthetically (mean $R^2 = 0.13 - 0.19$ for prediction of azimuth and elevation errors under the KTHMVR and KTHMBR conditions). These results support the conclusion that moving the head has little influence on kinesthetic perceptions of upper limb orientation or fingertip positions.

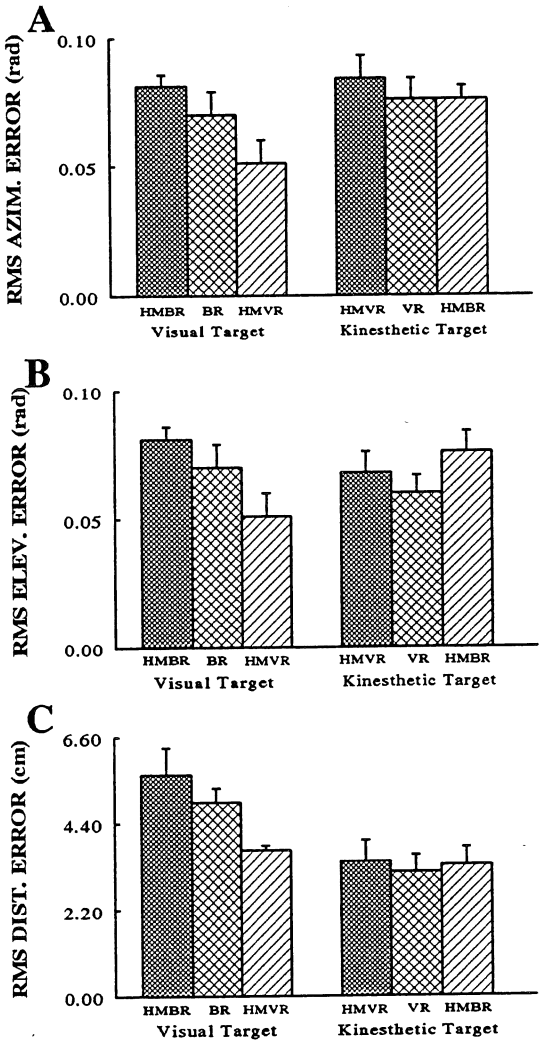

Fig. 1 Direction and distance errors for reaches to remembered visual and kinesthetic targets when head orientation was manipulated (HM) and reaches were visually guided (VR) or kinesthetically guided (BR). Each bar represents the mean rms error for six subjects. Error bars are 1 S.E.

Darling, W.G. ASB Proceedings, 17th annual meeting, 115, 1993.

Darling, W.G., Miller, G.F. Exp. Brain Res. 93, 534-547, 1993

Flanders, M. et al. Behav. Brain Sci. 15, 309-320, 1992

Soechting, J.F., Flanders, M. J. Neurophysiol., 62, 582-594, 1989

Smetanin, B. et al. Soc. for Neurosci. Abstr. 19, 549, 1993

QUANTITATIVE RELATION BETWEEN THE COMPLIANCE OF THE SUPPORTING SURFACE AND THE FORCE INPUT TO THE FEET DURING UPRIGHT BALANCE

Jin-Hsien Chiang and Ge Wu

Center for Locomotion Studies, The Pennsylvania State University
University Park, PA 16802

INTRODUCTION

Proprioceptive system is one of the sensory inputs that contribute to postural balance. In order to study its role in postural control, researchers have attempted to remove the proprioceptive information by changing the compliance of the supporting surface. For example, Shumway-cook and Horak[1] showed increased postural sway by adding foam to the bottom of the feet while both visual and vestibular systems remained intact. However, few study has been conducted to precisely determine the degree to which the proprioceptive information is being altered[2]. Therefore, the objective of this study is to investigate quantitatively the relation between the compliance of the supporting surface, by adding foam, and the force input to the feet, by measuring the pressure distribution under one's feet.

PROCEDURES

Ten young, healthy subjects, six males and four females, were recruited from the Pennsylvania State University, University Park. The mean age was 24.6 yrs (range 20 - 29) and mean weight 140.3 lbs (range 130 - 154).

A pressure detective insole (PEDAR system, NOVEL) was used to measure the peak pressure and maximum contact area. A movable, hard surfaced platform was used to generate a toes-up perturbation at 40°/s with acceleration of 400°/s^2 for maximum of 8°. The foam used was fomaex polyurethane sheet with thickness of 1" per layer.

The experiment consisted of eight different conditions: hard surface under perturbation (P) (1) and no perturbation (NP) (2); one layer of foam (1") under P (3) and NP (4); two layers of foam (2") under P (5) and NP (6); and three layers of foam (3") under P (7) and NP (8). Condition (1) was used as a control.

Subjects stood barefoot on the platform with heels 25 cm apart and toes 10° outward. The pressure insoles, as well as layer of foams as necessary, were inserted between the platform surface and the subject's soles. In all cases, the insoles were in direct contact with the soles. The subjects were asked to maintain his/her balance for four seconds while data were collected. The sequence of the test conditions was from condition (1) to condition (8) sequentially, two trials for each condition. Data were collected at 60 Hz.

Peak pressure[3] and maximum contact area were extracted. They were analyzed using repeated measures Analysis of Variance which included gender, four surface conditions, and two altered situations. A Bonferroni Correction was used to control the experiment-wise error rate for all comparisons to be 0.05 in each model. ($\alpha/12 = 0.0042$ for peak pressure and $\alpha/3 = 0.0167$ for maximum contact area).

RESULTS

Peak Pressure

The means of the peak pressure ($n = 20$) under eight different conditions are shown in Fig. 1. Statistical analysis revealed that the mean peak pressures were significantly different between gender ($F(1,8) = 6.825$; $p < 0.05$) and surface conditions by perturbation interaction ($F(3,56) = 7.762$; $p = 0.0002$). Based on the results of Least Squares Means, the peak pressure with foam decreased significantly compared to the ones on hard surface regardless perturbation ($p < 0.0003$). Without perturbation, peak pressure was significant lower than that with perturbation ($p < 0.0001$) regardless the surface conditions. However, significant differences were not found between two layers of foam and three layers of foam under NP and P situation ($p > 0.0042$).

Maximum contact Area

Figure 2 shows the result of maximum contact area. The mean maximum contact areas were not significantly different between male and female ($F(1,8) = 0.117$; $p > 0.5$). However, there were significant differences among four surfaces ($F(3,56) = 153.55$; $p = 0.0001$) and two perturbation conditions ($F(1,56) = 20.89$; $p = 0.0001$). The Least Squares Means of surface conditions showed that the maximum contact areas with foam were significantly increased compared with the ones on hard surface ($p < 0.0001$).

Without perturbation, the maximum contact area was significantly lower than that with perturbation.

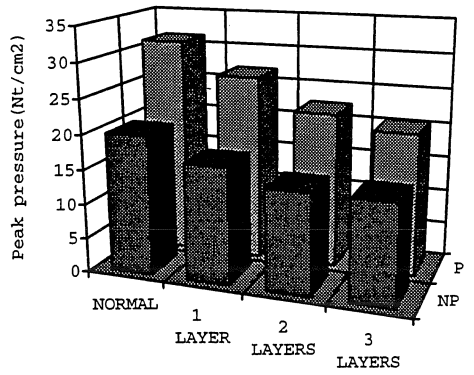

Fig. 1 Peak pressure of different conditions

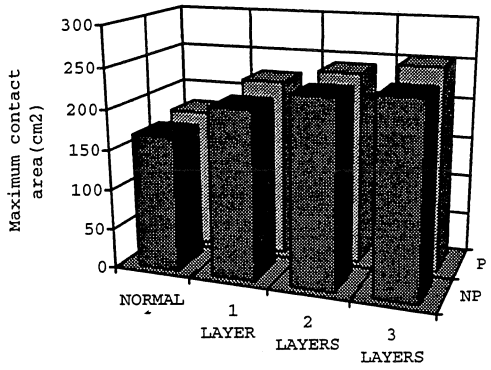

Fig. 2 Maximum contact area of different conditions

DISCUSSION

The result of this study showed that as the supporting surface becomes more compliant (by adding more layers of foams to one's soles), the peak pressure becomes smaller and the maximum contact area becomes larger.

Without perturbation, peak pressure was reduced by 16.4% with one layer of foam and 27.8% with two layers of foam and 28.0% with three layers of foam. This saturation in peak pressure increasing suggests that additional layers of foam might not be necessary (Fig. 3). Similarly, the maximum contact area was increased 24.4% with one layer of foam; 36.9% with two layers of foam; and 40.5% with three layers of foam (Fig. 4).

With toe-up perturbation, the changes in peak pressure and maximum contact area are similar to those with no perturbation except that the peak pressure at three layers of foam showed higher decrease (from 0.2% NP to 6% P), and the maximum contact area showed higher increase (from 3.6% NP to 7.4% P) (see Figs. 3 and 4). This difference results in a rather linear relation between the change in peak pressure and the surface compliance.

In summary, the use of foam to change the compliance of the supporting surface does alter the pressure input to the proprioceptive system. However, the change in peak pressure is not linearly related to the compliance of the surface. Furthermore, the pressure change depends on perturbation condition.

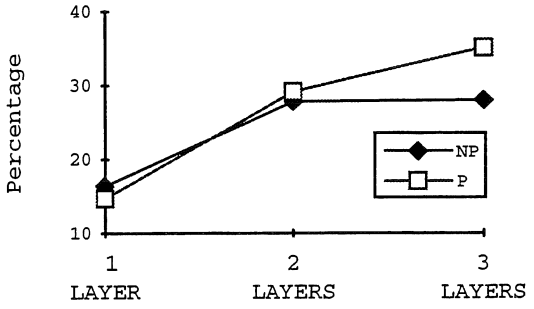

Fig. 3 Percent decrease of the peak pressure

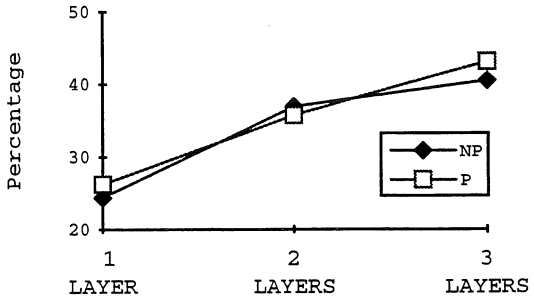

Fig. 4 Percent increase of the maximum contact area

REFERENCES

1. Shumway-cook, A.; Horak F. B., Assessing the influence of sensory interaction on balance: suggestion from the field. Phys. Ther. 66: 1548-1550, 1986
2. Teasdale, N.; Stelmach, G. E.; Breunig, A., Posture sway characteristics of the elderly under normal and altered visual and support surface conditions. J. of Geronotology. 46(6): 238-244,1991.
3. Mcpoil, T.G.; Cornwall, M.W., Effect of insole material on force and plantar pressures during walking. J. of the American Podiatric Medical Assoc. 82(8), 412 -416, 1992.

ACKNOWLEDGMENTS

This work was supported by a grant from the Gerontology Center at The Pennsylvania State University.

REPRESENTATION OF A VIRTUAL TRAJECTORY DURING MOVEMENT OF A SINGLE-LINK SAGITTAL ARM

S. McGlamery and M. Parnianpour

Department of Electrical Engineering, The Ohio State University, Columbus, OH 43210
Department of Industrial and Systems Engineering, The Ohio State University, Columbus, OH 43210

INTRODUCTION

The equilibrium point theory of motor control has advocated the use of a virtual trajectory to plan and execute voluntary movements. Point to point movement of a single-link sagittal arm can be achieved by sampling a virtual trajectory to control the firing rates for the system's actuators. It was observed that the number of virtual points between the initial and final points can greatly affect the performance of the system. The purpose of this study was to investigate energetics and the overall system performance of arm movement as a function of the stiffness and the number of samples used to represent the virtual trajectory.

METHOD

The one-link sagittal arm model developed by Dinneen and Hemami (1993) is used as the system model, with spindle feedback neglected. For point to point movement, a brief initial phase of the movement in which the actuators were actively controlled was followed by a second phase in which the system characteristics brought the system to rest. The present movement strategy actively controls the actuator outputs throughout the range of motion

The muscles are modeled as nonlinear springs, with the passive elasticity increasing linearly with the firing rate. The force produced by a muscle is given by

$$F = (R + Cl)^2 + B\dot{l}u(-\dot{l}) \qquad (1)$$

where R is the firing rate, l is the actuator length, and C is a constant describing the passive elastic behavior. The forces developed by the system's two actuators, the extensor and flexor, are referred to as F_1 and F_2, respectively, with firing rates R_1 and R_2. The differential equation of motion is given by

$$J\ddot{\theta} - mgd\sin\theta = k(F_1 - F_2) \qquad (2)$$

where J is the moment of inertia of the arm about the hinge, m is the system mass, g is the constant of gravity, d is the distance from the hinge to the center of gravity, and k is the moment arm of the actuators. The desired movement is achieved by using a virtual trajectory to calculate the values of R_1 and R_2.

The virtual trajectory used is a fifth order polynomial function which minimizes jerk, from Stein et al. (1986). The trajectory provides the position, velocity, and acceleration throughout the movement for any desired movement time and final position. This function can be sampled n times for a movement consisting of n steps. For each sample, the position, velocity, and acceleration for the corresponding time are substituted into equation (2), providing one relationship between R_1 and R_2. To ensure the stability of the system, a perturbation analysis was performed, yielding a second equation containing R_1 and R_2

$$K = [2k^2C(R_1 + R_2 + 2Cl_o) - mgd\cos\theta]. \qquad (3)$$

K is defined as the stiffness coefficient for the system, and l_o is the actuator length at $\theta = 0$. The system is stable for $K > 0$. Solving equations (2) and (3) simultaneously for each sampled point in the virtual trajectory gives us the series of values for R_1 and R_2 needed for the system to follow the motion specified by the virtual trajectory.

RESULTS

A computer simulation was created to compare the present method of point to point movement to the previous method. Using the same system constants as Dinneen and Hemami (1993), the position and velocity trajectories for both methods were produced (figure 1). The movement time required for the present method was determined from the 90% settling time of the previous method, in which the movement time is not directly controllable. Throughout both movements, a constant stiffness of $K = 2$ was used, and for the present method, 30 steps ($n = 30$) were utilized. In figure 1b, the movement for the present method is shown. By controlling the actuators throughout the movement, the peak velocity and overshoot are significantly reduced in comparison to the previous method. Figure 2 shows the firing rates for both actuators and the corresponding forces developed for the movements in figure 1. Figure 2 illustrates the difference in control strategy for the two methods. In the previous method, during the first .05 seconds of movement the firing rates are set such that the forces developed accelerate the arm towards its final equilibrium point, after which the firing rates are set at their final equilibrium values. With the firing rates set at their constant final values, the force-velocity and force-length characteristics of the actuators bring the system to rest, as can be seen in figure 2b. In the present method, the firing rates are controlled throughout the range of motion to bring the system to its final equilibrium point, which allows us to control the duration of the motion as well as reduce the peak overshoot by a factor of 10.

To determine the appropriate number of steps to use, we examined what effect increasing the number of steps, n, had for a range of stiffness values. Peak overshoot and the total mechanically adjusted work done throughout the range of motion are plotted in figures 3 and 4. For computation of mechanically adjusted work, the work done by an actuator is reduced by a factor of 2/3 when the contractile velocity is negative, to model the more efficient eccentric action of muscles. From figure 3, we can see that as the number of steps increases, the peak overshoot decays exponentially. The overshoot also decreases as the stiffness increases. Figure 4 shows a decrease in total work done by the system as the number of steps increases, and an increase in work as the stiffness increases, as would be expected. For 30 steps or more the overshoot and work become fairly constant for any given stiffness. Choosing the minimum number of steps which can produce the desired response provides us with the optimum number of steps for this movement time. As the movement time increases or decreases, the number of steps required correspondingly increases or decreases. As the stiffness increases, the magnitude of the firing rates increases correspondingly, while the difference between the firing rates remains constant. For lower firing rates, less energy is expended throughout the movement, but the system is also more susceptible to perturbations and overshoot. The CNS apparently sets K to reduce energy expenditure based on the expected degree of perturbation.

References

Dinneen, J.A. and H. Hemami. Stability and Movement of a One-Link Neuromusculoskeletal Sagittal Arm, IEEE Transactions on Biomedical Engineering, 541-548, 1993.

Stein, R.B., Oguztoreli, M.N., and C. Capaday. What is Optimized in Muscular Movements? in N.L Jones, N. McCartney, and A.J. Jones (Eds.), *Human Muscle Power* (pp 131-149), Human Kinetics Publishers Incorporated, 1986.

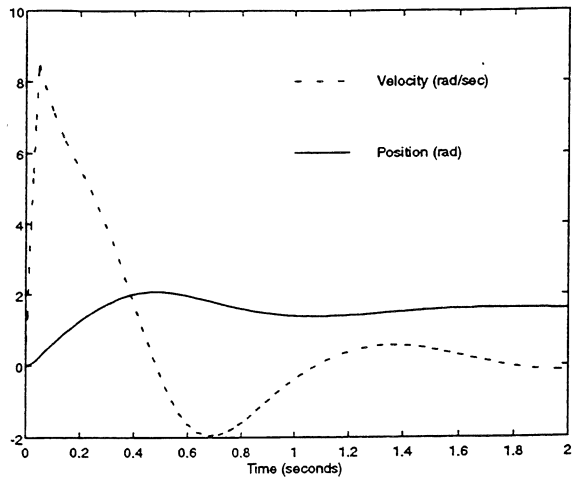

(a)

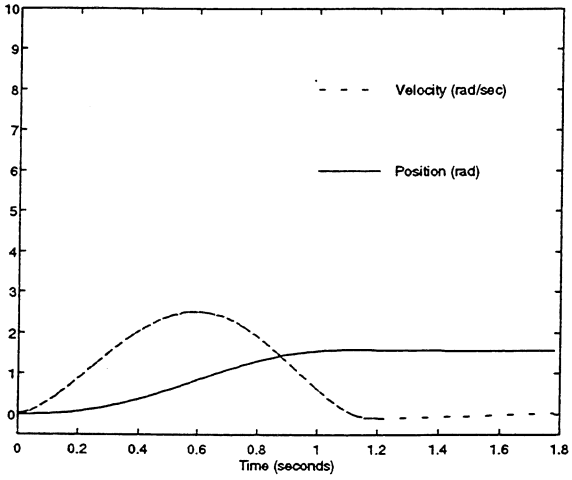

(b)

Figure 1. Position and velocity for : (a)Dinneen and Hemami, (b) present method

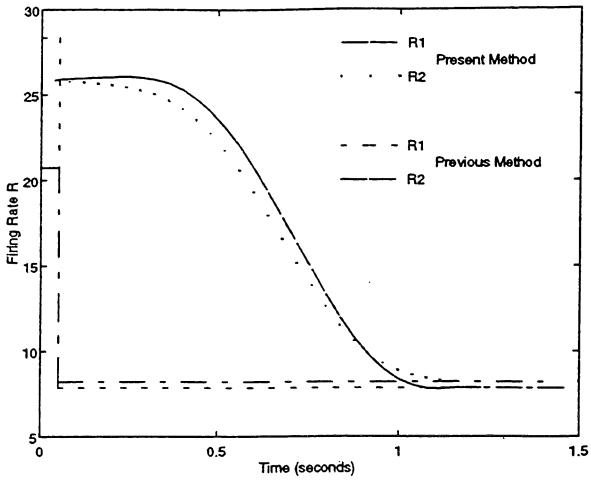

(a)

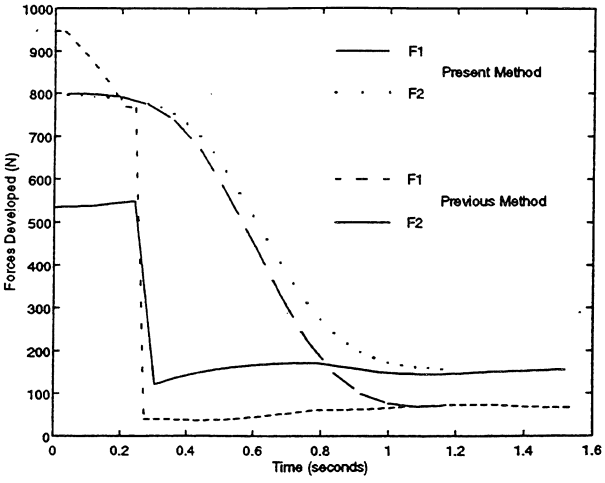

(b)

Figure 2. System control: (a) firing rates throughout motion for both methods, (b) corresponding forces developed.

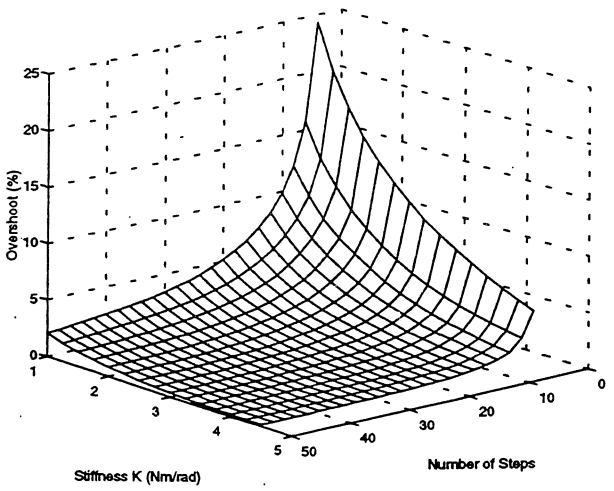

Figure 3. Peak overshoot as n and K are varied for the present method of point to point movement.

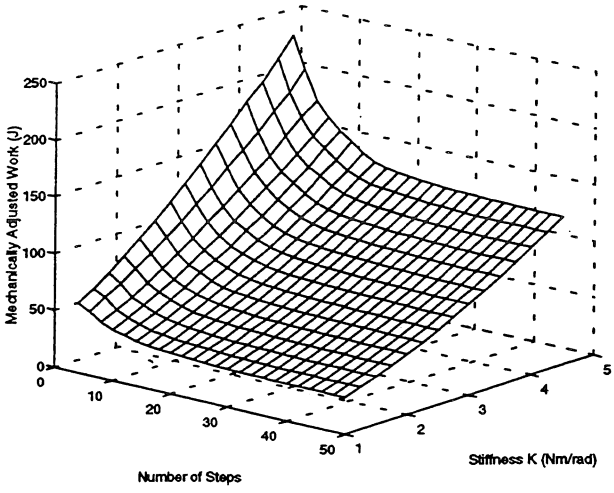

Figure 4. Total mechanically adjusted work done in point to point movement as n and K are varied, using the present method.

SESSION 12:

SPINE

MUSCLE ACTIVITY AND SPINAL LOADS DURING DYNAMIC TORSIONAL EXERTIONS

K.P. Granata and W.S. Marras

Biodynamics Laboratory
The Ohio State University

INTRODUCTION

Axial twisting of the torso has been identified as a significant risk factor for low back disorders (Punnet et.al., 1991). However, previous studies have had difficulty describing how the spine is loaded during twisting motions. Electromyographic activity of ten trunk muscles have been measured while 12 subjects performed twisting exertions under various force, velocity, position, and direction conditions. Muscle activity and coactivity as well as spine loading predicted from a validated biomechanical model were influenced by the twisting velocity, torsional load, and torsional direction, i.e. clockwise vs. counter-clockwise.

REVIEW AND THEORY

Torsional exertions are accompanied by significant muscle coactivation (Zetterberg et. al., 1987) which greatly influence spinal loads (Granata and Marras, 1994). Previous biomechanical models have had difficulty realistically representing muscle coactivity and spinal loading while generating valid biomechanical results.

The objectives of this study were to document the behavior of trunk muscles during isometric and isokinetic torsional exertions, and to examine how muscle activities contribute to spine loads during twisting exertions.

PROCEDURES

Twelve male subjects performed isometricand isokinetic, torsional exertions at 100% and 50% of their MVC effort. Isometric twisting exertions were achieved with the trunk rotated axially 20^{o} to the right, 20^{o} to the left, and sagittally symmetric. Isokinetic exertions were performed at twisting velocities of 10 and 20 deg./sec. through a $\pm 24^{o}$ range from a symmetric posture in both clockwise and counter-clockwise directions. Subject positions and motions were controlled by a Kin/Com isokinetic dynamometer while kinematic and kinetic data were precisely measured via a Lumbar Motion Monitor and force plate (Bertec 4060A) respectively.

Myoelectric activity of trunk muscles were collected using bipolar surface electrodes over the right and left pairs of the latissimus dorsi, erector spinae, rectus abdominis, external oblique and the internal oblique as reported in Mirka and Marras (1993). The EMG signals were processed and normalized using activity levels collected during MVC exertions.

	FORCE	DIR	ANGLE	VEL
Rt Lat	**p<.01**	**p<.01**	**p<.01**	p<.04
Lt Lat	**p<.01**	**p<.01**	p<.42	p<.82
Rt ErSp	**p<.01**	**p<.01**	p<.57	p<.49
Lt ErSp	**p<.01**	p<.93	p<.70	p<.02
Rt RAbd	**p<.01**	p<.15	p<.23	p<.07
Lt RAbd	**p<.01**	**p<.01**	p<.61	p<.27
Rt ExObl	**p<.01**	**p<.01**	p<.20	p<.84
Lt ExObl	**p<.01**	**p<.01**	p<.11	p<.25
Rt InObl	**p<.01**	**p<.01**	p<.06	p<.16
Lt InObl	**p<.01**	**p<.01**	p<.32	p<.53

Table 1. Statistical ANOVA results of EMG analyses. Interaction terms had no significant MANOVA values. Levels significant at p<.1 have been shaded. Levels significant at p<.01 have been noted in bold.

RESULTS AND DISCUSSION

During twisting exertions, EMG activity (Table 1) as well as EMG per unit torsional moment increased significantly (p<.01) with torsional force in all of the measured trunk muscles, both agonists and antagonists. Increased antagonist coactivity, reduces the optimality of the applied force, and has not been successfully predicated from biomechanical optimization functions attempting to minimize spinal load, muscle force or stress (Hardt,1978). Evidence that the rectus abdomini are influenced significantly by force and not by torsional direction indicate these muscles are employed as trunk stabilizers, but are not recruited to contribute to the torsional moment. Both Pope et. al. (1986) and McGill (1991) also found large amounts of coactivity during axial twisting that they attributed to the need for trunk stability.

The EMG per unit of torsional moment increased with twisting velocity in all ten of the measured muscles. Similar results were reported by (Granata, 1993; Marras and Mirka, 1994) for sagittally symmetric and asymmetric lifting exertions. The phenomena has been attributed to the need for increased stability at higher velocities (Gracoketsky

et. al., 1985). The results indicate that static modeling may have difficulty representing spinal loads that occur during dynamic lifting or twisting exertions.

Muscle coactivity was described as the average activity level of the co-contracting muscles relative to the prime mover, i.e. most active muscle. In general, average coactivity during twisting exertions (42%) was about twice the coactivation noted during lifting (Granata, 1993) exertions (26%) (Figure 1). Thus, more muscles are recruited at higher activation levels for twisting than for lifting exertions.

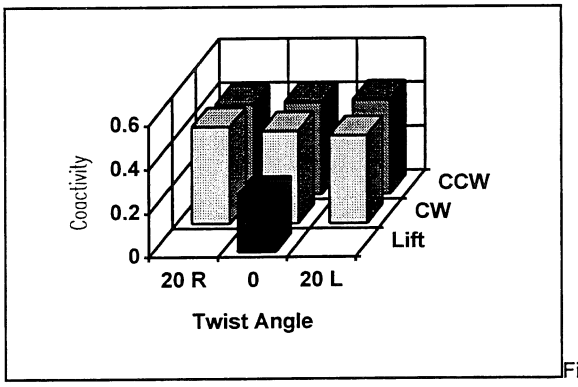

Figure 1. Torsional exertions generate significantly greater muscle coactivity than lifting exertions.

Spine loading, predicted from a validated, EMG-assisted model (Marras and Granata, 1994), was significantly ($p<.01$) affected by twisting velocity (Figure 2), torsional force and direction (clockwise vs. counter-clockwise) of the exertion. It is particularly noteworthy that relative spinal compression (per unit of twisting moment) at 10 deg./sec. is twice that of isometric compression. The trend of increased spinal load with velocity agrees with results from published lifting analyses. (Frievalds et. al., 1984). Shear loads also significantly ($p<.01$) increased with twisting velocity. These findings agree with the epidemiologic assessment of Marras et. al. (1993) who found that high risk jobs in industry were associated with significantly greater twisting velocities.

A pairwise comparison of relative spinal loads indicated that a significantly elevated isometric compression was present when the trunk was rotated to the right (14.32 N/unit Mz) compared to the loading when pre-rotated to the left (8.63 N /unit Mz). The analyses indicated that dynamic counter-clockwise motions resulted in about twice the anterior shear loading (10.18 N/unit Mz) compared to dynamic clockwise exertions (5.37 N/unit Mz).

Results from this research indicate EMG

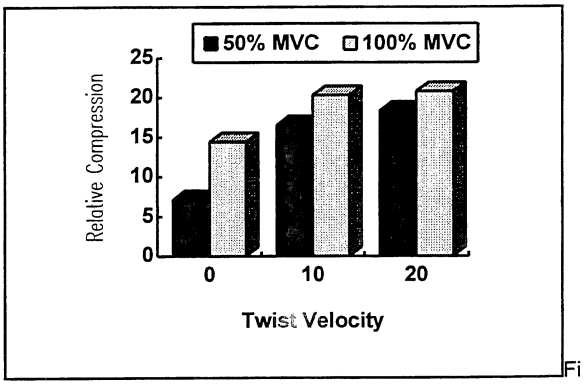

Figure 2. Spinal compression per unit torsional moment increased significantly with twisting velocity and force

activity and spinal compression and shear forces increase with exertion load, twist angle, velocity, and torsional direction. Thus twisting exertions may generate a combination of spinal forces that place one at higher risk of exceeding spinal tolerance (Shirazi-Adl A. et. al., 1986). These results support epidemiological findings that indicate risk of low-back pain are related to exertion load, velocity, and twisting angle (U.S. Dept. Labor, 1982).

REFERENCES

Freivalds A. et. al. (1984) *J. Biomechanics*, 17 (4), 251-262

Gracovetsky S. et. al. (1985) *Spine*, 10, 317-324

Granata K.P. (1993) Ph.D. Dissertation, The Ohio State University

Hardt D.E. (1978) *J. Biomech. Eng.*, 100, 72-78

Marras W.S. et. al. (1993) *Spine*, 18 (5), 617-628

Marras W.S. and K.P. Granata (1994) *Spine*, in review

Marras W.S. and G.A. Mirka (1994) *J. Orthop. Res.*, 9 (1), 91-103

McGill S.M. (1991) *J. Orthop Res*, 9 (1) 91-103

Mirka G.A. and W.S. Marras (1993) *Spine.* 18 (11), 1396-1409

Pope M.H. et. al. (1986) *J. Orthop. Res.*, 4 (3), 288-297

Punnet L. et. al. (1991) *Scand. J. Work Envir. Health.* 17, 337-346

Shirazi-Adl A. et. al. (1986) *Spine,* 11 (9), 914-927

Zetterberg C. et. al. (1987) *Arch. Phys. Med. Rehab.*, 50, 613-620

U.S. Dept. Labor (1982) Bulletin 2144

ACKNOWLEDGMENT

Funding was provided by the Ohio Bureau of Worker's Compensation, Division of Safety and Hygiene. The authors wish to thank G. Alread and F. Fathallah for their invaluable assistance.

ISOLATED ERECTOR SPINAE FATIGUE AND LIFTING MECHANICS

J.F. Hivon BSc and J.R. Potvin PhD
Human Biology, University of Guelph, Ontario, Canada, N1G 2W1

INTRODUCTION

Evidence provided in the past has led to the belief that muscular fatigue may lead to a higher risk of injury for the tissues of the lower spine. Parnianpour et al. (1988), as pioneers in biomechanical studies of low back fatigue, demonstrated that decreases in spine flexion occurred with fatigue, however, due to experimental procedures, application of these results to lifting is difficult. Potvin et al. (1991), in a study involving 2 hour and 20 minute lifting sessions, concluded that erector spinae muscle fatigue was accompanied by a significant increase in spine flexion and a subsequent increase in the strain on passive extensor tissues. However, it was difficult to establish whether the causal factor of the observed changes was the back fatigue or the leg fatigue. Since no leg fatigue was quantified, the extent of its effect could not be determined. Trafimow et al. (1993) presented evidence for increases in trunk inclination due to fatigue of the thigh musculature, however, quantification of this fatigue was not performed and the use of trunk inclination to represent spine flexion is questionable.

In summary, there is some evidence to suggest that a relationship exists between low back injury risk and 1) isolated leg fatigue and 2) some combination of leg and erector spinae fatigue. It was the objective of this study to investigate a third possibility by determining the effects of isolated erector spinae fatigue on the risk of lumbar spine tissue injury.

REVIEW AND THEORY

It would appear that repetitive lifting and its resultant fatigue may serve to predispose workers to low back injuries, however, the mechanisms through which these injuries occur are not completely understood. It is hypothesized that fatigue may act in numerous ways to put spine tissues at risk of injury. If an increased spine flexion were to result, there may be an increased risk of injury to the supra and interspinous ligaments (Adams et al., 1990), and the intervertebral disc. (Adams and Hutton, 1983, Potvin et al. 1991). Parnianpour et al. (1988) have demonstrated an increase in lateral bend and axial twist rotations about L4/L5 with erector spinae fatigue. Both movements have been linked to lumbar injury (Farfan et al, 1970, Andersson, 1981).

PROCEDURES

Six healthy, male subjects performed a series of lifts in the sagittal plane. Each subject was instrumented with 3 bilateral pairs of surface electrodes (lumbar, thoracic erector spinae (ES) and vastus lateralis (VL)) as well as a magnetic three dimensional kinematics monitoring device (3SPACE).

Individual sessions began with maximum voluntary contractions (MVC) of the thigh muscles and the ES. ES MVC's were performed in an apparatus that maintained an erect standing posture during isometric trunk extensor contractions. All EMG data was rectified and low pass filtered at 2.7Hz, non-linearly normalized using the MVC value as 100% and then sampled at 50Hz. Spine kinematic data was sampled at 20.4 Hz and normailized using upright standing and full flexion to represent 0% and 100% of maximum respectively.

The first lifting trials (rested) consisted of approximately 25 lifts at a frequency of 10 lifts/minute with a load of 20kg. The task required the lifting of an inertial load from a table at waist height, touching it to the ground and then lifting back up onto the table. Following the rested lifting session, the subjects performed a prolonged isometric contraction of their trunk extensors at 50% MVC until they could no longer maintain the load (exhaustion). It was assumed that these contractions resulted in substantial fatigue of the erector spinae muscles with no substantial fatigue of the leg muscles. Immediately following the prolonged isometric contractions, subjects began lifting for another 25 lifts.

Individual subject data was windowed to determine the start and end of each lift using spine flexion data and EMG data. Means, peaks and lift durations were calculated for each lift for the 6 EMG channels as well as the flexion, axial twist and lateral bend data. In addition the lift durations and RMS difference between right and left electrode pairs was calculated over the duration of each lift. Each lift time was normalized to 51 points (2% intervals). An analysis was performed to determine differences between the means for the rested and fatigued lifts variables using a one factor, repeated measure ANOVA.

RESULTS AND DISCUSSION

Fifty percent decreases in force generating capacity of the trunk extensors were demonstrated for each subject. Therefore, it was assumed that changes in lifting mechanics after the prolonged contraction could be attributed to fatigue in these muscles and not those of the legs.

Significant increases in peak lumbar and thoracic EMG were demonstrated (Figure 1). The average lift durations decreased by 20%, therefore subjects appeared to have a tendency to lift faster in a fatigued state. The increase in peak lumbar and thoracic EMG may have contributed to an increased load acceleration. The mean right/left differences were not observed to change significantly from the rested to the fatigued conditions. This variable was calculated to represent the bilateral coordination of each subject during the sagittal plane lifts.

It did not appear that isolated erector spinae fatigue increased spine flexion or increased the demands on the lower extremity as expected (Figure 1). The present results in combination with those of Trafimow et al. (1993) suggest that changes in lifting mechanics may be due to fatigue of the leg muscles. Thus, it is possible that leg fatigue was a major contributor to the conclusions drawn by Potvin et al. (1991). It would then follow that the increased risk of injury to the lumbar spine that has been hypothesized to accompany repetitive lifting may be due to either leg fatigue or other, as of yet, unmeasured factors.

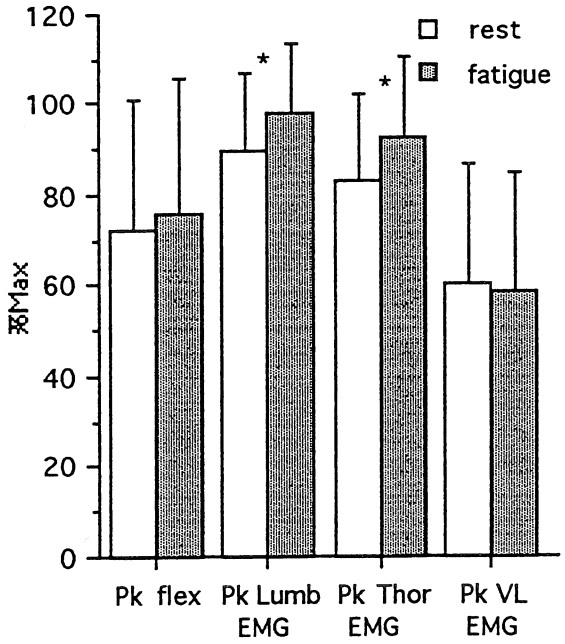

Figure 1: Graphical representation of selected variables. * indicates significant changes with fatigue. (pk = peak)

Isolated erector spinae fatigue did not appear to result in any generalizable trends towards an increased risk of injury to the tissues of the lower spine. However, it has been observed that some individuals may predispose themselves to a high risk of injury when in fatigued states. For example, one subject demonstrated an increase in flexion beyond their original maximum. Due to a possible increase in stress on the posterior spine ligaments resulting from this increased spine flexion, it is hypothesized that this subject was progressing towards an increased risk of injury in response to erector spinae fatigue (Figures 2 and 3). This subject also decreased his average lift duration from 7.8 s to 6.3 s (19%). This appeared to indicate an increased acceleration of the load and may explain the increased EMG amplitudes observed for the erector spinae (Figure 2).

Further work is needed in this area to further delineate the relative contributions of leg and trunk fatigue to a relationship between repetitive lifting and low back tissue injury risk.

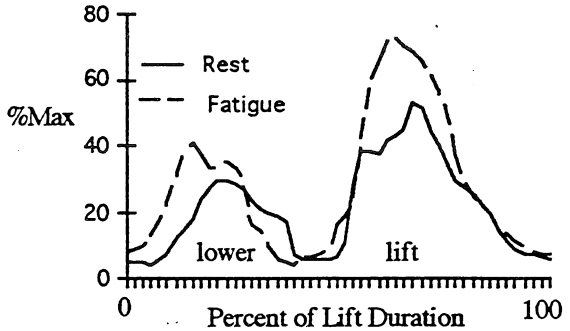

Figure 2: The ensemble average of lumbar EMG curves for one subject during the rested and fatigued lifting trials (n=25 for each curve)

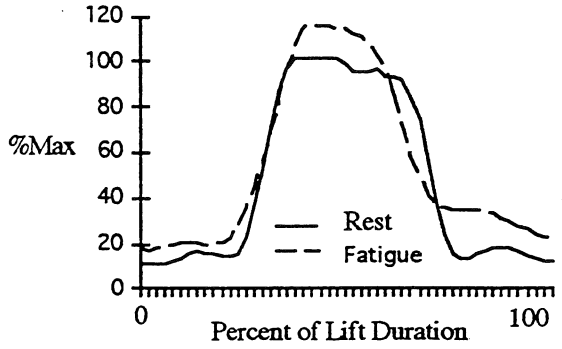

Figure 3: The ensemble average of spine flexion curves for one subject during the rested and fatigued lifting trials (n=25 for each curve)

REFERENCES

Adams, M.A. et al., *J. Bone Jt. Surg.*, 65:199-203, 1983.

Adams, M.A. et al., *Spine*, 3:245-253, 1990.

Andersson, G.B.J., Spine, 6:53-60, 1981.

Farfan, H.F. et al., *J. Bone Jt. Surg.*, 52-A:468-497, 1970.

Parnianpour, M. et al., *Spine*, 13:982-992, 1988.

Potvin, J.R. et al., *Spine*, 16:1099-1107, 1991.

Trafimow, J.H. et al., *Spine*, 18:364-367, 1993.

TORSO MUSCLE RECRUITMENT IN RESPONSE TO SAGITTAL PLANE L4/L5 SHEAR AND MOMENT LOADING

U. Raschke and D.B. Chaffin

Center for Ergonomics, The University of Michigan, Ann Arbor, MI 48109

INTRODUCTION

Current lumbar torso biomechanical prediction models utilizing optimization approaches to predict muscle activity do not predict observed antagonistic muscle activity well. It has been proposed that the performance may be improved if additional factors are included in the optimization formulations. Shear force is one such constraint. Toward this end, this study tested the hypothesis that shear force influences torso muscle activity. Statistical linear regression analysis of the muscle EMG activity during sagittal plane flexion loading lead to the rejection of this hypothesis. It is concluded that although antagonistic muscle activity was observed during this study, it was due to some other as yet unknown cause.

REVIEW AND THEORY

Empirically, antagonistic torso muscle activity has been observed during sagittal plane flexion loading and has been estimated to increase the spinal compression forces by 11-14% (Hughes, 1991, Thelen, 1992). Currently, optimization methodologies used in biomechanical models of the lower back to predict torso muscle activity (Bean et al. 1988, Crowninshield et al. 1981) do not adequately predict this muscle antagonism (Hughes, 1991). It has been theorized, however, that the CNS might be responding to physiologic requirements not currently represented in these prediction methodologies, such as minimization of shear loading on the spine or the production of intra-abdominal pressure. These omitted factors may be responsible for the observed antagonistic muscle recruitment. Hughes et al. (1987) found that inclusion of shear constraints in an optimization approach could lead to improved model predictions, yet the results were not conclusive. Cresswell's (1993) studies do not support a strong correlation between the antagonistic muscle activity and the IAP. Therefore, the objective of this study was to investigate the effect of sagittal plane moment and shear loads at the lower spine on the muscle activity of the lumbar torso. It was hypothesized that the lumbar torso muscle activity, as measured using normalized EMG, is influenced by moment as well as shear loading at the L4/L5 intervertebral joint.

METHODS

An experimental setup was designed in which moment and shear loads could be independently applied to the lumbar torso (Figure 1). Subjects stood in the neutral upright posture, with their ankles and knees strapped to padded braces on a rigid frame. The pelvis was fixed to the external rigid frame to neutralize the hip moment.

The loading conditions used for the experiment consisted of three levels of flexion loading (25, 112, 230N), applied horizontally at approximately the T9 vertebral level, and three levels of shear loading (0, 80, 180N), applied horizontally at the L4/L5 inter vertebral joint, as diagrammed in Figure 1.

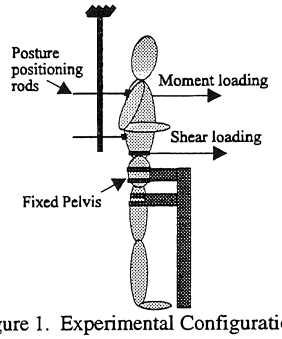

Figure 1. Experimental Configuration.

The actual L4/L5 moment loads for each subject varied slightly depending on the subject's L4/L5 to T9 distance. The average L4/L5 moments and standard deviations were 6.52 (0.21), 29.42 (0.94), and 59.6 (1.9) Nm. These load values were chosen to fall within the range of typical loads handled by manual materials handling (MMH) workers in industry (Marras et al., 1993). The load application location of the L4/L5 inter vertebral joint was palpated, while the application of the load at the T9 level was determined by the location of the harness to which the loads were attached. This harness passed around the subjects' torso and under his arms, and the most superior possible location of this harness was used. The moment error caused by modeling the L4/L5 interspace at the height of the palpated interspace level was assumed negligible (estimated to be less than 1.0%).

EMG activity from four muscle groups were recorded unilaterally from the right body side using surface electrodes. The muscles included the erector spinae, latissimus dorsi, external oblique, and rectus abdominus.

Linear regression analysis was used to evaluate the effects of the loading on the activity of the measured muscles. Equation 1 shows the model used in the regression analysis.

$$EMG_i = a_i + b_i*S_{L4/L5} + c_i*M_{L4/L5} + d_i*M_{L4/L5}*S_{L4/L5} + e_i \quad (1)$$

EMG_i	= normalized EMG activity of muscle *i*.
$M_{L4/L5}$	= L4/L5 moment.
$S_{L4/L5}$	= applied shear at the L4/L5 joint.
$M_{L4/L5}*S_{L4/L5}$	= moment shear interaction.
a_i, b_i, c_i, d_i	= regression parameters.
e_i	= residual error.

Five male subjects with no prior histories of back pain or injury participated voluntarily in the study (average age (std dev.) : 29.6 (4.9) years, height: 179.6 (8.3) cm, weight: 73.7 (8.4) kg). Subjects were instructed to maintain their upright neutral posture under the various loading conditions. Two positioning rods (wooden slates) were used to provide posture feedback. These slates could be felt by the subject but caused no discomfort or bracing. The loading conditions were randomized and two trials

of each loading condition were recorded. Each trial was five seconds long and EMG data were sampled at 80 Hz. EMG data were normalized with respect to baseline and maximum exertion values and smoothed using a FFT based filter with cutoff frequency of approximately 15Hz. The mean of the middle three seconds of each data trial were used for analysis. Subjects were given rests between trials to minimize fatigue effects.

RESULTS

Linear regressions were computed using the model described in Equation 1 for each muscle and each subject independently. Figure 2 shows the EMG response to the moment and shear loading conditions for the four muscles for a typical subject.

Table 1 provides a summary of the statistical results for each subject. For each subject and muscle (ES: erector spinae, LD: latissimus dorsi, EO: external oblique, RA: rectus abdominus), the significant ($p < 0.05$) predictor(s) is indicated. Only the L4/L5 moment was found to be a significant predictor of any of the torso muscle activities.

Table 1. Summary of the regression analysis significant predictors ($p<0.05$) for each subject and muscle. M=L4/L5 moment (see text for details)

	Muscle			
Subject	**ES**	**LD**	**EO**	**RA**
1	M	-	M	M
2	M	-	-	-
3	M	-	-	-
4	M	-	M	-
5	M	M	M	-

DISCUSSION AND CONCLUSION

The statistical results found from the shear loading experiments provide evidence that the CNS does not recruit muscles in response to shear loads on the spine as had been previously proposed. It seems therefore, that the antagonistic muscle activity observed in this study and by others is the result of some other yet undetermined mechanism. Therefore, this study provides evidence against the hypothesis that the inclusion of lumbar shear forces in biomechanical prediction models will enhance the predictability of the torso muscle activity. The source of the observed antagonistic activity remains unclear.

REFERENCES

Bean, J.C. et al. Biomechanical Model Calculation of Muscle Contraction Forces: A Double Linear Programming Method. J. Biomechanics 21(1):59-66 (1988)

Cresswell, A.G. On The Regulation of Intra-Abdominal Pressure During Different Motor Tasks. Ph.D. Dissertation, Karolinska Institute, Sweden.

Crowninshield D. et al. A Physiologically Based Criterion Of Muscle Force Prediction In Locomotion. J. Biomechanics, 14:793-801 (1981)

Hughes R. Empirical Evaluation of Optimization-Based Lumbar Muscle Force Prediction Models, Ph.D. Dissertation, University of Michigan (1991).

Thelen, D.G.,, A System Identification Approach to Quantifying Lumbar Trunk Loads. Ph.D. Dissertation, University of Michigan. (1992)

Marras W.S. et al. , The Role of Dynamic Three-Dimensional Trunk Motion in Occupationally-Related Low Back Disorders. Spine 18(5):617-629.(1993)

Acknowledgments: The authors would like to thank Coca-Cola USA for the support of this work.

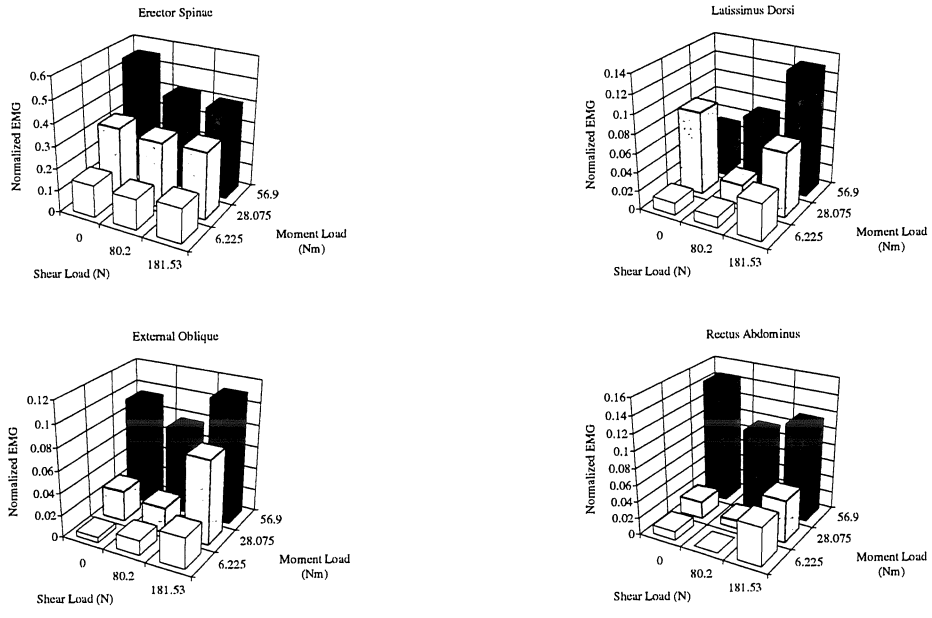

Figure 2. EMG response of four torso muscles to lumbar L4/L5 moment and shear loading conditions

STABILITY OF THE LUMBAR SPINE IN MAXIMAL EFFORTS

M Gardner-Morse*, IAF Stokes* and JP Laible+

*Department of Orthopaedics and Rehabilitation,
+Department of Civil and Environmental Engineering
University of Vermont, Burlington, Vermont 05405-0084

INTRODUCTION

The spinal column is inherently unstable, and *in vivo* a combination of muscle forces, muscle stiffness and motion segment flexibility stabilizes it. Clinically, instability is a controversial concept used to describe pathological conditions or variable pain symptoms. Here we investigated the classic mechanical definition of stability, in which a structure is stable if it returns to its equilibrium position in response to small disturbances.

This was investigated in a model of the spine with flexible motion segments and muscles whose stiffness was a function of their activation. Eigenvalue buckling analyses were used to determine the stability of the model. The aim is to use quantitative analyses to define the relative role of muscles in stabilizing the spine under conditions of maximal efforts in different spinal postures.

Under these conditions, active muscle stiffness was found essential to prevent the lumbar spine from buckling. The spine was unstable under the action of muscle forces if active muscle stiffness was ignored. For the range of published values of muscle stiffness as a function of activation, the spine was stable with a margin of safety up to two. It was inferred that certain loading conditions, spinal configurations and muscular activation patterns may place the spine at risk for 'self-injury' if the muscle activation strategy is not adequately controlled.

REVIEW AND THEORY

If the isolated spine (without muscles) is analyzed from the point of view of Euler buckling, it is unstable for very small applied forces. The idea that the active component of muscle stiffness (the component which is dependent on the degree of activation) stabilizes the lumbar spine has been put forward and investigated quantitatively by Bergmark (1989) and Crisco et al. (1990 and 1991). Muscles have two components of axial stiffness: passive (nonlinear elastic) and active stiffness. Here, the passive stiffness was assumed to be small in comparison to the active component. The active component is a complex function of activation, length and rate of shortening or lengthening. There is disagreement in the literature about what is an adequate representation of active muscle stiffness. Here, the simple linear formulation based on Bergmark (1989), was used:

$$k_m = q^*T/l_m$$

where k_m represents axial muscle stiffness (N/mm), T represents active muscle force (N) found in the muscle force distribution analysis, l_m represents muscle length (mm) and q is a dimensionless parameter. Thus, the global muscle stiffness depends on the forces in the muscles as well as the value of the active muscle stiffness parameter q, for which there is a wide range of published values (Crisco et al., 1990). In these analyses q was treated as a variable, and the critical value necessary for spinal stability was determined.

PROCEDURES

We constructed a model with 66 symmetric pairs of multi-joint muscles which attach to five rigid lumbar vertebrae and rigid bodies representing the thorax and the sacrum/pelvis. Vertebral positions, and attachments and physiologic cross-sectional areas (PCSA) of extensor muscles and psoas were taken from values reported by Bogduk et al. (1992). We also included the rectus abdominis, but omitted quadratus lumborum, unisegmental dorsal muscles and the oblique abdominals for lack of accurate data. Therefore, the analyses were limited to loadings in the sagittal plane (flexion and extension efforts). The motion segments were represented as elastic beams (Gardner-Morse et al., 1990) matched to experimental data. The initial position of the lumbar spine was assumed to be a resting position, in which no forces or moments (due to bodyweight or elastic stresses) were present.

To determine the muscle force distribution under conditions of maximal external effort, linear programs (linear optimization) were run with the objective of maximizing external moments (effort). Constraints on the solution were: simultaneous force and moment equilibrium at all vertebral levels, muscle stress bounds (0-0.46N/mm^2), and the physiologic range of motion permitted in the joints (5 mm translation and 5° rotation for sagittal plane; 2 mm translation and 2° rotation for the other planes).

The stability of the muscle force distribution was checked *post hoc*. The active muscle stiffness was variable based on variation of the active muscle stiffness parameter q. Both elastic and geometric stiffness in both the muscles and the spine were used in an eigenvalue buckling analysis. The spine is unstable if the value of the lowest positive eigenvalue λ is less than one, metastable if equal to one, and stable if greater than one.

These analyses are considered to be novel because 1) they recognize that equilibrium conditions must be satisfied at all the articulations crossed by multi-joint muscles. 2) they use published motion segment elastic properties to define the otherwise unknown location of the center of pressure for load transmission through motion segments. 3) they recognize that the spine must be in stable equilibrium.

RESULTS

Maximal efforts: In these simulations of maximal efforts, many muscles could not be maximally activated and still be compatible with equilibrium constraints. Antagonistic muscle activity occurred in the flexion effort in order to maintain simultaneous equilibrium at all six joints. Flexion of 7.5° at each joint (producing a slightly flexed posture) increased the maximal efforts in all planes. The maximum

compressive load on the spine was 2260 N. The addition of a 340 N vertical compressive load (upper body weight) only reduced the extension effort by 4%.

Structural stability: Under conditions of maximum voluntary effort, it was found that active muscle stiffness was essential to prevent the lumbar spine from buckling (Figure 1). It was stable with a margin of safety up to two for active muscle stiffness in the range of published values of muscle stiffness as a function of activation. The buckled shapes of the spine (the eigenvectors associated with the eigenvalues from the buckling analyses) were primarily lateral bending with a little torsional twisting of the spine. This suggests that lateral muscles may increase the stability of the spine even in sagittal plane loading.

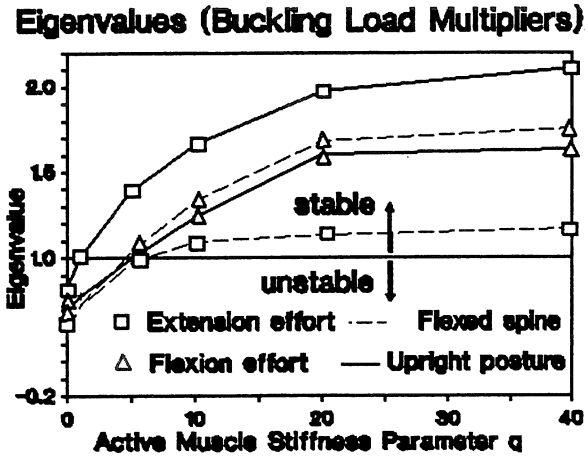

Figure 1 Graph showing model stability (lowest eigenvalue) as a function of muscle stiffness 'q', for flexion and extension efforts; flexed and upright posture.

DISCUSSION

These analyses showed quantitatively that a well controlled muscular activation strategy is required to maintain simultaneous equilibrium at all of the lumbar articulations. It also demonstrated that the active component of muscle stiffness is required to stabilize the lumbar spine. The stability of the lumbar spine did not necessarily depend on the magnitude of the external load (effort). This model should be able to identify loading conditions, spinal configurations and muscular activation patterns which may place the spine at risk for 'self-injury' if the muscle activation strategy is not adequately controlled.

REFERENCES

Bogduk N, Macintosh JE, Pearcy MJ: A universal model of the lumbar back muscles in the upright position. *Spine* 17:897-913, 1992

Bogduk N, Pearcy M, Hadfield G: Anatomy and biomechanics of psoas major. *Clin Biomech* 7:109-19, 1992

Bergmark A: Stability of the lumbar spine. A study in mechanical engineering. *Acta Orthop Scand* Suppl 230:1-54, 1989

Crisco JJ 3d, Panjabi MM: The intersegmental and multisegmental muscles of the lumbar spine. A biomechanical model comparing lateral stabilizing potential. *Spine* 16:793-9, 1991

Crisco JJ 3d, Panjabi MM: Postural biomechanical stability and gross muscular architecture in the spine. In: *Multiple muscle systems: Biomechanics and movement organization*, ed by JM Winters and SLY Woo. pp 438-450. New York, Springer-Verlag, 1990

Gardner-Morse MG, Laible JP, Stokes IAF: Incorporation of spinal flexibility measurements into finite element analysis. *J Biomechanical Eng* 112:481-483, 1990

ACKNOWLEDGEMENT

Supported by NIH R01 AR 40093, PHS Biomedical Research Support Grant S07 05429, and Fogarty International Center Fellowship TW 01948.

THE INTERACTION OF SPINE FLEXION AND PELVIS ROTATION CONTRIBUTIONS TO TRUNK INCLINATION DURING DYNAMIC LIFTING TASKS

D.C. Ursulak and J.R. Potvin
School of Human Biology, University of Guelph, Ontario, Canada, N1G 2W1

INTRODUCTION

The amount of spine flexion that occurs during a lift will influence the deleterious effects of stresses placed on the intervertebral joints and surrounding soft tissues. Anterior shear forces on the disc increase with extreme flexion due to increased stress in the anteriorly oriented interspinous ligaments and decreased force in the posteriorly oriented lumbar erector spinae muscles due to the flexion relaxation response (Potvin et al. 1991). Increased spine flexion also causes an anterior shift in the compressive force on the discs and vertebrae, resulting in posterior pressure on the nucleus and increased strain on annulus fibers. Progressive spine flexion also increases strain in the posterior ligaments (McGill, 1988). It has been suggested that during lifting the ligaments are preferentially utilized to the flexion moment (Gracovetsky et al., 1977). However, Potvin et al. (1991) have demonstrated that peak ligament moment contributions did not generally exceed 60 Nm even during stoop lifting (straight leg, inclined trunk).

Rotating the trunk to perform a lift, can be accomplished through two mechanisms; spine flexion and rotation of the pelvis about the hips. Some studies have attempted to estimate spine flexion by monitoring trunk inclination (Gracovetsky et al., 1977. Freivalds et al., 1984). This method neglects the substantial contribution of pelvic rotation as demonstrated by Potvin et al., (1991) and Burgess-Limerick et al., (1991).

The purpose of this study was to determine the interaction between spine flexion and pelvis rotation contributions to trunk rotations during dynamic lifting.

METHODS

Seven female subjects (age 22.7±1.25 yr., height 1.66±.05 m, mass 62.4±8.33 kg.) and four male subjects (age 24.5±2.38 yr., height 1.79±.07 m, mass 82.8±14.3 kg.) participated in the study after informed written consent. All subjects were screened for low back traumas or recurrent pain.

The subjects performed three types of lifts in the sagittal plane: 1) bending predominantly at the knee (squat lift), 2) bending primarily with the trunk (stoop lift), and 3) subjects were allowed to lift in the style that they felt most comfortable (freestyle lift). Each technique required lifts with three loads (female: 7, 13, 20 kg., male: 9, 18, 27 kg.), with three repetitions of each. The total number of lifts equaled 27. The highest loads for males and females were chosen to correspond with the maximum acceptable loads recommended by Mital et al. (1993). All loads and lifting techniques were presented in random order. The different techniques were incorporated to ensure that all the ranges of trunk rotation would be observed. There were no constraints placed upon speed of lift or time allowed between lifts.

Lifts were performed using a load pan with handles 15 cm from the floor and parallel to the sagittal plane, spaced approximately shoulder width apart. Subjects were allowed ten warm up lifts with the medium load to help avoid injury and to facilitate a prediction of the exertion required.

Reflective markers were affixed to the lateral malleolus, lateral epicondyle, greater trochanter, L_4L_5, C_7T_1, with sacral and thoracic triangular frames cemented to the sacrum and $T_{12}L_1$ respectively. Videography was recorded at 30 Hz, with digitizing completed on a Peak 5 system at 15 Hz. Erect standing biases were used to determine the zero reference point for normal lordosis and pelvic rotation. Pelvic rotation was monitored with the rotation of the sacrum triangle. Spine rotation was defined as the ($T_{12}L_1$ - sacrum) triangle rotations. Trunk inclination was defined as the angle created by the line joining the L_4L_5 and C_7T_1 markers. For each lift maximum spine flexion, pelvic rotation and trunk inclination were recorded. Statistics used a repeated measures one way Anova's, with a Scheffe's post hoc analysis.

RESULTS

Only the lift data is presented for this paper. Mean peak trunk inclination varied across lift techniques (squat 48.1°, free 74.2°, stoop 102.2°), as did pelvic rotation (squat 19.2°, free 25.8°, stoop 51.1°), while spine flexion remained relatively constant (squat 40.2°, free 51.3°, stoop 53.3°). Peak trunk inclination was largely dependent of the lift technique, while spine flexion remained relatively constant across the three lift techniques. It appears that pelvic rotation was predominantly responsible for any differences in peak trunk inclination observed between lifting techniques. Peak trunk inclination was not found to correlate with either peak spine flexion (r^2=0.17 males, r^2=0.40 females) or pelvic rotation (r^2=0.13 males, r^2=0.34 females).

There was some load effect for pelvis rotation with medium and heavy loads values being significantly greater than those for the light conditions($P<.008$). There was a significant difference in mean peak trunk inclination (72.3° males, 77.3° females, $p<0.05$)) for the three lift styles compared to mean peak spine flexion (52.4° males, 44.1°, females) ($P<.0001$) and

pelvic rotation (26.5° males, 37.8° females; P<.0001; see Figs. 1&2).

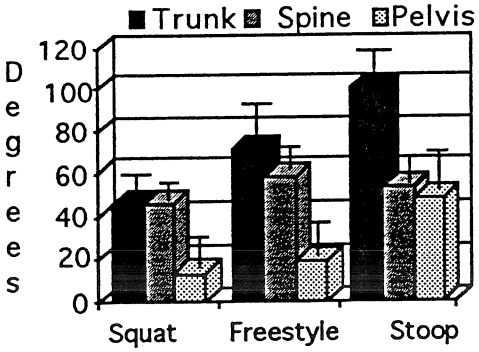

Fig.1 Mean Peak Trunk vs Spine vs Pelvic Rotations for Males

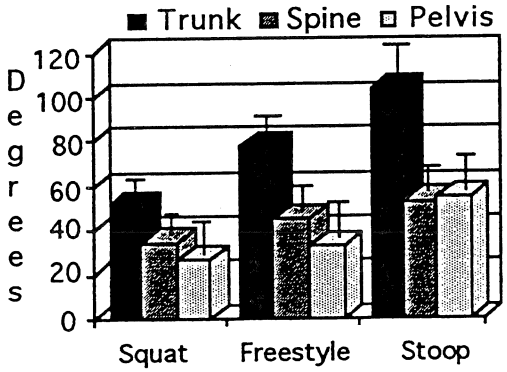

Fig 2. Mean Peak Trunk vs Spine vs Pelvic Rotations for Females

Table 1: Mean Maximum Male - Female Differences in Trunk, Pelvic & Spine Rotations(°) for Lifts & Loads

Lift Type	Load Type	Male - Female Diff. (°) Trunk	Pelvis	Spine
Stoop	Light	2.5	7.8 *	-2.0
	Medium	-0.7	-13.1 *	8.4
	Heavy	-10.2	-15.1 *	-0.1
Squat	Light	3.6	-3.4 *	10.0 *
	Medium	-7.4	-19.5*	10.5 *
	Heavy	-11.1	-16.5*	13.0 *
Free-style	Light	-3	-6.5 *	13.2 *
	Medium	-8.6	-17.1 *	9.1 *
	Heavy	-10.3	-18.6 *	19.1 *
	Mean	-3.4	-11.3 *	9.0 *

n=4 (male), n=7 (female)
* indicate significant differences

Differences were observed between male and female subjects in the relative contributions of spine flexion and pelvic rotation to the peak trunk inclinations measured. On average, females demonstrated higher pelvic rotations (by 11.3°, P<.0017) and lower spine flexions (by 9.0°, P<.0173) over the three lifting conditions (Table 1). These differences were most profound for the two heaviest load conditions. There was no significant difference in mean peak trunk rotations between male and females for any of the lifting techniques.

DISCUSSION

As was expected, the squat and stoop techniques had the lowest and highest trunk inclinations respectively, while the freestyle technique appeared to be a compromise between squat and stoop lifting. Increasing trunk inclination from the squat to the stoop technique were not accomplished with an increase in spine flexion, but instead, with increasing pelvic rotation. In fact, spine flexions were observed to remain relatively constant across techniques. Similarly there was no observed increase in spine flexion with an increase in load. These results may suggest that muscles, and not posterior ligaments, are primarily responsible for meeting the demands of increased loads. This has been observed previously by Potvin et al. (1991).

There is evidence to suggest that flexion can predispose the tissues of the spine to injury. A number of studies have used trunk inclination to represent spine flexion (Gracovetsky et al., 1977. Freivalds et al., 1984). However, the current data suggests that their is very little relationship between trunk inclination and spine flexion. In fact, trunk angle must be seen as a combination of spine and pelvic rotations. In light of this finding, caution must be exercised when drawing conclusions about tissue stresses or possible low back injuries as trunk inclination will most likely over estimate the true spine flexion. This is especially true as lifting progresses more towards a stoop technique, since this was observed to be accomplished essentially by an increase in pelvic rotation.

It was observed that females rotated about the hips more and flexed the spine less, when compared to males who tended to involve more spine flexion with less pelvic rotation. This difference became much more apparent as the loads increased. It must be noted that only four male subjects were studied and a further investigation of this possible phenomenon is currently being conducted.

REFERENCES

Burgess-Limerick et al. *Spine.* (1992)
Chaffin, D.B. *Am. ind. Hyg. Ass. J.* 38:662-675 (1975)
Farfan, H.F. *Orthop. Clin. N. Am..* 8:9-21 (1975)
Freivalds, A., et al. *J. Biomech..* 17(4):251-262 (1984)
Kippers, A. & Parker, W.J. *J. Biomech.* 22(1):67-75 (1989)
Gracovetsky, S. et al. *Orth. Clin. of N. Am.* 8(1):135-153 (1977)
McGill, S.M. *Spine.* 13(12):1395-1402 (1988)
Mital et al. *A Guide to Manual Materials Handling* (1993)
Potvin, J.R. *Spine.* 16(9):1099-1107 (1991)

MEASURING MOMENTS AND FORCES IN 6 DOF IN A SPINE MOTION SEGMENT

Daniel R. Baker, James D. Kang, Glen A. Livesay and Savio L-Y. Woo

Musculoskeletal Research Center - Department of Orthopaedic Surgery
University of Pittsburgh, Pittsburgh, PA 15213

INTRODUCTION

Injury to the cervical spine can develop from many different sources ranging from acute trauma to degenerative changes associated with aging. Treatment of these problems requires a detailed knowledge of the relationship between adjacent vertebrae. This relationship can be more easily understood by knowing the manner in which the forces and moments are transmitted between such adjacent vertebrae. We have applied a standard force-moment transformation to data from a 6 degree-of-freedom sensor to study this transmission.

Results obtained from studies of canine C4-C5 cervical spine motion segments demonstrate force and moment coupling. This coupling is diminished at the joint space – indicating that proper transformation of the forces and moments is necessary to understand the transmission of forces and moments across a motion segment. The observed coupling is consistent with studies who have examined vertebral motion, instead of forces and moments, under similar conditions.

REVIEW AND THEORY

Previous studies have shown that the cervical spine motion is highly coupled (Panjabi et al., 1986; Mimura et al., 1989; Greene and Heckman 1994). Further, this coupling has been shown to change after transection of spinal ligaments (Panjabi et al., 1975).

The 6 DOF measurements in our investigation are gathered via a universal force/moment sensor or UFS (Figure 1). By decomposing the applied forces and moments into their principle components the transmission of those forces and moments across a motion segment then can be studied under varying conditions. The technique presented here is based on Fujie, et al. (1993).

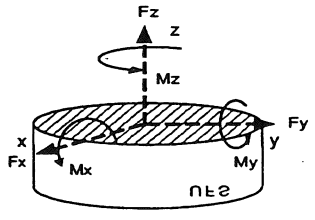

Figure 1. A schematic of the UFS with the sensor coordinate system attached.

The forces and moments measured by the UFS are then transformed using a [6x6] Jacobian matrix so that the forces and moments are those at the joint and not at the sensor. The Jacobian takes the form:

$$\begin{bmatrix} F_x' \\ F_y' \\ F_z' \\ M_x' \\ M_y' \\ M_z' \end{bmatrix} = \begin{bmatrix} 1 & 0 & 0 & 0 & 0 & 0 \\ 0 & 1 & 0 & 0 & 0 & 0 \\ 0 & 0 & 1 & 0 & 0 & 0 \\ 0 & -d_z & d_y & 1 & 0 & 0 \\ d_z & 0 & -d_x & 0 & 1 & 0 \\ -d_y & d_x & 0 & 0 & 0 & 1 \end{bmatrix} \begin{bmatrix} F_x \\ F_y \\ F_z \\ M_x \\ M_y \\ M_z \end{bmatrix}$$

with F and M as the component parts at the UFS face, F' and M' being the forces at the joint after a translation over a distance, d (for the current application there are no rotations between the sensor and the specimen). Note that the forces remain the same but that the moments are scaled by the translation. The only other transformation done is to convert the sensor coordinate system into the spine-centered coordinate system (White and Panjabi, 1990). This right-handed coordinate system has the y-axis vertical and the z-axis pointing anterior. For this investigation the coordinate system is located at the disc center.

PROCEDURES

The cervical spines from two 20 kg canines were harvested within 2 hours of death and were kept frozen (-20°C) until each test. After thawing, the C4-C5 motion segment was dissected and then potted in a custom testing jig. The motion segment was positioned in the jig and the inferior vertebra was held in place by four 2.8 mm Steinman pins placed orthogonally through the vertebral body. PMMA was then poured around the vertebral body, and care was taken to ensure that the segment was centered in the jig. The PMMA cured and the jig was inverted and the same procedure performed for the superior vertebra.

The jig was placed in an Instron™ 8521 bi-axial material testing machine, aligning the segment along the vertical axis of the test machine. The jig allowed adjustments to be made along the anterior-posterior axis. Once aligned, the jig was clamped into place and the trials began.

The test machine was programmed to apply displacements of ±0.09 rads about the y-axis at 0.63 rad/s. A 6 degree-of-freedom UFS (ATI, 350/2100), attached to the base of the

jig, measured the forces and moments exerted on the inferior vertebra. The rotational displacement of the superior vertebra and the forces and moments of the inferior vertebra were all recorded on the computer which controlled the test machine.

RESULTS

One trial consisted of two pure sinusoidal rotations about the y-axis. The jig was moved either anteriorly or posteriorly and the test was run again. A typical result, from the second canine C4-C5 motion segment tested, is shown in Figure 2. Note that all forces and moments are coupled given only an axial rotation to the superior vertebra. The solidlines are the forces and moments at the sensor and the dashed lines are the transformed forces and moments now located at the joint.

DISCUSSION

These results confirm that the force and moment transmission through a motion segment is highly coupled. Since the canine C4-C5 motion segment is morphologically different than a human it is surprising how similar the coupling is to other studies (e.g., Mimura et al., 1989).

Another interesting result is that all three forces have active components during an axial rotation. The y-axis force (the second down in Figure 2) was expected and illustrates the importance of the facet joints. The orientation of the facet joints at this motion segment allowed a downward component to be developed during each half of the applied sinusoidal motion. The facet joints may also account for the side forces and the moments about the x- and z-axes. These results show the necessity of measuring all forces and moments during this type of experiment.

The differences seen in the moments about the x- and z-axes between the moments measured at the sensor and those at the joint itself are an important reason for careful transformation of the forces and moments. Because of the test setup the moments were actually smaller than those seen at the sensor. Under certain geometric configurations the relative rotations would also need to be considered thus making the Jacobian somewhat more complicated.

While it is true that under these test conditions the applied motion may not be exactly physiologic, these results confirm previous work thus supporting the use of a UFS for further studies. Knowing how all of the forces and moments are transmitted across a joint will allow a detailed evaluation of the relative roles of the ligaments holding a motion segment together. This information would be quite useful to implant design engineers and clinicians alike.

REFERENCES

Fujie, H. et al., XIVth Int'l. Society of Biomechanics, Paris, (pp. 39-42), 1993.

Greene, W. and Heckman, J., The Clinical Measurement of Joint Motion, AAOS, 1994.

Mimura, M. et al., Spine, 14(11), 1135-1139, 1989.

Panjabi, M. et al., Ortho. Res., 4, 152-161, 1986.

Panjabi, M. et al. J. Biom., 8, 327-336, 1975.

White Jr., A. and Panjabi, M., Clinical Biomechanics of the Spine, J. B. Lippincott, 1990.

ACKNOWLEDGEMENTS

The authors wish to thank Greg Bijak for his help interfacing the sensor with the existing equipment and for his help during the testing and the Department of Orthopaedic Surgery at the University of Pittsburgh for providing support for this research.

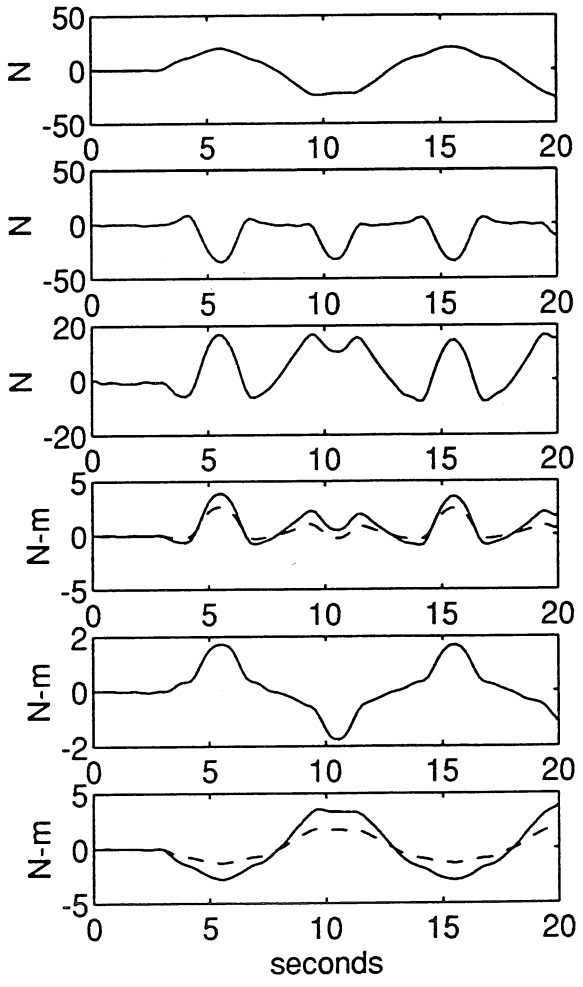

Figure 2. This is a typical force and moment result after transformation. From the top the forces and moments are: $[F_x, F_y, F_z, M_x, M_y, M_z]^T$. The solid line represents the forces and moments at the face of the UFS, in the White and Panjabi coordinate system for comparison, and the dashed line represents those transformed to the joint center.

POSTER SESSION

II

LOAD ON THE THUMB OF THE OBOIST'S

W.P. Smutz, A.T. Bishop, H. Niblock, M. Drexler, K.N. An, M. Johnson
Orthopedic Biomechanics Laboratory, Mayo Clinic/Mayo Foundation, Rochester, MN

INTRODUCTION

The forces acting on the right thumb while playing the oboe were measured. A simulated oboe was constructed, instrumented with loadcells and fitted with an adjustable thumb rest. The force and position of the thumb were measured for 5 different thumb rest position. Results showed that the position of the thumb rest affects the forces on the thumb.

REVIEW AND THEORY

Among the recent occupational groups to be identified as being susceptible to overuse injuries are musicians. Within members of symphony orchestras studied in Australia, England and the United States, the incidence rate of overuse injuries among woodwind players was more than 70 percent (2,3). Among oboe and clarinet players, injuries to the right thumb were the most common problem. In both the oboe and the clarinet the weight of the instrument is borne almost entirely by the right thumb. Supporting the weight of the instrument entirely by the tip of the thumb has been hypothesized to cause repetitive stressing of the ligaments of the joint. A variety of modified thumb rest are presently available that may help to reduce this overstressing. The Dutch thumb rest modifies the position of the thumb by increasing the distance from the instrument in the radial direction. The Loree thumb rest moves the thumb distally, which brings it closer to the balance point.

Although the weight of the instrument has been implicated as an injury mechanism, the loads that an oboe or a clarinet place on the thumb have not been quantified, either for the standard thumb rest or for a modified thumb rest. Therefore the purposes of this study are; 1) develop a methodology to measure the magnitude, direction, and point of application of the forces on the right thumb while playing the oboe, 2) use this methodology to perform measurements on a group of experienced oboe players, and 3) determine how changing the position of the thumb rest effects the forces on the thumb.

METHODS AND PROCEDURES

A simulated oboe was designed for the study. The simulated oboe is made of plastic and is of the same size and weight and has the same key position and balance point as an actual oboe (Figure 1). The simulated oboe has a thumb-rest that is adjustable in 2 planes, longitudinally and radially. In order to measure thumb force two loadcells have been attached to the thumb-rest, to measure forces ordinarily applied to the thumb at the thumb rest and the body of the instrument (Figure 2).

The position of the right thumb was measured using a electromagnetic tracking system. (3Space Tracker, Polhemus Navigation). The accuracy of the 3Space Tracker is 0.5 mm or 0.5 degrees (1). Sensors were attached to the proximal phalanx, distal phalanx, thumb metacarpal, and third metacarpal. A number of easily identifiable anatomic landmarks were digitized to relate the sensor positions and orientations to the underlying anatomy.

Ten adults (20-45 yrs) were used in this study. All the subjects were experienced oboists (one profession, a semiprofessional, and eight university students majoring in oboe performance). The test protocol consisted of 5 configurations; 1) thumb rest in the normal position, 2) thumb rest 1 cm distal to the normal thumb rest position along the longitudinal axis, 3) thumb rest 1 cm proximal to the normal thumb rest position along the longitudinal axis, 4) thumb-rest positioned normally in the longitudinal axis but moved out 0.4 cm radially to simulated a custom thumb rest that is presently being marketed, and 5) thumb rest positioned normally in the longitudinal axis but moved out 0.8 cm radially. Two different fingerings were measured in each configuration; left index finger only (B natural) and index, middle, and ring fingers of both hands (6 fingers total, D natural). Each fingering was held for 5 seconds. Both the force and 3Space Tracker data were collected for each configuration at a frequency of 15 Hz and stored on a PC computer. A photograph of the test subject's right hand was taken during each configuration. The photographs were used to determine the point of contact between the thumb rest and the thumb as well as the position of the oboe relative to gravity using a plumb line.

RESULTS

Results of the force measurements for the semiprofessional oboists on the thumb is shown in Figure 3. In general, the force on the pulp of the thumb ranged between 4 and 10 N, and the force on the lateral aspect of the thumb at the interphalangeal joint level ranged between 2 and 4 N. The location of the thumb rest definitely affects the amount of force applied. By using the thumb rest distal to the normal position (closer to the center of gravity of the oboe)

the force was found to be minimal. The fingering of the instrument also influenced the load on the thumb as shown for playing a B (1 finger) and a D (6 fingers).

DISCUSSION

A method has been developed for the measurement of joint position and force application of the thumb during oboe playing. These data could be used to estimate the loading on the ligament. The force on the ulnar aspect directly create a radial deviation moment and stress the ulnar collateral ligament. On the other hand, the friction on the pulp of the thumb would generate such a moment as well. Thus the normal force ia also an important measurement. The results from this study will be used to find the optimal position of the thumb rest that will minimize the injury potential to the thumb.

REFERENCES

1. An KN, Jacobsen MC, Berglund LJ, Chao EYS: Application of a magnetic tracking device to kinesiologic studies. [Technical Note] Journal of Biomechanics 21(7):613-620, 1988

2. Fry HJH: The treatment of overuse syndrome in musicians. Results in 175 patients. The Royal Society of Medicine 81:572-575, 1988

3. Fry HJH: Incidence of overuse syndrome in the symphony orchestra. Medical Problems of Performing Artists 1:51-55, 1986

Figure 1. Photograph of simulated oboe.

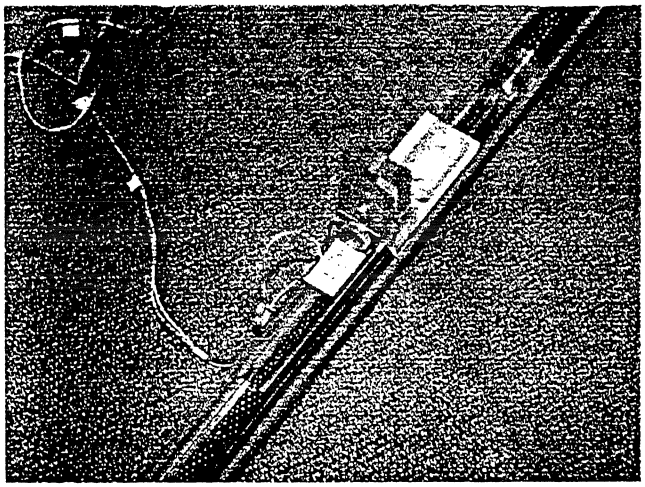

Figure 2. Adjustable thumb rest with loadcell installed.

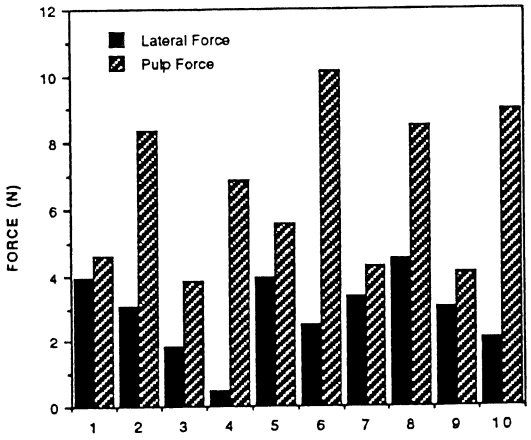

Figure 3. Thumb forces for semiprofessional oboist. 1) Normal position 1 finger, 2) normal position 6 fingers, 3) 1 cm distal 1 finger, 4) 1 cm distal 6 fingers, 5) 1 cm proximal 1 finger, 6) 1 cm proximal 6 fingers, 0.4 cm radial 1 finger, 8) 0.4 cm radial 6 fingers, 9) 0.8 cm radial 1 finger, 0.8 cm radial 6 fingers.

ACKNOWLEDGEMENTS

This study is supported in part by NIH Grant AR 08249

INVARIANT RELATIVE FOOT POSITION DURING RECOVERY FROM AN IMPENDING FORWARD FALL

J.W. Feuerbach and M.D. Grabiner
Department of Biomedical Engineering (Wb-3)
The Cleveland Clinic Foundation
Cleveland, OH 44195

INTRODUCTION

Because falling is a major cause of injuries and the sixth leading cause of death in persons over 65, characterizing the motor requisites of fall prevention is important. By characterizing these requisites, the effect of age-related performance deficits on the ability to restore balance subsequent to large perturbations may be more accurately depicted.[1] In Do et al.[2] the stepping response of a forward fall initiated from a static inclined position was partitioned into two phases: preparation and recovery. The preparation phase was defined as the time from the initial perturbation to recovery foot toe-off; and the recovery phase was defined as the time from recovery foot toe-off to recovery foot touchdown. These investigators stated that temporal aspects of the preparation phase were invariant and did not depend on initial conditions prior to the perturbation. However, recent evidence[3] contends that the preparation phase may not be invariant as Do et al. suggested. Do et al. also described the recovery phase as being "adaptable" to initial conditions. For example, step length increased with increasing inclination of the body prior to the perturbation.

In the present study we investigated the "adaptability of the recovery phase" in greater detail than that of the study by Do et al. A component of the step length was examined, namely the horizontal distance between the whole body center of gravity (CG) and the recovery foot CG. This variable was referred to as the *relative foot position*. The purpose of the present study was to investigate the relationship between the initial inclination prior to a sudden release and forward fall, step length, and relative foot position. It was expected that the relative foot position would demonstrate less "adaptability" than other kinematic and kinetic parameters.

METHODS

Each subject (N=10 males) was leaned anteriorly to one of five specified angles while supported by a horizontal rope, then released without warning. Prior to release, subjects were instructed to maintain a linear body position, arms folded across the chest, and the barefeet in full contact with the floor. Subsequent to release, the subjects avoided a fall by recovering with a single step while maintaining the arms folded across the chest, and also maintaining at least partial ground contact of the contralateral foot (hereafter referred to as the support foot). The subjects completed three successful

recoveries from initial inclinations of 5, 10, 15, 20, and 25 degrees from the vertical.

The body was modeled as seven linked segments -- trunk combined with the head and arms, thighs, shanks, and feet -- marked with twelve hemispherical markers. The motions of the markers were recorded at 60 Hz for two seconds with a six camera Motion Analysis System (Santa Rosa, CA). The recovery foot began and ended each trial on a 61 by 122 cm force plate (AMTI, Newton, MA). Ground reaction forces were recorded for 2 seconds, digitized at 1 KHz and stored on a microcomputer for processing.

The locations of the recovery foot CG and whole body CG were calculated at the time of recovery foot touchdown, which was identified from the vertical force record. *Relative foot position* was defined as the horizontal distance between the recovery foot CG and the whole body CG at the time of recovery foot touchdown. *Step length* was defined as the horizontal distance between the recovery foot CG prior to release and at touchdown. Relative foot position and step length were both entered into a 1 by 5 ANOVA with repeated measures. The level of significance was set at 0.05.

RESULTS

Mean normalized step lengths and relative foot positions for each of the five angles of lean are shown in Table 1. The differences between the relative foot positions were not significant ($p > 0.05$). There was a significant effect of inclination angle on step length ($p < 0.05$). Post-hoc Tukey's test revealed that, with the exception of the 10 and 15 degree conditions, the step lengths were significantly different from one another.

Table 1. Mean (sd) of normalized relative foot position and step length.

lean angle (degrees)	foot position (% height)	step length (% height)
5	11.9(2.4)	26.7(0.8)
10	13.1(2.8)	32.6(2.7)
15	12.8(3.0)	34.5(2.8)
20	14.6(3.0)	40.6(3.1)
25	13.0(2.2)	44.9(2.5)

DISCUSSION

Similar to Do et al., the step length of a successful recovery from an impending forward fall varied as a function of inclination angle, reflecting the adaptability of the recovery phase. However, *the relative foot position was invariant,* regardless of the inclination angle. Thus, relative foot position may represent a control parameter specified by the central nervous system.

Other conditions, such as various types of visual feedback[3], need to be examined to determine if the relative foot position of a successful recovery from an impending forward fall maintains invariance. The "adaptable recovery process" described by Do et al. may have invariant characteristics.

REFERENCES

1. Grabiner et al. *J Geront* 48:M97-102, 1993
2. Do et al. *J Biomech* 15:933-939, 1982
3. Hoshiyama et al. *Neurosci Res* 18:121-127, 1993.

GROUND REACTION FORCE ANALYSIS OF CHANGING DIRECTION DURING WALKING

Dali Xu* and Manssour H. Moeinzadeh**
*Department of Kinesiology, University of Illinois at Urbana-Champaign IL 61801
**Department of General Engineering, University of Illinois at Urbana-Champaign IL 61801

INTRODUCTION

Walking is a basic means of locomotion for human beings. Many researchers have studied various aspects of walking, including level walking straight forward and backward, and walking up and down stairs. Changing direction during walking has not been seriously considered by researchers, although, this type of walking often happens in every day life. People walk with feet step by step whenever walking straight forward and changing direction, however, altering direction during walking is an asymmetric movement. What are the unique characteristics of changing different direction during walking? What are the basic factors which influence human walking while changing direction? These important questions need to be investigated for a better understanding of human locomotion.

REVIEW AND THEORY

There has been limited studies of changing direction during locomotion. Stucke et al. (1984), investigated static and dynamic friction in rotation of running. Hamill et al. (1987) examined the changes in kinetics and kinematics of the lower extremity during the support phase of the running stride in track turns. Patla et al. (1991) evaluated the visual control of locomotion of the dynamics of gait adjustments on changing direction. These studies explained the characteristics of running and adaptation of human locomotion while changing direction, but there were not enough information for determining unique characteristics of changing direction during walking. Human motion depends upon the motor control and interaction between the internal and external forces. The ground reaction force (GRF) is the external force which can only be used by a person for creating different movement. From the biomechanical point of view, the ground reaction force plays an important role in human locomotion. The footwear design for walking is partially depend upon the information of the interaction between foot and ground. On a given surface, the shoe is the major means of attenuating the impacts which the body experiences during running (Cavanagh, et al. 1980) as well as walking. GRF, shoes and playing surfaces are the major factors in the human slip and fall. Information about these factors should be important in the understanding of the changing direction while walking, and in designing of shoes and playing surfaces. The purpose of this study was to investigate the properties of GRF while changing direction during walking so as to identify the unique characteristics of GRF patterns for altering direction. The insights gained in this study will be helpful in the clinical diagnosis of dysfunctional walking and also in the decision-making process of shoe manufactures.

PROCEDURES

Subjects: There were 33 volunteers consisting of 21 males and 12 females from the University of Illinois who participated in this study. The age range was from 18 to 23 years. The height was from 5'2" to 6'3" and the weight ranges from 119 lbs to 195 lbs.
Task: The subjects were asked to walk on a force platform while walking straight forward and while changing direction. Two elementary turning movements were defined to represent the walking while changing direction. They were turning to the right at 45 degrees and 90 degrees respectively. It was assumed that the result of turning in the right direction was the same as turning in the left direction. Two walking speeds of natural cadence (108 step/min.) and fast cadence (138 step/min.) were evaluated. The right foot and the left foot were used to support the body for changing direction at 45 degrees and 90 degrees respectively. Each subject performed thirty trials on the force platform for these different conditions. The performance for each different walking condition was in random order.
Instrumentation: One AMTI force platform was used to collect GRF data. The sampling frequency was 200 Hz/sec with the sampling duration of 2 seconds. The metronome was used to control the subject's walking speed.
Data Analysis: The data, from each trial, were statistically analyzed. A mixed design(2 x 2 x 3) of analysis of variance with repeated measurement was adopted to determine the significant difference between a)the support of each foot when changing direction, b)the walking speeds and c)changing angle conditions at the 0.05 alpha level. The data, which were used for analysis of the force-force diagrams and force-time curves, were normalized before being averaged and plotted.

RESULTS AND DISCUSSION

Results in general indicate that, the values of force variables of the left foot support were slightly different from those of the right foot support in most cases when subjects changed direction during walking. There were statistically significant differences between most of the dependent variables for walking in different speeds. There were statistically significant differences for altering angles in all dependent variables.

Both maximum absolute values of Fx and Fy were increasing while the turning angle of walking was increasing under the braking phase. The absolute value of Fx became larger also during the propelling phase when turning angle of walking increased. The value of Fy decreased during the propelling phase for changing direction during walking. The value of Fy was decreasing from the positive value to the negative value

while the turning angle of walking was increasing to 90 degrees. The regular propelling phase did not appear for Fy during the turning angle at 90 degrees. These are unique characteristics of GRF for walking straight forward and changing direction during walking.

There were common characteristics of force-time curves patterns of the vertical component (Fz) of GRF for both walking straight forward and changing direction. These results were similar to the study reported by Winter (1987). In contrast, the patterns of the force-time curves of medial lateral force (Fx) and anterior posterior force (Fy) were much different between walking straight forward and changing direction. The duration of the braking phase increased for Fy while the turning angle of walking increased. The more the turning angle was changed, the longer was the duration of the braking force. At 90 degrees, the propelling phase was totally gone. It was very clear that the stance phase of altering direction during walking at 90 degrees did not include propelling period. This is why the subjects could move to sideways. To change different directions during walking, Fx became larger when changing angle increased, and finally replaced Fy during this phase.

The significant differences in Fx and Fy between the different altering walking direction may be examined with dynamic analysis and display of the Fx vs. Fy profile (Figure 1). The analysis shows that these differences of the dynamic patterns include: 1) the absolute value of Fx increased under stance phase from walking straight forward to altering direction during walking. The slope of the plotted line from a to b for Fx was larger for changing direction at 90 degrees than for changing direction at 45 degrees; 2) in the propelling phase, when the absolute value of Fx increased from d to e, the value of Fy was almost unchanged for changing direction at 90 degrees. The slope of the plotted line was flat. However, in the same phase of changing direction at 45 degrees, the value of Fy increased simultaneously with the absolute value of Fx with the same scale. These phenomena indicated that the thrust forces of Fx and Fy were coincident with turning angles. There were high correlation coefficient between altering angles and Fx. Similar patterns observed for other foot supporting and speed conditions. These patterns could be used as force-force profiles for identifying changing different directions during walking.

In conclusion, Peak values and patterns of Fx and Fy were unique characteristics of GRF for walking straight forward and changing direction during walking. Patterns of Fx could be the most important characteristics of GRF for changing directions. Fz pattern of GRF was the common characteristics for various walking conditions. The results of force-time curve patterns and force-force diagrams give us a dynamic image for changing direction during walking. They could be used as the force profile for identifying the changing direction during walking.

REFERENCES

Cavanagh, P.R., and Lafortune, M.A. (1980). Ground reaction forces in distance running Journal of Biomechanics, 13, 397-406.

Hamill, J., Murphy, M., & Sussman, D. (1987). The effects of track turns on lower extremity function. International Journal of Sport Biomechanics. 3, 276-286.

Patla, A. E. et. al.(1991). Visual control of locomotion: strategies for changing direction and for going over obstacles. Journal of Experimental Psychology: Human Perception and Performance. Vol. 17, No. 3. 603-634

Stucke, H., Baudzus, W. & Baumann, W. (1984). On Friction characteristics of playing surfaces. Sport Shoes and Playing Surfaces. Human Kinetics Publishers, Inc. Champaign, IL. pp. 87-97.

Winter, D. A. (1987), The biomechanics and motor control of human gait. University of Waterloo Press.

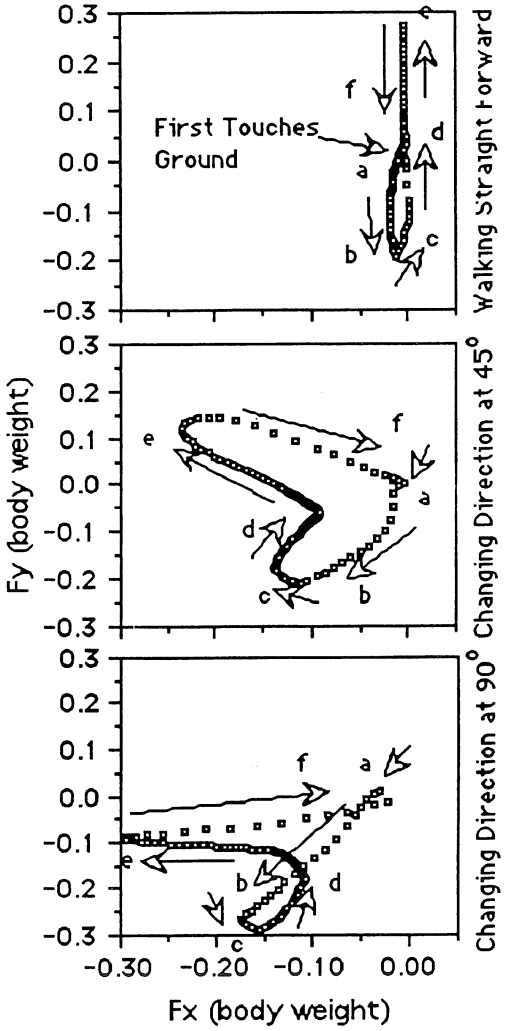

* a-b-c-d-e-f represent foot from heel touching ground to toe-off

Figure-1 Fx vs. Fy diagram: changing direction or walking straight forward under natural cadence with left foot supporting.

THE EFFECTS OF UNILATERAL MUSCULAR FATIGUE ON THE BILATERAL DEFICIT

T. OWINGS AND M. GRABINER

EFFECTS OF ANTI-FATIGUE FLOOR MATS ON POSTURAL SWAY

K. Barin, M. Parnianpour and P.J. Sparto

Department of Otolaryngology, The Ohio State University, Columbus, OH, 43210
Department of Industrial and Systems Engineering, The Ohio State University, Columbus, OH, 43210
Biomedical Engineering Program, The Ohio State University, Columbus, OH, 43210

INTRODUCTION

The so-called anti-fatigue floor mats are often used in industrial settings to relieve worker fatigue. Some investigators have hypothesized that these mats increase postural sway by creating a more unstable support base. The increased sway is thought to facilitate blood flow to the muscles thereby reducing fatigue. To test this hypothesis, postural responses of twelve subjects were measured as they stood on a solid support and two types of mat surfaces. The results showed that mats did not significantly increase postural sway during a short-duration standing task. However, further studies are needed to determine if floor mats increase postural sway for prolonged standing tasks.

REVIEW AND THEORY

Fatigue and other physical discomforts in the lower back and legs are common complaints among industrial workers who are subject to prolonged standing (see Kim, et al., 1994 for a review). In recent years, a variety of floor mats have been marketed aimed at reducing fatigue and minimizing other adverse effects of prolonged standing. The effectiveness of these anti-fatigue mats however, is still a matter of controversy.

Cook et al. (1993) measured EMG activities of the paraspinal muscles and the anterior tibialis muscles while standing either on a linoleum-covered concrete surface or on a surgical floor mat. Although the subjective data suggested that standing on the mat was more comfortable, the investigators found no difference in the EMG activities of the paraspinal and anterior tibialis muscles for standing on either support surface.

Kim et al. (1994) analyzed the spectral electromyographic responses of the lower back and leg muscles after prolonged standing on a concrete surface, on a thin mat, and a thick but less compressible mat. They found that standing on the more compressible floor mat did reduce the fatigue in the lower back muscles but had no effect on the leg muscles. Standing on the thick mat had no effect on either the back or leg muscles. Kim et al. (1994) suggested that the reduction in muscle fatigue was due to the more compressible mat providing a less stable support which resulted in increased body sway. The increased sway was thought to cause contraction of the trunk muscles which caused increased blood flow to those muscles.

The purpose of this study was to determine if standing on anti-fatigue floor mats increases postural sway and if so, whether the mat compression is a factor in the amount of sway. The results of this study are not only relevant to the association of fatigue reduction and postural sway, but they are also applicable to the issue of worker safety. That is, if certain floor mats reduce fatigue by increasing sway, one must weigh their benefit against potential hazards caused by a decrease in postural stability.

PROCEDURES

Subjects. Ten male and two female students were recruited to participate in this study. Their mean age was 28.4 with a range of 23 to 46 years. Their mean height and weight were 172.9 cm (range 152 to 188 cm) and 68.4 kg (range 50 to 91 kg) respectively. The subjects had no prior history of any balance problems.

Apparatus. The dynamic posturography platform, Equitest, manufactured by NeuroCom, was used to measure postural sway. The operation of the device has been previously described in detail (Nashner & Peters, 1990). Only the sensory organization test (SOT) was used in this study. In this portion of the test, postural responses are recorded in six different conditions as visual and proprioceptive inputs are varied. In the first three test conditions, the support surface remains fixed. In the next three conditions, the support surface rotates in proportion to the body sway, thereby providing the postural control system with inaccurate proprioceptive cues. For each support condition, the test is performed with 1) eyes open and fixed visual surround, 2) with eyes closed, and 3) with eyes open and visual surround rotating in proportion to the body sway.

Experimental design. Each subject stood on a solid surface (steel covered by a linoleum-like material) and on two different types of mats. The mats were the same material used by Kim et al. (1994). The thin mat (Mat 1) was roughly three times more compressible than the

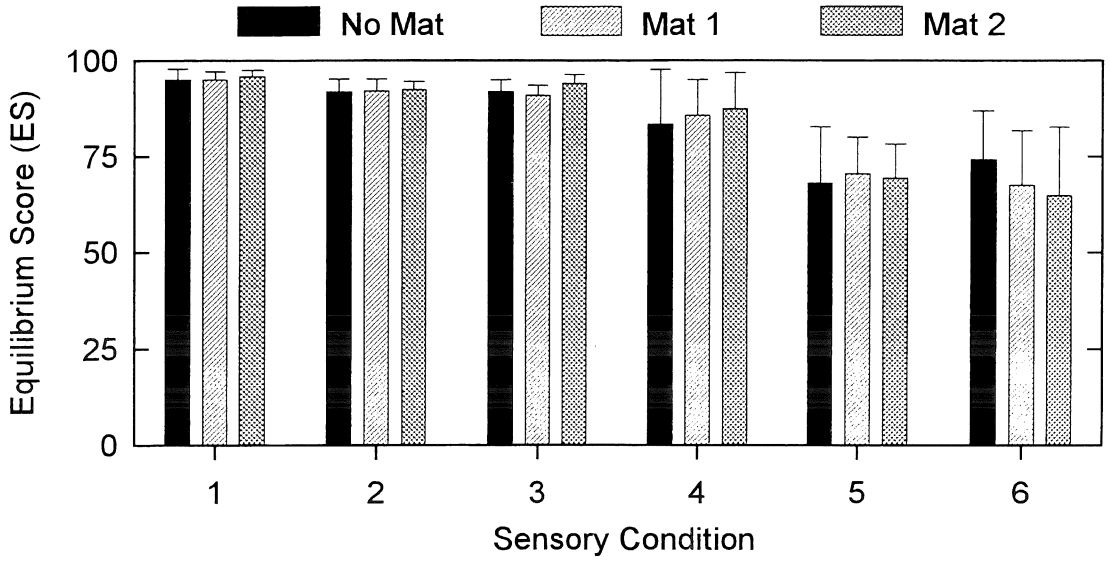

Figure 1. Mean and Standard Deviation of the ES (Conditions 1 through 6) for standing on a solid surface (No Mat), a thin more compressible mat (Mat 1), and a thick less compressible mat (Mat 2).

thick mat (Mat 2). Each subject underwent a single trial for each of the six sensory conditions in the SOT battery. After a brief rest, they repeated the same sequence for a different support surface. To overcome possible learning effects of successive SOTs, the order of the test presentation was fully randomized.

Data Analysis. In accordance with standard EquiTest protocol, for each of the six sensory conditions in the SOT battery, ground reaction forces were recorded for a 20-second period. An Equilibrium Score (ES) was determined for each trial on the basis of the ratio of the peak-to-peak body sway to the maximum possible sway without falling. The results were analyzed using MANOVA and ANOVA on the ES for the main effects of floor condition, sensory condition, and their interaction.

RESULTS

Figure 2 shows the means and standard deviations of ESs for the six sensory conditions in the SOT. The MANOVA on the ESs for the main effects of support and sensory conditions showed no significant difference in the postural sway that could be attributed to the use of floor mats. When individual ANOVAs were considered, there was a significant difference between the ES while standing on Mat 1 and the ES while standing on Mat 2 for the sensory condition 3 (ANOVA, $p < 0.02$). In condition 3 the support is fixed and the visual surround is sway-referenced. There was no significant difference between standing with no mat and standing on either Mat 1 or Mat 2 in this condition. In view of the overall MANOVA results and the fact that ESs for condition 3 are near maximum, the significance of the difference between Mat 1 and Mat 2 in this condition is doubtful.

DISCUSSION

The result of this study does not support the notion that an increase in postural sway is responsible for the reduction of muscle fatigue. However, this conclusion must be viewed with caution for a number of reasons. First, in this study we have used the center of pressure measurements as an indicator of sway. It is possible that subjects could produce hip sway with the upper and lower body moving in opposite directions. This kind of movement will generate little or no center of pressure movement but may serve the purpose of reducing fatigue. Second, this study was based on a short-duration standing task. In these tasks, highly compressible mats similar to those used in upholstery, have been shown to generate increased sway in subjects by reducing the proprioceptive cues arising from the ankle joint. The kind of mats used in this study are significantly less compressible and do not immediately influence ankle proprioception. However, it is conceivable that their effect could become more prominent after a prolonged standing task.

REFERENCES

Kim, J.Y. et al. *Applied Ergonomics*, 25(1), 29-34, 1994.

Cook, J. et al. *J. Biomed. Eng.*, 15, 247-250, 1993.

Nashner, L.M. and Peters, J.F. *Neurol. Clin.*, 8, 331-349, 1990.

YOUNG AND ELDERLY ADULTS ADOPT DIFFERENT STEPPING STRATEGIES WHEN CLEARING OBSTACLES

J.E. Kasprisin and M.D. Grabiner

Department of Biomedical Engineering
The Cleveland Clinic Foundation, Cleveland, OH 44195

INTRODUCTION

Falls in the elderly continue to be a growing medical and socioecomonic concern. Falls often affect both the physical and mental capacities of an individual, and can lead to decreased independence and institutionalization. Many falls are the direct result of tripping over an obstacle. In the present study, twelve three-dimensional obstacles were used to examine the stepping strategies of young and elderly adults during obstacle clearance. Results indicated that both age groups altered their stepping strategy as a function of obstacle height. However, as a function of obstacle length, the stepping strategy of the young group was affected to a greater extent than that of the elderly. The elderly group took longer to step over the obstacles and produced greater vertical forces that may reflect a larger vertical bias of the center of mass.

REVIEW AND THEORY

Research regarding stepping strategies and obstacle clearance has mainly focused upon the influences of obstacle height or length, as independent components (Patla, 1993; Patla, 1991; Chen, 1991). However, in order to successfully clear an obstacle, a strategy must account for the multi-dimensional characteristics of the obstacle. Implementing obstacles in which height and length have been simultaneously altered, may induce stepping strategies different than those when only one component is altered. The resulting strategies may provide better insight regarding age-related motor behaviours when encountering obstacles.

The purposes of this study were to:
1. Investigate the stepping strategies in young and elderly subjects, as the height *and* length of an obstacle were altered.
2. Investigate age-related differences in stepping strategy during obstacle clearance.

It was anticipated that:
1. Both age groups would alter their stepping strategies as a function of obstacle height and of obstacle length.
2. A significant difference in the stepping strategies used when clearing the obstacles would be found between age groups.

PROCEDURES

Fifteen young (29.1(8.6)yrs) and 16 elderly (75.2(6.8)yrs) heathy, active adults were required to step over an obstacle that was located between two force plates. From a standing position, the subjects were instructed to take a single step onto a force plate (P1), step over the obstacle with their contralateral limb, step onto a second force plate (P2), clear the obstacle with the trailing limb and continue walking for a few more steps. Subjects performed the task at a self-selected speed, and also selected the limb with which they would initially clear the obstacle (lead leg), and the stance limb on the first force plate (trail leg). The starting position was marked, and all trials were initiated from that mark. The selected lead leg was used as such for all trials in the collection.

Twelve dense foam blocks of varying height and length were used. Each obstacle measured 18 inches across (width) and was 0, 6, 8 or 12 inches in height and 6, 8 or 12 inches in length. The order of obstacle administration was randomized, and three trials were executed for each obstacle. Two practice trials were given for each obstacle.

The durations of limb support were extracted from the force plate data. The time from initial foot contact on P1 to foot contact on P2 reflected the time in which the lead leg cleared the obstacle. The time in which the trail leg cleared the obstacle was calculated as the time from the offset of force on P1 to the offset of force on P2. The duration of double support was also extracted.

The anterior-posteriorly directed force profiles were separated into "braking" and "propulsion" phases (Patla, 1991). The vertical impulse was calculated over the entire support phase on each force plate. The variables extracted for analysis were the braking, propulsion, and vertical

impulses on both force plates. The force values used in the calculation of impulse were normalized to body weight on the force plates.

Along with the support durations, the impulses are associated with basic stepping strategy and changes in these variables are representative of a change in the pattern of gait. For example, increases or decreases in a variable can reflect shortening or lengthing of stride, deceleration or acceleration of gait, center of mass elevation, or limb trajectory (Patla, 1991).

A between-groups height by length repeated measures ANOVA was implemented. Significant ANOVA effects were further investigated using t-tests with a Bonferoni adjustment.

RESULTS

Chen et al. (1991) reported that changes in strategy resulted mainly as a function of obstacle height and not as a function of the length of the obstacle. In the present study, an effect of obstacle height was revealed in both age groups (all $p \leq .001$) for all but one of the impulse variables (young braking on P2, $p = .271$). Generally, as obstacle height increased, the impulses increased. An effect of height was also revealed for the durations of limb support, in the young group (all $p \leq .003$), showing increased time as obstacle height increased.

An effect of obstacle length was revealed in the young group (all $p \leq .008$) for the propulsion and the vertical impulses, on both force plates. The impulses were greater for the longest obstacle than for the two shorter obstacles. A single effect of obstacle length was revealed in the elderly group ($p = .042$), in which the propulsion impulse on P1 for the longest obstacle was greater than that of the shortest. The young group revealed an effect of obstacle length for the two single support durations (both $p = .001$).

One purpose of this study was to investigate the manner in which height and length affected stepping strategy. Height by length interactions were found in the young group only (all $p \leq .044$) for the vertical impulses on both force plates, the propulsion impulse on P2, and both of the single support durations.

A second purpose of the study was to examine *age-related* differences in stepping strategies, which were primarily observed in durations of support. The elderly group had longer single and double support times than the young. The elderly group also produced greater vertical impulses on both force plates. Qualitatively, larger differences between groups in the braking and propulsion variables were not observed to be significant, perhaps influenced by large within-group variability present in the elderly.

DISCUSSION

The results support our first anticipated outcome in that both groups altered their stepping strategy (impulses) as a function of obstacle height. Both groups also made adjustments as a function of obstacle length, the elderly group, however, to a lesser extent. The interactions found in the impulse variables, as well as the support durations for the young group, suggest that changes were made in the stepping strategy due to increases in obstacle size in either dimension. However, stepping strategy changes made by the eldery group, appear mainly to be due to changes in obstacle height. The lack of interaction within the support durations also suggest that the elderly group did not increase their stance times in reaction to dimension changes, whereas the young group increased their stance times as either dimension of the obstacle changed.

In general, when clearing obstacles, young and elderly subjects appear to have adopted different stepping strategies. Whether the adjustments were made in order to minimize or to overcompensate foot clearance is indefinite. The current results warrant further investigation using motion analysis, in order to determine lower limb mechanics and foot-obstacle clearances.

REFERENCES

Patla AE. Adaptability of Human Gait, (pp. 55-96), Elsevier Science Publishers, 1991.
Patla, AE. *et al.* Gait & Posture, 1, 45-60, 1993.
Patla, AE. *et al.* J Exp Psych., 17, 603-634, 1991.
Chen, HC. *et al.* J Geron., 46, M196-M203, 1991.

EFFECT OF AGE AND VELOCITY ON THE RELIABILITY OF DETECTING ANKLE PLANTAR- AND DORSIFLEXION MOTIONS IN UPRIGHT STANCE

D.G. Thelen, C. Brockmiller, J.A. Ashton-Miller, A.B. Schultz, N.B. Alexander

Biomechanics Research Laboratory, Department of Mechanical Engineering and Institute of Gerontology, University of Michigan, Ann Arbor, MI 48109-2125

INTRODUCTION

Afferent feedback of lower extremity joint rotations is widely accepted as being important for the control of unipedal and bipedal stance and locomotion. This is particularly true in the dark or with support surface movement when visual and vestibular feedback can be unreliable. Because difficulty with balance and the incidence of falls increases with age (for example, Tinetti et al. 1988) it is important to determine whether age affects the reliability with which individuals can detect joint rotations. Present tests for quantifying proprioceptive thresholds at a joint are usually conducted under the non-weightbearing conditions. Usually they involve finding the threshold for detecting joint rotation (Barrack et al. 1983), though seldom with any estimate of detection reliability, and quantifying errors in the ability to match left and right joint angles in a passive or active manner (for example, Horch et al. 1935). Our recent study (Gilsing et al. 1994) indicates that the detection of ankle inversion and eversion motion with a 75 % probability of success is nearly an order of magnitude better in the weight-bearing state than in the non-weight-bearing state. The same study found the threshold did not depend on rotation velocity in the range of 2.5 to 200 degrees/sec. We are unaware of corresponding data describing the ankle dorsiflexion and plantarflexion thresholds, or their velocity sensitivity for lower velocities more typical of quiet stance. The purpose of the present study, then, was to test the null hypotheses that (a) age does not significantly affect the threshold for detecting ankle dorsi- or plantarflexion rotations during upright stance, and (b) the threshold for detecting ankle rotation is independent of velocity in the range 0.1 to 2.5 degrees/sec.

METHODS

Twelve young (YF; mean age = 22±2 years) and twelve old (OF; 70±4 years) healthy females participated in this study. YF were recruited from university staff and students. OF were independent dwelling community members who underwent a standardized medical history and physical examination by a physician geriatrician, and were found to have no significant neurological and/or musculoskeletal abnormalities. Subjects stood bipedally with their dominant foot placed on a servo-controlled plate which could rotate about the assumed ankle joint center (midway between the malleoli). Their contralateral foot supported half their weight on a fixed platform of equal height. Headphones with generic backround music were worn to occlude cues from motor noise. Subjects were asked to gaze at a visual light display in front of them. Following a random 0.5-1.0 second delay after a warning light cue, the platform rotated at a constant velocity to a specified angle. The subject was then asked to indicate verbally whether their foot had rotated (a) up, (b) down, (c) not at all, or (d) their foot had moved, but in an unknown direction. Subjects were tested using plate rotational velocities of 0.1, 0.5, and 2.5 °/s to angles of 0.05, 0.1, 0.2, 0.4, 0.8 ° in both dorsiflexion and plantarflexion. Subjects performed 5 trials at each velocity-angle combination and 30 dummy (no movement) trials for a total of 180 trials. The protocol was presented in 5 blocks of 36 randomly-ordered trials; first and last blocks were identical in order to be able to quantify learning effects (which proved non-significant). Directional success rates (SR: the percentage of correctly identified movements in a given direction) were determined for each velocity-angle. Repeated measures analysis of variance was used to determine the effects of angle, velocity, age and direction on SR.

RESULTS

Mean SR ranged from 8% for the OF at the 0.1 °/s and 0.05° motions to 100% for the YF at the 2.5 °/s velocity and 0.4° motions (Figure 1). Angle ($p<0.0001$, ANOVA), age ($p<0.0001$) and velocity ($p<0.0001$) all had highly significant effects on SR while, in comparison, directional effects were small ($p<0.05$). Mean SR improved with increasing angle and velocity, and were generally greater in DF than in PF. Both YF and OF had approximately 20%

higher SR in simply detecting motion at a given velocity-angle than in identifying the direction. Mean SR were always greater for the YF than for the OF at a given velocity-angle. YF correctly identified DF and PF motions of 0.05°, 0.2°, and 0.8° with a 75% SR at the high, moderate and low velocities, respectively. The equivalent data for OF were 0.2° and 0.8° at the high and moderate velocities, but did not reach 75% at the low velocity. Thus OF required approximately 4 times larger ankle rotations to achieve similar 75% SR to YF.

DISCUSSION

The lack of reliable afference from the feet and ankles, for example, in patients with peripheral neuropathy has been associated with a twenty-fold increase in injurious falls (Richardson 1992). Afferent information on ankle joint dorsi- and plantaflexion would seem an important sensory modality for planning the recovery from forwards or backwards falls. Indeed, motion sensation deficits may degrade postural control performance (Lee 1993). The results of this study demonstrate that healthy YF could reliably perceive surprisingly small ankle rotations during upright stance; these were an order of magnitude smaller than previously reported non-weight bearing values, but similar to the inversion/eversion values we found earlier. Although their performance was still impressive, OF required substantially larger (4 times greater) rotations to determine the direction with the same reliability as YF.

Motion sensitivity at the slow angular velocity (0.1°/s), representative of postural sway (Fernie et al. 1982), was an order of magnitude worse than sensitivity at the high velocity (2.5°/s) demonstrating an attentuated dynamic range not uncommon in biological receptors. Fluctuations in the cues from the forefoot plantar pressor afferents caused by random phase differences between the directions of ankle rotation and body sway may have contributed to decreased detection reliability at the slow velocity.

In summary, substantial age differences in the detection of ankle motion were demonstrated which may contribute to age-related difficulties with challenging postural balance tasks.

REFERENCES

Barrack R.L., *et al.* (1983) *Am. J. Sports Med.* 11:258-61.

Collins, J. J. and De Luca, C.J. (1993) *Exp. Brain Res.* 95:308-18.

Fernie, G. R., *et al.* (1982) *Age and Ageing* 11:11-16.

Gilsing, M.G., *et al.* (1994) Submitted to *J Brit. Ger Soc.*

Horch K.W., *et al. J. Neurophys.* 38:1437-47.

Lee, S-G. (1993) Ph.D. Thesis, Mech. Eng., University of Michigan, Ann Arbor.

Magnusson, M.,*et al.* (1990) *Acta. Otol.* 110: 182-88.

Richardson, J.K., *et al.* (1992) *JAGS 40:1008-12.*

Tinetti, M.E. *et al.* (1988) *New Engl. J. Med.* vol. 319: 1701-1707.

ACKNOWLEDGMENTS

We gratefully acknowledge the financial support of the Institute of Gerontology, an undergraduate Parker scholarship and NIH grants AG 06621 and AG 10542.

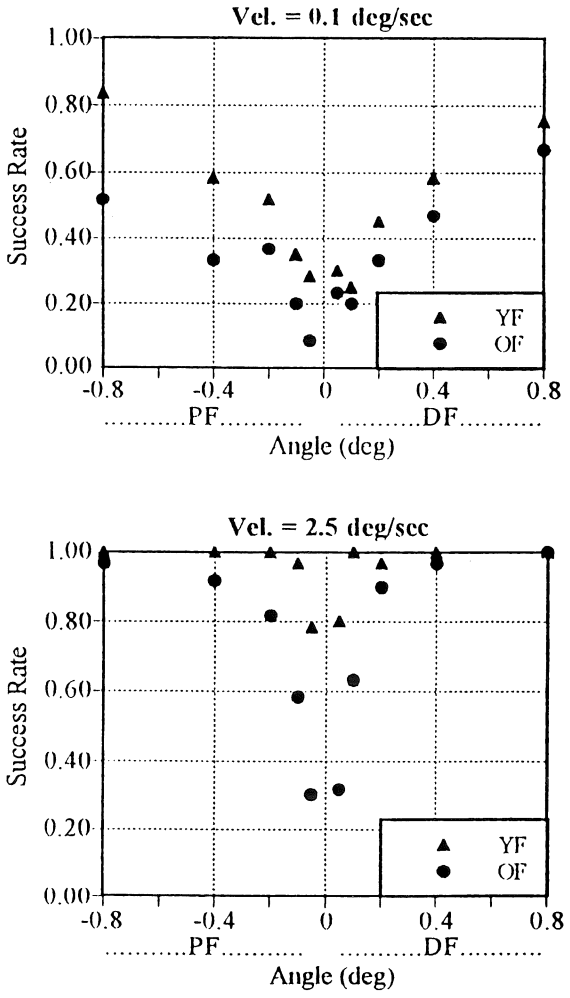

Figure 1. Success rates of young and old females.

KINETICS OF PREFERRED AND NON-PREFERRED SPEEDS OF WALKING AND RUNNING

M.M. Ryan and R.J. Gregor
Department of Health and Performance Sciences
The Georgia Institute of Technology, Atlanta, GA 30332-0110

INTRODUCTION

Kinematic analyses of locomotion at speeds at which one can either walk or run have been reported (Grillner et al., 1979, Thorstensson and Roberthson, 1987); however, kinetic analyses for extreme speeds of walking and slow jogging are lacking. The stance phase kinetics of natural walking and jogging at preferred speeds and walking and jogging at nonpreferred speeds were studied. Ground reaction force (GRF) patterns were similar for the preferred and nonpreferred jogging trials, with larger magnitudes in the faster preferred jog. Initial stance phase GRFs for the walking conditions displayed values consistent with increases in speed, however at the end of stance the lower speed preferred walking trials had higher vertical and A/P forces. Generalized muscle moment (GMM) patterns for jogging exhibited magnitude changes which were attributed to differences in speed. The walking trials showed a change in magnitude and direction of the GMMs during late stance to accommodate for increased speed.

REVIEW AND THEORY

Kinematic and kinetic analyses of walking, jogging and running at various speeds have been reported in the literature (Winter, 1983a, Mann, 1981). These studies however have not addressed the slowest speeds of jogging or the fastest speeds of walking, which are considered nonpreferred speeds. Two studies (Grillner et al.,1979, Thorstensson and Roberthson, 1987) employed nonpreferred speeds of walking and jogging to study what kinematic changes occur when one transitions from walking to running. Knee angle and support length differences between walking and jogging were suggested as two possible variables which may indicate the natural transition speed between these forms of locomotion (Grillner et al.,1979, Thorstensson and Roberthson, 1987). Kinetic data, however, are needed to support these kinematic outcome measures to determine the forces which produce these movements.

The purpose of this study was to examine the kinetics of both preferred (P) and nonpreferred (NP) walking and jogging to provide information about lower extremity mechanics during the transition between these forms of locomotion. As speed increases the magnitude of the GRFs and GMMs are expected to increase. It is hypothesized that the GRF patterns for the NP speeds will be similar to the other type of locomotion or some combination of the two. We hypothesize that the generalized muscle moments (GMMs) for the NP'd and P'd conditions change sign at different times during stance. For example, the ankle dorsiflexor moment may become extensor earlier in the stance phase for the NP'd compared to the P'd.

PROCEDURES

A linked segment rigid body model of the lower extremity was used for a 2-dimensional kinetic analysis of the stance phase of walking and jogging. Data for 3 subjects were collected on the track at Drake Stadium on the UCLA campus. The two P'd and two NP'd locomotor conditions included: (1) natural walking (P-walk), (2) natural jogging (P-jog), (3) walking as fast as possible (NP-walk), and (4) slow jogging (NP-jog). Lower extremity movement was captured at 200 Hz using high speed video cameras (NAC, Inc.) and synchronized with GRF data obtained from a force plate mounted within the track surface. Standard inverse dynamics equations were used to calculate GMMs at the hip, knee and ankle.

RESULTS

Vertical and anterior/posterior (A/P) components of GRF are presented in Figures 1 and 2 for conditions of walking and jogging, respectively. These data are the average of 10 trials for each condition for one subject and are presented as a percent of stance time.

A/P GRF for the NP- walk indicated minimal propulsive force generated at the end of stance (50-100N) compared to the P-walk (200N) (Figure 1). The P-walk condition had larger vertical GRF values during pushoff (750N) than the NP-walk (600N), despite a lower average locomotor speed (P-walk - 1.51 m/s vs. NP-walk - 3.33 m/s).

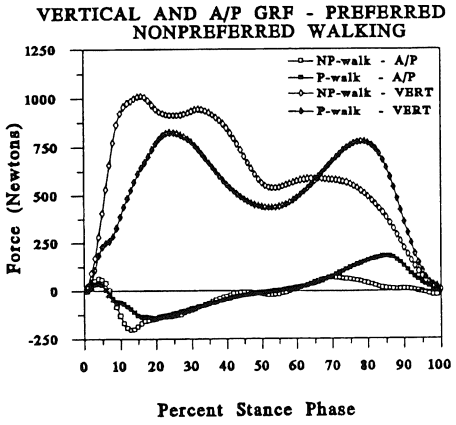

Figure 1. Vertical and A/P GRFs for P-walk and NP-walk.

Both jogging conditions showed similar GRF patterns, with the P-jog condition having higher vertical and A/P values than the NP-jog.

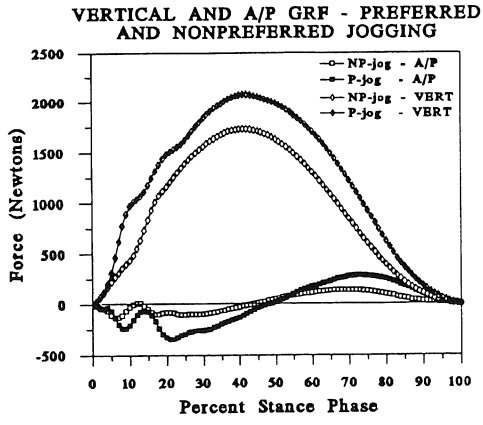

Figure 2. Vertical and A/P GRFs for P-jog and NP-jog.

Figures 3 and 4 are the GMMs for the hip, knee and ankle for P-and NP- walking and jogging, respectively. Positive moments represent ankle dorsiflexion, knee extension and hip flexion.

Ankle moments for the walking conditions were similar during the early portion of stance but differed greatly during the later stance phase (Figure 3). Peak PF moment occurred earlier in the NP-walk condition (70% of stance) compared to 80-85% of stance for the P-walk. In addition, the NP-walk had a lower peak PF moment than the slower P-walk (100 Nm vs. 175 Nm). These findings are consistent with the lower GRF values for the NP-walk. Large hip flexor and knee extensor moments at end of stance were apparent in the NP-walk condition, while the P-walk moments were opposite in sign (hip extensor and knee flexor moments).

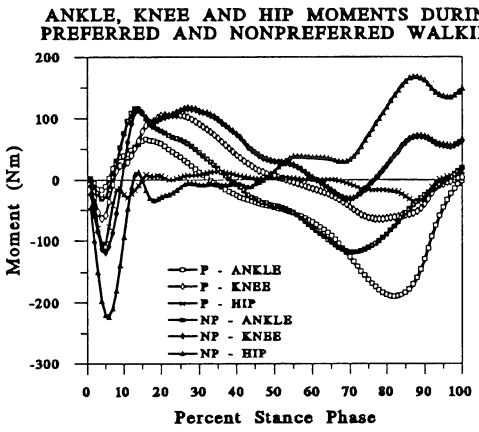

Figure 3. GMM for the hip, knee and ankle for P-walk and NP-walk.

Ankle and knee GMMs for NP- and P-jogging displayed similar patterns. NP-jog peak ankle plantarflexion (PF) occurred earlier in stance (55%) while the P-jog peak PF moment occurred between 60-65% of stance. The knee moments had a similar trend, with greater peak extensor and flexor moments produced in the P-jog condition. Considerably smaller hip extensor moments occurred during stance in the NP-jog (50 Nm) compared to the P-jog (175 Nm).

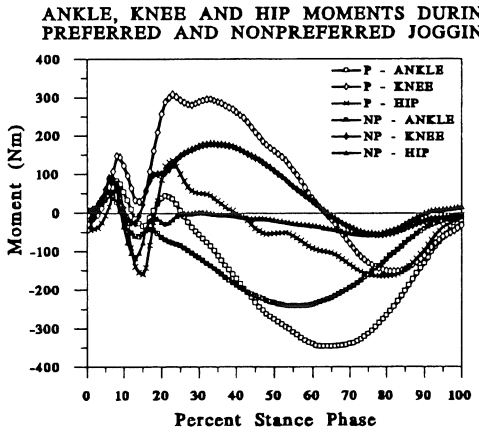

Figure 4. GMM for the hip, knee and ankle for P-jog and NP-jog.

DISCUSSION

The P-walk had typical GRF patterns which were consistent with data previously presented for walking (Winter, 1983a).

The NP-walk condition however displayed very different patterns. A bimodal pattern in the vertical GRF at the beginning of stance appears to be unique to the NP-walk. This type of pattern was not reported for fast walking in data presented by Winter (1983a). During the last 40% of stance the NP-walk had lower vertical and A/P GRF values indicating that minimal force was generated for pushoff. This is contrary to what would be expected for the faster NP-walk compared to the P-walk.

The GMM data indicate that there was minimal assistance at the ankle joint to maintain the NP-walk speed, however a knee extensor moment acted to compensate during pushoff. The large hip flexor moment observed at the end of stance in the NP-walk may have been needed to help bring the leg through at the beginning of swing. The contribution by the more proximal segments in the NP-walk was not observed in the P-walk. The P-walk condition had a large PF moment with low hip extensor and knee flexor moments. This change in the sign of the moments between the two conditions showed a change in the mechanics used to accomplish the NP-walk task.

The GRF data for the N-jog and NP-jog were consistent with data reported in the literature (Williams, 1987, Cavanagh et al., 1980, Munro et al., 1987). Both jog conditions showed similar GRF patterns with differences in magnitude attributed to the increase in speed.

GMM patterns for the NP-jog were in general agreement with data reported by Winter (1983b) for slow jogging. Increased peak GMM magnitudes for the P-jog were expected and supported by the increased GRF magnitudes at this faster speed. A phase shift in the peak ankle PF moment was apparent between the two jog conditions. The peak moment in the NP-jog indicates that pushoff began earlier than in the P-jog condition. During the last 15% of stance, the NP-jog showed minimal GMMs produced at all joints. The role of the hip at the end of stance became more important in the P-jog as the hip flexor moment increased to over three times the peak magnitude of the NP-jog. It was expected that the NP-jog condition would have markedly different GRF and GMM patterns. The similarity across jog speeds indicates that the NP-jog condition may not have been at a slow enough speed to elicit any apparent changes in the mechanics compared to the P-jog condition. Additional trials at lower velocities are needed to determine if the kinetics do change.

While the NP-walk hip and knee moments changed sign compared to the P-walk, both jog conditions had GMM of the same sign. Interestingly, the NP-walk and NP-jog conditions had earlier peak PF ankle moments than the P'd conditions. This would indicate a NP'd gait trend and not a speed dependent change because the NP-walk speed was greater than the P-walk, while the NP-jog speed was lower than the P-jog.

REFERENCES

Cavanagh, P.R. et al. J. Biomechanics, 13,397-406,1980.
Grillner, S.J. et al. Brain Res., 165,177-182,1979.
Mann, R. et al., Res. Quarterly. Exer. Sport. 51,334-348, 1980.
Munro, C.F. et al. J. Biomechanics, 20,147-155, 1987.
Thorstensson, A. and H. Roberthson, Acta. Physiol. Scand., 131,211-214, 1987.
Williams, K.R. et al.. Int.. J. Sports Med., 8,107-118,1987.
Winter, D.A., J. Motor Behav., 15, 302-330,1983a.
Winter, D.A., J. Biomechanics, 16,91-97,1983b.

ACKNOWLEDGMENTS

The authors would like to acknowledge John Franco, Jean Young, Scott Gregor and Barry Munkasy for their time and effort in collecting these data and Dr. Jill McNitt-Gray, USC Biomechanics Laboratory, for the use of the NAC video system.

SIMULATION OF HYPO- AND HYPER-GRAVITY LOCOMOTION

R.T. Whalen[1], G.A. Breit[1], D. Schwandt[2]
[1]NASA/Ames Research Center, Moffett Field, CA 94035
[2]RR&D Center, Veterans' Administration, Palo Alto, CA 94304

INTRODUCTION

We have proposed a novel method of using air pressure to apply an external axial force to the body, coincident with the body's center of mass, that has the potential of enabling Earth-equivalent musculoskeletal forces in space (Whalen *et al.*, 1991; Hargens *et al.*, 1991; Whalen, 1993). By reversing the direction of the pressure differential, walking and running at reduced musculoskeletal levels are possible on Earth.

We hypothesize that hypo- and hyper-g walking and running can be adequately simulated by this method of loading since gait is primarily governed by gravity acting at the center of mass and only secondarily by its distributed action on limb segments (He *et al.*, 1991; McMahon and Cheng, 1990). We report here results from simulated hyper-g walking and running.

METHODS

The method of developing a "non-contact" force at the mass center of the body is illustrated in Figure 1. In the figure, body weight on Earth, the pressure force, seal shear force, and inertia forces all contribute to the resultant ground reaction force (GRF). We have previously demonstrated that a one Earth body weight force can be generated by air pressure along. (In these studies about 33 per cent of the additional force was applied by the seal.)

We have built a treadmill and computer-controlled upper body air pressure system (Figure 2) and used the system to simulate hyper-gravity locomotion on Earth. A 3 foot diameter inflatable sphere, constructed from a lightweight coated fabric, enclosed the upper body from the waist. The sphere was tethered to the side rails of the treadmill with 4 tension straps that balance compression forces applied to the body by the pressure, and shear loading.

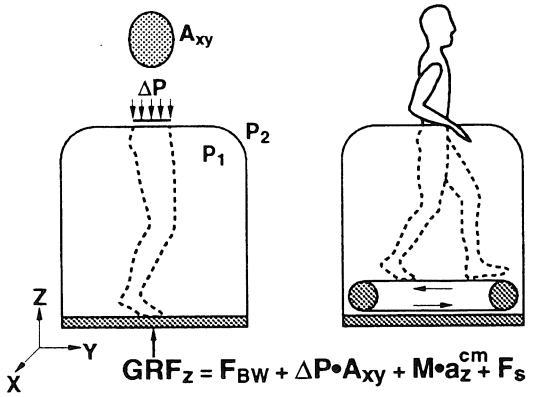

Figure 1. The upper and lower body are separated by a flexible air-tight waist seal that permits free lateral and vertical movement. A negative lower body pressure increases the vertical ground reaction force (GRF_Z); a positive lower body pressure (LBPP) decreases the force. Legend: F_{BW}= body weight; DP• Axy= pressure force; $M \bullet a_Z$= inertia force in z-direction; F_S= seal shear force.

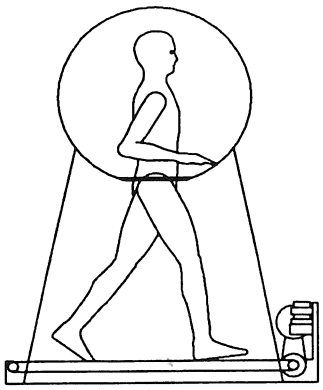

Figure 2. Schematic of the upper body positive pressure (UBPP) system

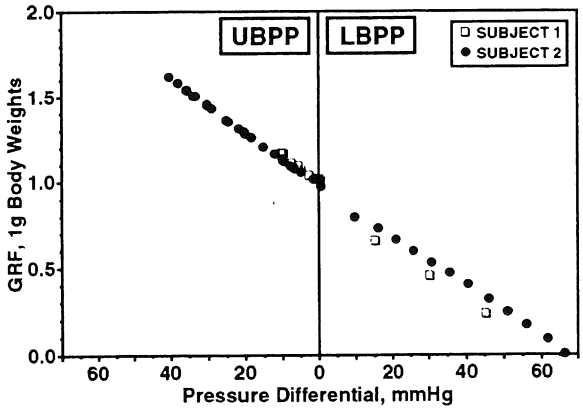

Figure 3. Static upright calibration of the GRF_Z versus chamber pressure using a force plate. The pressure differential is expressed in terms of positive upper or lower body pressure.

RESULTS

Ground reaction force data while walking and running on the treadmill were collected at 1.0, 1.3, and 1.6 g (0, 20, 40 mm Hg) using a capacitance insole force sensor. Typical gait cycles of treadmill walking at 2.0 m/s and treadmill running at 3.0 m/s at 1.0 g and 1.6 g are plotted in Figure 4. Peak force levels at toe-off increased as expected with increasing "g-level". Running data collected at different g-levels were normalized by the stride period (T_{stride}) and the effective body weight, computed by multiplying Earth body weight by the effective gravity (Figure 5).

Normalized peak GRF_Z decreased with increasing "g-level" indicating muscle force generation as a limiting factor to hyper-g gait. Interestingly, ground contact time at a fixed gait speed was constant, i.e., independent of gravity (Figure 6). Our data fit well with results of hypo-g running reported by He *et al.* who used a spring pulling vertically on a bicycle seat to simulate hyper-gravity (Figure 7).

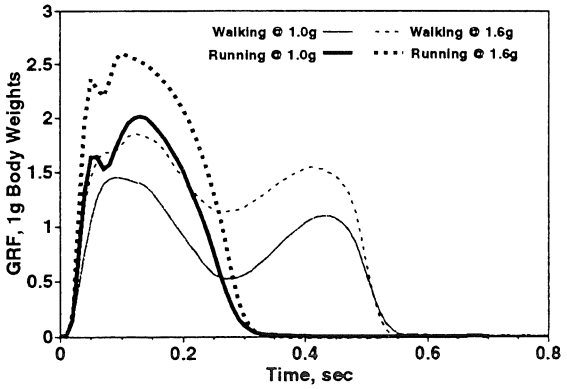

Figure 4. Ground reaction force-time profiles of a single gait cycle of treadmill walking at 2.0 m/s and treadmill running at 3.0 m/s collected at 1.0 g and 1.6 g (40 mm Hg UBPP).

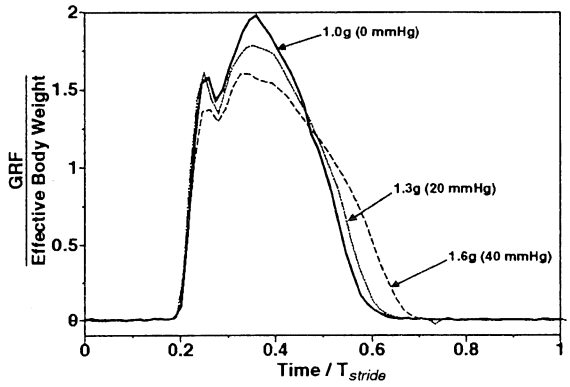

Figure 5. Running data collected at three force levels normalized by the effective static body weight and the stride period. Note the reduction in the normalized peak ground reaction force as "body weight" increases indicating muscle force generation as a limiting factor to hyper-gravity gait. Note that ground contact takes up a greater percentage of the stride period as g-level increases. A limiting condition occurs when the foot cannot leave the ground.

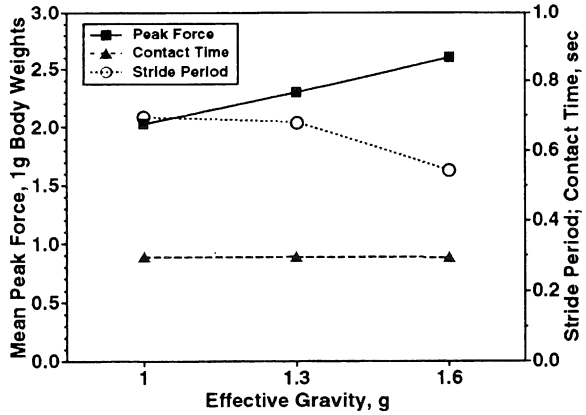

Figure 6. Values of contact time, stride period (T_{stride}), and peak vertical force averaged over a minimum of 10 cycles.

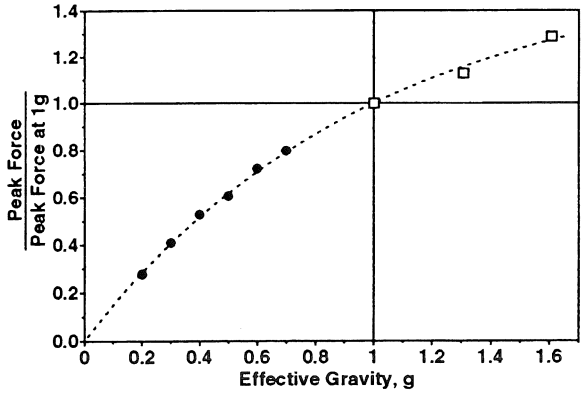

Figure 7. Normalized peak force versus "gravity" level. To accommodate differences in running style among subjects, we normalized peak GRFzs to each subject's GRFz at 1.0 g. Results extrapolated to hypo-gravity locomotion fit with recent hypo-gravity locomotion studies (He *et al.*, 1991).

DISCUSSION

We have verified that differential pressure loading is an effective and feasible method of altering the vertical component of the ground reaction during gait. Although we have only measured GRF_Z, McMahon and coworkers have shown that the horizontal (fore-aft) component should be similarly scaled. The general similarity in the GRF_Z force-time profiles with respect to different "gravity" levels further suggests a proportional scaling of internal lower limb musculoskeletal forces. The scaling cannot be exact, however, since ground contact time remains relatively constant as peak forces increase during "hyper-g" running. Furthermore, we observed important qualitative changes during simulated hyper-g gait (Figure 5). The reduction in peak GRF relative to the effective body weight and the relative lengthening of the contact time suggest that hyper-g running approaches what has been described previously as "Groucho running." (McMahon *et al.*, 1987) The increased load rate will require faster and more intense muscle activation likely recruiting new motor units. We have speculated about possible high-performance training applications.

We believe this device can be used in space to produce Earth-equivalent lower limb musculoskeletal forces and loading histories. We are also pursuing, in collaboration with the Palo Alto Veterans' Administration, the application of differential pressure as a method of unloading the lower limbs during rehabilitation.

REFERENCES

Hargens, A. *et al.* Aviat. Space Environ. Med., 62, 934-937, 1991.

He, J. *et al.* J Appl. Physiol., 71, 863-870, 1991.

McMahon, T.A. et *al.* J. Appl. Physiol., 62, 2326-2337, 1987.

McMahon, T.A. and Cheng, G. J Biomech 23/s1, 65-78, 1990.

Whalen, R. *et al.* Transactions of the 37th Meeting of the ORS 16/2, 628, 1991.

Whalen, R. Physiologist 36/s1, 127-130, 1993.

POSTURAL SYNERGIES DURING FAST MOVEMENTS IN A JOINT OF A TWO-JOINT LIMB SEGMENT

M.B. Shapiro, A.S. Aruin and M.L. Latash

Department of Physical Medicine & Rehabilitation
Department of Molecular Biophysics and Physiology
Rush University, Chicago, IL 60612

INTRODUCTION

Healthy human subjects performed fast, discrete elbow or wrist flexion or extension movements in a sagittal plane under the instruction to move one of the joints "as fast as possible". Both muscle pairs demonstrated commonly observed tri-phasic EMG patterns. Irrespective whether the primary movement took place in the elbow or in the wrist joint, and irrespective of the movement direction, the elbow flexor and the wrist flexor tended to demonstrate similar EMG patterns, while the elbow extensor and the wrist extensor also showed similar patterns of activation. Analysis of the time delays between pairs of the EMGs confirmed virtually simultaneous bursts in the wrist and elbow flexors and in the wrist and elbow extensors with high peak values of the cross-correlation functions. We consider the EMG patterns in postural muscles to be primarily of a central origin. We suggest that the formation of postural synergies (postural anticipation) is not a separate process, but a separate peripheral pattern of a single control process that may involve a number of joints and muscles. The two-joint task is a promising paradigm for studying the basic features of postural synergies, in particular in clinical populations.

REVIEW AND THEORY

Nicholai Bernstein (1967) was probably the first to consider voluntary movements as sources of postural perturbations. Because of inertial forces and joint coupling, virtually any movement induces torque changes in numerous joints. In order to preserve the equilibrium of the body and/or a required posture of the limbs and the head, the system of motor control must undertake corrective actions before the actual perturbation occurs. Fast voluntary limb movements are virtually always associated with changes in the activity of postural muscles some of which occur prior to the movement and can be called anticipatory while others occur later and can be considered corrective (for a recent review see Massion 1992). Anticipatory reactions are generated by the subject's central nervous system without an obvious external stimulus, while later, corrective reactions are initiated by the sensory feedback triggering signals. Anticipatory reactions are generated based upon predictions of the postural perturbations associated with a planned movement, while corrective reactions emerge in response to actual perturbations of posture that occur due to suboptimal efficacy of the anticipatory components. Both anticipatory and corrective reactions are assumed to be pre-programmed and differ in their relative timing with respect to the limb movement and method of triggering, feedforward or feedback.

Many studies investigated anticipatory changes in the activity of postural muscles during fast voluntary movements performed by standing subjects (Belenkiy et al. 1967; Cordo, Nashner 1982; Bouisset, Zattara 1987). However, the task of maintaining vertical posture involves many joints and muscles, thus complicating the analysis. This inspired us to search for a procedure that would allow studies of postural synergies and in a much more simple system. The chosen paradigm involves movements in a sagittal plane in only two joints, wrist and elbow, one of which performs a primary movement while the other carries out a postural task. We hypothesize that, when an instruction requires voluntary movement in only one joint and does not specify behavior in the other, postural joint, the muscles controlling the postural joint will display changes in their levels of activation tightly coupled to the primary movement, i.e. a synergy.

PROCEDURES

Seven healthy male volunteers participated in the study after giving an informed consent. The subjects sat comfortably in a chair and placed their right upper arm on a horizontal surface so that the shoulder joint was flexed 90°. The elbow joint was 90° into flexion, so that the forearm was vertical. The forearm was supinated 90°. The fingers were extended. The experimental procedure involved 4 series. In each series, the subjects were instructed to perform unidirectional movements "as fast as possible", not to bother about accuracy, and not to correct the final position. Different series (10 trials each) involved elbow flexions, elbow extensions, wrist flexions, or wrist extensions over a nominal distance of 40°.

A Mac-IIci computer controlled the experiment, digitized, and recorded joint angles and EMGs. Two goniometers (Penny & Giles) were taped on the subject's arm and measured wrist and elbow joint angle changes in a sagittal plane. The signals from the goniometers were sampled at 500 Hz. Velocity was derived from the goniometric signals by differentiation after filtering at 100 Hz with a second-order Butterworth filter. EMGs of biceps, lateral head of triceps, flexor carpi radialis and extensor carpi ulnaris longus were recorded. Pediatric electrocardiographic self-adhesive electrodes were taped over the muscle bellies and used for a bipolar EMG recording. The EMGs were amplified (1600X), band-pass filtered (60-500 Hz), and digitized at 500 Hz.

After the EMG signals were rectified and filtered with a 100 Hz filter, all the trials were viewed on the monitor screen, and the time of the beginning of the

first agonist burst was defined visually. This time was used for alignment and for all the further data processing as "time zero". The aligned trials of each series were averaged for each subject. The EMGs of the averaged trials were integrated over certain time intervals, corrected for the background EMG activity and normalized. The cross-correlation functions between the pairs of averaged EMG signals were calculated for each series and for each subject separately after filtering the EMGs at 40 Hz. Peak values of the cross-correlation functions and time shifts of the peaks were measured.

RESULTS AND DISCUSSION

All the subjects demonstrated relatively small, irregular deviations in the postural joint. Typically, EMG patterns in both muscle pairs demonstrated a commonly observed, so-called "tri-phasic" pattern. During primary movement requiring flexion or extension in the elbow or in the wrist, the two flexor muscles tended to demonstrate similar patterns of activity while the extensors also showed similar patterns of activation (Fig 1). Muscles acting at the "postural" joint (P-muscles) demonstrated levels of integrated activity comparable to those of the prime movers. The beginning of the antagonist burst in P-muscles could coincide with shortening of the muscle due to inertial forces. Thus, at least for the tri-phasic EMG patterns observed in postural muscles, the relative role of central programming in the initiation of the antagonist burst may be dominant as compared to the role of the local stretch-reflexes.

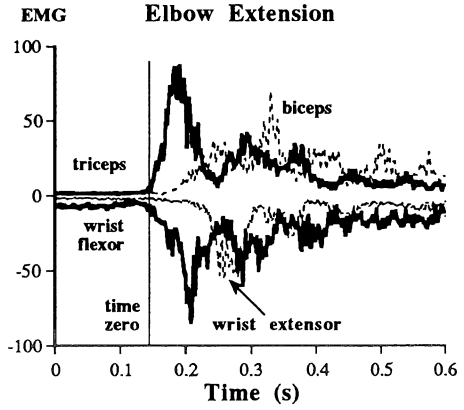

Figure 1

Averaged across 10 trials EMG patterns of one of the subject during elbow extension movements. Time zero (time of alignment) is shown by a vertical line. Note very similar patterns for the elbow and wrist extensors and for the elbow and wrist flexors. EMG scale is in arbitrary units. Time scale is in s.

The analysis of the cross-correlation functions between pairs of the EMGs demonstrated virtually no delay between elbow flexors and wrist flexors and between elbow extensors and wrist extensors in all four tasks, and similar flexor-extensor delays for both joints (about 60-80 ms) with the peak values of the cross-correlation functions in the range of 0.85 to 0.95. Thus, in our very simple paradigm, the EMG patterns in prime movers and postural muscles were tightly coupled allowing us to consider the mechanism giving rise to these patterns a universal postural synergy.

There were only few cases of an anticipatory activation of P-muscles; more commonly, P-muscles were activated simultaneously with the prime movers. A simple biomechanical model suggests that the patterns of simultaneous activation may be used to prevent flapping in the postural joint. Anticipatory activation may be required in cases of large differences in the inertia of moved segments and/or considerable differences in the properties of the muscles (fast vs slow).

The classical approach to the organization of postural control during voluntary movements (Bernstein, 1967) considers an hierarchical organization of the motor control system involving multiple parallel commands coordinated in order to fulfill a certain goal. One of the parallel commands may be related to the process of generation of anticipatory postural reactions (Massion 1992). The very tight coupling between the EMG patterns in the prime movers and postural muscles in our experiments lead us to suggest an alternative movement-posture control hypothesis implying that postural synergies are not separate processes, but separate peripheral patterns of a single control process. These patterns occur as results of a decomposition of a multi-joint control parameter into signals to individual joints and muscles. This view is compatible with the dynamic pattern generation approach to motor control.

REFERENCES

Belenkiy, V.I. et al. Biofizika, 10: 135-141, 1967.
Bernstein, N.A. The co-ordination and regulation of movements. Pergamon Press, 1967.
Bouisset, S., Zattara, M. J Biomech 20: 735-742, 1987.
Cordo, P.J., Nashner, L.M. J Neurophysiol 47: 287-302, 1982.
Massion, J. Prog Neurobiol 38: 35-56, 1992.

ACKNOWLEDGMENTS

The study was in part supported by an NIH grant HD30128.

BIOMECHANICS OF DESCENDING ON RAMPS

M.S. Redfern[1,2] and J. DiPasquale [1]

1. Department of Industrial Engineering, University of Pittsburgh, Pittsburgh, PA 15213

2. Department of Otolaryngology, University of Pittsburgh, Pittsburgh, PA 15213

INTRODUCTION

The biomechanics of gait while descending ramps at varying angles was examined in a young population. Joint angles and moments were calculated for the lower extremities. Stride length and cadence did not change as a function of ramp angle. Angle trajectories were found to be affected by ramp angle, primarily at the knee between mid-stance and toe-off. Joint moments for the knee and hip changed as a function of ramp angle between heel contact and mid-stance. The results suggest that large joint moments are generated at the knee and hip as ramp angle is increased in order to maintain relatively constant gait kinematics.

REVIEW AND THEORY

Falls continue to be a significant contribution to injuries in the work place, home and public accessible areas. Changes in elevation are a particular risk for fall injuries (Bureau of Labor Statistics, 1984). Ramps present a falling hazard due to both slips and loss of balance, particularly when descending. An understanding of the biomechanics of gait while descending an inclined surface is important because of the injury risks involved. Slips on ramps are a potential problem due to the higher shear forces that are created as the ramp angle is increased (McVay and Redfern, 1994; Buczek, et al.,1990; Harper, 1967).

Strength requirements while walking on ramps may also influence falls, particularly for individuals with reduced strength capabilities (such as the elderly). The purpose of this study is to determine the effect of ramp angle on the kinematics and kinetics of descending ramps in young, healthy subjects. Implications towards other populations, particularly the elderly, are discussed.

PROCEDURE

A ramp which incorporated a force plate was designed and built to capture foot forces during gait. The apparatus consists of a hydraulic platform with a hinged ramp (1.8 m length) attached. A force plate (Bertec, Inc) is bolted to the superstructure of the ramp two thirds from the top and is flush to the surface. The surface of the ramp is removeable, allowing for changes in surface characteristics during the trials. A harness system with an overhead trolley was used to prevent injury from falling. Foot forces were recorded on a 486 microcomputer via an analog-to-digital converter at a sampling rate of 240 Hz. Whole body movements in the sagittal plane were recorded using a standard Panasonic DV5100 video camera.

Six healthy young subjects (20-29 yrs) participated. Subjects presented with negative histories for neurologic, orthopedic, and vestibular disease. Small reflective markers were placed on the left side of the subject, located at the lateral malleolus, lateral femoral epicondyle, greater trochantor, anterior superior illiac spine, radial styloid process, lateral humeral epicondyle, acromion and two markers on the head in line with the Frankfort plane.

The video recordings were digitized using the Peak Performance (Peak 5.0) motion analysis system. The kinematic data are combined with the foot force data to calculate joint torques at the ankle, knee and hip. Segmental masses and moments of inertia were used based upon Dempster (1955), adjusted by Clauser et al. (1969).

The experimental protocol included five ramp angles (0, 5, 10, 15, and 20 degrees), and two floor surfaces (vinyl tile and slip resistant paint). A full factorial design was used with three replications per cell (5x2x3). Ramp angles were presented in random order, with all trials at that angle collected consecutively. Subjects were required to wear shoes with a standard 3/4 inch heel. They were instructed to walk at a comfortable pace during the experiment and were allowed practice at each ramp angle. During the trials, subjects walked to the top of the ramp, waited for approximately 30 s, then walked to the bottom of the ramp. Foot forces and video were recorded while walking down the rampway.

RESULTS

Gait parameters calculated from the kinematic data showed that step length, step period, and walking speed were not correlated with ramp angle in this young population. Mean step period, length, and velocities across subjects and ramp

angles were .54(.09) s, 0.35(0.05) steps/stature, and 1.1 (0.3) m/s, respectively.

Joint angles during the step varied as a function of ramp angle, primarily between mid-stance and toe-off. These angles varied only slightly as a function of ramp angle between heel strike and mid-stance. The most pronounced changes were found at the knee.

Knee and hip moments increased and ankle moments decreased as a function of ramp angle (Figure 1). For ramp angles of 5 degrees and above, flexion moments at the hip and extension moments at the knee remained elevated throughout stance. Also, knee extension moments were twice the magnitude of the hip flexion moments.

DISCUSSION

Gait parameters (gait speed, step length and step period), were unchanged in this young population. Joint angle trajectories changed primarily at the knee from mid-stance to toe-off in order to lower the body to the next step on the ramp. A consequence of constant step length and minimal changes in gait kinematics is that joint moments change as ramp angle is increased. Higher knee extension moments and hip flexion moments are required to maintain the same gait parameters seen in level walking. These prolonged high moments may be a problem for an elderly population with strength limitations. Different gait kinematics may be required by this population as ramp angle is increased in order to reduce the required moments. Knee strength, in particular, may be a critical factor in determining the ability to descend ramps safely. An investigation of the biomechanics of gait on ramps for an elderly population is currently underway to examine these questions.

REFERENCES

BLS Bulletin 2214. Washington, D.C.: Government Printing Office, 1984, pp. 1-19.

Buczek, et al. In Slips, Stumbles and Falls, ASTM STP 1103, ed. Gray, 1990, pp 39-54.

Clauser et al.AMRL-TR-69-70 (Ohio: Aerospace Medical Research Laboratories, 1969.

Dempster , Space Requirements of the seated operator, WADC-TR-55-159, 1955.

McVay and Redfern, J. of the AIHA, In Press, 1994.

Harper, NMSR 32, London: Her Majesty's Stationary Office, 1967.

ACKNOWLEDGEMENTS

This research was supported by the CDC , grant no. R49/CCR308848

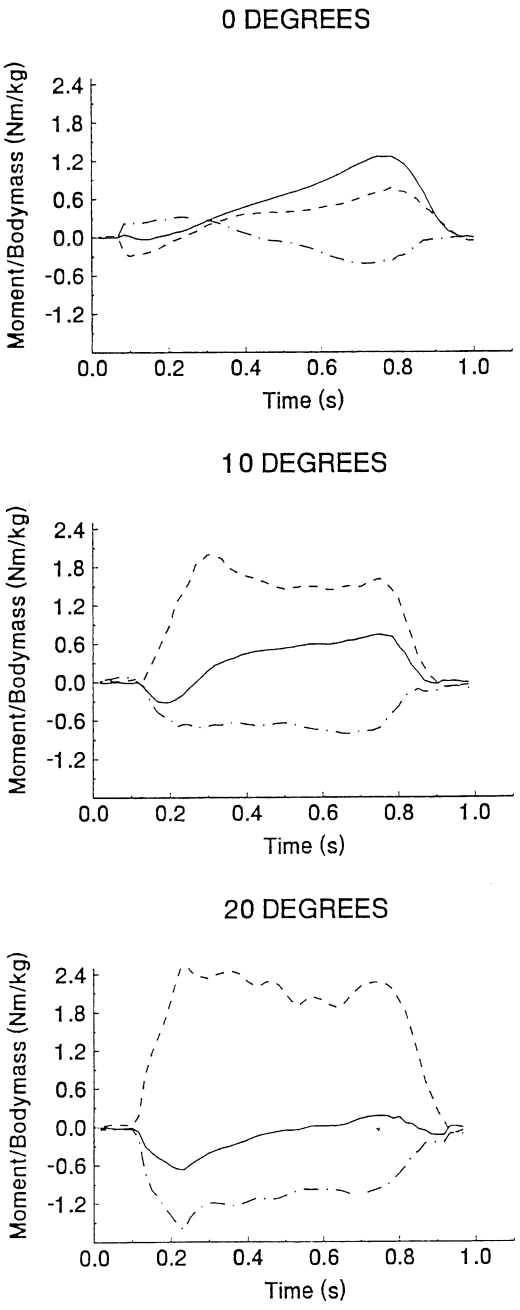

Figure 1. Joint moments as a function of ramp angle for the ankle, knee and hip. Solid line indicates ankle moment, dashed line indicates knee moment and dot-dash line is hip moment. (positive moment = extension)

MOMENTUM ANALYSIS OF RISING FROM A CHAIR

P. O. Riley, R. Popat, B. Kaya and D. E. Krebs
Biomotion Laboratory, Massachusetts General Hospital, Boston, MA, 02114
Institute of Health Professions, Massachusetts General Hospital, Boston, MA, 02114

INTRODUCTION

The sit to stand task is challenging particularly to the elderly (Weiner, Long et al. 1993). It requires both strength and coordination. Using a quasistatic whole body model we have previously inferred that the generation and control of momentum, especially upper body momentum, has an important role (Schenkman, Berger et al. 1990; Riley, Schenkman et al. 1991). Pai et al. have reported similar findings (Pai 1989; Pai and Rogers 1990; Pai and Rogers 1991) Momentum generation is quantified using a whole body dynamic analysis.

METHODS

Whole body kinematic data was acquired at 153 Hz. using a SELSPOT II/TRACK system (Antonsson and Mann 1989; Riley, Hodge et al. 1990). Body segment parameters were estimated (McConville, Clauser et al. 1980; Young and al. 1983) and segment linear and angular velocities were estimated using a fifth order Lagrangian estimator. Body segment and whole body linear and angular momenta were calculated (Hutchinson, Riley et al. 1993).

Subjects (3F,1M) were community dwelling elders 71.0±1.2 years of age. They rose from a backless, armless chair without using their arms. Chair heights of 80 and 100% of knee height were used. Freespeed and paced (1.2 sec) sit to stands were performed from the 80% chair. Parameters of interest were whole body and upper body (HAT) linear and angular momentum. We also evaluated the hip, knee and lower back torques. These parameters were normalized to body weight in newtons. Differences in the mean were evaluated using paired 2 tail t-test ($p<0.05$).

RESULTS

Lower back torques at maximum ground reaction force, just after clearing the seat were significantly greater rising from an 80% chair compared to a 100% chair. The same was true for maximum HAT AP linear and Sagittal plane angular momenta. Momentum and torque parameters were not significantly different for the freespeed and paced chair rises.

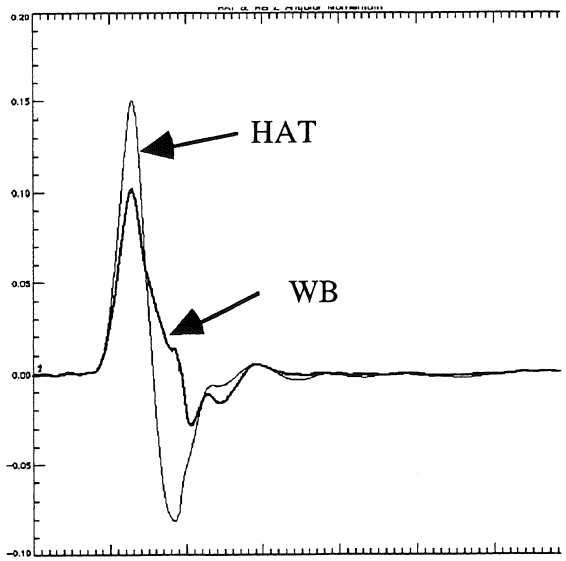

Typical Sagittal Plane Angular Momentum Plot. HAT head arms and trunk about hip. WB whole body about CG.

DISCUSSION

These findings are consistent with our previous studies (Schenkman, Berger et al. 1990; Riley, Schenkman et al. 1991). Healthy individuals compensate for the increased difficulty in rising from a lower chair by increasing upper body momentum generation before liftoff. Momentum analysis directly measures

this dynamic effect that was previously inferred from CG linear kinetic energy and liftoff CG-CoP moment arm.

HAT momentum dominates AP and Vertical linear momentum not only because most of the body mass is in the upper body, but also because of greater excursions and velocities. AP linear momentum rise during the forward flexion phase reaching a maximum just as seat unloading begins. Sagittal plane angular momentum peaks simultaneously. Peak Vertical linear momentum occurs during the extension phase after liftoff. While this is chiefly due to extension of the knee and hips, there is also a significant component due to extension of the HAT. More momentum is generated when rising from a lower chair. Non zero momentum parameters at full extension may be a measure of the degree of instability at the beginning of the stabilization phase.

REFERENCES

Antonsson, E. and R. Mann (1989). " Automatic 6-D.O.F. kinematic trajectory acquisition and analysis." ASME J Dynam. Syst. Measmt. Control **111**(1): 31-39.

Hutchinson, E. B., P. O. Riley, et al. (1993). "A dynamic analysis of the joint forces and torques during rising from a chair." IEEE Trans Rehab Eng **Submitted**:

McConville, J. T., C. E. Clauser, et al. (1980). Anthropmetric relationships of body and body segment moments of inertia. Air Force Aerospace Medical Research Laboratory.

Pai, Y.-C. (1989). Segmental contributions to total body motion in sit-to-stand. XII Congress, International Society of Biomechanics, ISB, Pergamon Press.

Pai, Y. C. and M. W. Rogers (1990). "Control of body mass transfer as a function of speed of ascent in sit-to-stand." Med Sci Sports Exerc **22**(3): 378-84.

Pai, Y. C. and M. W. Rogers (1991). "Speed variation and resultant joint torques during sit-to-stand." Arch Phys Med Rehabil **72**(11): 881-5.

Riley, P. O., W. A. Hodge, et al. (1990). "Modelling the biomechanics of posture and balance." J. of Biomechanics **23**: 503-505.

Riley, P. O., M. L. Schenkman, et al. (1991). "Mechanics of a constrained chair rise." J. of Biomechanics **24**(1): 77-85.

Schenkman, M., R. A. Berger, et al. (1990). "Whole-body movements during rising to standing from sitting." Phys Ther **70**(10): 638-48.

Weiner, D. K., R. Long, et al. (1993). "When older adults face the chair-rise challenge. A study of chair height availability and height-modified chair-rise performance in the elderly." J. American Geriatriac Society **41**: 6-10.

Young, J. W. C., R. F. and e. al. (1983). Anthropometric and mass distribution characteristics of the adult female. FAA Civil Aeromedical Institute.

BIOMECHANICAL COMPARISON OF FUNCTIONAL ELECTRICAL STIMULATION - INDUCED AND ACTIVE KNEE EXTENSION EXERCISE

Mary M Rodgers, PhD, PT and Roger M Glaser, PhD
Department of Veterans Affairs Medical Center, Dayton, OH; and
Institute for Rehabilitation Research and Medicine, Wright State University School of Medicine, Dayton, OH 45420.

INTRODUCTION

The purpose of this study was to compare biomechanical responses for knee extension (KE) exercise performed via functional electrical stimulation (FES)-induced contractions of the paralyzed quadriceps muscles of spinal cord injured (SCI) individuals with the same exercise being performed voluntarily by able-bodied (AB) individuals. SCI subjects were tested using a progressive intensity KE protocol to determine maximum KE resistance load. AB subjects were evaluated at three loads using a speed matched to the FES-KE exercise and at two loads using their freely chosen speed. Freely chosen velocity of KE exercise for AB was comparable to the FES-induced KE at the maximum load, but 35% faster at the no load condition. The EMG pattern of quadriceps muscle activity demonstrated by the AB subjects was comparable to the stimulation pattern used for the SCI subjects. Maximum knee extension angle decreased 47% from 0 load to maximum load for the SCI subjects. Maximum loads for knee extension varied among the SCI individuals (64.4±27.0 N). Based on these findings, the FES-KE exercise appears to appropriately simulate AB KE exercise except at the 0 load level. Hip and knee angles do not reflect differences which might indicate safety impairment. Loads are well within safe limits for the SCI population.

REVIEW AND THEORY

FES-induced knee extension exercise for SCI individuals has been used primarily for strengthening weak quadriceps muscles in preparation for more strenuous types of exercise (i.e. FES-induced leg cycle ergometry, FES-assisted ambulation) (Rodgers et al., 1991). Due to the artificial nature of the induced movement with FES, and how well it simulates active knee extension there have been questions about the safety of the knee joint biomechanics (Fournier et al., 1984). Previous work has focused on the physiologic effects of training with FES-induced KE exercise (Figoni et al., 1991). The purpose of this study was to examine the similarities and differences in the biomechanics between voluntarily performed AB and SCI FES-induced KE exercise so that the issues of simulation and safety might be addressed.

PROCEDURES

Subjects were 10 SCI males (mean age 40±13 yrs.) and 10 AB males (mean age 34±8 yrs.). SCI subjects had lesion levels from C6-T10 and time since injury of 12±8 yrs. All SCI subjects had previous experience with FES-induced exercise. Leg lengths were not significantly different between the two groups (SCI: 39±9 cm, AB: 33±2 cm). Quadriceps maximum isometric strength was determined for the AB group using a KinCom isokinetic dynamometer.

The exercise chair and electrical stimulator system used to induce KE activity includes unique instrumentation features which have been previously described in detail (Ezenwa et al. 1991). In summary, this system enabled asynchronous left-right KE exercise through approximately 70^{o} at a rate of approximately 6 KE/min./leg. External resistance was applied via load weights placed upon the lever arms at ankle level. The stimulation current was automatically ramped up and down to allow safe and smooth concentric and eccentric contractions. A knee angle-feedback system, incorporating potentiometer and microswitch sensors in the lever arms, ensured appropriate range of KE motion. In addition, threshold current and stimulation output current ramp parameters were continuously adapted (with each contraction) to maintain appropriate range of KE motion via gradual increases in FES current as fatigue occurred. Knee joint hyperextension, which can occur with spasticity, can be detected with this system and would initiate a reduction of stimulation current. The chair back support was fixed to maintain a hip angle of approximately 110^{o}. This hip angle reduced stretching of the hamstring muscles, thereby minimizing resistance to knee extension from spastic or tight hamstrings. Strap stabilization at the hips, knees and ankles were used to maintain joint alignment during exercise. The weight arms were instrumented with strain gauges to provide force data.

Each SCI subject was evaluated using a continuous, progressive intensity KE exercise protocol to determine a "maximum" KE resistance load. For this test, KE exercise was performed for five repetitions at each of several loads, starting with zero load and progressing in 0.5-kg increments to a maximum of 15.0 kg (147 N). The quadriceps muscles were considered fatigued when the KE failed to reach 50% of the 70^{o} target angle. Since the disuse osteoporosis which accompanies SCI may markedly decrease bone strength, the maximal load was limited to 147 N (Glaser, 1986; Gruner et al., 1983).

All motion data were collected at 60 Hz using a video based motion analysis system (Peak Performance Technologies, Inc.). Strain gauge readings of force and potentiometer measurements of knee angle were also collected for both groups (1000 Hz sampling rate). The quadriceps and hamstring muscles of the AB subjects were monitored using radio-telemetry electromyography (EMG) collected at 1000 Hz. FES current was recorded for the SCI subjects. Five conditions were evaluated for the AB subjects: freely chosen speed 0 load (T1), controlled speed 0 load (T2), controlled speed 7.5 kg (74 N) load (T3), controlled speed 15 kg (147 N) load (T4), and freely chosen speed 15 kg (147 N) (T5). Three conditions from the continuous, progressive intensity KE exercise protocol described above were evaluated for the SCI subjects using a maximum stimulation level of 300 mA: 0 load (T1), 1/2 maximum load (T2), and maximum load (T3). Maximum torques (Nm) were calculated from the force output, limb length, and maximum knee extension angle.

Knee range of motion (ROM) and knee joint kinetics were compared for 0, 1/2 maximum loads, and maximum loads between SCI and AB groups using independent *t tests* and a .05 level for significance. Stimulation vs EMG patterns were subjectively compared between the two groups.

RESULTS AND DISCUSSION

Since the stimulation timing was a set ramp of current for the FES-KE exercise, the time for each knee extension cycle was 7.4 sec for the SCI group (figure 1). The velocity freely chosen by the AB group was comparable to this stimulation rate at the 15 kg load level (6.2±1.4 sec), but was significantly faster for the AB group in the 0 load condition (4.9±1.5 sec). Based on these findings, the velocity of KE used in the FES-induced KE exercise appropriately simulates that of AB exercise provided the exercise is performed against resistance.

The pattern of quadriceps muscle activity in the AB subjects was comparable to the stimulation pattern used for the SCI subjects. The hamstrings were relatively silent at all load conditions for the AB group. For the SCI subjects, maximum stimulation occurred 1/3 sec before maximum strain gauge output and maximum knee extension angle. This gap was smaller at the higher loads, indicating a closer stimulation-force relationship with heavier loads in paralyzed muscle.

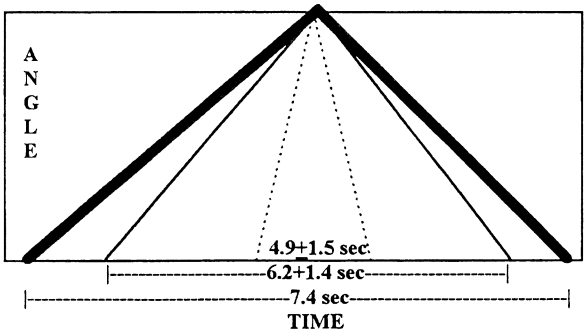

Figure 1. Diagram showing mean time-angle curves for the FES-KE exercise (bold line), the freely chosen trial for the AB subjects using 0 load (thin line), and the freely chosen trial for AB subjects using 15 kg load (dotted line).

Hip ranges were similar for both AB and SCI groups throughout the trials indicating little change in trunk position with the exercise. Maximum knee extension angle for the AB group did not change with freely chosen speed or with the different load levels (figure 2). Mean maximum knee extension angle decreased 21% from the 0 load to the maximum load condition for the SCI subjects. This indicates that with this exercise set-up, training at higher loads will take place within a more restricted range (less knee extension). If strengthening is desired in the more terminal knee extension range, the exercise device would need to be mechanically altered to enable full extension at high load levels (i.e., via pulley weight system).

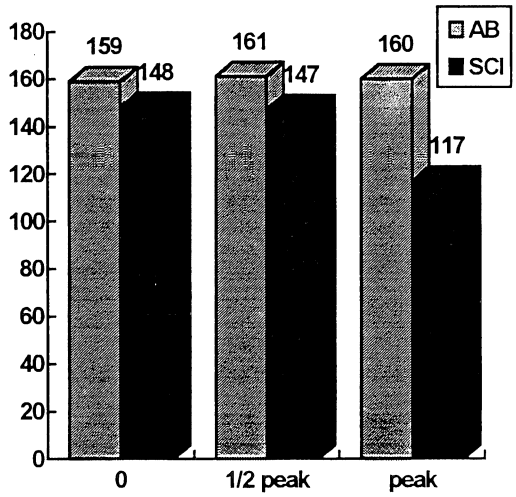

Figure 2. Mean maximum knee extension angle for each subject group at 0 load, 1/2 peak load, and peak load levels.

Maximum load for the AB subjects was arbitrarily set at 15 kg (147 N) to match the maximum load used for the SCI group. Maximum load varied among the SCI individuals based on their quadriceps muscle strength and endurance. Mean maximum load for the SCI subjects was 64.4±27.0 N (approximately 44% of the 147 N maximum AB load). All 10 SCI subjects required a current level greater than 150 mA to attain their 1/2 maximum and maximum torques. Maximum torques for the SCI group ranged from 9.9 Nm to 29.7 Nm (mean 23.6±8.9 Nm or approximately 52% of the mean maximum AB torque). In half of the SCI subjects, maximum torques occurred at 1/2 maximum load because of the reduction in knee extension angle at the full load levels (figure 3). Knee extension for the maximum load trial was an average of 47% of the extension ROM achieved with 0 load. Maximum torque for the AB group was 21% of their quadriceps isometric maximum torque.

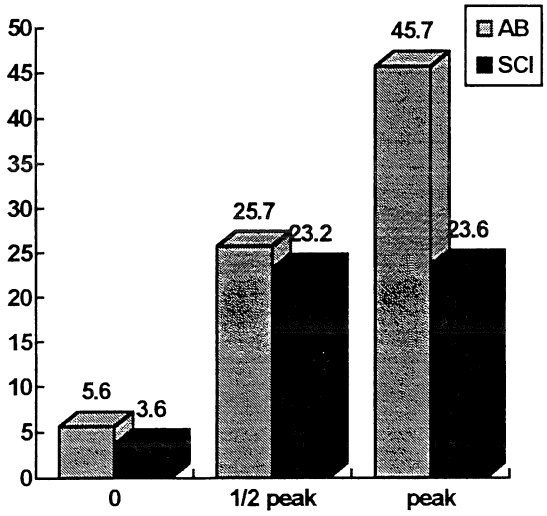

Figure 3. Maximum calculated torques at three load levels for each subject group.

CONCLUSIONS

Biomechanical responses for FES-KE exercise appear to appropriately simulate AB KE exercise except at the 0 load level. Higher load strengthening is not effective for terminal knee extension with this exercise device. Ranges and loads appear to be well within safety limits for the SCI population.

REFERENCES

Ezenwa BN, et al. Adaptive control of functional neuromuscular stimulation-induced knee extension exercise. *J Rehabil Res Dev* 28:1-8, 1991.

Figoni SF, et al. Acute physiologic responses of spinal cord injured individuals to functional neuromuscular stimulation-induced knee extension exercise. *J Rehabil Res Dev* 28:9-18, 1991.

Fournier A, et al. A medical evaluation of the effects of computer induced muscle stimulation in paraplegic patients. *Orthopaedics* 7:1129-1133, 1984.

Glaser RM. Physiologic aspects of spinal cord injury and functional neuromuscular stimulation. *Centl Nerv Syst Trauma* 3:49-62, 1986.

Gruner JA, et al. A system for evaluation and exercise-conditioning of paralyzed leg muscles. *J Rehabil Res Dev* 20:21-30, 1983.

Rodgers MM, et al. Musculoskeletal responses of spinal cord injured individuals to functional neuromuscular stimulation-induced knee extension exercise training. *J Rehabil Res Dev* 28:19-26, 1991.

ACKNOWLEDGEMENTS

This work was supported by the Rehabilitation Research and Development Service of the U.S. Department of Veterans Affairs (grant #B433-2RC).

ERROR ANALYSIS OF TWO SYSTEMS TO MEASURE IN-SHOE PRESSURES

Bin Xia, John C. Garbalosa, and Peter R. Cavanagh.

Center for Locomotion Studies, Penn State University, University Park, PA 16802

INTRODUCTION

Pressure measurements were obtained during two pressure loading protocols using two different in-shoe pressure measuring systems, the Tekscan and Pedar systems. The Tekscan insole had greater inter-sensor variability (standard deviation (S.D.) ranging from 53.3 to 90.8 kPa) and a larger increase in the recorded pressure from cycle 1 to 190 (26.0% to 36.7% increase) than the Pedar insole (S.D. ranging from 7.2 to 17.5 kPa and 6.3% to 10.1% increase) during pressure loading protocol 1. During pressure loading protocol 2, the coefficients of variation (C.V.) ranged from 9.5% to 20.8% ($\overline{c.v.}$= 12.9%) for the Tekscan insoles and 0.6% to 3.1% ($\overline{c.v.}$ = 1.4%) for the Pedar insoles respectively. Pedar insoles showed better linearity than Tekscan during protocol 2. The measurements of the applied load of 400 kPa by both insole systems varied significantly over cycles. Statistically, within each device the measurements produced by each insole varied significantly from each other. Measurements between days also varied significantly in the two systems with Pedar having smaller variances.

REVIEW AND THEORY

The measurement of plantar pressures is gaining recognition as a diagnostic tool in the management and prevention of foot related problems due to Diabetes Mellitus and orthopedic disorders (Novick, et al. 1993). The two most common methods to measure plantar pressures are pressure platforms and in-shoe pressure systems. Plantar pressure measurements using in-shoe devices offer important additional possibilities compared to platforms. They directly measure the interaction between the foot and footwear and allow the collection of data from many successive steps under various walking surface conditions without a targeting effect (Lee, 1980).

There are however some limitations in the use of in-shoe pressure systems which can be divided into two categories: time-dependent and time-independent. Time-independent problems, such as inter-sensor variation and non-linearity of sensor response, should be resolved by calibration prior to use. Each manufacturer provides procedures intended to perform these calibration functions. Time-dependent problems, such as between day variance and the effect of duration and frequency of loading on sensor response drift, are not well documented and, in general, manufacturers provide no methods to compensate for such change over time. The variance of different sensors may change on a day-to-day basis.

The purpose of this study was to examine both the time-dependent and time-independent variance of two commercially available in-shoe sensors: Pedar (Novel, Minneapolis, MN), and Tekscan (Tekscan, Boston, MA).

PROCEDURE

Two new Tekscan and Pedar insoles were used in the study. In the present paper a sensor refers to a single pressure sensing element. An insole is a collection of n such sensors where n equals 99 and 501 (trimmed prior to use) for the Pedar and Tekscan insoles respectively. The average pressure measurement of n sensors is denoted as the mean pressure measurement (MPM) of an insole. Pedar insoles are a capacitance based pressure sensor matrix with an effective sensor area of 1.5 cm^2. Tekscan insoles are a resistance based pressure sensor matrix with an effective sensor area of 0.26 cm^2. The FSCAN system (Tekscan, Boston, MA) was used to collect the data from the Tekscan insoles while the Pedar system (Novel, Minneapolis, MN) was used to collect the data from the Pedar insoles.

The Pedar insoles were calibrated according to the manufacturer's specifications prior to testing. The Tekscan insoles were calibrated prior to testing by loading the insoles to 400 kPa in a pressure loading device. This procedure insured that all sensors were calibrated as opposed to the manufacturer's procedure where the insoles are calibrated by stepping on them and only the sensors that are loaded are actually calibrated. Each insole was then put in a pressure loading device and loaded using two protocols. Protocol 1 consisted of cyclically loading the insoles to 400 kPa. The insoles were loaded using a 5 to 1 duty cycle (5 seconds load on to one second load off). Data were collected after the first cycle and then every ten cycles for 190 cycles at a sampling rate of 50 Hz. During each data collection period the insoles were unloaded for 30 seconds. This procedure was repeated the next day.

Protocol two used the same 5 to 1 second duty cycle, to load the Tekscan and Pedar insoles at 100 kPa increments from 100 kPa to 600 kPa to explore the linearity of the sensors. The data were collected at each pressure at a sampling rate of 50 Hz. C.V's were calculated for each insole at the different pressures and a mean C.V. ($\overline{c.v.}$) for the 6 pressure values was determined.

An analysis of variance was performed to determine the effect of collection period, insole and day on MPM. The level of significance for all tests were set at the $\alpha = .05$.

RESULTS AND DISCUSSION

Inter-sensor variability. As seen in Table 1 and Figure 1, the inter-sensor variability of the Pedar insoles during protocol 1 loading is small relative to the Tekscan insoles. The S.D.'s of each of the 20 collection periods of the Pedar insoles varied from 7.2 to 17.5 kPa as opposed to the 53.3 to 90.8 kPa range of the Tekscan insoles. Further, this variability is seen in the increase in the MPM from collection period 1 to collection period 20 of the two Tekscan (n=501 sensors) and Pedar (n=99 sensors) insoles.

Table 1. The response characteristics of protocol 1 test to a normal 400 kPa pressure

Insole type	Day 1 Range (kPa)	Range of S.D. (kPa)	Δp_1	Δp_2	Day 2 Range (kPa)	Range of S.D. (kPa)	Δp_1	Δp_2
Tekscan #1	384 - 484	53.3 - 86.6	1.32	0.21	338 - 462	56.6 - 90.8	1.45	0.32
Tekscan #2	381 - 514	55.3 - 82.8	1.45	0.43	390 - 505	61.1 - 82.2	1.52	0.27
Pedar #1	410 - 448	7.2 - 14.4	0.27	0.17	399 - 424	14.3 - 16.0	0.16	0.13
Pedar #2	390 - 419	12.6 - 17.5	0.32	0.28	385 - 424	7.7 - 9.6	0.28	0.18

In protocol 2 loading, the C.V. of the 99 Pedar sensors ranged from 0.6% to 3.1% ($\overline{c.v.}$ =1.4%) and the 501 Tekscan sensors ranged from 9.5% to 20.8% ($\overline{c.v.}$=12.9%). A decreasing trend was exhibited by the C.V.'s of the Pedar and Tekscan insoles as the applied load increased (Figure 2). Once the applied load surpassed 400 kPa, the Tekscan insole curves leveled off.

Inter-cycle variability. During protocol 1 loading, the Tekscan insoles had a greater increase in MPM ranging from 26.0 to 36.6% compared to the 6.3 to 10.1% range for the Pedar insoles (A change of approximately 100 - 133 and 25- 39 kPa respectively). In the first 50 cycles, the rate of change ($\Delta p1$) of the Tekscan insole MPM is greater than the remaining 140 cycles where the rate ($\Delta p2$) is leveling off (Figure 1a and Table 1). This event does not occur in the Pedar insoles where the rate of change lowered slightly from the first 50 cycles to the remaining 140 cycles (Figure 1b and Table 1). The MPM between cycles for the Tekscan insoles varied significantly ($F=17.53, 19, 58, p < .0001$). Although smaller in magnitude, the MPM between cycles for Pedar also varied significantly ($F = 7.72, 19, 58$ respectively; $p < .0001$).

Within device variance and response linearity. Mean pressure measurements produced by the two insoles of the Tekscan system varied significantly from each other ($F=75.79, 1, 58, p < .0001$) as did the two Pedar insoles ($F = 94.97, 1, 58, p < .0001$), even though the magnitude is much smaller. Day 1 MPM varied significantly from day 2 MPM for the two Pedar ($F = 55.90, 1, 58, p < .0001$) and Tekscan ($F = 28.92, 1, 58, p < .0001$) insoles (Figure 1). The response linearity of the Pedar insoles was better than the Tekscan insoles Figure 3 shows the averaged responses of two Tekscan and two Pedar insoles.

From the differences noted in the time independent and time dependent characteristics of the two systems, if the spatial resolution is not an important factor in the experiment, Pedar shows advantages in in-shoe pressure measurements.

REFERENCES

1. Novick A et al. Reduction of plantar pressure with the rigid relief orthosis. Jour Amer Pod Assoc. 83, 115-122, 1993.
2. Lee D N. Tutorials in motor behavior, (pp 281-295), Stelmach and Requin, 1980.

This work was supported by the National Institutes of Health under grant DK-5RO1DK4292.

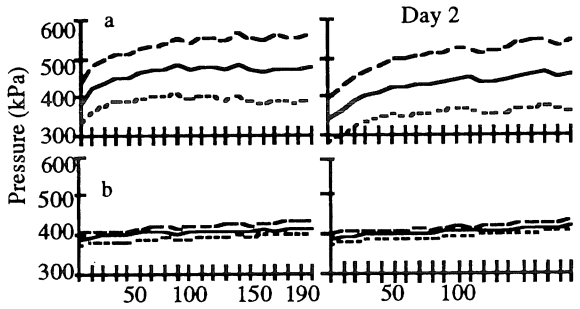

Figure 1. The mean and ± standard deviations of the 20 collection periods for the two days of protocol 1 loading of the Tekscan (a) and Pedar (b) insoles

This work was supported by the National Institutes of Health under grant DK-5RO1DK4292.

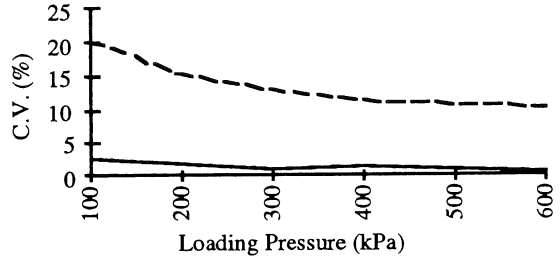

Figure 2. Coefficients of Variation of Tekscan insole (upper curve) and Pedar (lower curve) insole

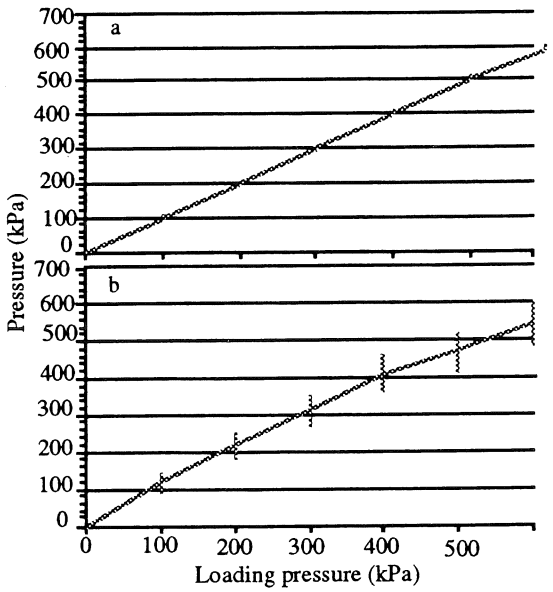

Figure 3. The response linearity of a) Pedar insoles and b) Tekscan insoles.

Effect of Transducer Size on Plantar Pressure Profiles: Analysis of Spatial Frequency Using the 2D Fast Fourier Transform

S.B. Hanson, B.L. Davis, R.M. Cothren, P. Quesada*, J.E.Perry

Department of Biomedical Engineering, Cleveland Clinic Foundation, Cleveland, OH 44195
*Center for Biomedical Engineering, Ohio State University, Columbus, OH 43210

INTRODUCTION

The measurement of plantar pressure profiles (PPS) is becoming a standard part of clinical management of diabetic patients with sensory neuropathy. This is due to convincing evidence that elevated plantar pressures are an important biomechanical factor in the etiology of foot problems in diabetic patients (Stokes et al., 1975, Cterctko et al., 1981, and Sims et al., 1988). At present there are numerous systems available to measure peak pressures during gait. Amongst these devices there is a noticeable variation in spatial resolution. Pressure transducers range in size from $6mm^2$ to $900mm^2$, making it difficult to draw comparisons between different clinical investigations.

The effect of transducer size can be analyzed by examining the spatial frequencies of the PPPs. An appropriate sampling frequency can be determined after identifying the highest frequency components that significantly contribute to the PPP. This technique has often been used to determine sampling rates to collect data at time increments small enough to prevent aliasing. In this study, the Fast Fourier Transform (FFT) was used to determine (i) the spatial frequency content of diabetic and non-diabetic PPPs and (ii) the effects of increasing the transducer size (from 5mm square to 10mm square). The objective was to determine how small pressure transducers need to be to accurately measure pressure profiles under normal and diabetic feet and the effect of measuring the pressures with larger transducers.

PROCEDURES

Foot pressure data were collected during gait from six non-diabetic and five diabetic patients using an EMED-SF Pressure Platform (manufactured by Novel Electronics Inc.) with a 19cm by 36cm rectangular array of 5mm square transducers (i.e., a spatial frequency of $0.2mm^{-1}$). During data collection, subjects did not target the platform; starting positions were adjusted in order to obtain clean footfalls. The data were converted to digital images where each pressure cell corresponded to a brightness of the pixel in the image matrix. A two dimensional Fast Fourier Transform (2D FFT) was performed on each image to determine the spatial frequency content of the image (Gonzalez et al., 1992). The 2D FFT images were scaled using the function $log(1+|F(u,v)|)$ where $F(u,v)$ is the original magnitude of the FFT image at $x = u$ and $y = v$. Cutoff frequencies (f_{cx} and f_{cy}) were defined as the boundaries enclosing 99% of the spectral magnitude in the x and y directions. Using a non-symmetrical second order Butterworth filter, the FFT images were filtered at the bandwidth cutoff frequencies f_{cx} and f_{cy}. The FFT images were also filtered at a cutoff frequency corresponding to 10mm square transducers (i.e. $0.05mm^{-1}$).

To quantify the difference in pressures that would be measured from 5mm and 10mm square transducers, maximum pressures were found in five areas (Fig.1) for each foot image: the toes; the heel; and three areas of the metatarsal region divided by the ratios 0.3,0.25, and 0.45 (Cavanagh et al., 1987). Maximum pressures from the original foot data were compared with those obtained from images filtered to simulate measurements from 10mm square transducers.

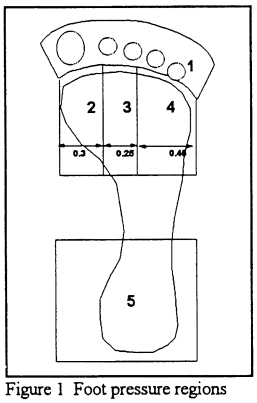

Figure 1 Foot pressure regions

RESULTS

The average cutoff frequencies for 99% of the spectral bandwidth in the x and y directions corresponded to a transducer size of 6.05mm by 5.83mm . No significant difference was found for the cutoff frequencies between normal and diabetic subjects.

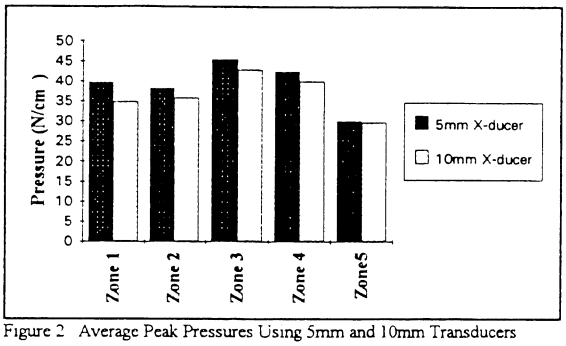

Figure 2 Average Peak Pressures Using 5mm and 10mm Transducers

The largest reductions in pressure (difference between using 10mm transducers instead of 5mm transducers) were found in the toe region (Fig. 2). Reductions in this area were on average 5 N/cm^2 (50kPa) or around 17.7% of the mean peak pressure. Across all regions the average pressure reduction for diabetic patients was 2.85N/cm2 (28.5kPa) and for normal patients 1.54N/cm2 (15.4kPa). Pressure

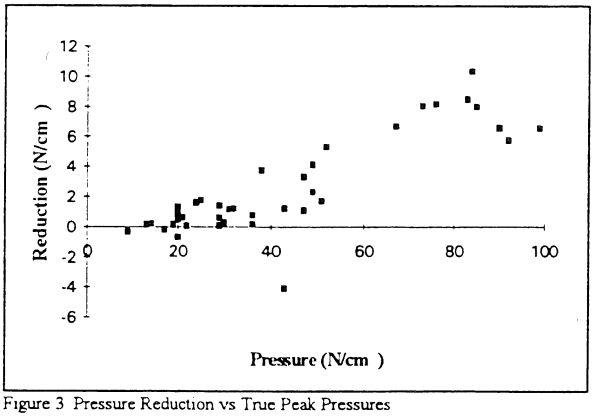

Figure 3 Pressure Reduction vs True Peak Pressures

reductions in the metatarsal region were found to be significantly correlated ($p<0.01$) with measured peak pressures in that region (Fig. 3).

DISCUSSION

The results from this study show that an effective transducer size for measuring PPPs is 6.05mm by 5.83mm. There was no significant difference in effective transducer size between diabetic and non-diabetic subjects; however, because the larger transducer underestimated peak pressures more in diabetic patients, it is proposed that the spectra for the diabetic PPPs have higher, more significant components at higher spatial frequencies.

This study also suggests that pressure measurement systems with larger transducers will give significantly poorer quality data (Fig. 4). When the transducer size was increased from 5mm square to 10mm square, loss of accuracy was demonstrated by average pressure reductions of 50kPa in the toe region. Pressure reductions found in the toe region were statistically greater than reductions in all other areas, and reductions in the metatarsal region were greater than those found in the heel area. These findings demonstrate that the 10mm transducer can accurately measure peak pressures in the heel region where there is little variation in local pressures, yet it underestimates peak pressures in the toe and metatarsal region where there is greater variation in pressure. Correlations between pressure reduction and peak pressure were as high as 0.82 and 0.9 for the regions of the first and second metatarsal heads. This implies that the higher peak pressures found in these regions will be underestimated to the greatest extent.

Underestimation of peak pressures was, on average, 28.5 kPa for diabetic patients compared to 15.4 kPa for non-diabetic subjects. Furthermore, the greatest underestimate of peak pressures (due to larger transducers) occurred in the toes and metatarsal regions of diabetic patients and there were high correlations between underestimates of pressure and true peak pressure in the 1st and 2nd metatarsal head regions. Of clinical significance is the fact that the toe and metatarsal regions are most prone to skin breakdown in diabetic patients; underestimating pressures in these regions could, therefore, pose substantial problems. Because of dense neuropathy and poor circulation , a difference in pressure of 50 kPa may be more detrimental for diabetic patients than for patients with intact sensation and good perfusion. Researchers and clinicians should be aware that measurements from systems with larger transducers may not accurately reflect the true pressure.

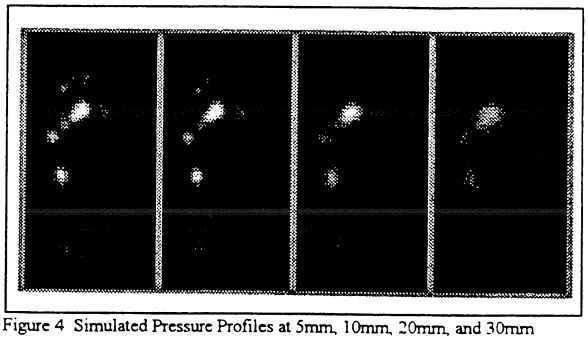
Figure 4 Simulated Pressure Profiles at 5mm, 10mm, 20mm, and 30mm

REFERENCES

Cananagh, P. et al. Foot & Ankle, 7, 5, 262-276, 1987.
Cteretko, G. et al. Bri. J. Sur., 68, 608-614, 1981.
Gonzalez, R. & Woods, R. Digital Image Processing, (pp. 111-119), Addison Wesly, 1992
Sims, D. et al. Physical Therapy, 68, 12, 1887-1902, 1988
Stokes, I. et al. Acta Orthop. Scand., 46, 839-847, 1975.

ARCH INDEX AS A PREDICTOR OF ARCH HEIGHT

J.L. McCrory, M.J. Young+, A.J.M. Boulton+ and P.R. Cavanagh

Center for Locomotion Studies, The Pennsylvania State University, University Park, PA 16802

+University Department of Medicine, Manchester Royal Infirmary, Manchester, UK

INTRODUCTION

The efficacy of arch index as a valid and convenient predictor of medial longitudinal arch height has recently been questioned (Hawes et al 1992). In the present study, arch index was measured in 45 elderly subjects and navicular height was measured directly from weight bearing radiographs of the same individuals. Normalized navicular height was determined by dividing navicular height by the total length of the foot as measured from the radiographs. A correlation coefficient of r=0.67 was found between navicular height and arch index and the correlation coefficient between arch index and normalized navicular height was found to be r=0.71. These data show, in the subjects used, that arch index provides a simple quantitative means from which the height of the medial longitudinal arch can be assessed with the limitation that only half of the variance in arch height can be explained.

REVIEW AND THEORY

The functional mechanics of the human foot are greatly influenced by the structure of the foot, in particular, by the height of the medial longitudinal arch. A convenient and reliable method of determining the medial longitudinal arch height is of considerable scientific and clinical value. At present, some controversy exists regarding the meaning and validity of several indirect measures of foot structure. Hawes, Nachbauer, Sovak, and Nigg (1992) have stated categorically that several footprint parameters, including arch index, are "invalid as a basis for prediction of categorization of arch height". They reported, for example, a correlation of only 0.3 between arch index and navicular height. Their measurement of navicular height was determined by palpation of the navicular tuberosity.

The purpose of this study was to determine the relationship between arch index and navicular height as measured by radiography. Our hypothesis was that arch index would be a useful predictor of arch height.

PROCEDURES

The subjects for this study were 14 females and 31 males, with a mean age of 63.3 years (S.D. 13.1 yrs), height of 1.69 meters (s.d. 0.08 m), body mass of 70.02 kg (s.d. 10.5 kg), and foot length of 0.0252 meters (s.d. 0.013 m). All subjects were free of prior foot surgery and exhibited no major foot deformity.

Arch index was measured using the method described by Cavanagh and Rodgers (1987). Briefly, a walking footprint was obtained from each of the 45 subjects. Arch index was defined as the area of the midfoot divided by the total area of the footprint. An arch index of less than 0.21 is indicative of a cavus foot, while an arch index greater than 0.26 is indicative of a planus foot.

Radiographs were taken of each foot while the patient was in the stance position, with each foot bearing approximately half of the patient's weight. Using calipers, a radiographic measurement called "true navicular height" was measured as the distance between the navicular tuberosity and the floor. The total length of the foot, from the most posterior aspect of the calcaneus to the tip of the most anterior phalanx, was obtained and termed "foot length." Navicular height was subsequently normalized to foot length by dividing navicular height by foot length.

RESULTS

Linear regression analysis was used to determine the relationship between arch index and true navicular height. The correlation coefficient was determined to be r=0.67. Likewise, a linear regression analysis was performed to quantify the relationship between arch index and true normalized navicular height, yielding a correlation coefficient of r=0.71. These results are illustrated in Figures 1 and 2.

DISCUSSION

The above results show that Hawes et. al (1992) may have been too eager to dispose of indirect measures of foot structure that can be collected easily from footprints. In contrast to the approximately 10% of explained variance in the study by Hawes et al (1992), the correlation coefficient in the present study indicates that approximately 50% of the variance in navicular height can be explained on the basis of arch index. Subsequent studies may well be able to add other variables which will explain additional components of the variance.

There are a number of possible reasons for the differences between our results and the results of Hawes and coworkers. First, palpation of a bony landmark is subject to considerable inaccuracy. Palpation errors may result from an incorrect estimation of the navicular tuberosity, or from other factors such as skin movement and soft tissue distribution. Navicular height determined by radiographic measurements is a more exact measure because the projection of the most inferior point on the tuberosity can be easily and reliably measured. Secondly, our sample is much older than that used by Hawes et. al. Though little quantitative evidence exists, it is widely believed that the atrophy of fat and muscle that accompanies the aging process results in losses of those tissues in the feet. Thus, the arch index values in an older subject group such as that used in the present study are less likely to be affected by soft tissue than similar values in young subjects.

While the debate continues on the validity of the various footprint parameters, the present data indicate that, in the subject group used, arch index provided a useful indirect measure of medial longitudinal arch height.

Figure 1
The Effect of Navicular Height on Arch Index

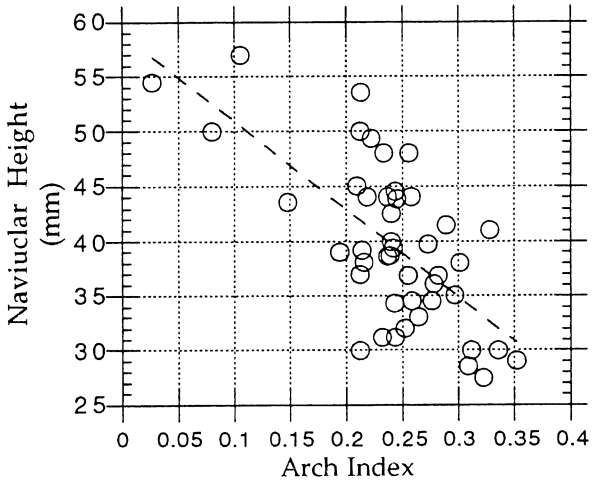

Figure 2
The Effect of Normalized Navicular Height on Arch Index

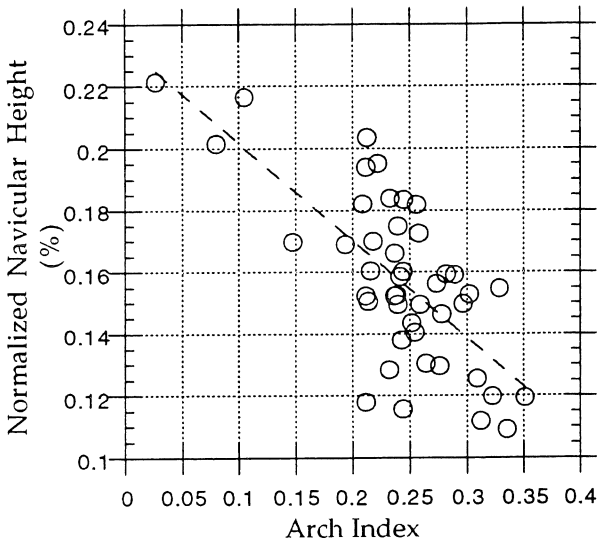

REFERENCES

Cavanagh, P.R. and Rodgers, M.M. J. Biomech., 20, 547-551, 1987.

Hawes, M.R. et al. Foot & Ankle, 13, 22-26, 1992.

A Comparison of Coupling Parameters between Runners who Pronate and Normals

I McClay and K Manal

Motion Analysis Laboratory, University of Delaware, Newark, DE 19716

INTRODUCTION

In a closed chain activity, motion at one joint is thought to effect the motion of an adjacent joint. In the case of running, this suggests that motion of the foot influences movement at the knee. The purpose of this research was to begin to investigate how the foot and knee are coupled during the support phase of running and to determine whether differences in this coupling exist between subjects with normal rearfoot motion (NL) and those who pronate (PR). 18 subjects (9 NL, 9 PR) were studied during treadmill running at 3.35 m/s. Excursion ratios between rearfoot eversion (EV) to tibial internal rotation (TIR) were compared between the two groups. In addition, the timing between peak eversion, knee flexion and knee internal rotation of the knee were also examined. Finally, correlations between various foot and knee angles were assessed. Findings suggest that timings between peak knee and rearfoot angles were not significantly different between the NL and PR group. Overall excursions were also similar between groups with the exception of tibial internal rotation which was greater in the PR group. The EV/TIR excursion ratio was significantly greater in the NL subjects. This was due to the equal EV excursion between the groups, but greater TIR in the PR group. Regression analysis revealed significant relationships between a number of the peak foot and knee parameters (R values between 0.327-0.733).

REVIEW AND THEORY

The knee is the site of the majority of running-related injuries. Abnormal motion of the foot is often implicated as a contributory cause. This is related to the functional link the tibia provides between the rearfoot and knee joint. In closed chain pronation, as the calcaneus everts, the talus (and consequently the tibia) internally rotates. It has been suggested that in the normal foot, there are approximately equal excursions of calcaneal eversion to tibial internal rotation. Nigg et al. (1993) examined the relation between arch structure and the EV/TIR excursion ratio. He found that subjects with flat feet had significantly higher ratios than those with high arch feet. This suggests relatively greater eversion as compared to tibial internal rotation in this group. This ratio has not been examined in subjects who pronate versus those with normal rearfoot motion.

Since tibial internal rotation is associated with flexion at the knee joint and eversion at the rearfoot, it has also been proposed that these motions should be synchronous. That is, peak knee flexion and internal rotation would occur with peak STJ pronation so that both joints would be reversing their motion at the same time. It is not known how close the timing of these peaks are in the normal runner, nor how excessive rearfoot eversion affects this timing. Bates et al (1979) found no significant difference between time of peak knee flexion and peak pronation in either runners with normal mechanics or those who pronated. However, the mean value of the pronator group was only 11 degs.

Therefore, the purpose of this research was to investigate the coupling parameters in runners with normal rearfoot mechanics and compare these to runners with excessive pronation. Coupling of within-joint motions were also examined.

PROCEDURES

18 recreational runners, previously screened for rearfoot mechanics were used in this study. 9 subjects each were assigned to the Pronator (PR) or the Normal (NL) group based upon their peak 2D eversion values measured during running. Values between 8-15 degrees placed one in the NL group while values greater than 18 degrees placed on in the PR group. The right foot was used in all cases, except when the left foot demonstrated the greater amount of eversion.

Three markers were placed on the femur, lower tibia and rearfoot segments (figure 1) in a manner similar to that described by Soutas-Little et al (1986). These markers served both to define the anatomical coordinate system and to track the motion of the segments.

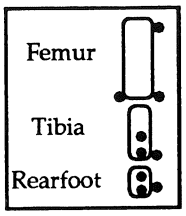

Figure 1. Lower Extremity Marker Placement (rearview of right lower extremity)

Following a standing calibration trial, subjects ran on a treadmill operating at 3.35 m/s. Data were collected with a 4 camera (200 Hz) Motion Analysis System (Motion Analysis Corp., Santa Rosa, CA). Five footstrikes were collected from each subject. The contact phase of three of these trials was used for analysis. Custom software was developed in order to calculate 3-D joint coordinate system angles (Grood and Suntay, 1983) of the calcaneus with respect to the tibia (rearfoot) and the tibia with respect to the femur (knee). In addition to these angles, tibial rotation with respect to the foot was also calculated in order to compute a calcaneal eversion (EV) to tibial internal rotation (TIR) ratio according to Nigg et al. (1990). All angles were referenced to standing with the exception of inversion/eversion of the foot. Excursions were calculated as the peak range of motion during the first 60% of stance (Figure 2)

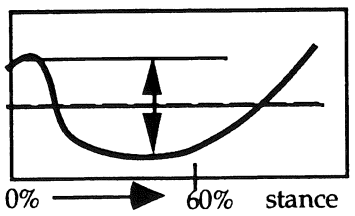

Figure 2. Calculation of excursion values

The EV/TIR ratio was calculated between the eversion excursion of the calcaneus (wrt tibia) and the internal rotation excursion of the tibia (wrt calcaneus) during the first 60% of stance. In order to examine the coordination of timing between the rearfoot and the knee joints, the time to peak eversion, knee flexion and knee internal rotation (KIR - tibia wrt femur) were determined (Figure 3). A positive EV-FL or EV-KIR time indicated that eversion occurred prior to knee flexion or internal rotation.

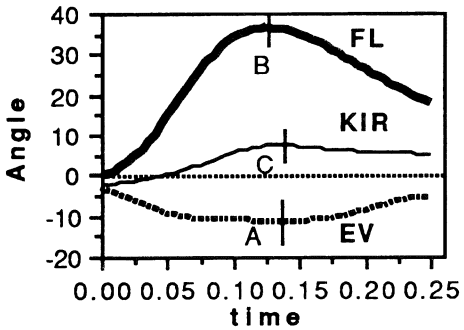

Figure 3. Calculation of timing variables. EV-FL time =(time at B - time at A) , EV-KIR time = (time at C - time at A)

Analysis of variance techniques were utilized to compare excursions and coupling parameters between the two groups. Regression analyses was used to assess the relationship between inter and intra-joint motions. Separate correlations were determined for the NL and the PR, as well as for the combined group.

RESULTS and DISCUSSION

The following results are based upon the mean data of three footstrikes for each of the subjects tested. Due to problems encountered during data reduction, knee data were only available for 10 subjects (5 NL and 5 PR). Table 1 presents the comparisons of excursions and coupling parameters for the PR and NL subjects.

Variable	n	PR (sd)	NL (sd)
Peak Eversion	18	-11.2 (2.6)	-21.2 (4.8)
Excursions			
Flexion	10	29.7 (4.8)	27.1 (6.9)
IR Knee	10	10.7 (5.4)	8.3 (6.0)
IR Tibia	18	13.3 (2.7)*	9.4 (2.4)
Eversion	18	-12.8 (4.1)	-12.7 (3.5)
Coupling Parameters			
EV/TIR	18	1.23 (0.44) *	1.53 (0.62)
EV-FL time	10	0.015 (0.026)	0.008 (0.048)
EV-KIR time	10	0.026 (0.024)	0.013 (0.060)

Table 1. Comparison of excursions and coupling parameters between the PR and NL. Significant differences are marked by * ($p<.05$) .

Despite the large difference in rearfoot mechanics, few significant differences were noted between the two groups. Knee joint excursions were similar, however, tibial rotation with respect to the calcaneus was greater. One explanation for this is that the tibia itself rotated more in the PR group. However, their femurs may have also rotated more, resulting in similar relative knee rotation to the NL subjects.

The PR and NL subjects had clearly different peak eversion values, however their mean excursions were almost identical. This resulted from the fact that the PR landed in greater eversion, but moved through the same range of motion. These subjects also had larger eversion angles in standing. Caution must be exercised when referencing eversion angles to standing. If PR subjects (with larger standing angles) move through similar eversion excursions to NLs, then resulting peak eversion angles might be very similar, masking the marked difference in rearfoot mechanics.

A significant difference was found between the EV/TIR excursion ratio in the NL and PR groups. However, the direction of this difference was unexpected. Although the PR group had significantly greater peak eversion, eversion excursions were similar. This was coupled with the greater TIR excursion for the PR group, resulting in a lower EV/TIR. The mean EV/TIR (1.38) found in this study was very similar to the 1.31 reported by Nigg et al. (1990). These researchers found a significant relationship between the EV/TIR ratio and arch height. As arch height decreased, EV/TIR increased. It is often suggested that pronators tend to have flatter feet than normals which might lead one to the conclusion that pronators would also have higher EV/TIR ratios. However, Nigg et al. also reported that arch height was not significantly related to eversion which challenges this oversimplified view.

Timings between eversion, knee flexion and knee internal rotation were similar between the groups. Peak knee flexion and KIR were slightly later with respect to peak EV in the PR group, however knee data were only available for 5 subjects. This small subject number and large variability may have contributed to the non-significance seen here.

The results of the regression analyses are presented in Table 2. Significant foot-knee relationships found were between dorsiflexion and knee flexion (DF-FL) across all groups and EV-FL in the NL group. These findings are not surprising as DF, EV, and FL are all thought to be part of the cushioning mechanism of the lower extremity and typically occur in concert. However, what has interesting was that in the NL group, as knee FL increased, eversion decreased. Reasons for this are not readily apparent. A significant relationship between AD-EV was also found with AD decreasing as EV increased. This may be due to the increasing valgus posture (less AD) of the knee as pronation occurs. EV was not found to be related to KIR challenging a commonly upheld belief that greater EV translates into greater KIR.

Variables	n	R	R^2	p
foot-knee				
DF-FL. (ALL)	10	0.612	0.353	0.0003
EV-FL (NL)	5	0.827	0.684	0.0001
EV-AD (ALL)	10	0.524	0.274	0.003
within foot				
EV-DF (NL)	9	0.398	0.158	0.039
within knee				
FL-AD (NL)	5	0.733	0.537	0.002
FL-AD (PR)	5	0.548	0.300	0.034

Table 2. Significant results of linear regression analysis. Rearfoot measures: DF-dorsiflexion, AB-abduction, EV-eversion. Knee measures: FL-flexion, AD-Adduction, IR-Internal Rotation. NL-normals, PR-Pronators, ALL-NL and PR

Significant within-joint coupling was seen at the knee between FL-AD which was not surprising as these motions typically occur together. At the foot, EV was found to be related to DF with EV increasing as DF decreased. It has been suggested that increased EV may be associated with lack of DF range which may, in part, explain these findings. However, this relationship did not hold in the excessive pronators.

Further work is need to continue to establish normative values for these coupling parameters and to examine their relative importance in the etiology of running injuries. Studies focusing on specific foot or knee injuries may lend more insight into the significance of these parameters.

REFERENCES

Bates, BT et al. MSSE 11(4):328-331 , 979.
Grood,ES &Suntay, W. J. Biom. Eng. 105,136-144. 1983
Nigg , BM et al. J. Biom 26(8): 909-916, 1993
Soutas-Little et al. MSSE 19(3):285-293, 1983

BILATERAL VERTICAL FORCE SYMMETRY FOR NORMAL TREADMILL AND OVERGROUND GAIT

Scott C. White, Carole A. Tucker, Kimberly A. DiVincenzo, & H. John Yack
Department of Physical Therapy & Exercise Science
State University of New York at Buffalo, Buffalo, NY 14214

INTRODUCTION

Symmetry indices (SI) derived from foot-ground reaction forces have been advocated as a means of quantifying gait. This paper reports SI values determined from vertical force curves for six subjects walking on a treadmill housing two force plates. None of the subjects exhibited perfect symmetry for treadmill gait but mean SI values were less than 4% from perfect symmetry. Walking on a treadmill did not increase bilateral differences compared to overground walking forces. SI values determined using a force measuring treadmill (FMT) may prove to be useful as criterion measures for quantifying gait changes and for gait re-education.

REVIEW AND THEORY

Foot-ground reaction forces have been advocated as a means of quantifying gait since they are kinetic based, accurate, sensitive, and can be collected and analyzed expeditiously. Reaction force data for overground gait (OGF) are available in the literature for normals (Herzog et al., 1989; Winter, 1991). Force plate targeting, obtaining multiple trials, collecting successive steps in a stride and walking direction biases are common problems when recording and interpreting OGF. SI values based on foot-ground reaction forces have been proposed as a useful means of assessing bilateral gait differences (Herzog et al., 1989; Stussi et al., 1990). However, data collection problems inherent in overground trials can influence SI values (Herzog et al., 1989). Using a treadmill which can distinguish successive foot-ground reaction forces alleviates a number of these limitations. Treadmill gait SI values have not been reported previously. This study reports SI values determined from vertical forces for normal subjects walking at different speeds on a FMT, and compares these values to OGF values.

PROCEDURES

Bilateral, vertical foot-ground reaction forces were recorded for six subjects walking on a treadmill housing two force plates (Kistler Instrument Corp.). Forces were monitored for subjects walking at three treadmill speeds. The speeds were set to match previously collected overground trials in which subjects walked at cadences 20 steps/min faster or slower than their self-selected normal gait. Cadences were controlled using an audio metronome. Forces were A-D converted online at 500 Hz and then low passed filtered at 100 Hz. Stance time (ST), average force (F_{ave}), vertical force impulse (F_{imp}), distinctive forces (F_1, F_2, F_3) and their time of occurrence (t_1, t_2, t_3) were determined from the vertical force curves (Figure 1). Force data were normalized to subject mass and time values were normalized to stance time. Data for the three speeds were averaged for ten sequential right and left steps, windowed from a 60 s sample of treadmill gait, and for 5 trials of overground gait. Symmetry indices (SI) across limbs were calculated using: $SI = 200\ ((X_{left} - X_{right})/(X_{left} + X_{right}))$.

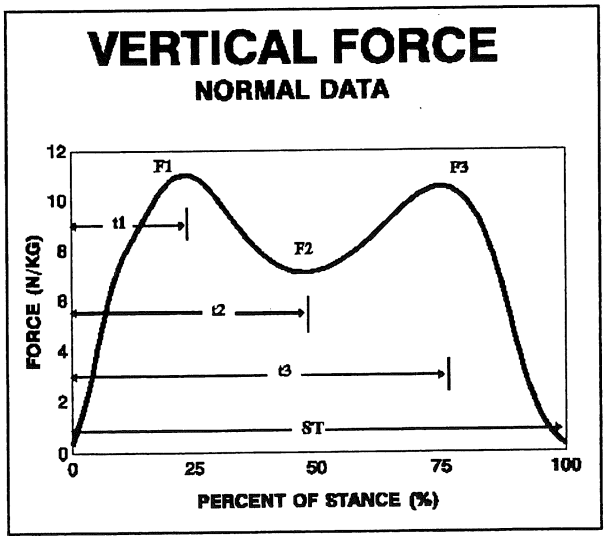

Fig. 1: Measures from vertical force records for determining SI values.

RESULTS AND DISCUSSION

None of the subjects exhibited perfect symmetry for overground or treadmill gait. These results are consistent with SI values reported for normal overground walking (Herzog et al., 1989). Mean

SI values for treadmill gait that were determined relative to the total stance (ST, F_{ave}, F_{imp}) were 2% or less (Table 1). SI measures based on peak forces and time to peak, were more variable but all were still less than 4 % for treadmill gait. Herzog et al. (1989) have also reported SI values consistently less than 4 % for a larger group (N = 33) of normal subjects walking overground. There were no distinct differences in SI values for the subjects walking overground compared to walking on the treadmill (Table 1). Peak vertical force values and the timing of the peak values were more variable for the overground walking but the differences can be attributed to having fewer repeated trials of OGF to average per subject compared to the treadmill trials. Walking on a treadmill did not increase bilateral differences in force production during gait for the different speeds and cadences tested in this study.

SI values based on a large number of successive vertical reaction force curves are easy to generate with the FMT. Based on this preliminary data, the measures are bilaterally stable with less than a 4% across limb difference. Although vertical foot-ground reaction force values do not identify reasons for asymmetries, they do reflect their existence. This type of data analysis may prove to be useful for determining criterion measures for differentiating between normal and pathological gait, objectively quantifying the efficacy of clinical intervention strategies, and for gait re-eduction of patients. The utility of this type of analysis should be investigated further by analyzing treadmill gait for individuals afflicted with different pathologies.

REFERENCES

Herzog, W. et al. *Med. Sci. Sports Exerc.* 21, 110-114, 1989.

Stussi, E. et al. *Proc. 24th Annual Meeting German Society of Biomed. Engng.*, Berlin, Sept., 1990.

Winter, D. *Biomechanics and Motor Control of Human Gait*, U. Waterloo Press, 1991.

ACKNOWLEDGEMENTS

This project was support by a grant from New York State Science and Technology Foundation. The authors gratefully acknowledge assistance from Kistler Instrumentation Corp. and Kristal Systems Inc.

Table 1: Vertical force symmetry values (%) for treadmill (FMT) and overground (OGF) gait.

Measures	Slow		Normal		Fast	
	FMT	OGF	FMT	OGF	FMT	OGF
Contact Time (ST)	0.7	-0.1	0.1	-0.4	0.2	0.9
Average Force (F_{ave})	0.0	-1.2	0.5	-0.6	-0.9	-1.7
Vertical Impulse (F_{imp})	-0.3	-0.9	2.0	-1.0	-1.6	-1.8
First Peak Force (F_1)	0.4	-1.0	1.7	0.5	-1.3	-0.5
Time to F1 (t_1)	0.5	-3.3	-1.1	-3.9	2.0	-3.7
Minimum Force (F_2)	0.9	-4.6	-2.9	-8.9	-2.3	-5.2
Time to F2 (t_2)	1.6	-5.8	-1.3	-2.7	-1.5	-0.1
Second Peak Force (F_3)	0.1	-0.7	1.6	1.0	1.1	-1.0
Time to F3 (t_3)	-3.7	0.2	-0.8	0.2	0.4	-0.2

A GROUND-REACTION-FORCE MEASURING TREADMILL

D. Fuglewicz & W. Klavoon

Kistler Instrument Corporation, Biomechanics Department, Amherst, NY 14228.

INTRODUCTION

The problems and limitations of acquiring valid ground-reaction-forces (GRF's) from overland walkways are well-known. Several groups have experimented with different methods of obtaining multiple foot strike records by combining force-measuring equipment and treadmills in various orientations with mixed results [1-5]. Some of these system offered valid data during running alone [3,4], while others force unnatural gait in certain instances [1,2]. In this paper, a new approach is used to combine force-measuring equipment with a treadmill to record vertical GRF's for both walking and running. This system offers the capability to record an unlimited number of consecutive left/right foot strikes with minimal noise artifacts, while allowing normal gait.

REVIEW & THEORY

GRF's are usually recorded from one or more force plates that are embedded into a walkway. Many problems and limitations of getting valid GRF's on overland walkways exist. Subjects (especially the handicapped) fatigue or become frustrated due to the need of performing multiple, consistent trials on long walkways. The subject's normal gait may be affected due to the necessity of making sure the foot actually strikes the force plate. In order to get valid and repeated data, walking speed should be controlled - something that can be difficult to do in the traditional setting. Because subject populations vary in height and physical ability, even if the subject strikes the first force plate correctly, the subject may miss the second force plate due to stride length variations.

In order to alleviate these problems, several groups have tried combining force plates and treadmills [1-5]. These designs suffered from many different problems. When only one force plate was used, separate left/right foot strikes could not be determined during walking gait [3,4,5]. Other designs had force plates placed in the treadmill in a manner that prevented natural gait for walking and running in the same system [1,2,5]. Substantial noise from the drive system or treadmill structure of some designs contaminated the force data [3,4].

We have developed a new design and fabricated a prototype ground-reaction force measuring treadmill (FMT). Two tandem force plates are incorporated within the treadmill belt which eliminates a number of previous instrumented treadmill design limitations, as well as the problems and limitations of overland gait force measurements. This paper presents instrument specifics for the FMT.

PROCEDURES

A treadmill (Trotter - Model 545 Supertrainer) and 2 force plates (Kistler - Type 9286) were used as the basis of the system. The force plates were placed into custom "cradles" which were in-turn attached to the treadmill frame in a tandem (one force plate in front of the other) orientation (Figure 1). Several stiffening pieces were added to ensure a rigid system structure. Care was taken to ensure that the system was stiff in order to prevent the treadmill from acting as a "spring" as the subject ambulates on the mill. In addition stiffness is needed to maintain as high a system natural frequency as possible.

A modified data acquisition and analysis program was used to acquire data from both force plates simultaneously (BioWare® Kistler - Type 2812). Because of the orientation of the force plates, there are occurrences where each foot is on each force plate (double support phase) and others when one foot is on both force plates (middle of swing phase). A custom algorithm which allows the analysis of consecutive, separate left and right foot strikes for walking and running was needed to handle these occurrences correctly. This algorithm was developed and then applied to the data. It combined the data from both force plates when only one foot was on both force plates, and kept the force plate data separated when both feet were on both force plates. Figure 2 - Upper Graph shows the "raw" forces from both force plates while Figure 2 - Lower Graph shows the separated foot strikes.

The vertical force signals from the force plates represent the vertical GRF's from the subject on the treadmill. The shear forces were also recorded to monitor the forces due to the friction between the belt and the top of the force plates in order to evaluate the effectiveness of various lubricants and force plate surfaces.

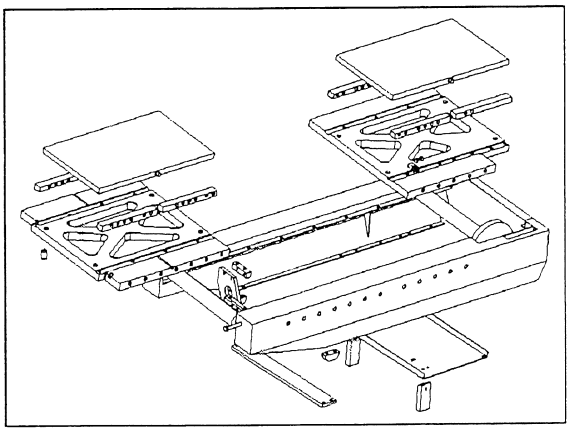

Figure 1. Exploded View of the Prototype FMT (Belt Removed)

RESULTS & DISCUSSION

The key performance specifications of the treadmill/force plate system are shown in Table 1 below.

Table 1. Key Specifications of the Prototype FMT

Speed Range	1.6-16	km/h
Bed Incline	0-15	%
Force Range	0-5	kN
Linearity	±1	% FSO
Threshold	0.01	N
System Noise (unfiltered)	≈2	% FSO
Primary System Natural Frequency	150	Hz

The initial results from the system were very promising as shown in the GRF's recorded during the transition from walking to running (Figure 3). The top graph shows the GRF from one foot, the bottom graph shows the GRF from the contralateral foot. Subjects adjusted quickly to walking and running on the treadmill and were quite comfortable after only a few minutes. The amount of noise due to mechanical vibration was small (Figure 2 - Lower Graph).

The primary natural frequency was determined to be 150 Hz. In examining the spectral frequencies of the data, most "noise" seems to come from moving parts of the treadmill (primarily the motor and

belt) because the frequency content of the noise increased with an increased treadmill operating speed. The noise measured was < 2% of the full scale value and is very acceptable for a prototype design. If the foot strikes are averaged, this noise will tend to be removed since the noise is random. This implies that while the foot strikes are averaged, the noise cannot accumulate.

Minimizing friction is important because it lowers the loading on the drive motor, reduces wear on the force plates, and lowers the noise induced on the force plates from the moving belt. The current design uses a low-friction Ultra-High Molecular Weight Polyethylene (UHMWP) to protect the force plate along with a silicone lubricant to lubricate the UHMWP/treadmill belt interface.

The coefficient of friction (COF) was determined by the following ratio:

$$COF = \sqrt{\frac{F^2_{Anterior-Posterior} + F^2_{Medio-Lateral}}{F^2_{Vertical}}}$$

The COF of the treadmill belt and standard aluminum force plate top surface was 0.25, while the COF of the belt and UHMWP with silicone lubricant was 0.14.

While this design uses a separation algorithm that correctly separates the raw data into left & right foot strikes, it does not determine which set of consecutive foot strikes is left or right. An infrared LED emitter/detector pair and retro-relfective tape on one foot is used to make this determination. As the taped foot passes by the emitter/detector, a pulse is recorded by the data acquisition system. This pulse is then correlated to the set of foot strikes and the appropriate step side is identified.

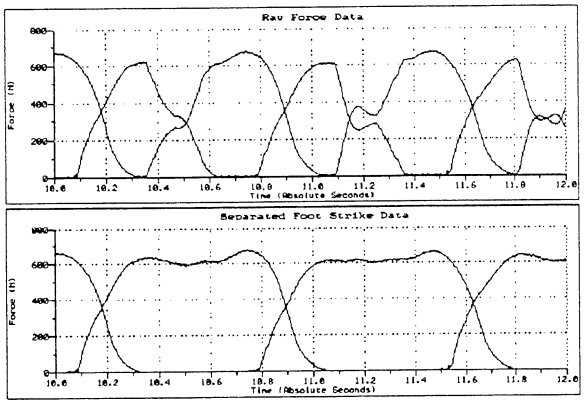

Figure 2. Raw Forces (Upper) & Separated Foot Strikes (Lower)

There are some limitations of this system. Only the subject's vertical forces can be recorded because the shear forces from the subject do not accurately pass through the treadmill belt to the force plates. In addition, in order for the separation algorithm to correctly determine two feet on both plates and one foot on both plates, there must be a time when there is no force on either plate. This means that the heel of one foot must pass completely in front of the toe of the other. This may prevent some patient populations from using the FMT.

One key question is how the GRF signatures compare to overland gait GRF signatures. If the data is equivalent, then much of the existing GRF analyses done on walkways will carry over directly to treadmill studies. In addition, the capability of getting a large number of foot strikes very quickly should add to the accuracy of the gait analysis. The FMT also enables GRF symmetry measures to be used to determine differences between left and right foot strikes. These measures could be used to follow a subject through a treatment protocol or could be used to differentiate various subject pathological populations.

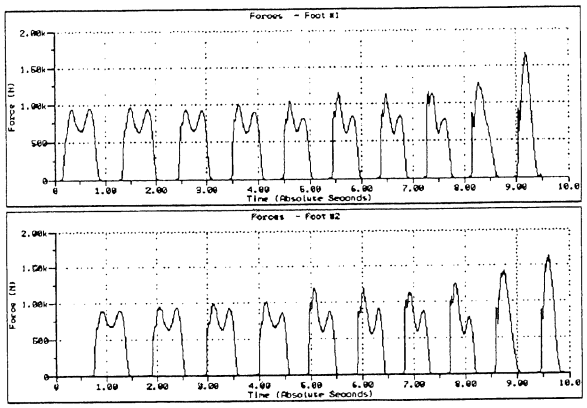

Figure 3. Vertical GRF's for Transition from Walking to Running

This design allows an unlimited number of consecutive vertical GRF foot strikes, free of targeting bias, to be recorded from a walking and/or running subject. The possibility exists of gait training/re-education via bio-feedback because the subject is relatively stationary and can view a monitor for visual feedback which is unlike previous feedback systems which required the subject to push a cart down the walkway [6]. In addition, other data (EMG, Video, Accelerometry, Goniometry...) can be easily acquired due to this relatively stationary position. Treadmills allow incline and speed to be controlled and varied throughout a trial so repeating the conditions of a trial are easily accomplished.

This patented system provides a new tool for continued investigations into current gait research. In addition, there are many new research areas that can be explored by utilizing the FMT's unique capabilities.

REFERENCES

[1] Horstmann G. et. al., Special Treadmill for the Investigation of Standing and Walking in Research and Hospital, Biomed Technik, 32 (1987), 250-254.

[2] Jansen E. et. al., Normal Gait of Young and Old Men and Women, Acta orthop. scand., 53, 193-196, 1982.

[3] Johnson L. et. al., Instrumenting an Exercise Treadmill for Evaluation of Vertical Ground Reaction Forces, SEM Proceedings, Dearborn, 988-998, 1993.

[4] Kram R. et al., A Treadmill-Mounted Force Platform, J. Appl. Physiol., 67(4): 1692-1698, 1989.

[5] Roemer R. et. al., Rotating Treadmill for the Continuous Measurement of Anterior-Posterior Forces During Walking, Med. & Biol. Eng. & Comput., 20, 519-522, 1982.

[6] Hirokawa S. et. al., Biofeedback Gait Training System, ISB Proceedings, Amsterdam, 1004-1009, 1987.

ACKNOWLEDGMENTS

This research and development was funded in part by a grant from the New York State Science and Technology Foundation - Technologies & Disabilities Program.

The authors wish to thank Scott C. White and H. John Yack of the University at Buffalo - Dept. of Physical Therapy & Exercise Science for their cooperation and consultation in this project.

QUANTIFICATION OF CYCLIC GROUND REACTION FORCE HISTORIES DURING DAILY ACTIVITY IN HUMANS

G.A. Breit and R.T. Whalen

Life Science Division, NASA Ames Research Center, Moffett Field, CA 94035-1000

INTRODUCTION

In this study, a portable monitoring system is used to measure and record the vertical component of ground reaction force (GRF_z) during walking and running. Load cycles of significant magnitude are categorized in terms of their range and offset using a "rainflow" algorithm. Towards the goal of simplifying the instrumentation, and exploiting the fact that an increase in gait speed yields an increase in peak ground reaction force and a concomitant decrease in foot-ground contact time, we investigated contact times as indicators of peak GRF_z during gait. Using an empirically-determined regression equation, a history of cyclic loads was estimated from a record of contact times collected during 40 minutes of walking and running. This profile correlated well to the loading history determined by direct measurement of force. We conclude that meaningful and quantitative information related to the magnitude of cyclic skeletal loading can be gathered using relatively simple observations of foot-ground contact times during gait.

REVIEW AND THEORY

Theoretical models and experimental studies of bone remodeling suggest that bone density and structure are influenced by local cyclic skeletal tissue stress and strain histories. Estimation of long-term loading histories in humans is usually achieved by assessment of physical activity level by questionnaires, logbooks, and pedometers, since the majority of lower limb cyclic loading occurs during walking and running. These methods provide some indication of the mechanical loading history, but fail to consider the true magnitude of the lower limb skeletal forces generated by various daily activities. These techniques cannot account for individual gait characteristics, gait speed, and unpredictable high loading events that may influence bone mass significantly.

We have developed portable instrumentation to measure and record GRF_z during normal daily activity. This equipment allows long-term quantitative monitoring of musculoskeletal loads, which in conjunction with bone mineral density assessments, promises to elucidate the relationship between skeletal stresses and bone remodeling.

PROCEDURE

The GRF_z monitoring system consists of a single capacitance insole force sensor and signal conditioner (EQ; Plymouth Meeting, PA) coupled with a battery-powered data logging system (Tattletale; Onset Computer; North Falmouth, MA) interfaced to a 2-megabyte RAM card and LCD display (Figure 1). GRF_z data are sampled continuously at a rate of 100 Hz. For short-term high-resolution studies, force data are stored directly to RAM for off-line analysis, allowing for a maximum of 3 hours of data collection. For long-term studies, a real-time filtering algorithm stores only significant data peaks and valleys to RAM, increasing the data capacity to approximately two weeks duration. A record of peak loading rate during each significant cycle and a histogram of time at force are also retained in real time. The signal conditioner and data logging system are packaged together in a single unit, 1.5" x 2.5" x 5", which is worn on a belt around the waist.

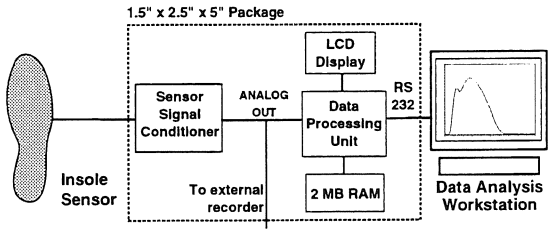

Figure 1: Schematic of GRF_z monitoring system.

A "rainflow" algorithm (Nelson *et al.*, 1977) is used to categorize each significant GRF_z cycle in terms of its magnitude (range) and offset from zero. These data are presented as range-offset histograms such as those in Figures 2a-b, which summarize data collected from one subject over a typical 40-hour laboratory work week, and over 40 minutes of walking/running outdoors, respectively. These plots are effective tools to visualize cyclic loading histories associated with various activities.

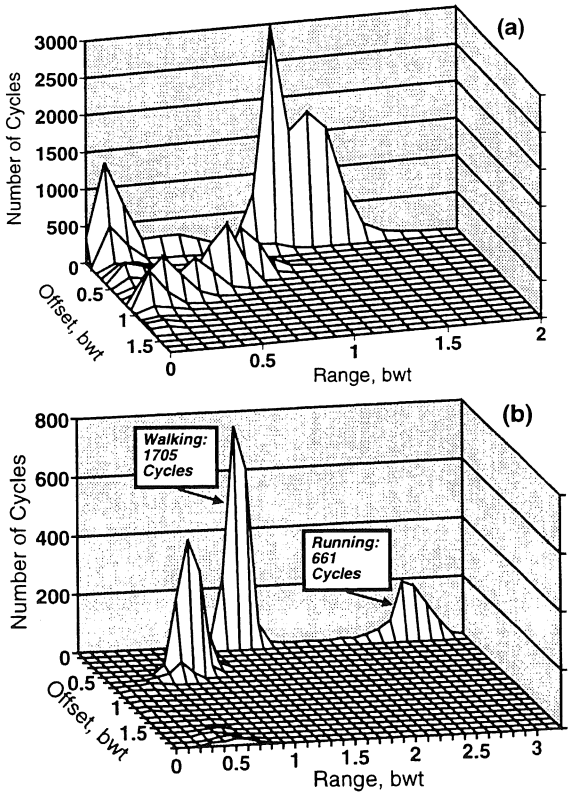

Figure 2a-b: Range/Offset histograms summarizing cyclic loading histories for two types of activity: (a) 40 hours of sedentary laboratory work; (b) 40 minutes of walking/jogging. The vertical axis indicates the total number of cycles which occurred at a particular range and offset. Cycles which occur at an offset of zero and possess a range ≥1 body weight (bwt) are associated with gait, with those cycles in excess of 1.8 bwt

attributed to running. An electronic step counter worn during data collection for Figure 2b indicated that 2390 steps were taken, which differs by 1% from the total of 2366 found by counting cycles. Cycles offset from zero with ranges <1 bwt usually occur midstance during walking and running.

We have recently developed an alternative approach to logging cyclic GRF_z loads during human gait that overcomes limitations due to nonlinearity and fatigue in the force sensors. During walking or running, the principal determinant of peak ground reaction force, from cycle to cycle, is the gait velocity. In general, an increase in gait speed results in higher peak GRF_z, *as well as* a concomitant decrease in the foot-ground contact time (McMahon *et al.*,1990). In other words, increased walking and running speed results in a taller, narrower GRF_z time profiles during the contact phase of the gait cycle. Consequently, we hypothesized that during gait, contact times are reliable indicators of peak GRF_z, and can be used in lieu of direct force measurements to determine cyclic loading histories during daily activity.

For an individual subject, an empirical GRF_z/contact-time relationship is established in a laboratory setting, using an instrumented force plate connected to a microcomputer equipped with data acquisition hardware and software. Subjects are instructed to walk and run over the plate at a variety of speeds. Gait speed is determined by measurement of transit time between two points of known separation. Because of the disparity between typical contact times for walking (0.5-0.8s) and running (0.1-0.35s), these two types of gait are easily distinguishable. Linear regression equations for peak GRF_z vs. contact time are calculated separately for running and walking. The regression standard error s_{yx}, (Zar, 1984), is noted to account for the normal step-to-step variability of peak GRF_z.

For the 40 minutes of GRF_z data summarized in Figure 2b, a step-by-step contact time history was generated by noting all time intervals between upward and downward crossings of a critical GRF_z level (≥0.2 bwt). Each interval was identified as either walking or running on the basis of its duration, and was converted to a peak GRF_z by the appropriate regression equation. To simulate the variability of these forces, a Gaussian random number of variance s^2_{yx} was added to each estimated GRF_z.

RESULTS

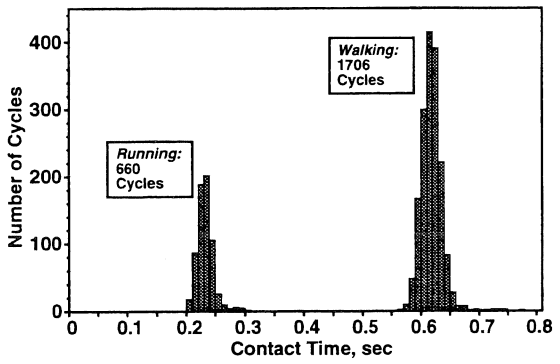

Figure 3: Contact time histogram for the data in Figure 2b. Characteristic times for walking and running are evident in the distribution's biphasic nature. Splitting the distribution at 0.50s, mean contact times (±SD) were 0.614±0.021s (walking) and 0.229±0.018s (running). Discrepancies in step counts from Figure 2b are attributed to errors in mapping of histogram bins.

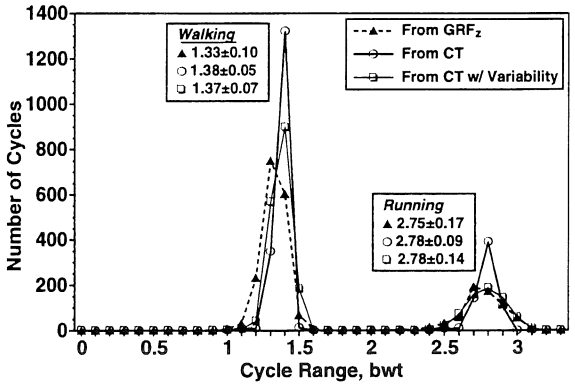

Figure 4: Estimated cyclic loading histories for the data shown in Figure 2b, calculated from GRF_z history, contact time history (Figure 3), and contact times plus GRF_z variability estimate. The GRF_z profile is by definition identical to the zero-offset cross section of Figure 2b. Means ±SD (in bwt) are given for each phase of the distribution (split at 1.8 bwt).

DISCUSSION

Current models of bone remodeling identify cyclic loading as a crucial determinant in skeletal adaptation. Accurate determination of long-term GRF_z histories may be essential to our understanding of the relationship between mechanical loads and bone remodeling and may be a useful approach to examine activity decline with age and its influence on bone density (Whalen *et al.* 1988).

In terms of instrumentation, estimation of GRF_z cycles by means of contact times is an attractive alternative to direct force measurement. The sensor, signal conditioner, and A/D converter in our current system could be replaced by a simple binary switch, connected to a single digital input on the microcontroller. As seen in Figure 4, the cyclic loading history estimated from contact times matches closely that determined directly from GRF_z measurements--the distribution means differ by less than the histogram resolution (0.1 bwt). This approach has limitations, however. This technique does not measure static loading, such as that experienced during upright standing. Furthermore, force/contact time calibration data are collected on level ground and may be inappropriate to situations such as stair climbing or walking on inclined surfaces. Nevertheless, the loads believed to have the greatest influence on bone occur during gait over level ground, minimizing the significance of these limitations.

REFERENCES

McMahon TA and Cheng GC. J. Biomech. 23 (Suppl. 1): 65-78, 1990.

Nelson DV and Fuchs HO. Fatigue Under Complex Loading: Analyses And Experiments, (pp. 163-187), SAE, Warrendale, PA, 1977.

Whalen RT *et al.* J. Biomech 21:825-838, 1988.

Zar JH. Biostatistical Analysis, (pp. 268-271), Prentice-Hall, 1984.

MUSCLE ACTIVATION AFFECTS SKELETAL MUSCLE CONTUSION INJURY IN RAT GASTROCNEMIUS

J.J. Crisco, W. Jackson, K. Hentel, J. Choi, P. Jokl

Biomechanics Laboratory, Department of Orthopaedics and Rehabilitation
Yale University School of Medicine, New Haven, CT USA.

INTRODUCTION

As participation in sports increases, so does the prevalence of sports related injuries. According to NCAA data collected from 1989-1993, muscle contusion injuries, caused by the impact of blunt non-penetrating objects, rank third in morbidity through time lost for training and competition (NCAA, 1989-1993). In an effort to increase our understanding of the mechanisms of contusion injury and muscle's tolerance to impact, previous work examined the impact response and injury in relaxed muscle using a rat model. The purpose of this study was to determine the effect of activation on a muscle contusion injury. Contracted muscle had a significantly different mechanical response to impact than relaxed muscle. Furthermore, contracted muscle was less susceptible to injury.

REVIEW AND THEORY

Impact biomechanics has primarily focused on the protection of occupants involved in vehicular accidents. In order to analyze whole body impacts knowledge of the impact behavior and tolerance of the tissues that make up the body is essential. Previous impact studies of soft-tissues have included spinal cord, lung tissue, and cardiac muscle. Little attention has been given to the impact characteristics of skeletal muscle. Studies that have been done have employed animal models and one of two methods to produce a reproducible injury: a spring driven hammer (Kvist et al. 1974) or a dropped mass (Walton and Rothwell, 1983).

Previously, we developed a model of muscle contusion in the rat based on a drop mass technique (Crisco et al., 1993). In addition to histological and biomechanical methods used by the previous studies to document injury, this new model documented the mechanical response (force-time-displacement) of impact and the loss of contractile function. With this model, the healing process of muscle contusion injuries as well as the effect of impactor shape on the injury produced were investigated. Though most muscle contusion injuries may occur in muscle that is in a state of contraction, all previous studies have been done in relaxed muscle. We hypothesized that during contraction, the transverse stiffness of the muscle tissue would increase, resulting in changes in the impact response as well as a change in injury severity. The purpose of this study was to compare the mechanical response and resulting injury of a defined muscle contusion injury in contracted and relaxed muscle.

PROCEDURES

A total of 18 male Wistar rats (320-350 g, Charles River Company) were used in this study. (All animal protocols were approved by the Yale Animal Care and Use Committee). All animals were anesthetized and received a single impact to the mid-sagittal plane of the belly of the gastrocnemius muscle of each limb using a drop mass technique (mass =171 g, height = 102 cm, impactor radius = 6.4 mm). For both limbs, the muscle was placed in a lengthened position by flexing the foot to 90°. One limb was impacted in this relaxed position.. The other limb was impacted while being electronically stimulated (70 V, 70 Hz) through electrodes (Grass Instruments) attached (Benzion USP, Fernadale Laboratories, & Steri-Strip, 3M) to the shaven skin on the sides of the muscle belly. The activated limb and limb impacted first were chosen randomly. For all impacts (n=18), force supporting the limb and displacement of the muscle belly were recorded by computer as a function of time (10 Khz). From this data, peak force (N), peak displacement (mm), energy (Nm), and impulse (Ns) were calculated. Stiffness (N/mm), defined as the least-squares fit of the load-displacement curve from 0-25% of the peak force, and delay (ms), defined as the time between peak force and peak displacement, were also computed.

Two hours after impact, the maximum tetanic tension of both limbs was determined.

Maximum tetanic tension was measured at optimal length in the anesthetized animal by fixing the femur with a K-wire, fixing the disarticulated calcaneus with attached Achilles tendon to a load cell, and stimulating the branch of the sciatic nerve that innervated the muscle complex using a standard protocol. The gastrocnemius muscle belly remained covered by skin throughout the procedure and the animal core temperature was maintained between 98-100° F. The significance of the differences was determined using a paired Student's t-test.

RESULTS & DISCUSSION

There were notable differences in the behavior of the impact response for contracted and relaxed muscle (Figure 1). The peak force of the impact was significantly less ($p < 0.01$) in the contracted muscle, while the peak displacement was significantly less ($p < 0.01$) in the relaxed muscle. The stiffness of the contracted muscle was significantly less ($p < 0.01$) than the stiffness in the relaxed muscle. The impact response variables are summarized in Table1.

Our results clearly illustrate that there is a difference in the response of muscle to blunt trauma dependent on the state of contraction. However, our hypothesis that the activated muscle would exhibit higher transverse stiffness was in error. Whether this is an actual property of the muscle tissue or is due to influence of the underlying bone remains to be investigated.

As expected for a rate-dependent material, there was a significant linear correlation between increasing delay and the energy absorbed. However, the mechanism by which contracted muscle absorbs less energy and transmits less peak force is unclear.

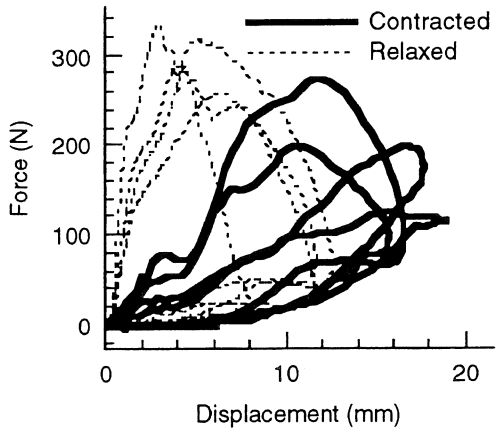

Figure 1. Impact response of four randomly chosen rats. Duration of the impacts was approximately 10 ms.

The mean maximum tetanic tension (n=9) for the relaxed leg was 27±4 N, significantly lower compared to the 31 ± 4 N for the activated leg. It is unclear whether the reduced susceptibility to injury of contracted muscle is due to changes in the gross mechanical behavior, changes in the ultrastructure, or both.

At the present it is important to note that contracting muscle reacts significantly differently to blunt trauma than does relaxed muscle and, in our model, is less prone to injury

REFERENCES

Crisco et al., 17th Trans. Amer. Soc. Biom., Iowa City, Iowa, Oct. 22-23, 1993.
Kvist et al. Scan. J. Rehab. Med., 6, 134-140, 1974.
NCAA: Injury Surveillance Systems, Overland Park, Kansas, 1989-1993.
Walton et al., Clin. Ortho., 176, 273-281, 1983.

ACKNOWLEDGMENTS

This work was partially supported by a grant from THE WHITAKER FOUNDATION. We gratefully acknowledge the assistance of James Huddleston.

Table 1. Average [s.d.] impact response variables (n=18).

	Peak Force (N)	Peak Disp. (mm)	Energy (Nm)
Relaxed	301 [77]	11.4 [1.4]	2.0 [0.3]
Contracted	193 [38]	17.4 [1.9]	1.4 [0.5]

	Impulse (Ns)	Stiffness (N/mm)	Delay (ms)
Relaxed	0.9 [0.07]	71.9 [14.5]	2.7 [0.5]
Contracted	0.8 [0.08]	17.3 [11.4]	1.5 [0.6]

ESTIMATE OF FUNCTIONAL COMMON TENDON BETWEEN TWO PARTS OF CAT SOLEUS MUSCLE

T. G. Sandercock and C.J. Heckman
Department of Physiology, Northwestern University School of Medicine, Chicago, IL 60611

INTRODUCTION

Muscle fibers terminate in microtendons which run together to form the aponeurosis and external tendon of the whole muscle. The goal of this study was to determine to what degree the tendon should be viewed as a collection of independent parallel tendons versus a fused common tendon. Cat soleus (SOL) muscle was stimulated as two independent parts by dividing the ventral roots into two bundles. The extent to which one part of the muscle stretched the tendon of the other part was measured. Results indicate approximately one half of the total elasticity should be viewed as common--stretched by both parts of the muscle. The methods used to measure the common tendon and its estimated stiffness are presented.

REVIEW AND THEORY

Our long term objective is to develop a model predicting whole muscle behavior based on the properties of its constituent motor units. Such a model requires a quantitative understanding of the physical interaction between motor units through their connective tissue links. That is, to what extent does the contraction of one fiber stretch neighboring fibers or their tendons. It is not clear how tightly the microtendons from individual fibers are cross linked to each other. In addition, the muscle fibers themselves are surrounded by a collagenous meshwork with unknown function (Trotrer 93). This project was undertaken to estimate the functional importance of tendenous links between fibers in a muscle.

In this study the soleus was divided into two large pseudo-motor units by splitting the ventral roots into two bundles, thus allowing each portion of the muscle to be stimulated independently. The specific purpose of this study was to measure how contraction in one part on the muscle stretched the tendon shared by the other part of the muscle. Essentially muscle is viewed as a lumped parameter model, where each part of the muscle is assumed to have its own independent series elastic (representing the elasticity of the cross bridges plus the independent portion of the tendon) which are in turn connected to a common tendon. The physical location of the common tendon is not restricted to the external tendon, but rather represents any compliance stretched by both parts of the muscle.

PROCEDURES

Experiments were performed on the SOL muscles of 4 cats. The data reported in this abstract are based on a single cat. Three cats were used to obtain preliminary data which are qualitatively similar but less accurate due to slightly different protocols. The cats were anaesthetized with Halothane for the initial surgery followed by sodium pentobarbitone (iv). The left hindleg was partially denervated, with care taken to preserve the nerve and blood supply to the SOL, and mounted in a rigid frame. The calcaneus was cut and attached to a servomechanism allowing the soleus to be moved under computer control while simultaneously measuring muscle force. The ventral roots were exposed and used to stimulate the SOL. The roots were divided into two bundles, each part innervating roughly half of the SOL, and placed on separate hook electrodes so that each part could be stimulated independently. At the end of the experiment the cat was killed with an overdose of sodium pentobarbitone.

Four different techniques were used to estimate the stiffness of the common tendon. Each techniques relies on first stimulating the whole muscle, then parts A, and B individually. It was essential that there was no cross-stimulation. The possibility of cross-stimulation was ruled out since tetanic tension from the two parts of the muscle summed linearly when the muscle was stimulated near maximum physiological length, even when the stimulating voltage was increased by a factor of two.

RESULTS

The length tension relationship was measured during stimulat ion of both the whole muscle, and part of the muscle, to determine if stretch of the common tendon can be detected as a shift in the length tension relationship. Force was measured every 2 mm, over a range -12mm to +6mm from the maximum physiological length for the SOL, using 100 Hz trains 500ms in duration. Passive tension was subtracted from the total force measured. Tetanic force was measured on the plateau region to minimize the dynamic effects of tendon stretch. Figure 1 shows the length tension relationship. The curves have been normalized by the peak tension. In addition, the length-tension curve obtained during partial stimulation, was visually right shifted by 0.8mm to produce the optimal alignment. The peak tetanic tension for whole muscle was 8.70N and for part A of the muscle, 4.62N, leading to a stiffness estimate of 5.1 N/mm for the common tendon.

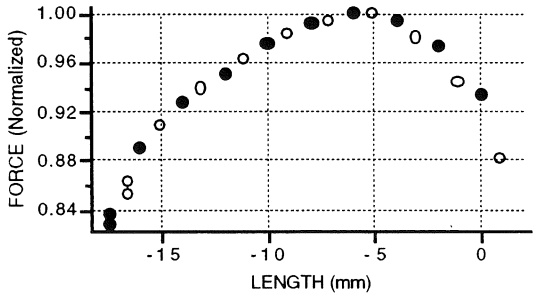

Figure 1 Length-Tension. Measured during whole muscle (solid circles) and partial muscle (open circles) stimulation. The data obtained during partial stimulation has been right shifted by 0.8mm.

Another technique used to estimate stiffness of the common tendon relies on measuring how stimulating, or terminating the stimulus, from one part of the muscle influences the tension measured from the other part. This will be referred to as the stretch-recoil test. Part A of the muscle was stimulated at 100Hz, beginning at 0.05s and ending at 0.80s. Part B of the muscle was stimulated with a 100Hz train beginning at 0.20s and ending at 0.50s. Parts A and B were stimulated together and then themselves. The heavy line in Figure 2 shows the tension measured by stimulating parts A and B

together minus the tension from stimulating part B alone. The depression seen in the plateau region shows the degree of nonlinear summation.

To test the hypothesis that tendon movement could explain the nonlinear summation measured via the stretch-recoil test, the expected tendon movement was mimicked using the servomechanism. If the common tendon is assumed to act as a linear spring, force from part B of the muscle will stretch the tendon by a length proportional to the force it produces. So, the force waveform measured during stimulation of part B alone, was scaled and used to stretch the SOL. The light line in Figure 2 shows the results obtained when only part A of the muscle was stimulated and the servomechanism was driven by a waveform (force from Part B) scaled to move a total of -0.5mm. Since the maximum tetanic force from part B was 4.16N this leads to an assumed common tendon stiffness 8.32N/mm. Movements with larger excursions better fit the rise in tension towards the end of stimulation, but exaggerated the initial fall in tension.

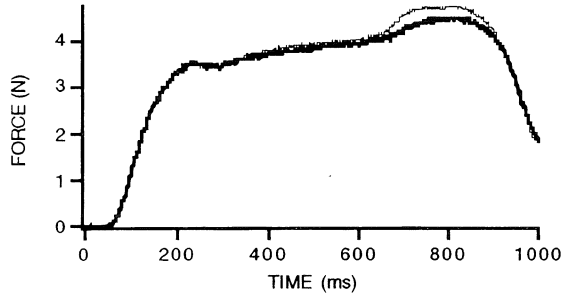

Figure 2. Stretch-Recoil Test. Heavy line -- digital subtraction of isometric tetnus waveform during stimulation of parts A and B together, minus the isometric tetnus waveform when part B was stimulated alone. Light line -- force from stimulation of part A with the servomechanism programmed to simulate tendon movement.

The third method used to estimate of stiffness in the common tendon was derived from the 'slack-test' method originally used to measure the maximum velocity of shortening in a muscle (Edman 1979). During tetanic stimulation a muscle is shortened, using a step decreases in length large enough to unload the series elastic in the muscle. The time needed to redevelop tension is then measured. If steps of different lengths are plotted against the respective times to redevelop tension, a straight line is obtained where the slope represents the maximum velocity of shortening for the muscle. This measurement was performed during both whole muscle and partial muscle stimulation. Tension redeveloped more quickly when only part of the muscle was stimulated, presumably because the common tendon was not as stretched as far. The difference in time to redevelop tension, multiplied by the velocity of shortening, provides an estimate of how much the common tendon is stretched. Figure 3 shows the results obtained using steps of magnitude 17, 15, 13, 11, 9, and 7mm. The estimated maximum velocity of shortening for whole muscle was 291mm/s and for part A of the muscle was 280mm/s. The average difference in time to reuptake tension was 4.0ms. Using whole muscle maximum velocity of shortening, this provides an estimate of stretch of 1.2mm for the common tendon going from 3.9N during stimulation of part A to 8.2N for the whole muscle (stiffness of 3.58N/mm). It is interesting to contrast the stretch of the common tendon with the step of approximately 4mm that was needed to fully unload the series elastic when the whole muscle was stimulated. This indicates the common tendon contains approximately one half the total muscle elasticity.

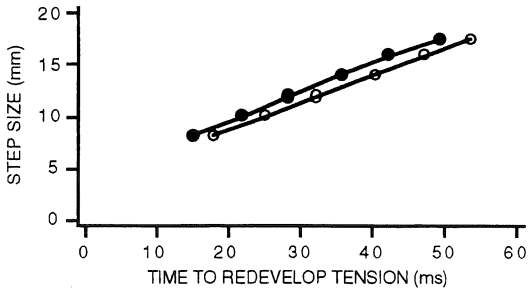

Figure 3. Results of Slack-Test. Time needed for whole muscle (solid circles) and part A of the muscle (open circles) to reuptake slack following a step decrease in muscle length.

Finially the alpha method (Proske and Morgan, 87) was used to estimate the stiffness of the common tendon. The method assumes a linear tendon and uses stiffness measured during full and partial activation of the muscle to separate crossbridge stiffness from tendon stiffness. Quick stretches of 1mm were used to measure muscle stiffness when the whole muscle, and part A alone, were stimulated at 100, 20, 13, and 10 Hz. During whole muscle activation at 100Hz (force of 8.43N), whole muscle stiffness was measured as 3.41N/mm. Stiffness of the common tendon was estimated at 7.18 N/mm and stiffness of the complete tendon 4.85 N/mm. So, the compliance of the common tendon is estimated as 47% of the whole muscle compliance. Expressed in the same form as the other methods, when the whole muscle is stimulated, compared to part A alone, the common tendon is stretched an additional 0.56mm.

DISCUSSION

Four methods were presented to measure the stretch of the common tendon when the whole muscle was stimulated versus part of the muscle. The estimates of tendon stretch ranged from 0.5 to 1.2mm for a change in muscle force of about 4 N. This rather small stretch is not surprising considering the short stiff tendon in cat SOL (Rack and Westbury, 83). Results from the slack-test and alpha test indicate the common tendon may represent approximately 1/2 the total elasticity fully active cat SOL.

The four methods provide fairly consistent estimates of common tendon stretch considering they are rough measures of a rather small amount of stretch. They all have the disadvantage that they are not direct measures of tendon properties. They measure the stretch at a single point rather than measuring stiffness as a function of tendon length. This is important since the length-tension properties of tendon are not linear but have been reported as exponential or exponential-linear (Zajac, 89). The methods are also not capable of measuring the known hysteresis during the stretch and release of a tendon. Sources of error will be discussed.

REFERENCES

Edman, K.A.P. *J. Physiol.* 291:143-159, 1979.
Proske, U. and D.L. Morgan. *J. Biomech:* :20:75-82, 1987.
Rack, P.M.H. and D.R. Westbury. *J. Physiol.* 347:479-495, 1984.
Trotter, J.A. *Acta. Anat.* 146:205-222, 1993.
Zajac, F.E. *C.R. Biomed. Engin.* 27:359-411, 1989.

THE EFFECT OF RANDOM, WHOLE-BODY VIBRATION AND HEAD-SUPPORTED MASS ON NECK MUSCLE ELECTROMYOGRAPHIC ACTIVITY AND PSYCHO-PHYSIOLOGICAL PERFORMANCE OF U.S. ARMY HELICOPTER PILOTS

S.A. Lantz and B.P. Butler

Department of Mechanical Engineering, University of Utah, Salt Lake City, UT 84112
Impact, Trauma, & Protection Division, U.S. Army Aeromedical Research Laboratory, Fort Rucker, AL 36362-0577

ABSTRACT

Volunteer military subjects were exposed to 2 hours of whole-body random vibration while wearing a helmet with a mass of 4.1 kg. The vibration was similar to that experienced in a UH-60 helicopter flying at 125 knots. Target acquisition times in a simple vigilance task were computed and recorded while EMG activity was measured and recorded at six points around the circumference of the neck. Degradations in vigilance performance, due to increased target acquisition times and/or to a greater percentage of missed targets, occurred at 45-60 minutes, 75-85 minutes, and 105-120 minutes with corresponding changes in the EMG patterns.

INTRODUCTION

The effectiveness of U.S. Army helicopter pilots in performing their combat missions has been greatly enhanced by extensive use of helmet-supported devices, such as night vision goggles, head-up displays, and chemical protective masks. Helmet-supported devices add to the total head-supported mass and lead to variations in the location of the mass. The trend to use the helmet as an equipment mounting platform is continuing, but the effects of these additional loads on the physiology of the neck and on pilot performance are not well understood.

Great emphasis has been placed on developing criteria for helmet mass and center of mass parameters based on the physiological and psychological performance of U.S. Army aviators. Recent studies at the U.S. Army Aeromedical Research Laboratory (USAARL) have examined neck muscle electromyographic (EMG) activity under different types of whole-body vibration and under different head-supported loads. In this study, psycho-physiological performance was assessed using a vigilance (target acquisition) task. Performance degradation, which is an indication of physiological and/or mental fatigue, was determined from increased acquisition times and increased numbers of missed targets on the vigilance task.

METHODS AND MATERIALS

Eleven volunteer military subjects (Table 1) were exposed to 2 hours of random whole-body vibration while wearing a helmet with a mass of 4.1 kg for which the center of mass was located 3.08 m superior and 1.96 m posterior to the head center of mass. The vibration was similar to that experienced in a UH-60 helicopter flying at 125 knots. The subject scanned for one of four light-emitting diode (LED) targets located at the periphery of his field-of-view. The order in which the LEDs turned on was controlled by a PDP 11/23 computer, which also measured and recorded the amount of time needed for the subject to acquire the targets. Target acquisition occurred when the subject aimed a collimated light beam atop his helmet at a photocell located just below the LED and held it there for 0.01 s. The LEDs were arranged in a diamond pattern (pattern 1) or in a rectangular pattern (pattern 2), as shown in Figure 1. The LEDs turned on in a pre-determined five-minute pattern and remained on for 3-7 s (average time 4.48 s),. The pattern repeated 24 times during the vibration exposure. To minimize the effect of the subjects learning the pattern, the subjects were told to return to their neutral position (looking straight ahead) after acquiring each target.

Vigilance pattern 1 was used for seven tests on seven subjects; vigilance pattern 2 was used for eleven tests on seven subjects. (Four subjects were tested using both patterns.) Pattern 1 required torsion movements to acquire targets 1 and 4 and either flexion or extension movements in the midsagittal plane to acquire targets 2 and 3. Pattern 2 required a combination of torsion and either flexion or extension movements to acquire all targets. Since pattern 2 required more head/neck motion and, therefore, was more likely to produce fatigue, the two sets of vigilance data were analyzed separately.

RESULTS AND DISCUSSION

To analyze the vigilance data, the average acquisition time for each subject for each target was calculated for the two-hour period and for each 5-minute vigilance "window" The subject groups were divided into "experienced" pilots and "rookie" pilots (those beginning their flight training). Table 2 presents the average acquisition times and the standard deviation of the acquisition times of all targets in both patterns.

Statistical analyses, using Student's t-test, were performed to determine if there were any differences in performance between the experienced pilots and the rookie pilots and to determine if any targets were "easier" to acquire than others. Values of $\alpha > 0.05$ were considered to be significant differences.

Pattern 1. The average acquisition time of the rookie pilots for target 4 was significantly greater than that of the experienced pilots. For the subjects as a group, the average acquisition time for target 2 was significantly less than that for the other three targets. For the experienced pilots, the average acquisition time for target 2 was significantly less than that for the other three targets and the average acquisition time for target 3 was significantly less than that for target 4. For the rookie pilots, the average acquisition time for target 2 was significantly less than that for target 4.

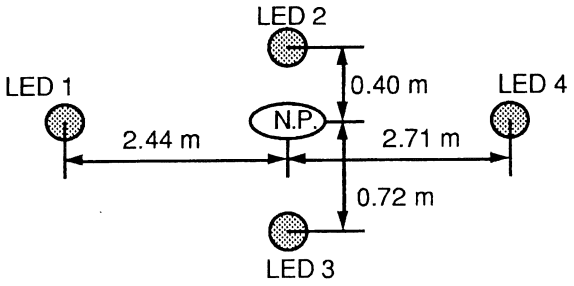

Figure 1a. Vigilance target pattern #1
(N.P. is the neutral position)

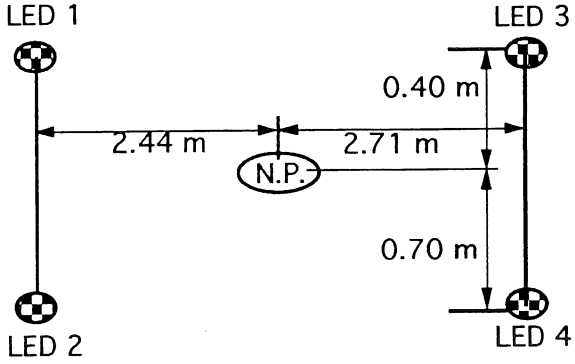

Figure 1b. Vigilance target pattern #2
(N.P. is the neutral position)

Table 1
Subjects Age, Height, and Weight

Subject Number	Age (yr.mo)	Height (cm)	Weight (kg)
1	28.01	188	98
2	29.09	170	66
3	23.09	178	73
4	26.11	178	73
5	26.02	183	84
6	24.05	188	82
7	23.07	170	82
8	24.00	185	79
9	22.02	183	68
10	23.09	180	73
Mean:	25.03	180	77

Pattern 2. The average acquisition time of the rookie pilots for all targets was significantly greater than that of the experienced pilots. For the subjects as a group, the average acquisition time for target 4 was significantly greater than that for target 1. For the experienced pilots, the average acquisition time for target 4 was significantly greater than that for targets 1 and 3. For the rookie pilots, there were no statistically significant differences (i.e., all targets were equally "difficult" to acquire).

To further analyze the vigilance data, the target acquisition times were divided into five categories: less than 1 s, 1-2 s, 2-3 s, more than 3 s, and "Did Not Acquire" For each target, the acquisition times in each window were separated into the appropriate categories and then were tabulated and plotted. The average performance during the time interval from 5-25 minutes was used as a baseline. (The 0-5 minute window was not used because of anomalies which were considered to be a "learning curve".) A chi-squared analysis was used to compare the data for each target from each window to determine trends in performance over time.

Increased target acquisition times and/or a greater percentage of missed targets were considered to be degradations in performance. There were significant differences between the performance of the experienced pilots and that of the rookie pilots: the rookie pilots had greater average acquisition times, had a greater percentage of targets requiring more than 3 s to acquire, and had a greater percentage of targets not acquired. For experienced pilots for target pattern 1, degradations in performance occurred at 75-90 minutes and at either 105-110 minutes or 115-120 minutes for all targets and at 45-60 minutes for target 3. For targets requiring turning of the head/neck, there was a period of improved performance at 50-55 minutes. For target pattern 2 for experienced pilots, degradations in performance occurred at 75-85 minutes, 90-100 minutes, and 105-120 minutes for all targets and at 45-60 minutes for all targets except target 1. For target pattern 2 for rookie pilots, degradations in performance occurred at 65-70 minutes for all targets, and at 45-60 minutes and 95-100 minutes for all targets except target 1. Improved performance for targets which required turning and lifting the head, occurred at 80-85 minutes and at either 110-115 minutes or 115-120 minutes.

Table 2
Averages and Standard Deviations of Target Acquisition Times for Various Groupings of Subjects[1]

Group	Target 1	Target 2	Target 3	Target 4
1--All	1.74	1.27	1.58	1.77
(n=7)	± 0.25	± 0.15	± 0.19	± 0.26
1--Exp'd.	1.64	1.21	1.50	1.67
(n=5)	± 0.19	± 0.11	± 0.14	± 0.07
1--Rookies[2]	2.00	1.441	1.77	2.04
(n=2)	± 0.20	± 0.12	± 0.15	± 0.16
2--All	1.83	1.91	1.88	2.03
(n=11)	± 0.18	± 0.24	± 0.21	± 0.24
2--Exp'd.	1.72	1.74	1.74	1.88
(n=5)	± 0.11	± 0.18	± 0.03	± 0.09
2--Rookies	1.93	2.04	2.00	2.16
(n=6)	± 0.18	± 0.19	± 0.23	±0.25

[1](All values in seconds (average ± standard deviation.).
[2]There was a large variation between the two subjects, so the average behavior for these subjects probably is not representative of the behavior of a group of rookie pilots.

ACKNOWLEDGMENTS

The authors wish to thank the following persons for their contributions to this research: Mr. John Jenkins, Mr. James "Al" Lewis, SGT Bradley Erickson, and Miss Lydia Woodcox. This research was supported by Battelle Contract DAAL03-86-D-0001, Delivery Order 2514 and by U.S. Army Contract DABT01-92-P-2326.

Exercise Decreases Ligamentous Stiffness In The Wrist

J J Crisco, S Chelikani, R Brown, SW Wolfe
Biomechanics laboratory, Department of Orthopaedics and Rehabilitation
Yale University Medical School, New Haven, CT USA

INTRODUCTION

The scaphoid bone plays a significant role in wrist stability since it is considered the primary mechanical link between the distal and proximal rows of carpal bones. This linkage is achieved via a complex arrangement of ligaments. The purpose of this study was to determine if increased loading of the wrist, via exercise, alters the mechanical behavior of the scaphoid ligaments. Healthy volunteers were tested on three days: after rest, after griping exercise, and after push-up exercise. Each test measured the load-displacement behavior of the scaphoid. We found that exercise significantly altered the load-displacement behavior of the scaphoid. After exercise the displacement at 40 N significantly increased with both exercises. Hysteresis energy also increased significantly. The linear estimate of stiffness significantly decreased with exercise. There were no changes with rest.

REVIEW AND THEORY

Repeated loading of ligamentous structures *in vitro* incrementally shifts the load-displacement curves along the displacement axis. These increments decrease with repeated loading and convergence is typically established in 3 to 10 loading cycles, depending on the structure. This phenomena is well documented during testing of cadaveric specimens, and protocols often include this preconditioning to enhance repeatability. The mechanism associated with preconditioning remains unclear. We hypothesized that preconditioning is an inherent property of ligamentous tissue and is not an artifact due to harvesting or storage of cadaveric material. This study was designed to determine if repeated loading *in vivo* alters the mechanical properties of a joint whose stability is dominated by ligamentous structures.

PROCEDURES

Both wrists of seven volunteers (n=14) were studied on separate days with three protocols. Each protocol consisted of three tests at time 0, at 5 minutes, and at 65 minutes. The first protocol was Rest: the volunteers were asked to refrain from any strenuous activities during the test period. The second protocol was called Grip: identical to the first protocol, but at t = 3 min., simulated gripping was performed with a generic grip exerciser calibrated to close with 138 N at mid grip. Thirty repetitions were performed in a period of 2 min. The third protocol was Push-up: identical to the first protocol, but at t = 3 min., a push-up was simulated by placing the extended wrist on a scale and maintaining a load of 138 N for 2 min.

At each specified point in time the mechanical behavior of the scaphoid bone was documented. The wrist was strapped supinated to a custom jig. A plunger, positioned above the wrist, traveled freely in the dorsal-palmar direction. The displacement of the plunger and the load applied to the plunger were recorded by computer. The tip of the plunger was dimpled and was positioned on the tubercle of the scaphoid, which can be palpated. An examiner applied a dorsally directed load to a maximum of 40 N. Each test consisted of five load-unload cycles. The data from the fifth cycle was analyzed. The maximum displacement was defined as the displacement corresponding to 40 N. Stiffness was the linear least squares fit of the loading portion of the load-displacement curve. The energy was the integral of the load-unload cycle.

Significant differences in mechanical behavior were determined using a repeated measures format ANOVA, with a Fisher LSD post-hoc test at level of 95%.

RESULTS AND DISCUSSION

Exercise had a significant effect on the mechanical behavior of the scaphoid. Maximum displacements (at 40N) increased on average by 2.2 mm and 3.2 mm after Grip and Push-up exercises. Stiffness values showed a corresponding decrease of 2.4 N/mm and 2.6 N/mm. The energy in the fifth load-unload cycle increased by 13.0 N·mm and 19.4 N·mm after Grip and Push-up, respectively. All

differences were statistically significant ($p < 0.05$).

There was no intra-day differences with the rested wrists. There was also no inter-day difference at t=0.

For both exercise protocols, there was partial recovery at t = 65. Maximum displacements decreased by 1.6 mm and 1.3 mm for Grip and Push-up, respectively, and these values were still significantly greater ($p < 0.05$) than the corresponding resting values. This indicates that recovery had initiated, but a rest of one hour was insufficient for a complete return to the original state. Likewise, stiffnesses and the energy absorbed displayed a similar trend.

Between the two types of exercise, the maximum displacement for Grip was 1 mm more ($p < 0.05$) than for Push-up at t = 5 min. This difference may be due to the cyclic loading associated with the Grip versus the static loading associated with the Push-up protocol.

This study documents a decrease in stiffness associated with exercise. We hypothesize that this change in mechanical behavior is associated with a "preconditioning" of the ligamentous structures, but this remains to be explicitly tested. Such preconditioning may be compared with warm-up exercises. Although the types of warm-ups vary widely, all are aimed at minimizing injury during strenuous activity. The relationship between a preconditioned ligament and the risk of injury has not been established. Paradoxically, in terms of classical mechanics, decreases in joint stiffness implies a less stable joint, yet such exercises are known to be beneficial in minimizing injuries and optimizing performance.

Table 1. Average (s.d.) values describing the mechanical behavior of the scaphoid for the three protocols.

Protocol	Time of test (min)	Max. Displ. (mm)	Stiffness (N/mm)	Hysteresis Energy (N·mm)
Rest	0: rest	6.9 (1.7)	7.2 (1.3)	51 (13)
	5: rest	6.7 (1.5)	7.2 (1.5)	57 (19)
	65: rest	6.6 (1.4)	7.3 (1.4)	52 (15)
Grip	0: rest	6.8 (1.4)	7.3 (1.4)	46 (14)
	5: Grip	10.0 (1.7)	4.7 (1.1)	66 (17)
	65: rest	8.4 (2.1)	5.7 (1.0)	68 (15)
Push-up	0: rest	6.7 (1.2)	7.6 (1.3)	50 (12)
	5: Push-up	9.0 (2.0)	5.2 (1.0)	63 (16)
	65: Rest	7.6 (1.5)	5.8 (1.1)	60 (18)

Figure 1. Both Grip and Push-up exercise performed prior to testing at t = 5 min. significantly increased maximum displacement. After 1 hour rest, neither displacement fully recovered. No differences at t = 0 indicated that 24 hours was sufficient for full recovery.

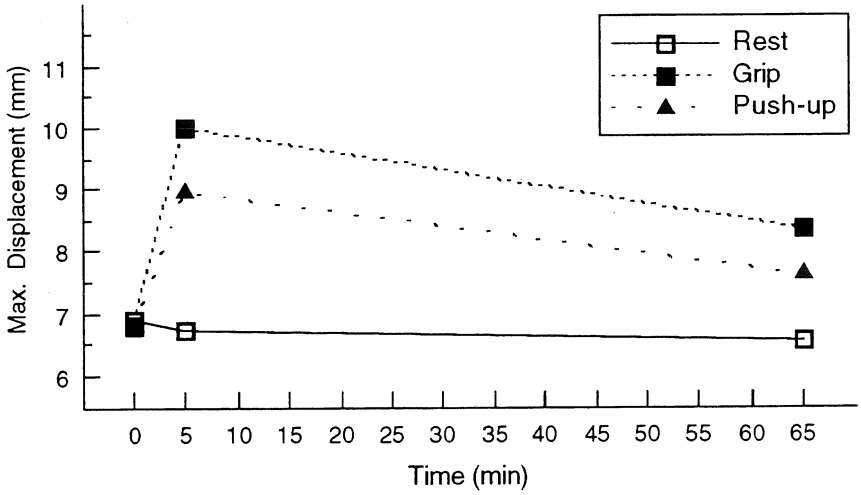

ACCURACY OF A VIDEO STRAIN MEASUREMENT SYSTEM

W.P. Smutz, M. Drexler, L.J. Berglund, E. Growney, K.N. An
Orthopedic Biomechanics Laboratory, Mayo Clinic/Mayo Foundation, Rochester, MN

INTRODUCTION

The accuracy of the Expert Vision System when used for soft tissue strain measurements was determined. Accuracy was determined for 5 camera distances, 5 marker sizes, and 5 loading rates. The accuracy was found to depend on the size of the marker, field of view of the camera, and strain rate.

REVIEW AND THEORY

Strain measurement of soft connective tissues such as tendons and ligaments is an important component in the characterization of their mechanical behavior. While many different techniques for measuring soft tissue strain have been reported in the literature they can be divided into general types non-contact video systems and mechanical contact systems. In recent years non-contact video systems have increased in popularity. The main advantage of the non-contact video system is that the measuring device is not attached directly to the specimen thereby reducing the effect that the measuring system has on the loading response of the specimen. Our laboratory has been using the Expert Vision System (Motion Analysis Corporation, Santa Rosa, CA) to measure soft tissue strain. A review of the literature revealed that the accuracy of the Expert Vision System when used to measure strain has not been reported. Therefore, the purpose of this study is determine the accuracy of the Expert Vision System when used to measure strain and to determine how camera distance, marker size, and loading rate effect the accuracy.

PROCEDURES

Two marker sets were constructed for the test. Each marker set was constructed by drilling a series of holes in a plexiglass plate. Ten holes for each of five different sizes were drilled in each plate. The five different holes sizes were; 0.8, 1.6, 1.9, 2.4, 3.2 mm. The holes were then filled with an epoxy resin mixed with florescent powder to form the markers. The marker sets were then be placed in a hydraulic test machine. One set of markers was attached to the base of the test machine and remained stationary throughout the test. The other marker set was attached to the hydraulic actuator of the test machine. A sliding rail was constructed and attached to the base of the hydraulic test machine (Figure 1). One camera of the Expert Vision System was attached to the rail. The purpose of the rail was to keep the markers perpendicular to the field of view of the camera and to allow for precise positioning of the camera.

Five camera distances were used; 174, 116, 87, 58, and 29 cm. These distances corresponded to a camera field of view of 120, 80, 60, 40, and 20 mm respectively. Field of view is defined as the largest horizontal distance that can be seen by the camera for a given camera distance. Incandescent black lights were used to illuminate the markers. Five loading rates were used. The loading rates were 2.5, 5, 10, 25, and 50 percent of the field of view of the camera per second. The input to the hydraulic actuator consisted of a single triangle wave. Displacement of the hydraulic actuator was 50 percent of the field of view of the camera. The motion of the moving markers were also measured using the LVDT of the hydraulic test machine. Data was collected at a rate of 60 hz.

The position of the markers was recorded using the video system. The movement of the marker images were tracked using the Expert Vision Software. The centroids of the images were used to calculated the location of markers using a Sun workstation. The absolute and relative coordinates of these markers were then transferred to a PC for further analysis.

Static accuracy of the system was defined as the amount of movement reported by the video system for the stationary markers. Dynamic accuracy of the system was defined as the difference between the position of the moving markers as reported by the video system and the LVDT. All errors were expressed in pixels. The Expert Vision System has 256 pixels horizontally and 240 pixels vertically.

RESULTS

For the static accuracy, the distances between static markers were calculated. Theoretically, these markers should remain stationary. Therefore, any changes in the distance between markers with time represents error or noise. In general, it was found that the mean error was 0.06 pixels. For a given

camera field of view, the error is dependant on the size of the markers (Figure 2) and for a given marker size, the error is dependant on the camera field of view (Figure 3). It seems that there is an optimal combination of size which gives the best accuracy.

DISCUSSION

The video strain measurement system by taking advantage of the automatic tracking software by Expert Vision was found to be quite adequate for soft tissue testing. The accuracy was found to depend on the size of the marker, field of view of the camera, and strain rate. Proper selection of these parameters is required to accomplish a given requirement of strain accuracy. The advantage of the current system is that with multiple markers on the specimen the measurement of the strain field would be possible and efficient. Also, the software uses subpixel calculations which make it more accurate.

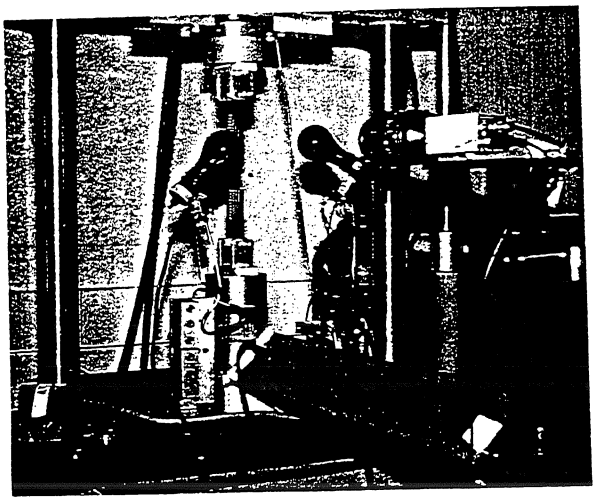

Figure 1. Photograph of test setup

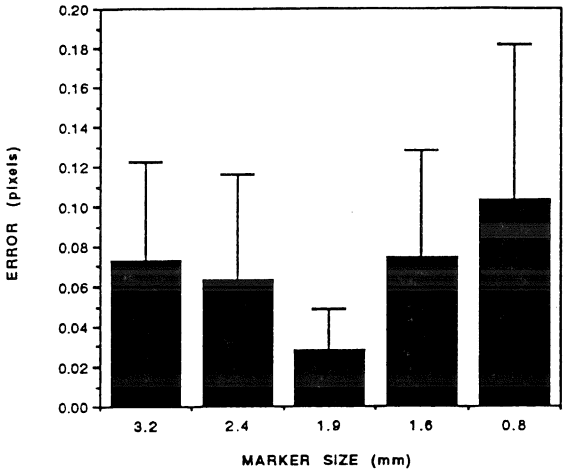

Figure 2. Static error for different marker sizes for a fixed camera distance of 87 cm.

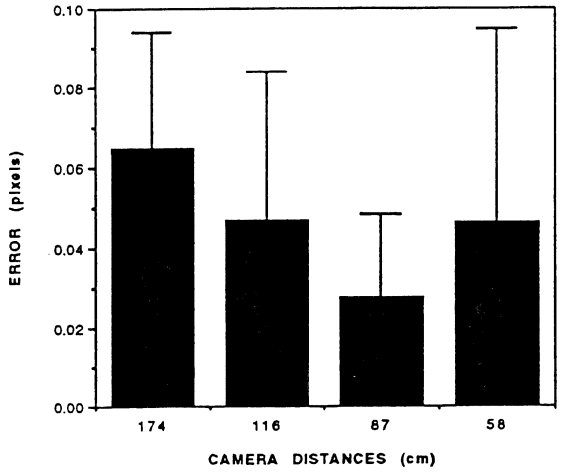

Figure 3. Static error for different camera distances for a fixed marker size of 1.9 mm.

ACKNOWLEDGEMENTS

This study was supported in part by NIH Grant AR 41171.

PRESSURE-VOLUME RELATIONSHIPS IN NORMAL EQUINE MIDCARPAL JOINTS

J. Hardy, A.L. Bertone, and W.W. Muir

Department of Veterinary Clinical Sciences,
The Ohio State University,
601 Vernon L Tharp,
Columbus, OH 43210

INTRODUCTION

Pressure-volume relationships in normal equine midcarpal joints were investigated by infusion of synovial fluid. A sigmoid pressure-volume curve was mathematically defined for sub and supra-atmospheric pressures. Effects of joint angle (90^0 or 135^0) infused fluid (saline or synovial fluid), compartmentation, hysteresis, and history-dependence on the pressure-volume curves were examined. Decreased joint angle caused decreased compliance (dV/dP), while compliance was greater with synovial fluid than with saline infusion. Compartmentation was not observed, but hysteresis was significant at all joint angles. Repeated infusion-withdrawal cycles cause decreased compliance in the high region (>30 mmHg) of the pressure-volume curve. These findings in normal joints will allow to further define alterations that may occur with disease.

REVIEW AND THEORY

Normal intraarticular pressure (IAP) is slightly negative. Joint effusion is a common finding in articular disorders and causes increased intraarticular pressure (IAP). Increased IAP results in decreased synovial membrane blood flow, and pain. The determinants of IAP include volume of infusion, joint angle, fluid infused, prior joint distention history, articular compartmentation and degree of pathology of the joint capsule. Knowledge of pressure-volume (PV) relationships in normal and diseased joints is important to understand the effects of joint effusion on articular health. Previous studies have examined PV relationships in normal and diseased joints, using electrolyte solutions or newtonian fluids such as oil. Synovial fluid exhibits non-newtonian viscoelastic properties, because of its high hyaluronate content. We hypothesized that the PV relationships of joints would differ from that previously reported if synovial fluid was used as the infusate. The purpose of the present study was to use synovial fluid to define the PV relationships of normal equine midcarpal joints and to determine the effects of joint angle (90^0 v s 135^0), infusate solution (saline or synovial fluid), compartmentation, and history-dependence on articular compliance (dV/dP) in normal equine midcarpal joints.

PROCEDURES

For this study, eighteen healthy adult horses (36 midcarpal joints, n=6/experiment) were anesthetized and positioned in dorsal recumbency, with both forelimbs suspended from a rack. The midcarpal joints were positioned at the desired angle with a goniometer. The dorsal lateral and medial, and palmar lateral and medial midcarpal joints pouches were cannulated for measurement of IAP. The dorsal midcarpal joint was cannulated through the extensor tendon for infusion of synovial fluid or saline. Fluid was infused and withdrawn with a calibrated pump set at a rate of 2.47 ml/min. All pressures tracings were continuously recorded on a physiograph. *Pressure-volume curves:* Volumetric elastance (dP/dV) was measured in all compartments at two joint angles (90^0 or 135^0), and with two different fluids (saline or synovial fluid) by infusion until an IAP of 80 mm Hg was reached in one compartment. *History-dependence:* The effect of prior distention on articular compliance at low (<30 mmHg) or high (30 to 80 mmHg) IAPs was determined by raising the IAP to 30 mmHg for 3 cycles, followed by increasing IAP from 30 to 80 mmHg for 3 cycles in 6 joints. Similarly, in 6 other joints, IAP was first increased from 30 to 80 mm Hg for 3 cycles, followed by 3 cycles at low pressure (up to 30 mm Hg).

For analysis, each PV curve was digitized to obtain data points which were used for mathematical modeling and statistical analysis.

Calculations: Each PV curve was fitted to the following exponential equation :

Pressure= $A*e^{(B*volume)}-C$, and the volume constant (1/B), a measure of compliance, was used for analysis. History dependence was tested by fitting a linear equation (Pressure = A + B*volume) to the low (up to 30 mmHg) or high (30 to 80 mmHg) pressure-volume curves.

Statistics: A four-way fixed-model analysis of variance was used to compare the non-linear equation B coefficients of the PV curves, with the following factors used: joint angle, fluid type, joint compartment, and infusion or withdrawal. Body weight of animals was tested and found not to be correlated with the data, so it was not included as a covariate. A four-way repeated measure analysis of variance (joint angle, compartment, low or high pressure, number of repetition (repeated measure)) was used

to compare the linear slopes of the low or high PV curves to test the history-dependence of the articular PV relationship. When a main effect or an interaction was detected, a Student-Neuman-Keuls post-hoc comparison test was used to identify the different means. Significance was set at $p<0.05$.

RESULTS

Equine midcarpal joint PV curves were best defined using two exponential equations: one for subatmospheric pressures:

Pressure= $-7.20 * e^{(-3.46*volume)}-3.61$ (Fig 1 and 2)

and one for supra-atmospheric pressures:

Pressure= $40.74 * e^{(0.11*volume)}-35.46$ (Fig 1)

Decreased joint angle significantly decreased subatmospheric ($p=0.028$) and supra-atmospheric ($p=0.006$) articular compliance (Fig 1). Saline infusion resulted in a significantly lower articular compliance (Fig 3). Significant hysteresis was detected for all joint angles (Fig 4). Differences in compliance were not detected among joint compartments. Sequential distention cycles (history-dependence) did not significantly affect PV relationships at IAP<30 mmHg. At high IAP (30 to 80 mmHg) a significant decrease in compliance was observed after the first distention cycle, particularly if the high pressure cycles followed low pressure cycles.

DISCUSSION

The sigmoid shape of the PV relationship (Fig 1) suggests that the joint is resistant to articular distention (low compliance) at subatmospheric pressures. With increasing intraarticular volume, the joint becomes more compliant, but as IAP reaches values > 30 mmHg, the joint becomes again less compliant. These findings are similar to that previously reported.[1] Use of synovial fluid as the infusate resulted in increased articular compliance as compared to saline, in contrast with previous results which showed a greater compliance with saline as compared to oil. These findings suggests that in normal joints, hyaluronate may increase the distensibility of articular soft tissues. Decreased joint angle resulted in decreased articular compliance, as previously reported.[1] Our inability to detect joint compartmentation in the present study may result from the non-weight bearing position of the joint. In the present study, significant hysteresis was detected at all angles, and may reflect fluid absorption, or more likely creep relaxation of the joint capsule. Joint distention cycles of up to 30 mmHg did not affect the biomechanical properties of the periarticular soft tissues. At IAP of 30 to 80 mmHg, a significant decrease in compliance was observed after the first cycle, which may result from initial fluid distribution within the joint cavity or to the rate of infusion.

In conclusion, this study describes the PV relationships of the equine midcarpal joint at sub and supra-atmospheric pressures and highlights the importance of joint angle, nature of infusate and prior history of distention as determinants of compliance in normal joints.

REFERENCES

1.Knight, A.D., et al. Pressure-volume relationships above and below atmospheric pressure in the synovial cavity of the rabbit knee. J Physiol, 328, 403-420, 1982.

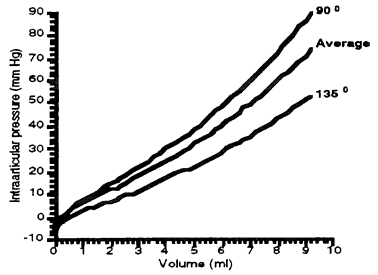

Figure 1: Pressure-volume relationship in the midcarpal joint at subatmospheric and supraatmospheric pressures and joint angles of 90° and 135°

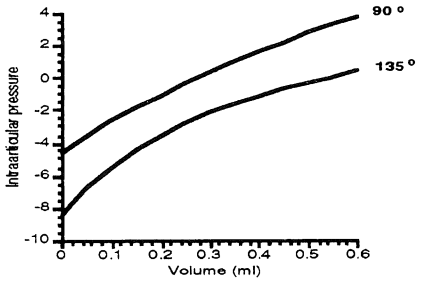

Figure 2: Pressure-volume relationship at subatmospheric (normal) intraarticular pressures

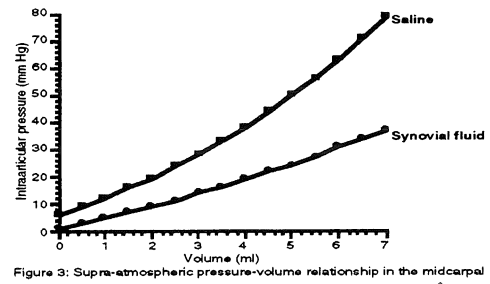

Figure 3: Supra-atmospheric pressure-volume relationship in the midcarpal joint with synovial fluid or saline infusion at joint angles of 135°

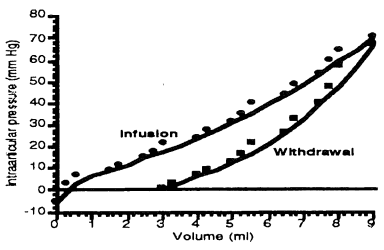

Figure 4: Pressure-volume relationship in the midcarpal joint during infusion or withdrawal of synovial fluid

A MECHANICAL MODEL OF VISCOELASTIC BEHAVIOR OF ACRYLIC BONE CEMENTS

D. N. Yetkinler and A. S. Litsky

Orthopaedic BioMaterials Laboratory,
Ohio State University, Columbus, Ohio, 43210.

INTRODUCTION

Aseptic loosening of implants is a major post-operative complication in total hip arthroplasty. Rose and Litsky (1989) stated the importance of local contact stresses in this progressive biomechanical phenomenon (1).

A reduced-modulus bone cement, polybutylmethylmethacrylate (PBMMA), was developed to reduce the local contact stresses at the bone-cement implant interface. The glass transition temperature (T_g) of the polybutylmethacrylate beads is 27°C so they are rubbery at body temperature. The elastic modulus of PBMMA is 0.27 GPa at 37°C compared to 2.1 GPa of standard PMMA bone cement. Therefore, PBMMA is viscoelastic at 37°C.

REVIEW AND THEORY

Saha and Pal (1984) stated the importance of the viscoelastic nature of bone cement and concluded that stress relaxation and creep deformation of PMMA can affect the load bearing capacity and eventually cause loosening of the prosthesis (2). An accurate model of viscoelastic behavior is essential in stress analysis as well as in finite element analysis of implant technology (3).

Pal and Saha (1982) analyzed the viscoelastic behavior of standard bone cement and showed a stress relaxation relationship of

$$\sigma_t = 18.907 \times e^{-0.2856 \times t} \ \text{MN/m}^2$$

when cylindrical specimens (30 mm length, 17 mm diameter) were subjected to 1% compressive strain (4).

In our study the collocation method was used to fit the experimental data into the generalized Maxwell model:

$$E_m(t) = E_\infty + \sum_{i=1}^{n} E_i \times e^{\frac{-t}{T_i}}$$

where E_m and E_R are the stress relaxation moduli of the mechanical model and the experimental data, respectively. E_∞ is the stress relaxation modulus of $E_R(t)\big|_{t\to\infty}$. $T_i = \frac{\eta_i}{E_i}$ is defined as relaxation time. The collocation method is based on the least squared error principle.

PROCEDURES

Short-term and long-term stress relaxation properties of both PMMA and PBMMA cement were investigated. Unconstrained stress relaxation tests were performed at 1%, 2.5%, and 5% strains on cylindrical compression specimens (26 mm length, 17 mm diameter). Long-term stress relaxation graphs were determined using the Time Temperature Superposition Principle on each 48 hour stress relaxation test. Both short-term and long-term results indicate a rapid initial stress redistribution followed by a slow steady-state decrease in stress.

Each curve was analyzed and stress relaxation moduli were determined at $t_0 = 0$, $t_1 = 0.01$ sec, $t_2 = 0.1$ sec, ...in one decade intervals. After processing this data according to the collocation method, moduli (E_i's) are determined by solving a 6×6 matrix.

$$\begin{bmatrix} a_{11} & a_{12} & a_{13} & a_{14} & a_{15} & a_{16} \\ a_{21} & . & . & . & . & . \\ a_{31} & . & . & . & . & . \\ a_{41} & . & . & . & . & . \\ a_{51} & . & . & . & . & . \\ a_{61} & . & . & . & . & a_{66} \end{bmatrix} \begin{bmatrix} E_1 \\ E_2 \\ E_3 \\ E_4 \\ E_5 \\ E_6 \end{bmatrix} = \begin{bmatrix} E_R(0) - E_\infty \\ E_R(.01) - E_\infty \\ E_R(.1) - E_\infty \\ E_R(1) - E_\infty \\ E_R(10) - E_\infty \\ E_R(100) - E_\infty \end{bmatrix}$$

where $a_{ij} = e^{\frac{-t_{i-1}}{T_j}}$ $(i, j = 1..6)$.

RESULTS

The comparison of several techniques used to fit the stress relaxation data into a model is shown in Table

	r^2
Linear Model	0.307
Logarithmic Model	0.836
Power-Law Model	0.987
Collocation Method (6 parameters)	0.998
Collocation Method (12 parameters)	0.999

Table 1. Several models and their determination coefficients (r^2) in the stress relaxation modeling of PBMMA.

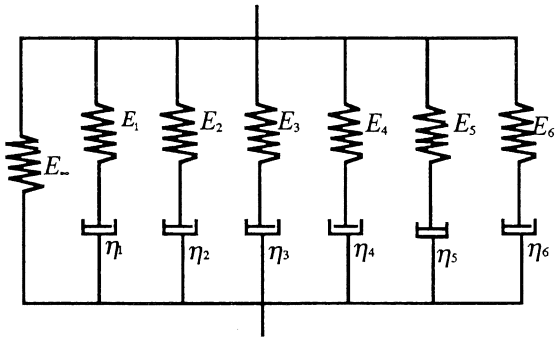

Figure 1. A generalized Maxwell model (6 parameters) of PBMMA acrylic bone cement calculated by the collocation method.

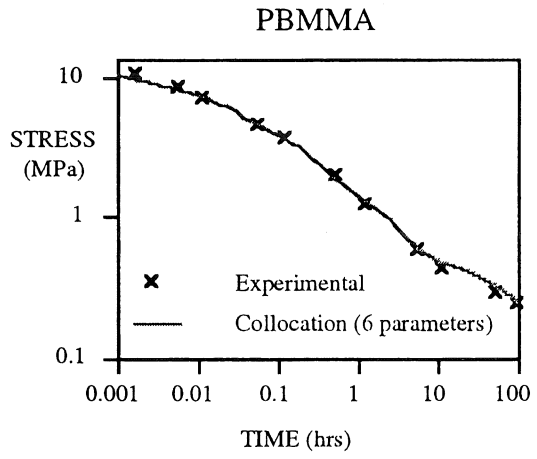

Figure 2. The model and experimental stress relaxation curve of PBMMA acrylic bone cement.

1. The coefficient of determination (r^2) for the collocation method (six parameters) is 0.998 compared to 0.987 for the power-law model. Figure 1 shows how the model is constructed mechanically with springs and dashpots. Figure 2 shows how the experimental data coincides with the results predicted by the collacation method.

DISCUSSION

The collocation method allows us to model viscoelastic behavior of acrylic bone cements accurately. Researchers can use the model as a numerical formula as well as a mechanical model.

Numerical interpretation of viscoelastic behavior is especially important in stress analysis experiments and finite element analysis.

REFERENCES

1. Rose, R.M. and Litsky, A.S. Biomechanical considerations in the loosening of hip replacement prostheses. Current Perspectives on Implantable Devices, 1:1-45, 1989.

2. Saha, S. and Pal, S. Mechanical properties of bone cement: A review. J. Biomed. Mater. Res., 18:435-462, 1984.

3. Chwirut, J.D. Long-term compressive creep deformation and damage in acrylic bone cements. J. Biomed. Mat. Res., 18:25-37, 1984.

4. Pal, S. and Saha, S. Stress relaxation and creep behaviour of normal and carbon fibre reinforced acrylic bone cement. Biomaterials, 3(4):93-6, 1982.

ACKNOWLEDGMENTS

Work supported by NIH - AR39684.

Orthopaedic BioMaterials Laboratory
S-2035 Davis Medical Research Center
480 West Ninth Avenue
Columbus, Ohio 43210

FINITE ELEMENT MODELING OF POLYTHYLENE STRESSES USING INDUSTRIAL TOLERANCES FOR FEMORAL HEAD SIZES IN TOTAL HIP REPLACEMENTS

T. A. Maxian, T. D. Brown, D. R. Pedersen, and J.J. Callaghan
Departments of Orthopaedic Surgery and Biomedical Engineering
The University of Iowa, Iowa City, IA, 52242

INTRODUCTION

A fully three-dimensional, nonlinear contact finite element (FE) model was used to investigate the effects of incongruencies between the femoral head and acetabular components on polyethylene stress distributions in the polyethylene liner. The model consisted of the femoral head, represented by a spherical rigid body, physiologically engaging a hemispherical FE meshed, metal-backed acetabulum, lined with interface contact elements. Parametric series were run for 22, 28, and 32 mm acetabular components, using head diameter ranges from a survey of current orthopaedic industrial tolerances. When the smallest allowable head sizes were modeled in the 22 mm and 32 mm series, peak polyethylene stresses increased 20% over the stresses that were obtained when mean sized heads were used. The increase was only 14% in the 28 mm series.

REVIEW AND THEORY

Increased polyethylene contact stress has been shown to lead to increased rates of polyethylene wear (Rostoker, W. and Galante, J. O., 1979). Consequently, any factors that lead to increased polyethylene stresses should be eliminated whenever possible. Using an axisymmetric FE model with prescribed surface tractions, Bartel et al. (1985) demonstrated that polyethylene stress is very sensitive to clearance between the femoral head and acetabular bearing surface. Implant manufacturers have different specifications for acceptable femoral head sizes (Ritter et al., unpublished data). Moreover, during revision surgery, an orthopaedic surgeon may use acetabular and femoral components from different manufacturers. We set out to investigate if plausible clinical variation in femoral head size could lead to wear-consequential polyethylene stress elevations in certain cases.

PROCEDURES

The model consisted of a fully three-dimensional hemispherical FE mesh representing a metal-backed acetabular component, inclined at 45°, in contact with a spherical rigid body representing the femoral head. All analyses were performed using the rigid body contact, large displacement features of ABAQUS. The FE mesh used 900 solid elements, with a combination of six-node wedge and eight-node brick elements. The metal backing used a single layer of elements with an elastic modulus of 210 GPa. The liner was four element layers thick with a polyethylene elastic modulus of 1400 MPa, corresponding to *in vitro* oxidation data (Rimnac et al., 1994). The inner surface of the acetabular component was lined with 180 frictionless rigid surface contact elements. Engagement was made using displacement control. To simulate the maximal loading occurring during the gait cycle, the femoral component was driven vertically upward until the reaction force reached 3.5 kN. Successive mesh refinement studies indicated that this level of mesh refinement provided adequate convergence (i.e., underestimation of the reaction force for the 28 mm head by less than 3%).

Since acetabular diameter variations were not known, the cup was selected to be 0.2 mm greater than the nominal diameter of the femoral head (i.e., 22.2, 28.2, and32.2 mm in the respective 22, 28, and 32 mm series). Models were generated (Table 1) corresponding to the mean, mean + 1 SD, mean - 1 SD, largest, and smallest diameters of industrially produced femoral heads.

RESULTS

As expected, peak polyethylene stress increased as the femoral heads became smaller in each series (Table 1). Peak polyethylene stresses increased 20% over the stresses obtained with mean-sized heads when the smallest-sized heads were used in the 22 mm and 32mm series, but only 14% in the 28 mm series (which had less variability). A representative contour stress distribution from the 27.97 mm femoral head (mean size) is shown in Figure 1.

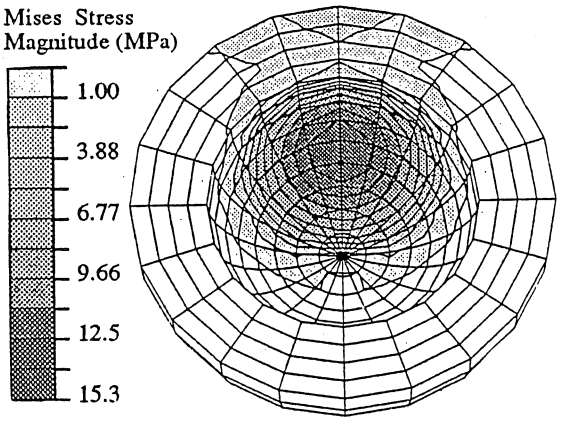

Figure 1. Polyethylene stress distribution.

The site of peak polyethylene stress occurs in the supero-lateral cup; thus, a considerable portion of the lateral margin experiences stress. Polyethylene stresses as a function of the distance away from the center of the acetabular component along the contact area are plotted in Figure 2 for the 28 mm series. For comparison, similar data from an axisymmetrically loaded, 27.97 mm model are also included.

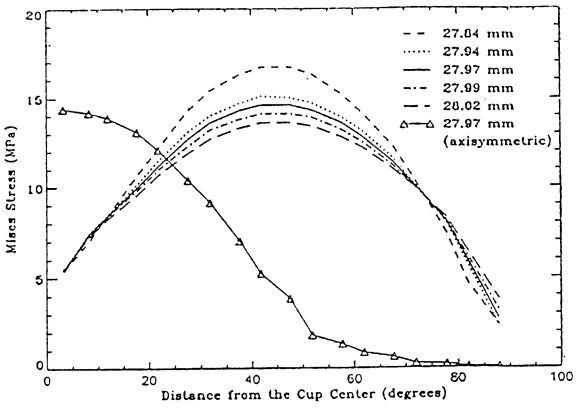

Figure 2. Polyethylene stress along a coronal section.

Stress in the axisymmetric case is near zero at the edge, while in the physiologically loaded case, considerable polyethylene stress occurs near the edge of the liner.

Table 1. Head diameters and peak polyethylene stresses.

Series	Diameter (mm)	Peak Polyethylene Stress (MPa)
22 mm		
largest	22.25	16.8
mean + 1 SD	22.20	15.4
mean	22.07	18.2
mean - 1 SD	21.95	20.7
smallest	21.87	22.1
28 mm		
largest	28.02	14.2
mean + 1 SD	27.99	14.7
mean	27.97	15.3
mean - 1 SD	27.94	15.8
smallest	27.84	17.5
32 mm		
largest	32.00	12.8
mean + 1 SD	31.98	13.4
mean	31.93	14.4
mean - 1 SD	31.88	15.3
smallest	31.75	17.4

The 22.25 mm case was special in that the largest femoral head was actually larger than the acetabular component. In this case, the peak contact stress was actually larger than the next smaller femoral head, as the femoral head impinged along the acetabular lip rather than loading within the acetabular cup.

DISCUSSION

This parametric FE series suggests manufacturers' tolerance variations for nominally same-sized femoral head components can have significant effects on the stresses in the polyethylene acetabular liner. These models underestimate the congruency variances encountered in clinical practice since the size of the acetabular component was kept the same within each series. Previous FE models of hip components have been predominantly axisymmetric. The results from this fully three-dimensional model indicate that axisymmetric models underestimate polyethylene stresses in the lateral margin of the cup due to use of an axially directed load.

Rostoker and Glanate (1979) showed that wear was an exponential function of polyethylene stress for stresses in the ranges developed in these models. With polyethylene wear debris implicated in aseptic loosening of total joint replacements (Amstutz et al., 1992), simple, practical measures to reduce polyethylene stresses and wear debris production should be undertaken whenever possible. Consequently, at revision, it may be prudent to ensure that components made by the same manufacturer are used, based on the assumption that components from a single manufacturer would be most congruent. Additionally, the rationale for current size tolerance standards may need to be re-examined.

REFERENCES

Amstutz et al., CORR, 276, 7-18, 1992.
Bartel et al., J Biomed Eng, 107, 193-199, 1985.
Rimanc et al., Trans of the ORS, pg. 175, 1994.
Rostoker, W. and Galante, J. O., J Biomed Mat Res, 13, 964-975, 1979.

ACKNOWLEDGMENTS

This work was supported by DePuy, Inc.

INITIAL EVALUATION OF A DIGITAL EDGE DETECTION TECHNIQUE TO MEASURE UHMWPe WEAR IN TOTAL HIP REPLACEMENTS

S. M. Shaver, T. D. Brown, J. J. Callaghan

Departments of Orthopaedic Surgery and Biomedical Engineering, The University of Iowa, Iowa City, IA 52242.

INTRODUCTION

Several techniques exist to estimate linear polyethylene wear in total hip replacements using conventional clinical anteroposterior radiographs. Some stages of these techniques rely on subjective measurements by the observer, leading to highly variable wear rates. To eliminate observer subjectivity and thereby improve accuracy and reproducibility, a digital image analysis based algorithm, incorporating edge detection techniques, has been developed. To test the reliability of the algorithm, total hip components were loaded in a materials testing machine, and x-rayed. A spherical wear track was milled into each of seven polyethylene cups and the preparation again x-rayed. The radiographs were digitized and the linear wear calculated using the new algorithm. Results show a very strong correlation between actual and calculated wear ($r^2 = 0.982$), with an average (RMS) error of only 0.059 mm. in measuring simulated wear over a range from 0.262 mm. to 1.981 mm.

REVIEW AND THEORY

Accurate measurement of polyethylene (UHMWPe) wear in total hip replacements is of great clinical importance due to biologic reaction to wear debris. Charnley et al. [1] first described a technique to estimate linear polyethylene wear from anteroposterior radiographs. Subsequently, new methods evolved that exhibited higher accuracy and lower variability. Probably the most widely accepted current technique is that of Livermore et al. [2], which employs templates of concentric circles to calculate magnification, and a draftman's compass to locate the direction of maximum wear. Linear wear is then calculated by subtracting the thickness of UHMWPe in the direction of maximum wear on the most recent radiograph from the UHMWPe thickness in the same direction on the original radiograph. Unfortunately, inaccuracies in most contemporary techniques, which require a certain degree of observer subjectivity, limit their application only to situations involving relatively large amounts of wear.

In hopes of improving the accuracy of current techniques, an algorithm was developed with a commercially available programming language (Precision Visuals, Boulder, Colorado) for operation on digitized anteroposterior radiographs. As a first step in calculating linear wear, the algorithm employed objective edge detection techniques to locate pixels constituting the femoral head-polyethylene cup and metal shell-PMMA interfaces (Figure 1). To initiate edge detection, the user cursor-selects a pixel near the center of the femoral head, and two pixels diametrically opposed near the lip of the head. The grayscale (G) values of pixels along a ray from the user defined center point to a lip point are stored. A five-point Lagrange-polynominal differencing formula (Eqn. 1) computes the radial grayscale gradient at each point.

$$\delta G/\delta r = 1/12\,[G_{-2} - (8G_{-1}) + (8G_{+1}) - G_{+2}] \quad (1)$$

Incrementing radially, the gradient is computed at each point until exceeding an empirically determined threshold. To ensure that this flagged pixel constitutes the actual head-cup interface, rather than simply a local background discontinuity, its grayscale value is compared to that of pixels lying just beyond the flagged pixel. The coordinates of a flagged point are stored only when this difference between pixels is large, representing a sustained decrease in grayscale values. The angle between the center point and the lip point is then incremented (typically by 1°) and the operation repeated along a newly defined ray. The angle increments are then continued circumferentially until encountering the second lip point. With an initially high threshold value, only pixels at sharp discontinuities exceed threshold. Repeating the process with successive threshold decrementation fills in a distribution of points along the interface. Using the coordinates of the points, a least-squares subroutine fits an ellipse to the head-cup interface. A similar procedure is invoked to yield an ellipse fitted to the back of the cup.

Once the equations for the two fitted ellipses are known, the distribution of separation distance between points on the metal shell-PMMA interface and the femoral head can be computed on radiographs of virgin versus worn cups (Figure 2). Changes in the separation distance indicate wear, with the linear wear defined as the magnitude of maximum change, and with the wear direction corresponding to the site of this maximum separation change.

PROCEDURES

To demonstrate the accuracy of the algorithm, a Harris/Galante-II shell with a size 58 mm. (actual diameter = 58.2) outside diameter was potted PMMA. One of seven 28 mm. inside diameter UHMWPe liners

(Zimmer, Inc.) was inserted into the metal shell for each trial. The acetabular component was articulated with a 28 mm. Iowa femoral head (actual diameter = 27.85 mm.) and mounted in a materials testing machine. Compressive loading to 100 N assured contact between (1) the back side of the UHMWPe liner and the inside of the metal shell and (2) the femoral component and inside of the liner.

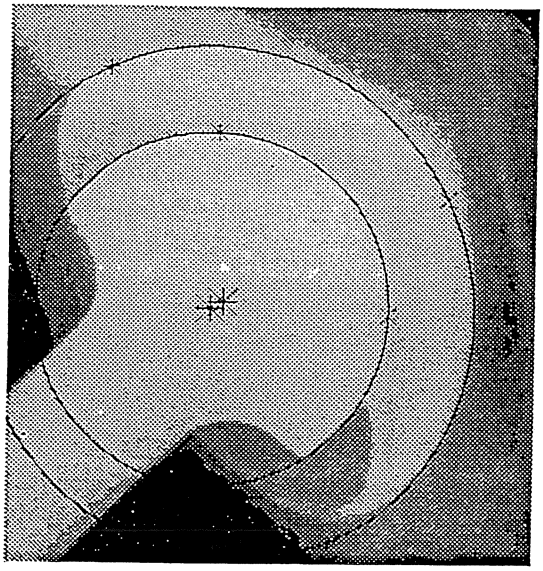

Figure 1. Digitized clinical radiograph with fitted ellipses

A portable x-ray machine was used to radiograph the loaded components using a clinically representative source to cassette distance of 127 cm. (50 in.). After exposure (95 kV, 1 mAS) the liner was removed for the creation of simulated wear. A ball end mill attached to a CNC milling machine was used to ablate material along a spherical front, simulating an ideal linear wear track. A dial gage attached to the milling machine measured the distance from the cup lip to inner apex before and after milling. The liner was then reinserted into the metal shell and again x-rayed, under the same conditions as previously described. The developed x-rays were digitized using a flatbed scanner (QCS-1260, Imapro Corp., Ottawa, Ontario, Canada) at a resolution of 300 pixels/inch (12 pixels/mm), and stored as two-dimensional grayscale arrays of 8-bit integers. Only the cup and the small area immediately surrounding the cup were digitized, to maximize resolution. Subsequent image analysis was run on a CRT screen of a 4000-60 VAXStation workstation (Digital Equipment Corporation, Maynard, MA.).

RESULTS AND DISCUSSION

Algorithm measurement repeatability was checked for a gold standard with respect to 0.914 mm. of simulated wear. The edge detection algorithm calculated an average linear wear of 0.887 mm. (s.d. = 0.038) over seven independent trials. A relative difference of 0.0296. Wear estimates for this same gold standard, performed by an experienced independent observer using the Livermore technique, averaged 0.981 mm. (s.d. = 0.149). Series wide, the image analysis technique had a strong (r^2 = 0.982) correlation with actual wear. The average (RMS) error was 0.059 mm over a simulated wear range from 0.262 mm. to 1.981 mm.

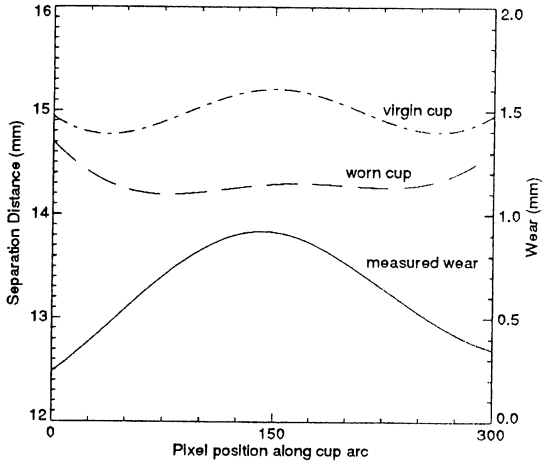

Figure 2. Minimum separation distances between metal shell and femoral head for serial radiographs

Better ability to detect small amounts wear could potentially improve early prediction of long-term outcome. For that reason, a digital image analysis algorithm, incorporating edge detection techniques, has been developed to measure UHMWPe wear in total hip replacements from routine anteroposterior radiographs. Variants of the algorithm can be applied to metal-backed and nonmetal-backed acetabular components, with either cemented or uncemented fixation. Although the program requires user interaction, observer subjectivity has been eliminated.

The digital image analysis approach to UHMWPe wear measurement appears to offer several fold better precision and reproducibility than does the best of current (subjective/manual) techniques, even when the latter is augmented by a stylus digitizer to encode points. Also, with the new digital analysis approach , full 3-dimensional reconstruction of head/cup position is possible, for an arbitrarily eccentric beam source location, subject only to the limits of the film grain size and the image capture resolution.

REFERENCES

1. Charnley, J. et al, 1973. Clin. Orthop., 95:9-26.
2. Livermore, J. et al, 1990. JBJS, 72A(4):518-528.

ACKNOWLEDGMENTS

The authors thank M.J. Rudert, R.L. Aper, D.R. Pedersen, and B. Christianson for their technical assistance. Financial assistance was provided by DePuy, Inc.

AN IN VITRO METHOD FOR QUANTIFYING THE EFFECTIVENESS OF THE LONGITUDINAL ARCH SUPPORT MECHANISM OF A FOOT ORTHOSIS.

Géza F. Kogler†, Stephan E. Solomonidis‡, John P. Paul‡
†Orthopaedic Bioengineering Research Laboratory, Southern Illinois University School of Medicine, Springfield, IL 62794-9230, U.S.A.; ‡Bioengineering Unit, University of Strathclyde, Glasgow, Scotland

INTRODUCTION

Foot orthoses are mechanical devices that provide an external support to the skeletal structure of the foot. Although their use is well-established within the clinical practices of the orthopaedic surgeon, orthotist, and podiatrist, most of the orthotic treatment plans have had little or no scientific testing to evaluate their performance (Nigg, 1986). One of the most common foot pathologies that patients seek medical attention for is plantar fasciitis. Excessive tension of the plantar fascia and repeated loading of the foot is considered to be the cause of the conditions of calcaneal heel spurs and plantar fasciitis which results in symptomatic heel pain and inflammation (Andrews, 1983). The intention of orthotic treatment is to support the skeletal structure of the foot, which in turn will reduce the tension of the plantar aponeurosis (Campbell et al., 1974; Torg et al., 1982, 1987). The purpose of the present study was to develop a quantitative technique for evaluating the longitudinal arch support mechanism of a foot orthosis.

REVIEW AND THEORY

The plantar aponeurosis, also referred to as the plantar fascia is of fundamental importance to the biomechanics of the foot for the transmission of forces to the ground (Sarrafian, 1987). As the foot is subjected to a load its arch elongates, producing a tensile force in the plantar fascia (Wright et al., 1964; Hicks, 1955). Foot morphology is often likened to the engineering structures of an arched beam and truss, referring to the arciform foot skeleton and the plantar aponeuroses contributions as a resistive 'tie' (Hicks, 1955; Lapidus, 1963). Hence, when the foot is loaded a proportion of that load is experienced by the plantar aponeurosis. Based on these principles and the orthotic treatment objectives for plantar fasciitis the following hypothesis was posed: If strain is alleviated with foot orthoses for the treatment of plantar fasciitis and calcaneal heel spurs, a quantifiable reduction in the tension of the plantar aponeurosis should be seen via fixation of a strain transducer.

PROCEDURES

3 fresh frozen right cadaveric lower legs disarticulated at the knee were used in the study, 2 males and 1 female aged 64, 75, and 65 respectively (mean age of 68). A Differential Variable Reluctance Transducer (The Microstrain Co., Burlington, VT.) was implanted into the plantar aponeuroses of cadaveric lower limb feet, through which the strain was calculated in three conditions, specimen barefoot, specimen with shoe, and specimen with shoe and orthosis. Each specimen was instrumented and mounted to a Scott electro-mechanical test machine Model CRE/500 (GCA Precision Scientific, Chicago, IL.) and subjected to ten cycles of preloading and unloading from 0-900 N with the crosshead speed set at 508 mm/min. The application of this load and crosshead speed were also the parameters of what constituted a 'test run'. The reference length and 'zero' position of the transducer was then determined. For this investigation the reference length corresponds to a condition of simulated 'partial weight bearing', with the plantar aponeurosis experiencing slight tension as it initially becomes load bearing. Percentage strain was calculated as a change in length divided by its original length through the formula $\left(\frac{L-Lo}{Lo}\right)\times 100$. 30 test runs were conducted with 10 for each test category. A shoe alignment plate and a mounting fixture assured that limb placement and position would be unchanged as a specimen was prepared for each treatment condition. The voltage output from the transducer and load cell were transferred via amplifier/signal conditioner to a data acquisition board (Real Time Devices Co., State College, PA.) for analog to digital conversion sampled at 750 Hz for a 1.5 second test. As data was sampled it was simultaneously stored on a micro-computer. Time, load, and strain data were collected and analyzed at four load levels (225, 450, 675, 900 N). In addition, the measurements and test design were evaluated for reliability.

RESULTS

The analysis consisted of a detailed evaluation of percent strain and time-to-load. Since the treatment by load interaction was significant ($p<0.05$) indicating that the treatment behaved differently over the four levels of load, the data was further analyzed by performing a one-factor repeated measures ANOVA at each level of load. These results indicate that the effect of treatment was marginally significant ($p = 0.055$) at load 225 N, significant ($p = 0.026$) at load 450 N, significant ($p = 0.016$) at load 675 N, and significant ($p = 0.011$) at the final load of 900 N, for percent strain. In order to determine specifically which treatments differed from one another three paired t-tests were performed between barefoot, shoe, and shoe with orthosis at each load. These results indicated, that in general, the shoe condition showed larger measurements of percent strain than the shoe with orthosis, at load 225 N it was marginally significant ($p = 0.077$), at 450 N significant ($p = 0.048$), at

675 N significant (p = 0.035), and at the final load of 900 N significant (p = 0.026).

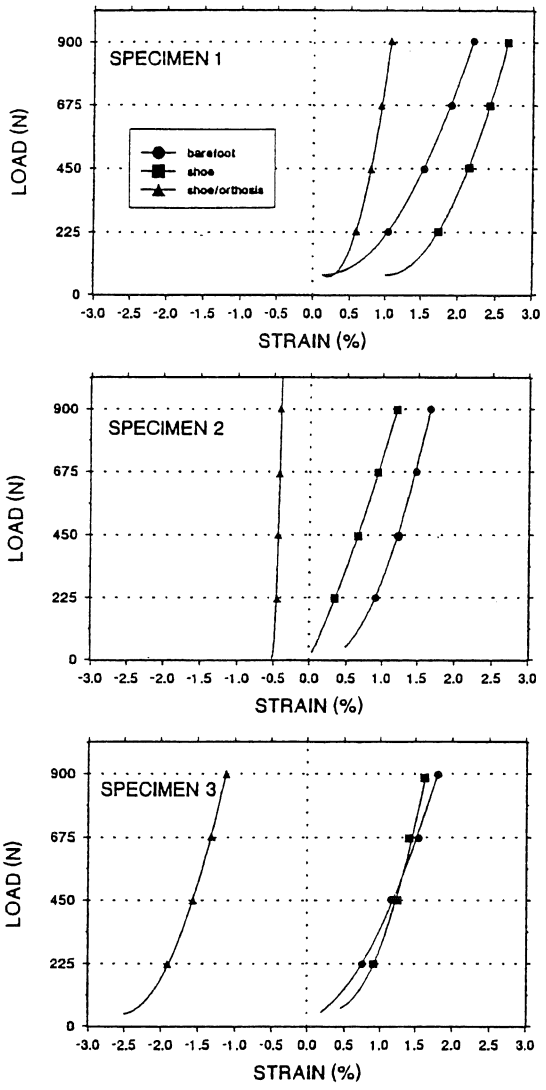

Figure 1. Load-strain curves of plantar fascia of each specimen and the three conditions. Each plot is displayed as a polynomial regression curve of a data set.

STRAIN %

load	barefoot	shoe	shoe / orthosis
225 N	0.69 (0.28)	1.17 (0.39)	-0.59 (1.04)
450 N	1.14 (0.38)	1.53 (0.45)	-0.40 (0.99)
675 N	1.46 (0.41)	1.78 (0.46)	-0.27 (0.95)
900 N	1.70 (0.40)	1.97 (0.46)	-0.14 (0.92)

Table 1. Mean values and (SD) for percent strain. (n=3)

The results for time-to-load, show the same general findings, in that the effect of treatment on time-to-load indicate significant differences for all levels of load in Newton's. Specifically, time-to-load is smaller in the barefoot condition compared to the shoe with orthosis condition under all four loads ($p < 0.05$).

TIME (s)

load	barefoot	shoe	shoe / orthosis
225 N	0.32 (0.03)	0.37 (0.04)	0.52 (0.05)
450 N	0.45 (0.03)	0.53 (0.05)	0.77 (0.08)
675 N	0.53 (0.03)	0.65 (0.04)	0.94 (0.10)
900 N	0.60 (0.04)	0.74 (0.04)	1.07 (0.11)

Table 2. Mean values and (SD) for time-to-load. (n=3)

DISCUSSIONS

Our investigations defined the patterns of strain in the plantar aponeurosis under three conditions (barefoot, shoe, shoe/orthosis). The findings support our hypothesis, demonstrating that the strain in the plantar aponeurosis is reduced with the application of an orthosis with a shoe. An in vitro method which measures the strain in the plantar aponeurosis can be used to quantify the effectiveness of the longitudinal arch support mechanism of foot orthoses. The relevance of this decreased strain is clinically noteworthy, since this is the primary objective for orthotic treatment of plantar fasciitis and calcaneal heel spurs. The orthoses' ability to treat these conditions may be further enhanced by its inherent "damping effect," observed in the time-to-load data. These results showed that the time-to-load was significantly increased with the shoe/orthosis condition compared to the barefoot situation. This delayed loading has also been suggested as a form of treatment for plantar fasciitis by cushioning the foot during weight bearing (Helal et al., 1988). The conventional oxford shoe tested did not show any arch support properties compared to the barefoot condition. It follows that further investigations be conducted with regard to the arch support capabilities of shoes.

REFERENCES

Andrews, J. R. Clin. Sports Med., 2(1): 137, 1983.
Campbell, J. W. et al. Clin. Orthop., 103: 57-62, 1974.
Helal, B. et al. Churchill & Livingston, NY, 2: 1004, 1988.
Hicks, J. H. Acta. Anat., 25: 34-45, 1955.
Lapidus, P. W. Clin Orthop., 30: 20-35, 1963.
Nigg, B. M. Human Kinetics Books,, Champaign, IL, 1986.
Sarrafian, S. K. Foot and Ankle, 8 (1): 4-18, 1987.
Torg, J. S. Clin. Sports Med., 1(1): 157-175, 1982.
Torg, J. S. et al. Clin. Sports Med., 6(2): 291-320, 1987.
Wright, D. G et al. J Bone Jt Surg., 46A: 482-492, 1964.

ACKNOWLEDGMENTS

This investigation was supported by a Central Research Committee Award from Southern Illinois University School of Medicine and (in part) by a grant from the Pedorthic Footwear Association Research Foundation.

TOTALS:

Printed 328 of the 366 records.

PRIMARY SORT FIELD: author

SELECTION CRITERIA:
All records